

Solution Properties of Polysaccharides

Solution Properties of Polysaccharides

David A. Brant, EDITOR
University of California

Based on a symposium
sponsored by the Division
of Carbohydrate Chemistry
at the 179th Meeting of the
American Chemical Society,
Houston, Texas,
March 24–27, 1980.

A C S S Y M P O S I U M S E R I E S **150**

AMERICAN CHEMICAL SOCIETY
WASHINGTON, D. C. 1981



Library of Congress CIP Data

Solution properties of polysaccharides.
(ACS symposium series, ISSN 0097-6156; 150)

Includes bibliographies and index.

1. Polysaccharides—Congresses. 2. Solution (Chemistry)—Congresses.

I. Brant, David A. II. American Chemical Society.
Division of Carbohydrate Chemistry. III. Series.

QD320.S5 547.7'8204541 81-236
ISBN 0-8412-0609-0 ACSMC8 150 1-580 AACR2

Copyright © 1981

American Chemical Society

All Rights Reserved. The appearance of the code at the bottom of the first page of each article in this volume indicates the copyright owner's consent that reprographic copies of the article may be made for personal or internal use or for the personal or internal use of specific clients. This consent is given on the condition, however, that the copier pay the stated per copy fee through the Copyright Clearance Center, Inc. for copying beyond that permitted by Sections 107 or 108 of the U.S. Copyright Law. This consent does not extend to copying or transmission by any means—graphic or electronic—for any other purpose, such as for general distribution, for advertising or promotional purposes, for creating new collective work, for resale, or for information storage and retrieval systems.

The citation of trade names and/or names of manufacturers in this publication is not to be construed as an endorsement or as approval by ACS of the commercial products or services referenced herein; nor should the mere reference herein to any drawing, specification, chemical process, or other data be regarded as a license or as a conveyance of any right or permission, to the holder, reader, or any other person or corporation, to manufacture, reproduce, use, or sell any patented invention or copyrighted work that may in any way be related thereto.

PRINTED IN THE UNITED STATES OF AMERICA

**American Chemical
Society Library
1155 16th St. N. W.
Washington, D. C. 20036**

ACS Symposium Series

M. Joan Comstock, *Series Editor*

Advisory Board

David L. Allara	James P. Lodge
Kenneth B. Bischoff	Marvin Margoshes
Donald D. Dollberg	Leon Petrakis
Robert E. Feeney	Theodore Provder
Jack Halpern	F. Sherwood Rowland
Brian M. Harney	Dennis Schuetzle
W. Jeffrey Howe	Davis L. Temple, Jr.
James D. Idol, Jr.	Gunter Zweig

FOREWORD

The ACS SYMPOSIUM SERIES was founded in 1974 to provide a medium for publishing symposia quickly in book form. The format of the Series parallels that of the continuing ADVANCES IN CHEMISTRY SERIES except that in order to save time the papers are not typeset but are reproduced as they are submitted by the authors in camera-ready form. Papers are reviewed under the supervision of the Editors with the assistance of the Series Advisory Board and are selected to maintain the integrity of the symposia; however, verbatim reproductions of previously published papers are not accepted. Both reviews and reports of research are acceptable since symposia may embrace both types of presentation.

PREFACE

This volume is the outgrowth of a symposium on the solution properties of polysaccharides and reflects the success of the symposium in bringing together an international group of experts engaged in studies of virtually every aspect of the solution behavior of polysaccharides. Thirty-seven chapters span the range from conformational analysis of dissolved polysaccharides using spectroscopic, scattering, hydrodynamic, and theoretical methods to experimental and theoretical investigations of the interactions between dissolved polysaccharide chains and between polysaccharides and a variety of high- and low-molecular-weight ligand species. Without exception these chapters are at the forefront of the activity in their respective fields, and the book represents an unmatched resource for persons who wish to remain or become conversant with current research on polysaccharide solution properties.

Chemical and biological interest in polysaccharides has begun to shift over the past decade from the structural and storage polysaccharides of plant origin, e.g. cellulose, carrageenan, and starch, toward polysaccharides of animal and, especially, microbial origin. The existing and potential commercial importance of extracellular microbial polysaccharides produced by fermentation using relatively inexpensive feedstocks has provided a major impetus for the increasing attention being given to these materials; the range of chemical and structural characteristics represented among the known microbial polymers and those potentially available by genetic engineering techniques can only further encourage this activity. Among polysaccharides of animal origin attention now is focused strongly on the mucopolysaccharides or proteoglycans that occur, usually in close association with protein, in the intercellular matrix of the connective tissues. This interest is motivated by evidence that abnormalities in the distribution of these substances accompany a number of serious metabolic diseases. Finally, the emerging recognition of poly- and oligosaccharides as immunochemical determinants has served as a strong stimulus for studies of polymers of both animal and microbial origin.

The polysaccharides derived from these two sources are almost always highly solvated, if not actually dissolved, in their native environment. Consequently it is appropriate that investigations of the relationships between the chemical structures and the physical and biological properties of these species should give special attention to their solution behavior.

Even for those polysaccharides that are crystalline or semicrystalline in nature, solution studies must play an important role. Investigations of the solution properties of all polymers are necessary not only to obtain fundamental data concerning the mean molecular weights and molecular-weight distributions of the macromolecular species, but also to provide information about relationships between chemical structure and the inherent conformational characteristics of individual macromolecules free of interactions with other like or unlike species. Such interactions are, of course, important for the biological function and physical behavior of polysaccharides, and solution studies also provide a unique avenue to information about interactions between small numbers of polysaccharide chains or between polysaccharides and other kinds of molecules and ions. This book illustrates the diverse modern techniques currently being exploited to investigate these properties of polysaccharides in solution.

University of California at Irvine
Irvine, CA 92717

DAVID A. BRANT

November 4, 1980

Quasielastic Light-Scattering Studies of Xanthan in Solution

J. G. SOUTHWICK, A. M. JAMIESON, and J. BLACKWELL

Department of Macromolecular Science, Case Western Reserve University,
Cleveland, OH 44106

We are using quasielastic light scattering to investigate the conformation and interactions of xanthan in aqueous solution. Xanthan is the extracellular polysaccharide produced by the bacterium *Xanthomonas campestris* and has a wide variety of uses, e.g. as a viscosity enhancer and food additive. The chemical structure is a repeating pentasaccharide: (1,2) a β -1,4-D-glucan backbone with a trisaccharide substituent on alternating backbone residues. The side chain is β -1,3 linked β -D-mannopyranosyl- α -1,4-D-glucopyranosyl- β -1,2-D-mannopyranoside 6-O-acetate. In addition, the terminal D-mannose residue of the side chain may have a pyruvic acid residue linked at the 4- and 6- positions. The degree of pyruvation typically varies from 0.31 - 0.56, (3) depending on the bacterial strain, history, and fermentation conditions. (4,5)

Early physical chemical studies of xanthan in aqueous solution at low ionic strength showed an unusual property in that there was a sigmoidal increase in the viscosity of a 1% solution at $T_m \sim 55^\circ\text{C}$. (6) Spectroscopic measurements using ORD, CD, and NMR methods have also detected this transition. (7) At room temperature a broad, featureless NMR spectrum is obtained, but the spectra become sharp and detailed above the transition temperature. As a result, the transition is explained as an order-disorder phenomenon, probably due to conversion of a helix to a flexible coil. It has also been shown that the transition temperature is variable, depending on the presence of trace ions. (8)

From x-ray diffraction studies of oriented crystalline films, Moorhouse *et al* (9) showed that the most likely solid state conformation is a 5_1 right-handed single helix, repeating in 47Å. A significant feature of this structure is that the trisaccharide side chains are arranged close to (and hydrogen bonded to) the glucan backbone, which could be expected to stabilize a stiff helical conformation in solution. However, the x-ray patterns were not of sufficient quality to determine the structure unambiguously, and other conformations including multiple strand helices also need to be considered. Electron microscopy by Holzwarth (10)

0097-6156/81/0150-0001\$05.00/0
© 1981 American Chemical Society

has shown that rod-like aggregates are precipitated from unheated xanthan solutions. Shorter, thinner chains are observed in preparations of heated (denatured) xanthan, and from the observed dimensions it is argued that the ordered form consists of a double helical aggregate of an average of 40 chains.

Our light scattering studies focused initially on the thermal transition, in order to compare the diffusion properties of xanthan above and below T_m . This led to an interest in the concentration dependence of diffusion and the development of chain overlap and entanglement points. Some of the work reviewed below has been published separately. (11,12,13,14)

Experimental

Xanthan Solutions. Specimens of xanthan were obtained from Kelco Co. (Kelzan) and from Dr. P. Sandford, then at U.S.D.A. Northern Regional Laboratory, and were purified by the method described by Holzwarth. (8) An aqueous stock solution containing $\sim 0.5\%$ xanthan was prepared by addition of distilled deionized water that had previously been filtered through $0.1\mu\text{m}$ Millipore filters (to remove bacteria, dust, etc.). This solution was dialyzed for four days against filtered distilled deionized water. Other than for the first solutions used for the thermal studies, sodium azide (0.02%) was added to the stock solutions to retard bacterial growth. Solutions at different concentrations were prepared by dilution with 0.02% aqueous sodium azide. Preparations before and at different intervals after filtration were checked for possible bacterial growth by examination of shadowed specimens in a Jeol 100B electron microscope. Bacterial cells were not seen in xanthan solutions that had been filtered through $0.22\mu\text{m}$ Millipore filters; these solutions remained sterile for over a month.

Aqueous xanthan solutions (in 0.02% sodium azide) were routinely filtered and centrifuged at $\sim 4350g$ for 30 minutes before collecting the light scattering data. These solutions showed a slow transition to lower values of D_t , at a rate that increased with the concentration, and this time dependence is one of the subjects of this paper. Solutions in filtered $4M$ urea were maintained at 90°C for three hours and then cooled slowly to room temperature.

Light Scattering. The thermal transition was studied using a laser light scattering instrument consisting of an argon ion laser ($\lambda = 4880\text{\AA}$), an EMI 9656KR phototube, a Keithley 104 wide band amplifier, and a Saicor SAI-52 real time 400 point spectrum analyzer and digital integrator; the homodyne data were recorded as the voltage spectra and converted to the power spectra by squaring 40 data points and subtracting the background. The latter data formed the input for a Lorentzian curve fitting program, from which the half width at half height, Γ , was deter-

mined. Γ can be related to the diffusion coefficient D through the equation

$$\Gamma = DK^2 \quad (1)$$

where K is the scattering vector ($\vec{K} = \frac{4\pi n}{\lambda} \sin \theta/2$).

In later work the above apparatus for spectrum analysis was replaced by a digital photon correlation spectrometer. Radiation at $\lambda = 6328\text{\AA}$ from a He-Ne laser was focused on the solution, and the scattered photons were detected using an ITT FW130 phototube with a Pacific Photometrics discriminator/amplifier system. The correlation function was computed by a Honeywell Saicor SAI-42A correlator and probability analyzer that was modified to permit digital photon correlation analysis. For a monodisperse specimen the time correlation function of the intensity fluctuations, $C(\tau)$ is given by

$$C(\tau) = Ae^{-\Gamma\tau} + B \quad (2)$$

where A is a constant, τ is the time, B is the background, and Γ , the time constant, (the half width at half height in the Lorentzian spectrum). Γ is determined from the slope of a plot of $\ln C(\tau)$ against τ . For a specimen containing a distribution of molecular weights, a plot of $\ln C(\tau)$ against τ exhibits a degree of curvature. We have applied the analysis procedure of Brown *et al.* (15) in which the following quadratic function is fitted to the data:

$$\ln|C(\tau)| - B = -\bar{\Gamma}\tau + \frac{1}{2!} \frac{\mu_2}{\bar{\Gamma}^2} (\bar{\Gamma}\tau)^2 \quad (3)$$

The initial slope of the plot, $\bar{\Gamma}$, is now the average time constant, and is related to the Z-averaged diffusion coefficient by equation (1). The degree of curvature of the plot is dependent on the polydispersity which can be quantified by the parameter $\mu_2/\bar{\Gamma}^2$.

Results and Discussion

In a quasielastic light scattering study of macromolecular solutions, it is essential to establish a clear relationship between the experimental conditions and the type of relaxation phenomena manifest in the light scattering data. To accomplish this, one must perform experiments over a range of scattering angles and solution concentrations. One of our objectives is to determine the translational diffusion coefficient (D_t) for xanthan, and to relate this parameter to a hydrodynamic size.

Effect of Scattering Angle

Akcasu *et al*(16) have recently shown that QELS is due simply to translational diffusion provided $\vec{K}R_g < 2.5$, where \vec{K} is the scattering vector ($\frac{4\pi n}{\lambda} \sin \theta/2$) and R_g is the radius of gyration. However, if $\vec{K}R_g > 2.5$, internal motions such as rotational diffusion and intrachain relaxations are also evident in the light scattering data. Figure 1 presents a plot of Γ against $\sin^2\theta/2$, where Γ is the half-width determined from the light scattering power spectrum for an 0.025% salt-free solution of xanthan. A linear relationship exists between Γ and $\sin^2\theta/2$ for $\theta < 60^\circ$, and in this region the translational diffusion coefficient, D_t , is given by $\Gamma = D_t \vec{K}^2$. Internal motions are evident in the data at $\theta > 60^\circ$ and these lead to positive deviations from the linear behavior. If we take $\theta = 60^\circ$ as the smallest scattering angle where internal relational motions are evident, and apply the equation of Akcasu *et al*(16) ($\vec{K}R_g = 2.5$), then $R_g = 1456\text{\AA}$ for xanthan in solution.

Effect of Concentration

The relaxational phenomena evident in the light scattering data also depend upon the concentration of polymer in solution, and D_t can only be determined in dilute solutions. With increasing concentration for flexible coil macromolecules, a critical concentration c^* is reached where molecular domains begin to overlap with each other, resulting in an entangled network structure. At concentrations above c^* , quasielastic light scattering detects the motion of chain segments between points of entanglement. Figure 2 presents a plot of the measured diffusion coefficient against concentration for xanthan solutions at low constant ionic strength. It is seen that the slope changes at a concentration of $c \approx 0.015\%$, and this transition could correspond to the onset of chain interactions. Extrapolation to $c = 0$ yields a hydrodynamic radius of $R_h = 1200\text{\AA}$, and, from the molecular weight of $\bar{M} = 2.16 \times 10^6$ (see below), overlap is predicted at $c \approx 0.03\%$, assuming spherical molecules. However, current investigations favor a more rod-like conformation for xanthan, in which case the transition at $c \approx 0.015\%$ could arise due to interparticle interference effects, and further studies are in progress on this point.

In later work we reexamined low (constant) ionic strength solutions of a second xanthan specimen (Kelzan) using the more sensitive method of photon correlation analysis. Figure 3 presents

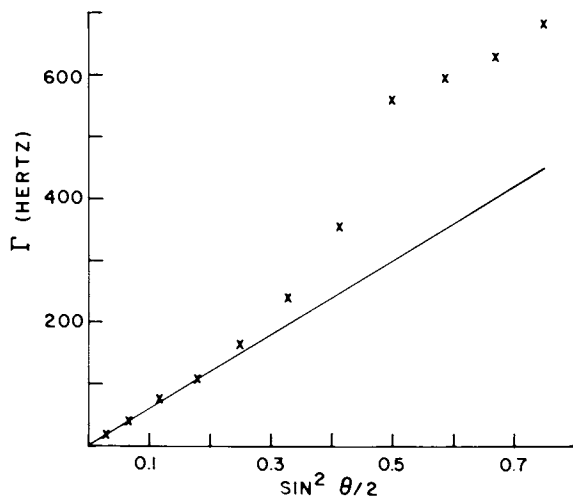


Figure 1. Plot of the halfwidth at half height ($\bar{\Gamma}$) against $\sin^2\theta/2$ (θ is the scattering angle) for a 0.025% solution of xanthan at 25°C and low ionic strength

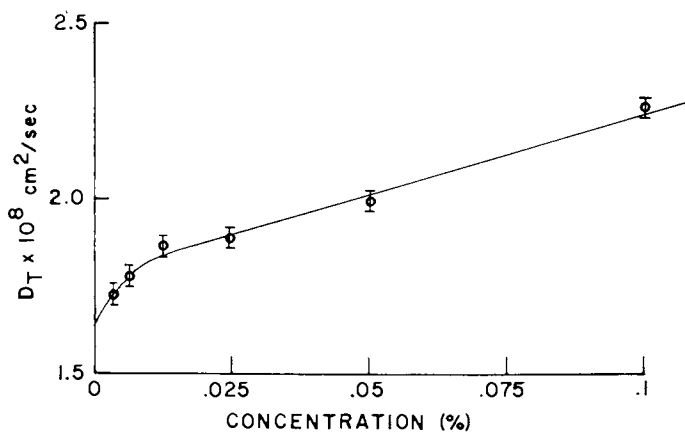


Figure 2. D_i vs. concentration for xanthan in aqueous solution at low ionic strength. The data were recorded at $\theta = 40^\circ\text{C}$ and 25°C .

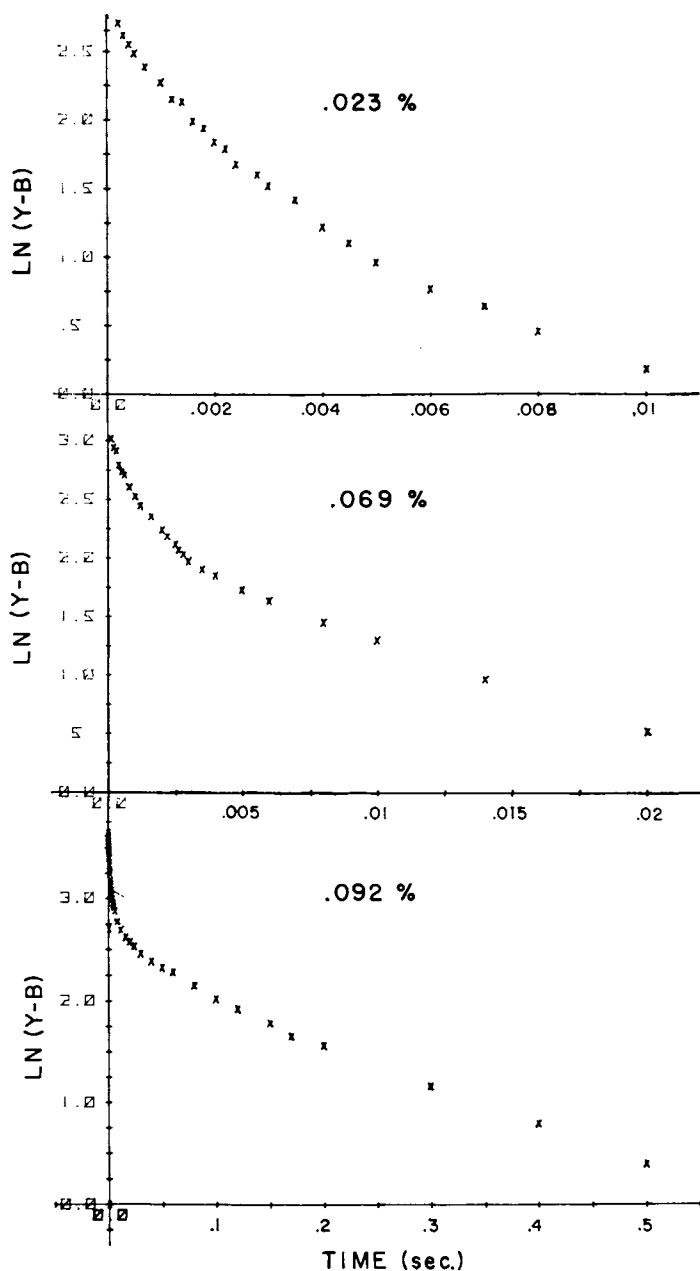


Figure 3. Plots of the logarithm of the correlation function vs. time for aqueous xanthan solutions at 0.023%, 0.069%, and 0.092% concentrations and low ionic strength (0.02% sodium azide). Data were collected at $\theta = 40^\circ\text{C}$ and 17°C . $Y - B$ is the experimental measurement minus the background; $(Y - B)^{1/2}$ is equal to $C(\tau)$ in Equation 2.

correlation functions plotted as $\ln(Y-B)$ vs time for QELS data obtained from low ionic strength xanthan solutions at three concentrations; 0.023%, 0.069%, and 0.092%. It is seen that the plot for the 0.023% xanthan solution shows a significant degree of curvature, which is probably due to the correlation length polydispersity. Correlation functions for 0.004% and 0.0115% solutions gave plots similar to the 0.023% plot in that they evidenced a single, polydisperse relaxation mode. However, the curves for the 0.069% and 0.092% solutions show a discontinuous change in slope: a degree of curvature similar to the data for $c=0.023\%$ is evident at shorter correlation times ($\tau < 0.005s$), but at longer correlation times the curves appear to be linear. The data obtained from a 0.14% xanthan solution give a plot of $\ln(Y-B)$ vs time which is qualitatively similar to 0.092% plot.

The first moments ($\bar{\Gamma}$) determined from the correlation functions are plotted against concentration in Figure 4. $\bar{\Gamma}$ increases with concentration up to $c \approx 0.015\%$ where it passes through an inflection, and then continues to increase to $c \sim 0.07\%$. At $\sim 0.07\%$ the data indicate that fast and slow relaxation processes coexist in solution, as evidenced by the discrete change in the slope of the 0.069% curve in Figure 3. As the concentration is increased above 0.07%, $\bar{\Gamma}$ decreases to an almost constant value for both the fast and slow processes. This transition is designated c_2 , and corresponds to a major effect in the quasielastic light scattering data: specifically, a transition from a single (polydisperse) relaxation mode to bimodal relaxation behavior, due to the appearance of an additional slow relaxation mechanism as well as a general slowing down of the relaxation times.

Presently we can see two possible explanations for the occurrence of the c_2 transition. Firstly, the transition could be due to a sol-gel transition, such that junction zones are formed at c_2 through intermolecular alignment of the stiff xanthan chain segments. Under these circumstances, the diffusion of the junction zones through the solution would be the source of the slow relaxation process. The fast relaxation process corresponds to the diffusion of non-aligned chain segments, i.e. sections of the chains between junction zones. A second possible explanation arises from the hydrodynamical model for semi-dilute solutions of rigid rods proposed by Doi and Edwards.(17,18) This theoretical model predicts that for semi-dilute solutions the correlation function will exhibit a transition to a non-exponential decay which bears a strong resemblance to a bimodal exponential relaxation. However our experimental results are only qualitatively in agreement with the predictions of Doi and Edwards, and further work is necessary to distinguish between these two possibilities, i.e. junction zones between semiflexible chains or a completely rigid rod conformation.

Thermal Transition

Our studies of the thermal transition in xanthan solutions were done using the spectrum analyzer, which was not sufficiently sensitive to allow us to perform experiments at high temperatures for concentrations below c^* . Nevertheless, we were able to look at the thermal properties of higher concentration solutions. Figure 5 shows the hydrodynamic radii determined from the Stokes-Einstein equation plotted as a function of temperature for a 0.1% salt-free (NRRL) xanthan solution. This concentration corresponds to semidilute conditions ($c^* < c < c_2$). However, we would expect that the behavior of the apparent hydrodynamic radius, R_h^{app} , which is calculated from our apparent diffusion coefficient, will be qualitatively similar to the behavior of the true R_h . From Figure 5 it is seen that heating the solution results in an increase in R_h^{app} from 840Å at 15°C to 940Å at 34°C, whereupon a further increase in temperature causes the measured radius to decline to 650Å at ~47°C. Above 47°C the macromolecular dimensions again increase with temperature to a value of 770Å at ~68°C. Upon cooling the solution a sigmoidal increase in the hydrodynamic radius is seen, with midpoint ~39°C, and the radius measured at room temperature (22°C) after heating and cooling is ~1100Å, which is ~200Å larger than the original value (i.e. before heating). Experimental spectra obtained in the region of the transition (35-40°C) could not be fitted to a Lorentzian curve regardless of the number of points skipped, and therefore Z-average hydrodynamic radii could not be determined at these temperatures.

The data indicate that the thermal transition evident in low ionic strength xanthan solutions results in a reduction in the apparent radius of the particle, a result which is consistent with a helix→coil transition. The poor fit to a single Lorentzian curve for the data in the transition region implies a greater polydispersity in relaxation times at these temperatures. This is a significant observation, since single relaxation behavior has been reported(19,20) in the transition region for other macromolecules that are known to undergo single helix-coil transitions in solution. Interpretation of this enhanced polydispersity near T_m is difficult in view of the concentration, but the most likely explanation is that intermolecular associations occur below T_m and these probably disengage just prior to the conformational transition. In support of this interpretation we note that quiescent birefringence has been observed in low ionic strength xanthan solutions for $c > 0.25\%$, (21) and that this birefringence is seen to disappear at a value equal to T_m . In addition the slow relaxation mode in low ionic strength solutions of Kelzan at $c > 0.07\%$ (as described above) points to intermolecular associations at these higher concentrations. The higher values of R_h^{app} observed on cooling below T_m are probably related to our observation of a time dependent aggregation in xanthan at low ionic strength.(12)

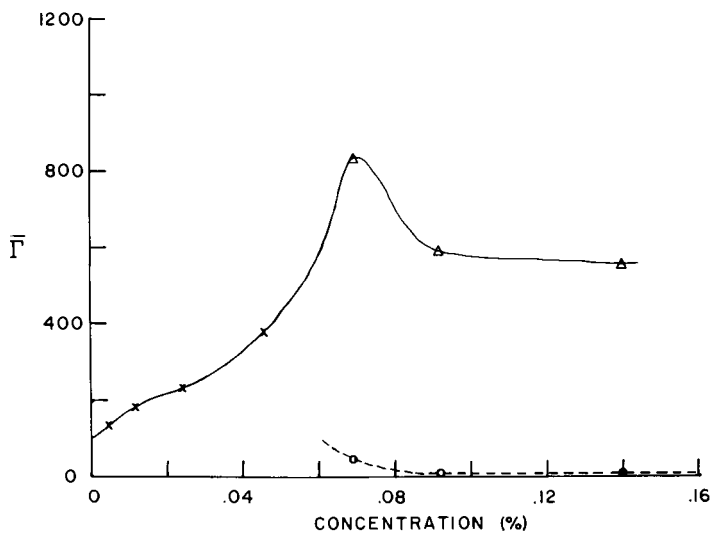


Figure 4. The z-average time constant $\bar{\Gamma}$ vs. concentration for xanthan solutions in 0.02% aqueous sodium azide: (X) values determined from single-mode correlation functions; (Δ and \circ) values determined for the fast and slow modes, respectively, from bimodal correlation functions.

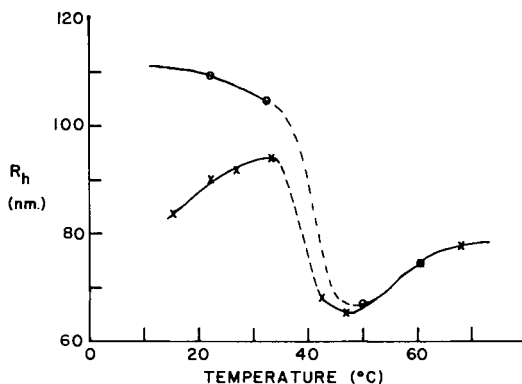


Figure 5. Apparent hydrodynamic radii vs. temperature for a 0.1% xanthan solution at low ionic strength: (X) data obtained on heating the solutions; (\circ) data obtained on subsequent cooling; (---) temperatures where the z-average diffusion coefficients could not be determined, probably due to polydispersity.

Characterization of the Random Coil Conformation

The solution properties of xanthan dissolved in 4M urea solutions ($c < 0.06\%$; low ionic strength) are distinctly different after the solution has been heated for three hours at 90°C and recooled to room temperature. The optical rotation at 365nm for unheated xanthan in 4M urea is $[\alpha]_{365} = -46^\circ$, as compared to $[\alpha]_{365} = -15^\circ$ for the heated and cooled solution; $[\alpha]_{365} = -35.8^\circ$ for xanthan in aqueous solution. Figure 6 shows plots of $[\alpha]_{365}$ against temperature for xanthan in aqueous solution (A), and heat treated xanthan in 4M urea (B). The aqueous solution shows data very similar to that reported by Morris *et al.*, (7) and probably corresponds to an order-disorder transition. However, for the heat treated 4M urea solution $[\alpha]_{365}$ is constant (-15°) up to 50°C , above which the negative rotation decreases to 20° at 60°C . Above 55°C it is seen that the behavior for the two systems is similar: $[\alpha]_{365}$ decreases with temperature at approximately the same rate. These data suggest that conformational differences exist between xanthan in aqueous (unheated) and heat treated 4M urea solutions, and that the molecular conformation in the heated urea solution is a random coil, which is also the conformation in low ionic strength solutions at high temperatures.

Distinct differences between the aqueous (unheated) and heat treated 4M urea solution are also seen in the hydrodynamic properties. Figure 7 is a plot of η_{sp}/c against shear rate ($\dot{\gamma}$) for 0.025% solutions of xanthan in three solvent systems; (A) 0.01M NaCl, (B) 1.0M NaCl, and (C) heat treated 4M urea. One can see that the urea solution does not show the large shear thinning effects evident in the sodium chloride solutions, which is again suggestive of a flexible coil conformation in (heated) urea. We have also determined the zero shear intrinsic viscosities and limiting translational diffusion coefficients for xanthan in both the ordered and random conformations, and have calculated the hydrodynamic radii using the Stokes-Einstein equation. These data are presented in Table I. Our values for the zero shear intrinsic viscosities are of limited accuracy since we have used a 4-bulb variable shear capillary viscometer for these measurements, and a low shear Newtonian viscosity regime was not detected. Nevertheless, this technique does demonstrate the large hydrodynamic differences between the two xanthan conformations. The hydrodynamic radii calculated for the ordered and disordered conformations agree qualitatively with our results obtained from a salt-free 0.1% solution as a function of temperature. The disordered conformation has a smaller hydrodynamic radius, which is probably sensitive to ionic strength. We note that Dintzis *et al.* (22) originally applied the solution preparation technique of heating 4M urea xanthan solutions, and concluded that such solutions were "true solutions" of xanthan, whereas unheated solutions in either 4M urea or ammonium acetate were not "true solutions", but formed dispersions. Our data show that conformational differences are apparent in these solutions.

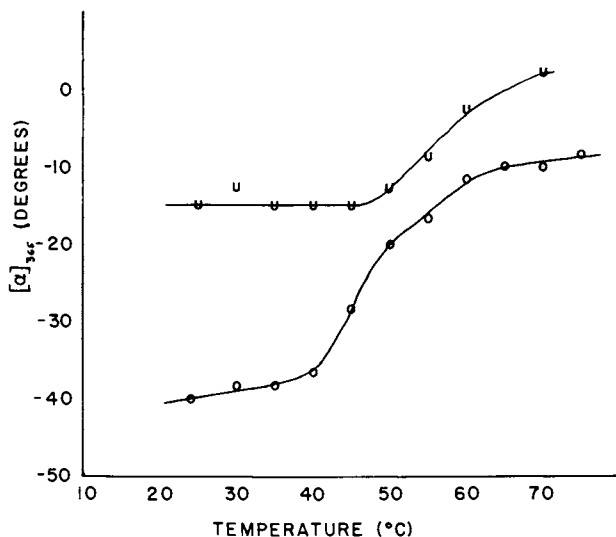


Figure 6. Specific optical rotation $[\alpha]_{365}$ vs. temperature: (O) data for a 0.06% solution of xanthan in 0.02% sodium azide; (X) data for a 0.047% solution of xanthan in 4M urea that had been maintained at 90°C for 3 h.

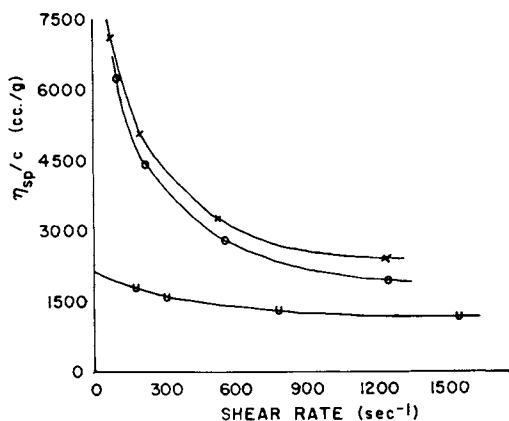


Figure 7. Plots of η_{sp}/c vs. shear rate ($\dot{\gamma}$) for 0.025% xanthan solutions in the following solvents: (X) 0.01M sodium chloride; (O) 1.0M sodium chloride; (U) 4M urea. The solution was maintained at 90°C for 3 h before collecting the data.

This research was supported in part by the National Science Foundation through grants PCM 18631 and ENG 76-20278.

Abstract

Quasielastic light scattering has been used to investigate the properties of xanthan gum in aqueous solution as a function of concentration, temperature, and solvent. With increasing concentration, a transition is seen at $c^* = 0.015\%$ corresponding approximately to the onset of molecular overlap. A second transition is also detected at a higher concentration $c_2 \approx 0.07\%$ where, in addition to a general reduction in the relaxation times, the single (polydisperse) relaxation mode observed below c_2 is replaced by bimodal behavior above the transition. Two possible explanations exist for such an effect: the slow mode could originate from intermolecular associations of semirigid chains; alternatively, xanthan chains could exist as rigid rods in solution and such a system would exhibit a slow mode due to librational motions (restricted rotations) above a critical concentration [Doi and Edwards(17,18)]. The thermal transition evident in low ionic strength xanthan solutions can be followed by light scattering, and it is observed that the apparent hydrodynamic radius significantly decreases with increasing temperature in the vicinity of the transition temperature, T_m . In addition there is an increase in the macromolecular polydispersity near to T_m . These results indicate that the thermal transition corresponds to a disruption of an aggregate structure which is coincident with the previously reported conformational change. Finally, the solution properties of xanthan solutions in 4M urea following heat treatment are interpreted in terms of a truly random coil conformation under these conditions.

Literature Cited

1. Jansson, P.E.; Keene, L.; Lindberg, B. Carbohydr. Res., 1975, 45, 275.
2. Melton, L.D.; Mindt, L.; Rees, D.A.; Sanderson, G.R. Carbohydr. Res., 1976, 46, 245.
3. Sandford, P.A.; Watson, P.R.; Knutson, C.A. Carbohydr. Res., 1978, 63, 253.
4. Cadmus, M.C.; Rogovin, S.P.; Burton, K.A.; Pittsley, J.E.; Knutson, C.A.; Jeanes, A. Can. J. Microbiol., 1976, 22, 942.
5. Cadmus, M.C.; Knutson, C.A.; Lagoda, A.A.; Pittsley, J.E.; Burton, K.A. Biotech. Bioeng., 1978, 20, 1003.
6. Jeanes, A.; Pittsley, J.E.; Senti, F.R. J. Appl. Polym. Sci., 1961, 5, 519.
7. Morris, E.R.; Rees, D.A.; Young, G.; Walkinshaw, M.D.; Darke, A. J. Mol. Biol., 1977, 110, 1.
8. Holzwarth, G. Biochemistry, 1976, 15, 4333.

9. Moorhouse, R.; Walkinshaw, M.D.; Arnott, S. Am. Chem. Soc., Symp. Ser., 1977, No. 45, 90.
10. Holzwarth, G.; Prestridge, E.B. Science, 1977, 197, 757.
11. Southwick, J.G.; McDonnell, M.E.; Jamieson, A.M.; Blackwell, J. Macromolecules, 1979, 12, 305.
12. Southwick, J.G.; Lee, H.S.; Jamieson, A.M.; Blackwell, J. Carbohydr. Res., 1980, in press.
13. Southwick, J.G.; Jamieson, A.M.; Blackwell, J. submitted to Macromolecules.
14. Southwick, J.G.; Jamieson, A.M.; Blackwell, J. submitted to Carbohydr. Res.
15. Brown, J.C.; Pusey, P.N.; Dietz, R. J. Chem. Phys., 1975, 62, 1136.
16. Akcasu, A.Z.; Benmouna, M.; Han, C.C. personal communication.
17. Doi, M.; Edwards, S.F. J. Chem. Soc. Faraday II, 1978, 74, 560.
18. Doi, M.; Edwards, S.F. J. Chem. Soc. Faraday II, 1978, 74, 918.
19. Jamieson, A.M.; Mack, L.; Walton, A.G. Biopolymers, 1972, 11, 2267.
20. Lee, W.I.; Schurr, J.M. Biopolymers, 1974, 13, 903.
21. Milas, M.; Rinaudo, M. Carbohydr. Res., 1979, 76, 189.
22. Dintzis, F.R.; Babcock, G.E.; Tobin, R.; Carbohydr. Res., 1970, 13, 257.

RECEIVED October 9, 1980.

Is Xanthan a Wormlike Chain or a Rigid Rod?

GEORGE M. HOLZWARTH

Exxon Research and Engineering Company, P.O. Box 45, Linden, NJ 07036

Xanthan is a high-molecular-weight polysaccharide of widespread utility as a viscosity-increasing additive for water. Aqueous xanthan solutions are markedly shear-thinning (non-Newtonian): the viscosity of a 1 mg/ml solution changes from 700 cP to less than 10 cP as the shear stress varies from 0.01 to 20 dyne cm⁻².

Shear thinning behavior of dilute polymer solutions can be qualitatively explained by two distinct models: (1) the molecule may be a non-deformable, highly elongated prolate ellipsoid which becomes oriented at high shear stresses; (2) the molecule may be a stiff but nevertheless wormlike chain which becomes oriented and deformed under high shear stresses.

The first model has been explored for xanthan by Whitcomb and Macosko (1), who show that an undeformable ellipsoid of length 1.5 μm and midpoint diameter 19 Å can fit data they observed for the variation of intrinsic viscosity with shear stress in distilled water. Rinaudo and Milas (2) have also adopted this model to fit their intrinsic viscosity and sedimentation data.

In contrast, a recent study from this laboratory (3) concludes that native xanthan molecules are better viewed as stiff but wormlike chains. This conclusion follows from measurements of zero-shear intrinsic viscosity for a homologous series of xanthans of different molecular weight: for native xanthan the exponent z in the relation $[\eta] = KM^z$ is only 0.96 rather than 1.8 as expected for rigid rods. It is the goal of this paper to explore whether a wormlike model is consistent with other experimental data, especially the dependence of intrinsic viscosity on shear stress (non-Newtonian behavior).

Chain stiffness can be quantitatively characterized by the persistence length a , defined as

$$a = \lim_{n \rightarrow \infty} h^2/2L$$

where h^2 is the mean-square end-to-end length of the polymer, L is the contour length of the chain, and n is the number of repeating units. For a flexible chain like polystyrene dissolved in benzene, a is less than 1 nm; for double helical DNA, $a=60$ nm (180 base-pairs (4)); for α -helical poly-benzyl-L- glutamate, which behaves as a rigid rod for all lengths synthesized to date (5), the persistence length is comparable to or exceeds the longest molecular length (300 nm).

What is the persistence length of xanthan? The ellipsoid model of Whitcomb and Macosko (1) would imply $a > 1.5 \mu\text{m}$. The ellipsoid model of Rinaudo and MiTas (2) implies $a > 0.6 \mu\text{m}$. On the other hand, the close similarity between the intrinsic viscosity of xanthan and of DNA (3) for the same molecular weight suggests that the persistence lengths of the two polymers are similar, i.e. $a \approx 50$ nm.

If $a=50$ nm, what is the ratio of contour length L to the persistence length? The pentasaccharide residue weight is about 950; the length ℓ of the residue (two β -(1 \rightarrow 4)-D-glucopyranose units) is about 10A. The polymer molecular weight is between 2×10^6 (2,6) and 15×10^6 (3). Taking $M=10 \times 10^6$ (a median value for various samples from my own work) as a guide, one finds that the degree of polymerization (DP) is 10^4 and the single strand contour length $DP \times \ell = 10 \mu\text{m}$. Although x-ray studies (7) favor a single-stranded structure, there is evidence that xanthan may be double-stranded (8); this would mean that the contour length is $5 \mu\text{m}$. Xanthan molecules in this length range have been seen in electron micrographs prepared under conditions which will stretch out the chains (8).

If the persistence length is 50 nm and the contour length is $50 \mu\text{m}$, then the contour length is on the order of 100 times the persistence length. Such a chain is coiled in solution. Another way of expressing this model is to say that xanthan ($M=10^7$) behaves hydrodynamically like a flexible chain with about 50 freely-jointed Kuhn-equivalent links each about 100 nm long.

Is such a deformable chain model inconsistent with the non-Newtonian intrinsic viscosity? Finding an answer to this question is the goal of this paper. To this end, the viscosity of xanthan solutions was measured over a broad range of shear stress, including especially the low-shear Newtonian limit which has not been measured by Whitcomb and Macosko. The intrinsic viscosity at various shear stresses was then determined and the resultant experimental curve was compared to theoretical expectations for a flexible chain (bead-and-spring) model.

Materials and Methods. The xanthan sample employed was a commercial dry powder (Keltrol) from Kelco Co. Samples were hydrated without further purification by overnight stirring in deionized water, then diluted with predissolved buffer concentrate to a final solvent containing 0.8M NaCl, 0.04 M PO_4 , .02% NaN_3 , pH 7.

Viscosity was measured with several instruments. For lowest shear rates a rotating-cylinder viscometer, constructed in this laboratory by using principles described by Zimm and others (9), was used. The inner cylinder (rotor) was suspended in the test solution by a feedback-controlled pressure regulator (Cartesian diver principle). This type of suspension eliminates all mechanical bearings except the solution in question and eliminates the possibility of interference by films at solution-air interfaces. The outer, stationary cylinder is made of precision glass-tubing. The rotor contains a lacquered aluminum ring to which a torque is applied by a rotating magnetic field. The rotating magnetic field is provided by the stator of a commercial electric motor. The driving torque on the aluminum ring in the rotor is varied by adjusting the electrical voltage applied to the motor windings. Shear stresses of .001 to .06 dyne cm^{-2} were employed; the corresponding shear rates were approximately 0.01-1 sec^{-1} . These shear stresses are so low that dilute xanthan solutions behave as Newtonian fluids. The sample temperature was 20°. The viscosity of buffer was used as a standard to convert the rotation period of the rotor into an absolute viscosity.

Two commercial viscometers were used at higher shear stresses: a Rheometrics Mechanical Spectrometer with sensitive transducer (data kindly provided by P. J. Whitcomb of General Mills Chemicals Co.), and a Contraves instrument (data kindly provided by W. Gale and B. Boseck of Exxon Production Research Co.). Viscosity standards from Cannon Instrument Co. were used to check the Contraves instrument.

Results. In Figure 1 are shown the viscosity versus shear stress data for xanthan solutions (.1 to 1 mg/ml) in 0.5M NaCl, 0.04M phosphate buffer, pH 7, containing 0.02% NaNO_3 as a preservative. The data show a Newtonian plateau between 0.001 and 0.08 dyne/ cm^2 for 0.1, 0.2, and 0.3 mg/ml. As the shear stress increases beyond 0.1 dyne/ cm^2 , a sharp drop occurs in the viscosity. The viscosity decreases until a second Newtonian plateau is reached at 2-20 dyne/ cm^2 . For higher xanthan concentrations the low-shear stress Newtonian plateau occurs at lower shear stresses and the transition between the two plateaus is broadened. Whitcomb and Macosko (1) have reported similar data except that their data did not extend into the low-shear Newtonian range at low concentrations.

In order to make a molecular interpretation from these data, it is necessary to obtain a plot of intrinsic viscosity versus shear stress. For this purpose the raw viscosity data in Figure 1 were first fitted to a simple equation, the Meter equation, which has four parameters

$$\eta = \eta_{\infty} + (\eta_0 - \eta_{\infty}) / (1 + (\tau/\tau_m)^{\alpha-1})$$

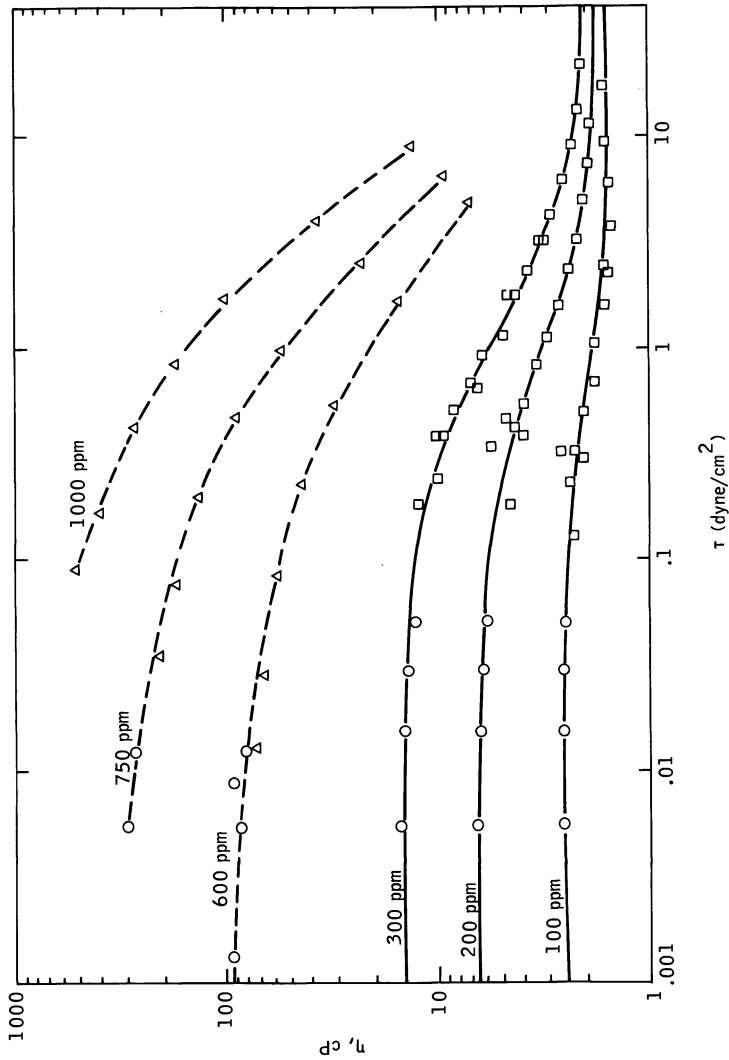


Figure 1. Viscosity vs. shear stress for xanthan dissolved in 0.8M NaCl, 0.04M PO_4 buffer, pH 7, 20°C. Xanthan concentrations are 100 to 1000 mg/L. The solid lines are computed from the Meter equation with least-squares fit to the experimental data. The dashed lines are drawn with a French curve.

Boger (10) has shown that this equation works remarkably well in fitting viscosity data for polyacrylamide solutions over four decades in shear stress including both the low and high shear Newtonian plateaus.

Table 1 lists the parameters obtained from a least-squares fit to the measured data at 100, 200, and 300 mg/l xanthan concentration.

Concentration mg/l	η_0 cP	η_∞ cP	τ_m dyne/cm ²	$\alpha-1$
100	2.5±0.1	1.6±.1	0.6±0.1	2.4±.8
200	6.5±0.3	1.7±0.4	0.5±0.1	1.1±.3
300	14.7±0.4	2.0±.3	0.48±0.04	1.2±.1

From the data in Figure 1 and Table 1, parameter values for the Meter equation describing the intrinsic viscosity can be estimated: $[\eta]_0 = 8000$ ml/g $[\eta]_\infty = 3000$ ml/g, $\tau_m = 0.5$ dyne cm⁻², $\alpha-1 = 1.5$ (geometric mean). Figure 2 shows a plot of $[\eta]/[\eta]_0$ vs. shear stress in 0.5M NaCl, 0.04M PO₄ pH 7 at 20°. Whitcomb and Macosko have previously reported the intrinsic viscosity of xanthan but in distilled water. Where the shear stresses overlap, the data are very similar to those in 0.5M NaCl. There is thus remarkably little effect of ionic strength on the shear stress at which $[\eta]/[\eta]_0$ drops sharply. However, the value of $[\eta]_0$ obtained by Whitcomb and Macosko, 24700 ml/g, is substantially greater than the value obtained here, 8000 ml/g.

The question now arises, what model(s) make these data understandable in molecular terms? In Figure 2 is shown the non-Newtonian intrinsic viscosity for the rigid rod model, with length 1.5 μ m and midpoint diameter 1.9 nm, as calculated by Whitcomb and Macosko (1). The model gives a satisfactory fit to the experimental data, including the new data for the first Newtonian plateau.

Testing the deformable chain model is more problematic. Only recently has the theory of chain dynamics been extended by Peterlin (11) and by Fixman (12) to encompass the known non-Newtonian intrinsic viscosity of flexible polymers. This theory, which is an extension of the Rouse-Zimm bead-and-spring model but which includes excluded volume effects, is much more complex than that for undeformable ellipsoids, and approximations are needed to make the problem tractable. Nevertheless, this theory agrees remarkably well (13) with observations on polystyrene, which is surely a flexible chain. In particular, the theory predicts quite well the characteristic shear stress at which the intrinsic viscosity of polystyrene begins to drop from its low-shear Newtonian plateau.

How well do predicted and observed non-Newtonian intrinsic viscosity agree for a wormlike model of xanthan? Fixman (Ref. 12, Fig. 4) gives the non-Newtonian intrinsic viscosity for a flexible chain model at various values of the excluded volume parameter a_η as a function of the normalized shear rate parameter K_η . The parameter K_η , which incorporates the effects of molecular weight and chain stiffness, equals $1.71[\eta]_0 M \eta_0 g / RT$ where $[\eta]_0$ is the polymer intrinsic viscosity at zero shear stress, η_0 is the solvent viscosity, g is the shear rate in sec^{-1} and the other symbols have their usual meaning.

The experimental parameters required in the theory to model the chain and its stiffness are M , $[\eta]_0$, and an excluded volume parameter. For xanthan we take a log-normal distribution in M between 1×10^6 and 30×10^6 , with peak at 10×10^6 and width approximating the observed distribution (3). The intrinsic viscosity at each molecular weight is fixed by the relation $[\eta] = 4.76 \times 10^{-4} M^{1.046}$ taken from $[\eta]$ - M data in earlier work (3). The excluded volume parameter (Fixman's I) is unknown, so we take two extremes with $a_\eta = 1.0$ (Fixman's $I=1$) and $a_\eta = 2.5$ (Fixman's $I=7$). Since xanthan is a polyelectrolyte (a factor not included in the theory), the large value of a_η may be more appropriate, although a large ionic strength (0.8 M NaCl) was chosen for the experimental work to suppress polyelectrolyte expansion.

In Figure 2 is shown the calculated curve of the ratio $[\eta]/[\eta]_0$ at various values of shear stress for the bead-spring (Fixman) theory with $a_\eta = 1.00$ and $a_\eta = 2.5$. It is apparent that Fixman's theory without any adjustable parameters can explain the data at least qualitatively, for $a_\eta = 2.5$. This bead-spring model can give a reasonably accurate representation of the specific shear stress at which $[\eta]$ first decreases, and the rate of decrease with shear stress is also predictable.

A critical reader might ask what effects a lower molecular weight, for example 2×10^6 rather than 10×10^6 , would have on the theoretical curve. The major effect would be to decrease K_η by the multiplicative factor 0.2. This would shift the theoretical curve to higher shear stresses (by a factor of 5) for a given value of $[\eta]/[\eta]_0$ in Fig. 2, making the agreement with experiment less satisfactory.

It should be emphasized that the agreement between the bead-and-spring model and the data for xanthan in Figure 2 does not mean that xanthan is a typical flexible chain. Rather, it means that, although the chain is very stiff (persistence length of order 50 nm and about 100 pentasaccharide repeating units per persistence length, the molecular weight of the native molecule is so high (contour length many times longer than the persistence length) that the chain behaves hydrodynamically as a random coil.

A qualitative view of the molecular basis for the non-Newtonian intrinsic viscosity can then be attempted. This is

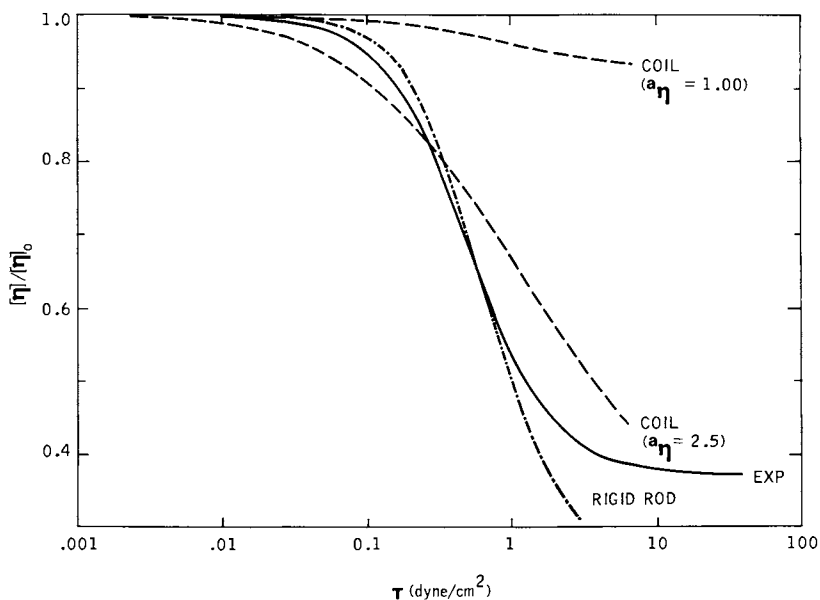


Figure 2. Normalized plot of intrinsic viscosity vs. shear stress: (—) experimental data derived from Figure 1; (---) $F(1)$ and $F(7)$ are calculated for the bead-and-spring model with Fixman's excluded volume parameter $\bar{V} = 1$ and 7 ($a_\eta = 1.0$ and 2.5, respectively); (- · -) calculated for a rigid ellipsoid with length = 1.5 μm and minor diameter = 1.9 nm (1).

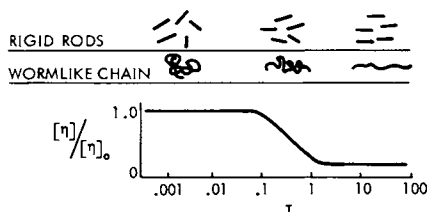


Figure 3. Diagram of the effect of shear gradient on shape and orientation of a wormlike xanthan chain and a rigid-rod model.

shown in Fig. 3. At low shear stresses, the molecule, with contour length about 100 times as long as the persistence length, is approximately spherical. At shear stresses for which the intrinsic viscosity begins to decrease from its zero shear limit, the chain is somewhat extended. Finally, at sufficiently large shear stresses, the chain becomes greatly extended. In contrast, the sole effect of shear gradient on a solution of rigid rods is orientation (Fig. 3).

Can the wormlike model fit other data? It was argued above that the Kuhn-equivalent approximation to the xanthan chain ($M=10^7$) is 50 freely jointed links each 100 nm long. For this chain, the root mean square radius of gyration s can be estimated:

$$(S^2)^{1/2} = (nL^2/6)^{1/2} = 3000 \text{ \AA}$$

The intrinsic viscosity of a sphere with equivalent radius $0.875 \times S$ is

$$[\eta]_0 = 10\pi N_A [0.875 S]^3/3M = 10,000 \text{ ml/g}$$

These values are in the observed range of xanthan (2,3,6,14).

When xanthan is denatured by heating above its "melting temperature" in a buffer of low ionic strength, the chain conformation is altered. The denatured form has a viscosity which depends much more strongly on ionic strength than the native form (15); this suggests that the persistence length of the denatured polymer is less than that of the native structure, although excluded-volume effects probably also contribute (16). Recently, it has also been shown that the viscosity of the denatured form shows a weaker non-Newtonian behavior than the native molecule (17). It would be very interesting to extend these observations by measuring the intrinsic viscosity at zero shear stress for the denatured molecule.

It is important to note that the typical application of xanthan uses a semi-dilute, not dilute solution. Interactions between the chains, which are not considered in this study, play an important role in the viscosity of these solutions.

Summary. The non-Newtonian intrinsic viscosity of xanthan can be explained either by a bead-spring model or by a rigid rod model with appropriate parameters. A Kuhn-equivalent chain with about 200 repeating units per link and about 50 links per molecule is in my view more consistent with all the data than is a rigid rod model.

Acknowledgement. I am grateful to P. J. Whitcomb, L. Soni, W. W. Gale, and B. Boseck for experimental data and to Chris Macosko and Don Siano for stimulating discussions.

References

1. Whitcomb, P. J.; Macosko, C. W. J. *Rheology*, New York, 22, 439-505, 1978.
2. Rinaudo, M.; Milas, M. *Biopolymers*, 17, 2663-2678, 1978.
3. Holzwarth, G. *Carbohydr. Res.* 66, 173-186, 1978.
4. Bloomfield, V. A.; Crothers, D. M.; and Tinoco, I. Jr., Physical Chemistry of Nucleic Acids, New York, Harper and Row, 1974, p. 258.
5. Fujita, H.; Teramoto, A.; Yamashita, T.; Okita, K.; Ikeda, S. *Biopolymers* 4, 781, 1966.
6. Dintzis, F. R.; Babcock, G. E.; Tobin, R. *Carbohydr. Res.* 13, 257-267, 1970.
7. Moorhouse, R.; Walkinshaw, M. D.; Annot, S. in Extra-cellular Microbial Polysaccharides (P. A. Sandford and A. I. Laskin, Eds.), ACS Symp. Ser. 45, 90-102, 1977.
8. Holzwarth, G.; Prestridge, E. B. *Science* 197, 757-759, 1977.
9. Uhlenhopp, E. L.; Zimm, B. H. *Methods in Enzymology* 27D, 483-491, 1973.
10. Boger, D. V. *Nature (London)* 265, 126-128, 1977.
11. Peterlin, A. J. *Chem. Phys.* 33, 1799, 1960.
12. Fixman, M. J. *Chem. Phys.* 45, 793-803, 1966.
13. Yamakawa, H. Modern Theory of Polymer Solutions, New York, Harper and Row, 1971, p. 314-317.
14. Holzwarth, G. American Chemical Society Preprint, Division of Petroleum Chemistry, Vol. 21, 281-296, 1976.
15. Holzwarth, G. *Biochemistry* 15, 4333-4339, 1976.
16. Odijk, T. *Biopolymers* 18, 3111-3113, 1979.
17. Rinaudo, M.; Milas M.; Moan, M. *Eur. Polym. J.* 15, 903-906, 1979.

RECEIVED December 2, 1980.

Investigation on Conformational Properties of Xanthan in Aqueous Solutions

M. MILAS and M. RINAUDO

Centre de Recherches sur les Macromolécules Végétales, Laboratoire propre du C.N.R.S., associé à l'Université Scientifique et Médicale de Grenoble, 53 X - 38041 Grenoble Cedex, France

The ordered conformation of the Xanthan chain is generally interpreted as an helix which is characterized by a melting temperature T_M depending on the polymer concentration, ionic strength, nature of the counterions (1-3). It seems that until now, the dependence of T_M on the degree of neutralization (or pH) of the polycarboxylic form and on the molecular weight has not been investigated.

The dependence of conformational transition on the pH.

In this part of the work, we report the results of potentiometry and optical rotation measurements. At different temperatures we have measured (Figure 1a) the dependence of the apparent pK_a on the degree of dissociation α_t . The pK_a is defined as :

$$pK_a = pH + \log \frac{1-\alpha_t}{\alpha_t}$$

where α_t is the total degree of dissociation ; $\alpha_t = \alpha_{H^+} + \alpha_N$ with α_{H^+} the degree of autodissociation of the carboxylic site during the titration ($\alpha_{H^+} = \frac{[H^+]}{C_p}$, C_p the concentration of xanthan expressed in equivalent per liter) and α_N the degree of neutralization. Under acid form of the polymer, one gets : $\alpha_t \equiv \alpha_H^0$ with α_H^0 the initial degree of ionization of the acidic groups. One observes that the curves change with increasing temperature. Above 40°C a shift in the position of the maximum can be observed. A similar behavior is found for the optical rotation as a function of α_t and the temperature (Figure 2a). Consideration of both figures leads us to the conclusion that there is a conformational change when α_t increases. This transition takes place for a given melting dissociation degree $(\alpha_t)_M$ which decreases when the temperature increases. $(\alpha_t)_M$ is taken as half transition at $[\alpha]^{300} = -75^\circ \text{ decig.}^{-1} \text{ cm}^2$). A plot of $(\alpha_t)_M$ as a function of the temperature in Figure 2b shows a transition around 40°C. This

0097-6156/81/0150-0025\$05.00/0
© 1981 American Chemical Society

temperature separates in fact the two realms of different behavior of Xanthan solutions as shown in Figure 1a.

Behavior above 40°C. The behavior is that of a polyelectrolyte with a charge-driven conformational change as monitored by optical rotation. The values of $[\alpha]$ increase for the values of α_t between 0.3 and 0.5 due to the conformational transition (Figure 2a). The pK_a changes (Figure 1a) are in agreement with the $[\alpha]$ curves and show a conformational transition with variation of the charge potential. In that range of temperatures both the initial degree of dissociation (Figure 1b) and the corresponding pK_a vary only slightly with temperature. In the presence of an excess of salt (Figure 3a) the pK_a is independent of the degree of titration and equal to 3.3 ; a correction based on the Debye-Huckel theory for the ionic strength gives an intrinsic $pK_o = 3.14$ for the carboxylic groups. The initial degree of dissociation is around 0.5 just as with other carboxylic polysaccharides (4) in the range of polymer concentration investigated.

Above 40°C the behavior is quite normal and controlled by the main helix-coil transition of the polysaccharide. This is not the case when the temperature is lower ; thus when the optical rotation of the acidic form of Xanthan $[\alpha]_H$ is investigated, there is a first small transition around 40°C and the value $[\alpha]_H$ is in agreement with a helical structure irrespective of the presence or absence of external salt (Figure 3b) ($[\alpha]$ under coil form is around $-50^\circ \text{ deg. cm}^2$).

Behavior below 40°C. The pK_a values are lower for low α_t and at the same time the initial apparent degree of dissociation is high (Figure 1). In Figure 1b, the initial degree of dissociation α_H^0 is plotted as a function of the temperature. A transition is confirmed around 30°C.

In excess salt at 10°C, the pK_a is exceptionally low ($pK_a = 2.8$ and the corresponding intrinsic pK_o should be lower than 2.64 and the initial degree of dissociation α_H^0 is very high in absence of external acid added.

From optical rotation, it is clear that the secondary structure is much more stable at temperatures below 40°C than above 40°C ; the degree of dissociation necessary for melting at 10°C is 0.7 (Figure 2).

From this set of experimental results, it is suggested that hydrogen bonds exist at low temperature. Intramolecular bonds could stabilize the secondary ordered structure, which exists at low temperature even when the apparent degree of dissociation reaches to 0.7. Such hydrogen bonds are presumed to involve the carboxylic and hydroxyl groups in the chain. This would increase the lability of the proton and correspond to a decrease of the pK_o .

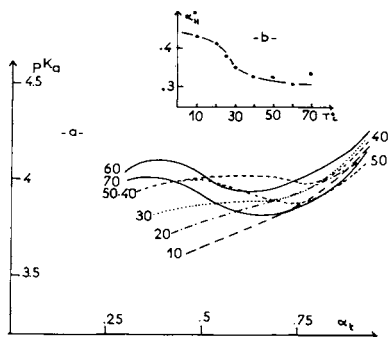


Figure 1. (a) Apparent pK_a of the carboxylic groups as a function of the total degree of dissociation (α_t) at different temperatures in water ($C_p = 7.10^{-4}$ equiv/L); (b) initial degree of autodissociation of the polyacid α_H^0 as a function of the temperature.

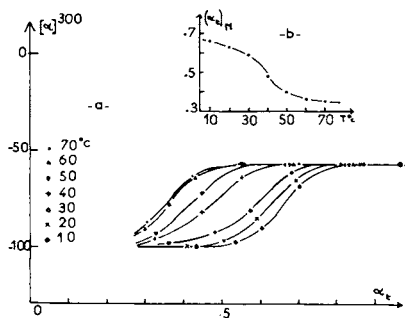


Figure 2. (a) Specific optical rotation $[\alpha]^{300}$ as a function of the total degree of dissociation (α_t) at different temperatures in water ($C_p = 7.10^{-4}$ equiv/L); (b) the degree of dissociation (α_H) (corresponding to the conformational change) as a function of the temperature. The data on Figure 2b have been obtained from Figure 2a.

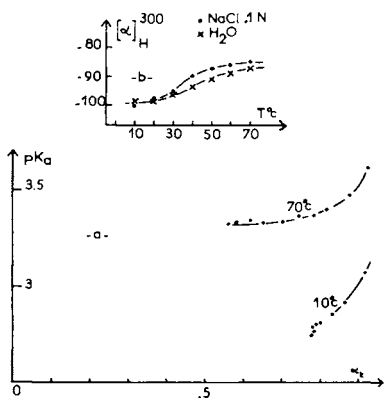


Figure 3. (a) Apparent pK_a of the carboxylic groups in excess of external salt (NaCl 0.1N) at 10°C and 70°C ($C_p = 7.10^{-4}$ equiv/L); (b) optical rotation $[\alpha]_H^{300}$ (acidic form) as a function of the temperature in water and in 0.1N NaCl. ($C_p = 7.10^{-4}$ equiv/L).

Structure of the solution and dependence on the molecular weight of Xanthan.

The different molecular weights of Xanthan were obtained by partial enzymic hydrolysis (5). It is shown in Figure 4 that the melting temperature T_M decreases with decreasing molecular weight although the slopes of the curves $T_M = f(\log \mu_t)$ which correlate with the heat of melting and with the charge parameter, are identical. This dependence is probably due to a cooperative conformational transition as suggested by Holzwarth (6) the degree of cooperativity decreases with a decrease in the molecular weight.

As previously described, when the conformation is ordered (as evidence by the optical rotation $[\alpha]$) the molecule is rigid and the solution becomes anisotropic; this birefringence appears between crossed polarizers. In Table I, the critical concentrations (in the absence of external salt) (C^*) for the appearance of helical conformation and (C^{**}) for the appearance of birefringence at 25°C are given as a function of different molecular weights.

TABLE I Critical concentrations at 25°C of ordered structure formation as a function of the molecular weights.

\bar{M}_w	C^* g/l (a)	C^{**} g/l (birefringence) (b)
$1.4 \cdot 10^5$	20 ± 3	33 ± 3
$2 \cdot 10^5$	10 ± 2	$22,5 \pm 2$
$7 \cdot 10^5$	7 ± 1	8 ± 2
$3.2 \cdot 10^6$	3 ± 0.5	3 ± 1

(a) from the curve $T_M = f(\log C_p)$ when $T_M = 25^\circ\text{C}$

(b) from observation between crossed polarizers.

The data in Table I suggest that the ordered helical conformation is necessary for birefringence to develop (which appears for a $C^{**} > C^*$). For the higher molecular weights $C^{**} \approx C^*$ due to the ionic strength necessary to induce the helical conformation at 25°C.

The values of C^{**} are a linear function of $(\bar{M}_w)^{-1}$ (Figure 5); the organization of the solution is correlated with the length of the molecule in agreement with the model of Flory (7).

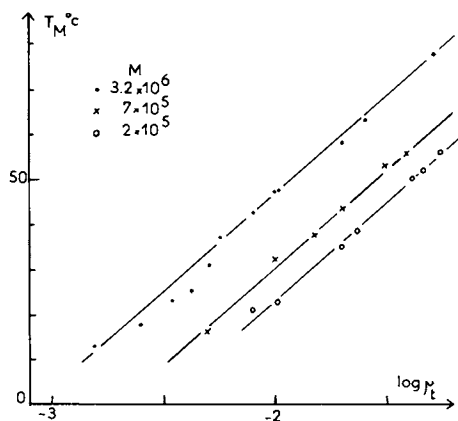


Figure 4. The temperature of conformational change for different molecular weight fractions of xanthan as a function of the total ionic strength ($\mu_t = \Phi C_p + C_s$), where Φ is the activity coefficient of sodium xanthan in the absence of external salt and is equal to 0.65 (8)

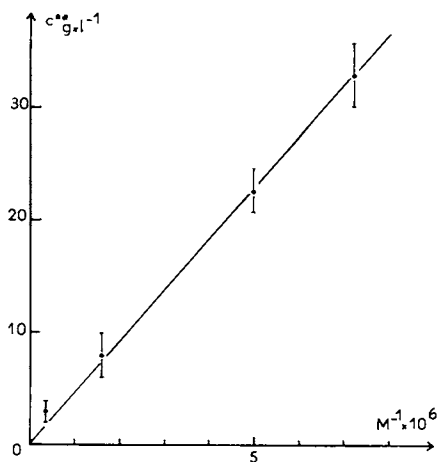


Figure 5. Critical concentration for the appearance of birefringence as a function of the inverse of the molecular weights

Experimental

The commercial sample of Xanthan has been purified and precipitated as the pure Na salt. Its characteristics were given in a previous work (1). The acidic form is obtained by percolation through an ion exchanger IR 120 H followed by progressive neutralization with NaOH. The carboxylic content is 1.58×10^{-3} equiv/g (Na form) in good agreement with the calculated value from the chemical structure proposed by Lindberg (9). The pH is measured using a TACUSSEL Minisis 6000 after calibration with buffer solutions pH \approx 7 and 4 at each temperature.

The anisotropy of the Xanthan solutions is observed between crossed polarizers. The optical rotation is expressed as the specific rotation $[\alpha]^{300}$ determined at a wavelength 300 nm in a 10 cm quartz cell with a spectropol 1 from FICA.

Literature Cited

- 1 Milas, M., Rinaudo, M., Carbohydr. Res. (1979) 76 186-196
- 2 Holzwarth, G., Biochemistry (1976) 15 4333-4339.
- 3 Morris, E.R., Rees, D.A., Young, G., Walkinshaw, M.D., Darke, A., J. Mol. Biol. (1977) 110 1-16.
- 4 Rinaudo, M., Milas, M., J. polymer Sci Part C (1974) 12 2073-2081.
- 5 Rinaudo, M., Milas, M., Int. J. of Biol. Macromol. (1980) 2 45-48.
- 6 Holzwarth, G., Ogletree, J., Carbohydr. Res. (1979) 76 277-280.
- 7 Flory, P.J., J. Polym. Sci. (1961) 49 105-128.
Proc. Roy Soc. (1956) A 234 60-89.
- 8 Rinaudo, M., Milas, M., Biopolymers (1978) 17 2663-2678.
- 9 Jansson, P.E., Kenne, L., Lindberg, B. Carbohydr. Res. (1975) 45 275-282.

RECEIVED September 26, 1980.

Xanthan Gum with Improved Dispersibility

P. A. SANDFORD, J. BAIRD, and I. W. COTTRELL

Kelco Division of Merck & Co., Inc., 8225 Aero Drive, San Diego, CA 92123

Xanthan gum (1) is the high molecular weight natural exopolysaccharide produced by the bacterium Xanthomonas campestris. Xanthan gum owes its commercial importance to its thickening, suspending and pseudoplastic properties in aqueous systems (2-9). Both industrial and food approved xanthan gum are available.

Factors Affecting Gum Dispersibility

Most high molecular weight hydrocolloids such as xanthan gum, guar gum, carboxymethylcellulose, etc., generally require a combination of vigorous and/or lengthy mixing times to produce uniform dispersion and complete hydration.

The problem of "fish-eye" formation is often encountered during dispersing of gums. When a gum particle begins to hydrate, often a gelatinous layer of partially hydrated gum forms on the outside of the particle and prevents water from penetrating to complete hydration and dissolution of the particle. Ideally, what is desired is a lump-free solution/dispersion that forms rapidly without vigorous agitation. However, in the industrial application of gums, often many difficult and varied hydration conditions are encountered (Figure 1). Often agitation is severely limiting thus making dispersion of gums difficult. Also, because of their many different uses, gums encounter a large variety of pH values, ionic environments, temperatures, etc., and gums are often mixed with surfactants, fats, oils, proteins, and various carbohydrates. Further, regulatory restrictions are placed on the use of gums in foods.

Methods of Improving the Dispersibility of Gums

The most common physical means of dispersing gums are listed in Figure 2. Some benefit can be obtained by generating bubbles (10) in situ (e.g., CO₂ evolution from reacting NaHCO₃

0097-6156/81/0150-0031\$05.00/0

© 1981 American Chemical Society

and citric acid), but often the high shear of a mixer or vigorous agitation encountered in the use of a dry powder eductor (aspirator) is more effective(1).

A technique (1) often used in dispersing gums into food preparations is the separation of gum particles by blending with the dry components of a formulation (e.g., sugar, starch). Another technique used to disperse gums is to slurry powder in either water miscible non-aqueous liquids such as vegetable oil prior to adding water. These non-aqueous solvents allow the gum particles to remain separated and hydrate slowly without forming lumps. Encapsulation of gums (11) also accomplishes the same effect of keeping hydrating gum particles separated.

Agglomeration (12) of gum particles can also result in a dispersible gum preparation. Agglomeration basically involves moistening gum particles which then stick together while the moisture is removed, and the agglomerated particles hydrate rapidly without lumping. However, agglomeration is quite costly. Sometimes by proper selection of particle size, lumping of some gums during dispersion in water can be minimized.

In addition to the various physical means used to obtain lump-free gum solutions/dispersions, various chemical treatments of hydrocolloids have been applied successfully (Figure 3). The most effective chemical methods for effecting dispersibility are the use of cross-linking agents.

The most common chemical method used in rendering gums dispersible is their reaction with aldehydes and, in particular, dialdehydes. Divalent metal ions can cross-link xanthan gum, particularly under alkaline conditions. For example, xanthan gum precipitated with calcium ions at pH 10-12 is insoluble at neutral pH (13, 14). Such a xanthan gum/calcium complex can be dispersed readily (since it is really insoluble) and, by adding acid (particularly if the acid complexes the calcium) such as citrate, the xanthan gum/calcium complex can be broken which allows the gum to hydrate and develop lump-free solutions. Knowledge of the behavior of the various salt forms of xanthan gum allows the design of other ways for dispersing the gum.

Borate also forms complexes with xanthan gum under alkaline conditions and allows the design of a system for increasing the dispersibility of xanthan gum in alkaline waters. More details on this process are presented later.

Other chemical derivatives of xanthan gum would be expected to have altered dispersibility and hydration behavior.

Glyoxal Treatment of Polyhydroxyls (14-19)

Glyoxal, because of its unique chemistry, is probably the most commonly used chemical agent for treatment of gums for improving dispersibility in non-food applications. The most important reactions of glyoxal are listed in Figure 5. Near neutral pH values, one glyoxal molecule tends to react

• Agitation	—	Very low to vigorous
• pH	—	2 to 12
• Metal ions	}	Soft water, hard water, brines Na ⁺ , K ⁺ , Ca ⁺⁺ , Mg ⁺⁺ , Al ⁺⁺⁺ , Cr ⁺⁺⁺
• Salts		
• Temperature	—	0 to 120°C
• Gum particle size	—	20- to 325-mesh (Tyler standard screen)
• Other components in hydration fluid	—	Surfactants, oils/fats, proteins, carbohydrates (sugar, starch, other gums)

Figure 1. Factors affecting gum dispersibility

Agitation

- low shear—*in situ* bubble formation (CO₂)
- high-shear mixer
- eductor/aspirator

Separation/coating of gum particles

- dry-mix dispersion (sugar, starch, clay)
- liquid-mix dispersion
 - miscible non-aqueous liquids (glycols, alcohols)
 - non-miscible non-aqueous liquids (vegetable oil)
- encapsulation

Selection of particle size

- mesh size
- agglomeration

Figure 2. Physical means of improving the dispersibility of gums

<u>Crosslinking/Insolubilization Agent</u>	<u>Resolubilization Method</u>
<ul style="list-style-type: none"> • Aldehydes <ul style="list-style-type: none"> — Formaldehyde — Glyoxal — Gluteraldehyde 	Base-catalyzed hydrolysis
<ul style="list-style-type: none"> • Metal ions <ul style="list-style-type: none"> — Divalent (Ca⁺⁺, Mg⁺⁺) — Trivalent (Al⁺⁺⁺) — Higher valences 	
<ul style="list-style-type: none"> • Borates 	pH adjustment
	Metal-complexing agents
	pH adjustment

Figure 3. Chemical means of improving the dispersibility of gums

with the single C-6 primary hydroxyl of the polysaccharide to form hemiacetal-I (Figure 4). At lower pH values, glyoxal tends to form a chemical bridge between two C-6 primary hydroxyls, hemiacetal-II (Figure 4). Increasing the temperature during glyoxal treatment at low pH values can result in complete reaction of the glyoxal with four primary hydroxyls. However, this acetal-III is much more stable to alkaline hydrolysis relative to the hemiacetals I and II.

It is the relative ease of hydrolysis of hemiacetals I and II from a polysaccharide that is so attractive in effecting dispersibility. Glyoxal-treated xanthan gum and other gums are very dispersible because of their relative insolubility but as the acetals are hydrolyzed, the gums begin to hydrate at a rate that allows each gum particle to remain separated to form lump-free solutions.

By altering the glyoxal treatment, a spectrum of glyoxal-treated gums results, each of which has different hydration and dispersibility properties.

Figure 6 lists representative methods disclosed in the literature used to treat various hydrocolloids such as xanthan gum with glyoxal. Gums have been treated using glyoxal in its liquid (e.g., 40% in water) form (14, 15, 16, 17, 19), solid (crystalline dihydrate, mp 15°C) form (18), and vapor (bp 77.6°C) form (15). The most commonly used glyoxal reagent is a 40 percent solution in water. Also to be noted in Figure 5 is that glyoxal has been added not only to gum solutions but also to gum precipitates and dry gum powder.

Factors Affecting Dispersibility and Hydration of Glyoxal-Treated Xanthan Gum

The data in the next five figures (Figures 6 through 11) highlight some of the most important factors affecting dispersibility and hydration of glyoxal-treated xanthan gum. These are shear rate during mixing, pH of the hydration fluid, salt content and levels in hydration fluid, mesh size, and temperature.

The effect of high pH (approximately 10) and shear rate on hydration of glyoxal-treated xanthan gum is shown in the next two figures (Figures 6 and 7). In both figures, the same hydration fluids and samples were used, the only difference being that the shear rate used for agitation in Figure 7 was lower (200 rpm) than that used in Figure 8 (800 rpm). Under both shear conditions, similar results were obtained. With no pH adjustment, viscosity developed rapidly, and actually exceeded that normally expected in the 10-30 minute time interval. The reason for this higher than-usual viscosity is not well understood. If more rapid hydration is desired, then NH_4OH or NaOH can be added to the dispersion as noted in Figure 7.

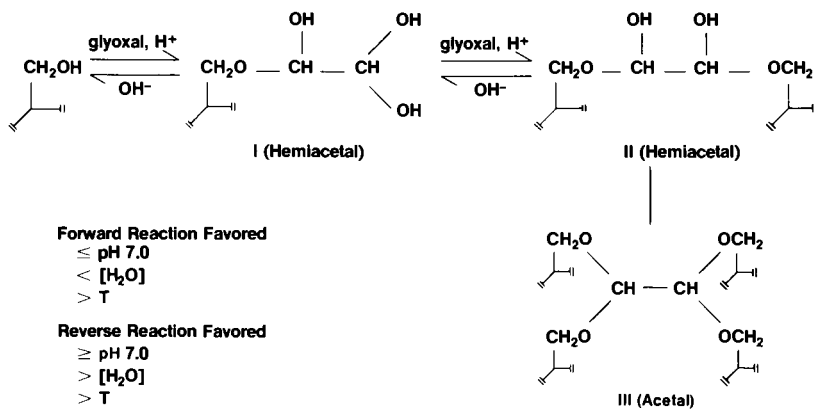


Figure 4. Glyoxal reactions with polyhydroxyls

Patent	Glyoxal Treatment	
	Gum	Glyoxal Reagent
U.S. Patent 2,879,268 (1959)	Powder	Acetone solution Glyoxal vapor
U.S. Patent 3,297,583 (1967)	Powder	Aqueous formic acid
U.S. Patent 3,489,719 (1970)	Powder	Aqueous acetic acid
U.S. Patent 3,997,508 (1976)	Powder	Dry powder (heated)
U.S. Patent 4,041,234 (1977)	Powder	Aqueous solution
U.S. Patent 4,041,234 (1977)	Isopropanol precipitate	Aqueous isopropanol
U.S. Patent 4,041,234 (1977)	Aqueous solution	Aqueous solution
U.S. Patent 4,041,234 (1977)	Fermentation beer	Aqueous solution
British Patent 1,547,030 (1979)	Fermentation beer	Aqueous solution
British Patent 1,547,030 (1979)	Aqueous solution	Aqueous solution

Figure 5. Glyoxal treatment of gums for improved dispersibility

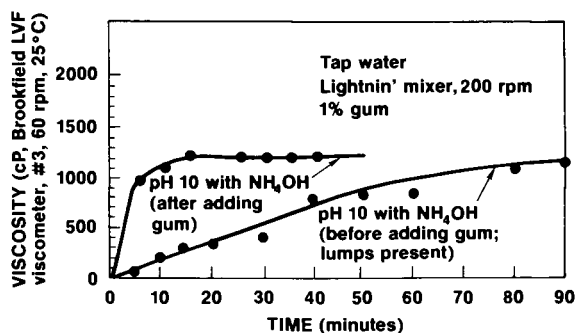


Figure 6. Hydration of glyoxal-treated xanthan gum (low shear)

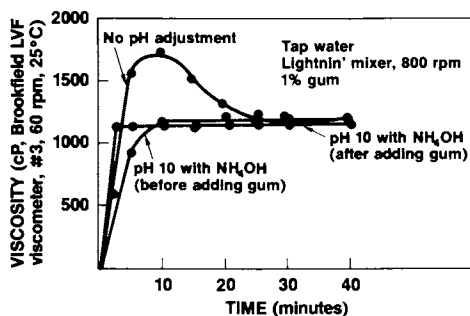


Figure 7. Hydration of glyoxal-treated xanthan gum (high shear)

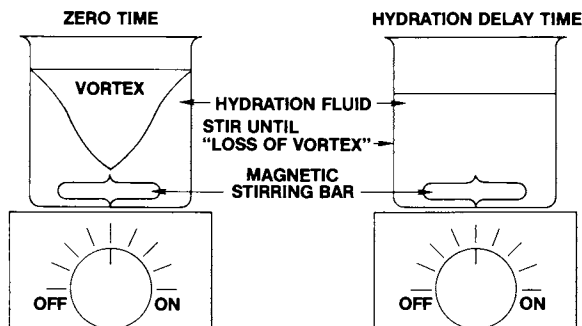


Figure 8. Hydration delay test

Particle Size (mesh ^a)	(μm)	Hydration Delay Time (min.)	Dispersibility
60	250	20.1	Excellent
100	150	20.8	Excellent
150	106	16.2	Excellent
200	75	19.5	Excellent
325	45	20.5	Excellent

^amesh size = Tyler standard screen

Figure 9. Effect of particle size on the hydration of glyoxal-treated xanthan gum

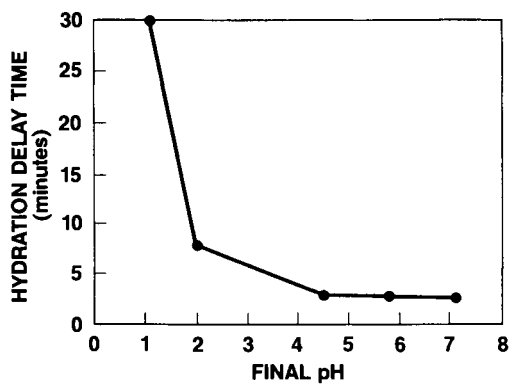


Figure 10. Hydration of glyoxal-treated xanthan gum: effect of pH

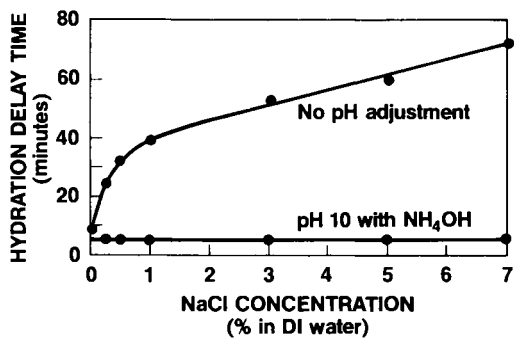


Figure 11. Hydration of glyoxal-treated xanthan gum in NaCl solutions

Since, in certain applications of glyoxal-treated xanthan gum, it is desirable to delay the development of viscosity (hydration delay), a simple test was developed to monitor this behavior (Figure 8). In the hydration delay test discussed, the gum is added to the vortex (created by a magnetic stirrer) of the hydration fluid (usually synthetic tap water) and the time that is required for the vortex to disappear because of viscosity development is called the hydration delay time.

The particle size of glyoxal-treated xanthan gum as seen in Figure 9 has little if any effect on the hydration delay time. The effect of pH of the hydration fluid on the hydration delay time (or viscosity development) is shown in Figure 10. The lower the pH, the greater the hydration delay time becomes. This results because hydrolysis of glyoxal from the gum is slower at low pH values. Thus, lowering the pH of the hydration fluid can be used to obtain longer hydration delay times with glyoxal-treated xanthan gum without adversely affecting dispersibility.

Hydration of gums in salt solution is generally more difficult than in deionized water. The effect on glyoxal-treated xanthan gum of adding NaCl to the hydration fluid is shown in Figure 11. Note that when the pH is unadjusted, hydration is delayed with increasing NaCl levels. If the pH of the salt solutions is adjusted to 10 with NH_4OH prior to adding the glyoxal-treated xanthan gum, hydration is rapid and independent of the NaCl levels. Hydration delay times of these adjusted samples are less than five minutes.

Borate-Treated Xanthan Gum

Although glyoxal-treated gums have excellent dispersibility in acid or neutral systems, they are not dispersible in strongly alkaline systems. The problem (attributed to alkaline hydrolysis of glyoxal) of dispersing glyoxal-treated xanthan gum in alkaline fluids, can be overcome by using a borate-treated xanthan gum (Figure 12). Borate treatment of xanthan gum at pH values above 8.0 results in a cross-linked xanthan gum that is essentially insoluble at this pH range (Figure 12). The presumed mechanism is by borate reacting with the vicinal hydroxyls of mannose to form crosslinks. This phenomenon has been explored in preparing dispersible guar gum derivatives (20, 21). Although the interaction of borate with xanthan gum is less pronounced at high pH values, it is sufficient to produce a dispersible product. Behaving almost opposite to that of glyoxal-treated xanthan gum, the alkaline borate/xanthan gum complex can be broken by the lowering of the pH. Borate-treated xanthan gum readily disperses above pH 7.0, and hydrates at pH values less than 7.0. This can be accomplished by lowering the pH by addition of common acids such as HCl, H_2SO_4 , and H_3PO_4 . Borate-treated

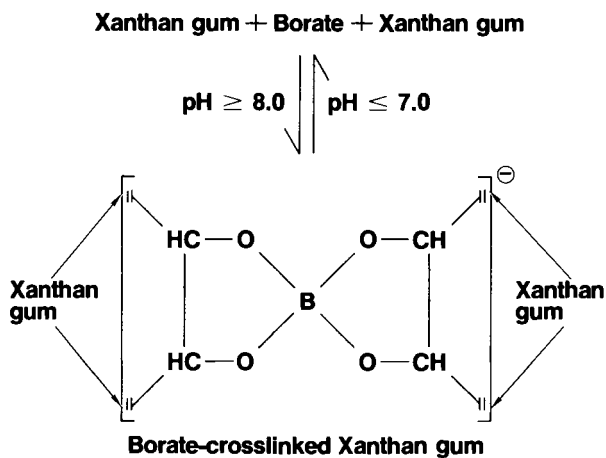


Figure 12. Borate-treated xanthan gum

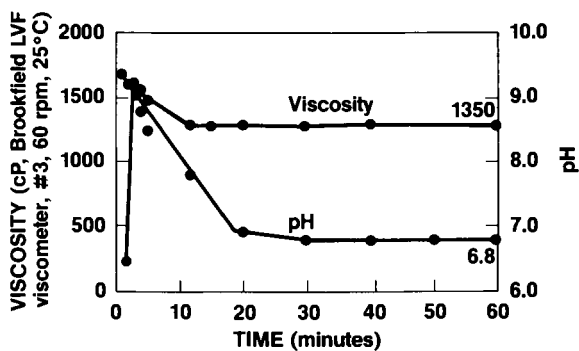


Figure 13. Hydration of borate-treated xanthan gum blended with fumaric acid (2%) and Na_2CO_3 (1%)

xanthan gum can be dispersed readily in tap water at pH less than 8.0 (Figure 13) by blending borate-treated xanthan gum with a base (e.g., Na_2CO_3 , 1%) and a slowly soluble acid (e.g., fumaric acid, 2%). The added Na_2CO_3 causes the pH to be alkaline sufficiently long to allow excellent dispersibility. The added fumaric acid eventually dissolves causing the pH to drop to near neutrality; this breaks the borate complex thereby allowing the xanthan gum to hydrate.

Summary

The dispersibility of xanthan gum can be improved most readily by treatment with glyoxal or alkaline borate. With glyoxal-treated xanthan gum, it has been shown that the mesh size, rate of shear of mixing, pH, and salt levels all affect the hydration and dispersibility. Borate-treated xanthan gum has excellent dispersibility and is especially suited to alkaline solutions. Borate-treated xanthan gum blended with a base (e.g., Na_2CO_3) and a slowly soluble acid (e.g., fumaric acid) are dispersible in neutral solutions. By proper selection of controllable factors, a dispersible xanthan gum with differing hydration rates can be produced and tailored to specific industrial needs.

Literature Cited

1. "Xanthan gum/KELTROL®/KELZAN®/A Natural Biopolysaccharide for Scientific Water Control", Second Edition, Kelco Div. Merck and Co., Inc., San Diego, California, 1975.
2. McNeely, W.H. and Kang, K.S., "Xanthan and some other biosynthetic gums", In Industrial Gums, Whistler, R. L. and BeMiller, J. N., Eds., Second Edition, Academic Press, New York, 1973, pp. 473-497.
3. Andrew, T. R., ACS Symposium Series No. 45, 1977, pp. 231-241.
4. Kovacs, P. and Kang, K. S., "Xanthan gum," In Food Colloids, Graham, H., Ed., Avi Publishing Co., Westport, Connecticut, 1977, pp. 500-521.
5. Cottrell, I.W. and Kang, K.S., "Xanthan gum, a unique bacterial polysaccharide for food applications", In Development in Industrial Microbiology, 1978, pp. 19, 117-131.
6. Racciato, J. S., Textile Chemist and Colorist 1979, pp. 11, 46-50.
7. Kang, K. S. and Cottrell, I. W., "Polysaccharides", In Microbial Technology, Vol. 1, Peppler, H. J., Ed., Second Edition, Academic Press, New York, 1979, pp. 417-481.

8. Pettitt, D. J., "Xanthan gum", In Polysaccharides in Food, Blanshard, J. M. V. and Mitchell, J. R., Eds., Butterworth, Boston, 1979, pp. 263-281.
9. Sandford, P. A., "Exocellular microbial polysaccharides", In Advances in Carbohydrate Chemistry and Biochemistry, Vol. 36, Tipson, R. S. and Horton, D., Eds., Academic Press, New York, 1979, pp. 265-313.
10. U.S. Patent 3,236,657 (February 22, 1966), Raymond E. Cox/General Foods Corp.
11. Sliwka, W., Angew. Chem. (International Ed.), 1975, pp. 14, 539-550.
12. U.S. Patent, 3,551,133 (December 29, 1970), Billy A. Sprayberry and Richard L. Urbanowski/Diamond Shamrock Corp.
13. Mehlretter, C. L., Biotechnol, Bioeng., 1965, pp. 7, 171-175.
14. U.S. Patent 4,095,991 (June 20, 1978), Pierre Falcoz, Pierre Celle, and Jean-Claud Campagne/Rhone-Poulenc Industries.
15. U.S. Patent 2,879,268 (March 24, 1959), Elof Ingvar Jullander/ Mo Och Domsjo Aktg.
16. U.S. Patent 3,297,583 (January 10, 1967), Wolfgang Dierichs and Werner Sammet/Henkel & Cie, GmbH.
17. U.S. Patent 3,489,719 (January 13, 1970), Albert B. Savage and Ronald L. Glomski/Dow Chemical Co.
18. U.S. Patent 3,997,508 (December 14, 1976), Horst Ziche/Henkel & Cie GmbH.
19. U.S. Patent 4,041,234 (August 9, 1977), Fred J. Maske/General Mills.
20. British Patent 1,547,030 (June 6, 1979), Ian William Cottrell and Henry George Hartnek/Merck & Co., Inc.
21. Goldstein, A. M., Alter, E. N., and Seaman, J. K., "Guar gum", In Industrial Gums, Whistler, R. L. and BeMiller, J. N., Eds., Second Edition, Academic Press, New York, 1973, pp. 303-321.

RECEIVED September 30, 1980.

Cellulose Viscosity–Molecular-Weight Relationships by Gel Permeation Chromatography–Low-Angle Laser Light Scattering

J. J. CAEL, R. E. CANNON, and A. O. DIGGS

International Paper Company, Corporate Research Center, P.O. Box 797,
Tuxedo Park, NY 10987

For years the determination of polymer molecular weights has served as an important process and quality control parameter as many final end use and physical properties of the polymer are closely related to its molecular weight and/or molecular weight distribution (MWD). Historically, such methods as membrane osmometry, light scattering, etc. have achieved considerable utility in determining polymer molecular weights (e.g. number and weight-average). At best, a knowledge of each of these averages for a given polymer yields information on the breadth of the distribution; however, the actual distribution is unknown and can only be inferred.

For MWD determinations, gel permeation chromatography (GPC) has gained wide acceptance as a preferred method. It is a liquid chromatographic technique based upon the principle of size exclusion whereby a macromolecule is separated on the basis of molecular size or hydrodynamic volume in dilute solution. This is achieved by the action of various column packing materials having controlled, pore size distributions. The weight fraction or concentration of polymer eluted during the separation process is measured by a concentration sensitive detector (e.g. UV, IR, or differential refractometer). In conventional GPC the raw data represent the elution volume distribution of the polymer sample by weight, and as a result, a transformation to molecular weights is required. This is generally achieved by a calibration procedure which uses Mark-Houwink coefficients (K and α) derived from both the polymer under investigation and usually narrow distribution, polystyrene standards. The accuracy of MWD data and associated molecular weight averages obtained from such a calibration method can be quite variable and is ultimately dependent upon the correctness of K and α for the polymer/solvent pair.

In the pulp and paper industry, GPC has been applied not only in measuring cellulose molecular weights and MWDs, but also in following its degradation as a consequence of various pulping, bleaching and viscose processes. In the initial applications of

0097-6156/81/0150-0043\$05.00/0
© 1981 American Chemical Society

GPC to study cellulose, cellulose trinitrate derivative was employed (1, 2). While this derivative is soluble in a wide range of organic solvents commonly used in GPC, the use of the trinitrate has several disadvantages (3). First, the nitration procedure can cause significant chain scission, thereby causing the MWD of the trinitrate to differ from that of the underivatized cellulose. In addition, the stability of the trinitrate is limited, and there can also be considerable variability in the degree of substitution. The latter effect is rather critical as both the GPC detector output and polymer hydrodynamic volume are a function of the degree of substitution. Recently, various workers have proposed that the cellulose tricarbonyl (CTC) derivative be employed in GPC applications (3, 4, 5, 6). This derivative is stable and complete trisubstitution is obtained. More importantly, degradation during the derivatization is believed to be eliminated. The structural formula for CTC is shown in Figure 1.

Ideally, the most accurate way to determine the MWD of a polymer by GPC is to link a molecular weight detector to the outlet of the last GPC column. To accomplish this, we have configured a low angle laser light scattering (LALLS) photometer to the GPC apparatus. Two inherent design features facilitate its use in absolute MWD determinations. The first is the ability to measure the intensity of scattered radiation at angles as low as $2-3^\circ$ from the primary beam, thereby circumventing the angular extrapolation of data to zero angle such as required in a Zimm plot (7). The second feature is the 0.008 ml flow-through sample cell which minimizes both post-column solute mixing and homodyne beating effects. An additional consequence of this configuration is the ability to determine Mark-Houwink coefficients on broad MWD linear homopolymers without recourse to fractional precipitation and intrinsic viscosity procedures.

Instrumentation

Figure 2 shows a schematic of the GPC/LALLS system. The GPC instrument is a Waters Associates model ALC-201 high pressure liquid chromatograph having four μ -Styragel columns₃ connected in series with porosities of 10^6 \AA , 10^5 \AA , 10^4 \AA , and 10^3 \AA . Connected to the last GPC column is a Chromatix KMX-6 low angle laser light scattering photometer utilizing polarized radiation from a 2.0 mW HeNe laser at 632.8 nm. Details of the LALLS photometer and its optical system have been described elsewhere (8). In order to measure the concentration of solute eluting from the GPC columns, the outlet of the LALLS 0.008 ml flow-through cell is connected to a Varian VARI-CHROM variable wavelength UV detector operating at 254 nm. All connections utilized 1/16" stainless-steel tubing having an internal diameter of 0.008" with low dead-volume, Luer type fittings in order to minimize mixing effects.

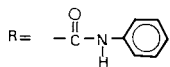
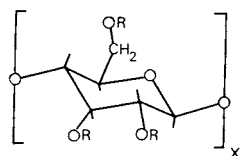


Figure 1. Structural formula for cellulose tricarbanilate

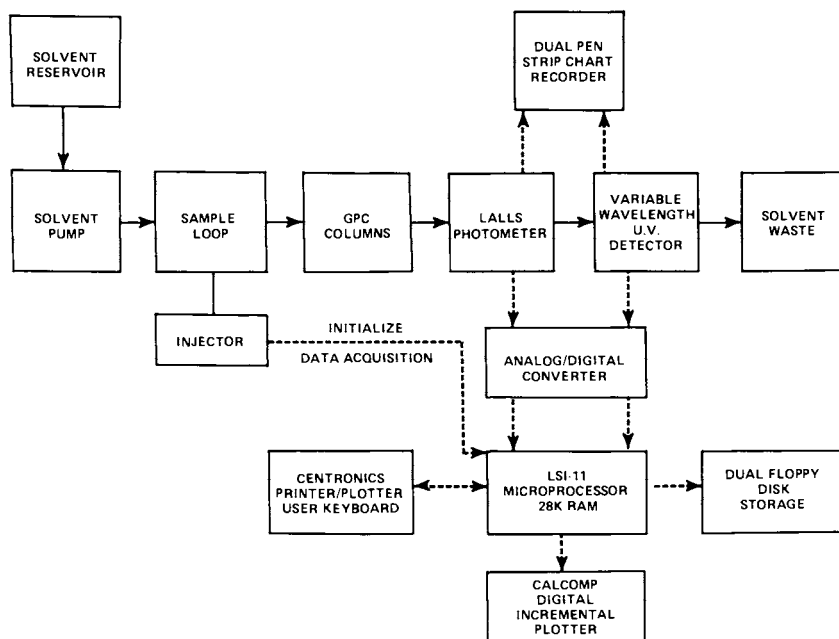


Figure 2. Schematic of the GPC/LALLS configuration

For on-line data acquisition and analysis the analog signals from both LALLS and UV detectors are digitized by a Chromatix LDS-2 laboratory data system. The essential components of this system are a Digital Equipment LSI-11 microprocessor having 28K words of random access memory, a FORTRAN compiler, a Centronics dot matrix printer/plotter and a dual floppy disk for mass storage. In addition, we have interfaced to this configuration a Calcomp model 1012 four-pen digital incremental plotter which provides added flexibility in the presentation of results.

Materials and Methods

All cellulose samples used in this work were derived from bleached, hardwood kraft pulps having a hemicellulose content of 2% or less. The basic procedure used for the preparation of CTC derivatives is to react the cellulose with phenylisocyanate in pyridine (3, 4, 6) at 80°C (9). Typically, 0.5 grams of dry cellulose is added to 540 ml of anhydrous pyridine followed by slow addition of excess phenylisocyanate. After reacting for 16-24 hours, the solution is cooled to 70°C, and 40 ml of methanol is added in order to remove unreacted phenylisocyanate. The CTC is isolated by precipitation into and washing by methanol, followed by dissolution into acetone, precipitation into water, and subsequent vacuum drying. The nitrogen content of all CTC preparations was determined by the semi-micro Kjeldahl method in order to assess the degree of substitution. All samples had nitrogen contents in the range 7.89-8.06% (theoretical content 8.08%) which corresponds to degrees of substitution from 2.91 to 2.99.

For both GPC/LALLS and intrinsic viscosity measurements, Burdick & Jackson distilled-in-glass, UV grade tetrahydrofuran (THF) was used. GPC/LALLS experiments were conducted at a constant, pulse-free solvent flow-rate of 1.0 ml/min. Solute concentrations were 0.1% (w/vol.) and the volume of injected solution ranged from 0.3 ml to 0.5 ml. Intrinsic viscosities for CTC in THF were measured at 25°C in a Cannon-Ubbelohde four-bulb shear dilution capillary viscometer (Size 50). Kinetic energy corrections were negligible and the data were corrected for shear effects by extrapolation of η_{sp}/c to zero shear rate (10).

GPC/LALLS Methodology

For a macromolecule in dilute solution in a one-component solvent, the relationship between the excess Rayleigh factor and the weight-average molecular weight, M_w , is given by the fluctuation theory of light scattering (11) as

$$Kc/\overline{R(\theta, c)} = 1/M_w P(\theta) + 2A_2 c/P(\theta) + 3A_3 c^2/P(\theta) + \dots \quad (1)$$

where

$$K = (2\pi^2 n^2 / \lambda_0^4 N) (dn/dc)^2 (1 + \cos^2 \theta) \quad (2)$$

and c is the solute concentration in g/ml, $\overline{R(\theta, c)}$ is the excess Rayleigh factor for unpolarized incident radiation at the scattering angle θ , n is the refractive index of the solution, λ_0 is the wavelength in vacuo, N is Avogadro's number, while A_2 and A_3 are the second and third virial coefficients. The term $P(\theta)$ is the form factor which is a function of the size and shape of the macromolecule in solution and represents the modulation of the intensity of scattered radiation due to the finite size of the molecule and to its deviation from sphericity. The term dn/dc is the specific refractive index increment and represents the change in solution refractive index as a function of solute concentration. If experiments are conducted in the limit of zero scattering angle where $P(\theta) = 1$ as well as at sufficiently low concentrations where only the second virial coefficient need be considered, then eq. (1) reduces to

$$Kc/\overline{R(\theta, c)} = 1/M_w + 2A_2c \quad (3)$$

For the determination of molecular weights and associated MWDs, both A_2 and dn/dc are measured in advance. Although the cellulose specimens used in this analysis have characteristic broad MWDs ($M_w/M_n = 1.8-4.0$), a single determination of A_2 from a representative CTC preparation was considered appropriate for all subsequent determinations of M_w and the MWD. This was achieved by using the LALLS photometer off-line and by extrapolating scattering data from a dilution series at $\theta = 4\frac{1}{2}-5\frac{1}{2}^\circ$ using eq. (3). The value of A_2 determined was 3.5×10^{-4} ml-mole/g². Likewise, dn/dc was determined for the same CTC preparation in THF at 632.8 nm on a Chromatix KMX-16 laser differential refractometer, and resulted in a value of 0.163 ml/g.

In Figure 3 are shown computer plots of the UV and LALLS detector response curves as a function of elution volume for a representative CTC. One obvious feature is the relative difference in the response of the two detectors as the sample molecular weight decreases with increasing elution volume. This is a consequence of the fact that the UV absorbance is a linear function of the solute concentration while $\overline{R(\theta, c)}$ is a function of both concentration and molecular weight. The molecular weight of solute eluting within a given volume element is calculated from a form of eq. (3)

$$Kc_i/\overline{R(\theta, c_i)} = 1/M_i + 2A_2c_i \quad (4)$$

The concentration of solute at the i^{th} point is given by

$$c_i = mx_i / (V_i \sum x_i) \quad (5)$$

American Chemical
Society Library
1155 16th St. N. W.
Washington, D. C. 20036

where m is the total mass of solute injected, V_i is the volume of solution corresponding to the i^{th} volume element, and x_i is the amplitude of the UV signal at V_i .

Typically, 100 values of M_i are calculated across the chromatogram which allow number, weight, and z-average molecular weights to be determined from the relations

$$M_n = \Sigma c_i / \Sigma (c_i / M_i) \quad (6)$$

$$M_w = \Sigma c_i M_i / \Sigma c_i \quad (7)$$

$$M_z = \Sigma c_i M_i^2 / \Sigma c_i M_i \quad (8)$$

In addition, both differential and integral absolute molecular weight distributions can be generated as shown in Figure 4a and b, respectively. It should be pointed out that in the calculation of M_i by eq. (4), the assumption is made that the resolution of the columns is perfect and that each i^{th} fraction which elutes is monodisperse in molecular weight. In actuality, M_i is a weighted average due to both the finite resolution characteristics of the columns and to mixing effects which can occur in each of the UV and LALLS detector cells. While this does not effect the accuracy of M_w , the derived values for M_n and M_z will tend to be somewhat greater and less than their true values z , respectively.

Results and Discussion

Accuracy and Reproducibility of GPC/LALLS. In Table I are shown molecular weight averages obtained from four successive analyses of the same CTC sample in order to assess the relative accuracy and consistency of the GPC/LALLS technique. As can be seen, the reproducibility of the technique is quite good with the average

TABLE I

REPRODUCIBILITY OF GPC/LALLS

Run #	M_n	M_w	M_z
1	331,269	577,855	1,035,150
2	318,615	579,268	1,016,520
3	320,666	581,239	1,024,100
4	<u>319,534</u>	<u>583,255</u>	<u>1,015,190</u>
Average =	322,521±2%	580,404±0.5%	1,022,740±1.2%

error of measurement ranging from 2% for M_n to 0.5% for M_w . Similarly, in Figure 5 is shown the agreement between M_w determined by GPC/LALLS and the corresponding zero shear intrinsic

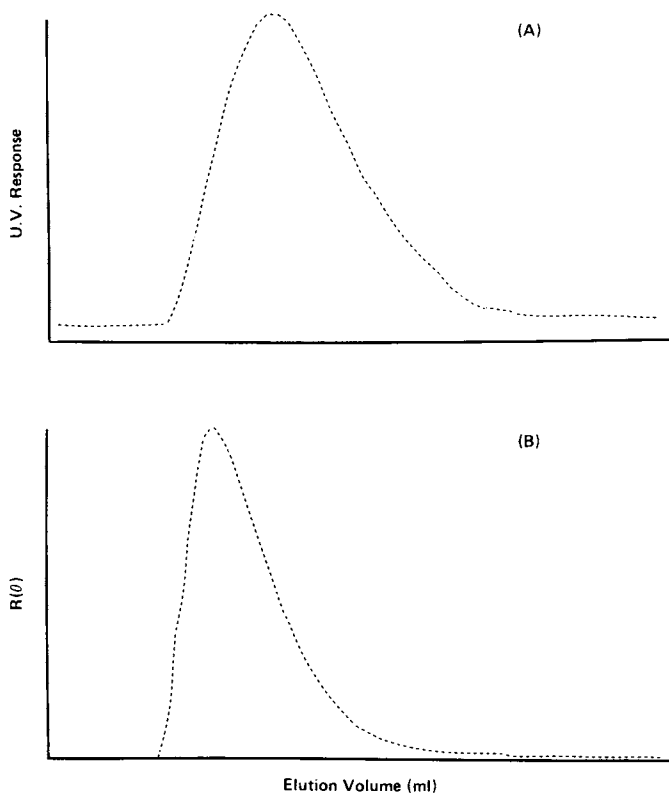


Figure 3. Experimental UV (A) and LALLS (B) detector response curves for CTC in THF

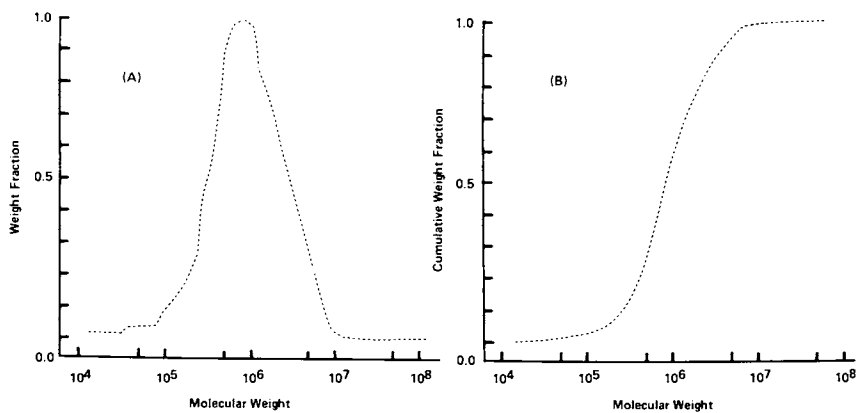


Figure 4. Differential (A) and integral (B) molecular-weight distributions derived from the data of Figure 3

viscosity obtained from a series of CTC preparations covering a wide range of sample molecular weights and having variable MWDs. In Table II, the values of M_w obtained by both GPC/LALLS and intrinsic viscosity methods are compared. As can be seen from Figure 5, the values of M_w determined by GPC/LALLS correlate

TABLE II

Sample	$[\eta]^a$	M_w^b	M_w^c
1	881.0	2,170,000	2,025,000
2	716.2	1,768,200	1,282,400
3	652.3	1,466,300	1,147,500
4	577.3	1,386,200	992,200
5	537.4	1,166,700	910,900
6	473.5	1,026,000	783,700
7	340.3	601,000	528,800
8	303.7	463,800	461,800
9	202.9	302,100	285,700

^a zero shear viscosity (ml/g) in THF at 25°C

^b from GPC/LALLS

^c from the relation $[\eta] = KM^\alpha$ with $K = 0.0053$ and $\alpha = 0.84$ (6)

well with the measured intrinsic viscosities; however, in all cases the M_w derived from GPC/LALLS is systematically larger than those determined from the Mark-Houwink relationship. Although the use of a single valued A_2 for the calculation of M_w throughout the MWD can be expected to introduce some uncertainty in the derived molecular weight averages, we do not expect the differences to be of the magnitude observed from the data of Table II. Rather, we believe the differences in molecular weight arising from these two techniques are a consequence of inherent errors in K and α for CTC in THF, since their accuracy is dependent ideally upon the ability to establish a $\log [\eta]$ vs. $\log M$ relationship from monodisperse fractions of the polymer. Conventional fractional precipitation methods rarely ever achieve monodispersity of the order attainable from anionic polymerization, and it is not uncommon for errors of 10% in K and α to result in a 20% error in the derived molecular weight. Likewise, while α is not strongly dependent on such dispersion effects, the value of K is considerably more sensitive due to the long extrapolation of data to vanishing molecular weight.

Determination of K and α from GPC/LALLS. The major assumption inherent in using GPC for the determination of polymer molecular weights and MWDs is that in solution the macromolecule is chromatographically fractionated according to its hydrodynamic volume. Unless monodisperse fractions of the polymer in question are available, one generally calibrates the GPC system by chromato-

graphing a series of anionically polymerized polystyrene (PS) standards which span several decades of molecular weight and which have nearly monodisperse distributions. Using this procedure most commercial GPC columns allow a linear relationship between $\log M$ vs. elution volume (V) such that

$$\log M_{PS} = a + b \cdot V \quad (9)$$

where a and b represent the y-axis intercept and slope of the $\log M$ vs. V plot. To convert the polystyrene calibration plot into a cellulose tricarbanilate plot, use is made of the theory of Flory and Fox (11) in which the hydrodynamic volume of a polymer in dilute solution is related to its molecular weight and intrinsic viscosity by a universal constant, θ :

$$\text{hydrodynamic volume} = [\eta]M = \theta \left(\frac{R_g^2}{g} \right)^{3/2} \quad (10)$$

and $\left(\frac{R_g^2}{g} \right)$ is the mean square radius of gyration. From the assumption that under the same experimental conditions different polymers having the same hydrodynamic volume will be eluted from the columns within the same volume element,

$$[\eta]_{PS} M_{PS} = [\eta]_{CTC} M_{CTC} \quad (11)$$

and the subscripts refer to the particular molecular species. Substitution of the Mark-Houwink relation for $[\eta]$ in eq. (11) yields

$$K_{PS}^{1+\alpha} M_{PS}^{1+\alpha} = K_{CTC}^{1+\alpha} M_{CTC}^{1+\alpha} \quad (12)$$

which upon logarithmic transformation results in the relation

$$\log M_{CTC} = \frac{\log K_{PS} + (1+\alpha)_{PS} \log M_{PS} - \log K_{CTC}}{(1+\alpha)_{CTC}} \quad (13)$$

As a result of eqs. (9-13), each PS molecular weight standard can be converted through use of Mark-Houwink coefficients from PS and CTC into a corresponding CTC molecular weight. These CTC molecular weights form the basis of a new calibration curve

$$\log M_{CTC} = a' + b' \cdot V \quad (14)$$

where a' and b' have the same meanings as in eq. (9) but are primed so as to distinguish them from the PS coefficients. In Figure 6 is shown the calibration curve for CTC in THF which results from eq. (13). The Mark-Houwink coefficients used for its generation are $K = 0.00203$, $\alpha = 0.678$ for polystyrene (4) and $K = 0.0053$, $\alpha = 0.84$ for CTC (6). Also depicted is the corresponding CTC molecular weight data obtained from a single, broad distribution sample by GPC/LALLS. With the exception of

the low molecular weight region of the distribution (i.e. $M_w \leq 70,000$), for a given volume element, the GPC/LALLS technique predicts larger molecular weights than calculated from eq. (13). The reversal of this trend at low molecular weights is probably due to imperfect column resolution at this extreme of the MWD and/or to expansion of the CTC coil at low molecular weights due to the bulkiness of the substituents and concomitant rigidity of the cellulose backbone (13). The former case will manifest itself in lower M_w values due to additional low molecular weight material while the latter would cause the solute to elute sooner than it would in an unexpanded state.

By combining terms in eq. (13) such that

$$\log M_{CTC} = mx + b$$

where

$$m = 1/(1+\alpha_{CTC})$$

$$x = \log K_{PS} + (1+\alpha_{PS}) \log M_{PS}$$

and

$$b = -\log K_{CTC}/(1+\alpha_{CTC})$$

it is possible from a plot of $\log M_{CTC}$ vs. x to calculate K and α for CTC in THF from a single broad MWD sample which has been chromatographically fractionated. This is achieved by taking appropriate values of M_{CTC} from the linear region of the GPC/LALLS data of Figure 6 and associating them with the corresponding molecular weights of the polystyrene calibration standards (i.e. pairwise values of M_{CTC} and M_{PS} are those which elute within the same volume element). Values of K and α resulting from this procedure are shown in Table III which also compares published values

TABLE III

COMPARISON OF MARK-HOUWINK COEFFICIENTS FOR CTC IN THF

<u>K</u>	<u>α</u>	<u>Method</u>	<u>Reference</u>
0.0043	0.84	GPC/LALLS	this work
0.0053	0.84	viscosity/light scattering	(6)
0.00201	0.92	viscosity/light scattering	(3)
0.00251	0.89	viscosity/light scattering	(4)

determined by other workers.

We have repeated this procedure on a number of CTC preparations and have found invariably excellent superimposition of GPC/LALLS molecular weight data in the linear domain of the $\log M_{CTC}$ vs. elution volume plot of Figure 6, which we view as indicative of the accuracy of the derived K and α . Certainly, our success with this method is due in part to the use of narrow distribution polystyrene standards in which K , α , and associated

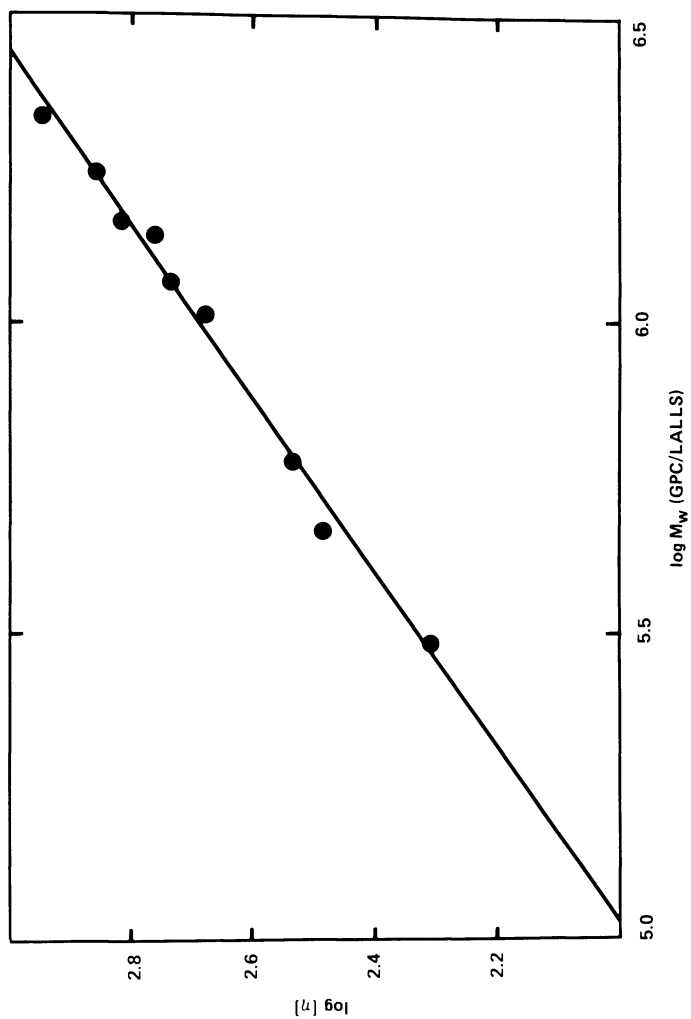


Figure 5. Correlation of \bar{M}_w determined by GPC/LALLS and measured zero shear intrinsic viscosity in THF for broad-distribution CTC

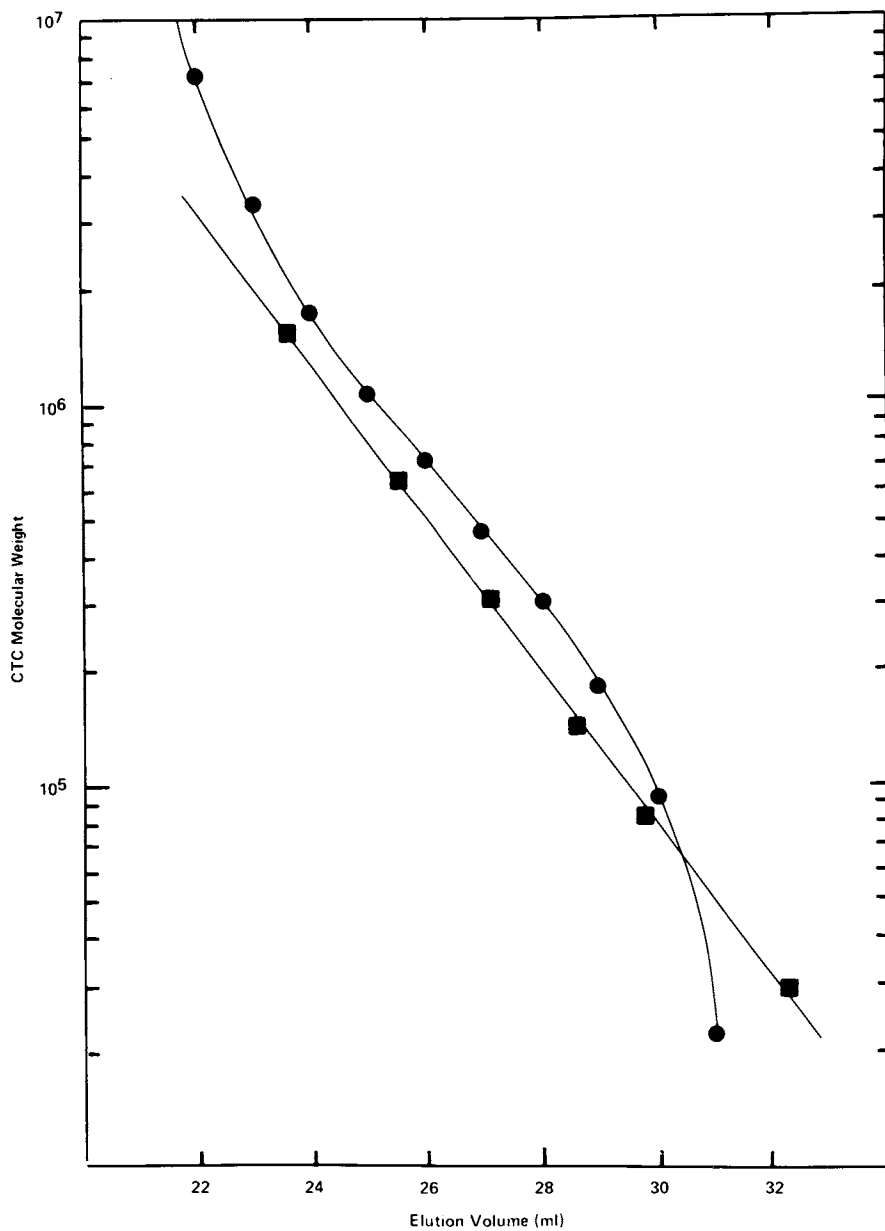


Figure 6. Comparison of GPC calibration curves for CTC derived from intrinsic viscosity (■—■) and GPC/LALLS (●—●) methods

molecular weights can be accurately determined. Two limiting features of our method for calculating K and α deserve comment. The first is that the $\log M$ vs. elution volume data for both the molecular weight standards and the polymer in question must be linear over a sufficient range of molecular weights. Fortunately, this is not a serious concern since most commercially available high performance GPC columns have been designed with this feature. A second limitation of the method is that it can only be applied to linear homopolymers. In the case of amylose tricarbanilate (ATC) which contains a small amount ($\sim 5\%$) of branched amylopectin tricarbanilate, the $\log M_{ATC}$ vs. elution volume data (Figure 7) determined by GPC/LALLS is devoid of any linearity. In fact, there is significant departure from the general trend of decreasing molecular weight with increasing elution volume which must be ascribed to the presence of the branched amylopectin. This is simply a consequence of the fact that within a given elution volume element where both linear and branched species have the same hydrodynamic volume there will be a distribution of molecular weights arising from the inherent greater density of chain segments for branched molecules relative to their linear analogs.

CED Viscosity - Molecular Weight Correlations. For convenient determination of cellulose molecular weight by viscometry, without recourse to chemical derivatization, a number of aqueous solvent systems have been advocated, e.g. cuprammonium hydroxide, cadmiumethylenediamine hydroxide (cadoxen), iron-sodium-tartrate (FeTNa) and cupriethylenediamine hydroxide (CED). In particular, the CED solvent system has gained considerable acceptance due to the wide range of celluloses that it is capable of dissolving. Unlike most polymers which permit the determination of both absolute molecular weight and intrinsic viscosity from the same solvent, cellulose generally requires chemical derivatization to facilitate both molecular weight determinations and solubility in common organic solvents. The aqueous cellulose solvents mentioned often are not practical for membrane osmometry or light scattering studies due to both the multicomponent nature and high alkalinity of the solvent. Some success has been achieved with light scattering studies using cadoxen (14) and FeTNa (15); however, the effect of preferential adsorption of one of the solvent components and, in the case of FeTNa, absorption of light by the solvent need be considered.

As with GPC analyses, the cellulose derivative used for the calibration of CED viscosities has been the trinitrate (16, 17). In Figure 8 are shown CED intrinsic viscosity-molecular weight (expressed as weight-average degree of polymerization, DP_w) relationships obtained from both nitrate and CTC derivatives. In the case of the nitrate, the data is taken from Sithola, *et al.* (17) while the CTC data is that determined by GPC/LALLS with CED intrinsic viscosities determined on the starting cellulose

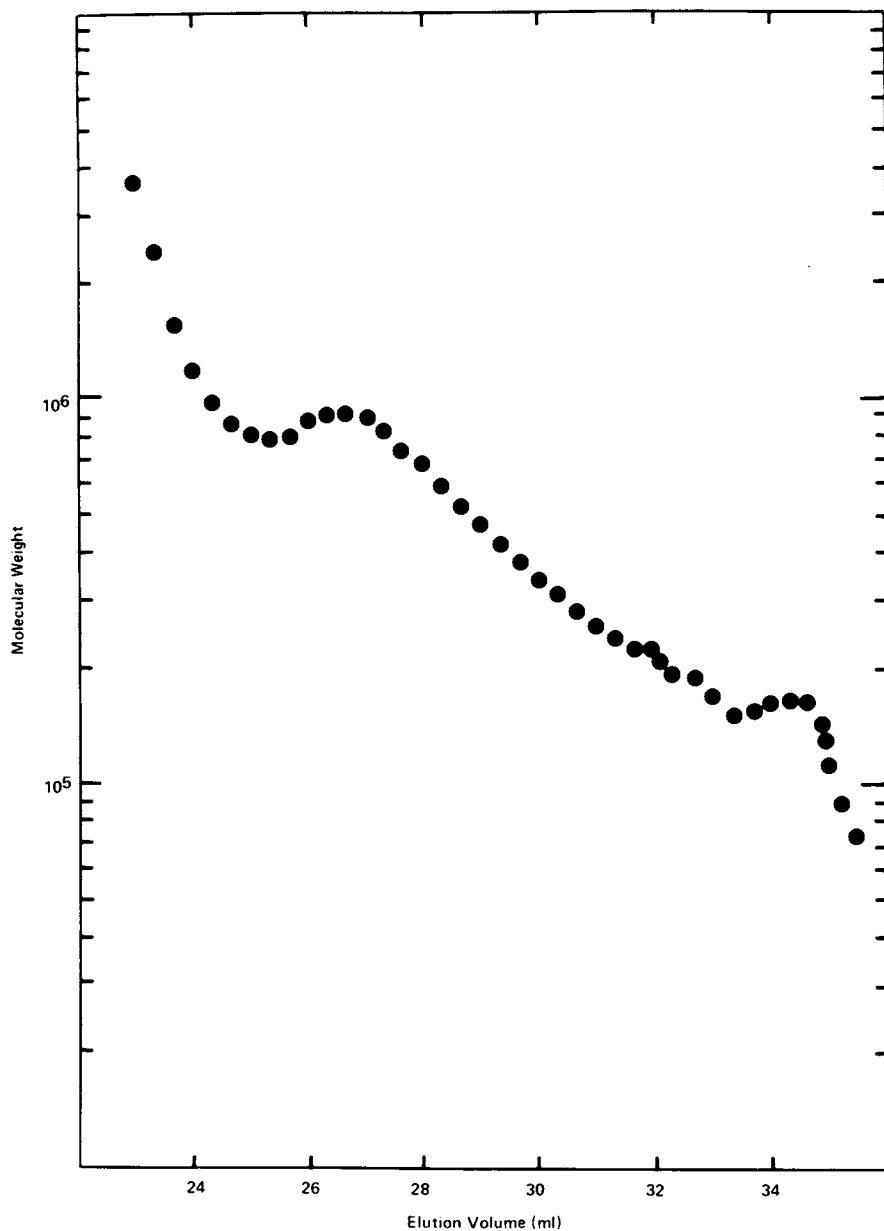


Figure 7. Molecular weight-elution volume relationship determined by GPC/LALLS for amylose tricarbanilate containing branched amylopectin tricarbanilate

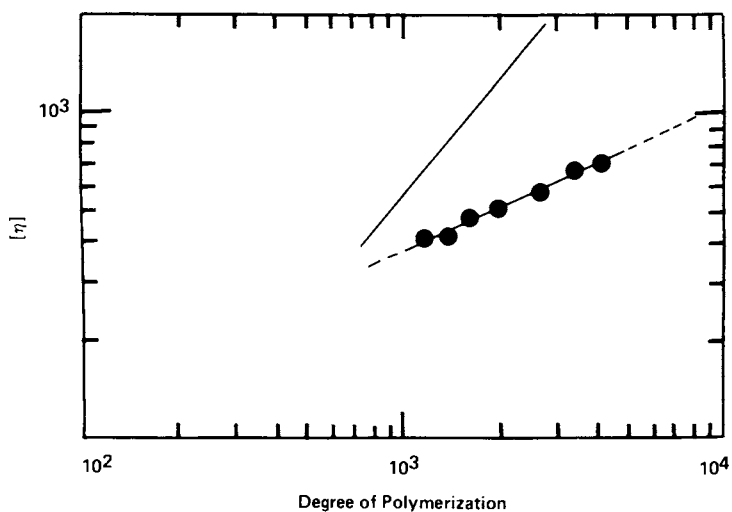


Figure 8. Effect of nitrate and carbanilate derivatives on the calibration of CED viscosity: (—) cellulose trinitrate; (●—●) cellulose tricarbamate.

specimens. Although the correlation based on the nitrate derivative yields a workable relationship, it is apparent that for a given CED viscosity, the degree of polymerization derived from carbanilation is substantially larger than that predicted from nitration. This is probably a consequence of chain scission occurring during the nitration procedure, and more importantly, indicative of the suitability of the tricarbanilate when assessing changes in cellulose molecular weight or MWD arising from various chemical treatments.

ACKNOWLEDGMENTS

The assistance of Mr. P.J. Christ of Chromatix Inc. for specific refractive index increment determinations and Mr. L.C. Hofmann of our Analytical Sciences group for nitrogen analyses is gratefully acknowledged.

ABSTRACT

For years the determination of cellulose molecular weights has served as an important process and quality control parameter in the pulp and paper industry since many final end use properties of cellulose are closely related to its molecular weight and/or molecular weight distribution (MWD). A particularly convenient technique which has met with considerable success and which is often considered an industry standard is the cupri-ethylenediamine or CED viscosity method. In order to place CED viscosity data on an absolute molecular weight basis, we have combined the techniques of gel permeation chromatography with low angle laser light scattering (GPC/LALLS) for MWD measurements on cellulose tricarbanilate (CTC) derivatives in THF. We have found CTC preparations to be ideally suited for such applications as the reaction yields a trisubstituted cellulose with little, if any, degradation. When applied to various CTC samples having a wide range of molecular weights, the GPC/LALLS technique predicts Mark-Houwink coefficients virtually identical to published values determined for CTC in THF by conventional methods. More importantly, the procedure predicts a useful relationship between the CTC degree of polymerization and the viscosity of the undervatized cellulose in CED, and the results are compared with CED viscosity-molecular weight data originally derived from cellulose nitrates.

LITERATURE CITED

1. Segal, L., J. Polym. Sci., 1966, B4, 1011-1018.
2. Meyerhoff, G.; Jovanovics, S., J. Polym. Sci., 1967, B5, 459-499.
3. Valtasaari, L.; Saarela, K., Paperi ja Puu, 1975, 57, 5-10.

4. El Ashmawy, A.E.; Danhelka, J.; Kössler, I., Svensk Papperstid., 1974, 16, 603-608.
5. Hall, D.M.; Horne, J.R., J. Appl. Polym. Sci., 1973, 17, 3727-3732.
6. Danhelka, J.; Kössler, I.; Bohackova, V., J. Polym. Sci., Polym. Chem. Ed., 1976, 14, 287-298.
7. Zimm, B.H., J. Chem. Phys., 1948, 16, 1099-1116.
8. Ouano, A.C.; Kaye, W., J. Polym. Sci., Polym. Chem. Ed., 1974, 12, 1151-1162.
9. Schroeder, L.R.; Haigh, F.C., TAPPI, 1979, 62, 103-105.
10. Flory, P.J., "Principles of Polymer Chemistry"; Cornell University Press: Ithaca, N.Y., 1953; p. 310.
11. Strazielle, C., in "Light Scattering from Polymer Solutions," Huglin, M.B., Ed.; Academic Press: New York, N.Y., 1972; p. 636.
12. Flory, P.J.; Fox, T.G. J. Amer. Chem. Soc., 1951, 73, 1904-1908.
13. Sutter, W.; Burchard, W. Makromol. Chem., 1978, 179, 1961-1980.
14. Henley, D. Arkiv Kemi, 1961, 18, 327-392.
15. Valtasaari, L., TAPPI, 1965, 48, 627-631.
16. Immergut, E.H.; Ranby, B.G.; Mark, H.F., Indus. Engr. Chem., 1953, 45, 2483-2490.
17. Sihtola, H.; Kyrklund, B.; Laamanen, L.; Palenius, I., Paperi ja Puu, 1963, 4, 225-232.

RECEIVED December 1, 1980.

Properties of Cellulose Acetate in Solution

Aggregation of Cellulose Triacetate in Dilute Solution¹

G. C. BERRY and M. A. LEECH

Department of Chemistry, Carnegie-Mellon University, 4400 Fifth Avenue,
Pittsburgh, PA 15213

There are very few published light scattering investigations of dilute solutions of cellulose triacetate, C(3.00)A [The notation C(D.S.)A indicates the degree of acetyl substitution (D.S.) of the cellulose acetate.] A study by Patel (1) and coworkers reports light scattering on fractions of C(2.96)A in a mixed solvent of methylene chloride and methanol (50:50 v/v), using procedures similar to those employed by Tanner and Berry (2) in their study on C(2.45)A in the same mixed solvent. The appropriate relation for the Rayleigh ratio R_{θ} reads

$$\frac{Kc}{R_{\theta}} = \frac{1}{M_w} (1 + \langle s^2 \rangle_{LS} h^2/3 + 2A_2 c + \dots) \quad (1)$$

with

$$K = K' \left(\frac{\partial n}{\partial c} \right)_{\mu, T}^2$$

where $\langle s^2 \rangle_{LS}$ is the light-scattering averaged mean-square radius of gyration, $h = (4\pi n/\lambda) \sin \theta/2$, K' is an optical constant, and $(\partial n/\partial c)_{\mu, T}$ is the refractive index increment of the polymer measured at constant chemical potentials of solvent components and temperature. For mixtures containing a solute in a two-component solvent, $(\partial n/\partial c)_{\mu, T}$ is related to the conventional refractive index increment $(\partial n/\partial c)_{c_3, P, T}$ measured at constant solvent composition by

$$\left(\frac{\partial n}{\partial c} \right)_{\mu, T} = \left(\frac{\partial n}{\partial c} \right)_{c_3, P, T} + \lambda \left(\frac{\partial n}{\partial c_3} \right)_{c_2, P, T} \quad (2)$$

¹ This is the fourth work in a series by the authors.

where the solvent mixture has components 1 and 3 present in volume fraction φ_1 and φ_3 (with $\varphi_1 + \varphi_3 = 1$) and

$$\lambda = (\partial c_3 / \partial c_2)_{p,T,\mu_3} \quad (3)$$

(See, for example, the discussion given by Eisenberg(3). When dealing with a mixture containing a solvent and a nonsolvent for the solute, we will let component 3 denote the latter.

In studies of C(2.45)A in a methylene chloride/methanol mixture (50:50 v/v), Tanner and Berry found λ equal to -0.2 (with $(\partial n / \partial c_3)_{c_2,p,T} = 0.0982$ ml/g), e.g., that methylene chloride preferentially solvated the polymer. Data of Patel and coworkers on C(2.96)A for the same solvent mixture gave $\lambda = -0.3$, also indicating preferential solvation of the polymer by methylene chloride. Data of Shakhparonov *et al.* (4) for C(2.45)A in methylene chloride/methanol mixtures containing 0 to 30% methanol indicate positive λ , or preferential solvation by methanol rather than methylene chloride. Their conclusions are based on apparent values of the molecular weight from light scattering, and are subject to error from the effects of the association discussed by Tanner and Berry.

Since the values of $\langle s^2 \rangle / M$ for C(3.00)A are large, it is convenient to discuss them in terms of the worm-like chain model for which (5)

$$\langle s^2 \rangle = \frac{L\rho}{3} S(L/\rho) \quad (4)$$

where L is the contour length

$$L = M/M_L \quad (5)$$

with M_L the mass per unit contour length, ρ of the persistence length, and $S(L/\rho)$ of the function

$$S(x) = 1 - 3x^{-1} + 6x^{-2} - hx^{-3} [1 - \exp(-x)] \quad (6)$$

For L/ρ greater than about 10, $S(L/\rho)$ is essentially unity. Approximating M_L by $m_0/1$, where the length of a repeating unit is taken to be 0.545 nm, we get $M_L = 490$ nm⁻¹ for C(3.00)A.

The light scattering data on C(2.96)A of Patel *et al.* in the 50/50 solvent mixture on fractions over the molecular weight range 10^5 to 1.7×10^5 give $3\langle s^2 \rangle_{LS}/L_w$ equal to 65 nm. This estimate is much greater than the value $\rho = 11$ nm reported for C(2.45)A by Tanner and Berry. Thus, the data of Patel *et al.* on C(2.96)A, suggest a much less coiled chain conformation than is indicated by rotational isomeric state computations for cellulosic chains. The value of $C_\infty = 6\langle s^2 \rangle / \rho L$ computed with the latter model is related to ρ by the equation

$$\rho = \frac{l}{2} C_{\infty} \quad (7)$$

or $\rho = 2.73 C_{\infty}$ for C(3.00)A. According to Yathindra and Rao (6), estimates of C_{∞} vary in the range 50 to 80, depending on the bond angle at the bridge oxygen atom. Consequently, ρ is expected to be in the range 13.1 to 22 nm, in reasonable agreement with the data of Tanner and Berry on C(2.45)A, but much lower than the estimate for C(3.00)A based on the data of Patel *et al.*

In some systematic studies on C(3.00)A, Moore and Russell (7) and later, Flory, Spurr and Carpenter (8) investigated the dependence of $[\eta]$ on solvent. It was found that $[\eta]$ was markedly dependent on solvent, but did not correlate with the second virial coefficient A_2 as is usual for flexible-chain polymers. Tanner and Berry showed that the chain expansion factor α is close to unity for C(2.45)A on the basis of the very small values of $A_2 M^2 / \langle s^2 \rangle^{3/2}$ observed experimentally. The low expansion of C(2.45)A is not necessarily due to small A_2 , but rather reflects a large value of $\langle s^2 \rangle / M$, which has the consequence that intramolecular excluded volume effects may be small despite large values of A_2 . Similar effects are discussed by Helminiak and Berry (9) in relation to studies on a polymer with limited flexibility, i.e., very few available rotational states, separated by high barriers. As they emphasized, the mere observation that α is near unity despite large values of A_2 cannot be taken as evidence for inflexibility. Presumably, α will also be nearly unity for C(3.00)A in which case, as with C(2.45)A, the variation of $[\eta]$ or ρ with solvent reflects short-range skeletal effects rather than long-range excluded volume effects.

Worm-like chain statistics have been used by Eizner and Pti-tsyn (10) for a bead model, and by Yamakawa and Fujii (11) for a cylinder model to calculate $[\eta]$ as a function of ρ , L and the chain diameter d . Their results can be put in the form ($[\eta]$ in dl/g).

$$M_L [\eta] = \frac{\pi N_A}{100} L^2 f(L/d, \rho/d) \quad (8)$$

The function $f(L/d, \rho/d)$ is discussed in more detail by Helminiak and Berry, who provide a graphical representation of $f(L/d, \rho/d)$. In the limit as L/ρ goes to zero, the worm-like chain adopts a rod-like conformation and $f(L/d, \rho/d)$ can be approximated by

$$\lim_{L/\rho=0} f(L/d, \rho/d) = 0.0257 (d/L)^{0.2} \quad (9)$$

so that

$$\lim_{L/\rho=0} M_L [\eta] \simeq 4.86 \times 10^{20} d^{0.2} L^{1.8} \quad (10)$$

In the opposite extreme (and for large L) Eqn. (8) takes on the form

$$\lim_{\rho/L=0} M_L [\eta] = 2^{3/2} \phi \rho^{3/2} L^{1/2} \quad (11)$$

with ϕ a constant equal to 2.65×10^{21} (of course, in Eqn. (11), ρ is independent of L).

The data of Patel *et al.* on $[\eta]$ versus M for solutions of fractions of C(2.96)A in chloroform give $[\eta] \propto L^{0.8}$. Consequently, even though ρ is large for C(3.00)A, the chain conformation cannot be considered to be rod-like on the basis of the viscometric data. Neither can $[\eta]$ be understood with the limiting form Eqn. (11) for very large L and small ρ/L . Even if Eqn. (8) is used with intermediate L/ρ , the dependence of $[\eta]$ on M observed by Patel *et al.* for chloroform solutions is not consistent with the large value of ρ calculated for their data on solutions in the methylene chloride/methanol mixed solvent. For example, application of Eqn. (8) gives ρ equal to 3.5 nm for the viscometric data on chloroform solutions, compared with 65 nm for the light scattering data on the solutions in the mixed solvent. Possible reasons for the discrepancy will be considered below.

Experimental

Materials. Solvents used in dilute solution experiments were freshly distilled prior to use, and the polymer was dried under vacuum (ca. 10^{-5} mm Hg) for several days before use in the preparation of solutions. These precautions were taken to reduce the possible influence of adsorbed water on the solution properties. The C(3.00)A polymer used here is that described by Tanner and Berry.

Studies on Dilute Solutions. The procedures and instrumentation for differential refractometry light scattering, viscometry and solution dialysis are those given by Tanner and Berry. The dialysis equipment, shown schematically in Figure 1, is similar to that used by Tanner and Berry, without explicit description. Dilute solutions were brought to osmotic equilibrium, using osmotic pressure membranes, over a several hour period by continuous feed of fresh mixed solvent with the desired concentration to the solvent side of the dialysis cell. About 20 ml of solution was retained on the solution side, agitated slowly with a magnetic stirring bar.

In order to aid identification and assessment of preferential loss of one of the mixed solvent components during the

differential refractive index measurement, a relatively nonvolatile solvent (or mixed solvent) of about the same refractive index n was used as the reference liquid in the refractive index cell, replacing the mixed solvent used to prepare the solution. The refractive index Δn_0 between the mixed solvent used for the solution and the reference was determined periodically during experiments on the solution.

Since some of the solvents used on this study are mixed solvents, with both components having a high vapor pressure, it was necessary to study the viscosity of dilute solutions with sealed viscometers. Commercially available suspended-level Cannon viscometers constructed to permit sealing under vacuum were used. The solution was filtered into the viscometer and degassed by successive freeze-thaw cycles, and the viscometer was sealed under vacuum. In use, the viscometer was mounted on a holder in a constant temperature bath to permit the rotation of the viscometer to the horizontal to fill the bulb, and rotation to the vertical for determination of the efflux time.

Results and Discussion

Refractive Index Increment. The refractive index increment $\partial n/\partial c_2$ of the polymer (component 2) in the solution was measured with both single and two-component solvents. With the latter, the increment was determined both with solutions at constant solvent composition and with solutions dialyzed to osmotic equilibrium of the low molecular weight solvents to obtain $(\partial n/\partial c_2)_\mu$, respectively.

Values of $(\partial n/\partial c_2)_{c_3}$ for solutions of C(3.00)A in several solvents are given in Table I and Figure 2. A value for $\partial n/\partial c_2$

Table I
Refractive Index Increments $(\partial n/\partial c_2)_{\varphi_3}$ for
Cellulose Triacetate

Component 1	Component 3	φ_3	n Solvent	$(\frac{\partial n}{\partial c_2})_{\varphi_3}$ (ml/g)
Methylene chloride	Methanol	0.50	1.368	0.108
Methylene chloride	Methanol	0.25	1.391	0.112
Methylene chloride	Methanol	0.20	1.398	0.069
Methylene chloride	--	0	1.424	0.054
Chloroform	--	0	1.446	0.041 ^a
s-Tetrachloroethane	--	0	1.494	0.009
m-Cresol	--	0	1.539	-0.028

^aValue given By Sharples and Sweenton (12)

Figure 1. Schematic of the equipment used to dialyze dilute solutions against a mixed solvent: solution chamber, C_1 ; solvent chamber, C_2 ; dialysis membrane, M ; supporting glass frits, F ; ground glass surface, S ; teflon-coated magnetic stirrer, T ; solvent inlet, I ; outlet, O , teflon tubing, A ; fresh solvent reservoir, R ; and solvent waste, W . The chambers hold approximately 20 mL each.

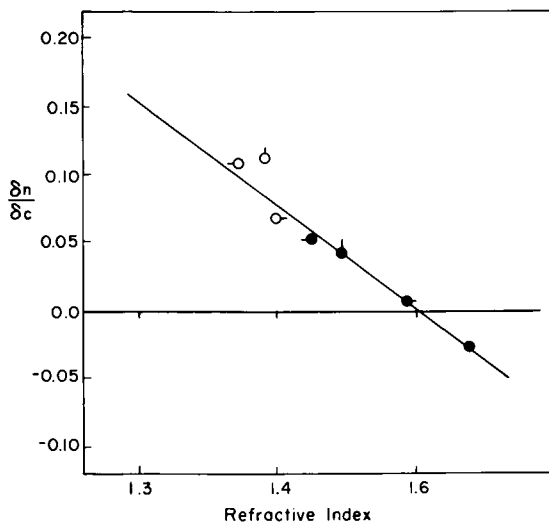
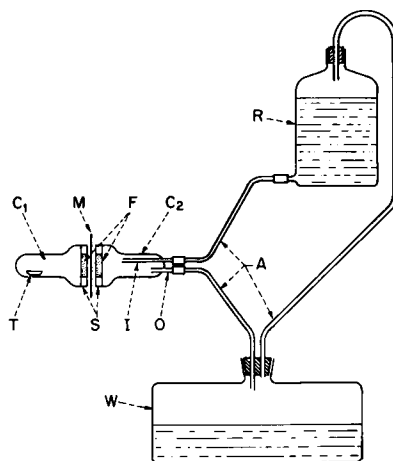


Figure 2. The refractive index increment $(\delta n/\delta C_2)\varphi_s$ for solutions of CTA in m-cresol (●); s-tetrachlorethane (●—); chloroform (●), methylene chloride (—●); and in mixtures of methylene chloride (1) and methanol (3) with $\varphi_s = 0.20$ (○); 0.25 (○); and 0.50 (—○).

for chloroform solutions due to Sharples and Sweenton (12) is included in Figure 2 for comparison. The data in Figure 2 are compared with the Dale-Gladstone relation

$$\left(\frac{\partial n}{\partial c_2} \right)_{c_3} = v_2(n_2 - n_s) \quad (12)$$

where n_s is the refractive index of the (mixed) solvent, to give the values $v_2 = 0.746$ ml/g and $n_2 = 1.505$. These may be compared with the corresponding constants $v_2 = 0.763$ ml/g and $n_2 = 1.495$ reported by Tanner and Berry for solution of C(2.45)A.

Inspection of Figure 2 reveals that with single component solvents for C(3.00)A, $\partial n / \partial c_3$ is generally small, e.g. $|\partial n / \partial c_3| < 0.05$. This is in accord with the limited range of solvents for CTA and the general principle that "like dissolves like." For example, an approximate correlation often obtains between the solubility parameter δ_s of the solvent and $|\partial n / \partial c_2|$, with $|\partial n / \partial c_2|$ being largest for solvents with δ most different from the solubility parameter δ_2 of the polymer and $|\partial n / \partial c_2|$ being nearly zero for solvents with $\delta_s \approx \delta_2$. Evidently, with CTA, the solvent-polymer contacts must be comparable to the polymer-polymer contacts for dissolution to occur.

Despite repeated attempts, the data for the mixed solvents are not as precise as should be expected. See, for example, the data for $(\partial n / \partial c_2)_{c_3}$ shown in Figure 2. Representative data of Δn versus c_2 are given in Figure 3. Since comparable measurements on C(2.43)A were more readily completed, we are at a loss for a definitive explanation for the difficulty experienced with solutions of C(3.00)A in mixed solvents. Possible explanations include the effects of solvent evaporation, incomplete dissolution of the polymer or (partial) absorption of the polymer on vessel walls during preparation and/or Δn measurement. In the only direct comparison with published data, we find $(\partial n / \partial c_2)_{\mu} = 0.178$ ml/g for C(2.96)A in a 1:1 (by volume) mixture of methylene chloride and methanol, in comparison with 0.130 ml/g for C(2.96)A reported by Patel and coworkers. The disparity is larger than should be expected. Values of $(\partial n / \partial c_2)_{\mu}$ found here are entered in Table II, together with $(\partial n / \partial c_2)_{\varphi_3}$ from Table I and λ calculated with Eqn. (1), using $(\partial n / \partial c_3)_{\mu} = -0.0982$ ml/g reported by Tanner and Berry. According to Casassa (13), for some systems for which λ exhibits no reversal of sign with φ_3 the quantity $\varphi_1 \varphi_3 / \lambda$ is nearly a linear function of φ_3 . Plots of λ and $\varphi_1 \varphi_3 / \lambda$ versus φ_3 for the data on C(3.00)A in mixture of methylene chloride and methanol are given in Figure 4a and 4b, respectively. The linear relation applies within the experimental error of our data giving the correlation

$$\frac{\varphi_3(1-\varphi_3)}{\lambda} = A(1+B \varphi_3) \quad (13)$$

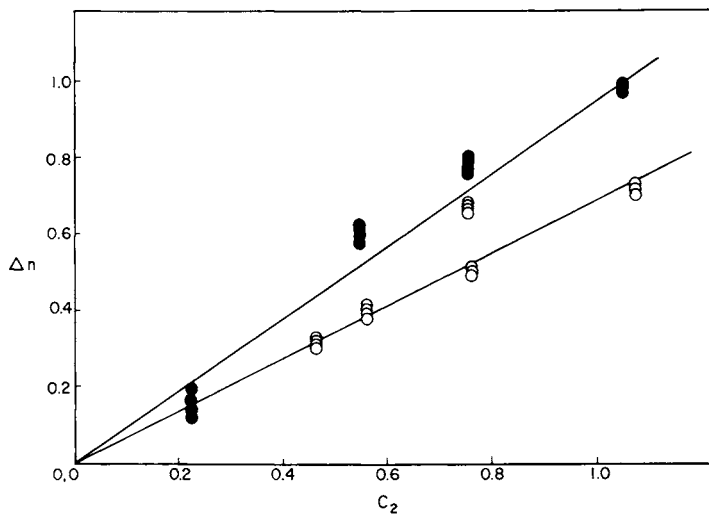


Figure 3. Representative plots of Δn vs. C_2 for CTA in solutions of CTA in the mixed-solvent methylene chloride (1) and methanol (3) with $\phi_3 = 0.20$. Data are for undialyzed (\circ) and dialyzed (\bullet) solutions.

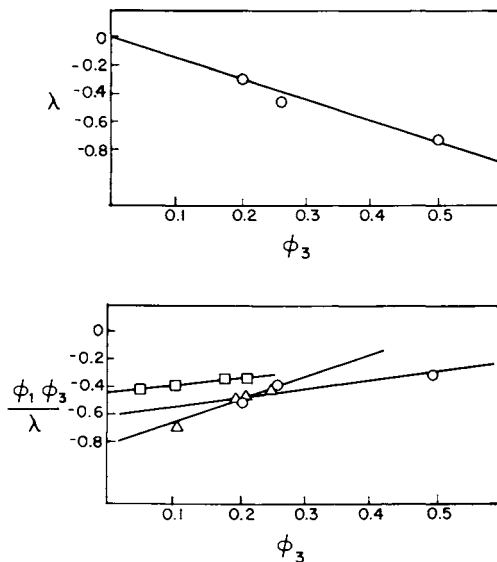


Figure 4. (a) The parameter $\lambda = (\partial C_3 / \partial C_2)_M$ vs. the volume fraction ϕ_3 of methanol for solutions of CTA in mixtures of methylene chloride and methanol; (b) The function $\phi_1 \phi_3 / \lambda$ vs. ϕ_3 for the data in Figure 4a (\circ), and for polystyrene in benzene (1) and methanol (3) and in carbontetrachloride (1) and methanol (3), according to Cassassa.

Table II
Refractive Index Increments of Cellulose Triacetate in
Mixed Solvent

Component 1	Component 3	φ_3	$\left(\frac{\partial n}{\partial c_2}\right)_\mu$	$\left(\frac{\partial n}{\partial c_2}\right)_{c_3}$	λ^a
Methylene Chloride	Methanol	0.20	0.099	0.069	-0.30
Methylene Chloride	Methanol	0.25	0.160	0.112	-0.49
Methylene Chloride	Methanol	0.50	0.178	0.108	-0.71

^aSee Eqn. (1) and (2) for a definition of λ .

for λ as a function of φ_3 with $A = -0.67$ and $B = -1.1$. Similar data for polystyrene in benzene (1) and methanol (3), and in carbontetrachloride (1) and methanol (3) discussed by Casassa are included in Figure 4b for comparison.

It was remarked by Casassa that a crude model for preferential solvation involving "specific binding sites" on the polymer with competitive binding of the two solvents to this site governed by an isotherm dependent on φ_3/φ_1 will lead to Eqn. (13). In this model, there are presumed to be ν binding sites per gram of polymer, each capable of binding either g_1 grams of component 1 or g_3 grams of component 3 so that the masses ξ_1 and ξ_3 of the two components bound to 1 gram of polymer at equilibrium are related by the mass balance

$$\frac{\xi_1}{g_1} + \frac{\xi_3}{g_3} = \nu \quad (14)$$

and by the isotherm

$$\frac{\xi_1/g_1}{\xi_3/g_3} = k \varphi_3 \varphi_1 \quad (15)$$

The model provides an interpretation of the constants A and B in Eqn. (13), with

$$A^{-1} = \nu k g_3 \bar{v} - \nu g_1 \bar{v}_1 \quad (16a)$$

and

$$B = k - 1 \quad (16b)$$

According to the results obtained here, for C(3.00)A in mixtures of methylene chloride (1) and methanol (3), $k = -0.1$. Although negative values of k are possible in general, they are not acceptable in the specific binding-site model under consideration. To proceed, we take k to be approximately zero, which is certainly possible within our experimental error. Then $-A^{-1} = 1.67 \approx v_{g1}v_1$, or C(3.00)A binds about 2.2 g methylene chloride per gram of polymer, or 6.9 mol methylene chloride per mol C(3.00)A repeating unit, and the amount of bound methanol is virtually nil.

To summarize, the refractive index data show that the few solvents for C(3.00)A are in some sense similar to the polymer (e.g. $\partial n/\partial c_2$ is small). Moreover, for the mixed solvent system studied here, interpretation of the preferential solvation with a specific binding site model indicates that the nonsolvent (methanol) of the mixed solvent pair is virtually excluded from the solvation domain of the polymer. These results suggest that dissolution of C(3.00)A requires solvents which can interact with the polymer in specific ways to compensate for the polymer-polymer interactions lost on dissolution.

Light Scattering. Light scattering measurements have been completed on solutions of an (unfractionated) C(3.00)A polymer in four single-component and three two-component solvents. In order to minimize effects of intermolecular association, solutions were treated with low level ultrasonic radiation using an ultrasonic cleaning bath (Bramson Ultrasonics Corp., Model LG40). Solutions were clarified by centrifugation in the light scattering cell. The light scattering data were analyzed with Eqn. (1) to obtain M_w , Γ_2 and $\langle s^2 \rangle_{LS}$:

$$\left(\frac{Kc}{R_0} \right) = \lim_{c \rightarrow 0} \frac{Kc}{R_\theta} = \frac{1}{M_w} \quad (17)$$

$h=0$

$$\lim_{c \rightarrow 0} M_w \frac{\partial(Kc/R_0)}{\partial c} = 2\Gamma_2 \quad (18)$$

$$\lim_{h \rightarrow 0} M_w \frac{\partial(Kc/R_\theta)}{\partial h^2} = \frac{1}{3} \langle s^2 \rangle_{LS} \quad (19)$$

With typical polymers, it is found that plots of Kc/R_θ versus h^2 have slopes that are independent of concentration, as required by Eqn. (1). Deviations from this behavior usually denote effects of intermolecular association. For example, Tanner and Berry reported that $\partial(Kc/R_\theta)/\partial h^2$ increased with increasing c for some solutions of C(2.43)A. The latter authors also reported experiments for which $\partial(Kc/R_\theta)/\partial h^2$ was independent of c , but which

revealed effects of association in large values of M_w .

The light scattering data on solutions of a C(3.00)A polymer (CMU-DI75) studied in seven different solvents are summarized in Table III. Data on Kc/R_θ versus h^2 are shown in Figures 5-8 for four systems, and data on Kc/R_θ versus c for two systems (the same mixed solvents, with $\varphi_3 = 0.25$ and 0.20) are shown in Figure 9. Values of $\partial n/\partial c_2$, or $(\partial n/\partial c_2)_\mu$ for the mixed solvents, given in Table II, were used to compute M_w . It may be noted that entries for Γ_2 and $\langle s^2 \rangle_{LS}$ do not require knowledge of $\partial n/\partial c_2$.

Inspection of the entries in Table III shows that the estimate for M_w is not independent of solvent with values of M_w in the range 5.7×10^4 to 2.2×10^6 (deleting a very large estimate in *s*-tetrachloroethane, for which $\partial n/\partial c_2$ is very small). In addition, values of $\langle s^2 \rangle_{LS}$ varied considerably among the solvents studied, and for most of the data the slope $\lambda(Kc/R_\theta)/\partial h^2$ is not independent of concentration. In obtaining the estimates of M_w and $\langle s^2 \rangle_{LS}$ given in Table III, the data at small scattering angle were neglected in cases for which Kc/R_θ versus $\sin^2\theta/2$ was sharply curved. It should also be remarked that phase separation occurred with the solution in the mixed solvent with $\varphi_3 = 0.50$ (methylene chloride/methanol) when the solution was allowed to stand at 25°C .

The variability of $\partial(Kc/R_\theta)/\partial h^2$ with concentration seen especially in Figures 6 and 8, and to some extent, in Figure 7 indicates that the degree of aggregation for C(3.00)A in those solvent systems increases with increasing polymer concentration. Similar results were reported for solutions of C(2.45)A by Tanner and Berry. The data obtained here indicate that C(3.00)A is aggregated to varying degree in most (or perhaps all!) of the solvents studied.

The lowest M_w is obtained in the methylene chloride/methanol mixed solvent with $\varphi_3 = 0.25$ (with neglect of the data for scattering angle less than about 60 degrees as the latter are much affected by the presence of the aggregated species). The second virial coefficient is smallest in the system with the least aggregation, similar to behavior reported by Tanner and Berry for C(2.45)A. Since the refractive index data suggest that C(3.00)A is completely solvated by methylene chloride when dissolved in mixtures of methylene chloride and methanol, it appears that the mixed solvent of the appropriate composition (e.g. nearly $\varphi_3 = 0.25$) acts to dissolve the methylene chloride-solvated C(3.00)A.

The values of $10^{18} \langle s^2 \rangle_{LS}/M_w$ entered in Table III vary from 16 to 59, with the largest value corresponding to the mixed solvent for which M_w was smallest. It is instructive to compare $\langle s^2 \rangle_{LS}/M_w$ with the value expected for a worm-like chain according to Eqns. (4)-(6) (using $M_L = 490 \text{ nm}^{-1}$). With $M_w = 5.7 \times 10^4$ Eqns. (4)-(6) give $10^{18} \langle s^2 \rangle/M = 590 \text{ cm}^2$ with $\rho = 50 \text{ nm}$, or

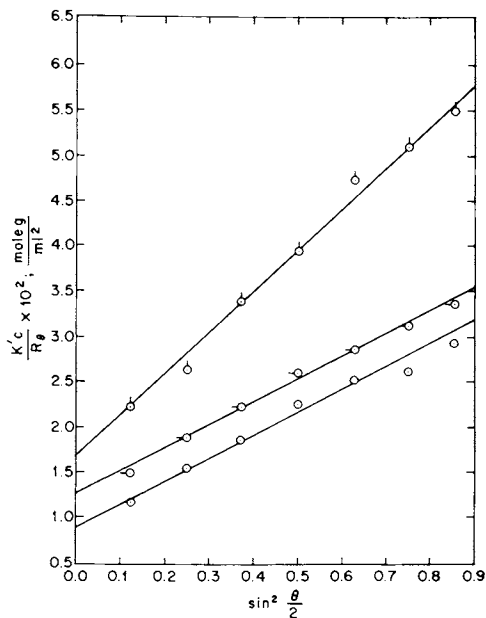


Figure 5. Light-scattering data for a dilute solution of cellulose triacetate in a mixture of methylene chloride (1) and methanol (3) with $\varphi_3 = 0.50$. $K' = K(\partial n/\partial c)\mu^{-2}$. The symbols \circ , $-\circ$, and \circ designate solutions with concentrations of 1.91, 3.01, and 4.81 g/L, respectively.

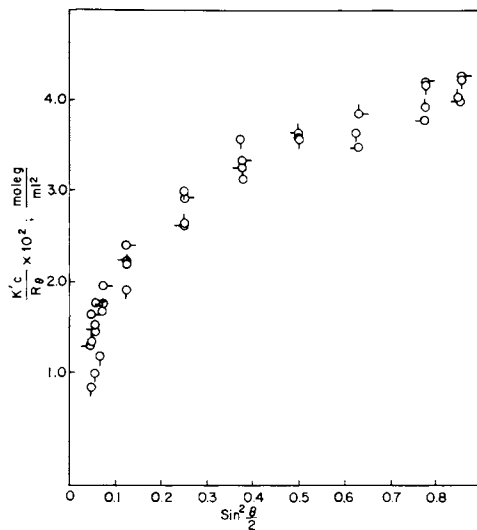


Figure 6. Plots of Kc/R_θ vs. h^2 for solutions of CTA in a mixture of methylene chloride (1) and methanol (3) with $\varphi_3 = 0.25$ for four concentrations: (\circ) 0.297 g/dL; (\circ) 0.194 g/dL; ($-\circ$) 0.132 g/dL; and (\circ) 0.091 g/dL.

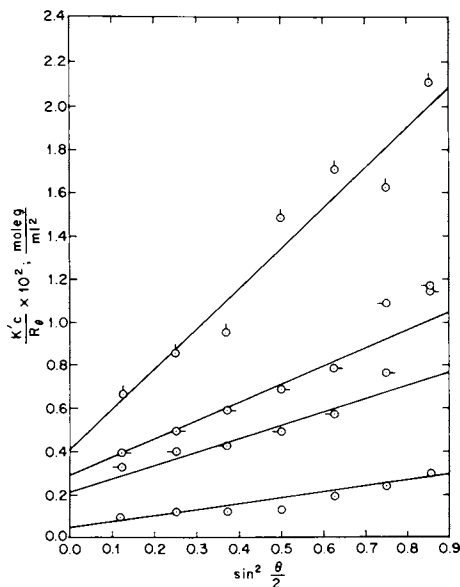


Figure 7. Light-scattering data for a dilute solution of cellulose triacetate in a mixture of methylene chloride (1) and methanol (3) with $\varphi_3 = 0.20$. $K' = K(\partial n / \partial c)_\mu^{-2}$. The symbols \circ , $\text{---}\circ$, $\text{---}\circ$, and $\text{---}\circ$ designate solutions with concentrations of 3.80, 5.04, 6.67, and 8.39 g/L, respectively.

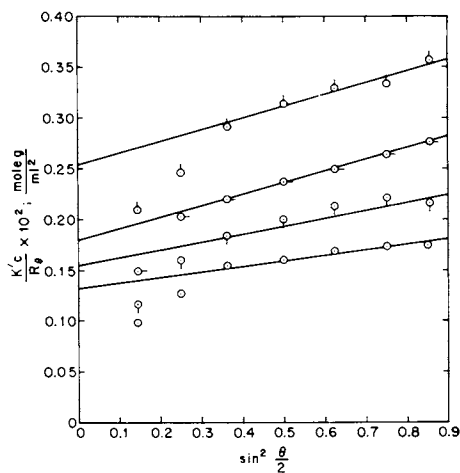


Figure 8. Light-scattering data for a dilute solution of cellulose triacetate in tetrahydroethane, $K' = K(\partial n / \partial c)^{-2}$. The symbols \circ , $\text{---}\circ$, $\text{---}\circ$, and $\text{---}\circ$ designate solutions with concentrations of 4.10, 6.22, 7.99, 8.93 g/L, respectively.

Table III
Light Scattering Parameters for a Cellulose Triacetate Polymer in Mixed Solvents:
Component 1 + Methanol

Component 1	ϕ_3	T (°C)	$10^{-4} \frac{(\partial n)^2}{\partial C^2} M_w$	$10^{12} \langle s^2 \rangle_{LS}$ (cm ²)	Γ_2 (ml/g)	$10^{-5} M_w$	$10^{18} \langle s^2 \rangle_{LS}$ $\frac{M_w}{w}$	Remarks
MeCl	0.50	35	2.37	225	300	7.5	300	precip. at 25°C ^b
MeCl	0.25	17	0.14 ₆	34	10	0.57	590	--
MeCl	0.20	20	0.28 ₆	80	350	2.9	280	--
MeCl	0	25	0.07	100	160	2.4	420	--
Chloroform	0	25	0.031	30	1060	1.9	160	--
s-TCE	0	25	(0.26) ^a	--	--	(300) ^a	--	marked ^b effect
m-cresol	0	25	0.174	620	1600	22	280	

MeCl = Methylene Chloride; s-TCE = s-Tetrachloroethane

^aValues in parentheses are for systems with low $(\partial n/\partial C_2)$.

^bThe quantity $\partial(Kc/R)/\partial h^2$ decreased with decreasing concentration; the value of $\langle s^2 \rangle_{LS}/M_w$ entered was calculated from the value of $\lambda(Kc/R)/\partial h^2$ extrapolated to infinite dilution.

$10^{18} \langle s^2 \rangle / M = 380 \text{ cm}^2$ with $\rho = 37.5 \text{ nm}$. The latter probably provides a reasonable estimate for C(3.00)A based on the data in the mixed solvent with $\varphi_3 = 0.25$, taking approximate account of the polydispersity of the sample used by approximation of $\langle s^2 \rangle / M$ by $\langle s^2 \rangle_{LS} / 1.5 M_w$. This estimate of ρ is somewhat larger than the value 11 nm reported for C(2.45)A by Tanner and Berry, but smaller than ρ found for C(2.96)A by Patel and coworkers in studies using the methylene chloride/methanol mixed solvent with $\varphi_3 = 0.5$.

The experimental estimate of 37.5 nm for ρ may be compared with the predictions of the rotational isomeric state model using the result for C_∞ of Yathindra and Rao mentioned above, for which ρ lies in the range 13 to 22 nm . The difference is small enough to be attributed to error in experimental light scattering, the effects of residual intermolecular association, the effects of molecular weight dispersity, or solvation effects, which are neglected in the theoretical estimate of ρ .

Summarizing the light scattering data, we find evidence for substantial association of C(3.00)A in most (if not all) of the solvents studied. The association is most pronounced in m-cresol and s-tetrachlorethane, and least in the mixed solvent methylene chloride (1) and methanol (3), with $\varphi_3 = 0.25$. In the latter, we find a persistence length of about 37.5 nm , compared with a contour length L_w of 116 nm ; the system is nearly a theta solvent at 17°C , as shown by the small value of Γ_2 .

Intrinsic Viscosity. Viscosities of dilute solutions determined with capillary viscometers were analyzed by the usual relations

$$\eta_{sp}/c = [\eta] + k'[\eta]^2 c + \dots \quad (20)$$

$$(\ln \eta_{rel})/c = [\eta] - \left(\frac{1}{2} - k'\right)[\eta]^2 c + \dots \quad (21)$$

where $\eta_{sp} = \eta_{rel} - 1$ and $\eta_{rel} = \eta/\eta_0$, with η and η_0 the viscosities of solution and solvent, respectively. Values of the intrinsic viscosity $[\eta]$ and the Huggins constant k' determined with five different solvents are given in Table 4.

The values of $[\eta]$ and k' are remarkably similar to each other in view of the association found in the light scattering results. Similar insensitivity of $[\eta]$ to the effects of association were reported by Tanner and Berry in studies on C(2.43)A. Presumably, this results from the insensitivity of the hydrodynamic volume to association at the level present in cellulose acetate solutions. In an approximate treatment of this effect Tanner and Berry estimated the effects of association by a model with random crosslinking of chains of primary molecules, calculating the number, weight and z -averages of the degree of

Table IV
Intrinsic Viscosity of CTA in Several Solvents

Component	Component 3	ϕ_3	T (°C)	k'	$[\eta]$ (dl/g)
Methylene Chloride	Methanol	0.25	25.0	0.346	1.19
Methylene Chloride	Methanol	0.20	24.7	0.55	1.16
Methylene Chloride	--	0	24.9	0.337	1.27
Chloroform	--	0	25.0	0.348	1.02
<u>m</u> -cresol	--	0	25.0	0.367	1.19

association ν given, respectively by

$$\nu_n = 1/\sum \nu^{-1} w_\nu \quad (22)$$

$$\nu_w = \sum \nu w_\nu \quad (23)$$

$$\nu_z = \sum \nu^2 w_\nu / \nu_w \quad (24)$$

where w_ν is the distribution of the weight fraction of ν -mers formed by the crosslinking (association). Further

$$\langle s^2 \rangle_{LS} = A \sum (M\nu)^2 g_{M\nu} w_{M\nu} / M_w \quad (25)$$

where $w_{M\nu}$ is the weight fraction of chains with primary molecular weight M , and degree of association ν , $g_{M\nu}$ is the ratio of the $\langle s^2 \rangle$ for such chains to $\langle s^2 \rangle$ for linear molecules with the same molecular weight, and A is a constant. The distribution $w_{M\nu}$ includes both distribution in ν and in the molecular weight of the primary molecule. With these relations, the ratio $\langle s^2 \rangle_{LS} / M_w$ for the associated (crosslinked) and dissociated (primary) chains is found to be

$$\left(\frac{\langle s^2 \rangle_{LS}}{M_w} \right)_{\text{ASSOC}} = \left(\frac{\langle s^2 \rangle_{LS}}{M_w} \right)_{\text{DIS}} \frac{\sum (\nu M)^2 g_{M\nu} w_{M\nu}}{(\sum \nu M_w M)^2} \quad (26)$$

Similarly, for the intrinsic viscosity,

$$[\eta]_{\text{ASSOC}} = [\eta]_{\text{DIS}} \frac{\sum (\nu M)^a g_{M\nu}^m w_{M\nu}}{M_w^a} \quad (27)$$

where a is equal to $\partial \ln[\eta] / \partial \ln M$, m is about unity, and M_w is the

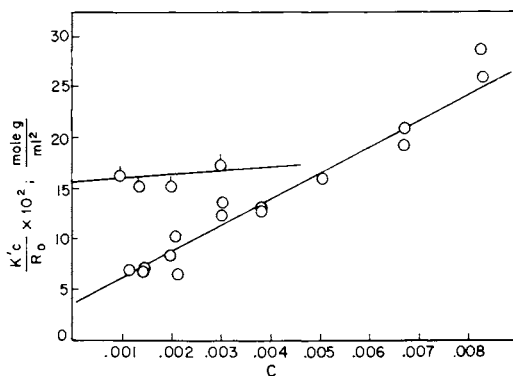


Figure 9. Plots of Kc/R_0 vs. C for solutions of CTA in the mixed-solvent methylene chloride (1) and methanol (3) with $\phi_3 = 0.25$ (○) and $\phi_3 = 0.20$ (○)

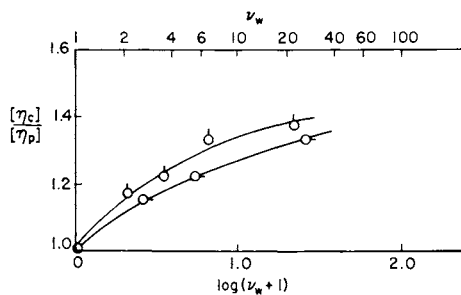


Figure 10. The ratio of the intrinsic viscosities $[\eta]_c$ and $[\eta]_p$ of radiation cross-linked and primary polymers, respectively, vs. $\nu_w + 1$, where ν_w is the number of crosslinks per molecule, for polystyrene and polydimethylsiloxane according to Shultz et al. and Kilb, respectively

viscosity-average molecular weight of the primary molecules.

Tanner and Berry considered the special case of primary molecules of uniform length, for which $w_{Mv} = w_v$, and

$$w_v = \frac{v^{v-1}}{\gamma^v} \gamma^{v-1} \exp\{-v\gamma\} \quad (28)$$

where $v_n = 1-\gamma$. For this case, association affects v_w much more than either $\langle s^2 \rangle_{LSM_w}$ or $[\eta]$ (the latter was estimated with $a = 0.8$ and $m = 0.85$). Although Eqns. (22)-(27) can also be studied with a polydisperse primary polymer (cf. Spiro, et al.) (14) a comparison with experimental data on polydisperse polymers crosslinked by high energy irradiation provides a more useful model. Data of Shultz, et al. (15) on irradiated polystyrene and Kilb (16) on irradiated polydimethylsiloxane are shown in Figure 10. It can be seen that substantial crosslinking gives rise to only modest increase in $[\eta]$, similar to the effects of association observed with C(3.00)A.

If it is accepted that the value of $[\eta]$ is nearly unaffected by the level of association present with C(3.00)A, then Eqn. (8) may be used to estimate ρ from data on $[\eta]$ and L using, for example, the function $f(L/d, \rho/d)$ calculated by Yamakawa and Fujii (11), or by Eizner and Ptitsyn (10). Since we do not have $[\eta]$ as a function of L (or M), we are unable to make a definitive comparison between data on C(3.00)A and Eqn. (8). We can, however, use the experimental values of $[\eta]$ and L_w to calculate ρ with Eqn. (8), using a range of plausible values for d . For example, with $L_w = 116$ nm and $d = 1.2$ nm, we find $\rho = 6$ nm. With $d = 0.5$ nm, the estimate for ρ increases to 8 nm. The estimate of ρ given by the light scattering data is not reached even with d as small as 0.1 nm.

The disparity between estimates of ρ based on the light scattering and the viscometric data may indicate that the light scattering data are affected by residual association, even with the methylene chloride/methanol mixed solvent with $\phi_3 = 0.25$. For example, if M_w of the C(3.00)A studied is less than the estimate 5.7×10^4 given by light scattering studies on the former mixed solvent, revision would decrease ρ_{LS} based on the light scattering data slightly (owing to the compensatory effects on $\langle s^2 \rangle_{LS/M_w}$ noted above) but would augment ρ_η deduced from the viscometric data. For example, 50 percent reduction in M_w would be expected to have little effect on ρ_{LS} , but ρ_η would be increased to about 17 nm.

Summary

The light scattering data on dilute solutions of C(3.00)A show effects of intermolecular association in all the single-component solvents studied, and in two of three mixed solvents examined. It is possible that association is minimal in mixtures

of methylene chloride (1) and methanol (3) with $\phi = 0.25$, but this is a tentative conclusion at present. Analysis of the data with the latter mixed solvent give a persistence length ϕ of 40 nm for C(3.00)A. Data on the refractive index increment of C(3.00)A show that $|\partial n/\partial c_2|$ is small for the available single-component solvents for C(3.00)A, indicating that polymer-polymer interactions lost on dissolution must be replaced by similar polymer-solvent interactions to effect solubility. In the mixed solvent methylene chloride and methanol, C(3.00)A is apparently nearly completely solvated by methylene chloride. Viscometric data on dilute solutions are relatively insensitive to association in the range encountered here. Analysis of the data gives a somewhat smaller value of ρ than that obtained from the light scattering data.

Acknowledgment

Partial support for this study from the Office of Water Research and Technology, Grant No. 14-34-0001-7528, is gratefully acknowledged.

Abstract

Properties of cellulose triacetate, CTA, in dilute solution have been investigated using light scattering, refractometry, and viscometry with moderately concentrated solutions. The weight average molecular weight M_w was determined with solutions in seven different solvent systems, including four mixed solvents (different ratios of methylene chloride and methanol). Values of M_w varied over a wide range, revealing the presence of severe intermolecular association of CTA in dilute solution. The most reliable M_w was obtained in a mixed solvent with 0.75 methylene chloride: 0.25 methanol. The best estimate for the radius of gyration based on the light scattering data results in a persistence length ρ of 37 nm for CTA. The relative insensitivity of $[\eta]$ to interchain association observed with CTA is similar to the effects reported on $[\eta]$ for linear chains undergoing radiation induced crosslinking. The sort of randomly branched structure produced in the radiation crosslinked polymer may also be dominant with intermolecularly associated CTA.

Literature Cited

1. Nair, P. R. M.; Gohel, P. M.; Patel, K. C.; Patel, R. D. Europ. Polym. J., 1977, **13**, 273.
2. Tanner, D. W.; Berry, G. C. J. Polym. Sci., Polym Phys. Ed., 1974, **12**, 941.
3. Eisenberg, H., "Biological Macromolecules and Polyelectrolytes in Solution", London, Oxford Univ. Press, 1976.

4. Shakhparonov, M. J.; Zakwedazeva, N. F.; Podgorodetskii, Ye. K. Polym. Sci. USSR, 1967, 19, 1349.
5. Yamakawa, H., "Modern Theory of Polymer Solution", New York, 1971.
6. Yathindra, N.; Rao, V. S. R. Biopolymers, 1970, 9, 783.
7. Moore, W. R.; Russel, J. J. Colloid Sci., 1954, 9, 338.
8. Flory, P. J.; Spurr, O. K. Jr.; Carpenter, D. K. J. Polym. Sci., 1958, 27, 231.
9. Helminiak, T. E.; Berry, G. C. J. Polym. Sci., Polymer Symp., 1978, 65, 107.
10. Eizner, Y. E.; Ptitsyn, O. B. Vysokonol Soedin, 1962, 4, 1725.
11. Yamakawa, H.; Fujii, M. Macromolecules, 1974, 7, 128.
12. Sharples, A.; Swinton, T. L. J. Polym. Sci., 1961, 50, 53.
13. Casassa, E. F. Polym. J., 1972, 3, 517.
14. Spiro, J. G.; Goring, D. A. I.; Winkler, C. A. J. Phys. Chem., 1964, 68, 323.
15. Shultz, A. R.; Roth, P. I.; Rathmann, G. B. J. Polym. Sci., 1956, 22, 495.
16. Kilb, R. W. J. Phys. Chem., 1959, 63, 1838.

RECEIVED September 22, 1980.

The Configurational Statistics of Pullulan and Some Related Glucans

DAVID A. BRANT and BRUCE A. BURTON

Department of Chemistry, University of California, Irvine, CA 92717

The work reported here has been carried out in the context of a program to develop reliable conformational energy functions for polysaccharides in solution (1, 2). A quite satisfactory model for aqueous amylose chains has been developed; details are reported at length elsewhere (3, 4, 5, 6). Here procedures applied successfully to amylose are extended to the closely related glucan pullulan as part of an effort to test the generality of the method. Information of potential applicability to the dextran family of polysaccharides is derived in the process. Owing to the current absence of appropriate experimental measurements of the configuration dependent properties (7) of pullulan, only an unrefined theory of the configurational statistics of pullulan can be developed at the present time (1, 2). It is nevertheless instructive to investigate the sensitivity of the calculated results to various parameters of the theory, and to contrast the behavior predicted for pullulan on the basis of an unrefined model with that of some other glucans. The results of these investigations are presented here primarily in the form of projection drawings of representative polymer chain conformations (2, 5).

Structure and Properties of Pullulan

Pullulan is an extracellular α -D-glucan produced by the organism Aureobasidium pullulans (8). Whereas the linear component of starch, amylose, is a homopolymer of α -1,4-linked D-glucose (Figure 1a), pullulan has the same structure with approximately every third α -1,4-linkage replaced by an α -1,6-linkage (Figure 1b) (9, 10, 11). For present purposes pullulan has been taken to be a regularly repeating polymer of maltotriose units linked by α -1,6-linkages. The term dextran refers to a widely studied family of microbial polysaccharides comprising homopolymeric α -1,6-D-glucan chains possessing variable degrees of chain branching (8). Pullulan and dextran are

0097-6156/81/0150-0081\$05.00/0
© 1981 American Chemical Society

amorphous polymers readily soluble in water whereas amylose is partially crystalline and displays only limited solubility in this medium. These differences are presumably related in part to the greater conformational freedom inherent in the α -1,6-linkages. Because pullulan is similar in chemical structure to amylose and is available in large amounts in pure form for experimental studies, it provides an ideal system in which to test the generality of methods developed to treat the conformational statistics of amylose. It represents, moreover, a logical step in the direction of a theoretical treatment of dextran.

Structural Parameters

As specified below, the structural geometry of the glucose residues (Figure 1) was taken to be that of either the mean α -D-glucose residue described by Arnott and Scott (12) or the mean α -D-glucose residue in crystalline cyclohexaamylose (13). The valence angle at the oxygen of the glycosidic linkage was chosen to be 111.5° for α -1,6-linkages (14) and either 114.5° or 117.0° for α -1,4-linkages (3, 4), as specified below.

Methods of Calculation

Conformational energies were estimated using methods described previously (1, 3). In the present calculations, however, terms were also introduced as indicated below to account for inherent barriers to bond rotation and for the anomeric effect, following methods proposed by Abe and Mark (15). Thus, threefold torsional barriers of 1.8 and 2.8 kcal mol⁻¹ were included in some cases for the C-O and C-C bonds, respectively; the energy maxima in these terms occurred for torsion angles 0, 120, and 240°. (See reference 1 for conventions pertinent to torsion angles and other geometric parameters.) A maximum anomeric stabilization energy of 1.1 kcal mol⁻¹ was associated with the ϕ rotation (Figure 1), which resembles the C-O bond rotation in poly(oxymethylene) (15). Rotation ω (Figure 1b) is similar to the C-C rotation in poly(oxyethylene) and, hence, realizes a maximum stabilization energy of 1.0 kcal mol⁻¹ (15). No significant anomeric effect attends the rotation ψ . Where included, the anomeric term operates in the torsion angle range 120 to 360° and provides maximal stabilization at about 180 and 300°.

Polymer chain dimensions, reported here as the dimensionless characteristic ratio C_∞ (1, 2, 4), were calculated from the structural geometry and conformational energy estimates using methods described earlier (16); approximations inherent in the calculations have been discussed in detail (1, 2, 4, 5, 16). The

characteristic ratio is defined to be proportional to the mean square end-to-end distance of the polymer chain, unperturbed by the long range excluded volume effect (1, 2); its observed value is close to 5 for aqueous amylosic chains (4). Projection drawings of representative conformations of the several glucans treated were generated by an elaboration of Monte Carlo methods described earlier (5). Details of the calculations will be presented later in the context of efforts to fit theoretical calculations of the characteristic ratio to experimental results.

Results and Discussion

Amylose. A conformational energy contour map for a dimeric segment of an amylosic chain is shown in Figure 2 (1-6). The Hybl et al. residue geometry(13) and potential functions without inherent torsional or anomeric terms (3) were used. The angle at the glycosidic oxygen was 114.5° . Energy contours are drawn at 1, 5, and 25 kcal mol⁻¹ relative to the global energy minimum; dashed contours imply negative absolute energies. Only one significant low energy domain appears in the conformation space of the amylose dimer near the position $\phi, \psi = 0, 0^\circ$. This conformer is depicted in Figure 1a. Throughout most of the conformation space of the dimeric segment intolerable steric conflicts occur as signified by the large domain of high energy where contour lines have been omitted. The energy surface in Figure 2 is refined in the sense that the characteristic ratio predicted from it (1, 2, 4, 5) agrees well with experimental measurements of C_∞ and its temperature coefficient for amylosic chains in aqueous media (17).

Figures 3 and 4 show projections into mutually orthogonal (xy and yz) planes of one conformation of a 100-residue amylosic chain. Circles represent the glycosidic oxygens. These oxygens are connected in the drawings by virtual bonds spanning the glucose residues, which, for clarity, are not shown. The ordinate and abscissa of the projection drawings are measured in Angstrom units and refer to axes of an arbitrary Cartesian coordinate system. Details of the computation are presented elsewhere (5).

The conformation depicted in Figures 3 and 4 was chosen to be representative of chains in a large Monte Carlo sample of such chains, all of which possess conformations consistent with the energy surface in Figure 2; its end-to-end extension is close to the mean value for chains in the sample. It is best to regard these projection drawings, and those which follow, as snapshots of a polymer chain, taken simultaneously from mutually orthogonal directions, which have served to capture the chain in one of the countless conformations available to it (2). In fact the shapes of all of the chains shown here are extremely labile, and the

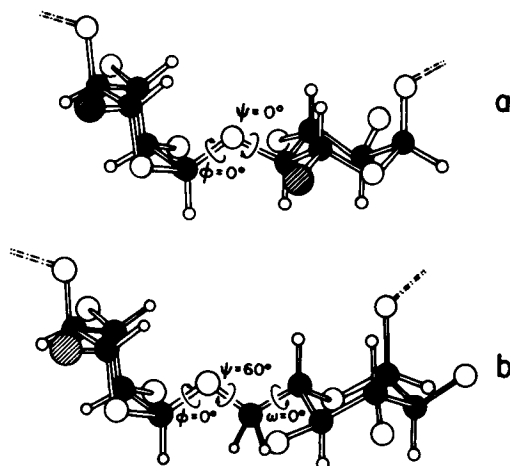


Figure 1. Projection drawings of dimeric α -D-glucan chain segments linked 1,4 (a) and 1,6 (b): (○) oxygens or hydroxyls; (◦) hydrogens; (●) carbons; and (⊗) hydroxymethyl groups. Conventions relating to torsion angles ϕ , ψ , and ω and other structural features are given elsewhere (1).

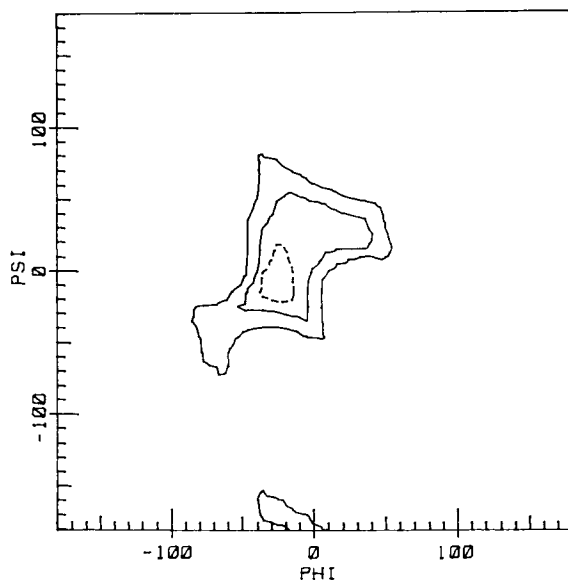


Figure 2. Conformational energy contour diagram for the dimeric segment in Figure 1a. Energy contours are drawn at 1, 5, and 25 kcal mol⁻¹ above the energy minimum; dashed contours correspond to negative absolute energies. References to details of the calculation are provided in the text.

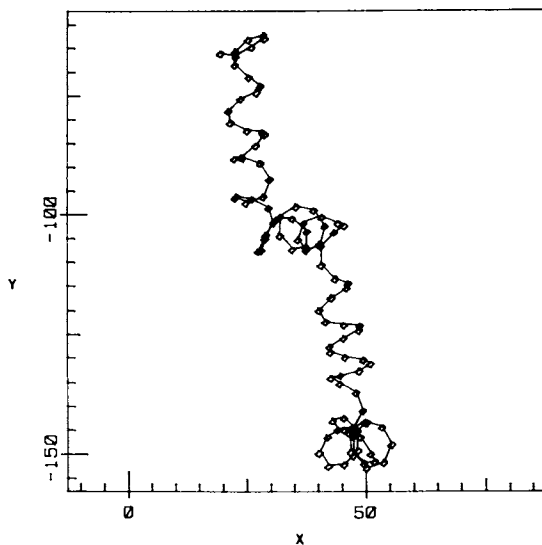


Figure 3. Projection into the xy plane of an arbitrary coordinate system of one particular amylose chain conformation consistent with the energy surface of Figure 2. Circles represent the glycosidic oxygens. These are connected by virtual bonds spanning the sugar residues; for clarity the residues are not shown.

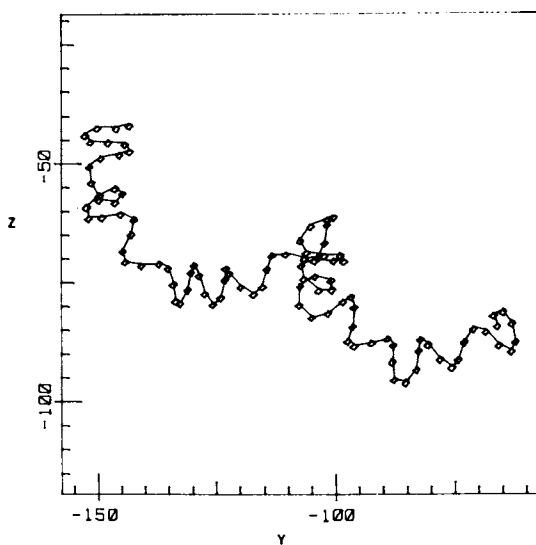


Figure 4. Projection into the yz plane of the same amylose chain conformation shown in Figure 3

projection drawings represent just a single fleeting conformation which will have changed substantially an instant later (2, 5).

Examination of the amylosic chain conformation in Figures 3 and 4 as well as numerous others in the Monte Carlo sample (5) discloses the statistical or random coil nature of the chain. At the same time the pseudohelical character of the chain's backbone trajectory is readily ascertained (2, 5). This latter feature plays an important role in the behavior of the chain, as discussed elsewhere in this volume (6, 18, 19, 20, 21, 22).

Among the several characteristics of the amylosic chain, it is of particular interest to characterize its stiffness as well as its extension. These questions have already been addressed at some length (5, 16). Here we would simply like to point out that, in addition to the characteristic ratio, the configurational entropy, and the persistence length, all commonly used as measures of stiffness and extension, it may be useful to consider a kind of correlation function defined by the mean projection of a unit vector along the final virtual bond of the chain onto a unit vector aligned with the initial virtual bond. This function is shown in Figure 5 for the conformational energy map of Figure 2; details of the calculation will be presented in another place. The oscillatory character of the correlation function is a clear reflection of the pseudohelical nature of the chain trajectory. We see in Figure 5 that correlation of the directions of the initial and final bonds of the chain persists even for chains (or chain segments) with degrees of polymerization of 100 or more. The correlation function has decayed to $1/e$ after 20 residues. This measure of the correlation length, expressed in numbers of glucose residues, may in some cases be more meaningful than the persistence length, which is a correlation length expressed in distance units (5). Certainly it is improper, as is sometimes done, to try to express the correlation length in residue units by taking the ratio of the persistence length to the (virtual bond) length of a single residue. If this is done for the amylosic chains of Figures 2-5, which possess a persistence length of about 28\AA and a virtual bond length of 4.25\AA , the correlation length in residue units is grossly underestimated. (The term "persistence length" in this paper refers to the magnitude of the mean end-to-end vector.)

Other skeletal geometries and potential functions can be justified for amylose in addition to those chosen to generate Figures 2-5. If, for example, the Arnott and Scott residue geometry (12) is used in conjunction with potential functions which include terms for inherent torsional barriers and the anomeric effect, the contour diagram of Figure 6 is obtained. Here the glycosidic bridge angle was taken to be 117.0° . This energy surface yields a characteristic ratio almost five times the

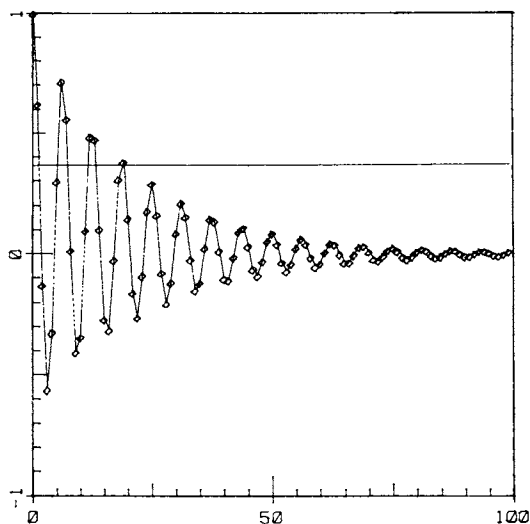


Figure 5. The ordinate displays the mean projection of a unit vector along the final virtual bond of an amylosic chain consistent with Figure 2 onto a vector aligned with the initial virtual bond. The abscissa is chain length, measured in glucose units. The horizontal line through the figure is the inverse of the base of natural logarithms.

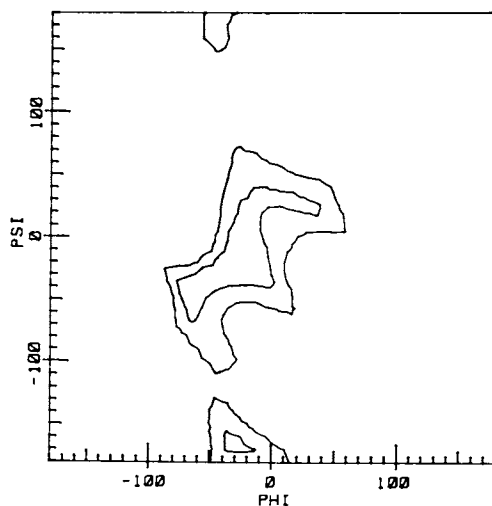


Figure 6. An energy surface as in Figure 2, but based on alternative assumptions about skeletal geometry and conformational energy functions as described in the text

experimental value, and, therefore, presumably represents a less realistic chain model. A typical chain conformation consistent with this surface is drawn in Figure 7, where the tendency toward pseudohelical trajectories seen in Figures 3 and 4 persists. Now, however, the chain is clearly more extended with greater mean pitch and fewer residues per turn in the pseudohelical segments. The associated correlation function shown in Figure 8 oscillates less dramatically because of the larger pseudohelical pitch, i.e., each virtual bond is, on the average, more nearly colinear with its predecessor. The persistence length calculated for this chain model is 66 \AA , but the correlation length measured in glucose residues (defined by the decay of the correlation function) is apparently smaller than in the case of the preceding, more realistic, chain model, which has a persistence length less than half as large.

Dextran. We will use the term "dextran" in the present context to denote the linear α -1,6-D-glucan homopolymer. A representative dimeric segment of this chain is shown in Figure 1b. To display the conformational energy hypersurface we present sections in ϕ, ψ space taken at constant values of $\omega = 60^\circ, -60^\circ,$ and 180° in Figures 9, 10, and 11, respectively. The three-dimensional contour diagram may be visualized as a stack of these two-dimensional sections. All of the low energy regions superimpose in this stack to produce a figure with a low energy "tunnel" parallel to the ω axis in the vicinity of $\phi, \psi = 40, -40^\circ$, as anticipated from simple steric considerations. This low energy region is depicted quite readily by a section in ϕ, ω space taken at $\psi = -60^\circ$ as shown in Figure 12. As expected, the α -1,6-linkages experience considerable freedom of rotation about the C(5)-C(6) bond. The energy surface shown in Figures 9-12 is based on Arnott and Scott residue geometry, a glycosidic bridge angle of 111.5° , and potential functions without torsional and anomeric terms. Contours in Figure 12 are drawn at absolute energies of $-2, -0.5, 8,$ and 25 kcal mol^{-1} ; as before, the dashed contours correspond to negative absolute energies. The present energy surface for the α -1,6-linkage resembles closely that previously published by Tvaroska, Pérez, and Marchessault (14).

Figures 13 and 14 depict mutually orthogonal projection drawings of a particular dextran chain conformation consistent with the preceding energy surface. The chain is quite disordered and undergoes abrupt changes in direction. It displays no obvious propensity for pseudohelical propagation and is, moreover, quite compact relative to the amylosic chain with $C_\infty = 1.8$ and a persistence length of just 6 \AA .

If we add torsional and anomeric terms to the potential function for dextran, then the freedom of rotation about ω

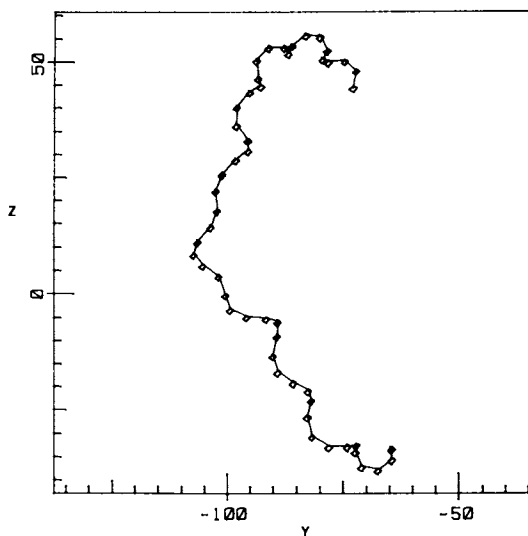


Figure 7. Projection of an amylosic chain conformation consistent with the energy surface in Figure 6

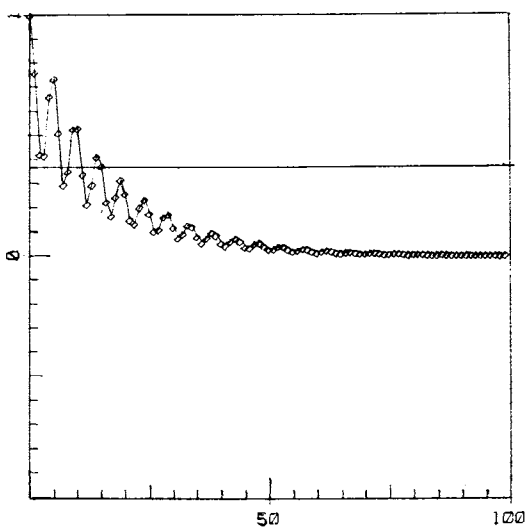


Figure 8. A correlation function as in Figure 5 for amylosic chains consistent with Figure 6

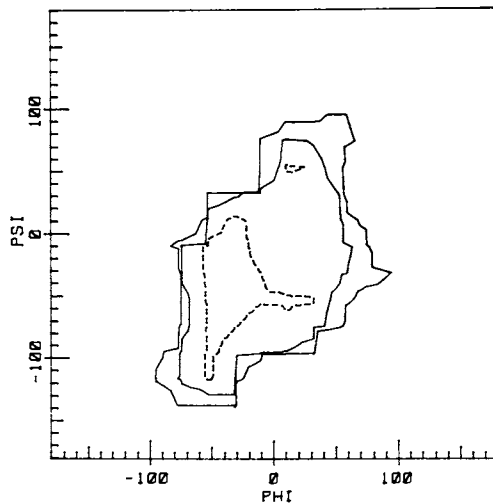


Figure 9. A section in ϕ, ψ space taken at $\omega = 60^\circ$ through the contour diagram of the conformational energy hypersurface for the dimeric segment in Figure 1b. Energy contours are drawn at 1, 5, and 25 kcal mol⁻¹ above the energy minimum; dashed contours correspond to negative absolute energies. References to details of the calculation are provided in the text.

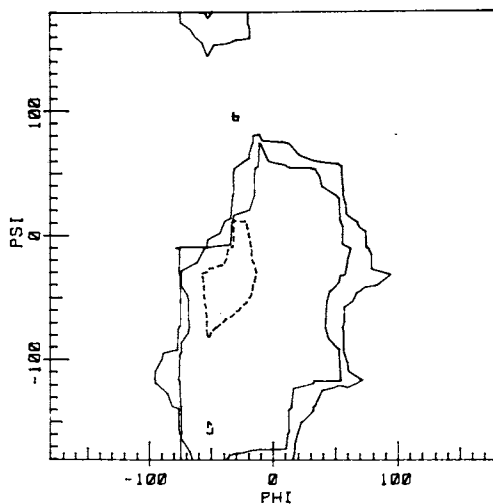


Figure 10. A diagram as in Figure 9 taken at $\omega = -60^\circ$

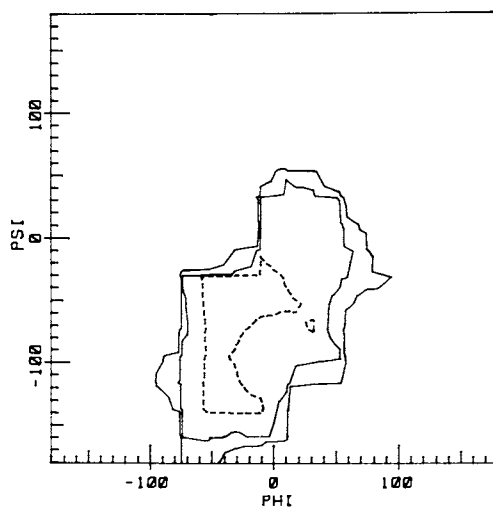


Figure 11. A diagram as in Figure 9 taken at $\omega = 180^\circ$

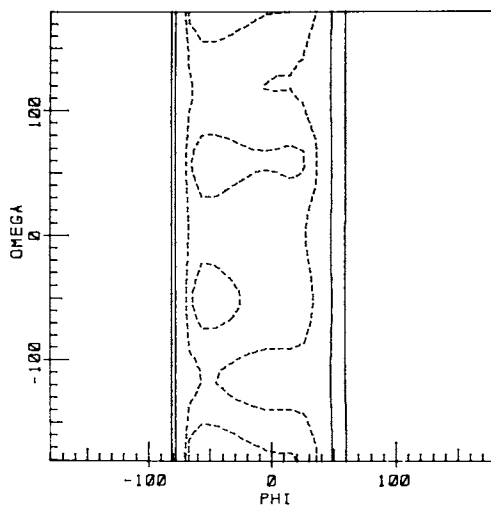


Figure 12. A section in ϕ, ω space taken at $\psi = -60^\circ$ through the contour diagram of the energy hypersurface described in Figure 9. Energy contours are drawn at absolute energies of -2 , -0.5 , 8 , and 25 kcal mol $^{-1}$; dashed contours refer to negative absolute energies.

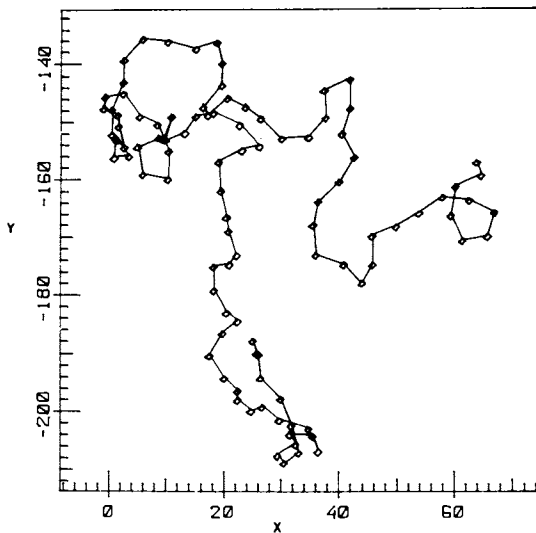


Figure 13. Projection into the xy plane of a linear dextran chain conformation consistent with the energy surface on Figures 9–12

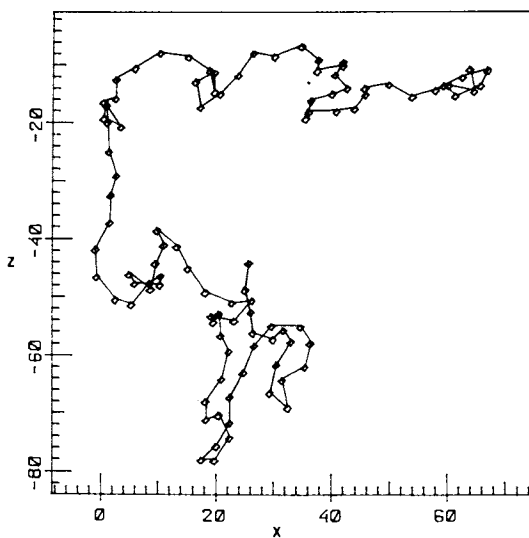


Figure 14. Projection into the xz plane of the same linear dextran chain conformation shown in Figure 13

decreases and three distinct minima appear. These are separated by barriers exceeding 2 kcal mol^{-1} along the ω axis as shown in Figure 15, where the energy contours correspond to those in Figure 12. This energy surface leads to more extended dextran chains with $C_{\infty} = 5$ and a persistence length of 13 \AA . As can be seen in Figure 16, chain conformations consistent with this energy surface are somewhat less tortuous than those associated with the surface of Figures 9-12, and there is some hint in the projection drawings of a tendency toward pseudohelical propagation. This latter suggestion could be investigated by examining the character of the associated correlation function, but we have not carried out the necessary calculation.

It is evident that inclusion of torsional and anomeric terms in the potential functions has a pronounced effect on the calculated chain dimensions and on the visual aspect of typical chain conformations. In the case of the dextran chain we currently have no basis for knowing which, if either, of the models discussed here is realistic. It may be possible to gain some insights that will help narrow the range of acceptable chain models for dextran by comparing theoretical and experimental values of the configuration-dependent properties of pullulan, which incorporates α -1,6-linkages. Alternatively, one would prefer to do the same for dextran itself, but this approach is complicated by the existence of chain branching in most, if not all, naturally occurring dextran samples.

Pullulan. When we construct a pullulan chain model by replacing every third α -1,4-linkage in amylose by an α -1,6-linkage, we find a polymer coil with compact dimensions and a tortuous trajectory. The pullulan conformation shown in Figures 17 and 18 was generated using the energy surface of Figure 2 for the α -1,4-linkages ($C_{\infty} = 5$ for the homopolymer) and the surface of Figures 9-12 for the α -1,6-linkages ($C_{\infty} = 1.8$ for the homopolymer). Mean coil dimensions predicted for pullulan by this model are small with $C_{\infty} = 2.4$ and a persistence length of 13 \AA . The effect of introducing into the amylose skeleton periodic α -1,6-linkages possessing considerable conformational freedom is to disrupt the pseudohelical tendency of the α -1,4-D-glucan homopolymer and reduce the chain extension significantly. The projection drawings nevertheless disclose occasional loops in the pullulan chain which are reminiscent of the pseudohelical trajectory of amylosic chains: occasionally the two α -1,6-linkages in each hexameric segment adopt conformations that combine with those of the four α -1,4-linkages in the segment to generate short sequences of amylose-like pseudohelical trajectory.

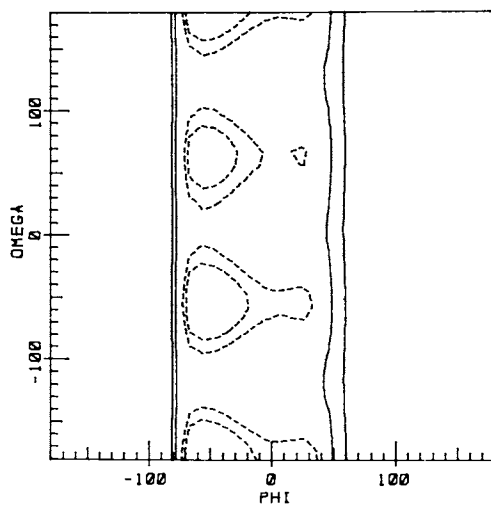


Figure 15. An energy surface as in Figure 12, but based on alternative assumptions about conformational energy functions as described in the text

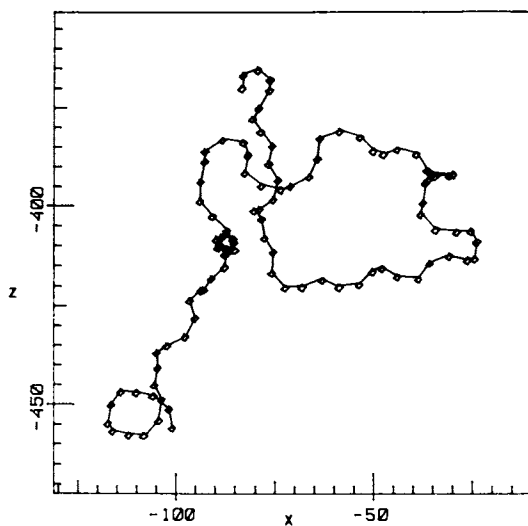


Figure 16. Projection of a linear dextran chain conformation consistent with the energy surface in Figure 15

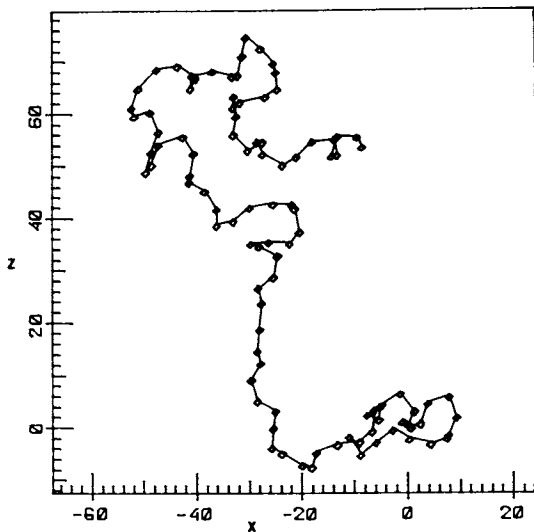


Figure 17. Projection into the xz plane of a pullulan chain conformation based on the chain model described in the text

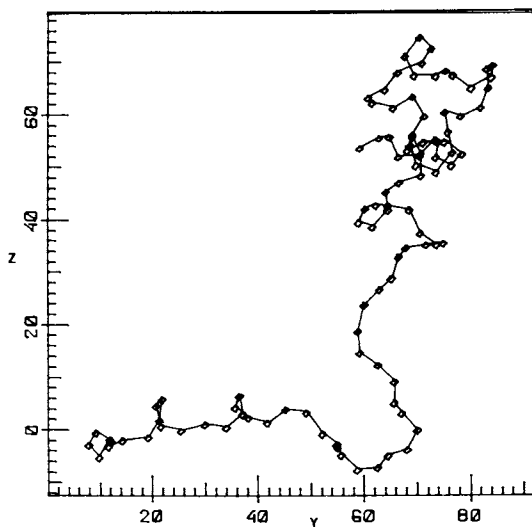


Figure 18. Projection into the yz plane of the same pullulan chain conformation shown in Figure 17

It is of interest to note that when different polysaccharide chains are compared, the correlation of characteristic ratio and persistence length, normally observed for various models of a particular type of chain, is no longer preserved. Thus the amylose chain based on the energy surface of Figure 2 has a characteristic ratio of 5 and a persistence length of 28 Å. The respective quantities for the dextran chain based on Figure 15 are 5 and 13 Å. For the pullulan chain just described, which also has a persistence length of 13 Å, the characteristic ratio is reduced to 2.4.

A second pullulan model has been constructed using again the energy surface of Figure 2 for the α -1,4-linkages but now incorporating the energy surface of Figure 15 for the α -1,6-linkage. A typical pullulan chain conformation based on this model is shown in Figure 19. The mean extension of such chains is described by a characteristic ratio and persistence length of 2.3 and 12 Å, respectively. Thus, even though the dextran homopolymer based on the energy surface of Figure 15 is much more extended ($C_{\infty} = 5$) than the one based on the surface of Figures 9-12 ($C_{\infty} = 1.8$), the pullulan model incorporating this second (Figure 15) type of α -1,6-linkage is slightly more compact than the pullulan chain based on the initial model (Figures 9-12). These results suggest that the chain dimensions predicted for pullulan chains will be rather insensitive to the details of the model employed for the α -1,6-linkages. If this impression persists after investigation of additional chain models, then comparison of theoretical and experimental studies of pullulan chain dimensions may not provide a very sensitive probe of the energy surface for the α -1,6-linkage. Investigation of temperature effects could, however, lead to additional information (1, 4).

Conclusions

Comparison of projection drawings and calculated chain dimensions for amylose, linear "dextran", and pullulan chains shows that the α -1,6-linkage is a source of considerable conformation freedom in D-glucan chains which incorporate this linkage. Experimental studies of the coil dimensions of pullulan and other polysaccharides containing α -1,6-linkages will be required to refine the parameters of the theoretical model for this linkage.

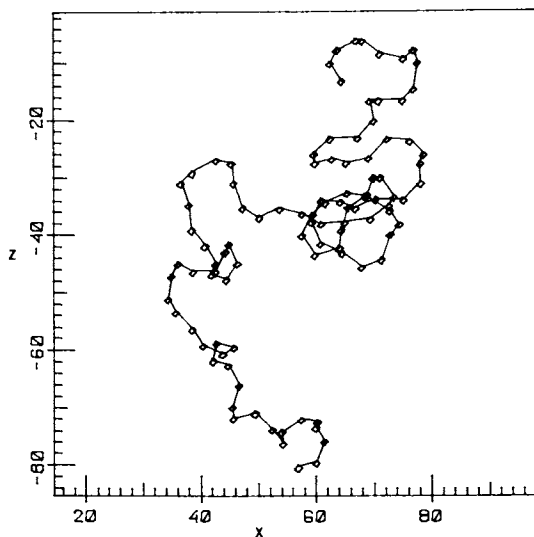


Figure 19. Projection of a pullulan chain conformation based on a chain model different from that used to generate Figures 17 and 18. See text for details.

Abstract

Theoretical chain models for the D-glucans amylose, linear "dextran", and pullulan have been constructed on the basis of realistic molecular geometries for the skeletal segments and estimates of the conformational energy as a function of the backbone torsion angles. Random coil chain dimensions have been calculated and are reported as the characteristic ratio of the mean square unperturbed end-to-end distance and as the persistence length. A correlation function designed as one measure of chain stiffness and extension is introduced. Projection drawings of representative conformations of amylose, dextran and pullulan chains are presented. Comparison of these drawings and the chain dimensions calculated for each chain discloses that the α -1,6-linkage is a source of substantial conformational freedom in D-glucan chains which incorporate this linkage. Experimental studies of the coil dimensions of pullulan and other polysaccharides containing α -1,6-linkages will be required to refine the theoretical model for this linkage.

Acknowledgement

This work has been supported in part by National Science Foundation Research Grants PCM79-23041 and PCM77-23603.

Literature Cited

1. Brant, D. A., Quart. Rev. Biophys. (1976) 9, 527.
2. Brant, D. A., in "The Biochemistry of Plants" (Preiss, J., Ed.), Vol. 3, Chapter 11, Academic Press: New York, 1980.
3. Goebel, C. V., Dimpfl, W. L., and Brant, D. A., Macromolecules (1970) 3, 644.
4. Brant, D. A., and Dimpfl, W. L., Macromolecules (1970) 3, 655.
5. Jordan, R. C., Brant, D. A., and Cesàro, A., Biopolymers (1978) 17, 2617.
6. Cesàro, A., and Brant, D. A., in "Solution Properties of Polysaccharides" (Brant, D. A., Ed.), ACS Symposium Series, Chapter 34, American Chemical Society: Washington, 1980.
7. Flory, P. J., Pure Appl. Chem. (1973) 26, 309.
8. Sandford, P.A., Advan. Carbohydr. Chem. Biochem. (1979) 36, 265.

9. Wallenfels, K., Keilich, G., Bechtler, G., and Freudenberger, D., Biochem. Zeit. (1965) 341, 433.
10. Catley, B. J., and Whelan, W. J., Arch. Biochem. Biophys. (1971) 143, 138.
11. Colson, P., Jennings, H. J., and Smith, I. C. P., J. Am. Chem. Soc. (1974) 96, 8081.
12. Arnott, S., and Scott, W. E., J. Chem. Soc. Perkin Trans. 2 (1972), 324.
13. Hybl, A., Rundle, R. E., and Williams, D. E., J. Am. Chem. Soc. (1965) 87, 2779.
14. Tvaroska, I., Pérez, S., and Marchessault, R. H., Carbohydr. Res. (1978) 61, 97.
15. Abe, A., and Mark J. E., J. Am. Chem. Soc. (1976) 98, 6468.
16. Brant, D. A., and Goebel, K. D., Macromolecules (1975) 8, 522.
17. Goebel, K. D., and Brant, D. A., Macromolecules (1970) 3, 634.
18. Cesàro, A., Konic, W., and Brant, D. A., in "Solution Properties of Polysaccharides " (Brant, D. A., Ed.), ACS Symposium Series, Chapter 32, American Chemical Society: Washington, 1980.
19. Handa, T., Yajima, H., and Ishii, T., ibid., Ch. 31.
20. Bhide S. V., Karve, M. S., and Kale, N. R., ibid., Ch. 33.
21. Pfannmueller, B., and Ziegast, G., ibid., Ch. 35.
22. Ohnishi, M., and Hirami, K., ibid., Ch. 36.

RECEIVED November 17, 1980.

Dilute Solution Properties of *Streptococcus salivarius* Levan and Its Hydrolysates

S. S. STIVALA and J. E. ZWEIG¹

Department of Chemistry and Chemical Engineering, Stevens Institute of Technology, Hoboken, NJ 07030

J. EHRLICH

Department of Oral Biology, College of Medicine and Dentistry of New Jersey, Newark, NJ 07103

Levan is a polymer composed of D-fructofuranose units joined by β -2, 6 bonds (1). Though it is found in plants (2), the levans of interest here are those obtained from the extracellular substance of cariogenic bacteria. The levans of bacterial origin are branched through β -2, 1 bonds, Figure 1. Levan, including dextrans (4) and mutans (5), have been implicated in dental caries and periodontal diseases by virtue of their acidogenic (6, 7), adhesive (8), and antigenic (9) properties in the oral cavity. The β -2, 6 and β -2, 1 linkages in *Streptococcus salivarius* levan was recently confirmed from chemical ionization mass spectroscopy (10).

The molecular weights of the levans produced from various bacterial cultures vary from about 12-100 x 10⁶ daltons, e.g., *S. salivarius*, 30-32 x 10⁶; *Bacillus subtilis*, 25 x 10⁶; *Aerobacter levanicum* from cell cultures, 17 x 10⁶; *Aerobacter levanicum* from isolated enzymes, 40-67 x 10⁶; *Bacillus vugatus* 50-100 x 10⁶ (see reference 11 for key references). Though the molecular weights of these levans can be as high as 100 x 10⁶, Long, Stivala and Ehrlich (12) reported that the molecular weight of levan produced by *S. salivarius* depends on the pH of the growth media, with value as low as 10⁶ obtained at pH = 5.7.

The breakdown of levan occurs through levan hydrolase, which is present in the mixed salivary sediment or plaque suspension and results first in the release of fructose which may be ultimately metabolized to organic acid (13). DaCosta and Gibbons (14) found that the hydrolase is an inducible enzyme since it is formed in broth containing levan, insulin or sucrose, but not in broth containing glucose or fructose. The *streptococcus* of plaque are believed to be responsible for the hydrolysis of levan (15) and since the bacteria can rapidly hydrolyze levan, it acts as storage polymer of carbohydrate which can be continually metabolized to organic acid (16).

¹ Current address: Shell Development Corporation, Houston, TX.

It has been suggested by Leach and co-workers (17) that levan might be as important as the more inert dextran in the caries process since levan is quite liable to be attacked by the oral bacteria and on hydrolysis and subsequent catabolism provides a prolonged acid habitat for the tooth. Thus, levan may serve as substrate for prolonged acid production even in the absence of exogenous sucrose or other simple dietary sugars, as for example, when the host is asleep or not eating. Therefore, one may assume that this polymer plays an important role in long term demineralization of the teeth and in long term ecological regulation via plaque pH depression. Stivala and co-workers (18, 19) examined the kinetics of the acid hydrolyses of *S. salivarius* levan under various conditions of pH and temperature. Bahary and Stivala (20) studied structural changes during the acid hydrolysis of this levan by observing changes in molecular weight and viscosity continuously in the light scattering cell and viscometer, respectively.

The solution properties of native *S. salivarius* levan, including fractionated moieties, were reported in earlier papers by Stivala and co-workers (11, 20, 21, 22, 23). A number of physico-chemical parameters of native *B. subtilis* levan, including the products from mild acid hydrolyses of molecular weights ranging from 100×10^6 to a low of several thousands, were reported by Dedonder and Silcewicz (24). This paper will review our earlier work on the solution properties of *S. salivarius* levan and extend our recent work (25) on the solution properties of fractionated moieties of the acid hydrolyzed levan.

Materials and Methods

Materials. (a). Levan Preparation: Levan was prepared and purified from cultures of *S. salivarius* strain ATCC 13419 according to procedures described elsewhere (12, 26). (b). Acid Hydrolyses: Native levan was hydrolyzed at pH \approx 2 at 35°C according to procedures described in earlier papers (18, 25). (c). Fractionation: The water soluble native levan was fractionated by fractional elution using varying ratios of water/tetrahydrofuran (11). The hydrolyzed sample was fractionated by fractional precipitation at about 4°C using ethanol as non-solvent (25, 27).

Methods. (a). Molecular Weights: Weight-average molecular weights, \bar{M}_w , (greater than about 5×10^4) were obtained in water and in various solvents, e.g. saline solutions, urea solutions, dimethylsulfoxide, from Zimm plots using light scattering data (21, 22). Sedimentation equilibrium was used to obtain \bar{M}_w for samples of $\bar{M}_w < 5 \times 10^4$ (25, 27).

Number-average molecular weights, \bar{M}_n , were obtained from colorimetric data from end-group analysis (reducing sugar) according to procedure described earlier (19).

(b). Dimensional Parameters: The z-average root-mean square radii of gyration, $(R_g^2)_z^{1/2}$, were calculated from the Zimm plots of light scattering, and z-sedimentation coefficients, S^0 , were obtained from sedimentation velocity data as described in earlier papers (21, 22). (c). Intrinsic viscosity, $[\eta]$, and partial specific volume, \bar{v} : The $[\eta]$ and \bar{v} were determined from viscosity and density measurements according to procedures described earlier (11, 21).

Discussion

I. Solution Parameters of Unhydrolyzed Levan. The fractional elution of the native levan reported by Ehrlich and co-workers (11) produced a total of 20 fractions with the 20th fraction recovered at 54/46 H₂O/THF. Turbidimetric titration showed that more than one-half of the levan is extracted in the narrow range of 50/50 to 53/47 H₂O/THF. The $[\eta]$, \bar{M}_w , S^0 , \bar{v} and $(R_g^2)_z^{1/2}$ reported by Stivala and co-workers (11, 21) for some of the fractions are summarized in Table I below. These investigators obtained values of 0.17 and 0.62 for the exponents of the linear double logarithmic plots of $[\eta]$ vs. \bar{M}_w and S^0 vs. \bar{M}_w , respectively. Exponent values of 0.5 to 0.9 in the former plot are exhibited by random coils whereas values below 0.5 and 2.0 indicate branched structures and rods, respectively. Exponent values of 0.57, 0.62, 0.71 for branched structures, 0.20, 0.29, 0.33 for rods, and 0.41, 0.43 and 0.47 for linear shapes have been reported from slopes of the latter plot (21), whereas 0.67 is expected for spheres. A value of 0.43 was obtained (21) from the slope of the log-log plot of $(R_g^2)_z^{1/2}$ vs. \bar{M}_w . For linear polymers values of 0.5-0.6 have been reported and for spheres the $(R_g^2)_z^{1/2}$ varies with $M^{1/3}$.

Table I. Solution Parameters of *S. salivarius* Levan in H₂O at 25°C (22).

Fraction	$[\eta]$ (dl/g)	$\bar{M}_w \times 10^{-6}$	$S^0 \times 10^{13}$ (sec)	\bar{v} (ml/g)	$(R_g^2)_z^{1/2}$ (Å)
F12	0.144	18.5	200	0.66	333
F14	0.148	20.0	194	0.63	340
F15	0.149	17.4	195	0.62	349
F17	0.151	19.0	182	0.64	403
F18	0.153	29.7	232	0.63	493
F19	0.156	32.5	299	0.61	410
F20	0.183	57.1	387	0.63	803

BIOPOLYMERS, Table II

The values of $[\eta]$ shown in Table 1 are extremely low for such extremely high molecular weight macromolecules. Further, it is noted that these high molecular weight fractions have corresponding low radii of gyration. Based on these observations and on the values of the exponents of the log-log plots of $[\eta]$ -, S^0 -, and $(R_g^2)^{1/2}$ - \bar{M}_w native *S. salivarius* levan is best described as a highly branched, compact structure of near-spherical symmetry (11, 21). This is in agreement with the electron micrograph studies of Newbrun and co-workers (28).

The $[\bar{\eta}]$ and $(R_g^2)^{1/2}$ of the native levan and its fractions were found (22) to be significantly higher in dimethyl sulfoxide than in water, reflecting the higher hydrodynamic volume of levan in the former. The $[\eta]$, $(R_g^2)^{1/2}$, and \bar{M}_w were also obtained in other solvents (23), e.g., 0.1 - 0.4 N NaCl, 4-8 M urea, ethanol-H₂O 11/9 by volume. The \bar{M}_w were constant, within experimental error, indicating that the levan in water is not aggregated by hydrogen bonds. Values of the radii of gyration were lower in water than in aqueous solutions of urea and lowest in the ethanol/water mixture. In the former, urea may break intramolecular hydrogen bonds, e.g., between branches, allowing the molecule to expand whereas in the latter, the ethanol, being a precipitant, renders the ethanol/water mixture a poor solvent causing the molecule to contract.

11. Solution Parameters of Hydrolyzed Levan. The hydrolysis of native levan effected a reduction in \bar{M}_w from 43×10^6 to 5.5×10^6 daltons. The fractionation of the partially hydrolyzed levan yielded 32 fractions varying in \bar{M}_w from 8×10^6 down to 10^4 (25, 27). Double logarithmic plots of $[\eta]$ vs. \bar{M}_w and S^0 vs. \bar{M}_w each yielded two linear segments intersecting at $\bar{M}_w \approx 10^5$. The exponents of the former were 0.05 and 0.67 for \bar{M}_w in the range of 8×10^6 to 2×10^5 and 9×10^4 to 10^4 , respectively, whereas those of the latter were 0.67 and 0.43, respectively. Examination of the values of these exponents suggested that the levan hydrolysates of $\bar{M}_w > 10^5$ are best characterized by spheres and those of $\bar{M}_w < 10^5$ exhibit random coil behavior (25, 27). Calculations, based on equivalent spheres and random coils, of various dimensional parameters from $[\eta]$, S^0 , and frictional coefficient data confirmed this observation (25).

Table II contains values of \bar{M}_n for the levan hydrolysates obtained from end-groups analyses, and sedimentation equilibrium. Values by the two methods are, within experimental error, in good agreement.

Figure 2 shows the plot of $\log [\eta]$ vs. $\log \bar{M}_n$ (values of $[\eta]$ from reference 25) of the levan hydrolysates for $[\eta]$ measured in water at 25°C. It is noted from this figure, that there are two linear segments. The linear segments can be expressed by the Mark-Houwink equation, $[\eta] = K \bar{M}_n^\alpha$ where the exponent α is obtained from the slope. The exponents calculated from Figure 2 are 0.50 for levan hydrolysates of $\bar{M}_n < 4 \times 10^4$ and 0.11 for values

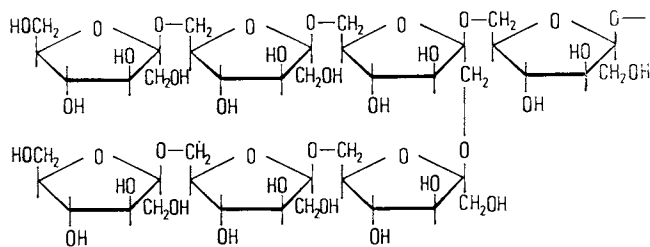


Figure 1. Structure of branched levan

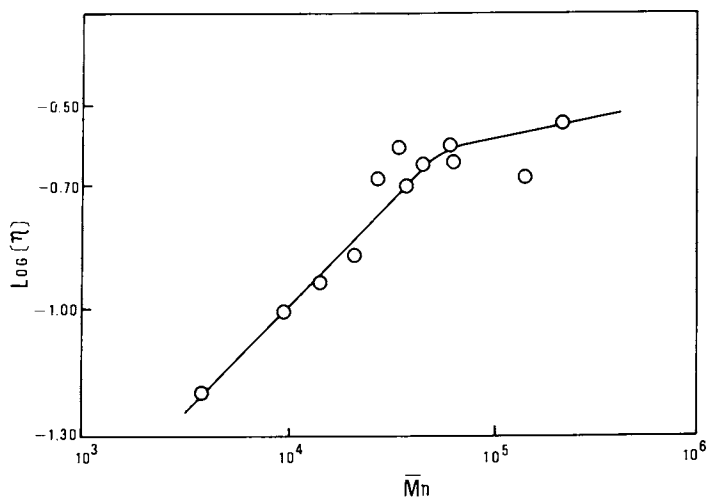


Figure 2. Log-log plot of intrinsic viscosity vs. \bar{M}_n for hydrolyzed levan fractions at 25°C

Table II. Number-Average Molecular Weights of Levan Hydrolysates

Sample	\bar{M}_n^a	Sample	\bar{M}_n^a	\bar{M}_n^b
Native	2.06×10^5	F17	3.36×10^4	
F1	2.27	F19	3.33	
F5	1.45	F21	2.80	
F7	6.63×10^4	E7	2.06	1.86×10^4
F10	6.21	E6	1.46	1.56
F13	3.51	E5	9.47×10^3	9.98×10^3
F15	4.62	E4	3.68	1.93

^aDetermined from end-group analysis

^bDetermined from sedimentation equilibrium

of $\bar{M}_n > 4 \times 10^4$. The nature of Figure 2 reflect the observations made from similar plots using \bar{M}_w values (25). However, as mentioned earlier the values of α in this case was 0.05 for $\bar{M}_w > 10^5$ and 0.67 for $\bar{M}_w < 10^5$. The difference in values of α obtained from \bar{M}_w and \bar{M}_n of the levan hydrolysates reflect the polydispersity of the samples in the weight range examined. The two different slopes observed in Figure 2 indicates that the structure of levan hydrolysates of $\bar{M}_n < 4 \times 10^4$ and $\bar{M}_n > 4 \times 10^4$ are different.

The dispersities, \bar{M}_w/\bar{M}_n , of native levan and hydrolysates are summarized in Table III (\bar{M}_w values are from reference 25). The hydrolysis of the native levan effected an appreciable drop in dispersity from 207 to values below 36 depending on the molecular weight of the hydrolysate. As a group, hydrolysate fractions of $\bar{M}_n > 4 \times 10^4$ exhibit dispersities in the range of 36-5.4 whereas those of $\bar{M}_n < 4 \times 10^4$ have lower dispersities in the narrower range of 2.7 - 1.3. Figure 3 shows

Table III. Dispersity, \bar{M}_w/\bar{M}_n of Native Levan and Its Hydrolysates

Sample	\bar{M}_w/\bar{M}_n	Sample	\bar{M}_w/\bar{M}_n
Native Levan	207	F17	6.5
F1	36	F19	2.7
F5	24	E7	1.3
F7	31	E6	1.5
F10	13	E5	1.9
F13	10	E4	2.7
F15	5.4		

the log-log plot of \bar{M}_n vs. \bar{M}_w . It is noted that the two linear curves of different slopes reflect the two structurally different levan hydrolysates.

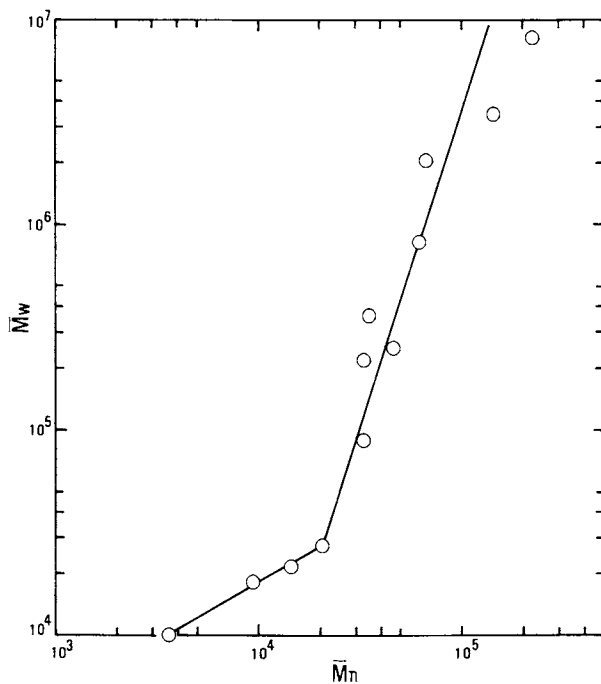


Figure 3. Log-log plot of \bar{M}_w versus \bar{M}_n

Exponent values of 0.05 and 0.67 of the Mark-Houwink relation for hydrolysates of $\bar{M}_w > 10^5$ and $\bar{M}_w < 10^5$, respectively, suggest that the former behave as spheres and the latter as random coils. The diameter, d , of hard sphere suspended in a liquid medium, may be calculated from $[\eta]$ using the Einstein equation, $[\eta] = 2.5/\rho$ where ρ is the density of the sphere; i.e., $\rho = m/v = m/(1/6)\pi d^3$ where m is mass and v is the volume. Since $m = M/N$ where M is molecular weight and N is Avogadro's number, the expression for d in terms of the measured M and $[\eta]$ is

$$d = [M[\eta]/(2.5)(1/6)\pi N]^{1/3} \quad (1)$$

The mean square end-to-end distance, \bar{r}^2 , for random coil may be calculated from $[\eta]$ and M using the Flory-Fox equation

$$[\eta] = \phi \bar{r}^2^{3/2}/M \quad (2)$$

where $\phi = 2.5 \times 10^{21}$. Using equations (1) and (2) the \bar{R}_g^2 for sphere and random coil may be calculated from the relationships $\bar{R}_g^2 = (3/20)d^2$ and $\bar{R}_g^2 = r^2/6$, respectively. Thus, Stivala and co-workers (25), calculated the values of \bar{R}_g^2 for the hydrolysates and from their corresponding values of \bar{M}_w^g , obtained the following relationships from log-log plots,

$$(\bar{R}_g^2)^{1/2} = 0.82 \bar{M}_w^{0.36} \quad \text{for } \bar{M}_w > 10^5 \quad (3)$$

$$(\bar{R}_g^2)^{1/2} = 0.13 \bar{M}_w^{0.57} \quad \text{for } \bar{M}_w < 10^5 \quad (4)$$

The exponent value of 0.36 is in good agreement with 0.33 for spheres, and the exponent value of 0.57 is in good agreement with 0.5-0.6 for random coils. Regarding native *S. salivarius* levan, Stivala and co-workers (11, 21) reported that in water it behaves as a highly branched compact structure of spherical symmetry.

The hydrolytic degradation of levan is catalyzed by the enzyme levan hydrolase which is found in the mixed salivary sediment or plaque suspension. DaCosta and Gibbons (14) reported that the enzyme preferentially cleaves the terminal fructose units suggesting that the hydrolysis is non-random. Stivala, Lauren and co-workers (18, 20) examined the acid hydrolysis of *S. salivarius* levan by observing changes in \bar{M}_w and $[\eta]$ continuously as a function of time, temperature, pH, and levan concentration. Two simultaneous first-order reactions were observed, an initial rapid reaction attributed to β -2,1 branch point cleavage and a slower reaction attributed to the β -2,6 non-branch points in the main-chain and branches. Specific rate constants for the two processes were obtained from Guggenheim plots. These studies suggested that the hydrolysis of levan proceeds by a non-random process.

This observation was supported from changes in \bar{M}_n observed during hydrolyses (19) with subsequent analysis of the data on a statistical model of a trifunctionally branched polymer. It was observed that the dispersity as a function of hydrolysis time, for given temperature and pH, exhibits a maximum. No maximum was observed for dextran hydrolyses, which is reported to follow a random path.

It is clear that hydrolytic attack of *S. salivarius* levan produces two structurally different degradation products, one that conforms to behavior in solution characteristic of spheres and the other characteristic of random coils. It should be mentioned that solution properties are greatly affected by the presence of even a few long branches but insensitive to many short branches. In this connection it was shown from ^{13}C NMR spectroscopy that the spectra of the high vs. low molecular weight levan hydrolysates do not differ (27) suggesting perhaps the presence of short branches in the samples of $M_w < 10^5$ or $M_n < 4 \times 10^4$.

It is noteworthy to mention, in support of the observation in Figure 2 on *S. salivarius* levan, the work of Dedonder and Slizewicz (24). These investigators examined the fractions of the partially acid hydrolyzed *B. subtilis* levan. They reported that a significant change in the structure of this levan occurs following hydrolysis.

Literature Cited

1. Whistler, R.L.; and Smart, C.L.; "Polysaccharide Chemistry"; Academic Press, New York, 1953; pp. 268-270.
2. Greenwood, C.T.; "Advanced Carbohydrate Chemistry"; 1952; 7, pp. 289-292.
3. Avigad, G.; "Encyclopedia of Polymer Science and Technology"; 1968; 8, pp. 711-718.
4. Sidebotham, R.L.; "Advan. Carbohydr. Chem."; 1974; pp. 371-444.
5. Guggenheim, B.; Helv. Odontol. Acta; 1970; 14, Suppl. V, 89-108.
6. Manly, R.S.; and Richardson, D.T.; J. Dent. Res.; 1968; 47, 1080-1086.
7. Bahn, A.N.; Cummings, S.G.; and Hayashi, J.S.; Dent. Res.; 1976; 55, Special Issue C, C134-C138.
8. de Stoppelaar, J.; Konig, K.G.; Plasschaert, A.J.M.; and van der Hoeven, J.S.; Arch. Oral. Biol.; 1971; 16, 971-975.
9. Shilo, M.; and Wolman, B.; Br. J. Exp. Pathol.; 1958; 39, 652-661.
10. Hancock, R.A.; Marshall, K.; and Weigel, H.; Carbohydrate Res.; 1976; 49, 351-360.
11. Ehrlich, J.; Stivala, S.S.; Bahary, W.S.; Garg, S.K.; Long, L.W.; and Newbrun, E.; J. Dental Res.; 1975; 54, 290-297.
12. Long, L.W.; Stivala, S.S.; and Ehrlich, J.; Arch. Oral Biol.; 1975; 20, 503-507.

13. Manly, R.S.; and Dain, J.A.; 1963; Proc. Int. Assoc. Dent. Res. Abstr: No. 359.
14. DaCosta, T.; and Gibbons, R.; Arch. Oral Biol.: 1968; 13, 609-617.
15. van Houte, J.; and Jansen, H.M.; Arch. Oral Biol.: 1968; 13, 827.
16. Gibbons, R.J.; Caries Res.: 1968; 2, 164.
17. Leach, S.A.; Kolendo, A.B.; and Saxton, C.A.; Caries Res.: 1967; 1, 104.
18. Lauren, M.D.; Stivala, S.S.; Bahary, W.S.; and Long, L.W.; Biopolymers; 1975; 14, 2373-2385.
19. Stivala, S.S.; Lauren, M.D.; and Garg, S.K.; Polymer; 1979, 20, 18-22.
20. Bahary, W.S.; and Stivala, S.S.; Colloid and Interface Sci.; 1978; 63, 212-217.
21. Stivala, S.S.; Bahary, W.B.; Long, L.W.; Ehrlich, J.; and Newbrun, E.; Biopolymers; 1975; 14, 1283-1292.
22. Bahary, W.S.; Stivala, S.S.; Newbrun, E.; and Ehrlich, J., Biopolymers; 1975; 14, 2467-2478.
23. Stivala, S.S.; Bahary, W.B.; Carbohydrate Res.; 1978; 67, 17-21.
24. Dedonder, R.; Slicewicz, P.; Bull. Soc. Chim. Biol.; 1958; 40, 873-886.
25. Stivala, S.S.; Zweig, J.E.; Biopolymers; in press.
26. Newbrun, E.; Baker, S.; Carbohydrate Res.; 1968; 6, 165-170.
27. Zweig, J.E.; "The Physico-Chemical Characterization of Acid Hydrolyzed *S. salivarius* Levan"; 1977; Ph.D. Dissertation: Stevens Institute of Technology, Hoboken, N.J.
28. Newbrun, E.; Lacy, R.; and Christie, T.M.; Arch. Oral. Biol.; 1971; 102 , 549-558.

RECEIVED August 26, 1980.

PS-60: A New Gel-Forming Polysaccharide

R. MOORHOUSE, G. T. COLEGROVE, P. A. SANDFORD,
J. K. BAIRD, and K. S. KANG

Kelco, Division of Merck & Co., Inc., 8225 Aero Drive, San Diego, CA 92123

PS-60 is an anionic heteropolysaccharide that forms viscous solutions and can under certain conditions, form thermoreversible gels with characteristics similar to those formed by both carrageenan and agar. The polysaccharide is produced by a bacterium that was originally isolated from a plant; the taxonomy⁽¹⁾ of the organism identifies it as a new species, Pseudomonas elodea.

Fermentation Conditions

A typical fermentation medium⁽²⁾ for PS-60 consists of a simple salts medium with glucose as C-source and both organic and inorganic sources of nitrogen (Figure 1). PS-60 is an anionic polysaccharide that gels after a heat treatment followed by cooling. The gelation properties are determined by the dominant counterion. Consequently, the counterion and the subsequent gel properties can be controlled by regulating the pH of the fermentation with Na⁺ or K⁺ phosphates and NaOH or KOH.

PS-60 is produced at a conversion efficiency of approximately 50% resulting in a very high viscosity fermentation beer (4000-8000 cP). It can be recovered from solution by precipitation with alcohol (e.g., two volumes of isopropanol) to produce a fibrous precipitate.

0097-6156/81/0150-0111\$05.00/0
© 1981 American Chemical Society

Chemical Composition

PS-60 is an acetylated polysaccharide containing 3- 4.5% O-acetyl groups which are readily removed by heating at ca. pH 10. The resultant deacetylated product has increased potential gel strength after heating. A deacetylation step is usually incorporated into any recovery process. Native PS-60 also contains a considerable amount of insoluble debris which can be removed by centrifugation or filtration. A typical purification scheme is shown in Figure 2. There are three basic forms of PS-60 which differ with respect to composition and properties and have different potential applications.

The compositions of the different forms of PS-60 are shown in Figure 3. Approximately 50% of native PS-60 is a carbohydrate fraction comprised of neutral sugars and a uronic acid. The neutral sugars were identified by paper chromatography and quantitated as the aldonitrile acetate derivatives after acid hydrolysis⁽³⁾: rhamnose and glucose were shown to be present in a molar ratio of 3:2. The uronic acid content was determined by decarboxylation⁽⁴⁾ and the carbazole procedure⁽⁵⁾ and identified as principally glucuronic acid by paper electrophoresis in an acidic buffer system⁽⁶⁾. One other minor uronic acid containing spot was detected but it is presumed that this was a uronic acid containing oligosaccharide, representing incomplete hydrolysis. As stated previously, the polysaccharide also contains 3- 4.5% alkali labile O-acetyl groups as determined by the procedure of Hestrin⁽⁷⁾.

With the exception of O-acetyl groups, the deacetylated polysaccharide has a similar composition. The removal of a large amount of insoluble debris is reflected in the composition of the purified polysaccharide fraction. The insoluble debris, which contains the bacterial cells, has not been completely characterized. The debris contains a large proportion of protein, but no carbohydrates.

Glucose	3.0%
K ₂ HPO ₄	0.05%
MgSO ₄ ·7H ₂ O	0.01%
NH ₄ NO ₃	0.09%
Promosooy	0.05%
Salt mixture*	1 ml/l medium
pH control with KOH	

* Salt mixture solution

ppm in Medium
0.05 B ³⁺
0.5 Mn ²⁺
1.5 Fe ²⁺
0.01 Cu ²⁺
0.02 Zn ²⁺
0.01 Co ²⁺
0.01 Mo ²⁺
1.80

Figure 1. PS-60: typical fermentation medium (for potassium form)

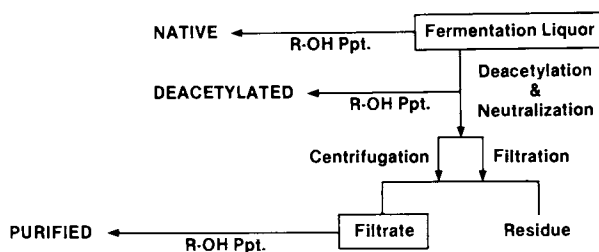


Figure 2. PS-60: isolation and purification scheme

	Native	Deacetylated	Deacetylated and Purified
Uronic Acid (%)	11	13	22
Acetyl (%)	3.0	0	0
Neutral Sugars (% molar ratio)			
Glucose	(40)	(40)	(40)
Rhamnose	(60)	(60)	(60)
Protein	10	17	2
Ash	7.0	8.0	9.5

Figure 3. Chemical composition of PS-60

While the complete primary structure of the PS-60 polysaccharide has not been determined the glycosidic linkages have been determined by methylation⁽⁸⁾ of the purified polysaccharide followed by hydrolysis and quantitation of the O-methyl sugars as the alditol acetate derivatives⁽⁹⁾. The derivatives were separated and identified by gas liquid chromatography mass spectrometry using a Hewlett-Packard Model 5992 GC/MS fitted with 1.5 ft. glass columns containing 3% OV-225 at 170°C. The derivatives of 2, 3 di-o-methylrhamnose and 2, 3, 6-tri-o-methylglucose were identified by comparing the GC/MS spectra and relative retention times with those of known O-methyl sugar standards and with published data⁽¹⁰⁾.

PS-60 is thus most likely a linear polymer formed from glucuronic acid, glucose and rhamnose. Glucose and rhamnose residues are linked 1,4 and the negative specific rotation $[\alpha_{589}] = -45^\circ$ indicates that the majority of the glucose units are β -linked.

Native PS-60

The native form of PS-60 is readily soluble in water and is characterized by high viscosity at low concentration. Typical viscosities are 40-80 cP at 0.1% concentration and 1000-2000 cP at 0.5% when measured on a Brookfield LVF viscometer, 60 rpm, at 25° (Figure 4). The gum also has a high rheological yield point; a 1% gum solution has a working yield value of 60 dynes/cm², defined by the shear stress at a shear rate of 0.01 sec. as measured using a Wells-Brookfield cone and plate viscometer in the spring relaxation mode⁽¹¹⁾.

The effect of pH on solution viscosity of native PS-60 is depicted in Figure 5. Changes of pH in the range of 3-11 do not substantially change the viscosity of 0.5% solutions of native PS-60.

The effect of temperature on the solution viscosity of native PS-60 is both characteristic and unusual. As shown (Figure 6) the viscosity of a 0.5% native PS-60 solution is stable in the range of 20-70°C and abruptly undergoes a reversible decrease when the temperature is increased above 70°C.

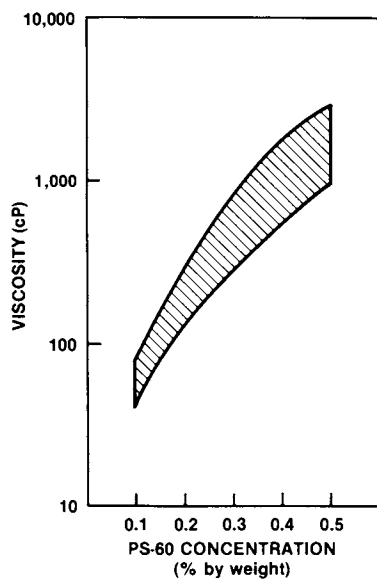


Figure 4. Native PS-60: effect of gum concentration on solution viscosity

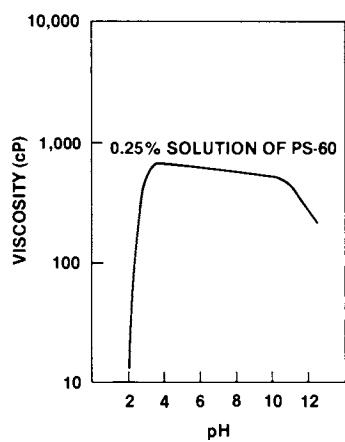


Figure 5. Native PS-60: effect of pH on solution viscosity

Although utility is anticipated for native PS-60 as a high viscosity biogum, perhaps the most significant property is the formation of gels after a sequence of heating and cooling. Both the native and deacetylated forms of PS-60 form thermoreversible gels after heating and cooling but the respective gels are significantly different in gel texture. Following heating in the presence of various cations, native PS-60 forms elastic or soft gels upon cooling, whereas the deacetylated PS-60 produced firm, non-elastic or brittle gels. (Figure 7).

Figure 8 summarizes the properties of the gels produced by heating 1% gum solutions to 90°C for 10 minutes in the presence of cations, followed by cooling. The native PS-60 forms weak elastic gels which have the same melting and setting temperatures with no hysteresis.

Deacetylated PS-60

Deacetylated PS-60 forms firm brittle gels similar to agar and carrageenan gels which also undergo thermoreversible gel-sol transition. However, these gels show considerable differences in setting and melting temperatures and in this respect PS-60 appears to be more similar to agar than to Kappa carrageenan, primarily because of the large hysteresis between setting and melting temperatures (Figure 8).

The strength of gels produced from deacetylated PS-60 solutions is a function of the gum concentration, the salt concentration and also the cations present. Figure 9 outlines the gel strength as a function of deacetylated PS-60 concentration and salt concentration as analyzed by a computerized response surface methodology⁽¹²⁾. Gels were prepared by heating deacetylated PS-60 in salt solutions at 90°C for 10 minutes and after cooling for 2 hours, gel strengths were measured using an Instron Model 1122 in conjunction with the large diameter Marine Colloids gel tester plunger. (Instron Corporation, 2500 Washington St., Canton, Mass. 02021).

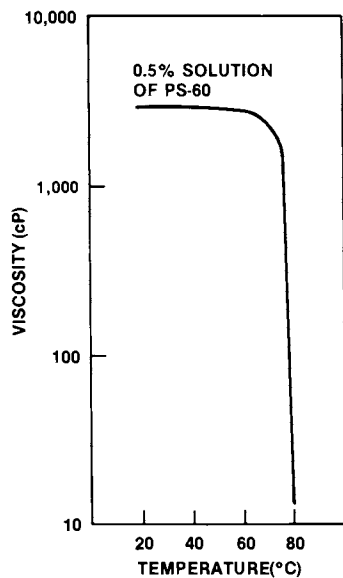


Figure 6. Native PS-60: effect of temperature on solution viscosity

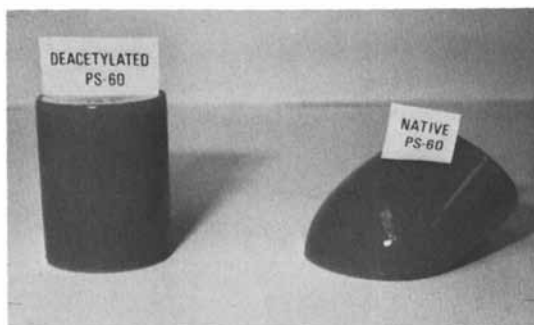


Figure 7. Comparison of native and deacetylated PS-60 gels. Native PS-60 forms an elastic or soft gel whereas deacetylated PS-60 forms a firm, nonelastic gel

Type	Gel Nature	Melts	Sets	Hysteresis	Minimum Gelling Conc.
Native PS-60	Very Elastic	65-70°C	65-70°C	None	—
Deacetylated PS-60					
K ⁺ Gel	Brittle	90°C	31-46°C	45-60°C	—
Ca ²⁺ Gel	Brittle	90°C	45-50°C	45-50°C	0.05%
Kappa Carrageenan	Brittle	40-95°C	25-75°C	15-20°C	0.3%
Agar*	Brittle	60-97°C	32-39°C	60°C	0.04%

* Bacteriological grade specs: gelling temperature range 33-39°C, melting temperature 70°C minimum.
(Whistler's Industrial Gums)

Figure 8. Comparison of the gel properties of PS-60 and other gums

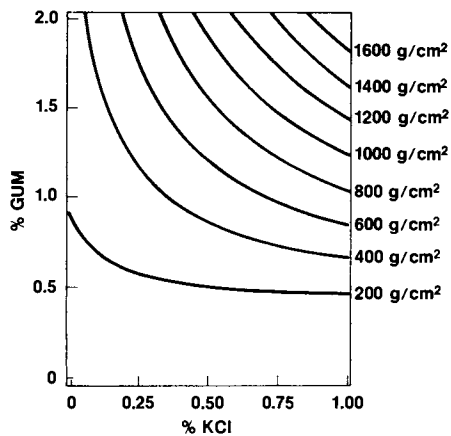


Figure 9. The effect of salt and gum concentration on the gel strength of deacetylated PS-60

A minimum of 0.5% potassium chloride is required for a strength of approximately 500 g/cm² at 1% gum concentration and under these conditions deacetylated PS-60 gels have 1.5 X gel strength of Kappa - carrageenan (GELCARIN HWG).

The gel strength as a function of cation type and concentration is shown in Figure 10. The gum is highly sensitive to the type of cation; a much lower concentration of the divalent cations magnesium and calcium is required to obtain maximum gel strength than for the monovalent cations sodium and potassium (e.g., 0.05% $MgCl_2 \cdot 6H_2O$ results in a similar gel strength to 0.5% KCl for a 1% gum gel). Other gelling cations include barium, strontium, rubidium and cesium. Practically any soluble salt can be used for gelation except borates which react readily with rhamnose and destroy gelling properties.

As a result of the high potential gel strength at low gum concentrations, it is anticipated that deacetylated PS-60 will find utility in many industrial applications where carrageenan is presently being used.

Clarified Deacetylated PS-60

PS-60 fermentation beer which has been deacetylated, can be readily clarified by sedimentation, centrifugation or filtration and this is facilitated at elevated temperatures due to the large decrease in apparent viscosity at temperatures greater than 70 °C. The gelling properties of the clarified, deacetylated product are similar to those of the unclarified product. Again firm and brittle thermoreversible gels are formed of excellent clarity with transmittance values approaching 100% at 0.5-1% gum concentrations. As with the unclarified product, the gel strength and setting temperature can be modified by the choice and concentration of monovalent and divalent cations.

The similarities of these properties with those of agar are obvious and Figure 11 summarizes the salient functional properties of both clarified PS-60 and agar gels.

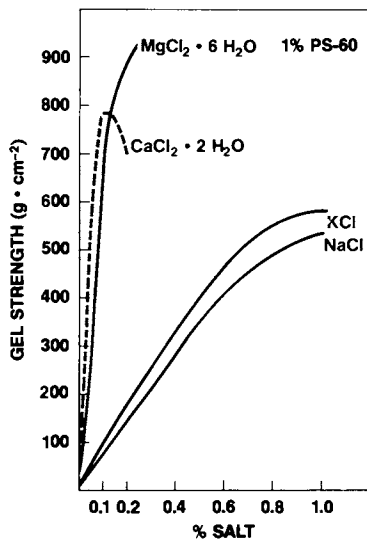


Figure 10. The effect of cation type and concentration on the gel strength of deacetylated PS-60

Figure 11. Similar properties of clarified deacetylated PS-60 and Agar gels

- Thermoreversible
- Heat stability
- Enzyme resistance
- No toxicity
- No chemical reactivity
- Optical clarity
- Gel structure

PS-60 and agar form thermoreversible gels with similar melting and setting temperatures. The most convenient method of preparing gels is by heating solutions to 90°-95°C or, in the case of media preparation, by autoclaving. PS-60 has excellent heat stability equivalent or superior to that of agar and gels can survive six cycles of autoclaving, (15 psi for 15 minutes) and cooling with a 50% reduction in gel strength.

PS-60 gels have been shown to be resistant to commercially available protease, carbohydrase and lipase enzymes. The gels have no toxicity and are chemically inert with respect to inhibition of growth of various organisms or with respect to colonial morphology. Laboratory prepared samples of PS-60 have optical clarity superior to that of agar in a variety of media. Furthermore, PS-60 may, in certain cases, be advantageous in the growth of various species of organisms. The potential of PS-60 as an agar replacer has been more completely covered in a recent paper.⁽¹³⁾

The most significant differences between PS-60 and agar are that PS-60 gels set almost instantly and the setting temperature is variable. Depending upon the media, setting temperatures of 40-50°C are encountered at normal use levels. As described previously, divalent cations are more efficient in obtaining high strength gels. In applications where PS-60 gels are used as an agar replacer, magnesium is generally used as the gelling cation due to its better melting characteristics. The gel strength is determined by both the concentration of PS-60 and the salt concentration. Most PS-60 media (which contain extra salts) can be prepared (by autoclaving) using approximately 0.5% PS-60 as the gelling agent, plus approximately 0.1% MgCl₂ to give equivalent gel strengths to that of agar at 1.5%.

Figure 12 outlines the effect of salt concentration, in this case magnesium, on gel strength and gel point of a typical purified deacetylated PS-60 sample. Solutions were prepared at 95°C in deionized water containing various concentrations of magnesium chloride using 0.5% gum. The viscosity of the samples was monitored upon cooling; an apparent increase was

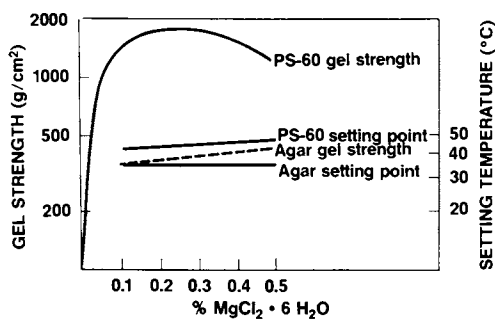


Figure 12. The gel strength and setting point of clarified deacetylated PS-60 (0.5% gum) and agar (1.5% gum) as a function of salt concentration ($\text{MgCl}_2 \cdot 6\text{H}_2\text{O}$)

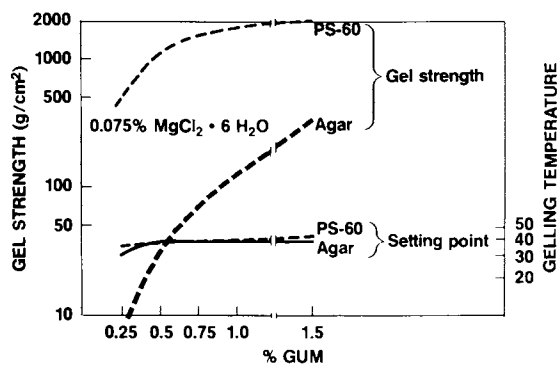


Figure 13. The gel strength and setting point of clarified deacetylated PS-60 and agar as a function of gum concentration in the presence of 0.075% $\text{MgCl}_2 \cdot 6\text{H}_2\text{O}$

considered the gel point. The gel strengths were determined after a minimum of 4 hours at ambient temperature. At constant gum concentration (0.5%) the gel strength maximized at 0.2% added $\text{MgCl}_2 \cdot 6\text{H}_2\text{O}$ with a gel point of approximately 43°C . Further, addition of salt results in decreased gel strength as seen for added calcium while the gel point rises slightly to 46°C . If the gum concentration is increased at a constant magnesium concentration (0.075% $\text{MgCl}_2 \cdot 6\text{H}_2\text{O}$) both gel strength and gel point increase (Figure 13). These results indicate that both the gel strength and gel setting point are strongly influenced by gum concentration and the salt concentration. PS-60 has equivalent or superior functionality to agar even at a lower use level.

In summary, a new strain of Pseudomonas has been isolated which produces an extracellular heteropolysaccharide PS-60, in an aerobic submerged culture. PS-60 has high viscosity, a high yield value and after heating following cooling forms weak, elastic gels. After deacetylation by alkaline treatment, PS-60 forms firm, brittle gels similar to those of Kappa carrageenan.

The deacetylated PS-60 fermentation beer is also readily clarified to give a product which forms optically clear gels with thermoreversibility, heat stability, and enzyme resistance properties characteristic of agar. The gel strength, melting point and setting point of these gels can be controlled by the concentration and type of cation employed. Further investigation is required on both the structure and conformation of this polysaccharide in solution in order to determine the origin of these gelation phenomena. Such studies will lead to a better understanding of the mechanism of gel formation and increase our knowledge of the potential industrial applications of this novel polysaccharide.

Literature Cited

1. Kaneko, T. and Kang, K. S. 79th Annual Meeting of American Society of Microbiology (1979) Los Angeles, CA.
2. Kang, K. S., Veeder, G. T., and Cottrell, I. W. 79th Annual Meeting of American Society of Microbiology (1979) Los Angeles, CA.
3. Baird, J. K., Holroyde, M. J., and Ellwood, D. C. Carbohyd. Res. (1973), 27 464-467.
4. Browning, B. L. Methods of Wood Chemistry (1967), 2 632-637.
5. Bitter, T. and Muir, H. M. Anal. Biochem (1962), 4 330-334.
6. Kosakai, M. and Yosizawa, Z. Anal. Biochem. (1975), 69 415-19.
7. Hestrin, S. J. Biol. Chem. (1949), 180 249-261.
8. Hakomori, S. J. Biochem. (Tokyo) (1964), 55 205-208.
9. Bjorndal, H., Hellerquist, C. G., Lindberg, B., and Svensson, S. Angew. Chem. Int. Edn. (1970), 9 610-619.
10. Jansson, P. E., Lennart, K., Kiedgren, H., Lindberg, B., and Lonngren. J. Chem. Commun (1976), No. 8 Univ. of Stockholm s-10405, Stockholm (Sweden).
11. Jeanes A. and Pittsley, J. E. J. Appl. Poly Sci. (1973), 17 1621-24.
12. "Strategy of Experimentation" (1973) published by the Applied Technology Division E. I. du Pont de Nemours and Co., Wilmington, Delaware, 19898.
13. Veeder, G. T., Kang, K. S. and Mirrasoul, P. J. 79th Annual Meeting of American Society of Microbiology (1979), Los Angeles, CA.

RECEIVED December 24, 1980.

Conformation, Dynamics, and Gelation Mechanism of Gel-State (1→3)-β-D-Glucans Revealed by C-13 NMR

HAZIME SAITŌ

Biophysics Division, National Cancer Center Research Institute,
Tsukiji 5-chome, Chuo-ku, Tokyo, Japan 104

(1→3)-β-D-glucans of higher molecular weight, in aqueous media, have a unique property to be able to form either elastic or soft gels (1-9), depending on their primary structures, linear or branched D-glucans. Undoubtedly, this property mainly arises from conformational and aggregation behavior of the polysaccharide chains. The energetically preferred conformation of (1→3)-β-D-glucans, determined by calculation of the energy contour diagrams, has been proposed to be wide and extended helix or more likely a double- or triple-stranded helix (10-13). The recent X-ray diffraction studies showed that conformation of curdlan, a linear (1→3)-β-D-glucan, is 7/1 single helix or 6/1 triple-helix depending on the extent of thermal treatment and hydration (14-16). In addition, (1→3)-β-D-glucans, from *Armillaria mella* and yeast (17, 18) and from *Lentinus edodes* (19), were revealed to take 6/1 triple helix, very similar to (1→3)-β-D-xylan (20). Consequently, the object of this article is concerned with whether such a helix conformation is retained in solution and gel states or not.

We emphasize here that ¹³C NMR spectroscopy is very useful for determining the conformation of polymer chains in the gel state, although very little work has been done along with this line (5-9, 21, 22). In particular, ¹³C chemical shifts of C-1 and C-3 carbons were found to be very sensitive to predict the portion of single helix conformation, with reference to those obtained in the solid state by cross-polarization magic-angle spinning (CPMAS) ¹³C NMR spectroscopy (23).

¹³C NMR CHARACTERISTICS OF GELS: CROSS-LINKED POLYMERS (24)

Before proceeding with the details of polysaccharide gels, it is worthwhile to examine the ¹³C NMR characteristics of gel samples of chemically cross-linked synthetic polymers in which the extent of the cross-links can be varied more easily.

In bulk materials including gels, all of the carbons in polymers do not always contribute to high resolution ¹³C resonances, since a sizable amount of loss of the peak-areas is found to occur

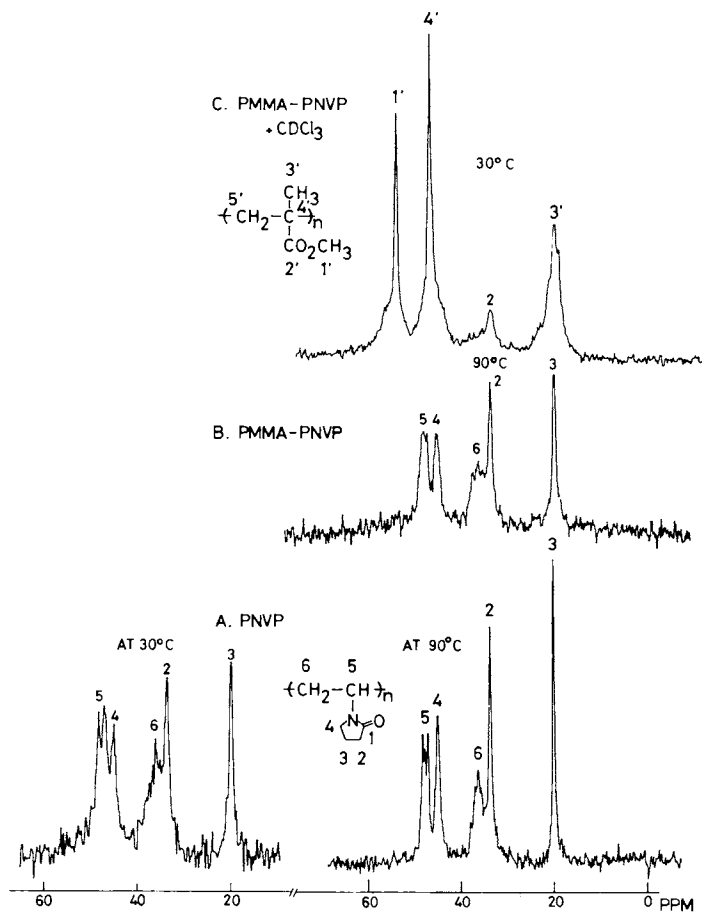
0097-6156/81/0150-0125\$05.75/0
© 1981 American Chemical Society

due to the presence of immobilized segments such as cross-links or crystalline portions (25-28). As an illustrative example, ^{13}C NMR spectra of chemically cross-linked gels of poly(N-vinylpyrrolidone)(PVP) are shown in Figure 1. Compared with the peak-intensities of PVP (without cross-linking) solution, it is estimated that only about 55 and 35% of the polymer chain contribute to the observed ^{13}C spectra of the gels, containing 0.1 and 1 mole % cross-linking, respectively. It is noteworthy that the ^{13}C signals of the gels are broadened together with increasing proportion of the cross-linking. The cause of the line-broadening is obviously interpreted in terms of the restriction of chain mobility due to the presence of cross-links and entanglement of polymer chains especially in the vicinity of cross-links, since the line-broadening is remarkable in samples of higher cross-linking (see Figure 1D). In spite of these obvious changes of line-widths, however, no chemical shift displacement was induced by changing the samples from gels to aqueous solution, because the conformation of the polymer chain is essentially disordered. In gels of cross-linked blend-type copolymer consisting of hydrophilic N-vinylpyrrolidone (NVP) and hydrophobic methyl methacrylate (MMA), swollen by water, no ^{13}C signals can be observed for the portion of hydrophobic MMA (Figure 2). Therefore, it is clear that the hydrophobic MMA portion is unable to be swollen and served as an additional cross-links. However, the ^{13}C NMR of the MMA portion is made visible by addition of chloroform to this system (Figure 2C) or by swelling with dimethyl sulfoxide. Therefore, acquisition of motional freedom by swelling with a good diluent is essential for the observation of high resolution ^{13}C NMR spectra in gel samples.

GEL OF A LINEAR (1 \rightarrow 3)- β -D-GLUCAN (CURDLAN)

Curdlan is an exocellular (1 \rightarrow 3)- β -D-glucan (DPn=540) containing no other linkages, isolated from Alcaligenes faecalis var. myxogenes by Harada et al. (1,2-4).

A. Gelation Behavior Curdlan powder was not soluble in water at neutral pH but formed a firm resilient gel when the aqueous suspension was heated at a temperature above 50°C (29). As shown in Figure 3, ^{13}C NMR spectra of the aqueous suspension (80 mg/ml) were recorded at various temperatures. The assignment of peaks was done in view of the data taken at higher alkaline condition and from water-soluble D-glucan (30). A noticeable feature of the ^{13}C NMR spectra is that the peak-intensities and the ^{13}C chemical shifts vary with temperature. The substantial loss of the peak-areas is obviously due to the presence of the cross-links in the gel state or insufficient swelling at lower temperature. To visualize this, the relative peak-intensities were plotted against temperature, with reference to those obtained in the presence of 0.3M NaOH at which full peak-areas are observed (as



Macromolecules

Figure 2. 15.03-MHz C-13 NMR spectra of PVP gel and blend-type copolymer of MMA and NVP (24)

will be discussed later)(Figure 4A). Interestingly, the abrupt change of the peak-intensities occurred at a temperature between 46° and 50°C, corresponding to the onset of gelation. Further heating of the sample resulted in the diminution of the peak-intensities, contrary to the cases of other thermally gelable polysaccharides such as ι -carageenan gel (31). The reduction of the peak-intensities is in parallel with the reduction of the transmittance of light which might be caused by aggregation of the polymer chain. It appears that the gelation behavior as viewed from the change of the peak-intensities (Figure 4A) is more drastic than that of the viscosity and transmittance previously reported (29,32). This discrepancy may arise from the difference in quantity of the D-glucan in the aqueous suspension.

Obviously, the C-3 (and C-1) ^{13}C chemical shift is displaced upfield abruptly at the temperature corresponding to gelation, and further displaced gradually with rising temperature. As will be discussed in the next section, the ^{13}C chemical shifts of C-1 and C-3 are very sensitive to the conformational transition of β -D-(1-3)-linked D-glucose chain, from helix to random coil, as viewed from the upfield displacement of the ^{13}C signals (6,7). Therefore, it is likely that swelling of curdlan molecules at 50°C is initiated by slight conformational change, possibly by a thermal fluctuation around the preferred dihedral angle.

B. Conformation Figure 5 demonstrates the comparison of the ^{13}C NMR signals of the resilient gel with those of low molecular weight fraction soluble in water (6). At ambient temperature (28°C), the peak-areas of the ^{13}C NMR signals in the gel state account for only 20-30% and 60% for C-1 -C-5 and C-6, respectively, with reference to those at 0.22M NaOH solution. These values are approximately half the intensities observed at 50°C and very close to those at 77°C (see Figure 4A). The remaining ^{13}C signals, invisible in the conventional high resolution spectrometer, should be ascribed to the portion of the cross-links (or junction-zones) of the gel network and the residues close to the cross-links.

The ^{13}C chemical shifts of C-1 and C-3 carbons of the resilient gel are clearly shifted downfield by 2.8 and 3.2 ppm, respectively, compared with those of a lower molecular weight fraction (DPn=13). Such substantial downfield displacements are limited to the carbons in the glucosidic linkages of (1-3)- β -D-glucans. This observation is very similar to the downfield displacements of C-1 and C-4 carbons (in the glucosidic linkages) of cyclodextrins (1.6-2.0 and 2.9 ppm, respectively) compared with those of the linear (1-4)- α -D-glucans such as amylose (30). In the formers, it appears that no overall internal rotation around the C-1-O and C-4-O linkages is allowed because of its cyclic structure. In a similar manner, the C-1 and C-3 signals, which exhibit the conformation-dependent downfield displacements observed in the gel state, can be ascribed to certain ordered conformations in which only a slight oscillation around the favored dihedral angle around the

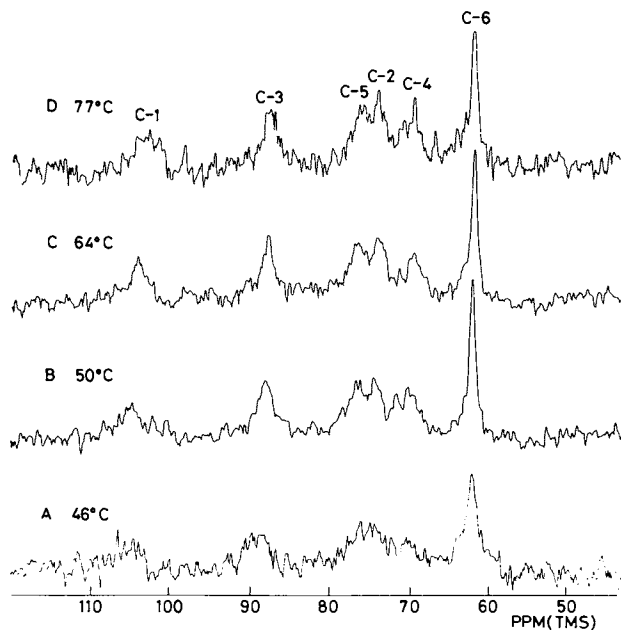


Figure 3. 25.03 MHz C-13 NMR spectra of curdlan in aqueous suspension or gel (80 mg/mL) recorded at various temperatures. Number of transients: 19200 (A), 9469 (B), 11260 (C), and 24134 (D).

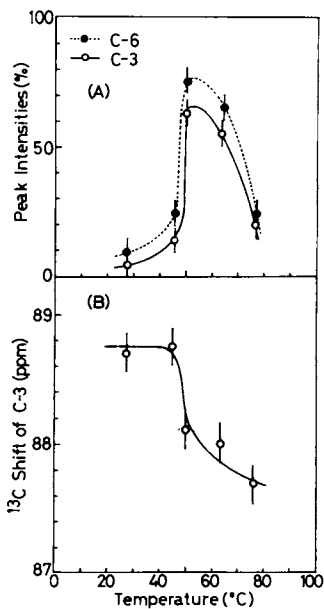


Figure 4. (A) A plot of the relative peak intensities of C-6 and C-3 signals, with reference to those obtained in the presence of 0.3M NaOH, against temperature; (B) a plot of the C-3 C-13 chemical shift against temperature.

C-1-0 and C-3-0 linkages is allowed (6). We attempted here to compare the ^{13}C chemical shifts of the gel with those of solid state curdlan, the conformation of which is mainly single helix at ambient temperature and triple-helix at higher temperature above 120° , as studied by X-ray diffraction (14,15). The newly emerging technique, cross-polarization magic angle spinning (CPMAS) ^{13}C NMR method (23) enables one to eliminate an enormous amount of line-broadening due to static dipolar field from neighboring proton nuclei and also chemical shift anisotropy in the solid state. Figure 6 shows the CPMAS ^{13}C NMR spectrum of curdlan powder, taken by courtesy of Professor Gary Maciel and Dr. Victor Bartuska of Colorado State University. Interestingly, the most mobile C-6 carbon gives rise to the least intense signal in the solid state because of insufficient CP transfer between proton and carbon. It was again found that the ^{13}C chemical shifts of C-1 and C-3 are displaced downfield appreciably in the solid state compared with the peak-positions of liquid state D-glucan, as shown in Table I.

Table I. Comparison of ^{13}C chemical shifts of curdlan observed in aqueous solution, elastic gel and solid state^a

	Aqueous solution (DPn=13, pH=7)	Elastic gel	Solid state
C-1	103.7	106.5 (2.8) ^b	105.1 (1.4) ^b
C-2	74.5	74.2 (-0.3)	74.8 (0.3)
C-3	85.3	88.7 (3.2)	90.1 (4.6)
C-4	69.3	70.2 (0.9)	70.6 (1.3)
C-5	76.8	76.8 (0)	76.6 (-0.2)
C-6	61.9	61.8 (-0.1)	62.1 (0.2)

^a ppm from TMS. ^b Displacements of ^{13}C chemical shifts with reference to those obtained in aqueous solution (DPn=13).

Therefore, the ^{13}C signals observed in the gel state are unequivocally ascribed to the portion of single helix, although there appears a slight difference of the chemical shifts between the gel and solid state around 1 ppm.

C. Conformational Transition Figure 7 shows that the ^{13}C NMR spectra of curdlan in the presence of dilute alkali up to 0.19M are essentially the same as those of the elastic gel (6). Therefore, molecular organization of the curdlan sample in dilute alkaline state is essentially the same as that of the elastic gel. When NaOH is increased to 0.22M, the linewidths of the ^{13}C NMR signals are abruptly narrowed, resulting in the conformational transition to the random coil. The transition behavior is consistent with that of optical rotatory dispersion, viscosity and flow birefringence (33). (In particular, a viscosity minimum was achieved at 0.2M NaOH, in contrast to that of amylose[33,33a]). It is expected that full peak-areas are revealed at 0.22M NaOH, because no cross-links can exist in curdlan of random-coil conformation.

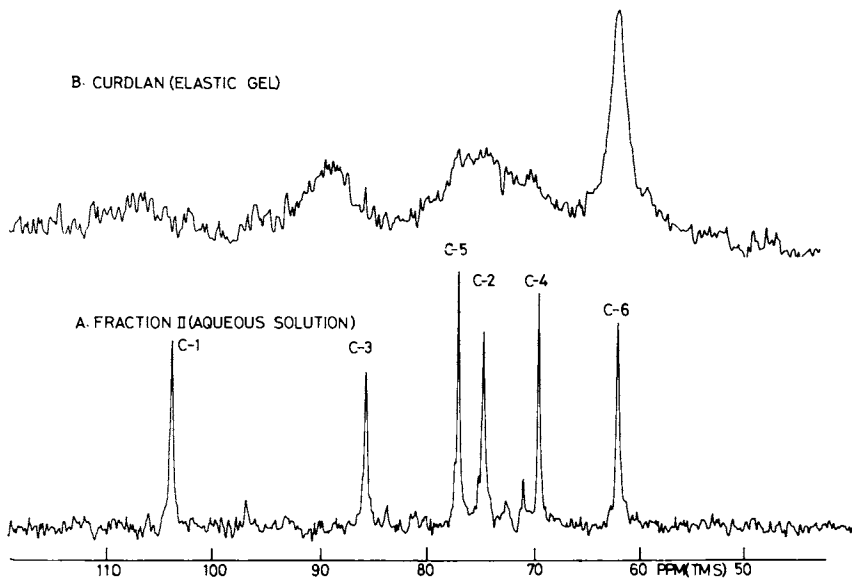


Figure 5. 25.03-MHz $C-13$ NMR spectra of low-molecular-weight (1 \rightarrow 3)-D-glucan soluble in water (A) and of curdlan in the elastic gel state (B) (6)

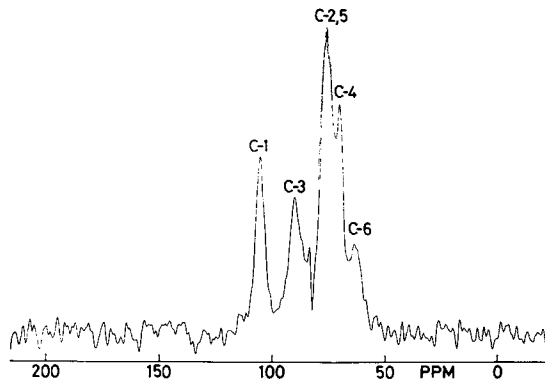
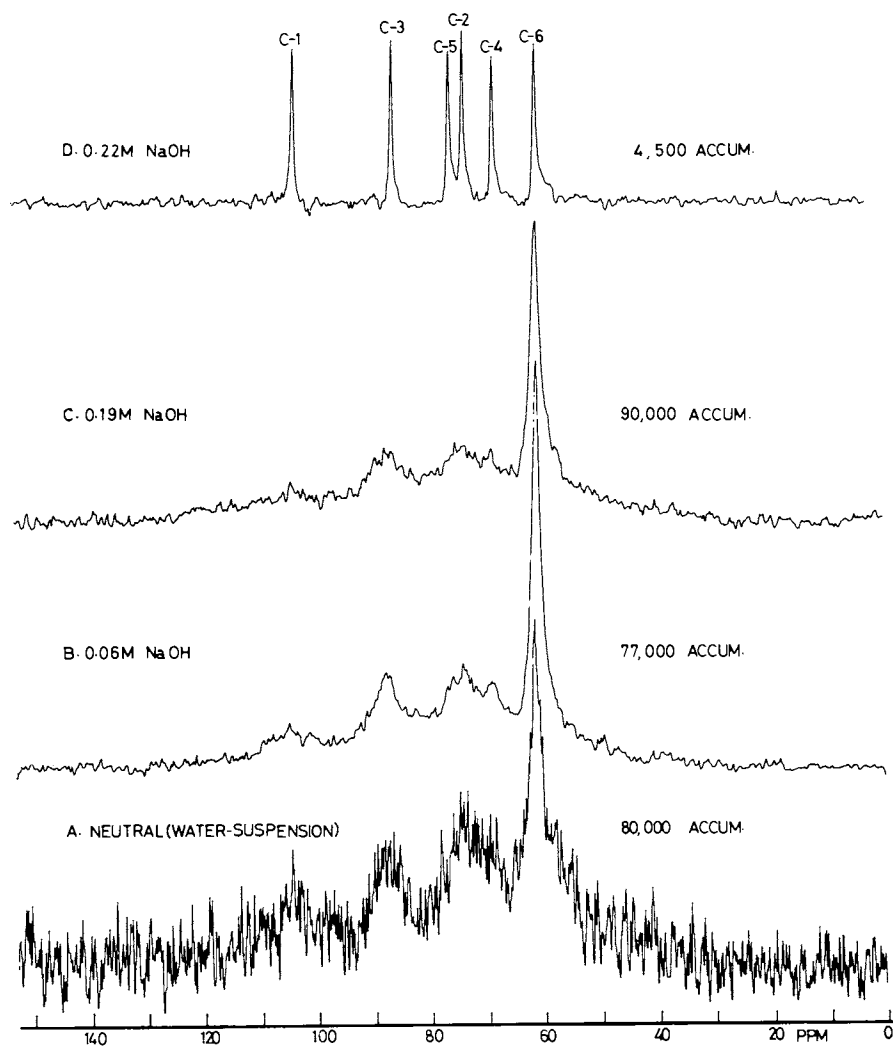
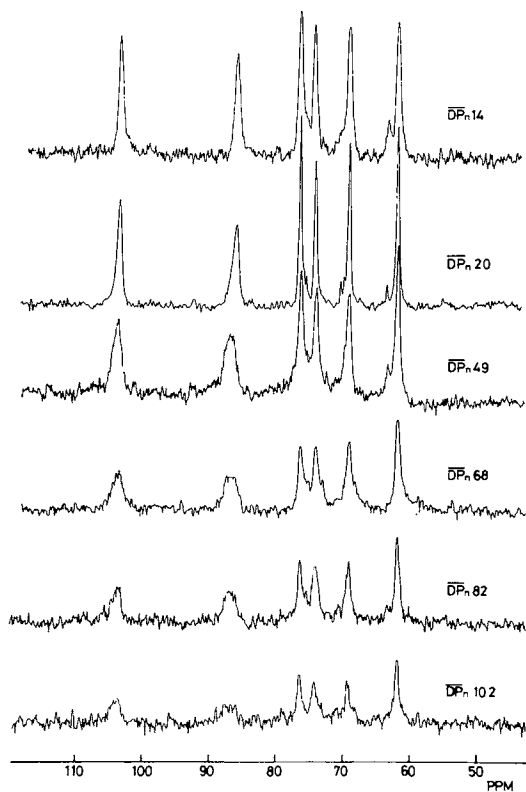


Figure 6. 15.03-MHz CPMAS $C-13$ NMR spectrum of solid-state curdlan, recorded by a modified JEOL FX-60Q spectrometer. Contact time—1 ms, 1000 transients, and acquisition time—64 ms.



Biochemistry

Figure 7. 25.03-MHz C-13 NMR spectra of curdlan of an aqueous suspension and in the presence of NaOH: (A) aqueous suspension; (B) in 0.06M NaOH; (C) in 0.19M NaOH; and (D) in 0.22M NaOH (6).



Macromolecules

Figure 8. 25.03-MHz C-13 NMR spectra of (1 \rightarrow 3)- β -D-glucans with DPn 14-540 in 0.06M NaOH. Accumulation times: 20000 for DPn = 14-82, 27198 for DPn = 102, 45900 for DPn = 131, 10941 for DPn = 380, and 77000 for DPn = 540 (7).

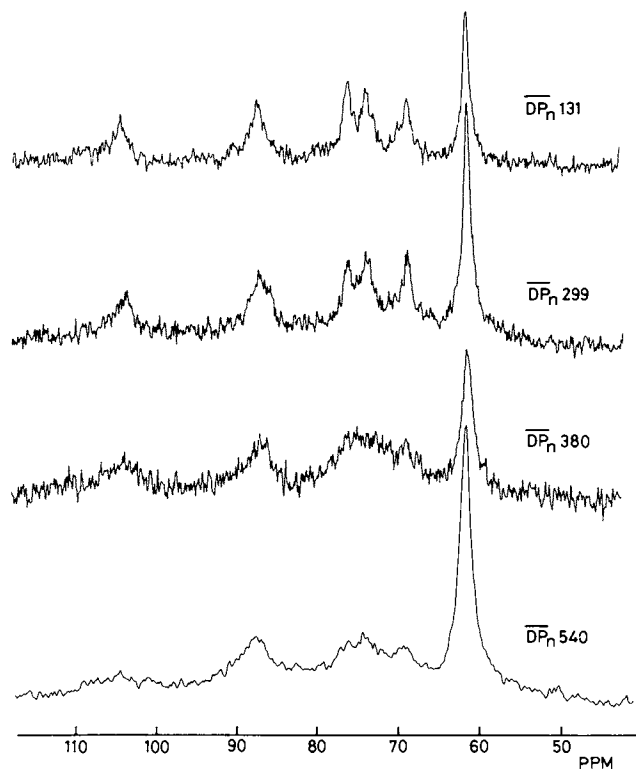


Figure 8. *Continued*

Contrary to the cases of agarose or κ -carrageenan gels (31,34), heating the curdlan sample did not induce a conformational transition at the temperature of gelation, although some distortion of the conformation was noted as viewed from the upfield shifts of ^{13}C peaks. In fact, a thermally induced helix-coil transition may occur at the temperature 140-160°C, as Kuge et al. showed that the gel sharply melts in this temperature range (35).

D. Molecular-Weight Dependence of Conformation (7) Obviously, (1 \rightarrow 3)- β -D-glucans of low molecular weight such as laminaran and some low molecular-weight fractions of the acid hydrolyzate of curdlan adopt a disordered conformation in solution (37). Thus, it is important to know at what chain-length does (1 \rightarrow 3)- β -D-glucan undergo conformational transition from random-coil to helical form, in neutral aqueous media, in order to understand the solution properties of this polysaccharide. For this purpose, the glucans with various chain-lengths were prepared from a hydrolyzate of curdlan by the procedure of gel-filtration. ^{13}C NMR spectra were measured under dilute alkaline conditions, because the D-glucans (DPn \geq 20) are insoluble in water at neutral pH. This approach may be justified, because it is already known that the conformation of (1 \rightarrow 3)- β -D-glucan is not altered in this alkaline condition, as described above.

Figure 8 shows ^{13}C NMR spectra of (1 \rightarrow 3)- β -D-glucans with various DPn's in the presence of 0.06M NaOH. It is found that the C-1 and C-3 signals of the glucans with DPn \geq 49 are appreciably displaced downfield with respect to those of DPn=14. On the basis of the argument described above, it is concluded that the glucans with DPn \geq 49 adopt the helix conformation, while those with DPn \leq 20 take a disordered conformation. As shown in a plot of the relative peak-intensities (with respect to those of the glucans with DPn 14) against DPn (Figure 9), the peak-intensities decrease with DPn. Such an apparent loss of the peak-areas is caused by the presence of a portion to which water can not penetrate to allow swelling (cross-links). It follows from Figure 9 that the longer the chain-length of the primary molecules the extent of forming such cross-links is higher. Interestingly, the relative peak-areas are found to level off at DPn 300, which is corresponding with the fractions capable of forming gels. It should be emphasized that the formation of the cross-links are accompanied simultaneously with the conformational change to the helix form.

E. Molecular Dynamics of Gel Network and Gelation Mechanism To characterize the molecular dynamics of a polymer-chain in the gel state, relaxation parameters such as the spin-lattice relaxation times, nuclear Overhauser enhancements and linewidths were compared among the gel state, solution state of the random-coil form for higher alkaline conditions and lower molecular weight fractions

Table II. Spin-lattice relaxation times (T_1 's), linewidths and nuclear Overhauser enhancements (NOE's) of curdlan in gel state and random-coiled form and of lower molecular fractions (Z)

	DPn=540						Lower molecular weight glucan					
	Elastic gel			In 0.22M NaOH			DPn=49			DPn=131		
	T_1	Line- width ^a	NOE	T_1	Line- width ^b	NOE	T_1	Line- width ^a	NOE	T_1	Line- width ^b	NOE
C-1	86 ^a	172 ^b	1.0	76 ^a	14 ^b	1.5	87 ^a	41 ^b	1.8	57 ^a	47 ^b	1.6
C-2	84		1.4	78	15	1.4	102	23	1.9	69	51	1.4
C-3	76	156	1.2	84	14	1.4	105	49	1.8	64	53	1.8
C-4				80	15	1.5	118	22	1.2	93	53	1.5
C-5	84		1.4	83	14	1.3	129	24	2.0	77	44	1.5
C-6	62	50	1.4	54	17	1.9	87	19	2.0	56	25	2.1

^a in msec. ^b in Hz.

incapable of forming gels (Table II). Irrespective of the greater change of the linewidths between the gel state (about 150 Hz) and sol state (14 Hz), the change of the T_1 's, and NOE's was found to be very little. Generally, the T_2 values tend to be affected by the slow motion of long correlation times, while the T_1 values are mainly determined by the fast motion. Therefore, the T_1 values are not strongly affected by the presence or absence of the cross-links.

The segmental motion of the backbone may be highly heterogeneous because of a possible distribution of segments in different physical environment. Thus, the segmental motions can be described by a distribution of the correlation times. Intrinsically, such molecular motions of helices should be anisotropic tumbling motions. Nevertheless, the use of isotropic tumbling as described by the $\log\text{-}\chi^2$ distribution of the correlation times (38) may be justified for the following reasons. First, there appears no specific difference of the relaxation parameters in the carbons of C-1 and C-3 in spite of the different orientation of the CH vectors with regard to the helical axis. Second, the isotropic tumbling model was successfully employed to reproduce the relaxation parameters of the helical forms of simple polypeptides (39,40).

We used the formula proposed by Schaefer (38) as follows:

$$F^{(p)}(s) = (ps)^{p-1} e^{-ps} / \Gamma(p) \quad (1)$$

$$\text{with } s = \log_b [1 + (b-1) \tau / \bar{\tau}] \quad (2)$$

where $F^{(p)}(s)$ is the probability density function of the correlation time τ and $\Gamma(p)$ is the gamma function. In eq.(1), p is used to describe the width of the distribution of the correlation times. As p becomes larger, the distribution becomes narrower. The logarithmic time scale b is usually taken as 1000. Since the long tail of the $\log\text{-}\chi^2$ function has a feature to overemphasize

the contribution of the longer correlation times (41), we used here the truncated form which truncates the long tail of the correlation time at 1000 ns. The average correlation time of gel state curdlan is thus obtained as 40 ns ($p=8$), while the correlation time of the random-coil state is 4.3-22 ns. Such a change of the correlation times from the gel state to sol state seems to be surprisingly small.

As pointed out in Section D, the cross-links are formed even for lower molecular oligomers incapable of forming gel. The average correlation times, calculated for those oligomers, are plotted against the DPn ($p=8$), as shown in Figure 10, and found to change in proportion to the DPn. As described above, there appears no drastic change in the correlation times between the gel with infinite network and the oligomers with finite network, in contrast to the change of the peak-intensities. This result may be quite reasonable since the molecular motions of the chain-segment other than the cross-links should be correlated with the density of the cross-links, which is a function of the DPn in view of the classical theory of gelation (42), mainly due to the entanglement of the chains in the presence of the cross-links.

In view of the gelation behavior of curdlan described in Section A, it appears that gelation may proceed with formation of two kinds of cross-links. In the first step (50°C), the polymer networks are swollen because of thermal oscillation of the helical chain by which water molecules can penetrate into the interstices held by the multiple-stranded helices (cross-links). The amount of such regions is not dominant for the sample without heat-treatment at higher temperature, as viewed from the X-ray diffraction study (15,16), but may be enough for gelation. Further heating of the gel sample was accompanied with the development of turbidity together with shrinkage of the gel. This finding implies that water molecules which had penetrated into the interstices are expelled again as a result of aggregation of the helical chains. Consequently, gel-strength was increased with temperature from 60° to 100°C (2). Harada et al. reported that microfibrils of 300-400 Å wide and 1000-1500 Å long are seen by electron microscope for the sample heated at a temperature 120°C for 4h(43,44). These microfibrils are clearly caused by the aggregation of the helical region. These regions serve as additional cross-links for the gel.

GELS OF BRANCHED (1→3)-β-D-GLUCANS (5,8,9)

A. Characterization of Branched Glucans Many branched (1→3)-β-D-glucans were isolated from cell wall of fungi and formed rather soft gels in aqueous media. Figure 11 shows ¹³C NMR spectra of lentinan (45,46) from *Lentinus edodes*, A₃ (5,47) from *Pleurotus ostreatus*, and schizophyllan (48) from *Schizophyllum commune*, taken in DMSO solution. Those are known to have branches for every 3-5 glucopyranosyl residues at 0-6. The side-chains are

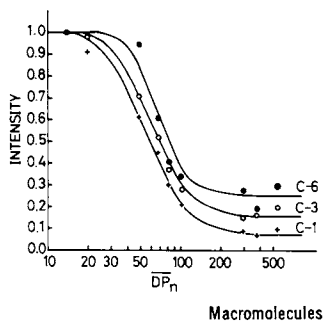


Figure 9. A plot of the peak intensities of C-1, C-3, and C-6 with respect to those of $DP_n = 14$ by taking into account the differences in NOE values vs. DP_n of $(1 \rightarrow 3)\text{-}\beta\text{-D-glucans}$ (in the presence of $0.06M$ NaOH) (7)

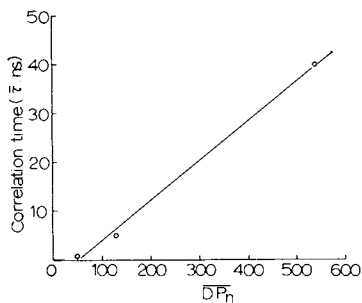
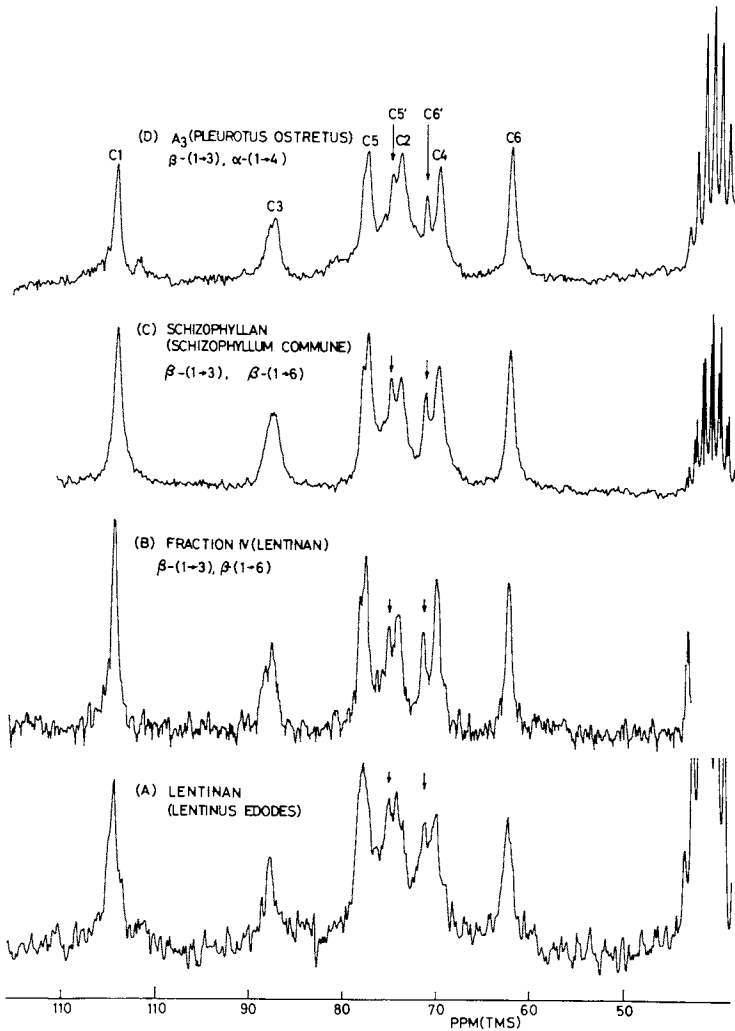


Figure 10. A plot of the average correlation time vs. DP_n of $(1 \rightarrow 3)\text{-}\beta\text{-D-glucans}$ (7)



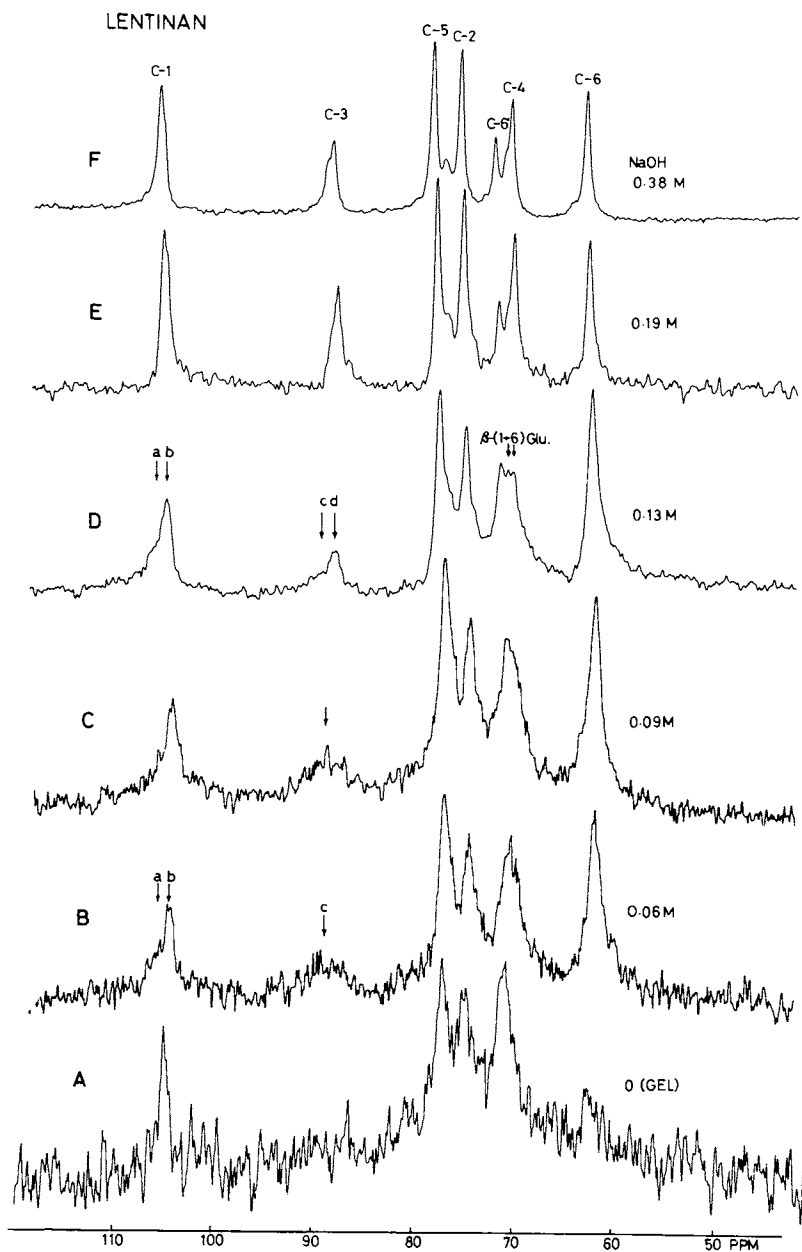
Carbohydrate Research

Figure 11. 25.03-MHz C-13 NMR spectra of various types of branched (1 → 3)-β-D-glucans in dimethyl sulfoxide (8)

β -D-(1 \rightarrow 6)-linked glucose residues (lentinan), α -D-(1 \rightarrow 4)-linked glucose (A_3) and D-glucose residue (schizophyllan). Regardless of differences in the types of the side-chains attached to the β -D-(1 \rightarrow 3)-linked backbone, the ^{13}C NMR spectra shown in Figure 11 are very similar to each other, suggesting that the peaks are ascribable to the β -D-(1 \rightarrow 3)-linked main-chains, which are common to all of the branched (1 \rightarrow 3)- β -D-glucans containing branches at 0-6'. ^{13}C signals arising from the side-chains are obviously buried under the intense peaks of the major β -D-(1 \rightarrow 3)-linked glucose residues. The extent of the branching can be easily evaluated by comparison of the peak-intensity of C-6' with that of C-6 at the unbranched portion.

B. NaOH-Induced Conformational Transition Figure 12 shows that the ^{13}C NMR signals of the major β -D-(1 \rightarrow 3)-linked glucose residues are completely suppressed in lentinan gel in contrast to the case of Figure 11. The less intense signals appearing in the neutral gel state are ascribed to the β -D-(1 \rightarrow 6)-linked glucose residue, present as a minor component in the side-chains of lentinan (8%). The ^{13}C signals of the major β -D-(1 \rightarrow 3)-linkages, however, are revealed on stepwise addition of NaOH to the gel sample (Figure 12B-12F). Interestingly, the peak-positions of the C-1 and C-3 carbons of the β -D-(1 \rightarrow 3)-linkages at lower alkalinity (0.03-0.13M NaOH) are essentially the same as those observed for the gel state curdlan. Under more alkaline conditions (>0.19M), on the other hand, all peaks except for C-5' and C-6', coincide with those of the random coiled curdlan. Therefore, it is clear that lentinan adopts a helix conformation in the less alkaline state and is a random-coil at higher alkalinity. Such a helix-coil transition of lentinan is completed at almost the same NaOH concentration as that of curdlan. At an intermediate stage of the helix-coil transition (0.13M), an asymmetrical peak-profile appears for C-3, which could be resolved into two components, a broad peak (c) and a narrow peak (d). The former and the latter peaks are readily assigned to the helical and the random-coil forms, respectively, in view of the individual peaks. This observation indicates that there exists some portion of lentinan that is readily convertible into the random-coil form in the less alkaline condition. Similar results were also obtained for other branched (1 \rightarrow 3)- β -D-glucans, schizophyllan and A_3 .

Figure 13 illustrates that the relative peak-intensities of C-1 and C-3 in the β -D-(1 \rightarrow 3)-linkages of lentinan and schizophyllan (with respect to those obtained under more alkaline conditions) gradually increase with the concentration of NaOH. We found that the change of the relative peak intensities agrees very well, qualitatively, with that of the linewidth (Figure 14) and of the absorption maximum of Congo Red. Undoubtedly, these broad transitions between 0.13 and 0.19M NaOH are characteristic of the branched (1 \rightarrow 3)- β -D-glucans. As mentioned already, the linewidth of the ^{13}C NMR signals strongly depends upon the extent of the



Carbohydrate Research

Figure 12. 25.03-MHz C-13 NMR spectra of lentinan in the gel state and the changes with concentration of NaOH (9)

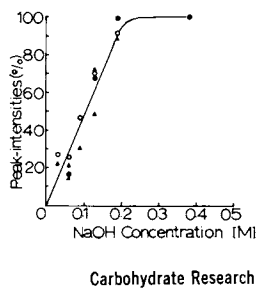


Figure 13. A plot of the relative peak intensities of C-1 and C-3 signals of β -D-(1 \rightarrow 3)-linked D-glucosyl residue for lentinan and schizophyllan with respect to those at 0.38M NaOH (lentinan) and 0.19M NaOH (schizophyllan) vs. the concentration of NaOH. Lentinan: (Δ) C-1; (\circ) C-3; and (\bullet) reference. Schizophyllan: (\blacktriangle) C-1; (\bullet) C-3; and (\bullet) reference (9)

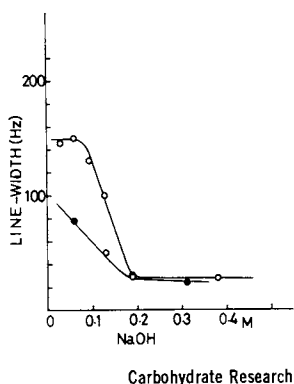


Figure 14. A plot of the C-13 linewidths (C-3) of lentinan and Fraction IV vs. the concentration of NaOH: (\circ) lentinan; (\oplus) narrow component of lentinan (Peak d); (\bullet) Fraction IV (9)

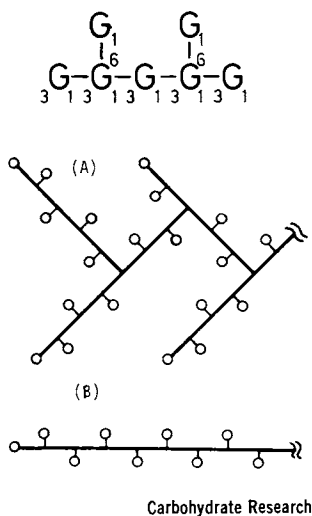


Figure 15. Schematic of the primary structure of branched (1 \rightarrow 3)- β -D-glucans: (A) tree-like, (B) linear (9).

cross-links in the gel state. Accordingly, the gradual change of the linewidths might well be explained by the gradual change of the degree of cross-linking which is a function of conformational state.

It is emphasized that the lower molecular weight fraction of lentinan (fraction IV: molecular weight 16200) exhibits a similar conformational transition to that of the original lentinan. It appears, however, that the linewidths of the single helical portion are much smaller than those of lentinan (approximately half the width of the latter)(see Figure 14, closed circles).

C. Gel Network of Branched (1→3)-β-D-Glucans There are some obvious differences between the physicochemical properties of the linear and branched (1→3)-β-D-glucans. In particular, branched D-glucans form soft gels without heating, whereas the linear D-glucan is capable of forming a firm resilient gel after heating at a temperature above 50°C. Furthermore, turbidity develops in the resilient gel of the linear D-glucan either when the gels are prepared at higher temperature or when the gels are prepared at a lower temperature (60°C) and kept for long time. In contrast, no elasticity was gained in the gels of the branched D-glucans. This distinction may be a reflection of a difference in the molecular organization of the gel networks. Nevertheless, it should be emphasized that, both for the linear and branched D-glucans, the conformation of the molecular chain is a single helix for the portion other than the cross-links, and the cross-links for the gelation are composed of the multiple-stranded helix.

From chemical analysis, the primary structure of lentinan and schizophyllan was elucidated as that of (1→3)-β-D-glucans having two branches for every five D-glucosyl residues (lentinan) or one for every three or four residues (schizophyllan). From chemical analysis alone, however, it cannot be definitely determined whether types (A) (tree-like) or (B) (linear) depicted in Figure 15 represent, at least, a plausible model of the primary structure. It is conceivable that a structure of type (A) would be more readily capable of forming physical cross-links by the multiple-stranded helices, because it is more highly branched than that of type (B) or a linear D-glucan. However, in type (A) many of the cross-links may be loosely formed in view of possible steric hindrance due to the presence of branching for the formation of the multiple-stranded helices, although the number of the cross-links may be increased considerably. The present ¹³C NMR results are consistent with this view. Namely, the complete suppression of the ¹³C NMR signals observed in the neutral gel state is obviously due to the increased number of cross-links in the gels of the branched glucans. The loosely formed cross-links (very short double- or triple-stranded helices) may be readily attacked by NaOH, resulting in diminution of the cross-links to cause a broader conformational change at lower NaOH concentration (0.1-0.2M). Firmly held cross-links resembling those in the linear D-glucans may be broken

finally at 0.2M NaOH, the same concentration as for the linear D-glucans. Further, the gels of highly branched (1→3)-β-D-glucans as type (A) may be unfavorable for the aggregation of the helical segments, as observed for the development of turbidity in curdlan gel.

CONCLUDING REMARKS

It is demonstrated that the presence of a single helical conformation, as revealed by ^{13}C NMR spectroscopy, plays a dominant role for the unique properties of higher molecular-weight linear and branched (1→3)-β-D-glucans. We are planning to analyze the conformation and dynamics of cross-linked region by means of CPMAS NMR spectroscopy.

Acknowledgements: The author is indebted to colleagues listed in the references, especially to Dr. T. Sasaki, for their collaboration at various stages of this work. He is grateful to Professor Gary E. Maciel and Dr. Victor Bartuska of Colorado State University for the measurement of CPMAS NMR, Professor T. Harada for stimulating discussion, and Takeda Chemical Industries for a gift of samples. This work was partly supported by a Grant-in-Aid for Scientific Research from the Ministry of Education, Science and Culture.

LITERATURE CITED

1. Harada, T.; Masada, M.; Fujimori, K.; Maeda, I. Agr. Biol. Chem. 1966, 30, 196.
2. Harada, T. In "Extracellular Microbial Polysaccharides", Sanford, P. A.; Laskin, A., Eds; American Chemical Society: Washington D.C., 1977; p.265.
3. Harada, T. In "Polysaccharides in Food", Blanshard, J. M. V.; Mitchell, J. R., Eds.; Butterworth: London, 1979; p.283.
4. Kasai, N.; Harada, T. ACS Symposium Series, to be published.
5. Saitô, H.; Ohki, T.; Yoshioka, Y.; Fukuoka, F. FEBS Lett. 1976, 68, 15.
6. Saitô, H.; Ohki, T.; Sasaki, T. Biochemistry, 1977, 16, 908.
7. Saitô, H.; Miyata, E.; Sasaki, T. Macromolecules, 1978, 11, 1244.
8. Saitô, H.; Ohki, T.; Takasuka, N.; Sasaki, T. Carbohydr. Res. 1977, 58, 293.
9. Saitô, H.; Ohki, T.; Sasaki, T. Carbohydr. Res. 1979, 74, 227.
10. Rees, D. A.; Scott, W. E. Chem. Commun. 1971, 1037.
11. Rees, D. A.; Scott, W. E. J. Chem. Soc. (B), 1971, 469.
12. Sathyanarayana, B. K.; Rao, V. S. R. Biopolymers, 1971, 10, 1605.
13. Blum, T. L.; Sarko, A. Carbohydr. Res. 1977, 54, 125.
14. Marchessault, R. H.; Deslandes, Y.; Ogawa, K.; Sundararajan, P. R. Can. J. Chem. 1977, 55, 300.
15. Takeda, H.; Yasuoka, N.; Kasai, N.; Harada, T. Polymer J. 1978, 10, 365.

16. Takeda, H. Ph. D. Thesis, Osaka University, 1978.
17. Jelsma, J.; Kreger, D. R. Carbohydr. Res. 1975, 43, 200.
18. Jelsma, J. Ph. D. Thesis, University of Groningen, 1979.
19. Bluhm, T. L.; Sarko, A. Can. J. Chem. 1977, 55, 293.
20. Atkins, E. D. T.; Parker, K. D.; Preston, R. D. Proc. Roy. Soc. B. 1969, 173, 209.
21. Saitô, H. Kagaku no Ryoiki, 1979, 33, 609.
22. Smith, I. C. P.; Saitô, H. Pure Appl. Chem. 1980, in press.
23. Schaefer, J.; Stejskal, E. O. In "Topics in Carbon-13 NMR Spectroscopy", Levy, G. C. Ed. Vol. 3. Wiley-Interscience: New York, 1979; p. 283.
24. Yokota, K.; Abe, A.; Hosaka, S.; Sakai, I.; Saitô, H. Macromolecules, 1978, 11, 95.
25. Schaefer, J. In "Topics in Carbon-13 NMR Spectroscopy", Levy, G. C. Ed. Vol. 1. Wiley-Interscience: New York, 1974, p. 149.
26. Duch, M. W.; Grant, D. M. Macromolecules, 1970, 3, 165.
27. Schaefer, J. Macromolecules, 1972, 5, 427.
28. Komoroski, R. A.; Maxfield, J.; Mandelkern, L. Macromolecules, 1977, 10, 545.
29. Kimura, H.; Moritaka, S.; Misaki, M. J. Food Sci. 1973, 38, 668.
30. Colson, P.; Jennings, H. J.; Smith, I. C. P. J. Amer. Chem. Soc. 1974, 96, 8081.
31. Bryce, T. A.; McKinnon, A. A.; Morris, E. R.; Rees, D. A.; Thom, D. Faraday Discussion Chem. Soc. 1974, 57, 221.
32. Konno, A.; Kimura, H.; Nakagawa, T.; Harada, T. Nippon Nogei-kagaku Kaishi, 1978, 6, 247.
33. Ogawa, K.; Watanabe, T.; Tsurugi, J.; Ono, S. Carbohydr. Res. 1972, 23, 399.
- 33a Banks, W.; Greenwood, C. T. "Starch and Its Components", Edinburgh Univ. Press., 1975; p. 175.
34. Dea, I. C.; McKinnon, A. A.; Rees, D. A. J. Mol. Biol. 1972, 68, 153.
35. Kuge, T.; Suetsugu, N.; Nishiyama, K. Agr. Biol. Chem. 1977, 41, 1315.
36. Maeda, I.; Saito, H.; Masada, M.; Misaki, A.; Harada, T. Agr. Biol. Chem. 1967, 31, 1184.
37. Ogawa, K.; Tsurugi, J.; Watanabe, T. Carbohydr. Res. 1973, 29, 397.
38. Schaefer, J. Macromolecules, 1973, 6, 882.
39. Allerhand, A.; Oldfield, E. Biochemistry, 1973, 18, 3428.
40. Saitô, H.; Ohki, T.; Kodama, M.; Nagata, C. Biopolymers, 1978, 17, 2587.
41. Torchia, D. A.; Hasson, M. A.; Hascall, V. C. J. Biol. Chem. 1977, 252, 3617.
42. Flory, P. J. "Principle of Polymer Chemistry", Cornell Univ. Press: Ithaca, N. Y., 1953, Chapter 9.
43. Koreeda, A.; Harada, T.; Ogawa, K.; Sato, S.; Kasai, N. Carbohydr. Res. 1974, 33, 396.
44. Harada, T.; Koreeda, A.; Sato, S.; Kasai, N. J. Electron Microsc. 1979, 28, 147.

45. Chihara, G.; Maeda, Y. Y.; Hamuro, J.; Sasaki, T.; Fukuoka, F. Nature, 1969, 222, 687.
46. Sasaki, T.; Takasuka, N. Carbohydr. Res. 1976, 47, 99.
47. Yoshioka, Y.; Ikekawa, T.; Noda, M.; Fukuoka, F. Chem. Pharm. Bull. 1972, 20, 1175.
48. Komatsu, N.; Ohkubo, S.; Kikumoto, S.; Saito, G.; Sakai, S. Gann, 1969, 60, 137.

RECEIVED August 26, 1980.

**American Chemical
Society Library**
1155 16th St. N. W.

Washington, D. C. 20036

In Solution Properties of Polysaccharides; Brant, D.;
ACS Symposium Series; American Chemical Society: Washington, DC, 1981.

Determination of Galactose-to-Galactose and Galactose-to-Mannose Structures in β -D-Galactofurano- α -D-Mannopyranans by C-13 NMR Spectroscopy

E. BARRETO-BERGTER and P. A. J. GORIN

Prairie Regional Laboratory, National Research Council,
Saskatoon, Saskatchewan, S7N 0W9 Canada

β -D-Galactofuranosyl units occur commonly as components of polysaccharides of fungi, bacteria and protozoa. They can be readily detected using ^{13}C -n.m.r. spectroscopy by virtue of their C-1 signals which occur at very low fields having δ_{C} values of 106.5-109.3 (1,2,3,4,5,6) (Table I). They are readily distinguishable from C-1 signals of α -D-galactofuranosyl units as in varianose [$\sim\delta_{\text{C}}101$ (7)] and those of α -D-galactopyranosyl units occurring at $\delta_{\text{C}}100.3$ with oligosaccharides (8) and at $\delta_{\text{C}}102.1$ (or 102.6) with a galactomannan (9). β -D-Galactopyranosyl units give C-1 signals at $\delta_{\text{C}}103.9$ to 105.9 (8,10,11) and values as high as $\delta_{\text{C}}107.0$ have been observed for the C-1 signal of a β -D-galactopyranosyl unit linked (1 \rightarrow 6) to a β -D-galactopyranosyl residue substituted at C-3 and C-4 by a pyruvic acid acetal (12). However, the ring-carbon atoms of furanoses are deshielded compared with those of their pyranose analogs (13) and five membered rings can also be detected by means of their C-2, C-3 and C-4 signals, which are at δ_{C} 82, 78 and 84, respectively. In this way minor β -D-galactofuranose structures can be detected in polysaccharide preparations from *Sporothrix schenckii* (5) (Fig. 1) and *Ceratocystis paradoxa* (14) (Fig. 2).

The variation of the δ_{C} values of C-1 of β -D-galactofuranosyl units from one galactomannan to another (Table I) suggested that, in structures with a mannan core and galactofuranosyl side-chains, that such shifts depend on the position of substitution of the galactosyl unit on the adjacent α -D-mannopyranosyl unit. Such a position of substitution could be determined by methylation analysis carried out on the galactomannan followed by a similar analysis on the mannan obtained by preferential removal of galactofuranosyl units with acid. However, such a method would be unreliable when the proportion of galactofuranosyl to mannopyranosyl units is small, as in galactomannans containing little galactose or having long side chains containing galactofuranose. (The galactomannans described herein are in these categories).

0097-6156/81/0150-0149\$05.00/0

© 1981 American Chemical Society

Table I. Chemical Shifts of C-1' Signals of Polysaccharides containing β -D-Galactofuranosyl units.

Chemical shift of C-1' Signal δ_C , p.p.m.	Chemical Structure
109.3	Single unit β -D-galactofuranosyl side-chains of galactomannan of <u>Sporothrix schenckii</u> , attached (1 \rightarrow 2), (1 \rightarrow 3), or (1 \rightarrow 6) to α -D-mannopyranosyl units.
109.4	Single unit β -D-galactofuranosyl side-chains of galactomannan of <u>Trichophyton interdigitale</u> attached (1 \rightarrow 2), (1 \rightarrow 3) and/or (1 \rightarrow 6) to α -D-mannopyranosyl units.
108.4 (major) 109.2	Approximately 4 unit side chains of β -D-(1 \rightarrow 5)-linked D-galactofuranosyl units in galactomannan of <u>Aspergillus niger</u> attached (1 \rightarrow 2)- or (1 \rightarrow 6) to α -D-mannopyranosyl units.
109.5 107.6 107.2	Galactomannan of <u>Ceratocystis stenoceras</u> containing single unit and β -D-(1 \rightarrow 6)-linked D-galactofuranosyl side-chains.
106.6	β -D-Galactofuranosyl units of galactomannan of <u>Trypanosoma cruzi</u> .
106.5	β -D-Galactofuranosyl units of polysaccharide of <u>Crithidia fasciculata</u> .
109.4	β -D-Galactofuranosyl non reducing end units of polysaccharide of spores of <u>Aspergillus fumigatus</u> .

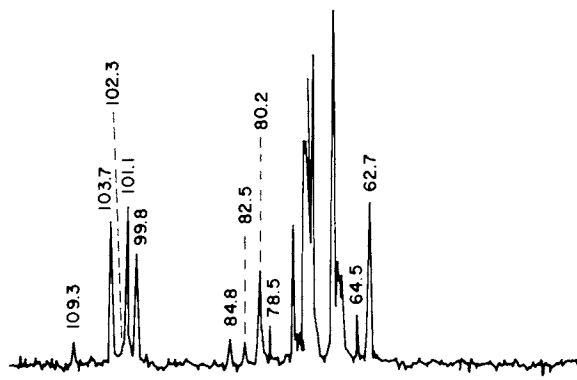


Figure 1. *C-13 NMR spectrum of galactofuranose-containing polymer from Sporothrix schenckii*

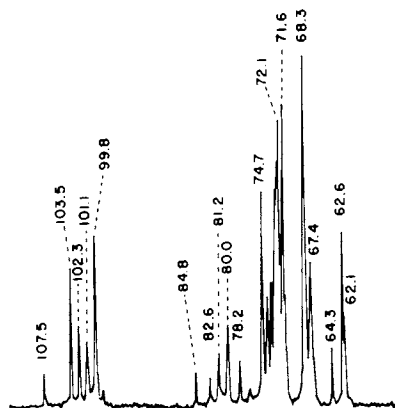


Figure 2. *C-13 NMR spectrum of galactofuranose-containing polysaccharide from Ceratocystis paradoxa*

Another common method, that of preparation of a β -D-galactofuranosyl mannose by partial hydrolysis or by partial acetolysis, is impractical since such a glycosidic linkage is relatively labile.

The structure-dependent variation of chemical shifts of β -D-galactofuranosyl units in galactomannans was confirmed by preparation of methyl glycosides of 2-O-(C-1', δ_C 107.7), 3-O-(C-1', δ_C 106.5) and 6-O- β -D-galactofuranosyl- α -D-mannopyranose (C-1', δ_C 109.7) (3). Shift values of δ_C 108.6 (2) and 109.5 (15) have been recorded for C-1 signals of β -D-galactofuranosyl units linked (1 \rightarrow 5)- and (1 \rightarrow 6), respectively, to adjacent β -D-galactofuranosyl residues.

The methyl glycosides were prepared via condensation of 3,5,6-tri-O-acetyl- α -D-galactofuranose 1,2-(methyl orthoacetate) with appropriate acceptors, in nitromethane containing mercuric bromide, following the procedure of Kochetkov and coworkers (16). When methyl 4,6-O-benzylidene- α -D-mannopyranoside was used as acceptor β -galactosylation took place exclusively at OH-3, since the disaccharide obtained on removal of the O-benzylidene and acetate groups gave a ^{13}C -n.m.r. spectrum (Fig. 3) with 13 signals and a C-3 signal which was displaced downfield by +5.8 ppm (α -O-glycosylation effect). β -O-glycosylation effects were observed for signals C-4 (-1.7 p.p.m.) and C-2, which underwent a strong shift of -3.2 p.p.m. since the attached hydroxyl group is axial (17). α -O-glycosylation effects (= α -shifts) refer to the change in shift of the O-substituted carbon signals on the transformation OH \rightarrow O Gly. β -glycosylation effects (= β -shifts) are the change in shift of the resonances of the adjacent β -carbon atoms.

The methyl glycoside of 2-O- β -D-galactofuranosyl- α -D-mannopyranose was isolated following use of methyl 3,4,6-tri-O-benzyl- α -D-mannopyranoside as acceptor (methyl 3-O-acetyl-4,6-O-benzylidene- α -D-mannopyranoside did not react). 2-O-galactosylation occurred since the derived methyl glycoside gave a ^{13}C -n.m.r. spectrum (Fig. 4) whose C-1 resonance underwent a strong β -shift of -2.5 p.p.m., by virtue of its appended axial OCH₃ group. The α -shift of C-2 was +4.8 p.p.m.

6-O- β -D-galactofuranosyl-(methyl α -D-mannopyranoside) was isolated following use of methyl 2,3,4-tri-O-benzyl- α -D-mannopyranoside as acceptor. Its structure was confirmed since there was no C-6 signal at δ_C 62.8, having been displaced downfield by an α -shift of 5.9 ppm. (Fig. 5).

The C-1' shifts obtained from the three above O- β -D-galactofuranosyl (methyl α -D-mannopyranosides) were used to characterize the galactose to mannose bridges in galactomannans with single-unit and longer side-chains, as follows:

1. *Sporothrix schenckii* galactomannan

β -D-galactofuranosyl-(1 \rightarrow 6)- α -D-mannopyranosyl linkages can be suggested for the galactomannan which gives a C-1 signal

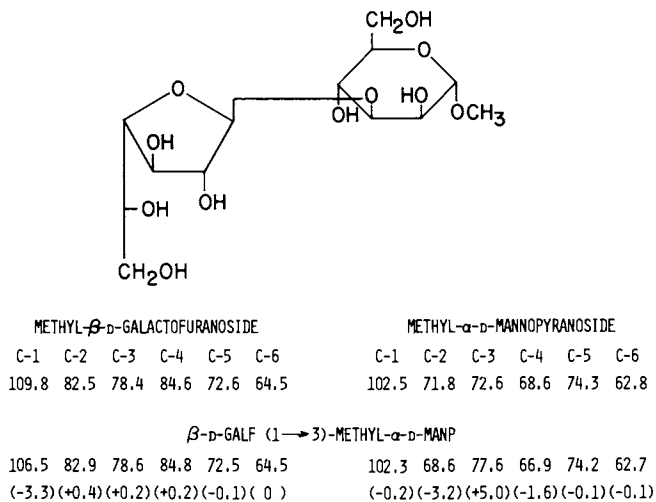


Figure 3. Assignment of signals in C-13 NMR spectrum of 3-O- β -D-galactofuranosyl-(methyl- α -D-mannopyranoside)

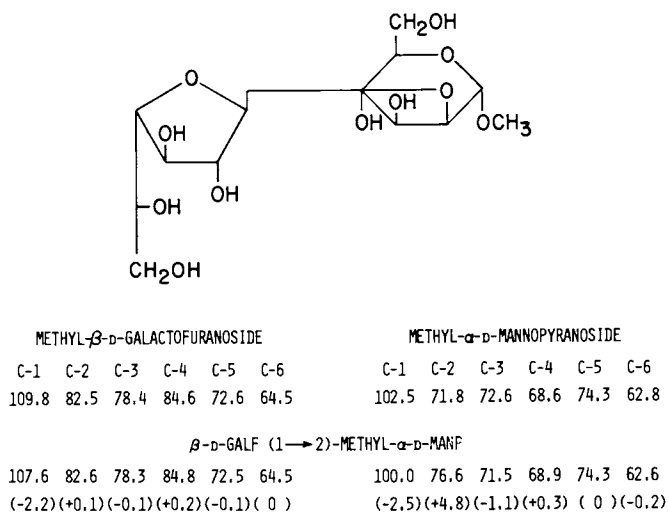


Figure 4. Assignment of signals in C-13 NMR spectrum of 2-O- β -D-galactofuranosyl-(methyl- α -D-mannopyranoside)

at $\delta_C 109.3$ (Fig. 1), which arises from single-unit side chains. Other signals attributable to β -D-galactofuranose, by virtue of their resemblance to signals of methyl β -D-galactofuranoside, are at $\delta_C 84.8$ (C-4), 82.5 (C-2), 78.5 (C-3) and 64.5 (C-6).

Other prominent signals correspond to α -D-mannopyranosyl units (18). These are C-1 signals of non-reducing end-units linked (1 \rightarrow 2) to adjacent units ($\delta_C 103.7$), 6-O-substituted units of the main chain ($\delta_C 101.1$) and 2,6-di-O-substituted units ($\delta_C 99.8$) of the main chain. A C-2 signal is present at $\delta_C 80.2$, corresponding to 2,6-di-O-substituted α -D-mannopyranosyl units.

Details of the methylation analysis of the polysaccharide are given in Table II.

Table II Methylated Fragments obtained from *S. schenckii* Galactomannan

	% Composition
2,3,4,6-Tetra-O-methylmannitol acetate	24
2,3,5,6-Tetra-O-methylgalactitol acetate	7
3,4,6-Tri-O-methylmannitol acetate	4
2,4,6-Tri-O-methylmannitol acetate	2
2,3,4-Tri-O-methylmannitol acetate	48
3,4-Di-O-methylmannitol acetate	15

Since the galactofuranosyl units are linked (1 \rightarrow 6) to mannopyranose it is not clear whether such a unit is mono-O-substituted by galactofuranose (2,3,4-tri-O-methylmannitol acetate) or di-O-substituted by galactofuranose and mannopyranose (3,4-di-O-methyl fragment).

2. Trichophyton interdigitale galactomannan

By virtue of its ^{13}C -n.m.r. spectrum (3), which contains a C-1 signal at $\delta_C 109.4$ (Fig. 6), a (1 \rightarrow 6) galactose to mannose linkage is suggested. Other ^{13}C signals corresponding to mannopyranosyl units are also similar to those of the *S. schenckii* galactomannan.

The partially methylated alditol acetates obtained previously (19) on methylation analysis were similar, although with different proportions (Table III)

Table III. Methylated Fragments Obtained from *T. interdigitale* Galactomannan

	% Composition
2,3,4,6-Tetra-O-methylmannitol acetate	15
2,3,5,6-Tetra-O-methylgalactitol acetate	12
2,3,4-Tri-O-methylmannitol acetate	47
2,4,6-Tri-O-methylmannitol acetate	2
3,4-Tri-O-methylmannitol acetate	24
3,5(2,4)-Di-O-methylmannitol acetate	1

Galactomannans having a single C-1 signal at $\delta_C 109.4$ seem to be quite common, another example being one from the spores of Aspergillus fumigatus.

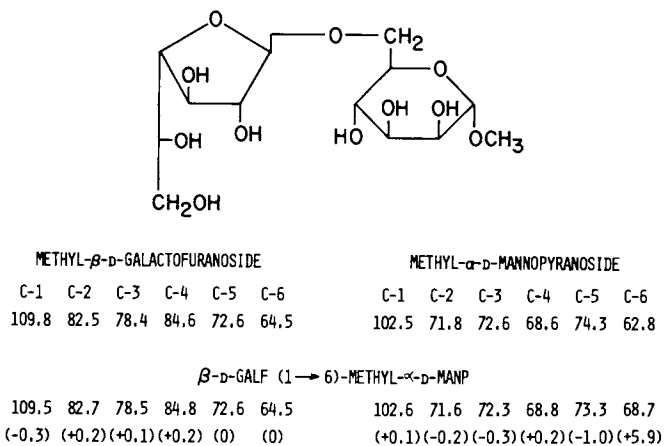


Figure 5. Assignment of signals in C-13 NMR spectrum of 6-O- β -D-galactofuranosyl-(methyl- α -D-mannopyranoside)

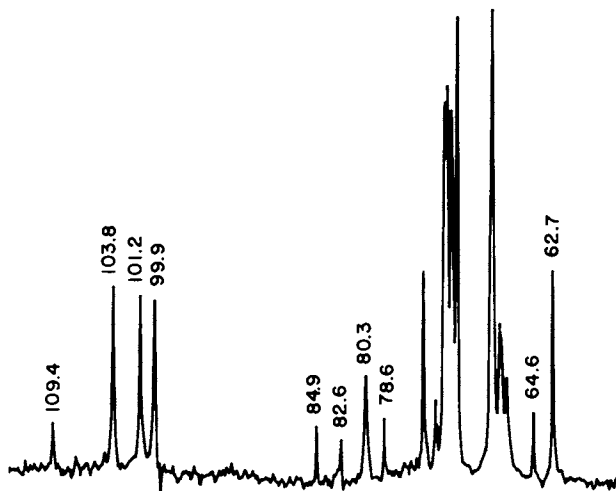


Figure 6. C-13 NMR spectrum of galactomannan of *Trichophyton interdigitale*

3. Aspergillus niger galactomannan

The galactomannan of A. niger contains (1→5)-linked β-D-galactofuranosyl side-chains of 3-4 units in length (C-1 δ_C108.4), the innermost unit giving a minor C-1 signal at δ_C109.2, which would represent a unit linked (1→6) to the adjacent α-D-mannopyranosyl unit in the mannan core (20; Fig. 7).

Once again it is not clear whether the unit is 6-0-substituted by galactofuranose or 2,6-di-0-substituted by galactofuranose and mannopyranose, according to the following methylation data (Table IV).

Table IV Methylated Fragments Obtained From A. niger Galactomannan

	% Composition
2,3,4,6-Tetra-0-methylmannitol acetate	23
2,3,5,6-Tetra-0-methylgalactitol acetate	14
2,3,6-Tri-0-methylgalactitol acetate	36
2,3,4-Tri-0-methylmannitol acetate	5
3,4,6-Tri-0-methylmannitol acetate	12
3,4-Di-0-methylmannitol acetate	9

4. Trypanosoma cruzi galactomannan

The ¹³C-n.m.r. spectrum of the galactomannan (Fig. 8) is consistent with β-D-galactofuranosyl single unit side chains (3) since it contains signals corresponding to those of methyl β-D-galactofuranoside at δ_C84.8(C-4), 83.0(C-2), 78.5(C-3) and 64.6(C-6), with no α- or β-0-substitution effects. The C-1 signal at δ_C106.6 corresponds to a α-D-galactofuranosyl residue linked (1→3) to a α-D-mannopyranosyl unit. Other C-1 signals correspond to non-reducing α-D-mannopyranosyl end-units linked (1→2) to an α-D-mannopyranosyl unit (δ_C103.7) and consecutive (1→2)-linked α-D-mannopyranosyl unit (δ_C102.3). Signals at δ_C79.9 and 80.1 correspond to C-2 of 2-0- and 2,6-di-0-substituted α-D-mannopyranosyl units (18), respectively. The methylation data is very complex, 2,3,4,6-tetra-0-methylmannitol acetate (25%), 2,3,5,6-tetra-0-methylgalactitol acetate (9%), and 3,4,6-tri-0-methylmannitol acetate (17%) being detected as major components. Also agreeing with the ¹³C data was the formation, following partial acetolysis, of a (1→2)-linked trisaccharide containing α-D-mannopyranosyl units.

5. Ceratocystis stenoceras galactomannan

The galactomannan gives 3 C-1 signals at δ_C109.5, 107.6 and 107.2 (Fig. 9). Methylation analysis gave rise to 2,3,5-tri-0-methylgalactitol acetate corresponding to 6-0-substituted galactofuranosyl units. 6-0-β-D-Galactofuranosyl- (methyl β-D-galactofuranoside) gives a C-1 signal at δ_C109.5, corresponding to the polysaccharide signal at δ_C109.5 arising from a β-D-galactofuranosyl unit linked (1→6) to a galactofur-

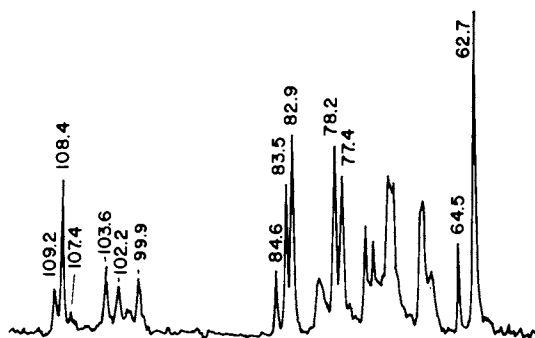


Figure 7. *C-13 NMR spectrum of galactomannan of Aspergillus niger*



Figure 8. *C-13 NMR spectrum of galactomannan of Trypanosoma cruzi*

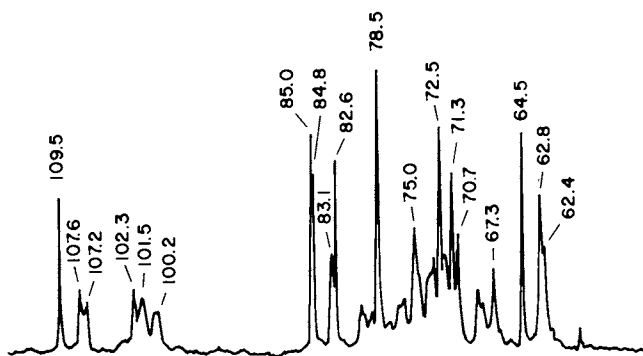


Figure 9. *C-13 NMR spectrum of galactomannan of Ceratocystis stenoceras*

anosyl residue. However, it is still possible that a contribution to this signal is made by galactofuranosyl residues attached (1→6) to mannopyranosyl units, since the C-1 shift would be similar.

The methylation data for the galactomannan are presented in Table V.

Table V Methylated Fragments obtained from C. stenoceras Galactomannan

	% Composition
2,3,4,6-Tetra-O-methylmannitol acetate	9
2,3,5,6-Tetra-O-methylgalactitol acetate	23
3,4,6-Tri-O-methylmannitol acetate	20
2,3,6-Tri-O-methylglucitol acetate (from starch)	7
2,3,5-Tri-O-methylgalactitol acetate	16
4,6-Di-O-methylmannitol acetate	2
3,4-Di-O-methylmannitol acetate	23

According to the C-1' shifts of the disaccharide glycosides the signal at δ_C 107.6 should arise from β -D-galactofuranosyl units linked (1→2)- to α -D-mannopyranosyl residues. Whether the mannosyl residues are mono-O-substituted in this way, or whether they are also substituted in the 6-positions by other mannosyl residues is not clear, since both 3,4,6-tri-O- and 3,4-di-O-methylmannitol derivatives were detected. The polysaccharide signal at δ_C 107.2 is intermediate between a (1→2)- and a (1→3) linkage. However the percentage (2%) of 4,6-di-O-methylmannitol from the methylation experiment was too low, in comparison with the size of the C-1 signal, to allow the possibility of (1→3) substitution by a β -D-galactofuranosyl unit.

Literature cited

1. Agura, M., Kohama, T., Fujimoto, M., Kuniaka, A., Yoshino, H. and Sugiyama, H. Agric. Biol. Chem. (Japan). 1974, 38: 2563-2564.
2. Gorin, P.A.J. and Mazurek, M. Carbohydr. Res. 1976, 48: 171-176.
3. Gorin, P.A.J., Barreto-Bergter, E. and da Cruz, F.S. Carbohydr. Res., submitted for publication.
4. Joseleau, J.P., Lepeyre, M., Vignon, M. and Dutton, G.C.S. Carbohydr. Res. 1978, 67: 197-212.
5. Mendonça, L., Gorin, P.A.J., Lloyd, K.O. and Travassos, L.R. Biochemistry. 1976, 15: 2423-2431.
6. Gorin, P.A.J., Previato, J.O., Mendonça-Previato, L. and Travassos, L.R. J. Protozool. 1979, 26: 473-478.

11. BARRETO-BERGTER AND GORIN β -D-Galactofurano- α -D Mannopyranans 159
7. Lindberg, B., private communication.
8. Cox, D.D., Metzner, E.K., Cory, L.W. and Reist, E.J. Carbohydr. Res. 1978, 67: 23-31.
9. Gorin, P.A.J., unpublished results.
10. Usui, T., Tsushima, S., Yamaoka, N., Matsuda, K., Tuzimura, K., Sugiyama, H., Seto, S., Fujieda, K. and Miyajima, G. Agric. Biol. Chem. (Japan). 1974, 38: 1409-1410.
11. Colson, P. and King, R.R. Carbohydr. Res. 1976, 47: 1-13.
12. Duarte, J.H., Iacomini, M., Gorin, P.A.J., Feijó, M.A.L. and Duarte, H.S., unpublished results.
13. Perlin, A.S., Cyr, N., Koch, H.J. and Korsch, B. Ann. N.Y. Acad. Sci. 1973, 22: 932-942.
14. Alviano, C.S., Gorin, P.A.J. and Travassos, L.R. Exp. Mycol. 1979, 3: 174-187.
15. Mendonça-Previato, L., Gorin, P.A.J. and Travassos, L.R. Infect. Immun., submitted for publication.
16. Kochetkov, N.K., Khorlin, A.J. and Bochkov, A.F. Tetrahedron. 1967, 23: 707.
17. Dorman, D.E., Angyal, S.J. and Roberts, J.D. J. Am. Chem. Soc. 1970, 92: 1351-1354.
18. Gorin, P.A.J. Can. J. Chem. 1973, 51: 2375-2378.
19. Bishop, C.T., Perry, M.B., Blank, F. and Cooper, F.P. Can. J. Chem. 1965, 43: 30-39.
20. Barreto-Bergter, E.M., Travassos, L.R. and Gorin, P.A.J. Carbohydr. Res., submitted for publication.

RECEIVED September 22, 1980.

Structure and Conformation of the Capsular Polysaccharides of Group B Streptococcus

HAROLD J. JENNINGS, CZESLAW LUGOWSKI, and KARL-GUNNAR ROSELL
Division of Biological Sciences, National Research Council of Canada,
Ottawa, Canada K1A 0R6

DENNIS L. KASPER

Channing Laboratory, Harvard Medical School and the Department of Medicine,
Peter Bent Brigham Hospital, Boston, MA 02115

Recently Group B streptococcal infections in the new-born have become a major problem resulting in a high rate of morbidity and mortality (1). Serological studies have suggested that a deficiency of type-specific antibody to the capsular polysaccharides in new-born infants may be an important factor in predisposing them to the development of group B streptococcal disease (2). Hence the importance of the development of a vaccine based on the capsular polysaccharides and also of an understanding of the structure-specificity relationships involved in the production of these protective antibodies.

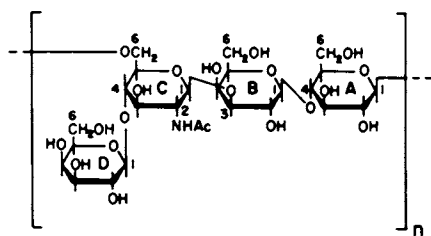
Lancefield characterised two polysaccharide antigens obtained from group B *Streptococcus*; a group antigen (rhamnan) common to all strains, and the type-specific capsular polysaccharides that distinguished four major serotypes designated Ia, Ib, II and III (3,4,5). The type-specific polysaccharides were isolated by the hot hydrochloric acid extraction of the whole streptococcal organisms and all had identical constituents; galactose, glucose and 2-acetamido-2-deoxy-glucose. The acid extracted antigens are immunologically incomplete and form a lower molecular weight core to the complete native antigen which contains additional terminal acid-labile sialic acid residues. Thus when neutral or buffered (pH 7.0) extractions of the whole organisms are carried out the loss of sialic acid is minimized and more complete antigens can be isolated (2,6,7,8). Recently it has also been established for the type Ia and III organisms that pH control during the growth of the organisms is also a factor in the production and isolation of a complete native antigen (9). This paper is mainly concerned with the structure-specificity relationship of the native type III polysaccharide although some reference will also be made to the structure of the isomeric type Ia polysaccharide (10). This structural study provides further evidence that only the native antigen is effective in the production of protective antibodies against type III group B streptococcal infections. It also defines the important role that sialic acid plays in the

0097-6156/81/0150-0161\$05.00/0

© 1981 American Chemical Society

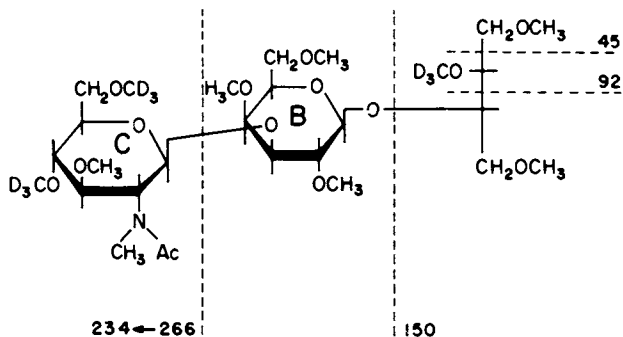
formation of conformational-dependent determinants which are responsible for the production of these protective antibodies.

The incomplete type Ia (10) and III (9) group B streptococcal antigens have D-galactose, D-glucose and 2-acetamido-2-deoxy-D-glucose constituents in a molar ratio of 2:1:1, whereas both native antigens contain additional sialic acid residues (9-10). The structure of the more complex type III native antigen was determined by first elucidating the structure of the incomplete core antigen obtained by the acid-extraction of the organisms. The structure of the type III incomplete antigen shown in Figure 1 proved to be identical to that proposed for the capsular polysaccharide of type 14 *S. pneumoniae* (11) and the structure was elucidated using similar procedures to those employed in the structural determination of this latter antigen. By methylation analysis of the type III incomplete antigen the individual specifically methylated component sugars were identified and quantified (GC-MS analysis) and are listed in Table 1. These components were consistent with the type III incomplete antigen having the above structure (Figure 1) although sequence and linkage configuration data were still required. The sequence was determined using two degradation procedures. The first involved a modified Smith degradation (9) in which the polyalcohol obtained was permethylated and the product was partially hydrolysed. This yielded a partially hydrolysed oligosaccharide which was further methylated using trideuteriomethyl iodide. Using this procedure labeled methyl groups were introduced at all the newly exposed hydroxyl groups. The resultant labeled oligosaccharide is shown in Figure 2 together with some of its major fragments when it was subjected to GC-MS analysis. The sequence of the individual methylated sugars in the oligosaccharide could be determined from the larger fragments obtained in this analysis. This sequence represents the sequence of the original sugar components, A, B and C of the repeating unit of the backbone of the incomplete type III antigen Figure 1; the erythritol residue of the methylated oligosaccharide originating from the oxidised backbone glucopyranose residue (A). Because the 2-acetamido-2-deoxy-D-glucose residue (C) is a branch point in the incomplete type III antigen a further degradation was required to elucidate its point of attachment to the terminal D-galactopyranose residue (D). This was achieved by the oxidation of the latter residues to β -D-galactopyranosyluronic acid groups and subjecting the modified polysaccharide to a uronic acid degradation (9). This degradation involved the methylation of the modified polysaccharide, removal of the methylated galactopyranosyluronic acid residues, and remethylation of the polymeric material with trideuteriomethyl iodide. The identification by GC-MS analysis of 2-deoxy-3-O-methyl-4-O-trideuteriomethyl-2-(N-methyl-acetamido)-D-glucose in the hydrolysis products of the above polymer demonstrated unambiguously that the terminal β -D-galactopyranose residues (D) of the incomplete type III antigen were linked to O-4 of the backbone



Canadian Journal of Biochemistry

Figure 1. Repeating unit of the incomplete Type III polysaccharide antigen of Group B Streptococcus (9)



Canadian Journal of Biochemistry

Figure 2. Methylated oligosaccharide degradation product obtained from the incomplete Type III streptococcal antigen (9)

Table I

Methylation analysis of the native and incomplete core type-III streptococcal polysaccharides.

Methylated glucose derivatives	Molar ratios	
	Incomplete core polysaccharide	Native polysaccharide
2,3,4,6-Tetra- <u>O</u> -methyl- <u>D</u> -galactose	1	-
2,4,6-Tri- <u>O</u> -methyl- <u>D</u> -galactose	1	1
2,3,6-Tri- <u>O</u> -methyl- <u>D</u> -glucose	1	1
2,3,4-Tri- <u>O</u> -methyl- <u>D</u> -galactose	-	1
3-Mono- <u>O</u> -methyl- <u>N</u> -methyl- <u>N</u> -acetyl- <u>D</u> -glucosamine	+	+
4,7,8,9-Tetra- <u>O</u> -methyl- <u>N</u> -methyl- <u>N</u> -acetyl- <u>D</u> -neuraminic acid	-	.+

NOTE: +, slight and nonquantitative response; -, not detected.

2-acetamido-2-deoxy-glucopyranose residues (C). That all the sugar components were in the β -D-configuration was ascertained from the ^{13}C NMR spectrum of the incomplete type III antigen which exhibited only one narrow signal in the anomeric region of the spectrum due to the coincidence of the anomeric signals of all the individual sugar residues. From previous studies on model compounds on the low field chemical shift (104.2 ppm) of this signal was only consistent with the β -D-configuration of all these residues (9).

The structure of the repeating unit of the native type III antigen is shown in Figure 3. This structure was clearly established by differences in the individual methylated sugars yielded by the hydrolysis of its permethylated product as compared to those yielded on hydrolysis of the permethylated core antigen (Table 1). The detection of only 2,3,4-tri-O-methyl-galactose in the former as compared to only 2,3,4,6-tetra-O-methyl galactose in the latter established that sialic acid residues of the native antigen were linked to O-6 of all the terminal β -D-galactopyranose residues of the core antigen. In addition the detection of only the fully methylated derivative of sialic acid established that all these sialic acid residues were terminally located. The α -D-configuration of these residues was determined by the characteristic chemical shift (12) of the signal of their carboxylated carbons in the ^{13}C NMR spectrum of the native type III antigen (Figure 3).

The native type Ia polysaccharide antigen from group B *Streptococcus* was shown to be isomeric with the native type III antigen as both contained D-galactose, D-glucose, 2-acetamido-2-deoxy-D-glucose and sialic acid in the molar ratio of 2:1:1:1 respectively (10). On removal of these sialic acid residues both also yielded isomeric core structures (incomplete antigens). However the native type Ia antigen proved to have some structural differences when compared with the native type III antigen (9). The structure of the native type Ia antigen was determined using identical procedures to those previously described for the native type III antigen and its repeating unit is shown in Figure 4. Methylation analysis of the incomplete type Ia antigen and of the oligosaccharide obtained from the modified Smith degradation of this antigen indicated that the type Ia and III incomplete antigens retain two common structural features in the form of both having terminal β -D-galactopyranose residues and a β -D-GlcNAcp-[1 \rightarrow 3]- β -D-Galp-[1 \rightarrow 4]- β -D-Glcp trisaccharide unit. However they differ in that the terminal β -D-galactopyranose residues of the incomplete type Ia antigen are linked to O-4 of the backbone β -D-galactopyranose unit instead of to the 2-acetamido-2-deoxy- β -D-glucose residues as they are in the incomplete type III antigen. In addition the common backbone trisaccharide is linked via O-4 of its 2-acetamido-2-deoxy- β -D-glucose residue (10) in the incomplete type Ia antigen and via O-6 of the same residue in the incomplete type III antigen (9).

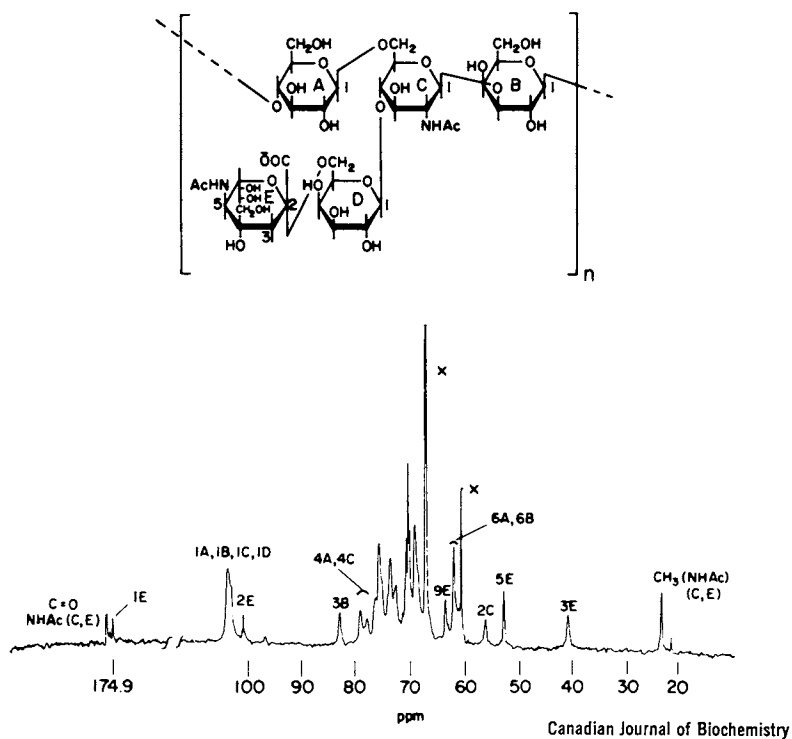


Figure 3. Repeating unit of the native Type III streptococcal polysaccharide antigen and its fourier-transformed C-13 NMR spectrum (25.2 MHz) taken with an aquisition time of 0.3 s and a spectral width of 5 kHz. The number of induction decays was 150,000 (9)

The native type Ia polysaccharide also differs from that of the native type III antigen in that its terminal sialic acid residues are linked to 0-3 of the side-chain β -D-galactopyranose residues of the type Ia core antigen and to 0-6 of the same residues in the type III core antigen.

Before using the above structural information to help interpret the serological properties of the type III group B streptococcal organisms it is of interest to note the high degree of structural homology between both the native type III and native type Ia antigens and some important human serum glycoproteins. The terminal α -D-NeuAcP-[2 \rightarrow 6]- β -D-Galp unit of the former exists as end-group in human serrotransferrin (13) and the α -D-NeuAcP-[2 \rightarrow 3]- β -D-Galp exists as end-group in the human M and N blood groups substances (14).

Antisera raised to group B *Streptococcus* type III organisms in rabbits contain two distinguishable populations of antibodies (9). One population has an exclusive specificity for the native type III antigen and is thus dependent on the presence of its sialic acid residues while the other has a specificity for the incomplete type III core antigen. There is evidence to suggest that this latter specificity is due to determinants terminating in β -D-galactopyranose (9) and also that this determinant could be functional in the production of protective antibodies (15). In serological studies in animals it was reported (15) that antisera to the structurally identical type 14 pneumococcal polysaccharide, the β -D-galactopyranose residues of which have been shown to be immunodominant (16), was both opsonic and protective against group B *Streptococcus* organisms. However in structural studies on the native type III antigen no terminal β -D-galactopyranose residues were detectable, all of them being masked by sialic acid residues. This latter observation would seem to be more compatible with the serological evidence for the essential participation of the native type III antigen in the development of human immunity to the type III group B streptococcal disease. In these experiments it was demonstrated that in human sera it was the antibody directed to the native polysaccharide antigen which correlated most highly with opsonic activity (2). One possible explanation for this apparent contradiction could be that in the experiments using the type 14 antipneumococcal serum the required functionally active determinants terminating in β -D-galactopyranose residues could have been generated on the type III organisms by the removal of sialic acid residues from the organism-associated native type III polysaccharide. Certainly it has been demonstrated, that these residues are extremely labile and that even rigid pH-control (pH 7.0) of growth conditions of this organism is necessary in order to produce a native polysaccharide having no terminal β -D-galactopyranose residues (9). On the above evidence it would appear that the determinant terminating in sialic acid is important in the production of protective antibodies against type III

group B streptococcal infections in humans and an attempt to structurally define this determinant was made.

Serological studies indicate that despite the dominant peripheral location of the sialic acid residues of the native type III antigen they are not themselves immunodominant. This was established when the related native type Ia antigen, also containing terminal α -D-linked sialic acid residues did not inhibit the homologous serological reaction of the native type III antigen (16). Therefore perhaps the high specificity of this determinant terminating in a sialic acid residue could be attributed to its large size. Because of the above evidence together with some highly characteristic structural features of the native type III antigen it was of interest to attempt to deduce the actual size of this determinant using the classical serological approach of determining by inhibition techniques (17) the relative contribution of different parts of the determinant to its overall serological specificity. One might anticipate that the disaccharide 6-O- α -D-[N-acetylneuraminy]- β -D-galactopyranose, which constitutes the branches of the native type III antigen (Figure 3) should be a strong determinant as has been demonstrated in other branched structures (18). However on a serological basis one could probably predict that this disaccharide would be a very unfavourable determinant in human antibody production. This is because antibodies would be formed to a determinant ubiquitous among human serum glycoproteins having been positively identified as a terminal disaccharide in human serotransferrin (13). Therefore in order to achieve serological specificity from serotransferrin it would be necessary to be larger than the trisaccharide α -D-NeuAc-(2 \rightarrow 6)- β -D-Galp-(1 \rightarrow 4)- β -D-GlcNAc which is also an integral part of the structure of human serotransferrin (13). This deduction proved to be correct when in serological studies (16) serotransferrin did not inhibit the homologous serological reaction of the native type III antigen. Therefore in classical terms one would expect this determinant to include residues from the backbone of native type III polysaccharide in order for it to achieve serological specificity from serotransferrin. Inclusive of the sialic acid residue this would now constitute a large determinant as Kabat has shown that the upper limit for a determinant consisting of linear glucopyranose residues is of the order of six residues (17). However if the determinant is large and extends into the backbone of the native type III antigen one might then anticipate that the incomplete type III antigen would still retain a large part of its structure. In fact it has been previously determined that the incomplete type III antigen does not cross-react (9) with antibodies specific for the native type III antigen and more importantly does not inhibit (16) the homologous serological reaction of this latter antigen. Thus by using classical inhibition techniques it was not possible to define the determinant responsible for the specificity as the native type III antigen.

In order to explain the above negative results one can only postulate the conformational dependence of this determinant. On the basis of the serological evidence (9) it is obvious that sialic acid must play an important role in this dependence, and this can be rationalised if it associates with the backbone of the native type III antigen thus forming a more complex ring structure. At the same time this would enable the sialic acid residues to assume a lower profile within the structure of the native type III antigen. Breakage of this ring structure by removal of the sialic acid residues should then involve conformational changes, and evidence for such changes can be obtained by a comparison of the ^{13}C NMR spectra of the native (Figure 3) and incomplete type III antigens. Chemical shift changes involving linkage carbons can be indicative of changes in torsion angles between glucose residues (19), and one of the three signals in the linkage region of the spectrum of the native type III antigen at 78.3 ppm undergoes such a characteristic displacement to 79.1 ppm. It now remains to assign those signals in order to discover at which point in the structure of the native type III antigen this conformational change had occurred. The lowest field signal at 83.4 ppm was assigned (9) to C-3 of the backbone β -D-galactopyranose residue (B) and the signals at 79.6 and 78.3 ppm to C-4 of either the 2-acetamido-2-deoxy- β -D-glucopyranose (C) or the penultimate β -D-galactopyranose residue (D) (9). Recently by removal of the terminal β -D-galactopyranose residue (D) from the incomplete type III antigen it became possible to assign the signal of the native type III antigen which underwent the previously mentioned displacement to C-4 of the 2-acetamido-2-deoxy- β -D-glucopyranose residue (C) (16). Thus the sialic acid of the native antigen controls the torsion angles of the glycosidic bond between the penultimate β -D-galactopyranose (D) and the backbone 2-acetamido-2-deoxy- β -D-glucopyranose (C) residues. This evidence indicates a conformational change involving the branches of the native type III antigen, rather than more extensive conformational changes in the backbone of the native antigen on removal of the sialic acid residues, and is consistent with the formation of a ring structure involving sialic acid (E) and residues D and C as shown in Figure 5.

Space filling models (CPK) suggest that such a structure is possible and also suggest that the interaction of the sialic acid residue (E) with the 2-acetamido-2-deoxy- β -D-glucopyranose (C) residue could occur by hydrogen bonding between the carboxylate group of the former and the hydroxyl group at C-3 of the latter (Figure 5). This hydrogen bonding would probably be augmented by additional hydrogen bonding between the carboxylate group of the sialic acid (E) residue and its own hydroxyl group at C-8. Chemical shift data (^{13}C) indicate that this type of internal hydrogen bonding occurs in sialic acid molecules which have the α -D-configuration (12). However the formation of this cyclic structure cannot be solely responsible for the specificity of the

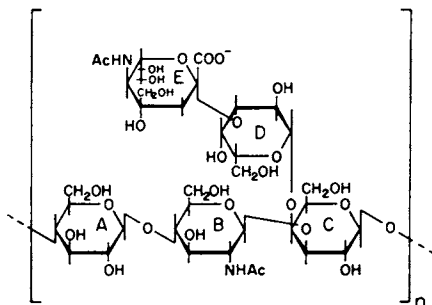


Figure 4. Repeating unit of the native Type Ia polysaccharide antigen of Group B Streptococcus (10)

Proceedings of the National Academy of Science

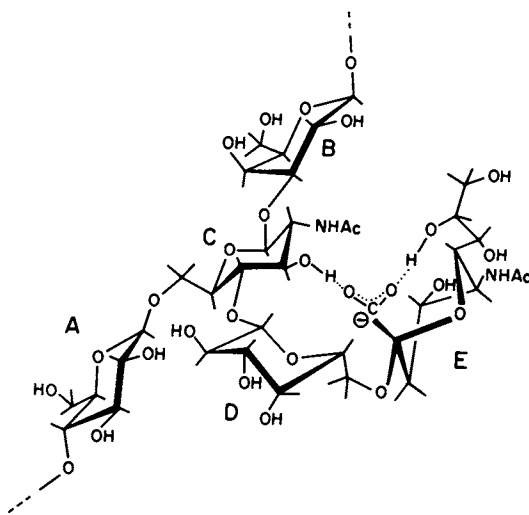


Figure 5. Proposed conformation of the repeating unit of the type III polysaccharide antigen of Group B Streptococcus

native type III antigen because in all probability serrotransferrin could also form an identical ring structure and yet does not inhibit the homologous serological reaction of the native type III antigen. Thus although the ring structure is probably necessary for the serological specificity of the native type III antigen it does not play a dominant role in this specificity. Obviously this specificity must involve additional backbone sugar residues although previous serological studies would suggest only a limited participation by these residues. Space-filling (CPK) models would suggest that the orientation of residues A, C and D (Figure 5) would be conformationally dependent on the presence of the ring system and that therefore this might constitute the critical side of this determinant. On this evidence it is conceivable that the determinant need not be too large to achieve specificity and in fact that sialic acid need not be involved directly in the determinant but simply function as an external factor in the conformational control of the determinant.

It is interesting to speculate on the role of this conformational control by sialic acid residues in other molecules having terminal sialic acid residues. Certainly the isomeric native type Ia antigen (Figure 4) also has a specificity dependent on its terminal sialic residues (10) and evidence is available to suggest that this specificity could also be attributed to a similar ring-type structure (16). In addition glycoprotein structures having terminal sialic acid residues are ubiquitous on all cell surfaces where they are probably involved in recognition processes which trigger different biological transformations (20). Perhaps similar conformational control by the sialic acid residues of these glycoproteins explains the high specificity of these recognition processes and thus the avoidance of random recognition.

Acknowledgements

One of the authors D.L.K. is the recipient of a United States Public Health Service research career and development award No. 1K0400126. Supported in part by U.S. Public Health Service Research Grant No. 1AI72538. This manuscript is NRCC No. 18535.

Literature Cited

1. Baker, C.J., *J. Inf. Dis.*, (1977) 136, 137-
2. Kasper, D.L., Baker, C.J., Baltimore, R.S., Crabb, J.H., Schiffman, G., and Jennings, H.J., *J. Exp. Med.* (1979) 149, 327-339.
3. Lancefield, R.C., *J. Exp. Med.* (1933) 57, 571-582.
4. Lancefield, R.C., *J. Exp. Med.* (1934) 59, 441-458.
5. Lancefield, R.C., *J. Exp. Med.* (1938) 67, 25-40.
6. Baker, C.J., Kasper, D.L., and Davis, C.E. (1976), *J. Exp. Med.* 143, 258-270.

7. Kane, J.A. and Karakawa, W.W. (1977), *J. Immunol.* 118, 2155-2160.
8. Tai, J.Y., Gotschlich, E.C., and Lancefield, R.C. (1979), *J. Exp. Med.* 149, 58-66.
9. Jennings, H.J., Rosell, K.-G., and Kasper, D.L. (1980), *Can. J. Biochem.* 58, 112-120.
10. Jennings, H.J., Rosell, K.-G., and Kasper, D.L. (1980), *Proc. Nat. Acad. Sci.* 77, 2931-2935.
11. Lindberg, B., Lönngren, J., and Powell, D.A. (1977), *Carbohydr. Res.* 58, 177-186.
12. Bhattacharjee, A.K., and Jennings, H.J. (1977), *Carbohydr. Res.* 55, 105-112.
13. Spik, G., Bayard, B., Fournet, B., Strecker, G., Bouglet, S., and Montreuil, J. (1975), *FEBS. Lett.* 50, 269-299.
14. Sadler, J.E., Paulson, J.C., and Hill, R.L. (1979), *J. Biol. Chem.* 254, 2112-2119.
15. Fisher, G.W., Lowell, G.H., Cumrine, M.H., and Bass, J.W. (1978), *J. Exp. Med.* 148, 776-786.
16. Jennings, H.J., Lugowski, C., and Kasper, D.L. Unpublished results.
17. Kabat, E.A., and Mayer, M.M. (1961) in *Experimental Immunochimistry* (Thomas, Springfield, Ill.) pp. 241-267.
18. Pazur, J.H., Anderson, J.S., and Karakawa, W.W. (1971), *J. Biol. Chem.* 246, 1793-1798.
19. Jennings, H.J., and Smith, I.C.P. (1978), *Methods Enzymol.* 50, 39-50.
20. Jeanloz, R.W., and Codington, J.F. (1976) in *Biological Roles of Sialic Acid* (Rosenberg and Schengrund, Plenum Press, New York, N.Y.) pp. 201-238.

RECEIVED September 22, 1980.

Light-Scattering Spectroscopy of Meningococcal Polysaccharides

A. DINAPOLI and B. CHU

State University of New York at Stony Brook, Long Island, NY 11794

TEH-YUNG LIU

Division of Biochemistry and Biophysics, Bureau of Biologics,
Food and Drug Administration, Bethesda, MD 20014

Groups A and C meningococcal polysaccharides are bacterial products responsible for the prevention of corresponding forms of meningitis in man. In this paper, we want first to review our earlier light-scattering work on the characterization of group C polysaccharides in KCl and sodium acetate buffers of varying ionic strengths with and without the addition of excess EDTA (2). By using the cumulants method of data analysis, we observed a large value of the normalized second moment of the linewidth distribution, evidence of a high degree of polydispersity (3). The polydispersity effect was further analyzed by means of an approximate histogram method which revealed a bimodal linewidth distribution for both groups B (4) and C polysaccharides. This conclusion was supported by agreements in the mean linewidth and the second moment of the linewidth distribution using two independent methods of data analysis. We shall present the temperature and the pH dependence of groups B and C polysaccharides as well as the effects of ion exchange on the group B polysaccharide using the more refined histogram technique, and secondly, present our polydispersity analysis in terms of distributions of molecular weight.

The bacteria Neisseria meningitidis produces several chemically distinct polysaccharides, three of which have been isolated and are designated Groups A, B and C meningococcal polysaccharides. Groups A and C polysaccharides are currently being used as vaccines for prevention of meningitis due to these organisms, whereas group B is non-immunogenic. It is believed that conformation and/or size may be related to immunogenicity, but the details are not clear. In this article, we hope to relate our light scattering data which have been accumulated over the past six years or so (1, 2, 3, 4) to our present studies

0097-6156/81/0150-0173\$06.75/0
© 1981 American Chemical Society

in order to formulate a more unified understanding on the solution properties of such clinically important polysaccharides.

Experimental

Isolation and Fractionation (5, 6). Cells of Groups A, B, and C *Neisseria meningitidis* were grown in a culture medium (about 60 l.) for a day. Group A had been isolated via a complex series of dialysis, extractions and treatment with pancreatic deoxyribonuclease. All the samples used for physio-chemical and light scattering studies referred to in this article were precipitated from the culture medium using cetavlon (hexadecyltrimethylammonium bromide). Yields were on the order of 1 g.

Preparative gel filtration was performed on an Agarose 4B column (5 x 80 cm) at 4°C. After the first filtration one lot of Group C was further fractionated using the same column and two pools were formed. The refractionated high and low molecular weight pools were designated as C-1 and C-2 fractions, respectively. A summary of the different samples used throughout this work is given in Table I.

Chemical Analysis. Group A polysaccharide is a homopolymer of D-N-acetyl-mannosamine phosphate which is partially O-acetylated. Groups B and C are both homopolymers of sialic acid, but group C is O-acetylated, whereas group B is not. The linkages for the three polysaccharides, as deduced from C¹³ NMR studies, as well as the number of monomeric units composing each chain, as measured by reducing group analysis with NaBH₄, are shown in Fig. 1.

Sample Preparation. We employed a variety of buffers and experimental conditions in our preparations. The techniques described here are general ones with the details noted where appropriate. All glasswares were boiled in soap solution and then rinsed exhaustively with deionized, distilled water. Small flasks for the stock solution and the light scattering cells were rinsed in an acetone vapor still to remove dust. Transfers of solutions were made through specially designed teflon septums (Reliance Glassworks) to further avoid contamination by dust particles in the air. Buffers were prepared using filtered (VM Millipore filters with a nominal pore diameter of 0.05 μ), deionized, doubly distilled water. Dry polysaccharides were stored below 0°C in dessicators between use. A stock solution was prepared at a concentration of about 6 mg/ml and allowed to equilibrate for 24 to 48 hours at room temperatures. The stock solution was then filtered (Millipore GS filter, pore diameter 0.22 μ) directly into the cell and diluted to known concentrations by weighing. The diluted solution was allowed to equilibrate over a period of another 24 hours before light scattering measurements. Each solution was centrifuged at 8,000 G for at least one hour immediately prior to measurements.

Table I
Sample Designation and Characteristics

	<u>C-1</u>	<u>C(II)</u>	<u>B(I)</u>
Fractionation	Agarose 4B	Refractionated	Unfractionated
M.W./Residue	290	290	289
Linkage	α 2-9	α 2-9	α 2-8
M.W./Chain	43,500	43,500	22,000
M.W. (M _w l.s.)	6.46×10^5	7.65×10^5	1.83×10^5
$\langle r_g^2 \rangle^{1/2}$ (Å)	345	414	263
A_2 ($\frac{\text{ml} \cdot \text{mole}}{\text{g}^2}$)	0.99×10^{-4} (pH = 7.0)	2.82×10^{-4} (pH = 5.5)	2.66×10^{-4} (pH = 5.6)

Buffer: 0.4 M KCl + 0.05 M NaAc.

t: 28⁰ - 30⁰C

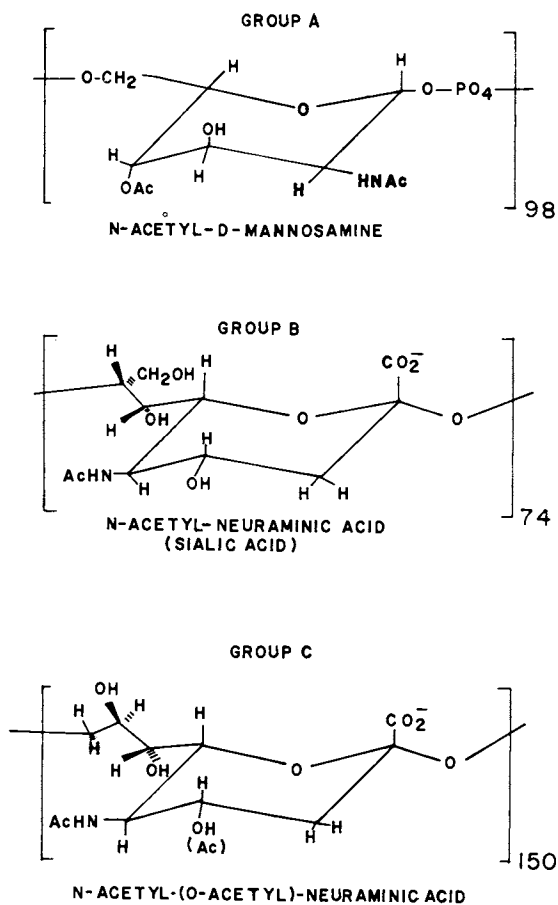


Figure 1. Chemical composition of Groups A, B, and C meningococcal polysaccharides (6)

A number of samples were dialyzed. We used dialysis tubing (A. H. Thomas H47) with a 3500 molecular weight cut-off. The dialyzate to sample ratio was about 500:1, and the dialyzate was changed on a daily basis. In one case, the solution was first dialyzed against 0.02 M EDTA for 3 days and then deionized water for five days. The dialyzed solution was used to study the pH dependence of the diffusion coefficient of the polysaccharide solution. Adjustments of pH were made using NaOH and HCl.

In order to study the effects of metal ion contamination, we passed 20 mg of group B polysaccharide dissolved in water through a 0.9 x 15 cm column packed with Dowex 50W-X2 (100-200 mesh) which had been washed with 6N HCl and rinsed until free of chloride ions. Polysaccharide concentrations were followed at $\lambda_0 = 210$ nm, pooled and lyophilized. The sample was then dissolved in 0.4M Tris (Trizma base, Sigma Chemical Co., No. T-1503) which has been titrated with H_3PO_4 to a pH of 6.74.

We also checked the gel fractionation procedure using a 1 x 90 cm column packed with Sephadex G-25 and a buffer of 100 mM KCl and 2 mM sodium cacodylate with a pH of 6 following adjustments using acetic acid.

Light Scattering Studies. Intensity and linewidth measurements were performed using primarily the instrument schematically shown in Fig. 2. The light source was a Spectra-Physics Model 165 argon ion laser operating at 488.0 nm with a power output typically between 100 and 500 mW. The beam was directed to the cylindrical light scattering cell (i.d. 8 mm) which was immersed in an index matching oil thermostat controlled to within 0.01°C. The detection system, consisting of a slit, a pinhole and an ITT FW130 photomultiplier tube, was mounted on a rotating arm which could be positioned to a precision of 2 minutes of arc. The entire spectrometer could be controlled by a Hewlett-Packard 9830A calculator. A similar set up utilizing Ortec ECL counting electronics was also used. The spectrometer was aligned and calibrated using pure benzene and various binary fluid mixtures which exhibited large amplitudes of local concentration fluctuations but small correlation lengths when compared with the wavelength of incident light.

We have checked that the measured correlation function at each scattering angle gives a linewidth which scales with K^2 to within 2%, where $K = 4\pi \cdot \sin \frac{\theta}{2} / \lambda$ with λ being the light wavelength in the scattering medium and θ , the scattering angle. The K^2 check, which was performed using both an aqueous suspension of Dow 910 Å latex spheres and NBS - 705A polystyrene in cyclohexane, insured that the spectrometer was properly calibrated for both intensity and linewidth measurements. In particular, we knew the amount of stray light which might give rise to a homodyne contribution and thereby distort the self-beating correlation function.

The angular distribution of scattered light was measured between 30° and 150° . Only those angles which were found during the alignment procedure to be accurate to within 1 (max. 2) percent were used. Two or three runs were made with each sample and the results at each angle typically agreed to within a few tenths of a percent. The Rayleigh ratio (R_{VV}) was then determined using Eq. (1):

$$R_{VV} = \left(I_{\text{ex}} - I_{\text{DK}} \right) \frac{\sin \theta}{\phi I_0} = \frac{R^*}{\phi} \quad (1)$$

Where I_{ex} is the measured, scattered intensity of the sample minus the measured scattered intensity of the buffer, both averaged over several runs, I_{DK} is the dark counts per second (~ 25 for our photomultiplier tube), I_0 is proportional to the laser incident intensity with variations in the 0.2% range, ϕ is an experimentally determined instrument constant relating the measured and the absolute values of the scattered intensity. The value of ϕ is determined each day using R_{VV} for pure benzene as measured by Ehl et al. (7).

The intensity correlation function was measured using a 96-channel Malvern single-clipped digital correlator which had been modified such that the last four channels were shifted 320 delay times to allow an accurate determination of the baseline. The measured and computed baselines typically agree to within 1%. Differences between these values indicated the presence of dust contamination. Correlation functions with greater deviations in baseline were analyzed only in a qualitative way since they were considered to be unreliable.

Analysis and Results

Intensity of Scattered Light. From measurements of scattered light intensity as a function of concentration and scattering angle, we can determine the weight averaged molecular weight, M_w ($= \sum N_i M_i^2 / \sum N_i M_i$ where N_i is the number of scatterers with molecular weight M_i); the z-averaged square of the radius of gyration, $\langle r_g^2 \rangle_z$ ($= \sum N_i M_i^2 r_{g,i}^2 / \sum N_i M_i^2$) and the second virial coefficient, A_2 . These parameters are related according to the classical Rayleigh-Gans-Debye theory, expressed in Eqs. (2) and (3) in limiting forms:

$$\lim_{\theta \rightarrow 0} \frac{HC}{R_{VV}} = \frac{1}{M_w} + 2 A_2 C \quad (2)$$

$$\lim_{C \rightarrow 0} \frac{HC}{R_{VV}} = \frac{1}{M_w} \left[1 + \frac{16\pi^2 n_o^2}{3\lambda_o^2} \langle r_g^2 \rangle_z \sin^2 \left(\frac{\theta}{2} \right) \right] \quad (3)$$

$H = 4\pi^2 n_o^2 (\partial n / \partial C)^2 / N_A \lambda^4$ with C, n, N_A , and $(\partial n / \partial C)$ being, respectively, the concentration (Wt/vol), the refractive index of the solvent, Avagadro's number, and the refractive index increment. The latter quantity has been measured for both Group B(I) (4) and C-1 (3) polysaccharides in buffers containing 0.4 M KCl and 0.05 M NaAc at 30°C and 488.0 nm. The results for our present study [C(II) polysaccharide] along with those from the literature (3, 4) are listed in Table I. Figure 3 shows a typical Zimm plot, which incorporates θ and C extrapolations on a single grid. The weight average molecular weight of C-1 polysaccharide determined by ultracentrifugation (5) appears to be lower. We can offer no explanation for the discrepancy. However, the molecular weight by light scattering does represent an absolute determination. We can obtain the concentration dependent radius of gyration by plotting HC/R_{VV} vs $\sin^2(\frac{\theta}{2})$ through Eq. (4):

$$\langle r_g^2(C) \rangle_z = \frac{\text{Initial Slope}}{\text{Intercept}} (1 + 2A_2 C M_w) \frac{3\lambda_o^2}{16\pi^2 n_o^2} \quad (4)$$

The results are shown in Fig. 4.

We must remember that the weight averaged molecular weight and, to a greater extent, the z-averaged radius of gyration are strongly influenced by the larger scatterers, i.e., by the higher molecular weight fraction of the polymer. Therefore, light scattering is enormously biased towards larger particles and only limited information is available on the smaller particles for both static and dynamical properties.

Time Correlation Function. The measured, self-beating intensity correlation function can be expressed as

$$G^{(2)}(\tau) = A(1 + \beta |g^{(1)}(\tau)|^2) \quad (5)$$

where A is the baseline, β is a function of the spectrometer and has a value of about 0.5 in our case, and $g^{(1)}(\tau)$ is the first order, electric field correlation function.

For a monodisperse sample of structureless particles, $g^{(1)}(\tau) = \exp(-\Gamma \tau)$, where Γ is the characteristic linewidth and

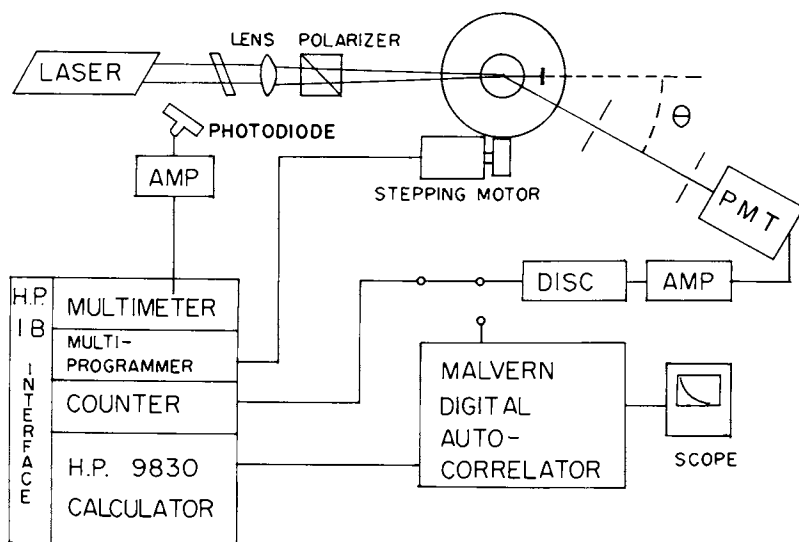


Figure 2. Schematic of instrument used for both light-scattering intensity and photon-correlation measurements

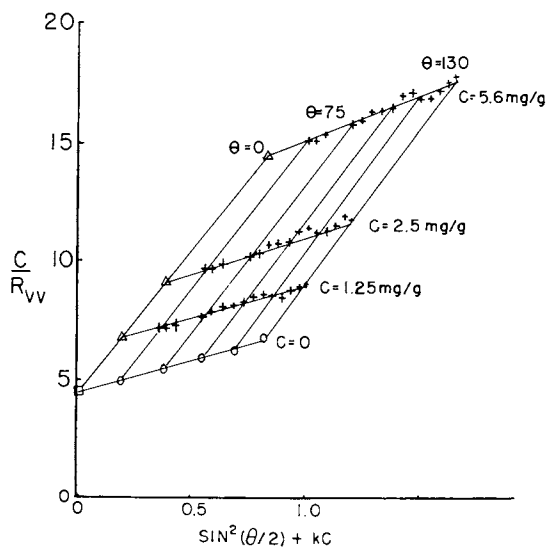


Figure 3. Zimm plot of *C*-polysaccharide (Sample C(II)) at 30°C

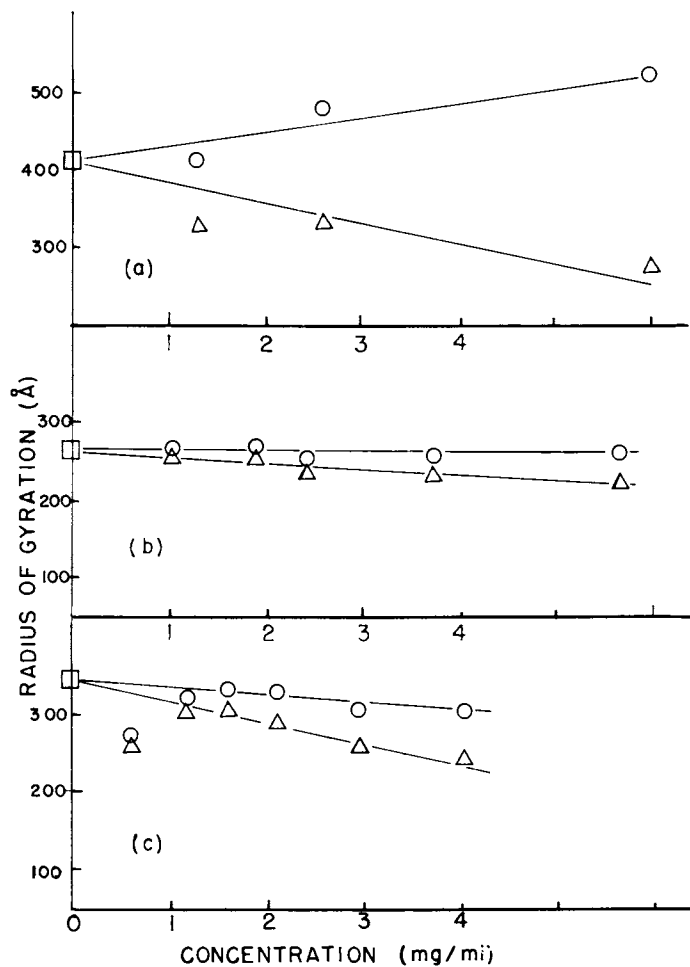


Figure 4. Plots of $\langle r_g^2(C) \rangle Z^{1/2}$ (○) and the apparent values, $\langle r_g^2(C) \rangle Z^{1/2} / (1 + 2A_2CM)$, (Δ) vs. concentration at 30° for Samples C(II): (a, present work), B(I) (b, Ref. 4), C-I (c, Ref. 3) polysaccharide.

τ ($\equiv J\Delta\tau$) is the delay time with J being the channel number and $\Delta\tau$, the delay increment, on the order of 2 to 40 microseconds for most of our samples. According to Eq. (5), the logarithm of the net, measured correlation function, $G^{(2)}(\tau) - A$, versus the delay time yields a straight line with a slope of $-\Gamma$. $\Gamma = DK^2$ where D is the translational diffusion coefficient. However, our solutions are polydisperse. Then,

$$g^{(1)}(\tau) = \int_0^{\infty} G(\Gamma) e^{-\Gamma\tau} d\Gamma \quad (6)$$

where $G(\Gamma)$ is the normalized distribution of linewidths.

The usual technique for handling Eq. (6) is to expand about $\bar{\Gamma} (= \int \Gamma G(\Gamma) d\Gamma)$. In practice, the resulting expression (7)

$$g^{(1)}(\tau) = \exp(-\bar{\Gamma}\tau) \left(1 + \frac{\mu_2\tau^2}{2!} - \frac{\mu_3\tau^3}{3!} + \dots \right) \quad (7)$$

is valid only for short delay times and fairly narrow distributions with

$$\mu_i = \int_0^{\infty} (\Gamma - \bar{\Gamma})^i G(\Gamma) d\Gamma \quad (8)$$

The width of the distribution can be characterized by the normalized variance, or polydispersity index, which is $\mu_2/\bar{\Gamma}^2$. For Dow "monodisperse" latex spheres, the value of $\mu_2/\bar{\Gamma}^2$ is less than 0.05. For a commercial polyacrylamide sample with molecular weights ranging from 4×10^4 to 4×10^6 , $\mu_2/\bar{\Gamma}^2$ can be between 0.25 and 0.35. The polydispersity index for "fractionated" meningococcal polysaccharide solutions is generally in excess of 0.6. Such a high value of $\mu_2/\bar{\Gamma}^2$ is suggestive of a multi-modal linewidth distribution and demands more sophisticated and careful data analysis in order to obtain meaningful results. The cumulants method (8), which was used in our earlier papers, (1, 2, 3) becomes more difficult to utilize, especially when Eq. (7) is truncated after the quadratic term. The technique remains useful if we hold the scattering angle and the delay time increment constant and study only changes induced by perturbing the system. However, we probe $G(\Gamma)$ differently when we vary the delay time range of our experiments. Therefore, different apparent values of $\bar{\Gamma}$ and μ_2 may appear for the same sample.

In our fourth paper (4) a new approach was introduced which approximates $G(\Gamma)$ by a histogram. The integration can then be done for each step, and we obtain

$$|g^{(1)}(\tau)| = \sum_{i=1}^N \frac{G(\Gamma_i)}{(-\tau)} \left\{ \exp[-(\Gamma_i + \frac{\Delta\Gamma}{2})\tau] - \exp[-(\Gamma_i - \frac{\Delta\Gamma}{2})\tau] \right\} \quad (9)$$

where N is the number of steps in a histogram, each step i is $\Delta\Gamma$ sec^{-1} wide with a height of $G(\Gamma_i)$. The fit is accomplished using a non-linear least squares technique described in detail elsewhere (9). Figures 5 and 6 show, respectively, typical histograms of Groups B and C polysaccharides in 0.4 M KCl and 0.05 M NaAc buffer at pH=5.5 and 30°C and a plot of the deviation of the correlation function computed from the fitted histogram and the measured correlation function. Deviation plots showing errors which are either non-random or greater than one to two percent are generally considered unreliable in view of the precision of our measurements. The advantages of the histogram technique can be enumerated as follows:

- 1) No a priori form of the distribution function is assumed.
- 2) The entire correlation function profile is taken into account in our data analysis.
- 3) We can deduce the linewidth (and therefore the diffusion coefficient) as well as the amplitude of each step in the histogram.
- 4) The resolution of the approximation, i.e., the number of steps, can be adjusted dependent upon the resolution and precision of the correlation function.
- 5) The moments of the distribution can be computed once $G(\Gamma)$ has been approximated.

Values of $\bar{\Gamma}$ and $\mu_2/\bar{\Gamma}^2$ by this powerful, new approach are in agreement with those obtained by the more established cumulants technique, as listed in Table II and offer a wealth of new information. In particular, we show the effects of temperature on the distribution in Fig. 7. The variation of the low salt sample produced by the pH changes is shown in Fig. 8. The concentration dependence of diffusion coefficients for C(II) polysaccharide in high salt buffer is tabulated in Table III. Figure 9 shows the angular dependence of $\bar{\Gamma}_{\text{high}}$, $\bar{\Gamma}_{\text{low}}$, and $\bar{\Gamma}$ for group C(II) polysaccharide. Finally, Figure 10 shows the results obtained after group B polysaccharide has passed through an ion-exchange column.

Interpretation of Data. In this article we strive to unify the accumulated data (1, 2, 3, 4) with the present study. However, in comparing results among different sample preparations many factors, such as the time of harvesting the polysaccharide, purification techniques, and preparative fractionation, will result in samples of slightly different characteristics. In one preparation, we could not even dissolve the group C polysaccharide in buffer solution before further treatment. Thus, we are not surprised to find the molecular weight difference between C-1 and C(II) polysaccharides as listed in Table I,

Figure 5. Histograms for C(II) (---) and B(I) (—) polysaccharides in 0.4M KCl, 0.05M NaAc buffer at pH = 5.5
 $D_{B(I)} = 1.74 \times 10^{-7} \text{ cm}^2/\text{s}$. $D_{C(II)} = 1.40 \times 10^{-7} \text{ cm}^2/\text{s}$.

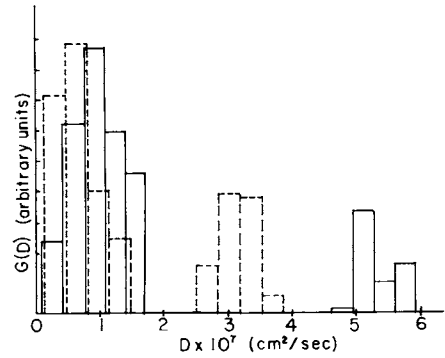


Figure 6. A deviation plot for the Group C histogram in Figure 5. $Dev = 100[\text{calculated } g^{(1)}(\tau) - \text{experimental } g^{(1)}(\tau)] / \text{experimental } g^{(1)}(\tau)$, $g^{(1)}(\tau)$ is plotted also.

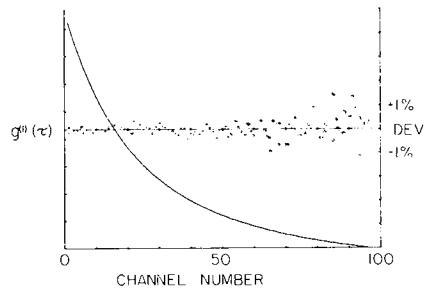


Table II

Comparison of Cumulants and Histogram Techniques

C(II) Polysaccharide in KCl-NaAc Buffer*
 pH = 5.5 ; t = 30°C

Concentration (mg/ml)	θ (deg)	Cumulants		Histogram	
		$\bar{\Gamma}(s^{-1})$ $\times 10^{-3}$	$\mu_2/\bar{\Gamma}^2$	$\bar{\Gamma}(s^{-1})$ $\times 10^{-3}$	$\mu_2/\bar{\Gamma}^2$
5.617	90	7.98	0.80	8.17	0.87
3.428	90	-	-	7.53	0.80
2.91	60	4.01	0.64	4.11	0.72
2.91	90	8.17	0.60	8.18	0.68
2.91	120	12.4	0.63	12.6	0.67
1.956	90	6.63	0.65	6.97	(0.77)
1.252	90	8.48	0.32	8.82	0.39

* 0.4 M KCl + 0.05 M NaAc.

Table III

Concentration Dependence of C(II)
 Polysaccharide in KCl-NaAc Buffer
 $\theta = 90^\circ$; t = 30°C

Concentration (mg/g)	\bar{D}	\bar{D}_{slow}	\bar{D}_{fast}	A_s/A_f
	$\times 10^7 \text{cm}^2/\text{sec}$	$\times 10^7 \text{cm}^2/\text{sec}$	$\times 10^7 \text{cm}^2/\text{sec}$	
1.252	1.5	0.4	2.8	-
1.956	1.2	0.7	3.0	-
2.591	1.4	0.6	3.0	2.0
3.428	1.3	0.7	-	(2.5)
5.617	1.4	0.5	3.1	1.8

Figure 7. Histograms of diffusion coefficients of Sample C(II) in KCl buffer at different temperatures. Diffusion coefficients corrected to the viscosity of water at 30°C $D_{w,30} = D_{KCl,T} \times \eta_{KCl}/T \times 303/\eta_{w,30}$.

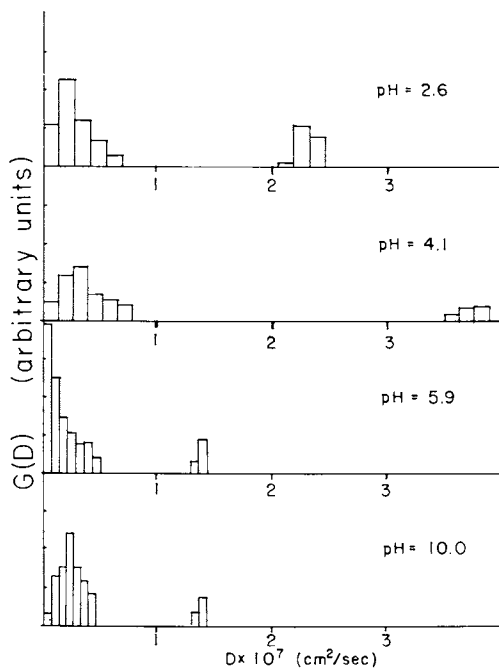
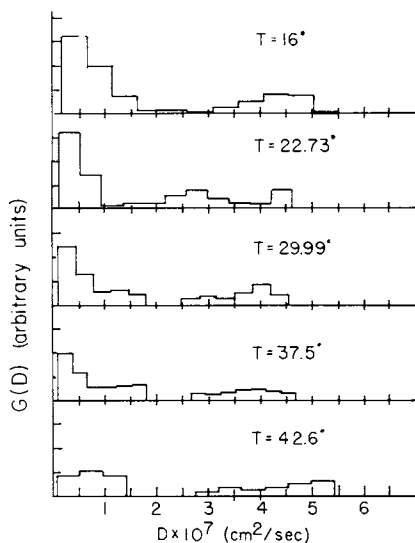


Figure 8. Histograms of diffusion coefficients of Sample C(II) at $t = 30^\circ\text{C}$ in water solutions adjusted to the indicated pH with HCl or NaOH. The natural pH is 4.1 at a concentration of about 1 mg/mL.

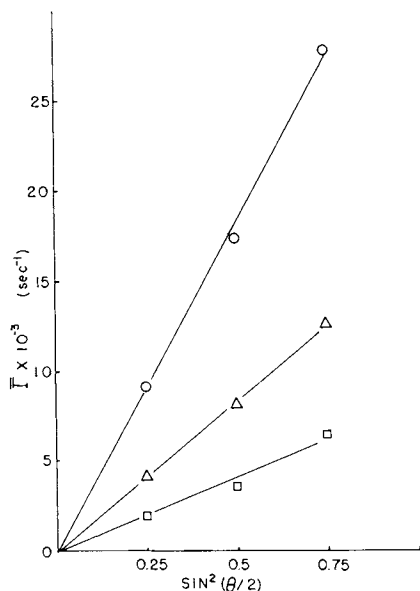


Figure 9. \bar{D} for the entire histogram (Δ), for the low frequency component (\square) and for the high-frequency component (\circ) vs. $\sin^2(\theta/2)$ for C(II) polysaccharide, 2.59 mg/gm, 0.4M KCl at pH 5.6.

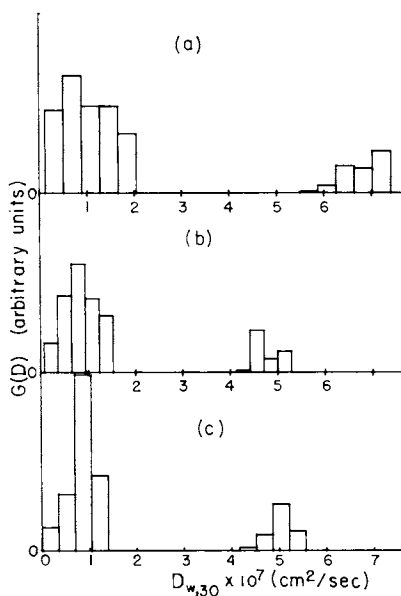


Figure 10. Histograms for B(1) polysaccharide under different conditions: (a) in 0.4M tris buffer, pH = 6.7, $t = 22.7^\circ\text{C}$ after ion exchange, $\bar{D}_{30,30} = 1.42 \times 10^{-7} \text{ cm}^2/\text{s}$; (b) in 0.4M KCl, pH = 5.6, $t = 35^\circ\text{C}$, $\bar{D}_{30,30} = 1.74 \times 10^{-7} \text{ cm}^2/\text{s}$; (c) in 0.4M KCl, pH = 5.6, $t = 28^\circ\text{C}$ $\bar{D}_{30,30} = 1.67 \times 10^{-7} \text{ cm}^2/\text{s}$. Diffusion coefficients corrected to the viscosity of water at 30°C .

The most striking and intriguing result of our analysis of the intensity correlation function is the bimodality of the linewidth distribution function. While we have observed that a broad molecular weight distribution of polyacrylamide can give rise to an apparent bimodal histogram (14), the ratio of the area of the slow peak to the area of the fast peak is generally in excess of 50:1 indicating the presence of a long tail in the low molecular weight portion of the distribution function. However, the polysaccharide solutions consistently yielded comparable area ratios in the bimodal linewidth distribution as shown in Table III. We are firmly convinced that the presence of a fast peak is neither an artifact of the histogram technique nor is it a result of improper solution preparation.

The existence of a bimodal linewidth distribution may be attributed to several factors. When a polymer is large, interference between segments of the same chain will give rise to an intramolecular scattering contribution to the linewidth. We have ruled out this possibility since $\langle r^2 \rangle^{1/2} \cdot K$ has a maximum value of 1.2 and is often much less than $\frac{1}{2}$ in our experiments. Thus, our experiments cannot observe the contributions due to internal motions and they amount to, at most, one to two percent of the total scattered intensity. (10) We have also made other studies whereby a second faster peak can be attributed to a pseudo-gel motion in semidilute solutions (11). This explanation is unreasonable because the concentrations of our solutions are very small. We should not have reached the semidilute regime.

A rigid rod model has been proposed for the meningococcal polysaccharides (6) as well as the bacterial polysaccharide produced by *Xanthomonas campestris* (12) (Xanthan gum). Such a model assumes the form of the correlation function to be (10)

$$g^{(1)}(\tau) \approx S_0(KL) \exp(-DK^2\tau) + S_1(KL) \exp[-(DK^2 + 6\theta)\tau] \quad (10)$$

where L is the length of the thin rod, θ is the rotational diffusion coefficient, $S_0(KL)$ and $S_1(KL)$ are complicated functions of KL . At low values of KL (up to about 2), the major contribution to $g^{(1)}(\tau)$ is from the first term in Eq. (10). As the angle and/or the length of the rod increases, S_1 increases and the correlation function decays with two characteristic times for a monodisperse sample. The analysis is generally complicated by the fact that we must assume a prolate ellipsoidal form to determine the length and the axial ratio from θ , an approximation which is valid only for very long, thin, rodlike molecules. Furthermore, corrections may exist for coupling between rotational and translational diffusion, flexure of the rod (13) and polydispersity. We have taken two approaches in comparing our results to the rigid rod model. First, we have used the literature value for the axial ratio (6), 50 to 60, and our measured value of the

translational diffusion coefficient, from the first peak of the histogram as indicated by Eq. (10), to compute the dimensions of the ellipsoid of revolution from Perrin's equation:

$$D = k_B T / \frac{6\pi\eta a (1 - b^2/a^2)^{1/2}}{\ln[(1 + (1 - b^2/a^2)^{1/2})/(b/a)]} \quad (11)$$

where a and b are the semi-major and semi-minor axes, respectively, η is the solvent viscosity, k_B is Boltzmann's constant and T is the temperature. The results indicate a molecule about 500 nm long and 10 nm in diameter with a volume of 10^{-17} cm³. The histogram for such a molecule at $\theta = 60^\circ$, using Eq. (10), should have peaks at 2600 sec⁻¹ and 3200 sec⁻¹ with the higher frequency peak having an area of about 60% as estimated from Fig. (8.7.1) of reference 10. In fact, at $\theta = 60^\circ$ our results typically show a slow peak at 2000 sec⁻¹ and a faster peak at 10,000 sec⁻¹, the higher frequency component being 30% of the total area. Furthermore, the partial specific volume (\bar{v}) for group C polysaccharide (both C-1 and C-2), 0.718 ml/gm (6), has been used to compute the molecular volume

$$v_m = \frac{\bar{v}M}{N_a} \quad (12)$$

The results for sample C-1 are 3.88×10^{-19} cm³ and 6.14×10^{-19} cm³ using the molecular weight measured by sedimentation and light scattering, respectively. The results in both cases are more than an order of magnitude smaller than what we have deduced using this model.

Our second approach was to subtract $\bar{\Gamma}$ (slow component) from $\bar{\Gamma}$ (fast component). The remainder, divided by six, should give θ independent of angle and concentration. The remainder we compute varies with angle, precisely as K^2 in fact, and is concentration dependent. Furthermore, an anisotropic, rodlike molecule of the dimensions necessary to produce a bimodal linewidth distribution function should give rise to a depolarized correlation function for either group B or group C polysaccharide. In light of the above analysis, we are forced to abandon the rigid rod hypothesis and seek another model which explains the behavior of the polysaccharides observed with the histogram technique.

We believe the most feasible explanation of the bimodal behavior in linewidth to be two distinct molecular weight fractions. The inability to separate the two may be due to an equilibrium between them, or unknown inadequacies in the gel filtration techniques used. The B-polysaccharide sample which we passed through an analytical column (1 cm x 90 cm packed with sepharose 4B) was diluted to the extent that the precise data required for a histogram analysis was difficult to obtain. Second order cumulants fits one, two, three and four days after

filtration showed significant scatter in values of $\bar{\Gamma}$ and $\mu_2/\bar{\Gamma}^2$, but the $\bar{\Gamma}$ value showed an increasing trend. On the fifth day we succeeded in obtaining correlation function data of sufficient quality to perform a histogram fit. The results were typical of those samples which had not been subjected to analytical fractionation. The fact that unfiltered, Millipore filtered, and gel filtered solutions all give bimodal distributions in linewidth shows that our clarification techniques have not altered the characteristics of the polysaccharides.

We have tried to perturb the equilibrium between the two fractions by varying the temperature from 16°C to 42°C. Any dissolution or further aggregation of the larger sized fraction would result in changes of the peak area ratios. Differential conformational changes of either fraction would be seen as changes in the diffusion coefficients. As seen in Figs. 7 and 11, and Table IV no significant changes in the group C sample were observed. The group B sample had been passed through an ion exchange column and dissolved in Tris buffer. Therefore, the comparison in Fig. 11 is not direct. Nonetheless, no trend is observed which would support a temperature dependent equilibrium.

We have used high salt buffers throughout the bulk of our work in order to avoid electrostatic interactions. The value of 0.4M KCl was chosen in light of the results of Paper II (2) which showed linewidth variations when the salt content of the buffer was changed from 0 to 1M. Above 0.4M no changes were observed. We have also removed cations from a group B sample by ion exchange in order to see if they have any effect on configuration or aggregation. Again, no clear trend is visible as shown in Fig. 10.

Finally, we have measured the correlation function of a group B sample which had been extensively dialyzed for many days. As seen in Fig. 8 and Table V, no significant changes are observed as the pH changes from 2 to 10. The interpretation of this data is complicated by the fact that we used pure water rather than a high salt buffer. Therefore, changing the pH, (with HCl or NaOH) changed the salt concentration by a small absolute amount, but a large relative amount. One would expect, however, to see a change in the diffusion coefficient as the polysaccharide becomes increasingly ionized at higher pH values and repulsions between the sialic acid monomers increase.

We do observe, however, a substantial difference in the relative areas of the two histogram peaks. Undialyzed group B polysaccharide (sample B(I)) has been measured in pure water (4) at a concentration of 2.975 mg/g at scattering angles of 60° and 90°. In both cases the ratio of the areas ($A_{\text{slow}}/A_{\text{fast}}$) is about 5, which is typical for most undialyzed samples we have measured. The values we observe for the exhaustively dialyzed sample (Table V) indicate that a low molecular weight component has leaked out of the dialysis sac. This interpretation suggests that the smaller molecules are less than 3500 gm/mole, the

Table IV

Temperature dependence of C(II) polysaccharide
5.6 mg/g in 0.4M KCl buffer

$T(^{\circ}\text{C})$	$D_{\text{Total}, 30^{\circ}\text{w}}^{(a)}$ $\times 10^7 \text{cm}^2/\text{sec}$	$D_{\text{slow}, 30^{\circ}\text{w}}^{(a)}$ $\times 10^7 \text{cm}^2/\text{sec}$	$D_{\text{fast}, 30^{\circ}\text{w}}^{(a)}$ $\times 10^7 \text{cm}^2/\text{sec}$	$\frac{\text{Area}(\text{slow})}{\text{Area}(\text{fast})}$
16.0 $^{\circ}$	1.4	0.58	3.5	1.9
22.7 $^{\circ}$	1.6	0.45	3.1	1.3
29.99 $^{\circ}$	1.7	0.64	3.6	1.9
37.5 $^{\circ}$	1.7	0.73	3.8	2.0
42.6 $^{\circ}$	2.4	0.74	4.3	1.2

(a) corrected to the viscosity of water at 30 $^{\circ}$ C. The results are qualitative and should not be taken on a quantitative basis.

Table V

pH dependence of B(I) polysaccharide at 30 $^{\circ}$ C

pH	D_{total} $\times 10^7 \text{cm}^2/\text{sec}$	D_{slow} $\times 10^{-7} \text{cm}^2/\text{sec}$	D_{fast} $\times 10^{-7} \text{cm}^2/\text{sec}$	$\frac{\text{Area}(\text{slow})^{(a)}}{\text{Area}(\text{fast})}$
2.6	0.39	0.26	2.3	14
4.1	0.44	0.34	(3.7)	34
5.9	0.18	0.16	1.4	44
10.0	0.27	0.25	1.4	40

(a) Dialysis has reduced the amount of the smaller size fraction significantly.

cutoff for our dialysis tubing and only a fraction of the molecular weight of a complete chain as deduced by reducing group analysis. In light of our second paper (2), which showed changes in Γ induced by an excess of EDTA, we cannot, with certainty, relate the depletion of the low molecular weight fraction to dialysis alone. Further investigations are under-way to separate the effects of dialysis alone and the presence of EDTA. We have also observed such a dialysis procedure with group B results in a significant weight loss of material, while dialysis of group C against water or buffer does not. The weight loss also suggests a leakage of a very low molecular weight component.

Transformation to Molecular Weight. If the linewidth distribution represents only translational diffusional motions of a bimodal molecular weight distribution, we may be able to transform the measured linewidth distribution to a molecular weight distribution. The procedure has been outlined in paper IV (4). Briefly, we make use of the Mark-Houwink expression relating the diffusion coefficient at infinite dilution (D_0), the molecular weight (M), an exponent which depends on the hydrodynamics of the particle (B) and a proportionality constant (k_T):

$$D_0 = k_T M^{-B}. \quad (13)$$

Furthermore, we use the relationship

$$G(\Gamma_i) \Delta\Gamma = f^*(M_i) \Delta M_i M_i^2 P(\theta, M_i) \quad (14)$$

where $f^*(M_i)$ is the unnormalized molecular weight distribution, $P(\theta, M_i)$ is the particle scattering factor at scattering angle θ for particles of molecular weight M_i and ΔM_i is the width of the i^{th} step. Equation (13) transfers the linewidth axis to molecular weight in a non-linear fashion, therefore although $\Delta\Gamma$, representing the width of each histogram step, is constant, ΔM_i is not. The value of M_i in Eq. (14) is computed from the value of Γ_i at the center of the step in histogram space. The value of B is known for certain special cases such as rods ($B=1$), coils ($B=1/2$) and spheres ($B=1/3$). The choice of a hydrodynamic model will also give expressions for $P(\theta, M_i)$ (15).

The values of D_0 for each step in the histogram are determined through Eq. (15).

$$D_{0,i} = D_i / (1 + k_D C) = \Gamma_i / k^2 \cdot (1 + k_D C) \quad (15)$$

where k_D is obtained by measuring the diffusion coefficient as a function of concentration C . We choose k_D by successive iterations until M_w , computed from $f(M)$, matches the measured value.

For the polysaccharides, we cannot assume that the two molecular weight fractions have the same shape. Therefore, equations (13) and (14) must be applied to each peak independently using $k_D^{(1)}$, $B^{(1)}$, $P(\theta, M_i)^{(1)}$, $k_D^{(2)}$, $B^{(2)}$, and $P(\theta, M_i)^{(2)}$ for the high molecular weight (low frequency) peak and the low molecular weight (high frequency) peak, respectively. The measured values of $k_D^{(1)}$ and $k_D^{(2)}$ are, respectively 16 g/g and 81 g/g. Furthermore, since the conformation of either peak is unknown, $B^{(1)}$ and $B^{(2)}$ are also unknown. We assume that each fraction consists of either random coils or hard spheres, for which B and $P(\theta, M)$ are well known. The transformation is then made using the four combinations of random coils and hard spheres for the two fractions and the results are checked against the measured values, both static and dynamical, using the scheme outlined in Fig. 12.

We start with the measured correlation function and compute the moments of the distribution using the cumulants technique and the approximate $G(\Gamma)$ using the histogram method. $\langle D \rangle_z = (\bar{\Gamma}/K^2)$ from both analysis must agree, as indicated in Table II. Then, $f(M)$ is computed, as described, and the values of M_z , M_w and M_n are determined. If the transformation is made using $G(\Gamma)$ deduced by the histogram technique directly, we find $M_n : M_w : M_z$ on the order of 1 : 2 : 200, which we consider reasonable. This is caused by the inherent tendency of the histogram fit to extend to very low frequency values, resulting in a very high molecular weight step in the molecular weight histogram. We have arbitrarily set a lower limit in Γ -space and refit the correlation function. Furthermore, by simply ignoring the lowest frequency step of the original histogram, we find the resulting value of $\langle D \rangle_z$ to remain essentially unchanged to within about 5%. It is this modified histogram in Γ -space which we use as the starting point for our transformation. The light scattering z -averaged diffusion coefficient, and z -averaged square of the hydrodynamic radius are then computed from $f(M)$ using Eqs. (16) and (17), respectively.

$$\langle D \rangle_{z, L.S.} = \frac{\sum P(\theta, M_i) N_i M_i^2 D_{o,i}}{\sum P(\theta, M_i) N_i M_i^2} \quad (16)$$

$$\langle r_h^2 \rangle_{z, L.S.} = \frac{\sum P(\theta, M_i) N_i M_i^2 r_{h,i}^2}{\sum P(\theta, M_i) N_i M_i^2} \quad (17)$$

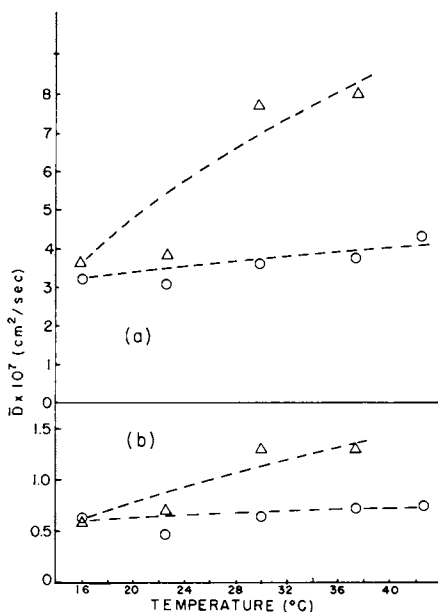


Figure 11. $D_{w,30}$ for the fast peak (a) and slow peak (b) for Sample C(II) (○) in 0.4M KCl buffer and Sample B(I) (△) in 0.4M tris buffer

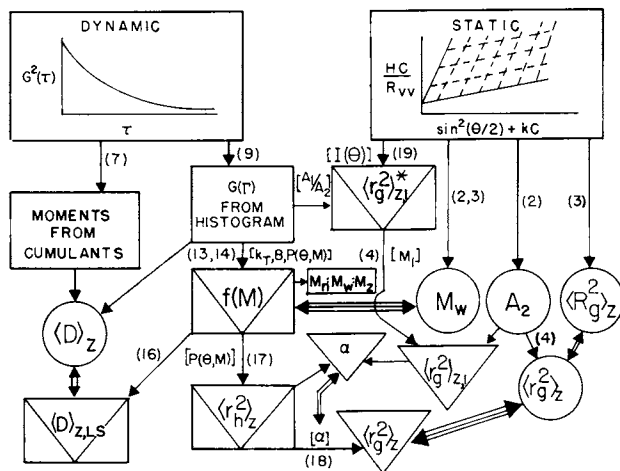


Figure 12. Flow chart indicating the scheme for deducing measurable properties from the linewidth distribution and molecular-weight distribution and comparing them to the observed, static, and dynamical results: (○) measured values and (△) model-dependent, deduced quantities. Parentheses refer to equation numbers and brackets indicate important parameters required for each step. Single arrows indicate direct calculations, double arrows are comparisons, and triple arrows show values that are forced to agree. Gyration radii not capitalized are concentration dependent, the argument, (C), being omitted for clarity.

N_i is the number of molecules with molecular weight $M_i (= f(M) \times \Delta M_i)$, $D_{o,i} = k_B T M_i^{-B}$ and $r_{h,i} = k_B T / (6\pi\eta D_{o,i})$ with k_B , T , and η being Boltmann's constant, the temperature ($^{\circ}K$) and the solvent viscosity, respectively. The particle scattering factors, $P(\theta, M_i)$, must be taken into account at finite angles in order to allow a comparison of the computed values with measured values, which are intrinsically weighted by $P(\theta, M_i)$. The results of the transformation using various hydrodynamic models ($B^{(i)}$'s and $P(\theta, M_i)^{(i)}$'s) are reported in Table VI for a variety of scattering angles and concentrations. We observe that the computed values of $\langle D \rangle_{z,0}$ are independent of the model chosen. Model dependent parameters are indicated in the flow chart by triangles, but we have emphasized those values which are functionally model dependent, yet in fact model insensitive by enclosing the triangle in a square. $\langle D \rangle_{z,0}$ values, when multiplied by $(1 + k_D C)$ give the measured $\langle D \rangle_z$ values precisely.

A further means of determining the characteristics of a macromolecule is to compare the radius of gyration, a static property, with the hydrodynamic radius, a dynamical property. The ratio of the two, $\alpha = r_h / r_g$, is known to be 1.29 for compact spheres and 0.665 for random coils. Again, we must deduce α_1 and α_2 independently, which can be done in two different ways. First, we compute $\langle r_g^2(C) \rangle_z$ from $f(M)$ using Eq. (18):

$$\langle r_g^2(C) \rangle_{z,j} = \frac{\sum_i P(\theta, M_i) N_i M_i^2 (r_{h,i} / \alpha_j)^2}{\sum_i P(\theta, M_i) N_i M_i^2} \quad (18)$$

The index j indicates either the first or second peak, while i runs over the peak in question. The values which correspond to $\langle r_g^2(C) \rangle_z$ are shown in Fig. 4. In a z -average weighting process, only α_1 , for the high molecular weight fraction, influences the radius of gyration for the entire system.

The second technique for determining α was partially outlined in paper IV. We use the ratio of the areas under the two histogram peaks, (A_1/A_2) in Γ -space, which are proportional to the scattered intensity from each fraction, to deduce the scattered intensity of the large fraction independently as a function of scattering angle. $\langle r_g^2(C) \rangle_z^*$ is then computed through Eq. (19):

$$\langle r_g^2(C) \rangle_z^* = \frac{\text{initial slope}}{\text{intercept}} \times \frac{3\lambda_o^2}{16\pi^2 n_o^2} \quad (19)$$

We have obtained the slope both by using (A_1/A_2) and the total intensity, $I_T(\theta)$, at 3 angles in a straight forward way (method A), and by assuming a form for the low molecular weight fraction to deduce $\langle r_g^2(C) \rangle_{z,2}$ (method B), where the subscript 2 denotes the smaller size fraction. From $\langle r_g^2(C) \rangle_{z,2}$, we compute $C/I_2(\theta)$ and

Table VI

Fitting parameters for molecular weight transformation

C, θ	$P(\theta)$ (1)	B (1)	B (2)	$\langle D \rangle^z$ $\times 10^7$ (a)	$\langle D \rangle_{z20}$ cm/sec (b)	$\frac{2}{g} \langle r^2 \rangle^{1/2}$ \AA	$M_h : M_w : M_z$
2.59 mg/g $\theta = 60$	R.C.	1/2	1/3	1.40	1.22	478	1 : 3 : 29
	H.S.	1/3	1/2	1.40	1.22	482	1 : 2 : 26
2.59 mg/g $\theta = 90$	H.S.	1/3	1/3	1.41	1.22	482	1 : 3 : 105
	H.S.	1/3	1/2	1.41	1.22	483	1 : 3 : 29
	R.C.	1/2	1/3	1.41	1.22	479	1 : 3.5 : 19
2.59 mg/g $\theta = 120$	H.S.	1/3	1/2	1.67	1.45	475	1 : 1.8 : 8.3
	R.C.	1/3	1/2	1.20	1.08	437	1 : 2.7 : 11.9

(a) measured value

(b) computed value from $f(m)$, corrected to infinite dilution(c) R.C. - Random coils $P(\theta, M) = 2/Q^2 \cdot [\exp(-Q) + Q - 1]$ $Q = K^2 r_g^2$ (d) H.S. - Hard spheres $P(\theta, M) = 3/Q^3 \cdot (\sin Q - \cos Q)$ $Q = Kr_h$

$I_T(\theta) - I_2(\theta)$ at all measured angles in order to obtain the desired $I_1(\theta)$. Since $\langle r_g^2(C) \rangle_{z,1}^{1/2}$ is small ($<100\text{\AA}$), the slope is flat and independent of the model chosen. Both means of obtaining $\langle r_g^2(C) \rangle_z^*$ are in agreement and the results are tabulated in Table VII. In order to make a correct comparison of $\langle r_g^2(C) \rangle_{z,1}$ to $\langle r_h^2(C) \rangle_{z,1}$ (note that this is not $k_B T / 6\pi\eta \langle D \rangle_{z,1}$, which is weighted differently) we must correct $\langle r_g^2(C) \rangle_{z,1}^*$ by $1 + 2CA_2^{(1)} M_w^{(1)}$. This was not done in Paper IV causing a disagreement between these results, and the results reported here. We have assumed $A_2^{(1)}$ to be equal to A_2 as obtained from the Zimm plot directly, but we can only estimate $M_w^{(1)}$ to be greater than the measured M_w for the solution (see Table VII).

Conclusions

Our analysis relies heavily on the histogram technique for determining the linewidth distribution, which we have found to be bimodal under all conditions. Numerous preparations of polysaccharide solutions using the same dry polysaccharide have been prepared during the course of our studies by means of the histogram method. In addition, we have used two light scattering spectrometers whose reliability had been checked independently a number of times by different operators. Therefore, we could rule out stray light contributions and dust contamination. If these effects were significant, we would have obtained different histogram profiles. The fact that we have obtained similar results throughout our studies supports our confidence in the histogram approach. However, we must concede that it is entirely a different matter when we try to relate the linewidth distribution to the physical properties of the solution. While such a bimodal linewidth distribution function suggests the dynamics due to rod-like molecules, in keeping with currently accepted models on similar polysaccharides, the details of the histogram, e.g. the way the peaks change with varying scattering angle and solution environment, force us to conclude that a rod-like molecular hypothesis is not tenable. Rather, we suggest the presence of two molecular weight fractions with different conformations. Gel permeation chromatography has failed to separate the two fractions. We have also shown that the ratios of the two fractions are virtually unaffected by changes in temperature and pH. Dialysis against an EDTA solution does deplete the smaller fraction preferentially, but the details of this process have not yet been explored fully.

We have attempted to transform the linewidth distribution to a molecular weight distribution and, in the process, determine the shape of the larger fraction. While actual values of M_w for each fraction are inaccessible, results indicate the smaller fraction to be on the order of 1.5×10^5 g/mole and the larger one about 1×10^6 g/mole or greater. These values correspond to aggregates of 4 and 15 or more of the polysaccharide chains. The shape of

Table VII
 α 's deduced from static and dynamic measurements
of C(II) polysaccharides in KCl buffer

Conc mg/g	$\frac{\langle r^2 \rangle_{z,1}}{(\theta=90^\circ) \alpha}$	$\frac{\langle r^2 \rangle_{h,z,1} * 1/2 \alpha}{\alpha}$	Method	$\frac{\langle r^2 \rangle_{z,1}^{1/2} (\text{assumed})}{M_v}$ g/mole	α_1
1.25	433	334	B	(610,000) (1 x 10 ⁶) (2 x 10 ⁶)	0.85 0.76 0.63
2.59	510	388 400	B A	(610,000) (1 x 10 ⁶) (2 x 10 ⁶)	0.89 0.76 0.59
5.61	608	349	B	(610,000) (1 x 10 ⁶) (2 x 10 ⁶)	0.92 0.76 0.57

the smaller fraction is undetermined, as is expected from the nature of the light scattering experiment. If we assume both fractions to be of the same conformation, ie, $B^{(1)} = B^{(2)}$, we must further assume $k_T^{(1)} = k_T^{(2)}$. The consequences are that $M_n : M_w : M_z$ is on the order of 1 : 2 : 100, even using the modified $G(\Gamma)$ histogram. We consider this ratio to be unreasonable and conclude that the two fractions have different shapes. The values of α range from 0.70 to 0.95, as can be seen from Tables VI and VII. We may rule out the hard sphere conformation and conclude that the larger fraction consist of molecules more like stiff coils.

It should be noted that our analysis does not preclude the possibility that there are impurities in our samples. Furthermore, the presence of even a trace amount of an unknown impurity in our sample may be the cause of the postulated aggregation process. Finally, the histogram procedure requires that segments with very small amplitudes be set equal to zero. Therefore, the region between the two histogram peaks may be taken as having a very small, but not necessarily zero, contribution to the total distribution. The observed bimodal distribution, in fact, could be a very broad unimodal distribution with peaks at the extremes and a central valley, or a more complicated multimodal distribution which our histogram approximation cannot accomodate.

Literature Cited

1. Chen, F.C., Tscharnuter, W., Schmidt, D., Chu, B., Biopolymers, (1974) 13, 2281.
2. Fujime, S., Chen, F.C., Chu, B., Biopolymers, (1977), 16, 945.
3. Tsunashima, Y., Moro, K., Chu, B., Biopolymers, (1978), 17, 251.
4. Gulari, E., Chu, B., Biopolymers, (1979), 18, 2943.
5. Liu, T.Y., Dunne, F.T., Gotschlich, E.C., Eur. J. Biochem, (1977).
6. Liu, T.Y., Gotschlich, E.C., Egan, W., Robbins, J.B., J. Infect. Dis., (1977), 136, 571.
7. Ehl, J., Loucheux, C., Reiss, C., Benoit, H. Makromolekular Chem., (1964), 75, 35.
8. Koppel, D.E., J. Chem. Phys. (1972), 57, 4814.
9. Chu, B., Gulari, E., Gulari, E., Phys. Scr. (1979) 476.
10. Berne, B., Pecora, R., "Dynamic Light Scattering" Wiley Interscience, New York Chapter 8.
11. Chu, B., Nose, T., Macromolecules (1979), 12, 599.
12. Rinaudo, M., Milas, M., Biopolymers, (1978), 17, 2663.
13. Loh, E., Biopolymers, (1979), 18, 2569.
14. DiNapoli, A., Ph.D. Thesis, SUNY/Stony Brook.
15. Kerker, M., "The Scattering of Light and other Electromagnetic Radiation" (1969), Academic Press, New York and London.
16. Tanford, C., "Physical Chemistry of Macromolecules" John Wiley and Sons, Inc., New York.

RECEIVED October 6, 1980.

Structural Characterization of Proteoglycan Subunit from Nasal Septum by Laser Light Scattering

H. REIHANIAN, A. M. JAMIESON, and J. BLACKWELL

Department of Macromolecular Science, Case Western Reserve University, Cleveland, OH 44106

L. H. TANG and L. ROSENBERG

Connective Tissue Research Laboratories, Montefiore Hospital, The Bronx, NY 10467

Proteoglycan subunit (PGS) is a class of macromolecular species which is found in mammalian connective tissue. Chemically, they consist of a linear protein backbone to which are grafted linear glycosaminoglycan side-chains. Physically, they are believed to exist in their native form as complexes¹ linked to hyaluronic acid as shown in Fig. 1. The complex or proteoglycan aggregate (PGA) is stabilized by a highly insoluble protein called link protein. PGS is isolated in purified form by ultracentrifugation in CsCl density gradients first under associative conditions as aggregate, PGA, and subsequently as PGS under dissociative conditions. Purified fractions are labelled Al-D1, Al-D1-D1 etc.

Recently, we have carried out a series of studies of the hydrodynamic properties of solutions of proteoglycan species isolated from bovine nasal septum²⁻⁴. We reported a limiting sedimentation coefficient, $S^0 = 23.4S$, diffusion coefficient $D^0 = 3.32 \times 10^{-8}$ cm²/sec and intrinsic viscosity $[\eta] = 861.4$ ml/g, for an Al-D1-D1 proteoglycan subunit fraction (PGS). These results lead to the conclusion^{2,4} that the weight-average molecular weight $M_w = 3.97 \times 10^6$.

Several interesting effects were observed in the light scattering properties of PGS at finite concentration²⁻⁴. In aqueous NaCl, the concentration-dependence of D_t is strongly negative. This result, coupled to reports of a large negative second osmotic virial coefficient^{5,6} suggests a self-association mechanism for PGS which is rather surprising in view of its high charge density. It was suggested²⁻⁴ that the locus for self-association may lie at the hook region where polysaccharide chains are absent (Fig. 1). It was further reported²⁻⁴ that, unlike the intermolecular aggregation of PGS with HA in the absence of link protein, the self-association of PGS is intensified with increase of temperature.

In the absence of added salt, anomalous light scattering properties of PGS solutions were observed. The apparent D_t , calculated from the first moment of the photon correlation func-

tions exhibited a strong dependence on scattering angle. It was suggested that these properties could be the result of a tendency for intermolecular ordering of the expanded macroions under the congested conditions which occur at very low ionic strength²⁻⁴.

Finally, it was demonstrated that D_t of a dilute solution of PGS at physiological ionic strength exhibited a sigmoidal decrease upon titration with HA indicating the formation of PGA. In the transition region, highly non-exponential correlation functions were observed but it was not possible to resolve these data into individual components²⁻⁴.

In this paper, we present additional evidence concerning these earlier observations. First, we describe a light scattering study of the solution properties of a PGS sample (A1D1 fraction) treated with cyanogen bromide (CNBr) to selectively, and irreversibly, destroy the native structure of the hook region. These show the absence of any self-association behavior. Then, a total intensity study of the light scattering properties of PGS in salt-free solutions was carried out. A comparison of these results with the earlier diffusion data under such conditions supports the conclusion that intermolecular ordering is present under these conditions. Finally, we present results of a dynamic light scattering study of the titration of PGS with HA in which an attempt to separate PGA and residual PGS monomer was made.

Methods and Materials

Materials

Highly purified proteoglycan fractions Al-D1-D1 and Al-D1 isolated from bovine nasal cartilage was used in this experiment. The samples had been determined to be free of contamination by hyaluronic acid or link protein. Details of isolation and purification of these fractions are described in the literature^{7,8}. Hyaluronic acid sample from Rooster's Comb was generously supplied by Dr. Swann, Harvard Medical School. An Al-D1 subunit fraction which had been treated with CNBr was supplied by Dr. E. N. Jaynes⁹. The CNBr cleavage in these samples had been performed as described by E. Gross¹⁰. It is anticipated that mild treatment of PGS with CNBr will destroy principally the globular hook region leaving the remainder of the core essentially intact. Solutions prepared using these samples were all buffered with 0.01M 2-(N-morpholino)ethane sulfonic acid (MES) to pH 7.0. All solutions were prepared for light scattering by Millipore filtration and adjudged suitable for light scattering when the intensity of light scattering was constant to within 1%.

Quasielastic Laser Light Scattering

The light scattering studies were carried out using two op-

tical mixing spectrometers. The first has been well described elsewhere^{11,12} and was used to study the spectrum of scattered light in the angular range $30^\circ < \theta < 75^\circ$. The second spectrometer is designed specifically for photon correlation analysis and again has been described elsewhere³. Analysis of the correlation functions obtained by this instrument was performed by the method of moments¹³ using the weighting procedure of Brown et al.¹⁴ in which a polynomial function is fitted to the points in the plot of $\ln c(\tau)$ against time:

$$\ln |c(\tau)| - B = -\bar{\Gamma}\tau + \frac{1}{2!} \frac{\mu_2}{\bar{\Gamma}^2} (\bar{\Gamma}\tau)^2 \dots \dots \quad (1)$$

This generates the first moment $\bar{\Gamma}$, of the correlation function $c(\tau)$ from which the z-averaged translational diffusion coefficient $D_{t,z}$ is computed

$$\bar{\Gamma} = D_{t,z} K^2 \quad (2)$$

where K the scattering vector

$$K = 4\pi/\lambda \sin\theta/2 \quad (3)$$

where λ is the wavelength of light in the medium and θ is the scattering angle. The second moment is also computed which is a measure of deviations from single exponential behavior¹³.

To investigate the possibility of intermolecular ordering at low ionic strength solution, we determined the apparent structure factor from the relation

$$\langle I(K) \rangle = NM^2BP(K)S(K) \quad (4)$$

where $P(K)$ is the particle scattering function, N is the number of particles per unit volume, M is the particle weight and B is optical constant. The apparent structure factor $S(K)$, characterizes the angular variation of the intensity of scattered light as a result of intermolecular interference. For macroion solutions with long-range intermolecular ordering, $S(K)$ is related to the relaxation times Γ_D^{-1} for concentration fluctuations by^{15,16}

$$\Gamma_D = D'(K)^2 S(K)^{-1} \quad (5)$$

where $D'(K)$ is the "self particle" translational diffusion coefficient.

Scattered intensities were determined from mean scattering count rates using an Ortec #9315 Photon Counter. Measurements of the polarized and depolarized scattering components of pure benzene were used to calibrate the photometer.

Results

a) Self-Association of PGS

In Fig. 2, we display results of a photon correlation study of solutions of Al-D1 PGS in 0.15M NaCl at pH 7.4 at temperatures $T = 25^\circ\text{C}$ and 37°C . At these concentrations, the correlation functions are close to single exponential decays ($\mu_2/\bar{\Gamma}^2 \sim 0.01$) and the data are well characterized by a single parameter, the mean time constant $\bar{\Gamma}$. As described in earlier work²⁻⁴, D_t decreases as concentration increases, reflecting an increase in particle size because of self-association. For comparison, in Figs. 3 and 4, we show the concentration-dependence of $D_t (= \Gamma/K^2)$ and the reduced scattering intensity of the CNBr-treated subunit. From the latter we compute $M_w = 3.0 \pm 0.3 \times 10^6$ g mole⁻¹ which compares favorably with $M_w = 3.2 \pm 0.3 \times 10^6$ g/mole for native PGS Al-D1 deduced from the Zimm plot shown below (Fig. 5) and $M_w = 3.97 \pm 0.2 \times 10^6$ g/mole for an Al-D1-D1 fraction reported earlier^{3,4}. We therefore deduce that the CNBr-treatment has degraded the subunit primarily in the 'hook' region at the chain end rather than in the core region. It is noted from Figs. 3 and 4 that the concentration-dependence of D_t and the second virial coefficient are each positive, displaying only a modest excluded volume effect. This result contrasts with the large negative concentration dependence observed for the intact subunit. Finally, it is pertinent to note that, as shown in Fig. 2, the concentration-dependence of D_t for PGS-ALD1D1 in 0.15M NaCl is more negative at $T = 37^\circ\text{C}$ than it is at 25°C .

b) PGS in the Absence of Added Salt

Figure 5 is a Zimm plot of the total intensity of light scattered by native PGS Al-D1 in water in the absence of added salt. Extrapolation of these data in the limit $c \rightarrow 0$, $\theta \rightarrow 0$ leads to $M_w = 3.2 \times 10^6$ g/mole and $\langle R_g^2 \rangle^{1/2} = 1450\text{\AA}$. The prime motivation for this study was to attempt to observe intermolecular interference effects as embodied in the parameter $S(K)$ in eq. (4). From Fig. 5, the Zimm plot ostensibly appears quite normal, permitting interpolation of M_w and $\langle R_g^2 \rangle^{1/2}$. We draw attention, however, to the curvature evident at low concentrations. We have estimated the static structure factor $S(K)$, using eq. (4), based on the assumption that the extrapolated values at $c = 0$ of the Zimm plot are a valid representation for $P(K)$, i.e. $(c/R_g)c \rightarrow 0 = 1/kMP(K)$. The results are shown in Fig. 8. Also included are a set of $S(K)$ values computed from our earlier small-angle heterodyne study of $D_t(c)$ for PGS in salt-free water²⁻⁴. These $S(K)$ values were calculated using eq. (5).

It is possible that errors may exist in the extrapolation to $c = 0$ in this strongly-interacting system. However, we note

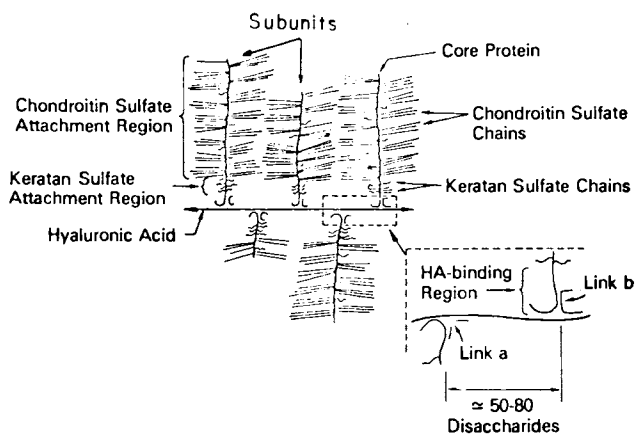


Figure 1. Currently accepted model for connective tissue proteoglycan aggregate (1)

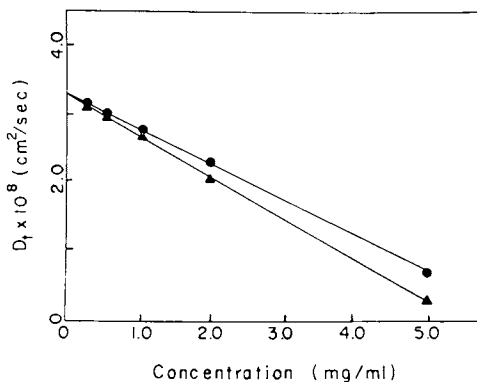


Figure 2. Concentration dependence of the translational diffusion coefficient of PGS A1-D1-D1 in 0.15M NaCl/0.01M MES, pH 7.0 at 25°C (●) and at 37°C (▲)

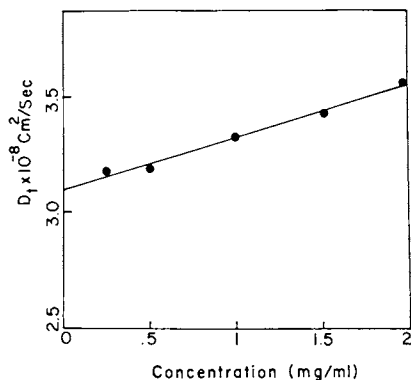


Figure 3. Concentration dependence of translational diffusion coefficient $D_{t,z}$ of PGS A1-D1 fraction treated with CNBr in 0.15M NaCl, pH 7.0 at a 40° scattering angle.

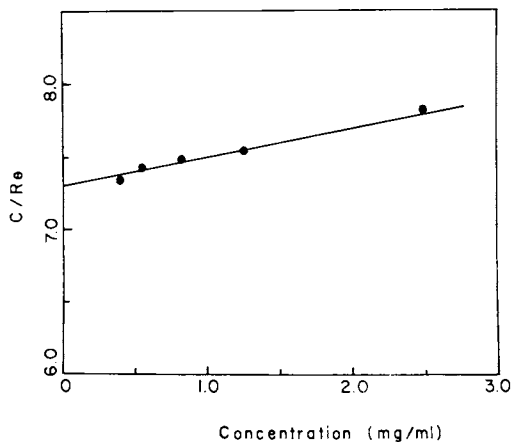


Figure 4. Concentration dependence of C/R_θ of PGS A1-D1 fraction treated with CNBr in 0.6M GdnCl. Optical constant $k = 6.82 \times 10^{-8} \text{ mL}^2 \text{ g}^{-2} \text{ cm}^{-4}$, particle scattering function $P(\theta) = 0.0675$.

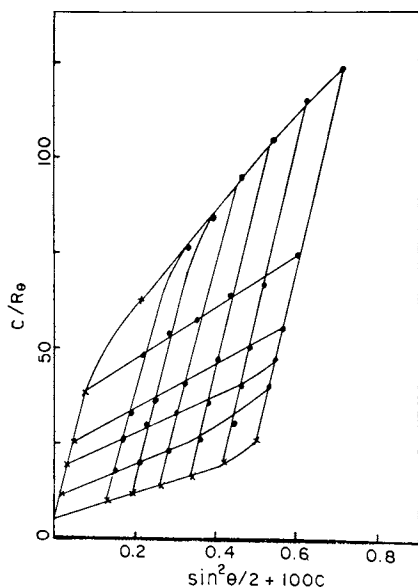


Figure 5. Zimm plot for PGS A1-D1 in water at the following concentrations: 0.32, 0.46, 0.71, 1.1, and 2.2 mg/mL. Optical constant $k = 6.17 \times 10^{-8} \text{ mL}^2 \text{ g}^{-2} \text{ cm}^{-4}$.

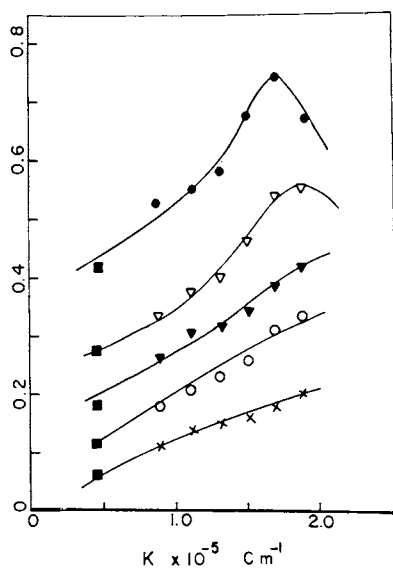


Figure 6. Angular dependence of apparent structure factor $S(\mathbf{K})$ for PGS A1-D1 in water: (●) $C = 0.32 \text{ mg/mL}$; (▽) $C = 0.46 \text{ mg/mL}$; (▼) $C = 0.71 \text{ mg/mL}$; (○) $C = 1.1 \text{ mg/mL}$; and (×) $C = 2.2 \text{ mg/mL}$; (■) values at small scattering vector calculated using Equation 5. Identical representation for $S(\mathbf{K})$ is obtained by assuming $P(\mathbf{K})$ for PGS to be that of a star polymer with polydisperse rays (see Equation 6).

that, within experimental error, an identical representation for $S(K)$ to that shown in Fig. 8 is obtained by assuming $P(K)$ for PGS to be that of a star polymer with polydisperse rays¹⁷

$$P(K) = \frac{1 + \mu^2/3f}{(1 + \mu^2(f+1)/6f)^2} \quad (6)$$

where $\mu^2 = K^2 \langle R_g^2 \rangle$, $\langle R_g^2 \rangle = 1450 \text{ \AA}^2$, and f is the number of rays. From electron microscope observations it is evident^{7,9} that this is indeed a reasonable structural model for the extended subunit. The parameter f represents the number of glycosaminoglycan side chains and is of the order 100.

c) Interaction with Hyaluronate

The variation of the photon correlation spectrum of a 0.25 mg/ml solution of PGS was studied during titration with aliquots of a .05 mg/ml solution of rooster comb HA. Analysis of these data was performed using an iterative least-squares fit to a series of equally-spaced exponentials. Amplitudes, A_i , and time constants of each exponential are independently varied. We found that a single exponential fit sufficed initially ($\mu_2/\Gamma^2 < 0.1$) but a sudden transition to a non-exponential decay occurs at higher (HA) concentrations ($\mu_2/\Gamma^2 > 0$). In this region, the correlation function is fit within experimental errors by the sum of three exponentials, one of which has the same time constant as that due to diffusion of subunit. These results are shown in Fig. 7. Species 1 represents unaggregated PGS, species 2 and 3 represent aggregate. We have also estimated values for the numbers n_i of each species and associated molecular weights M_i . These were computed based on approximation

$$A_i = n_i M_i^2 \exp(-k^2 R_{g,i}^2/3) \quad (7)$$

and using the known values for the molecular weight subunit $M_1 = 3 \times 10^6$ assuming $M_3 = 2.5 \times 10^8$ which corresponds to a saturated aggregate (one PGS per 60 disaccharide residues). A further useful relation is $(n_2 + n_3) = n_{\text{HA}}$, the total number of hyaluronate molecules in solution. It is not intended to imply that two discrete species of aggregate are formed. The sum of two exponentials represents the best fit to the distribution of aggregate sizes that can be achieved within the precision of our data. In Fig. 8, we plot the variation of number- and weight-average values for PGA as the titration proceeds.

Finally, it is observed that increase of temperature rapidly disrupts the aggregates formed by titration of PGS with HA. At $T = 45^\circ\text{C}$, aggregate is completely dissociated. This is in direct contrast to the temperature variation of the self-association process of PGS described above (Fig. 2).

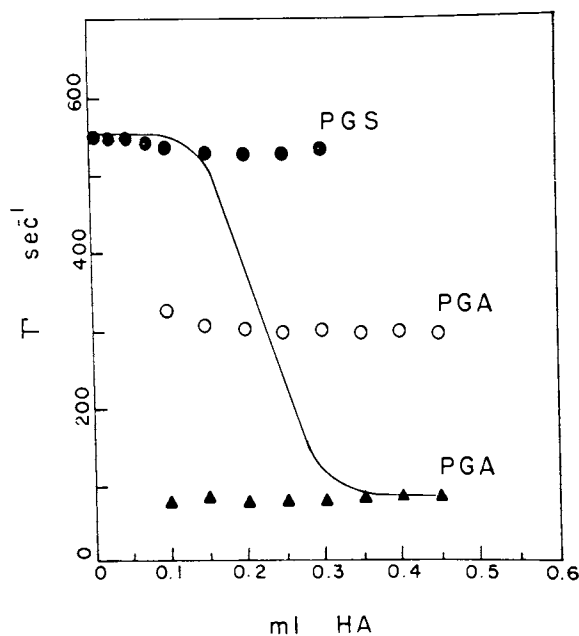


Figure 7. Variation of γ on titrating 10 mL of a solution of PGS A1-D1, $C = 0.25$ mg/mL, with an aqueous solution of hyaluronic acid, $C = 0.25$ mg/mL, with an aqueous solution of hyaluronic acid, $C = 0.05$ mg/mL at 22°C . Species 1 represents unaggregated PGS, Species 2 and 3 represent aggregate PGA.

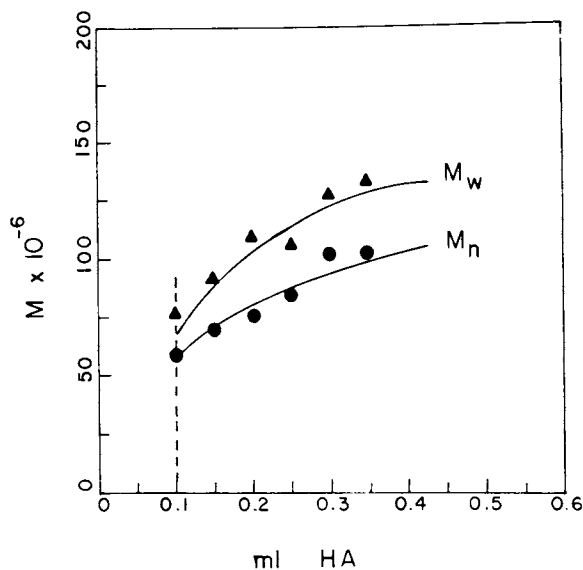


Figure 8. Variation of \overline{M}_n and \overline{M}_w for PGA as titration of PGS with hyaluronic acid proceeds

Discussion

a) Self-Association of PGS

In previous studies of PGS in aqueous NaCl at pH = 7.4, negative concentration dependence of D_t (Fig. 2) as well as negative osmotic virial coefficients were observed²⁻⁴. In view of the highly-charged character of the PGS macroion, these data indicate short-range attractive interactions occur between molecules. It was further discovered that this self-association behavior is disrupted by the protein denaturant guanidine hydrochloride²⁻⁴. In this work we have shown (Figs. 3 and 4) that the aggregation effect is not present in solutions of the CNBr-treated fragment. These results support the conclusion that the intermolecular interaction occurs at the hook region. We also find (Fig. 2) that the negative slope of D_t increases as the temperature is raised. This result suggests an enhancement of the attractive forces as temperature rises and the possibility that a hydrophobic interaction is involved. Finally, we recall that the concentration-dependent sedimentation coefficients of PGS in aqueous NaCl show little evidence of self-association²⁻⁴. We have suggested that the PGS aggregation process can be reversed by increase of hydrostatic pressure. Evidence for such an effect in other polysaccharide systems is well-established in the literature and again suggests the involvement of hydrophobic interactions^{18,19}.

b) PGS in the Absence of Added Salt

The light scattering experiments described in a previous publication²⁻⁴ together with the intensity data summarized in Fig. 5 have produced several apparently contradictory results. First, the apparent D_t depends on scattering angle and in fact appears to exhibit a minimum² at $c = 0.50$ mg/ml near $K = 10^5$ cm⁻¹. Further, the concentration dependence of D_t is very pronounced and negative in wide-angle experiments, but weak and positive in small-angle experiments. Third, the Zimm plot in the wide angle regime appears 'normal' with a large positive second virial coefficient.

The only reasonably plausible interpretation which reconciles this evidence in a self-consistent fashion appears to be that summarized in Fig. 6. This model argues that chain expansion at low ionic strength and the attendant increase in congestion in the solution lead to cooperative intermolecular interactions, viz. an 'ordering' tendency between near neighbors. As described above, it appears based on the known structural features of PGS that a reasonably accurate determination of the particle scattering function $P(K)$ can be obtained by extrapolation at each angle to $c = 0$. This permits a determination of $S(K)$ via eq. (4). These $S(K)$ data permit a rationalization of

the difference between small- and wide-angle behavior of the apparent diffusion coefficient via eq. (5) as shown in Fig. 6.

It is noteworthy that an apparent peak is observed in $S(K)$ for $c = 0.32$ mg/ml at $K \sim 1.75 \times 10^5$ cm⁻¹. This would correspond to a maximum in the radial distribution function at $r_{\max} \sim 2\pi/K_{\max} = 3500\text{\AA} \pm 500\text{\AA}$ for random close-packing of dense spheres. For comparison, when $c = 0.32$ mg/ml, the mean inter-particle spacing for close-packed spheres is $l \sim (1.5M/cN_A)^{1/3} = 3000\text{\AA}$, with an estimated uncertainty of $\sim 10\%$. It is noted, however, that the peak in $S(K)$ appears at a position which is significantly different (larger) from the position where a minimum is observed in Γ_D , $K \sim 10^5$ cm⁻¹ (see Fig. 10 of ref. 2). This suggests to us the possibility that the 'upturn' in Γ_D at wide angles is due to an enhanced contribution of internal chain dynamics to the kinetic factor $D'(K)$ in eq. (5) rather than to the effect of $S(K)$. The hazards of this decomposition of intensity data in such a complex scattering regime are obvious. However, we offer the above as the only reasonable means of correlating the apparently contrary experimental light scattering results derived from this system.

c) Interaction of PGS with Hyaluronate

Titration of PGS with hyaluronate clearly leads to formation of an intermolecular aggregate, as shown in Fig. 7. However, the aggregates formed are labile, easily decomposed by heating and rather polydisperse. This is in contrast to the properties of the native aggregate (A1) fraction which includes link protein. The correlation functions obtained from solutions of native aggregate A1 are very close to single exponential decays ($\mu_2/\bar{\Gamma}^2 < .1$) which means this species is much more homogeneous than the link-free aggregate ($\mu_2/\bar{\Gamma}^2 > .3$ for correlation function obtained from link-free aggregate). Also the aggregate A1, appears to be stable thermally to temperatures of the order 65°C in contrast to the link-free aggregate which is decomposed at 45°C. These results lead to the conclusion that the link protein stabilizes the bond between PGS and hyaluronate and is involved in making homogeneous aggregates.

Acknowledgement

This work was supported by NIH through grants HL 21622 and AG 00361.

Précis:

Solution studies of proteoglycan subunit are described. In dilute aqueous NaCl, self-association behavior of subunit is observed which occurs at the globular protein 'hook' region. Thus the association is banished by denaturation with guanidine hydro-

chloride or by removal of the 'hook' with cyanogen bromide. In salt-free solutions of subunit anomalous light scattering results are observed. While the concentration-dependence of the diffusion coefficient is large and negative, the intensity data indicate a large, positive second virial coefficient. A self-consistent interpretation of the results is achieved by assuming that at low ionic strength intermolecular interaction leads to transient 'ordering'. Titration of subunit with hyaluronate forms an intermolecular aggregate which is rather polydisperse and easily disrupted on heating when compared to the native aggregate. The latter contains link protein, is rather homogeneous, and resists thermal decomposition. This supports the notion that link protein stabilizes the bond between subunit and hyaluronate.

Literature Cited

1. Hascall, V. C. J. Supramol. Struct., 1977, 7, 101.
2. Reihanian, H., Jamieson, A. M., Tang, L. H., and Rosenberg, L. Biopolymers, 1979, 18, 1727.
3. Reihanian, H., Blackwell, J., and Jamieson, A. M. Biopolymers, submitted 1980.
4. Reihanian, H. Master Thesis, 1978, Case Western Reserve University.
5. Pasternack, S. G., Veis, A., and Breen, M. J. Biol. Chem., 1974, 249, 2206.
6. Sheehan, J. K., Nieduszynski, I. A., Phelps, C. F., Muir, H., and Hardingham, T. E. Biochem. J., 1978, 171, 109.
7. Rosenberg, L., Hellman, W., and Kleinschmidt, A. K. J. Biol. Chem., 1975, 250, 1877-1883.
8. Rosenberg, L., Hellman, W., and Kleinschmidt, A. K. J. Biol. Chem., 1970, 245, 4123-4130.
9. Walton, A. G., Volger, H. G., and Jaynes, E. N. Int. J. Biolog. Macromolecules, 1979, 1, 89-92.
10. Gross, E. Methods Enzymol., 1967, 11, 283-255.
11. McDonnell, M. E. and Jamieson, A. M. Biopolymers, 1976, 15, 1283-1299.
12. McDonnell, M. E. and Jamieson, A. M. J. Macro. Sci., Phys., 1977, 13, 67-88.
13. Koppel, D. E. J. Chem. Phys., 1972, 57, 4814.
14. Brown, J. C., Pusey, P. N., and Dietz, R. J. Chem. Phys., 1975, 62, 1136-1144.
15. Brown, J. C., Pusey, P. N., Goodwin, J. W., and Ottewill, R. H., J. Phys., 1975, A8, 664-682.
16. Schaefer, D. W. and Berne, B. J. Phys. Rev. Lett., 1974, 32, 110.
17. Burchard, W., Macromolecules, 1977, 10, 919.
18. Gilbert, L. M. and Gilbert, G. A. Methods Enzymol., 1973, 27, 273.
19. Harrington, W. F. and Kegeles, G. Methods Enzymol., 1973, 27, 306.

RECEIVED October 6, 1980.

Rheological Studies on Proteoglycan

GO MATSUMURA

School of Pharmaceutical Science, Showa University, Hatanodai 1-5-8,
Shinagawa, Tokyo 142, Japan

The physical and mechanical properties of cartilage are certainly important for the physiological role of this tissue. Proteoglycan in connection with collagen and other constituents of this tissue may affect its physical properties. Cartilage proteoglycan is a complex species. To a protein core, many chondroitin sulfate and keratan sulfate chains are attached. The molecular weight of a proteoglycan monomer prepared from bovine nasal septa has been reported as two to three million daltons (1), for example. This monomer is bound to a hyaluronic acid backbone reversibly and noncovalently. The gigantic proteoglycan thus formed is stabilized by link proteins.

In the present study, we attempted to elucidate the rheological behavior of proteoglycan in viscous solution, with special regard to the differences between free monomer and aggregate.

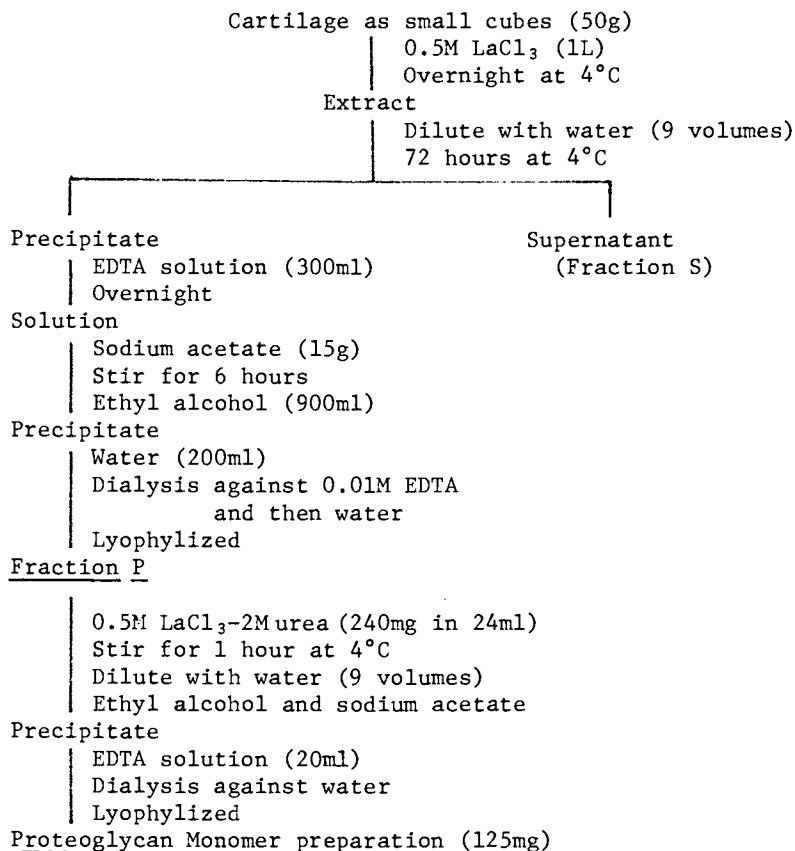
Materials

Proteoglycan monomer. From whale nasal cartilage proteoglycan was extracted with 0.5M LaCl₃ in the presence of protease inhibitors (38mM α -aminohexanoic acid, 5mM benzamidine HCl and 10mM EDTA-2Na). From bovine nasal cartilage proteoglycan was recovered in Fraction P (Scheme 1) in monomeric form binding with link protein(s) (2). However, most proteoglycan in Fraction P was characterized as aggregated in the present preparation by ultracentrifugation (Figure 1, top) and gel filtration profiles. So the preparation was reprecipitated in the presence of 2M urea in addition to LaCl₃. In this precipitate, proteoglycan was recovered mostly as monomer (Figure 1, middle). By polyacrylamide gel electrophoresis in the presence of sodium dodecyl-sulfate, the existence of link proteins was suggested. The presence of some contaminating proteins was also suggested by this electrophoresis and by the high protein content of the preparation.

An example of the **chemical** and physical analysis of this preparation follows: glucuronic acid 29%, hexose 7.1%,

0097-6156/81/0150-0213\$06.25/0
© 1981 American Chemical Society

Scheme 1
Preparation of Proteoglycan Monomer from Whale Nasal Cartilage



protein 18.6%, disaccharide constituent of chondroitin sulfate 6-sulfate/4-sulfate = 1/3, intrinsic viscosity 2.9dl/g, sedimentation constant 14.7s (main) and 11s (minor). Physical measurements were carried out with solutions in 0.1M Tris-HCl buffer, pH 7, containing 0.05M NaCl.

By the addition of hyaluronic acid, the viscosity of the proteoglycan solution was increased. Hyaluronic acid in an amount equal to one twentieth of the weight of proteoglycan seemed to be enough to reach the maximum value (Figure 2). By ultracentrifugation (Figure 1, bottom) and gel filtration most proteoglycan appeared to exist as aggregate under these conditions.

Hyaluronic acid. From a water extract of human umbilical cords hyaluronic acid was purified by the method originally reported for bovine synovial fluid (3). The preparation was practically free of protein and sulfated glycosaminoglycans. The molecular weight was estimated as about one and a half million by equilibrium centrifugation. Thus the aggregate used in the present study was not the native aggregate of the cartilage tissue, but an artificial one.

Methods

Viscosity of dilute solutions. A capillary viscometer (Cannon-Manning semimicro, No. 100) was used for determination of the intrinsic viscosity and for study of enzymatic degradation. Measurements were carried at 37°C. For the latter study specific fluidities, the reciprocal of specific viscosity, were plotted against reaction time. With random degradation of a chain polymer a straight line is obtained by this plotting, and the slope of the line is proportional to the reaction rate constant (4).

Viscosity with stational flow. A cone-plate type rotating rheometer (Shimadzu, RM-1, equipped with a reduction gear, RDG-1) was employed. The rate of shear available ranged from 7.48×10^{-3} to 74.8/sec. The apparent viscosity at a given rate of shear was calculated from the rate of shear and the observed shear stress. Samples were dissolved in the buffer solution mentioned before at 2 or 4% concentration and measured at room temperature ($22 \pm 1^\circ\text{C}$).

Dynamic viscoelasticity. From the oscillatory rotation of the plate dynamic viscoelasticity was estimated with the same equipment. The maximum shear was 0.250, and the angular frequencies employed ranged from 5.82×10^{-3} to 5.82×10^{-1} rad/sec. The rotation angle of the plate and the twist of the cone were recorded with an X-Y plotter. From the hysteresis loop obtained the storage modulus or dynamic elasticity (G') and the loss

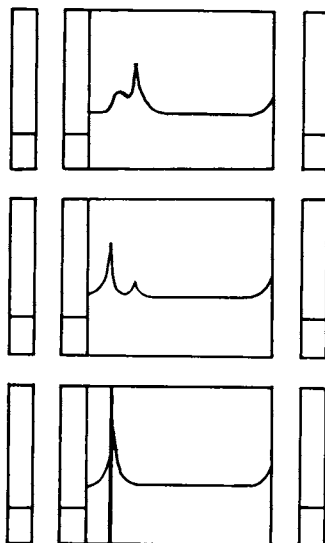


Figure 1. Sedimentation profile of proteoglycan: (top) Fraction P (see Scheme 1), 0.2%, 51,200 rpm, 6 min; (middle) Proteoglycan monomer, 0.3%, 60,000 rpm, 6 min; (bottom) aggregate, 0.3% proteoglycan monomer in the presence of 0.015% hyaluronic acid, 51,200 rpm, 6 min.

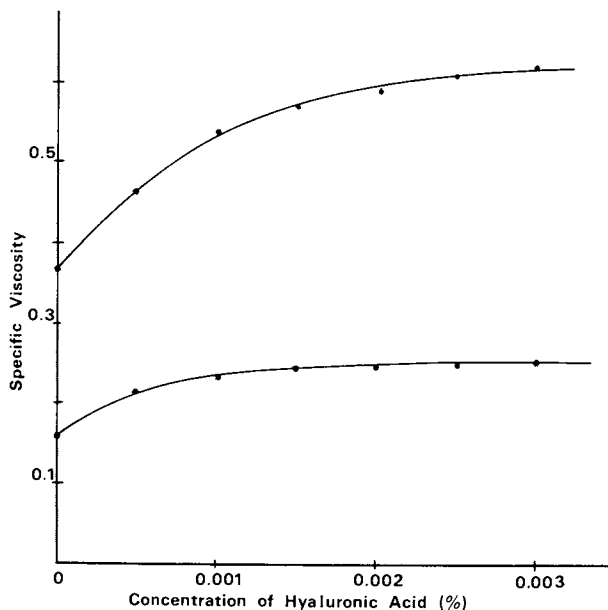


Figure 2. Effect of hyaluronic acid on the viscosity of proteoglycan monomer. Concentration of monomer: (upper curve) 0.1%; (lower curve) 0.05%.

modulus (G'') were calculated. The loss modulus can be converted to the dynamic viscosity by dividing by the angular frequency.

Results

Viscosity with stationnal flow. As is usual for solutions of high polymeric compounds, the apparent viscosity of proteoglycan solutions depended strongly on the rate of shear; the higher viscosity was observed at the lower rate of shear (Figure 3). The concentration of proteoglycan was 2% in each solution. To prepare the aggregate solution hyaluronic acid was added to the final concentration of 0.1%. The aggregate showed higher viscosity than monomer at any rate of shear. But the difference was more remarkable at high shear rates. For comparison the result with hyaluronic acid of the same concentration (2%) is also given in this figure with solid triangles. This solution behaved like a Newtonian liquid at shear rates less than 10^{-1} /sec. On the other hand, proteoglycan monomer seemed to remain in the power law region throughout the range examined (5).

Dynamic viscoelasticity. With same solutions used for the measurements of Figure 3 dynamic viscoelasticity was examined. It is clear that both moduli of proteoglycan increased significantly upon formation of aggregate with hyaluronic acid (Figure 4). This effect was more pronounced at higher frequencies and for the storage modulus. Thus the loss tangent, which is the ratio of the loss modulus to the storage modulus, was decreased by the presence of hyaluronic acid (Figure 5). Though the loss tangent of proteoglycan monomer was decreased by increasing the angular frequency, that of aggregate remained constant. As is well known, hyaluronic acid cannot be replaced by any other linear acid polysaccharide for aggregate formation. In the rheological examinations mentioned above only hyaluronic acid could affect the behavior of proteoglycan monomer solution.

The viscoelasticity of hyaluronic acid solution was much more influenced than proteoglycan, either monomer or aggregate, by the angular frequency of the plate. Thus the ordinate of Figure 6, which represents both moduli, is expressed logarithmically. In contrast to proteoglycan aggregate the loss modulus was bigger than the storage modulus especially at lower frequencies.

Effect of Streptomyces hyaluronidase. The effects of some depolymerizing enzymes on the viscoelastic properties of proteoglycan were examined. The first example was that of Streptomyces hyaluronidase (hyaluronate lyase, EC 4.2.2.1.), which is shown as strictly specific to hyaluronic acid (6). Thus this enzyme can degrade only the hyaluronic acid backbone of aggregate and should not attack the proteoglycan monomer. To 0.1% solution of aggregate 0.05TRU of Streptomyces hyaluronidase was added. As

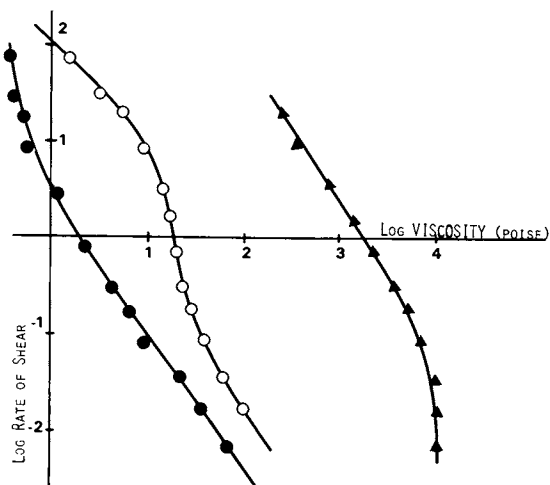


Figure 3. Rheogram of proteoglycan and hyaluronic acid: (●) monomer, 2%; (○) aggregate (2% monomer in the presence of 0.1% hyaluronic acid); (△) hyaluronic acid, 2%.

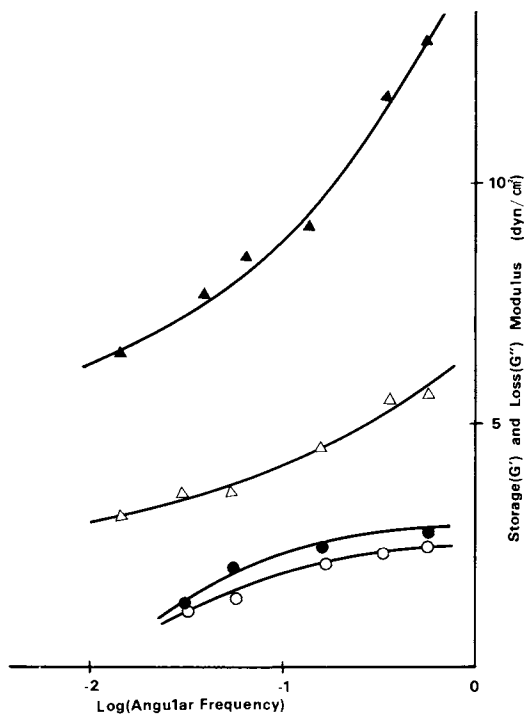


Figure 4. Dynamic viscoelasticity of proteoglycan: (○, ●) monomer; (△, ▲): aggregate (see Figure 3 for concentration); (●, ▲) storage modulus; (○, △) loss modulus.

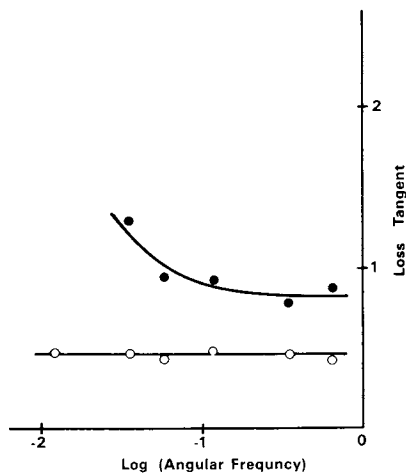


Figure 5. Loss tangent of proteoglycan: (●) monomer; (○) aggregate (see Figure 3 for concentration).

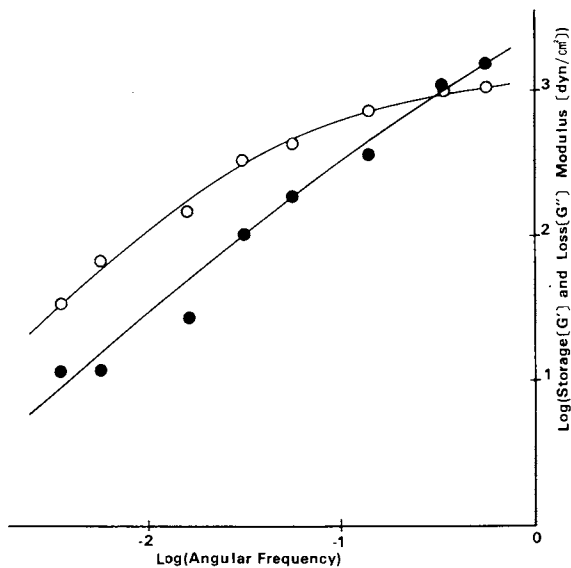


Figure 6. Dynamic viscoelasticity of hyaluronic acid: (●) storage modulus; (○) loss modulus (see Figure 3 for concentration).

shown in Figure 7, the specific fluidity of the aggregate increased gradually by this enzymatic treatment. This increase in specific fluidity seemed to level off after some incubation period, suggesting that macromolecular proteoglycan monomer remained even after prolonged digestion. Without the presence of hyaluronic acid, however, the specific fluidity of proteoglycan monomer solution also increased after treatment with this enzyme. The plateau value was similar to that obtained in the presence of hyaluronic acid. As shown in Figure 1 (bottom), this preparation contained some proteoglycan in the aggregated form, but the amount of the aggregate was too small to explain the decrease in viscosity produced by this enzymatic digestion.

To 4% solution of proteoglycan, either in the presence of or in the absence of hyaluronic acid, 1TRU of the enzyme was added. The viscoelasticity of these reaction mixtures were measured with appropriate intervals (Figure 8). With the aggregate solution the decrease of both moduli was observed. The decrease of storage modulus seemed to stop after some reaction period, but the decrease of loss modulus continued further. Again this enzyme affected the viscoelastic properties of the monomer solution. The effect on the loss modulus was little, if any. However, the storage modulus increased significantly.

Since the sedimentation constant of the monomer preparation was not affected by this enzymatic treatment, the depolymerization of proteoglycan was not likely. The increase of storage modulus is difficult to explain in terms of degradation. One might speculate that some proteoglycan monomer existed as a complex with small hyaluronic acid oligomer. The removal of this oligomer might cause some conformational change in the proteoglycan molecule to increase the specific fluidity of dilute solution and the storage modulus of concentrated solution. The possibility that this enzyme preparation was contaminated with proteolytic enzymes was not eliminated. As will be stated later, both moduli of the proteoglycan monomer increased with proteolytic digestion.

Effect of chondroitinase ABC. This enzyme (chondroitin ABC lyase, EC 4.2.2.4.) also depolymerizes the hyaluronic acid backbone of aggregate. In addition, it can degrade chondroitin sulfate chains of monomer, but not its keratan sulfate chains. To 0.1% solution of proteoglycan 0.005U of the enzyme was added. As shown in Figure 9, the specific fluidity of the solution, either in the presence of or in the absence of hyaluronic acid, increased in two stages. The first linear increase may indicate the break down of hyaluronic acid backbone. Then upward increase which follows may be due to the shortening or removal of chondroitin sulfate chains of monomeric proteoglycan.

The effect on viscoelastic properties of concentrated solution (4% proteoglycan and 1U chondroitinase ABC) was more or less similar to that with Streptomyces hyaluronidase treatment (Figure

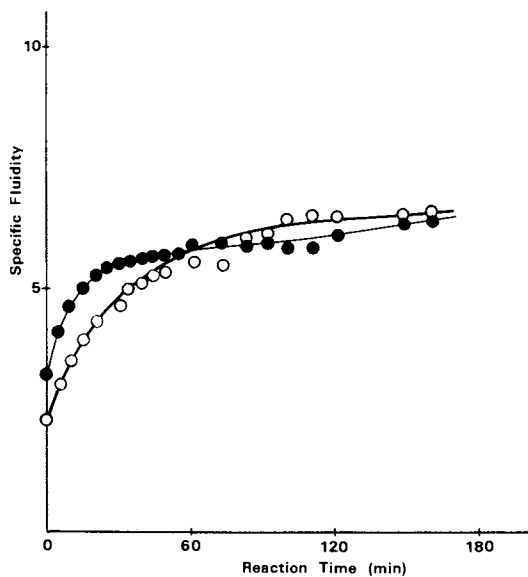


Figure 7. Effect of *Streptomyces hyaluronidase* on the specific fluidity of dilute solution of proteoglycan. Concentrations: proteoglycan, 0.1%; enzyme, 0.05 TRU; (●) monomer; (○) aggregate.

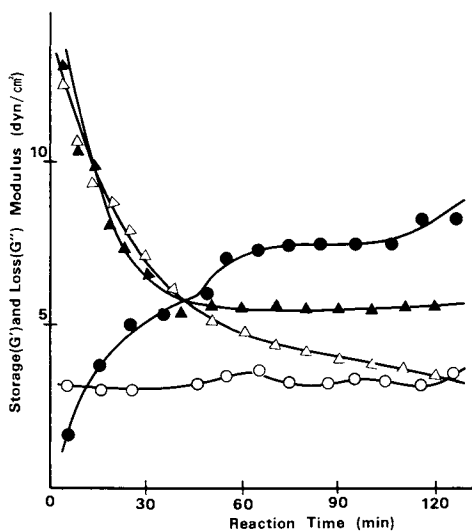


Figure 8. Effect of *Streptomyces hyaluronidase* on the dynamic viscoelasticity of proteoglycan. Concentrations: proteoglycan, 4%; enzyme, 1 TRU. Angular frequency: 0.349 rad/s; (○, ●) monomer; (△, ▲) aggregate; (●, ▲) storage modulus; (○, △) loss modulus.

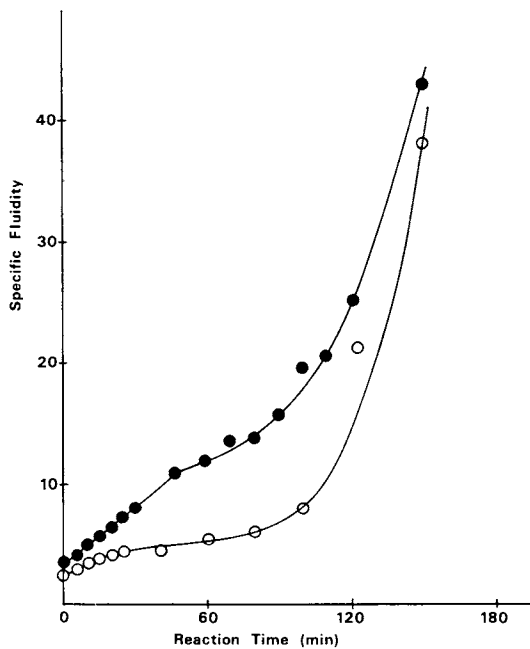


Figure 9. Effect of chondroitinase ABC on the specific fluidity of dilute solution of proteoglycan. Concentrations: proteoglycan, 0.1%; enzyme, 0.005 U; (●) monomer; (○) aggregate.

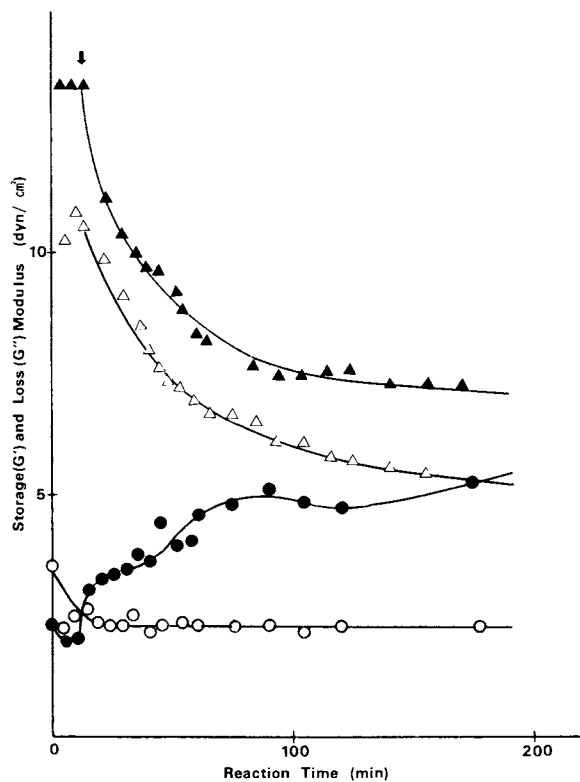


Figure 10. Effect of chondroitinase ABC on the dynamic viscoelasticity of proteoglycan. Concentrations: proteoglycan, 4%; enzyme, 1 U. Angular frequency: 0.349 rad/s; (○, ●) monomer; (△, ▲) aggregate; (●, ▲) storage modulus; (○, △) loss modulus.

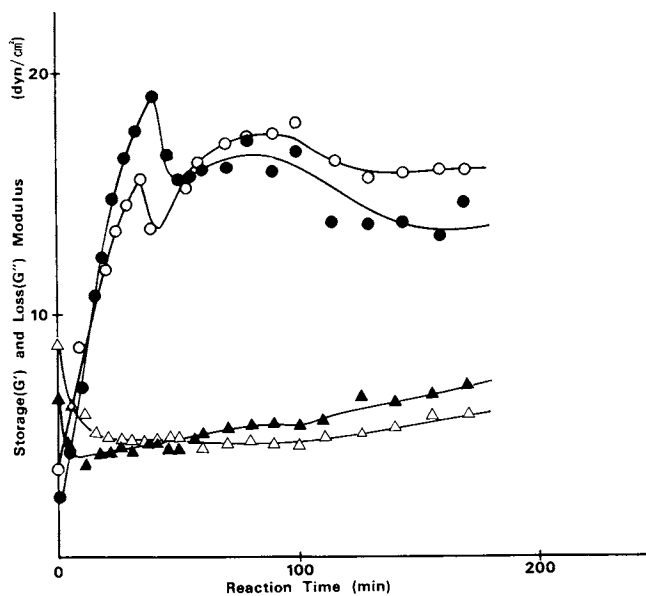


Figure 11. Effect of trypsin on the dynamic viscoelasticity of proteoglycan. Concentrations: proteoglycan, 4%; enzyme, 1 U. Angular frequency: 0.349 rad/s; (●, ●) monomer; (△, ▲) aggregate; (●, ▲) storage modulus; (○, △) loss modulus.

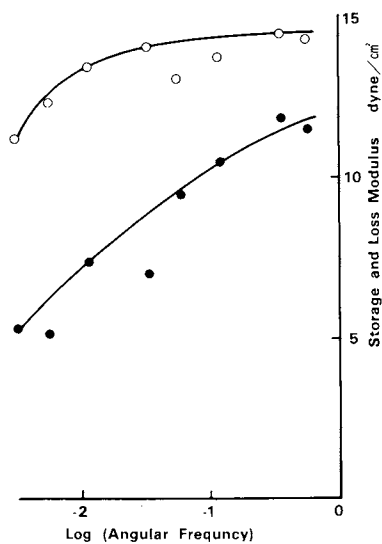


Figure 12. Dynamic viscoelasticity of proteoglycan monomer treated with trypsin for 2 h: (●) storage modulus; (○) loss modulus (see Figure 11 for concentrations).

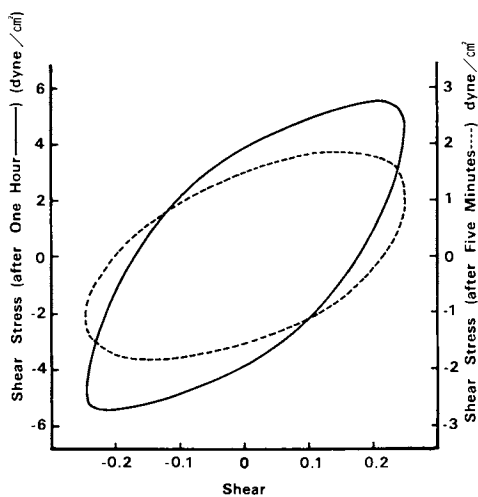


Figure 13. Hysteresis loop of proteoglycan monomer: (---) after 5 min; (—) after 1 h (see Figure 11 for concentrations and angular frequency).

10). After exhaustive digestion, however, viscoelasticity was almost completely abolished.

Effect of trypsin. This enzyme (EC 3.4.21.4) can degrade the protein core of proteoglycan. But in the aggregated form the hyaluronic acid linkage region of core protein and link proteins are said not to be attacked by this proteolytic enzyme (7). With a reaction mixture of 4% proteoglycan and 1U of trypsin the effect of this enzymatic treatment on viscoelastic properties was examined (Figure 11). With aggregate a rapid decrease of both moduli was observed at early stages of this treatment; then small increases followed. With monomer steep increases of both moduli were observed; then gradual decreases followed. The highest values were even higher than those of untreated aggregate.

A two hour digest of monomer was subjected to measurement of the viscoelasticity at various angular frequencies (Figure 12). In contrast to untreated aggregate (Figure 4), the loss modulus was bigger than the storage modulus. The loss modulus was less affected by the angular frequency.

The hysteresis loop of proteoglycan, either as monomer or as aggregate, was a typical ellipse suggesting normal viscoelastic behavior. As given in Figure 13 with a broken line, the reaction mixture of proteoglycan monomer and trypsin showed an elliptic loop at five minutes after addition of the enzyme. After one hour incubation, the hysteresis loop was distorted to a somewhat tetragonal shape. The direction of the loop is clockwise. Some plasticity might be induced in proteoglycan monomer by this tryptic digestion.

These anomalous rheological properties were found with monomer but not with aggregate. Since the hyaluronic acid linkage region of proteoglycan was protected from tryptic digestion by the formation of aggregate, this anomaly may be the result of a conformational change caused by processing of core protein in this region.

Conclusion

The apparent viscosity with stationnal flow and dynamic viscoelasticity of proteoglycan were increased by formation of aggregate. Enzymatic treatment with hyaluronidase or trypsin on proteoglycan monomer could increase the viscoelasticity. The former enzyme increased the storage moduls more remarkably, whereas the latter affected the loss modulus more significantly. These effects might be understood as conformational changes in the monomer molecule. Further studies are under the progress.

Litereture cited

1. Rosenberg, L.; Choi, H.; Pal, S.; Tang, L. "Carbohydrate-protein interaction (ACS Symposium Series 88)"; American Chemical Society: Washington, D.C., 1979; p. 186.

2. Mason, R. W.; Roughley, P. J. *Biochem. Soc. Trans.*, 1974, 2, 894.
3. Matsumura, G.; De Saiegui, M.; Herp, A.; Pigman, W. *Biochim. Biophys. Acta*, 1963, 69, 574.
4. Matsumura, G.; Pigman, W. *Arch. Biochem. Biophys.*, 1965, 110, 526.
5. Lenk, R. S. "Plastic rheology"; Wiley Interscience: New York, 1968; p. 12.
6. Ohya, T.; Kaneko, Y. *Biochim. Biophys. Acta*, 1970, 198, 607.
7. Heinegard, D.; Hascall, V. C. *J. Biol. Chem.*, 1974, 249, 4250.

RECEIVED October 15, 1980.

Solution Properties of Hyaluronic Acid

T. W. BARRETT

Department of Physiology and Biophysics, University of Tennessee Center for the Health Sciences, 894 Union Avenue, Memphis, TN 38163

Hyaluronic acid is a glycosaminoglycan polysaccharide composed of D-glucuronic acid (G), which possesses a carboxylate anion, and N-acetyl-glucosamine (N), which possesses an amide group, with linkages $\beta(1 \rightarrow 3)$ for G-N and $\beta(1 \rightarrow 4)$ for N-G. In previous papers, I reported the abrupt pH-dependent conformational transition present in potassium hyaluronate solutions buffered in phosphate at constant ionic strength 0.1, $I = 0.1 \text{ mol} \cdot \ell^{-1}$, observed using axial and radial birefringence, linear dichroism, and viscometry (1, 2, 3). Most of the transition for this particular buffer occurs in the pH range 7.0-7.5, i.e., across the physiological range, and consequently the transition has important consequences for many physiological systems (1).

Other investigators (4, 5) have recently reported a major conformational transition, but used other solvents; therefore, as this paper attempts to explain, the reported transition occurred in a pH range other than 7.0-7.5. In all instances, however, the transition occurs at a pH equal to the apparent equilibrium constant, $\text{pH} = \text{pK}_a$, of the hyaluronate in solution. As the transition is not solely a function of pH, nor ionic strength, but involves selective interaction of the amide group with monovalent versus divalent cations at $\text{pH} > \text{pK}_o$ (6), where pK_o is the equilibrium constant of the carboxylate ion, it seems that any analysis of the transition should proceed along thermodynamic lines, rather than stoichiometric, which neglects the interaction of solvent and polymer peculiar to polyelectrolytes in solution. These interactions include not only the interaction of polyelectrolyte and ions, but the interaction of the polyelectrolyte-ion complex and ions in the atmosphere of the complex (7). They would also include counterion condensation on the polyelectrolyte (8).

A thermodynamic analysis of solvent denaturation is applied here to the abrupt conformational transition occurring in hyaluronate solutions buffered in phosphate when the pH is changed

0097-6156/81/0150-0229\$05.50/0
© 1981 American Chemical Society

across the physiological range 7.0-7.5 with ionic strength kept constant at 0.1. The transition is described in terms of a thermodynamic binding parameter, Γ_{32} , which is the equivalent of the stoichiometric binding parameter in site-binding theory, but which includes all modes of interaction of the molecule with the solvent including stoichiometric binding. This difference enables the treatment of long-range interaction and counterion condensation effects on the apparent pK , pK_a , of hyaluronate solutions.

The ability of phosphate buffers to shift the pK_a of hyaluronate solutions far from the pK of the carboxylate ion, pK_o , is due to the demonstrated tendency of amide groups and phosphate ions to bind preferentially. As the abrupt conformational transition is accompanied by an equally abrupt change in the second virial coefficient, it is suggested that the transition is due to a change of control from site-binding to ionic-atmosphere-binding. The pH at which ionic-atmosphere-binding occurs is far higher for the phosphate-amide group subsystem than for the carboxylate-salt subsystem, and this difference accounts for the shift of the pK_a far from the pK_o in phosphate buffer. In solutions in which the electrolytes are less able to penetrate the hydration shell of the amide group, the pK_a is less removed from the pK_o , and consequently the change of control occurs at a lower pH.

Whereas in the case of protein denaturation the mechanism concerns a balance between a salting-out of newly exposed non-polar groups and the salting-in of simultaneously exposed polar groups, in the case of hyaluronate solutions, on the other hand, the mechanism concerns the relative degree of salt effects on the amide group and the anionic carboxyl group, both effects producing stabilization/destabilization in the same direction, but with the phosphate-amide binding preventing destabilization until a higher pH, when salting-in is occurring.

The implications of this point of view are explored for an understanding of 1) the elastic (energy storing) property of hyaluronate solutions and 2) the two kinds of energy dissipating properties (intrinsic and internal viscosity) of such solutions.

The observable properties of a polyelectrolyte depend upon the distribution of small ions in its neighborhood. This distribution is affected by two types of "binding" (20, 21). The first involves the binding of counterions to specific sites of the macroion, i.e., "site-binding" (20). The second involves the binding of counterions anywhere in the vicinity of the macroion, i.e., "ionic-atmosphere-binding". The site-binding of phosphates to nonpolar amides is unique.

Recently, Manning has proposed that the site-binding/ionic-atmosphere-binding distinction between bound counterions be classified as a distinction between site-binding and "territorial binding" (9). Site-binding refers to the direct contact between one or more charged groups on a polyion without the inter-

vention of water molecules (10, 11). Territorial binding is defined as binding other than site-binding, and may include interactions with the Coulomb field of the charged groups of the macroion. The distinction between two types of binding may be experimentally demonstrated (10-15). As, at the time of writing, there appear to be at least three names in use to refer to binding other than site-binding, we shall use "ionic-atmosphere-binding" as a disposable label for this binding other than site-binding, lest we choose an obsolescent name, and refer the reader to Manning's discussion of the matter (9). Moreover, the term "ionic-atmosphere-binding" will be used here as descriptive of the interactions of the counterion with specific locations on the polyion, as well as diffuse Debye-Hückel atmospheric screening. It is therefore descriptively broader than the term "territorial binding", which does not include atmospheric screening of the Debye-Hückel type within its scope, and is, moreover, related to the concept of "apparent ionic charge" of Magdelénat *et al.* (16, 17, 18, 19).

Theoretical

It is known that the presence of phosphate ions slows a denaturation reaction. Simpson and Kauzman (22) demonstrated in a study of the effects of various electrolytes on the rate of denaturation of ovalbumin in urea that phosphate (HPO_4^{2-} and H_2PO_4^-) slowed the denaturation reaction. Thus, the removal of the pK far from the pK of the carboxylate anions in the hyaluronate ^a studies examined here (1, 2, 3) may also be ascribed to the use of phosphate buffer. The following analysis proceeds, however, along thermodynamic lines, not kinetic.

The effect of phosphate on the amide group of hyaluronic acid is, however, expected to be different from the effect of the potassium cation on the carboxylate anion. This could be demonstrated by the obtainment of salting-out coefficients, \underline{K}_s , for the two sites, which is defined by the Setschenow equation (23-29):

$$\log a = \log S_0/S = \underline{K}_s c_s, \quad (1)$$

where a is the activity coefficient, S_0 is the solubility in water (grams/liter), S is the solubility in a given solvent at the same temperature, and c_s is the molar concentration of added salt.

For example, Robinson and Jencks (26) obtained a $\underline{K}_s = 0.5$ for ATGEE (acetyltetraglycylethyl ester), a polypeptide chain model, but a value of 3.0 was obtained for carboxyhemoglobin (30), and 6.48 for fibrinogen (31).

As ATGEE possesses amide dipoles it does not, however, provide the most appropriate model for the amide group of the N-

acetylglucosamine of hyaluronic acid. The monoamides N-methyl propionamide (NMP) and N-methyl acetamide (NMA), on the other hand, have been studied by Schrier and Schrier (27). These investigators noted that the salting-out coefficient for the amide group, \underline{k}_A , is quite independent of salt type except for charge. \underline{k}_A for uni-divalent salts is also 1.5-1.8 times the average value for uni-univalent salts.

If \underline{K}_S is divided into the group salting-out coefficients due to the amide group, \underline{k}_A , and the carboxylate group, \underline{k}_C , then the relative quantities of amide and carboxylate groups control the sign and magnitude of \underline{K}_S . As demonstrated by Schrier and Schrier (27) and others (32, 33), \underline{k}_A may be theoretically evaluated by utilizing an electrostatic model for salt effects, and the assumption of the additivity of group salting-out effects largely validated. It is the balance, therefore, of the degree of salting-out of amide groups and carboxylate groups which determines at what pH and ionic strength hyaluronic acid will be stabilized/destabilized. The process of stabilization/destabilization is complicated by the use of phosphate buffer due to the preferential binding of phosphate to the amide group previously mentioned. As this preferential binding is absent in the case of the destabilized carboxylate group, the conclusion is that this group is salted-in at a lower pH than the amide group. With phosphate buffer at constant ionic strength 0.1, this balance in the hyaluronate solution is such that a pH change from 7.0 to 7.5 salts-in, or denatures, the hyaluronate and permits water uptake. The requisite ratio of \underline{k}_A to \underline{k}_C is obtained for salting-in in the pH 7.0-7.5 range: i) by the buffering ratio of K_2HPO_4 and KH_2PO_4 ; ii) by the preferential binding of phosphates to the amide group, and potassium to the carboxylate group; and iii) by the prevention of a denaturation reaction of hyaluronic acid by phosphate until a higher pH - a prevention already observed kinetically in proteins (22).

Whereas in previous analyses of protein denaturation (28) a mechanism was proposed concerning a balance between a salting-out of newly exposed nonpolar groups and the salting-in of simultaneously exposed polar groups, which determines whether a particular salt will be a stabilizer or a destabilizer of a folded macromolecular structure, here, on the other hand, a mechanism is proposed concerning the relative degree of salt effects on the amide group and the anionic carboxyl group, both producing stabilization/destabilization in the same direction, but with the phosphate-amide site-binding producing a prevention in destabilization until a higher pH when salting-in is occurring. It is this prevention that shifts the pK_a of the molecule away from the pK_o of the carboxylate anion, and thus causes the

situation preceding the sudden transition in optical and rheological measures when the pH is changed from 7.0 to 7.5, while ionic strength remains constant at 0.1 (1, 2, 3).

It is recognized (26, 27) that electrostatic theories of salting out of the kind developed by Debye and Kirkwood (23) do not account for the large differences between the effects of different salts, such as is evident in the preference of phosphate for amide group binding. Whether this preference and relative prevention of the denaturation reaction implicates an interaction with a changing structure of liquid water has yet to be determined (26, 28).

The interpretation offered here depends on the feasibility of phosphate-amide group binding. In the discussion section below, evidence is presented concerning both this feasibility and also concerning the unique nature of this form of site binding.

The analysis to follow provides a thermodynamic parallel to the polyelectrolyte theories of Manning (34), Record (35), and Oosawa (36). These theories, although primarily addressing the case of ionic-atmosphere-binding, also recognize the effects of site-binding. For example, it is suggested that site-binding is to be expected for a polyelectrolyte with monovalent charged groups if the chain is sufficiently flexible [Ref. 34, p. 186]. Hyaluronic acid is such a flexible polymer, and additional reasons why site binding occurs in the case of the amide group are stated in the discussion section.

Numerical

The thermodynamic measure of binding, Γ_{32} , is defined (7):

$$\Gamma_{32} = \frac{-m_3\beta_{23}}{1 + m_3\beta_{33}} = -\left(\frac{\partial\mu_2}{\partial\mu_3}\right)_{m_2} = \left(\frac{\partial m_3}{\partial m_2}\right)_{\mu_3}^{m_2 \rightarrow 0} \quad (2)$$

where $m_{\underline{i}}$ is the molality; $RT\beta_{\underline{i}}$ is the excess free energy; $\mu_{\underline{i}}$ is the chemical potential for component \underline{i} ; $\beta_{\underline{ij}} = (\partial\beta_{\underline{i}}/\partial m_{\underline{j}})_{m_{\underline{k}}, T, P}$; and where the subscripts are standard for a three-component system (37). The superscript "d" will be used below to designate the differential measure of two solutions at different pH.

The $^d\beta_{23}$ s for five pH transitions: 6.0 \rightarrow 6.5, 6.5 \rightarrow 7.0, 7.0 \rightarrow 7.5, 7.5 \rightarrow 8.0, and 8.0 \rightarrow 8.5 for potassium hyaluronate buffered in phosphate solution at ionic strength 0.1, were calculated from the changes in free energy corresponding to changes in the molecular end-to-end chain length of the Rouse-Zimm-Peterlin description (38, 39, 40) with internal viscosity (1, 2, 3) given in Table IV of Ref. 2. We stress that these are difference measures, e.g., $^d\Gamma_{32} = \text{pH}_{\underline{i}}\Gamma_{32} - \text{pH}_{\underline{j}}\Gamma_{32}$, where $\text{pH}_{\underline{i}}\Gamma_{32}$ is

Γ_{32} for a solution at $\text{pH}_{\underline{i}}$ and $\mu = 0.1$ and $\text{pH}_{\underline{j}}\Gamma_{32}$ is Γ_{32} for a solution at $\text{pH}_{\underline{j}}$ and $\mu = 0.1$, where $\underline{i} \neq \underline{j}$ and in the experiments considered \underline{i} and \underline{j} take on the values 6.0, 6.5, 7.0, 7.5, 8.0, and 8.5, with constant ionic strength 0.1 throughout. The $\text{d}\Gamma_{32}$ s for these five pH transitions were calculated (Table I) and plotted in Fig. 1.

TABLE I

Binding parameters* for potassium hyaluronate solutions in phosphate buffers calculated by Eqs. (2), (3), (4), and (5) from data in Ref. 2.

pH	d Γ_{32} ^D	d Γ_{32} ^N	pH	$\Delta\Gamma_{32}$ & $\Delta\mu_0$	$\Delta\mu_s$
6.0 → 6.5	-1.03	~0	6.5	-1.03	-4.78
6.5 → 7.0	-2.16	~0	7.0	-2.16	-5.91
7.0 → 7.5	+18.49	~0	7.5	+18.49	+14.74
7.5 → 8.0	+15.12	~0	8.0	+15.12	+11.37
8.0 → 8.5	+16.84	~0	8.5	+16.84	+13.09

*in RT units.

The difference measure, $\Delta\Gamma_{32}$, for the solutions at pH 6.0, 6.5, 7.0, 7.5, 8.0, and 8.5 may be obtained by (7):

$$\Delta\Gamma_{32} = \text{d}\Gamma_{32}^{\text{D}} - \text{d}\Gamma_{32}^{\text{N}} = (\partial \ln K_a / \partial a_3)_{m_2, T, P}, \quad (3)$$

where $\text{d}\Gamma_{32}^{\text{D}}$ and $\text{d}\Gamma_{32}^{\text{N}}$ are the denatured and native difference state measures of binding, and $a_{\underline{i}}$ is the activity for component \underline{i} . In the case of the solutions considered here, $\text{d}\Gamma_{32}^{\text{N}}$ is slightly positive (Table I, Fig. 1). As it is a measure of a difference, and as it is reasonable to assume that Γ_{32}^{N} for pH 6.0 is negative (41), the slightly positive values for $\text{d}\Gamma_{32}^{\text{N}}$ indicate a difference from a negative baseline.

In the case of the solutions considered here, $\text{d}\Gamma_{32}^{\text{D}}$ is clearly positive. As β_{23} is equal to b_{23} (7), the second virial coefficient for a nonideal solution, Equ. (2) suggests that this coefficient is negative for all six solutions with an abrupt increase in value for the three solutions of pH 7.5, 8.0, and 8.5. Hyaluronic acid is expected to have significant virial coefficients higher than the second. Shaw and Schy (42) obtained a

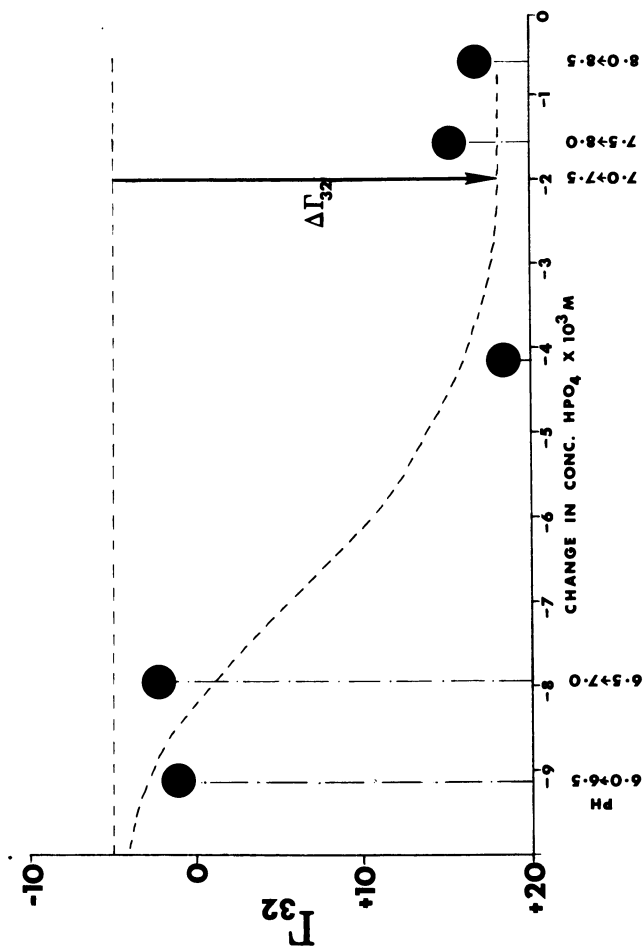


Figure 1. Binding parameters for potassium hyaluronate in phosphate buffer ($\text{pK}_a = 7.2$) based on Refs. 1 and 2 and demonstrating conformational change. Dotted curve is $\Delta\Gamma_{32}$.

virial coefficient value of 5.08×10^{-3} (ml/gm) for low molecular weight hyaluronic acid buffered in saline at pH 7.2. Comparable values based on calculations for the third virial coefficient using the presently considered data (1, 2, 3) for high molecular weight human umbilical cord hyaluronic acid in this pH range are 8.50×10^{-3} and 8.92×10^{-3} (ml/gm) for solutions at pH 7.0 and 7.5, respectively (41).

Positive measurements of second virial coefficients are considered due to attraction of solvent across a membrane to a second compartment containing the macromolecules considered (43, 44). The second virial coefficient is also a function of the cohesion between molecules, whereas, according to the theories of Van der Waals and Berthelot, the third virial coefficient is not. As hyaluronic acid tends to associate at low pH, the theoretical assumption of force additivity is denied.

In the case of hyaluronate solutions, acidification reduces the mutual repulsion of negatively charged chain elements through the protonation of carboxyl groups of the glucuronic acid moiety (5). The neutral amide groups of the N-acetylglucosamine moiety are also protonated during acidification, but to positively charged groups (56). This protonation of the amide groups is of importance in removing the apparent equilibrium constant of the hyaluronate solution (which is 7.2 for hyaluronate in phosphate) far from the equilibrium constant for the carboxyl group alone, i.e., from the pK, which is 3.23. As acidification leads to a highly compact^o form, a reduction of intermolecular repulsion is implied and, hence, a slightly negative second virial coefficient. Measurements of nonideality are thus likely to reflect the sum total of negative second virial coefficient and positive third virial coefficient.

Negative second virial coefficients for hyaluronate solutions at low concentration have been measured by light scattering (45), and are reflected in the $d_{\Gamma_{32}}^N$ values at or near zero and the negative $d_{\Gamma_{32}}^D$ values at low pH (Table I). The expansion of hyaluronic acid in alkaline solution is reflected in the positive $d_{\Gamma_{32}}^D$ values of Table I, i.e., in positive third virial coefficients.

The free energy of unfolding of the polymer is (7):

$$\Delta\mu_o = \Delta\Gamma_{32} (1 + \beta_{33}m_3); \quad (4)$$

and the change in standard chemical potential or free energy on adding reagents is (7):

$$\Delta\mu_s = \Delta\mu_o + RT\Delta b_2, (m_2 \rightarrow 0), \quad (5)$$

where Δb_2 is defined:

$$\Delta b_2 = \ln K_o - \ln K_a, (m_2 \rightarrow 0). \quad (6)$$

As the pK of the hyaluronate carboxyl group is 3.23 and that of hyaluronate in phosphate-buffered solution is 7.2, Δb_2 is -3.97 in RT units. $\Delta\mu_o$ and $\Delta\mu_s$ for five solution pHs are given in Table I.

Theoretical binding parameters for hyaluronate solutions based on Refs. 1, 2, 4, and 6 are sketched in Figure 2. Conformational changes are demonstrated for pK_a s at a, b, c, and d.

The line $\Gamma_{32}^N = (\Gamma_{32}^N C + \Gamma_{32}^N A)$ indicates the site-binding for both the carboxylate group and the amide group, and the line $\Gamma_{32}^D = (\Gamma_{32}^D C + \Gamma_{32}^D A)$ indicates the ionic-atmosphere-binding for both the carboxylate and the amide group. The conformational change lines a, b, c, and d also indicate a switch from site-binding to ionic-atmosphere-binding in a joint action for both the carboxylate and amide group, although the carboxylate group switches at lower pH, and the amide group switches at higher pH. As the conformational transition is a joint action, therefore, the conformational change line actually seen for hyaluronate in phosphate buffer is at a pK_a which is a compromise between the low and high pH switches. This compromise induced by the amide-phosphate interaction, which switches from site-binding to ionic-atmosphere-binding at a solution pH higher than in the case of the carboxylate-counterion interaction, accounts for the removal of the pK far from the pK_o . For example, if $\Gamma_{32}^N A > \Gamma_{32}^N C$ and $(\Gamma_{32}^N C + \Gamma_{32}^N A) > (\Gamma_{32}^D C + \Gamma_{32}^D A)$, then the binding parameter for the molecule in solution will be represented on the Γ_{32}^N line, even if $\Gamma_{32}^N C < \Gamma_{32}^D C$. Only when $(\Gamma_{32}^N C + \Gamma_{32}^N A) < (\Gamma_{32}^D C + \Gamma_{32}^D A)$ will there occur a switch to the Γ_{32}^D line, and this will be at a pK_a removed from the pK_o determined only with respect to the carboxylate group.

The remainder of this paper explores the detailed implications of this point of view for hyaluronate solutions which exhibit the properties of both 1) elasticity or energy storage behavior and 2) two kinds of energy dissipation behavior - intrinsic and internal viscosity.

Discussion

It is relevant to this discussion that membrane equilibrium measurements have shown that under certain conditions the lithium ion is bound more strongly to long-chain phosphates than the sodium ion (46), as this reversal of the normal binding order implies penetration of the phosphate groups through the hydration shell of the alkali metal ions, and thus site binding. This binding order was also observed by electrophoresis (47),

conductivity (48), and dilatometric (49) experiments. In the hyaluronate solution experiments under discussion here the phosphate ions exist in solution, and the amide group of N-acetylglucosamine performs the function of the alkali ions; i.e., the ionic composition of molecule and solution are reversed. Nonetheless, the result is the same consequence of site binding.

We note that DNA in alkali metal ion solution, due to the phosphate groups along its backbone, also offers the situation converse to hyaluronic acid in phosphate buffer regarding the siting of neutralized ion and phosphate ion, i.e., whether on the macromolecule or in the solution. Both situations, however, offer the opportunity of an abrupt transition, which is due to site-binding regardless of which of the binding groups exists on the macromolecule. Because, in the case of nucleic acids, the phosphates reside on the macromolecule, the apparent association constant of, e.g., poly(A)·poly(U)-oligolysine, is a function of alkali metal ion concentration (50, 51).

It is relevant to mention that those theoretical treatments of polyelectrolytes only in terms of ionic-atmosphere-binding have failed in the case of alkali metal ions. For example, Kottin and Nagasawa (52) examined only those cases in which the degree of ionization did not allow site binding of alkali metal ions; and Alexandrowicz and Katchalsky (53) were only able to account for membrane equilibrium and osmotic pressure results obtained for polyacrylates and polyphosphates by assuming a much higher charge per unit length than was used for potentiometric titrations. It is interesting, therefore, that alkali metal ions also site-bind to polyacrylate, although not as much as to polyphosphate (49).

It does not appear that the solvation of the amide groups hinders phosphate binding. A similar case exists for the flavins (54, 55). In the case of clostridial flavodoxin, the phosphate group is not bound to a basic arginine or lysine side chain but to a cluster of neutral polar groups - four hydroxyl groups from serine and threonine residues and four backbone NH groups. Thus, the penetration of the amide group's solvation shell by the phosphate ion is also likely in the case of hyaluronate solutions.

For the reasons outlined above, and in the case of hyaluronate in phosphate buffer, the two measures of binding, $d_{T_{32}}^D$ and $d_{T_{32}}^N$, may be designated functions of the degree of solvation of the amide group (i.e., degree of ionic-atmosphere-binding) and of the degree of protonation (i.e., degree of site-binding), respectively, of the amide and carboxylate groups. The solvation properties of the electrically neutral amide group are not only affected by the presence of phosphate divalent anions, as discussed, but also by the presence of divalent cations, but to a lesser degree (6). This influence on the ability of the amide group to bind water results in a change in the pK_a , osmotic

pressure, and in the abrupt conformational change. As the conformational change occurs at $\text{pH} = \text{pK}_a$, and as (7):

$$\left(\frac{\partial \ln K_a}{\partial C_3} \right)_{T,P} = - \frac{\Delta b}{2} \left(\frac{C}{3} \rightarrow 0 \right), \quad (7)$$

where $C_3 = (1,000 \text{ m}^3)/V_m$ and $V_m = (1,000/\text{m}_1)\bar{V}_1 + \sum_{i=2}^n m_i \bar{V}_i$, one may predict a relation between the degree of abruptness of the conformational change and the extent of the difference between pK_a and pK_o . This theoretical relation is demonstrated in Fig. 2.

According to Equ. (1), the free energy of unfolding of hyaluronic acid is related to the free energy of transfer from one medium to another. In the instances considered here, in which $\text{pK}_a > \text{pK}_o$, the free energy of transfer was between polymer and solution. Equ.s (1) and (6) suggest that for a solution of $\text{pH} = \text{pK}_o = 3.23$, i.e., the pK of the carboxylate ion, this transfer cannot occur. At solution $\text{pH} 2.5$, hyaluronic acid is a viscoelastic putty (56); but when the solution pH is raised, the dissolved hyaluronic acid becomes less elastic and more viscous (57). That is to say, for a change in pH so that solution $\text{pH} > \text{pK}$, whether the pK is pK_o or pK_a , an increase in viscosity is to be expected - as has been demonstrated (1). Furthermore, according to the analysis of Fig. 2, this means that if the binding of the polymer is best described by Γ_{32}^D (i.e., it is predominantly ionic-atmosphere-binding), then viscous behavior is to be expected; if it is best described by Γ_{32}^N (i.e., it is predominantly site-binding), then elastic behavior is to be expected. When $\Gamma_{32}^D = \Gamma_{32}^N$, the polymer is in a "viscoelastic putty" state; i.e., it is viscous as well as elastic, of small volume, with both bound water and bound salt.

We may indicate these various states as follows.

A. For the predominantly elastic state occurring with a solution buffered at a $\text{pH} \leq \text{pK}_o$ and $|\Gamma_{32}^D| - |\Gamma_{32}^N| < 0$, $\Gamma_{32}^N > 0$, $\Gamma_{32}^D \approx 0$, we define the following measure of binding:

$$\Gamma_{24} = - \frac{\partial \mu_2}{(\partial \mu_4)} = -\Gamma_{32}^N = + \left(\frac{\partial \mu_2}{\partial \mu_3} \right)^N, \quad (8)$$

where μ_4 is a stress (pressure) induced chemical potential.

B. For the hyaluronate system in the viscoelastic putty state buffered at $\text{pH} = \text{pK}_o$, we have:

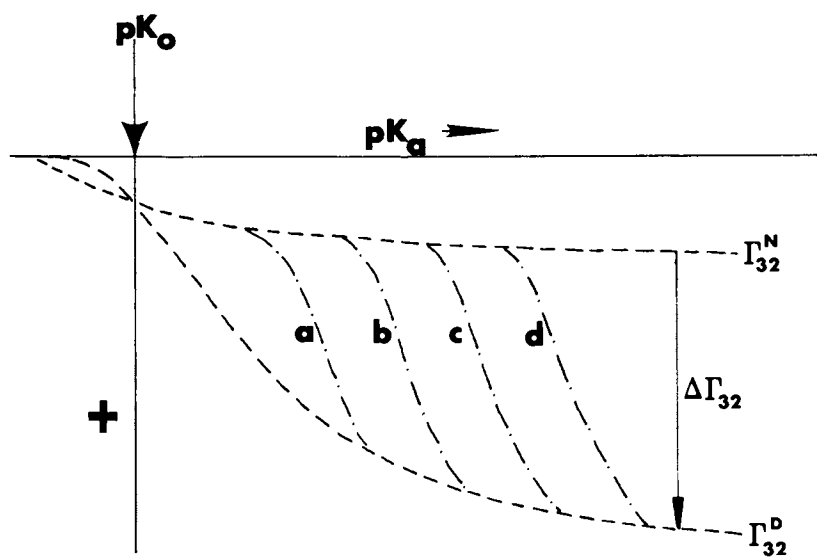


Figure 2. Theoretical binding parameters for hyaluronate solutions. See text for explanations.

$$-\Gamma_{24} - \Gamma_{32}^D = \Gamma_{32}^D - \Gamma_{32}^N = 0, \text{ i.e., } \Gamma_{24} = -\Gamma_{32}^N. \quad (9)$$

C. For those instances when $pK_o < pH < pK_a$ and $|\Gamma_{32}^D| - |\Gamma_{32}^N| > 0$, the solution is more elastic than viscous; i.e., $G'' < G'$, where G'' is the dissipative shear modulus, and G' is the storage shear modulus for hyaluronate solutions subjected to oscillatory shear (57).

D. For those instances when solution $pH > pK_a$ and $|\Gamma_{32}^D| - |\Gamma_{32}^N| > 0$, the system is more viscous than elastic; i.e., $G'' > G'$. At solution $pH \sim pK_a$, there is an abrupt increase in intrinsic viscosity and also internal viscosity (1, 58, 59, 60); i.e., there is a correlation of changes in elasticity and internal viscosity with changes in the binding theory measures of Γ_{32}^N and Γ_{32}^D .

In effect, the amount and sign of the difference between measures of ionic-atmosphere-binding and site-binding, i.e., $\Delta\Gamma_{32} = \Gamma_{32}^D - \Gamma_{32}^N$, describes the degree of elasticity, intrinsic viscosity, and internal viscosity as follows:

i) Predominantly elastic, or energy storing, behavior implies $\Delta\Gamma_{32}$ is negative, $|\Gamma_{32}^N| > |\Gamma_{32}^D|$, $\Gamma_{32}^D \sim 0$, and thus site-binding predominates.

ii) Predominantly viscous, or energy dissipating, behavior, i.e., as indicated by an intrinsic viscosity measure, implies $\Delta\Gamma_{32}$ is positive, $|\Gamma_{32}^N| < |\Gamma_{32}^D|$, $\Gamma_{32}^N \sim 0$, $\Gamma_{32}^D > 0$, and ionic-atmosphere-binding predominates.

iii) The presence of internal or bulk viscosity, determined by an order parameter and relaxations of excited long-range macromodes, in the presence of an intrinsic viscosity, which represents relaxations of excited micromodes, implies, again, that $|\Gamma_{32}^N| > |\Gamma_{32}^D|$, but requisite relaxation times apply; e.g., if τ_M and τ_m are the relaxation times for macro- and micromodes, respectively, then $\tau_m \geq \tau_M$, and internal viscosity is appreciable. On the other hand, in the less entropic state, $\tau_M > \tau_m$ (62, 63, 64), and internal viscosity is negligible. Thus, the absence of internal viscosity at solution pHs 6.0, 6.5, and 7.0 and its presence at 7.5, 8.0, and 8.5 is due to the adiabatic elimination of internal viscosity at the lower pHs, by which slowly varying degrees of freedom are exhausted (65). Whereas intrinsic viscosity is essentially low frequency viscosity based on Markovian processes, internal viscosity is essentially high frequency viscosity based on non-Markovian processes with memory (65, 66). Internal viscosity is correlated with the magnitude of $|\Gamma_{32}^D|$ or ionic-atmosphere-binding in the presence of an intrinsic viscosity approximating the same time order or greater;

intrinsic viscosity is also correlated with the magnitude of $|\Gamma_{32}^D|$ or ionic-atmosphere-binding, but is unrelated to the time order of the internal viscosity.

The states described by i), ii), and iii) may exist to varying degrees simultaneously. Hyaluronic acid, unlike DNA, exhibits internal viscosity (1), and thus all three types of behavior. There is an abrupt increase in both intrinsic and internal viscosity across the pH range 7.0-7.5 in phosphate buffer (1, 2, 3), and these changes are indicative of the conformational transition.

The abruptness of the change from site-binding to ionic-atmosphere-binding, at the change of solution pH from 7.0 to 7.5, may be described as follows. In the case of a limiting model of an electrical double layer, in which there is no penetration of the inner layer by mobile ions, the relation of the measure of binding to polyelectrolyte theory is expressed by (67):

$$\Gamma_{32} = \frac{\xi}{2} + V_2 n_3^* \quad (10)$$

where V_2 is the molar volume of the polymer, n_3^* is the number of free ions determined by a membrane electrode, and thus $V_2 n_3^*$ is the excluded volume. The reduced linear charge density, ξ , introduced by Manning (8) and Oosawa (26) is defined:

$$\xi = \frac{q^2}{\epsilon kT} \frac{Z}{L} \quad (11)$$

where q is the protonic charge, ϵ is the bulk dielectric constant of solvent, L is the length of the molecule, k is the Boltzmann factor, T is the absolute temperature, and Z is the number of elementary charges within the molecule's cylindrical surface.

If ξ becomes greater than unity (i.e., if $Z/L > 7.14 \text{ \AA}$ in water at 25°C), then a switch occurs from site-binding to ionic-atmosphere-binding. This means that both the carboxylate anion and the amide group ionic-atmosphere-bind when this occurs, and the amide groups' hydrophilicity determines an abrupt conformational change. Thus, in the experiments considered, as solution pH is increased, ξ increases, ionic-atmosphere-binding occurs, and sufficient counterions "condense" on the polyion to lower the net value of ξ to unity in a feedback type of control. Letting $-\xi/2 \sim \Gamma_{32}^N$ (for solution pH 6.0, 6.5, and 7.0 in the experiments considered) and $V_2 n_3^* \sim +\Gamma_{32}^D$, then Equ. (10) is related to Equ. (3). At solution pHs 6.0, 6.5, and 7.0, the value of ξ is less than unity; at solution pHs, 7.5, 8.0, and 8.5, the value of ξ exceeds, then is returned to unity by feedback control, i.e., counterion condensation. In terms of Equ. (3) and the

carboxylate and amide groups, we have $\Delta\Gamma_{32} = (\Gamma_{32}^D \underline{C} + \Gamma_{32}^D \underline{A}) - (\Gamma_{32}^N \underline{C} + \Gamma_{32}^N \underline{A})$, where the subscripts \underline{C} and \underline{A} refer to the carboxylate anion and the amide group, respectively. $\Delta\Gamma_{32}$ is thus the independent variable for the observed conformational transition. However, as this is a limiting model, the description is only of the conformational transition stage.

Considering now a model in which the fixed charges are in an inner layer and mobile charges may enter this layer, site-binding or incomplete dissociation is assumed to occur whenever an ion is so close to the macroion that desolvation takes place. The degree of dissociation is $1/Q$ (20), where

$$\alpha Q = 2\xi = \left(-x \frac{d\phi}{dx}\right)_{x=E}; \quad (12)$$

$\phi = e\psi/kT$, ψ = absolute value of the Poisson-Boltzmann electrostatic potential, $x = \kappa_0 r$; r = distance from the axis of a cylindrical rod molecular model; and where the degree of site binding is $1 - \alpha$, α being the degree of ionization or the fraction of ionic groups of the macroion which are not neutralized by site-binding counterions; i.e., $1 - \alpha$ is the degree of neutralization within the inner layer of an electrical double layer model. At zero ionic strength (i.e. $E = 0$, where $E = \kappa_0 a$ and $\kappa_0 = (8\pi N_A q^2 n_3 / 1,000 \epsilon kT)^{1/2}$, n_3 is the concentration of the electrolyte far from the macroion, and a is the assumed cylindrical rod molecular model), the measure of binding is defined (20, 21):

$$\lim_{E=0} 2\Gamma = \alpha - \frac{\alpha^2 Q}{4}, \quad 0 \leq \alpha Q \leq 2, \quad \text{for site binding} \quad (13A)$$

$$\lim_{E=0} 2\Gamma = \frac{1}{Q}, \quad \alpha Q > 2, \quad \text{for ionic atmosphere binding.} \quad (13B)$$

In aqueous solution at 25°C, the critical condition $\alpha Q = 2$ corresponds to an average axial distance of $\sim 7 \text{ \AA}$ between the nearest ionized (i.e., non-site-bound) polyelectrolyte groups. When this distance is smaller than $\sim 7 \text{ \AA}$, 2Γ does not depend on α (21). Thus, the critical value of $\xi = 1$ is when $\alpha Q = 2$.

Equ. (10) is now (67):

$$\Gamma = \alpha/2\beta\epsilon + V_2 n_3^*, \quad (14)$$

where β is a correction factor for the surface potential; and we redefine $\Gamma_{32}^N = -\alpha/2\beta\epsilon$. Just as in the impenetrable model, above, $\Delta\Gamma_{32} = (\Gamma_{32}^D \underline{C} - \Gamma_{32}^D \underline{A}) - (\Gamma_{32}^N \underline{C} - \Gamma_{32}^N \underline{A})$; and, as before, $\Delta\Gamma_{32}$ is the independent variable of the observed conformational transitions.

We have suggested (Fig. 1) that during the conformational change to the more disordered configuration there is a switch in control (of the determination of configuration entropy) from site-binding to ionic-atmosphere-binding. Evidence has been discussed concerning the site binding of phosphates and alkali metal ions, and we presented evidence to suggest that this type of binding could occur on the amide groups of hyaluronic acid. The switch, therefore, from a description in terms of Equ. (13A) to one in terms of (13B), when $\xi > 1$ for initially the carboxylate group, and finally the amide group, means that ionic-atmosphere-binding becomes the major determinant of hyaluronic acid conformation at high pH; i.e., in phosphate buffer at ionic strength 0.1, a change in solution pH 7.0 to 7.5 results in an abrupt increase in hyaluronate entropy. It seems reasonable, therefore, to identify Γ , as defined by Equ. (13A), with $(\Gamma_{32}^N \underline{C} + \Gamma_{32}^N \underline{A})$ and Γ , as defined by Equ. (13B), with $-(\Gamma_{32}^D \underline{C} + \Gamma_{32}^D \underline{A})$.

X-ray diffraction studies (68-78) of the possible conformations available in hyaluronic acid in solution indicate that helices packed together in various arrangements are possible. It is therefore appropriate to relate the present analysis to the theory of the helix-to-coil transition. In the model developed by Zimm and Rice (79) for helix-to-coil transitions in charged macromolecules, the fraction, θ , of intact hydrogen bonds in the helix is given by:

$$\theta = \frac{1}{z} \frac{\partial \ln \Xi}{\partial \ln s} = \frac{\partial \ln m}{\partial \ln s} \quad (15)$$

where Ξ is a semi-grand partition function for a polymer of many identical subunits, each of which may ionize, and each of which may also hydrogen bond to the appropriate other segment of the same chain to form an α -helix; z is the number of charge sites on the polymer; and s is the equilibrium constant for the addition to a section of helix of the appropriate segment from the adjacent section of randomly coiling chain. Therefore, in the event that the conformational structure of hyaluronic acid is dependent on the assumptions of the Zimm-Rice model, we have the following relation with the present model:

$$\theta = 1 - \frac{|\Delta\Gamma_{32}|}{|\Delta\Gamma_{32}|_{\max}} \quad (16)$$

In fact, the Zimm-Rice model describes qualitatively similar changes in the titration curves for polyglutamic acid (Ref. 79, p. 402, Fig. 3) as those changes plotted in Fig. 2: an increase in ionic strength shifts the pK_a to the left and increases the slope of the wave. We also have a relation between solution pH

and pK_a in (80):

$$0.434 \ln a_3 = pH - pK_a = \frac{0.434}{ZkT} \frac{\partial RT \beta_j}{\partial \alpha}, \quad (17)$$

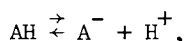
where α is the degree of ionization and defined:

$$\alpha = \frac{1}{Z} \frac{\partial \ln \Xi}{\partial \ln a_3} \quad (18)$$

In the case of a cylindrical polyion with the boundary condition at the surface of the cylinder determined self-consistently, so that the only input required is the density of ionizable groups on the cylinder surface and their dissociation characteristics, Equ. (17) is more aptly given by (81):

$$pH = pZ + \log_{10} \frac{\alpha}{1-\alpha} - \frac{0.434 e \phi_s}{kT}, \quad (19)$$

where Z is the equilibrium constant for the dissociation reaction



$-e$ is the electronic charge, and ϕ_s is the uniform surface potential.

Due to the self-consistent boundary condition, the pH at the surface of the polyion, pH_s , is the pH the acid group "sees", not the reservoir pH. Thus, pH_s is always less than the pZ of the ionizable groups and is written as (81):

$$pH_s = pH - \log_{10}(1 + \phi_s^*), \quad (20)$$

where $\phi_s^* = -e\phi_s/kT$. The movement of the curves of Fig. 2 to the right thus indicates an increasing ϕ_s^* .

According to this theory, the Debye screening length $1/\kappa$:

$$\frac{1}{\kappa} = \frac{(1,000 \epsilon kT)^{1/2}}{8\pi e^2 N_0} I^{-1/2} \text{ in cm}, \quad (21)$$

where $I = \frac{1}{2} \sum_j z_j^2$, and N_0 is Avogadro's number, is a measure of

the penetration depth into the solution of the electric field produced by the surface charge distribution. A large value for the Debye screening length corresponds to a "thick" double-layer, and a small value corresponds to a "thin" double-layer. The potential at the surface of the cylinder is due to the surface charge distribution and the ionic atmosphere surrounding the cylinder, which is diffuse. This diffuseness of the ionic atmosphere does not permit a balance with the surface charge, so the surface potential remains negative (81). There are theoretical

reasons for believing that charge structures play very little role in polyelectrolyte molecular interactions at distances greater than the Debye length of the solution in which the molecules are immersed (82). At greater distances, attractive forces of electrodynamic origin are important; and, at distances near the Debye length, a balance exists of repulsive electrostatic forces and attractive forces (83).

The problem of hyaluronic acid conformational transitions also involves consideration of these transitions as examples of changes in amounts of hydrogen bonding, or of changes in amounts of bound water.

The study by Scheiner and Kern (84), using quantum mechanical methods, of the effects of hydrogen-bonded water on peptide bonds is relevant in this regard. The peptide unit was modeled by trans-N-methylacetamide (NMA). It was found that many of the effects of a full hydration shell can be simulated by the interaction of two water molecules, and interpeptide hydrogen bonding is found to have much the same effects as hydration. Whereas previous studies of amide group interactions and hydration of amides dealt mostly with amide units in their fully planar conformation, Scheiner and Kern studied conformations other than this preferred conformation, as relatively little energy is required for significant deviations from planarity to occur. They found that, apart from water binding to oxygen and the NH group, the possibility exists of water hydrogen bonding to the π system of an amide, and considered the possible effects of those species, such as phosphate, which interacts with the amide through the intermediary of a second moiety, e.g., a second hydration shell.

Further evidence for an alkali-induced conformation change (disorder-order, this time) comes from ^1H nuclear magnetic resonance studies (85, 86). The addition of alkali was seen to cause the hyaluronate spectrum to sharpen, indicating that segmental motion is enhanced by disruption of presumed inter-residue bonding upon the ionization of hydroxyl groups. The authors of these studies indicate that changes in the configuration of the acetamidodeoxyhexose residue are critical in influencing the overall conformation of hyaluronic acid, a result in agreement with the thesis of the present view. On the other hand, Mathews and Decker (87) report that increasing the pH of a neutral salt solution of sodium hyaluronate (0.4 M NaCl, pH \sim 5.5) to pH 12.5 (2.5 M NaOH) produces a rapid drop in viscosity. This result is understandable from the present view not as a pH-increase-induced order-disorder transition, but as a salt-induced disorder-order transition, as ionic strength was uncontrolled.

The possibility of salts acting through a second hydration shell on amide groups is relevant to the change in osmosis by salt action. As Bjerrum (88) and Onsager (89) have pointed out, electrostatic interaction at close range may be so strong that pairs of ions and, of more relevance to this discussion, anions

around a cation will stay together for a long time and act like a single molecule. The result of this close range interaction will be electrostatic screening, and hence a change in long range interaction. This observation is relevant in the following regard. Although the pH-dependent conformational transition of hyaluronic acid in phosphate has been observed by optical and rheological methods (1, 2, 3), it is not observable using laser Raman spectroscopy (90), which is a probe of only primary and secondary structure. This finding, together with the observation of a small limiting birefringence but a large limiting extinction angle with minimum change in monomer anisotropy (1), strongly suggests that the pH-dependent conformational transition of hyaluronic acid is due to a change in long-range interaction. This aspect of the conformational transition is treated in Ref. 91.

Finally, we address the physiological consequences of this conformational transition. The major intracellular buffer is phosphate buffer (92). Furthermore, although the bicarbonate buffer system is present in higher concentration in the eye, the phosphate buffer exists even in intraocular fluid (93). We may thus have one answer to the question: "What molecular mechanisms in cells are so extraordinarily sensitive that a change in H^+ concentration of as little as 3×10^{-8} M (approximately the difference between blood at pH 7.4 and blood at pH 7.0) can be lethal?" [Ref. 92, p. 51], in the particular buffering action of phosphates on hyaluronates.

Synopsis

Potassium cations, at low solution pH, site-bind to the carboxylate anions, and at a high solution pH ionic-atmosphere-bind; and, similarly, the phosphate anions selectively site-bind to the amide group at low solution pH, but at a high solution pH - higher than in the case of the potassium-carboxylate complex - also ionic-atmosphere-bind. The abrupt transition occurs at a pH at which there is a switch from control of conformation by the amide group site-binding (in the presence of the carboxylate group already switched to ionic-atmosphere-binding) to both an amide and carboxylate ionic-atmosphere-binding. In all instances, the transition referred to will be from low entropy to high.

Literature Cited

1. Barrett, T. W.; Harrington, R. E. Biopolymers, 1977, 16, 2167.
2. Barrett, T. W. Biopolymers, 1978, 17, 1567.
3. Barrett, T. W. Biopolymers, 1979, 18, 351.
4. Park, J. W.; Chakrabarti, B. Biopolymers, 1977, 16, 2807.
5. Park, J. W.; Chakrabarti, B. Biopolymers, 1978, 17, 1323.

American Chemical
Society Library
1155 16th St. N. W.

6. Chakrabarti, B. Arch. Biochem. Biophys., 1977, 180, 146.
7. Schellman, J. A. Biopolymers, 1978, 17, 1305.
8. Manning, G. S. J. Chem. Phys., 1972, 51, 3249.
9. Manning, G. S. Accounts of Chemical Research, 1979, 12, 443.
10. Spegt, P.; Weill, G. Biophys. Chem., 1976, 4, 143.
11. Karenzi, P. C.; Meurer, B.; Spegt, P.; Weill, G. Biophys. Chem., 1979, 9, 181.
12. Zana, R.; Tondre, C.; Rinaudo, M.; Milas, M/ J. Chim. Phys. Physicochim. Biol., 1971, 68, 1258.
13. Zana, R.; Tondre, C. Biophys. Chem., 1974, 1, 367.
14. Tondre, C.; Kale, K. M.; Zana, R. Eur. Polym. J., 1978, 14, 139.
15. Ikegami, A. J. Polym. Sci., 1964, Part A 2, 907.
16. Magdelénat, H.; Turq, P.; Chemla, M. Biopolymers, 1974, 13, 1535.
17. Magdelénat, H.; Turq, P.; Tivant, P.; Chemla, M.; Menez, R.; Drifford, M. Biopolymers, 1979, 18, 187.
18. Magdelénat, H.; Turq, P.; Tivant, P.; Menez, R.; Chemla, M.; Drifford, M. J. Chem. Educ., 1978, 55, 12.
19. Schmitt, A.; Meullenet, J. P.; Varoqui, R. Biopolymers, 1978, 17, 1249.
20. Gross, L. M.; Strauss, U. P. In Conway, B. E.; Barradas, R. G. (eds.) "Chemical Physics of Ionic Solutions"; Wiley: New York, 1966; pp. 361-389.
21. Strauss, U. P.; Helfgott, C.; Pink, H. J. Phys. Chem., 1967, 71, 2550.
22. Simpson, R. B.; Kauzman, W. J. Am. Chem. Soc., 1953, 75, 5139.
23. Long, F. A.; McDevit, W. F. Chem. Rev., 1952, 51, 119.
24. Flory, P. J. J. Cell. Comp. Physiol., 1957, 49, 175.
25. Von Hippel, P. H.; Wong, K-Y. Biochemistry, 1962, 1, 664.
26. Robinson, D. R.; Jencks, W. P. J. Am. Chem. Soc., 1965, 87, 2470.
27. Schrier, E. E.; Schrier, E. B. J. Phys. Chem., 1967, 71, 1851.
28. Von Hippel, P. H.; Schleich, T. In Timasheff, S. N.; Fasman, G. D. (eds.) "Structural Stability of Biological Macromolecules"; Dekker: New York, 1969; pp. 417-574.
29. Hofmeister, F. Arch. Exptl. Pathol. Pharmacol., 1888, 24, 247.
30. Green, A. A. J. Biol. Chem., 1931, 93, 517.
31. Florkin, M. J. Biol. Chem., 1930, 87, 629.
32. Nandi, P. K.; Robinson, D. R. J. Am. Chem. Soc., 1969, 94, 1308.
33. Jencks, W. P. "Catalysis in Chemistry and Enzymology"; McGraw-Hill: New York, 1969.
34. Manning, G. S. Quart. Rev. Biophysics, 1978, 11, 179.
35. Record, T. M. Jr.; Anderson, C. F.; Lohman, T. M. Quart. Rev. Biophysics, 1978, 11, 103.

36. Oosawa, F. "Polyelectrolytes"; Marcel Dekker: New York, 1971.
37. Casassa, E.; Eisenberg, H. Adv. Protein Chem., 1964, 19, 287.
38. Rouse, P. E. Jr. J. Chem. Phys., 1953, 21, 1272.
39. Zimm, B. H. J. Chem. Phys., 1956, 24, 269.
40. Peterlin, A. J. Chem. Phys., 1963, 39, 224.
41. Barrett, T. W. In preparation, 1980.
42. Shaw, M.; Schy, A. Biophysical J., 1977, 17, 47.
43. Hirschfelder, J. O.; Curtiss, C. F.; Bird, R. B. "Molecular Theory of Gases and Liquids"; Wiley: New York, 1954.
44. Tombs, M. P.; Peacocke, A. R. "The Osmotic Pressure of Biological Macromolecules"; Clarendon: Oxford, 1974.
45. Barrett, T. W.; Baxter, J. E. In preparation, 1980.
46. Strauss, U. P.; Ross, F. D. J. Am. Chem. Soc., 1959, 81, 5299.
47. Strauss, U. P.; Woodside, D.; Wineman, P. J. Phys. Chem., 1957, 61, 1353.
48. Strauss, U. P.; Bluestone, S. J. Am. Chem. Soc., 1959, 81, 5292.
49. Strauss, U. P.; Leung, Y. P. J. Am. Chem. Soc., 1965, 87, 1476.
50. Latt, S.; Sober, H. Biochemistry, 1967, 13, 2579.
51. Record, M. T. Jr.; Lohman, T. M.; De Haseth, P. J. Mol. Biol., 1976, 107, 145.
52. Kotin, L.; Nagasawa, M. J. Chem. Phys., 1962, 36, 873.
53. Alexandrowicz, A.; Katchalsky, A. J. Polym. Sci., 1963, A1, 3231.
54. Müller, F.; Hemmerich, P.; Ehrenberg, A. In Kamin, H. (ed.) "Flavins and Flavoproteins"; University Park Press: Baltimore, Md., 1971; pp. 107-120.
55. Watenbaugh, K. D.; Sieker, L. C.; Jensen, L. H.; Legal, H.; Dubourdieu, M. Proc. Nat. Acad. Sci. U.S.A., 1972, 69, 3185.
56. Balazs, E. A. Fed. Proc. Am. Soc. Exp. Biol., 1966, 25, 1817.
57. Gibbs, D. A.; Merrill, D. W.; Smith, K. A.; Balazs, E. A. Biopolymers, 1968, 6, 777.
58. Cerf, R. J. Phys. Radium, 1958, 19, 122.
59. Cerf, R. Fortschr. Hochpolym.-Forsch., 1959, 1, 382.
60. Cerf, R. J. Phys., 1977, 38, 357.
61. Schellman, J. A. Biopolymers, 1975, 14, 999.
62. Volkenshtein, M. V.; Gotlib, Y. Y.; Ptitsyn, O. B. Soviet Physics - Solid State, 1961, 3, 306.
63. Gotlib, Y. Y. Soviet Physics - Solid State, 1962, 3, 1574.
64. Careri, G. In Haken, H.; Wagner, M. (eds.) "Cooperative Phenomena"; Springer-Verlag: New York, 1973; pp. 391-394.
65. Kawasaki, K. In Haken, H. (ed.) "Synergetics: Cooperative Phenomena in Multi-component Systems"; B. G. Teubner: Stuttgart, 1973; pp. 35-44.

66. Mori, H. In Haken, H. (ed.) "Synergetics: Cooperative Phenomena in Multi-component Systems"; B. G. Teubner: Stuttgart, 1973; pp. 45-53.
67. Schellman, J. A.; Stigter, D. Biopolymers, 1977, 16, 1415.
68. Atkins, E. D. T.; Sheehan, J. K. Nature, 1972, 235, 253.
69. Atkins, E. D. T.; Phelps, C. F.; Sheehan, J. K. Biochem. J., 1972, 128, 1255.
70. Stone, A. L. Biopolymers, 1972, 11, 2625.
71. Dea, I. C. M.; Moorhouse, R.; Rees, D. A.; Arnott, S.; Guss, J. M.; Balazs, E. A. Science, 1973, 179, 560.
72. Atkins, E. D. T.; Sheehan, J. K. Science, 1973, 179, 562.
73. Guss, J. M.; Hukins, D. W. L.; Smith, P. J. C.; Winter, W. T.; Arnott, S.; Moorhouse, R.; Rees, D. A. J. Mol. Biol., 1975, 95, 359.
74. Winter, W. T.; Smith, P. J. C.; Arnott, S. J. Mol. Biol., 1975, 99, 219.
75. Sheehan, J. K.; Gardner, K. H.; Atkins, E. D. T. J. Mol. Biol., 1977, 117, 113.
76. Morris, E. R.; Rees, D. A.; Robinson, G.; Young, G. A. J. Mol. Biol., 1980, 138, 363.
77. Welsh, E. J.; Rees, D. A.; Morris, E. R.; Madden, J. K. J. Mol. Biol., 1980, 138, 375.
78. Morris, E. R.; Rees, D. A.; Welsh, E. J. J. Mol. Biol., 1980, 138, 383.
79. Zimm, B. H.; Rice, S. A. Mol. Physics, 1960, 3, 391.
80. Harris, F. E.; Rice, S. A. J. Phys. Chem., 1959, 31, 526.
81. Brenner, S. L.; McQuarrie, D. A. J. Theoret. Biol., 1973, 39, 343.
82. Kennedy, C. M.; Smith, E. R. J. Theoret. Biol., 1977, 65, 203.
83. Brenner, S. L.; McQuarrie, D. A. Biophys. J., 1973, 13, 301.
84. Scheiner, S.; Kern, C. W. J. Am. Chem. Soc., 1977, 99, 7042.
85. Darke, A.; Finer, E. G.; Moorhouse, R.; Rees, D. A. J. Mol. Biol., 1975, 99, 477.
86. Welti, D.; Rees, D. A.; Welsh, E. J. Eur. J. Biochem., 1979, 94, 505.
87. Mathews, M. B.; Decker, L. Biochim. Biophys. Acta, 1977, 498, 259.
88. Bjerrum, N. Kgl. Danske Vid. Selsk. Mat. Fys. Medd., 1927, 7, 9.
89. Onsager, L. Science, 1969, 166, 1359.
90. Barrett, T. W.; Peticolas, W. L. J. Raman Spectroscopy, 1979, 8, 35.
91. Barrett, T. W. Adv. Colloid & Interface Sci., 1980, 12, 85.
92. Lehninger, A. L. "Biochemistry: The Molecular Basis of Cell Structure and Function"; Worth: New York, 1970.
93. Kinsey, V. E.; Reddy, F. V. N. In Prince, J. (ed.) "The Rabbit in Eye Research"; Thomas: Springfield, 1964.

RECEIVED October 13, 1980.

Anticoagulant Activity, Anionic Density, and the Conformational Properties of Heparin

ROBERT E. HURST and SEYMOUR S. WEST

Department of Public Health, University of Alabama in Birmingham,
University Station, Birmingham, AL 35294

JULIAN M. MENTER

Dermatology Research Laboratory, Atlanta VA Hospital, Decatur, GA 30033

Heparin is a sulfated polysaccharide with a number of biological activities, the most important of which is its inhibition of blood clotting. The biochemical basis for this activity is emerging from recent work in a number of laboratories. Heparin binds to the protein antithrombin, which induces a conformational change in the antithrombin (1,2,3) and activates it towards thrombin, Factor Xa, and possibly other clotting factors as well. However, this is not the only mechanism by which heparin can interfere with clotting, since a heparin fraction has been identified which does not activate antithrombin, but still exerts an appreciable anticoagulant effect by interfering with binding of Factor X with phospholipid (4). The heparin-antithrombin interaction exhibits "biochemical" specificity, and only about 1/3 or less of the chains in most commercial heparin preparations contain the "antithrombin-binding sites" which enable binding to antithrombin (5,6). Only a small portion of the heparin chain, about 4-6 disaccharides, is responsible for the binding to antithrombin, and heparin chains which lack these "antithrombin-binding regions" are unable to bind to antithrombin. However, these sequences themselves do not produce anticoagulant activity (7); thus the remainder of the chain is also required in some way. While the remainder of the chain provides a site for the binding of thrombin or factor Xa, its structure and physical properties may also affect the anticoagulant activity.

In spite of this increased understanding of the biochemical basis of heparin's action, the physical basis is not well understood. That the high sulfation plays a role was first suggested by Jorpes and Bergstrom (8) in 1937. Although correlations have been made between anticoagulant activity and the visco-elastic properties of various heparins (9) or the linear charge parameters of different heparin preparations (10) only general relationships have emerged. Moreover, separating effects on anticoagulant activity due to these physical factors from effects produced by modifying the "biochemical" factors as discussed above, is difficult.

0097-6156/81/0150-0251\$05.00/0
© 1981 American Chemical Society

Recently we reported that partition in two-phase solutions of butanol/aqueous NaCl containing excess quaternary ammonium salt could be used to isolate a series of heparin fractions from a commercial heparin preparation. These fractions varied mainly in their degree of sulfation and showed minimal variation in molecular weight (11). This now opens up the possibilities of relating both physical and biological properties to defined structural or compositional variables through systematic studies of a homologous series of fractionated heparins. In this report we review the principles and applications of this technique for isolating heparins with different linear charge densities from the same heparin preparation.

As an example of the potential usefulness of such fractions, we also report their use as a probe of the physical basis of the photochemical fading of acridine orange bound to heparin. Fluorescence fading under continuous irradiation is a second-order photochemical reaction of adjacently-bound acridine orange ions in which photooxidation leads to irreversible loss of fluorescence, with the role of heparin being catalytic (12). A quite unexpected finding was that anticoagulant activity and fluorescence fading both showed qualitatively the same peculiar dependence upon anionic density. This suggested that the same physical forces were acting in both cases. In the case of fluorescence fading, the differences in fading constants arose from differences in dynamic conformational properties which accompanied differences in linear charge density. This led us to speculate that anionic density is most likely a structural variable governing anticoagulant activity through the dynamic conformational properties of the heparin (13).

Materials and Methods

The hog mucosal heparin sample subjected to fractionation was provided by Cohelfred Laboratories, Chicago, IL. It was obtained prior to the bleaching and refractionation stages and still contained some nonheparin glycosaminoglycans. It is not sold commercially, but was chosen because it has not been fractionated. The anticoagulant activity is 143 USP units/mg. Three heparin preparations, fractionated by affinity chromatography on antithrombin-Sepharose into high-affinity (HA), low-affinity (LA), and very low-affinity (NA) fractions (6), were provided by Dr. Ulf Lindahl. The anticoagulant activity of the HA fraction was 222 units/mg in the APTT test against a secondary standard heparin of 163 USP units/mg.

Heparin fractions were chemically characterized as described (11) by measurements of uronate (UA), sulfaminohexose (SAH) and sulfate (SO_4). Anticoagulant activities were determined on aqueous solutions of heparin fractions containing a known amount of uronate using the USP assay in recalcified sheep

plasma. The results are expressed in terms of the anticoagulant activity (USP units) per micromole of heparin uronate. These somewhat unusual units are employed since the fractions were not actually weighed, being too small. These units can be at least approximately converted to the more familiar units of units/mg by multiplying by the uronate content of ultra-dry heparin (1.85 $\mu\text{mol/mg}$), or ordinary hydrated heparin (1.62 $\mu\text{mol/mg}$).

Isolation and Characterization of Heparin Fractions. Preparative scale fractionation was carried out by sequential extraction of eight tubes, each containing 10 mg of heparin in 20 mL of 1-butanol (upper phase) and 20 mL of 0.01 M NaCl (lower phase). The biphasic solution contained 30 g HPC/ of butanol phase. After removing the lower, aqueous phase, the upper butanol phases of each tube were successively extracted with 4 mL of aqueous butanol-saturated solutions of NaCl containing 2 g/L HPC as listed in Table I. Fractions are identified by the NaCl concentration at which the fraction was extracted. Equivalent fractions from different tubes were combined, and, after making each tube at least 0.5 M in NaCl, the heparin was precipitated with three volumes of acetone. A more detailed description of the procedure was published previously (11). Analytical-scale fractionation of the three affinity-fractionated heparins was carried out similarly, except that only 1 μmol (as uronate) of each was fractionated. Molecular weight distributions of the fractions were determined on 6% agarose as described (11).

Structural sensitivity of partition fractionation. The phenomenon of partition is uniquely different from that usually encountered in that the glycosaminoglycan-HP complex appears to be soluble in either the upper or the lower phase, but not in both simultaneously (14,15,16). With homogenous preparations, the change in solubility from one phase to the other occurs over an 0.005 M change in NaCl concentrations (14,15,16). The change in solubility is characterized in terms of the parameter C50, which is defined as the concentration of inorganic salt (NaCl in this case) at which half the uronate is in each phase (17). (It should be noted that the composition of the glycosaminoglycan in each phase under such conditions is different.) The structural sensitivity of the parameter C50 to polymer sulfation and molecular weight was determined with two homologous series of chondroitin sulfate fractions prepared by a combination of gel-filtration and ion-exchange chromatography of partial hyaluronidase digests. One series varied in molecular weight, but not in sulfation, while the other varied in sulfation, but not in molecular weight (15).

Fluorescence Fading. The fluorescence fading constant, r'' , was measured for each of the heparin fractions in 8 μM

Table I. Distribution and Properties of Heparin Fractions

No.	[NaCl] at which extracted	% of total UA in fraction	molar ratios				Anticoagulant Activity (USP U/ μ mol)	Z ²
			SO ₄ UA	SAH UA	HEX UA			
1	0.10	0.7	0.85	-	-	-	-	
2	0.110	1.9	0.85	-	-	-	-	
3	0.120	4.1	0.91	0.42	-	-	-	
4	0.130	5.7	1.21	0.57	1.03	44	4.88	
5	0.140	11.3	1.36	0.84	0.83	68	5.55	
6	0.145	10.4	1.39	0.87	0.77	84	5.69	
7	0.150	10.7	1.41	0.93	0.80	94	5.81	
8	0.155	10.0	1.42	0.98	0.79	102	5.93	
9	0.160	13.2	1.54	0.99	0.73	114	6.45	
10	0.165	11.5	1.57	0.95	0.79	114	6.60	
11	0.170	8.2	1.62	1.03	0.75	119	6.84	
12	0.175	5.6	1.82	1.03	0.74	131	7.95	
13	0.200	6.8	1.93	1.01	0.76	106	8.58	

acridine orange with a molar ratio of heparin uronate to acridine orange of 2.2. These conditions ensure that the photochemical fading, and not the formation of acridine orange-heparin complex, is rate determining (18). The fading kinetics of 660 nm fluorescence of bound acridine orange excited at 546 nm, were measured on an instrument constructed in our laboratories as previously described (13). This instrument provides the fluorescence intensity (I_f) directly as its inverse as a function of time on an X-Y recorder. The intensity of the exciting light was separately measured with a thermopile. The plot of $1/I_f$ vs time is linear and its slope (r) and intercept (A) are used to calculate r'' from equation 1:

$$r'' = r/(AE_0) \quad (1)$$

It should be noted that r'' is measured in absolute units of m^2/J and, hence, its measurement is not tied to the use of an arbitrary standard. It is directly related to the molecular rate constant for the reaction leading to fading (18) and is independent of exciting light intensity.

In order to obtain information concerning the molecular basis for the observed differences in fading constants, the temperature-dependence of fading was determined for the four fractions showing the largest differences (0.140, 0.145, 0.150 and 0.155 M fractions). Since r'' is proportional to a molecular rate constant, the temperature dependence of r'' can be interpreted in terms of transition-state theory:

$$r'' = C(kT/h) \exp(\Delta S^\ddagger/R) \exp(-\Delta H^\ddagger/RT) \quad (2)$$

where R , k , T , and h have their usual meaning and ΔH^\ddagger and ΔS^\ddagger are the respective enthalpy and entropy of activation for the fading reaction. Since the numerical value of the constant c in equation 2 is not known, absolute preexponential factors cannot be determined from the Arrhenius plots. However, taking ratios of r'' with respect to an arbitrarily chosen "reference sample" (the 0.150 M fraction in this case) automatically results in elimination of the unknown constant and makes it possible to express the entropy terms for each fraction as differences in activation entropies:

$$\Delta\Delta S_i^\ddagger \equiv \Delta S_i^\ddagger - \Delta S_{ref}^\ddagger \quad (3)$$

These can then be interpreted in an absolute sense.

Results

Structural Sensitivity of Partition. The dependence of C50 upon polymer sulfation and molecular weight are displayed

in Fig. 1. In order to display both curves on the same plot, the independent variables of molecular weight and Z^2 are shown on the top and bottom abscissae respectively, with the dependent variable C50 given on the ordinate. The parameter Z is the sum of anionic groups (sulfate + carboxylate) per uronate residue, and if all are ionized, is equivalent to the linear charge density. The relation of C50 to sulfation was plotted as C50 vs Z^2 in an attempt to account for electrostatic factors (15) and, indeed, C50 is linearly related to Z^2 . In contrast, C50 is independent of molecular weight for polymers in excess of 12,000 daltons. Therefore we conclude that separations using sequential extraction partition procedures would separate heterogeneous mixtures according to anionic density, and independently of molecular weight, provided the polymer was larger than the critical lower limit of 10-12,000 daltons.

Properties of Heparin Fractions. Table I lists the distribution of uronate among the various fractions together with several molar ratios of the individual fractions. The uronate is broadly distributed among the 13 different fractions, which indicates a high degree of compositional variability in the original sample, although the majority of the material, 67%, is concentrated in the 0.140 - 0.165 M NaCl fractions. The molar ratios demonstrated that the major chemical difference in the heparin fractions is in their degree of sulfation, or anionic density. This is demonstrated by the steady increase in the SO_4/UA ratio. With the exception of the 0.130 M fraction, which contains some dermatan sulfate, the SAH/UA ratio, which measures the extent of N-sulfation, increases from the 0.130 through the 0.150 M fractions, but this ratio is constant for the fractions extracted at higher salt concentrations.

Further analysis reported elsewhere (11) has shown that the 0.100 - 0.120 M fractions contain predominately dermatan sulfate; the 0.130 M fraction consists of a mixture of dermatan sulfate and low-sulfated heparin; the 0.140 M fraction contains only a small amount of dermatan sulfate, and the higher fractions all consist exclusively of heparins of varying compositions.

The molecular weight distributions of the individual fractions were determined by gel-filtration and are described in more detail elsewhere (11). The average molecular weights and molecular weight distributions of the 0.155 M fractions and above were identical with each other and with the distribution afforded by a purified commercial heparin sample. However, the molecular weight of the 0.140 M fraction was about 2,000 daltons lower than the molecular weights measured for the higher fractions. Thus, molecular weight and anionic density of heparins are not completely independent, with smaller chains having a lower anionic density.

Correlation of Anionic Density with Anticoagulant Activity.

Table I lists the anticoagulant activities of each of the fractions. With the exception of the final fraction, the anticoagulant activities steadily increase with increasing sulfation, although the relationship is nonlinear. Fig. 2 displays both the anticoagulant activities of these fractions and the concentration of NaCl at which they were extracted as functions of Z^2 . The extracting NaCl concentration, which should be equivalent to C50, is a linear function of Z^2 over the entire range of fractions, and thus heparin behaves identically with the chondroitin sulfate fractions in Fig 1 in this respect. However, a quite different behavior is observed with regard to the anticoagulant activities. Although an initial linear portion is observed, the slope changes about four-fold at about $Z^2 = 6$.

One possible alternate explanation for Fig 2 is that fractionation by anionic density is accompanied by fractionation according to antithrombin affinity. Were such fractionation to occur, marked differences in anticoagulant activity among the fractions would result. In an effort to determine whether such is the case, the anionic density distributions of HA-, LA-, and NA-heparins were determined. Although some differences in these distributions were evident (11), it is also evident that HA-heparins exist within a similar range of sulfation as do the LA and NA heparins. Clearly, HA-heparin is not all high-sulfated heparin and LA-or NA-heparins are not all low-sulfated heparins. These results show that fractionation according to antithrombin affinity probably did not occur to any extensive degree and, hence, the results in Fig 2 do indeed demonstrate that anticoagulant activity varies with the linear charge density or factors related to it.

Fluorescence Fading. The anionic-density fractionated heparin fractions seemed to present an ideal means of investigating the role of polymer charge in the phenomenon of fluorescence fading. When the fading constants (r'') of the fractions were determined, a quite unexpected result emerged. As shown in Fig 3, r'' and anticoagulant activity both show qualitatively similar dependence upon Z^2 . Indeed, as shown in Fig 4, the two show a close correlation with each other. This striking similarity suggested there may be a similarity in the physical mechanisms by which both are governed by anionic density. Thus, a knowledge of the physical basis for fluorescence fading may yield information concerning the role of physical forces in governing anticoagulant activity.

In order to gain further information of the mechanisms by which r'' varies among heparins of different anionic density, the temperature dependence of r'' was investigated. When $\ln r''$ was plotted as a function of $1/T$, the several fractions afforded a family of parallel straight lines. Their vertical displacement

Figure 1. Structural sensitivity of partition fractionation to polymer structural variables of molecular weight (■—upper axis) and anionic density (●—lower axis) vs. Z^2 . Values shown are C_{50} for two homologous series of fractionated chondroitin sulfate fractions.

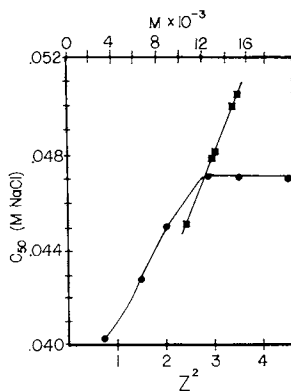
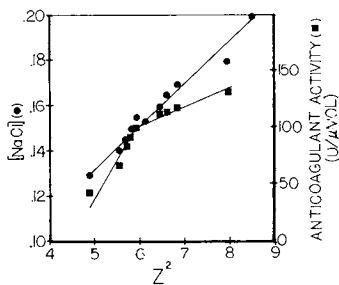


Figure 2. Relationships between anticoagulant activity in the USP assay (■—right ordinate), NaCl concentration (molar) at which the fraction was extracted (●—left ordinate) and Z^2 , where Z is the number of chemically measured anionic groups per uronate moiety



increased with increasing sulfation of the fraction. The average slope corresponds to an apparent activation energy of 12 ± 1 kcal/mol, or $\Delta H^\ddagger = 11$ kcal/mol. It is therefore evident that the differences in r'' among the heparin fractions are due only to preexponential (i.e. entropic) factors. Since anticoagulant activity and the fluorescence fading constant both depend in the same way upon Z^- , and are at least empirically related, $\Delta\Delta S^\ddagger$ should be related to the logarithm of the anticoagulant activity. This relationship is shown in Fig 5, which shows a clear empirical correlation between the magnitude of the anticoagulant activity and the ability of the heparin to bring reactive dye molecules into a configuration favorable for reaction.

Discussion

Anionic density fractionation of heparin presents some new insights and approaches to several problems in heparin research. At a purely practical level it presents some alternate approaches to isolation, characterization, and standardization of heparins. The technique affords highly purified heparins from which several contaminants are removed at lower salt concentrations. The technique also affords the possibility of isolating fractions which are much less variable in overall composition than are the usual preparations, and such fractions may prove very useful in providing more rational standards. In addition a convenient way of describing the compositional heterogeneity of heparins is provided. Finally, and perhaps most importantly, by presenting a means for isolating fractions which vary systematically in structural parameters, insight into mechanisms of action and the molecular origins of activity may be gained.

The mechanism of partition in these two-phase systems is itself an interesting problem in the conformational properties of charged polyions. As was shown earlier (14,15,16), the very sharp change in the solubility can be treated as the result of a cooperative change between two states. One state is soluble only in the butanol phase while the other is soluble only in the aqueous phase. The entropy change for the transition between these two states is highly dependent upon the concentration of salt and is related to the electrostatic field surrounding the polyion. This dependence upon salt concentration is responsible for the change in solubility since ΔH and $T\Delta S$ are similar in magnitude so that even small changes in the entropy change can result in a change in the sign of the free energy (16). We have postulated that this is due to a conformational change in the glycosaminoglycan-HP complex, although no changes in shape parameters were demonstrated. The phenomenon is quite clearly different from the behavior observed with the same substances in the absence of the butanol phase.

Figure 3. Relationship between fluorescence fading constant (r'') (●—left ordinate) and Z^2 . The anticoagulant activity (■—right ordinate) shown in Figure 2 are repeated in order to show the similarity in shape.

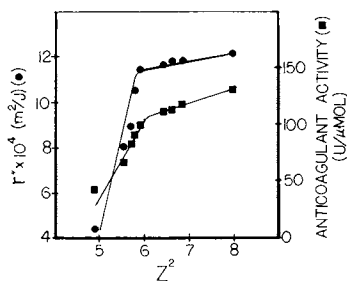


Figure 4. Relationship between anticoagulant activity and r'' for heparin fractions

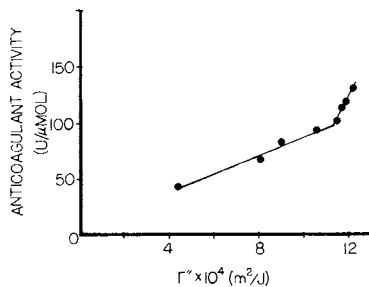
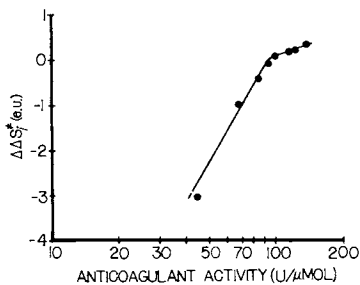


Figure 5. Relationship between relative activation entropies of fluorescence fading, ΔS_f^\ddagger (in eu) and the logarithm of the anticoagulant activity. Activation entropies are relative to the value observed with the 0.150M fraction.



Under such conditions the glycosaminoglycan is precipitated; however the molecular weight dependence is very different from that shown in Fig 1. For precipitation, the "critical electrolyte concentration" is a continuous function of the molecular weight (19), and separations are according to total molecular charge (20), which is the product of linear charge density and the number of subunits. In contrast, the separations with partition are according to the linear charge density. This is demonstrated with the fractionated chondroitin sulfate samples in Fig. 1. Further confirmation is seen in Fig 2, since the extracting salt concentration and Z^2 are linearly related for the heparin fractions.

These fractions have provided some new insights into the structural origins of the anticoagulant effect of heparin. The anticoagulant activities of the heparin fractions clearly increase with the salt concentration at which they are extracted. As shown in Fig. 2, we have attributed this behavior to factors related to the linear charge density of the heparin. While we cannot completely rule out some contribution to anticoagulant activity differences from "biochemical" mechanisms related to differences in the frequency of occurrence of antithrombin-active chains among different fractions, the similarities in the distributions of affinity-fractionated heparins argues against such a mechanism as being mainly responsible for the differences in anticoagulant activity among the fractions. The most significant point is that HA-heparin is not all highly sulfated with LA- and NA-heparins being low sulfated. Therefore, fractionation by anionic density is unlikely to produce much variation in the fraction of active chains. This is in sharp contrast to the behavior of fractions isolated by ion-exchange chromatography which show marked variation in this parameter (21).

Although anionic density appears to be a necessary condition for anticoagulancy, it is not sufficient, since chains which lack an antithrombin-binding oligosaccharide sequence show little or no anticoagulant activity. Just as clearly, antithrombin binding itself is not a sufficient condition, since these sequences show no anticoagulant activity themselves. We speculate that the anionic density of the remainder of the chain is related to the amount of anticoagulant activity induced. Thus, at least two approximately independent variables appear to govern the activity of heparin. The ability to bind to antithrombin appears to act as a "master on-off switch", whereas the anionic density related-factor appears to act as a "rheostat".

The work with fluorescence fading permits some speculation about a mechanism by which anionic density governs anticoagulant activity. This work suggests that the mechanism may involve the dynamic conformational properties of the heparin, and not the static conformational properties.

The photochemical fading of acridine orange-heparin fluorescence involves a second-order photooxidation whereby two molecules of acridine orange bound to adjacent sites react in the rate-determining step (12,18). The role of the heparin or other glycosaminoglycan appears to be to bring the acridine orange molecules together for the photooxidation reaction without itself undergoing detectable chemical alteration. In this respect it acts as a catalyst. The similarity of the activation energies for all the heparin fractions and for dermatan sulfate (13) shows that the chemical mechanism of fading is the same for different glycosaminoglycans, but that the large differences in the rate of fading for acridine orange complexes with different glycosaminoglycans arise from entropic factors.

The activation entropy is a measure of the dynamic conformational properties of the polymer; it reflects the conformational change that the polymer must undergo to accommodate a transition state between two reactive dye molecules. If the main difference among the heparins is their ability to bring reactive dye molecules into favorable conformations, it is certainly reasonable that this is linked to the ability to bring reactive protein molecules (e.g. thrombin and antithrombin) into configurations favorable to their reaction with each other. Thus, it is this dynamic conformational property which is important, and it may be that it is not directly related to the static properties. It is interesting that the extracting salt concentration is a linear function of Z^2 while anticoagulant activity is not. While it is certainly possible that this difference arises from some systematic error in the clotting assay, it is also possible that it reflects a basic difference between static and dynamic conformational properties. The transition between phases may be governed directly by the electrostatic field surrounding the polyion, which will be reflected in a linear plot. However, the dynamic conformational properties need not be directly related, although they bear a general relation to linear charge density.

It must be emphasized that the relationships between anticoagulant activities and r'' (Fig 4) and activation entropy (Fig 5) are strictly empirical. Nevertheless, the existence of an underlying physical basis is consistent with models of heparin action. As summarized by Laurent and coworkers (1) heparin promotes the interaction between thrombin and antithrombin which are bound to the same heparin chain. In this respect the heparin can be considered as a catalyst, and, as discussed above, its role in this process and fluorescence fading may well be quite analogous. A number of authors have shown that heparin induces conformational changes in antithrombin or, possibly, in the serine proteases of the coagulant cascade, and that this leads to an increase in the rate of inactivation of the serine protease by antithrombin. Our

studies suggest that the ability of heparin to induce such changes may be linked to its own ability to assume a special configuration. Interestingly, heparin has been reported to increase the activation entropy of the inactivation of thrombin by antithrombin (2), a finding which is in close accord with this hypothesis.

Thus we propose that the linear charge density itself does not govern the anticoagulant activity of heparin. Although the linear charge density does bear some relationship to the dynamic conformational properties of the heparin, it is these latter which govern the amount of anticoagulant activity induced by antithrombin-active heparin chains. Future work on the physical basis for the action of heparin might concentrate on properties related to the dynamic conformational properties of the heparin, but must control or account for "biochemical" effects on anticoagulant activity.

Acknowledgements

The authors wish to thank Belinda Perkins for her aid in preparing the manuscript. This work was supported in part by USPHS Grants HL 24509 and HL 22402.

References

1. Laurent, T.; Tengblad, A.; Thurnberg, L.; Hook, M.; Lindahl, U. J. Biochem., 1978, 175, 691-701.
2. Machovich, R.; Aranyi, P. Biochem. J., 1978, 173, 869-875.
3. Nordenman, B.; Bjork, I. Biochem. 1978, 17, 3339-3344.
4. Walker, F.J.; Esmon, C.T. Thromb. Res., 1979, 14, 219-230.
5. Lam, L.H.; Silbert, J.E.; Rosenberg, R.D. Bioch. Biophys. Res. Comm., 1976, 69, 570-577.
6. Hook, M.; Bjork, I.; Hopwood, J.; Lindahl, U. FEBS Letters, 1976, 66, 90-93.
7. Hopwood, J.; Hook, M.; Linker, A.; Lindahl, U. FEBS Letters, 1976, 69, 51-54.
8. Jorpes, E.; Bergstrom, S. J. Biol. Chem., 1937, 118, 447-455.
9. Stivala, S. Fed. Proc., 1977, 36, 83-88.
10. Edwards, H.E.; Diakun, G.P.; Davies, J.V.; Allen, J.C.; Phillips, G.O. Biochem. Biophys. Res. Comm., 1978, 85, 1602-1609.
11. Hurst, R.E.; Menter, J.M.; Settine, J.M.; West, S.S.; Coyne, E.H. Biochemistry, 1979, 18, 4283-4287.
12. Menter, J.M.; Hurst, R.E.; West, S.S. Photochem. Photobiol., 1979, 29, 473-478.
13. Menter, J.M.; Hurst, R.E.; Corliss, D.A.; West, S.S.; Abrahamson, E.W. Biochem., 1979, 18, 4288-4292.
14. Hurst, R.; Sheng, Y-p. Biochim. Biophys. Acta, 1976, 444, 75-84.
15. Hurst, R.; Sheng, J. Biochim. Biophys. Acta, 1977, 497, 539-547.

16. Hurst, R. Biopolymers, 1978, 17, 2601-2608.
17. Jennings, G.C.; Hurst, R.E. Biochim. Biophys. Res. Comm., 1974, 60, 1208-1214.
18. Menter, J.M.; Golden, J.F.; West, S.S. Photochem. Photobiol., 1978, 27, 629-633.
19. Laurent, T.C.; Scott, J.E. Nature, 1964, 202, 661-662.
20. Laurent, T. Arch. Biochem. Biophys., 1961, 92, 224-231.
21. Sach, E.; Choay, J.; Fareed, J.; Andersen, A.C.; Messmore, H.L. Chemistry and Biology of Heparin, 1980, in press.

RECEIVED September 22, 1980.

Configurational Entropy of Tethered Polymers and the Swelling Properties of Connective Tissue

PETER S. GEISSLER

Donner Laboratory, Bio-Med Division, Lawrence Berkeley Laboratory,
Berkeley, CA 94710

Experiments on excised rabbit corneas have shown that the swelling tendency of corneal stroma decreases markedly as the connective tissue becomes hydrated. The relationship between the swelling pressure, P , and the hydration, H , has been shown (Fatt and Goldstick, 1965) to be:

$$P \propto e^{\gamma p} \{-H\}$$

for a wide range of hydrations and several species of mammals. The hydration is defined as the grams of water per gram dry weight of the tissue. The swelling pressure is the mechanical pressure under which the connective tissue is in volumetric equilibrium. This relationship between pressure and tissue hydration is manifest in numerous physiological situations. For example, the discs that separate and cushion the vertebrae become compressed (dehydrated) under the weight of the body in the standing position; most humans are a full $\frac{1}{2}$ inch taller upon rising in the morning than they are after standing for several hours. Another example: the mammalian cornea is optically transparent because the light scattering protein fibers of this connective tissue are held in a lattice type arrangement by attractive forces that markedly decrease as the tissue becomes hydrated. At low hydrations, the restoring forces maintaining the periodic lattice structure are large; whereas swollen corneas have smaller restoring forces to maintain the periodic lattice of protein fibers. Thus, swollen corneas exhibit greater fluctuations about the periodic array than do normally hydrated corneas. These fluctuations of the spatial distribution within the protein fibers result in increased light scattering.

0097-6156/81/0150-0265\$05.00/0
© 1981 American Chemical Society

Thus, important optical properties of the cornea may be deduced from the relationship between swelling pressure and tissue hydration. An electromicrograph of osmiumtetroxide stained rabbit cornea is shown in Figure 1. At normal hydration the protein fibers are in a periodic array. Figure 2 shows a swollen cornea; substantial fluctuations occur in neighbor - neighbor distances between the protein fibers, and the array is no longer of the crystalline lattice type.

Connective tissue consists of large collagen fibers held together by flexible polysaccharide chain molecules. Figure 3 shows the large collagen fibers being held in a lattice array by the polysaccharide chain molecules. The ends of each polysaccharide molecule are tethered to the protein fibers. The exact details of bonding are unknown. It is not known, for instance, if polysaccharide molecules link only nearest neighbors in the protein fiber lattice, as has been assumed in the construction of Figure 3. As the connective tissue swells, the collagen fibers move farther apart, thereby increasing the distance, L , between the tethered ends of the polysaccharide chains. The tethering condition is simply a fixed end-point condition. The hydration, H , measured experimentally is linearly related to the mean distance between neighboring collagen fibers, and thus to the tethered length, L , of the polysaccharide chains. A simple calculation of the configurational entropy of these polymers as a function of end-to-end distance, L , qualitatively accounts for the observed decrease in osmotic activity associated with swelling. The calculation of the configurational entropy based upon a simple model is given below in equation 31. The principal aim of the calculation is the development of an equation that will enable one to predict the swelling, mechanical, and optical properties of connective tissues as the polysaccharides are affected by temperature, ionizing radiation, pH, and ester sulfate concentration, as compared to the normal state.

As noted above, the hydration, H , is linearly related to the end-to-end length, L , of the polysaccharide chains. We must then relate the swelling pressure, P , to the chemical potential of these chain molecules. For this, let us consider an osmotic experiment in which an excised piece of connective tissue is bathed in water. Mechanical equilibrium is maintained by the application of a pressure, P , on

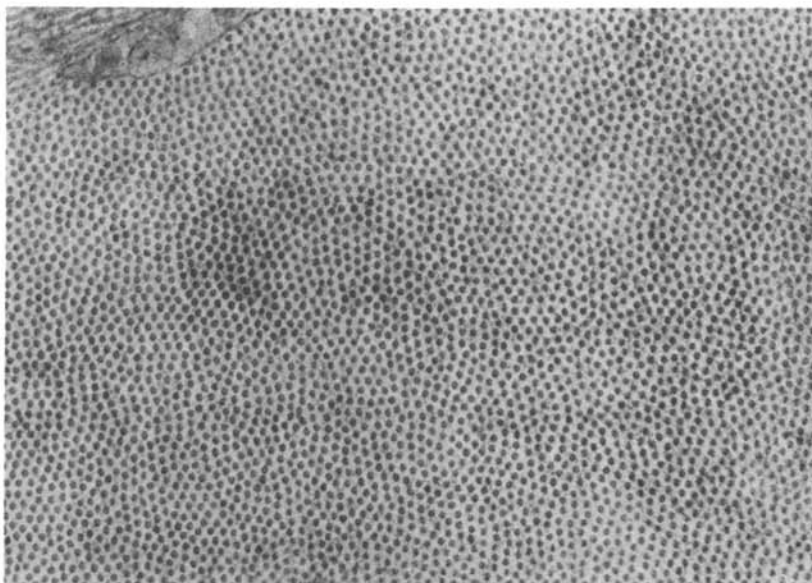


Figure 1. Cross-section of normally hydrated rabbit cornea

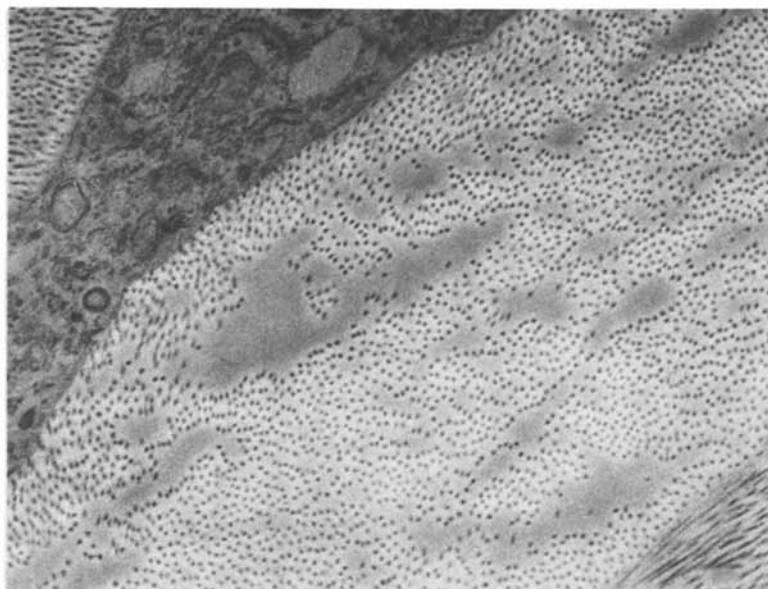


Figure 2. Cross-section of swollen rabbit cornea

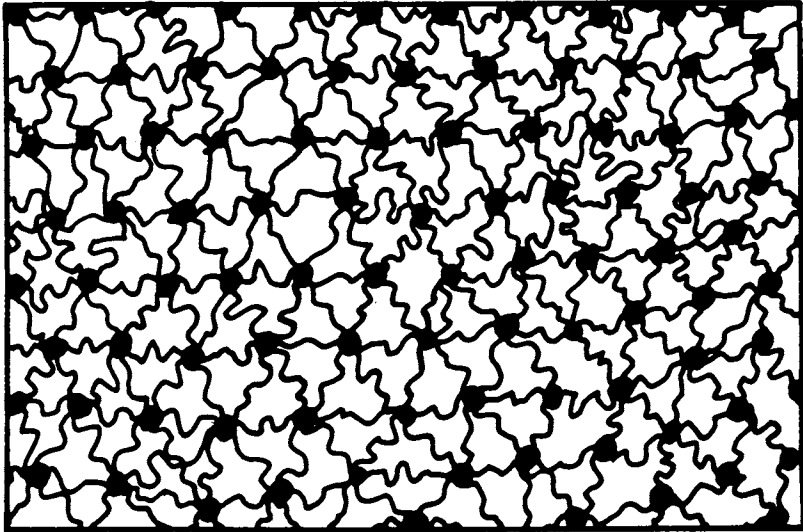


Figure 3. Model of protein fibers (dots) and polysaccharide chain molecules (lines) for rabbit cornea

the sample. The water can freely pass into the tissue from the infinite reservoir of bathing solution. The osmotically active solute molecules in the tissue are the polysaccharide chain molecules which are tethered to the protein fibers and hence not permitted to diffuse into the bathing solution, thereby giving rise to a swelling pressure. We denote the chemical potential of the solvent by μ_w and the chemical potential of the osmotically active solutes by μ_i . The condition of osmotic equilibrium may be expressed as

$$d\mu_w = \mu_w^{\text{tissue}} - \mu_w^{\text{bathing sol}^n} = 0. \quad (1)$$

This may also be written

$$d\mu_w = \bar{V}_w dP + d\mu_w^c = 0. \quad (2)$$

giving

$$d\mu_w^c = -\bar{V}_w dP. \quad (3)$$

The Gibbs-Duhem equation at constant temperature gives

$$\sum_{i=1}^k n_i d\mu_i^c = 0 \quad (4)$$

which can be rewritten

$$\sum_{j=1}^{k-1} n_j d\mu_j^c = -n_w d\mu_w^c \quad (5)$$

in which the summation goes over all the components except the solvent. Introducing Eq. (5) into Eq. (3) we obtain

$$\sum_{j=1}^{k-1} n_j d\mu_j^c = n_w \bar{V}_w dP. \quad (6)$$

Connective tissue is sufficiently dilute to make the volume contribution of the solvent, $n_w \bar{V}_w$, to the total volume of the solution V overwhelmingly larger than that of the other components, protein fibers and polysaccharide chains. Thus, to a good approximation,

$$n_w \bar{V}_w \cong V \quad (7)$$

and Eq. (6) can be written

$$dP = \sum_{j=1}^{k-1} \frac{n_j}{V} d\mu_j^c. \quad (8)$$

The number of moles of component j per unit volume is the molar concentration $C_j = n_j/V$. The equilibrium pressure of a solution maintaining osmotic equilibrium with the solvent is the osmotic pressure, π , so that, under present conditions, the variation in P is identical with the change in osmotic pressure:

$$dP = d\pi$$

Hence, Eq. (8) can also be written

$$d\pi = \sum_{j=1}^c c_j d\mu_j^c \quad (9)$$

Equation (9) is the basis for investigating how the swelling pressure will vary with hydration, pH, degree of ionization due to radiation, temperature, etc. It is necessary only to adopt a simple model of the tethered polysaccharide chains and evaluate the configurational entropy.

A very simple model has been chosen to represent the tethered polysaccharide chains that form the connecting links of the collagen fibers in connective tissue. The model is that of the Liquid Lattice Theory (Huggins, Flory). The density of polysaccharide chains is high enough to justify the mean field approximations; at normal hydration the corneal stroma contains 77 percent water, and the dry weight is 70 percent collagen (Polatnic et al., 1957) and 4.5 percent polysaccharide (Anseth and Laurent, 1961).

The segments of a chain polymer molecule are located in a liquid lattice of coordination number σ . However, the chain is not free to assume any configuration; the first and last segments are tethered to the large protein fibers of connective tissue. This end-to-end length will vary linearly with tissue hydration.

The total number of configurations of an untethered polymer in the liquid lattice theory is

$$\Omega_{\text{untethered}} = \sigma(\sigma-1)^{N-1} (1-\bar{f}(L))^N \quad (10)$$

or

$$\Omega_{\text{untethered}} = (\sigma-1)^N (1-\bar{f}(L))^N \quad (11)$$

where σ is the coordination number of the lattice, N is the total number of chain segments, and $f(L)$ represents the expectancy that a given cell adjacent to a previously vacant one is occupied.

Insofar as the liquid lattice theory may be viewed as a random walk process, where n_i steps can be taken in each of $i=1, 2, \dots, \sigma$ directions, each with a probability W_i , we see that the total number of different configurations W untethered is

$$W_{\text{untethered}} = \sum_{\sum n_i = N} \frac{N!}{n_1! n_2! \dots n_i! \dots n_\sigma!} w_1^{n_1} w_2^{n_2} \dots w_i^{n_i} \dots w_\sigma^{n_\sigma} \quad (12)$$

where W_i is chosen so that back-tracking is compensated. Thus we require that:

$$W(\sigma, w, N) = \Omega(\sigma, \bar{F}, N). \quad (13)$$

Thus,

$$W_{\text{untethered}} = (w_1 + w_2 + \dots + w_i + \dots + w_\sigma)^N \quad (14)$$

$$\Omega_{\text{untethered}} = (\sigma - 1)^N (1 - \bar{F}(L))^N \quad (15)$$

so

$$w_i = \frac{(\sigma - 1)(1 - \bar{F}(L))}{\sigma} \text{ for all } i. \quad (16)$$

Now we wish to calculate the total number of configurations accessible to a tethered polymer chain in the liquid lattice; subject to the condition that the chain is of definite end-to-end length, L . Thus we again compute the sum

$$W = \sum_{\{n_i\}} \frac{N!}{n_1! n_2! \dots n_i! \dots n_\sigma!} w_1^{n_1} w_2^{n_2} \dots w_i^{n_i} \dots w_\sigma^{n_\sigma} \quad (17)$$

where $\{n_i\}$ is subject to the condition that $\sum_{i=1}^{\sigma} n_i = N$ and the tethering condition:

$$\sum_{i=1}^{\sigma} \delta_i n_i = L \quad \text{or} \quad \sum_{i=1}^{\sigma} \delta_i n_i = L + N \quad (18)$$

where δ_i = Projection of i step type in the direction of the endpoint

and where $\gamma_i = \delta_i + 1$.

If the only restriction on the n_i were $\sum n_i = N$, this task would be solved immediately by the polynomial formula, and the sum would be

$$(w_1 + w_2 + \dots + w_i + \dots + w_\sigma)^N. \quad (19)$$

The second condition, $\sum_{i=1}^{\sigma} \gamma_i n_i = L + N$,

constitutes the real difficulty of the problem which consists of selecting only the terms complying with this condition as well.

To cope with this additional constraint, we use the following artifice. We compute the following sum without the second restriction:

$$F(w_i, z, \gamma_i, N) = \sum_{\sum n_i = N} \frac{N!}{n_1! n_2! \dots n_i! \dots n_\sigma!} w_1^{n_1} w_2^{n_2} \dots w_i^{n_i} \dots w_\sigma^{n_\sigma} z^{\gamma_1 n_1} \dots z^{\gamma_i n_i} \dots z^{\gamma_\sigma n_\sigma} \quad (20)$$

$$= \sum_{\sum n_i = N} \frac{N!}{n_1! n_2! \dots n_i! \dots n_\sigma!} (w_1 z)^{n_1} \dots (w_i z)^{\gamma_i n_i} \dots (w_\sigma z)^{\gamma_\sigma n_\sigma} \quad (21)$$

$$= (w_1 z^{\alpha_1} + w_2 z^{\alpha_2} + \dots + w_n z^{\alpha_n} + \dots + w_r z^{\alpha_r} + \dots + w_s z^{\alpha_s})^N \quad (22)$$

$$= f(z)^N \quad (23)$$

Nominally, we let the end-to-end distance, Z , take on any value. Our $f(Z)$ plays the part of the "sum-over-states".

The W , which we need is obviously the coefficient of Z^{N+L} in the function $f(Z)^N$; it can be computed by the method of residues in the complex plane. The solution is simply

$$W_{\text{tethered}} = \frac{1}{2\pi i} \oint z^{-L-N-1} f(z)^N dz \quad (24)$$

the integration to be conducted along any closed contour around the origin in the complex Z plane, within the circle of convergence of $f(Z)$. The integral may be evaluated by the method of steepest descent.

The integrand of equation (24) has an extremely sharp maximum at $Z = Z_0$. It is convenient to use logarithmic derivatives. Letting

$$e^{\gamma p} \{g(z)\} = z^{-N-L-1} f(z)^N, \quad (25)$$

Z_0 is determined by

$$g'(Z_0) = -\frac{N+L+1}{Z_0} + N \frac{f'(Z_0)}{f(Z_0)} = 0 \quad (26)$$

furthermore,

$$g''(Z_0) = \frac{N+L+1}{Z_0^2} + N \left(\frac{f''(Z_0)}{f(Z_0)} - \frac{f'(Z_0)^2}{f(Z_0)^2} \right) \quad (27)$$

For a purely imaginary increment iy of Z near $Z = Z_0$, the integrand can be written

$$z^{-N-L-1} f(z)^N = Z_0^{-N-L-1} f(Z_0)^N e^{-\frac{1}{2} y g''(Z_0)} \quad (28)$$

so

$$W_{\text{tethered}} = \frac{1}{2\pi i} Z_0^{-N-L-1} f(Z_0)^N \int_{-\infty}^{\infty} e^{-\frac{1}{2} y g''(Z_0)} dy \quad (29)$$

so

$$W_{\text{tethered}} = Z_0^{-N-L-1} f(Z_0)^N \frac{1}{\sqrt{2\pi g''(Z_0)}} \quad (30)$$

The logarithm of W_{tethered} is proportional to the partial molar free energy, the chemical potential,

$$\log W = -(N+L+1) \log Z_0 + N \log f(Z_0) - \frac{1}{2} \log (2\pi g''(Z_0)). \quad (31)$$

For a cubic liquid lattice with $\sigma = 6$

$$w = \frac{5}{6} (1 - \bar{F}(L)) \quad (32)$$

$$z_0 = \frac{(4L+1) + \sqrt{(4L+1)^2 + 4(N-L-1)(L+1)}}{2(N-L-1)} \quad (33)$$

$$g''(z_0) = \frac{N+L+1}{z_0^2} + N \left(\frac{2}{z_0^2 + 4z_0 + 1} - \frac{(2z_0 + 4)^2}{(z_0^2 + 4z_0 + 1)^2} \right). \quad (34)$$

Thus, the chemical potential can be expressed in terms of the number of segments of the polymer, N , and the end-to-end distance of the tethered polymer chains.

It may be seen from equation (31) that as the tissue becomes hydrated, and the end-to-end distance of the polymer chain increases to more nearly approach the contour length, the configurational entropy, and hence partial molar free energy, is tremendously reduced. Since any change in the partial molar free energy (chemical potential) gets expressed as a change in the swelling pressure according to Eq. (9), we can then anticipate the qualitative shape of the swelling pressure vs. hydration curve; it can be approximated by Equation (1).

Having satisfied ourselves that this model of connective tissue predicts that the swelling pressure does indeed decrease markedly with hydration (i.e. as $\frac{L}{N} \rightarrow 1$), it is useful to note that the partial molar free energy given in Equation (1) is an increasing function of N for constant $\frac{L}{N}$. The model here is a freely jointed chain of N segments with a fixed end-to-end distance of L segments. In the application of the model to real molecules, the assignment of N is somewhat artificial. One must decide how many saccharide units constitute one segment. Having decided that, the total number of segments, N , is simply the contour length divided by the contour length per segment. Presumably the assignment is related to the correlation length or persistence length of the molecule. Increased temperature increases the "play" in bond angles and permits increased rotation between saccharide units; the molecule becomes more flexible. Having adopted some criteria for the choice of N , one can calculate how N depends upon temperature. Thus, Equation (31) provides an avenue for predicting the mechanical and swelling properties as a function of temperature and for predicting the optical response

of the cornea to infra-red radiation. Similarly, Equation (31) provides a means of calculating the effect of ionizing radiation which alters bond angles between adjacent saccharide units. Further, one can use Equation (31) to predict how the degree of sulfation of acid mucopolysaccharides found in fish cornea reduces swelling of connective tissue by hindering rotations and decreasing N .

It may also be noted that tearing of connective tissue causes the polysaccharide chains to break or to be pulled from the collagen fibers. This results in increased configurational entropy and increased osmotic activity. Thus, the injured connective tissue swells.

REFERENCES

- Anseth, A., and Laurent, T.C., Exp. Eye Res., 1961, 1, 25
- Fatt, I., and Goldstick, J., Colloid Sci., 1965, 20, 434
- Flory, P.J., Chem. Phys., 1942, 10, 51
- Flory, P.J., and Krigbaum, W.R., Annual Review of Physical Chemistry, 1951, 2, 383
- Huggins, M.L., J. Phys. Chem., 1942, 46, 151
- Huggins, M.L., Am N.Y. Acad. Sci., 1942, 41, 1
- Huggins, M.L., J. Am. Chem. Soc., 1942, 64, 1712
- Polatnick, J., et al., Biophys., Biochim. Acta, 1957, 26, 365

RECEIVED November 3, 1980.

Carboxyl and Amide Transitions in the Circular Dichroism of Glycosaminoglycans

BIRESWAR CHAKRABARTI

Department of Ophthalmology, Harvard Medical School and Eye Research
Institute of Retina Foundation, 20 Staniford St., Boston, MA 02114

Glycosaminoglycans (GAG), a group of acidic polysaccharides, is a coined word from glycosamine (amino sugar) and glycans (polysaccharides). These polysaccharides are of animal origin. With the possible exception of hyaluronic acid, they are present in tissues as segments of larger macromolecules, the proteoglycans, which consist of carbohydrate chains (the glycosaminoglycans) covalently linked to protein. The structure, occurrence, physicochemical properties, and physiological function of glycosaminoglycans have been described in some recent articles (1,2,3). The conformation of hexose polysaccharides in solution including the earlier chiroptical studies of glycosaminoglycans was reviewed by Stone (4) and very recently by Chakrabarti and Park (5) who described in detail the structure and interaction properties of these macromolecules.

Glycosaminoglycans are linear polyelectrolytes with a repeating disaccharide unit consisting of a N-acetylglucosamine, and, with the exception of keratan sulfate, a uronic acid. They differ in parent monosaccharides, molecular weight, degree of sulfation, and homogeneity of these characteristics, and in types of backbone linkages. GAG structures are shown in Figure 1.

Because of the inherent properties of optical activity of sugar molecules, glycosaminoglycans exhibit a rather complex circular dichroism due to the presence of various chromophores in the sugar backbone and as substituents. Thus, interpretation of the optical activity of these compounds requires an understanding of the optical properties of each of its chromophores. In GAG, the chromophores are acetal, hemiacetal, hydroxyl, carboxyl, and acetamido groups. The optical characteristics in the observable range of a commercial spectropolarimeter (> 185 nm) are due mostly to carboxyl and acetamido groups but other chromophores may also contribute. Since most CD measurements of glycosaminoglycans have been made with commercial instruments, we will be concerned here primarily with the carboxyl and amide chromophores of these polymers.

Circular Dichroism of Uronic Acid Residues

Except in keratan sulfate, which has a galactose instead of uronic acid, all GAG have a carboxyl group-containing sugar monomer — glucuronic acid and/or its C-5 epimer, iduronic acid. GAG, in general,

0097-6156/81/0150-0275\$05.00/0
© 1981 American Chemical Society

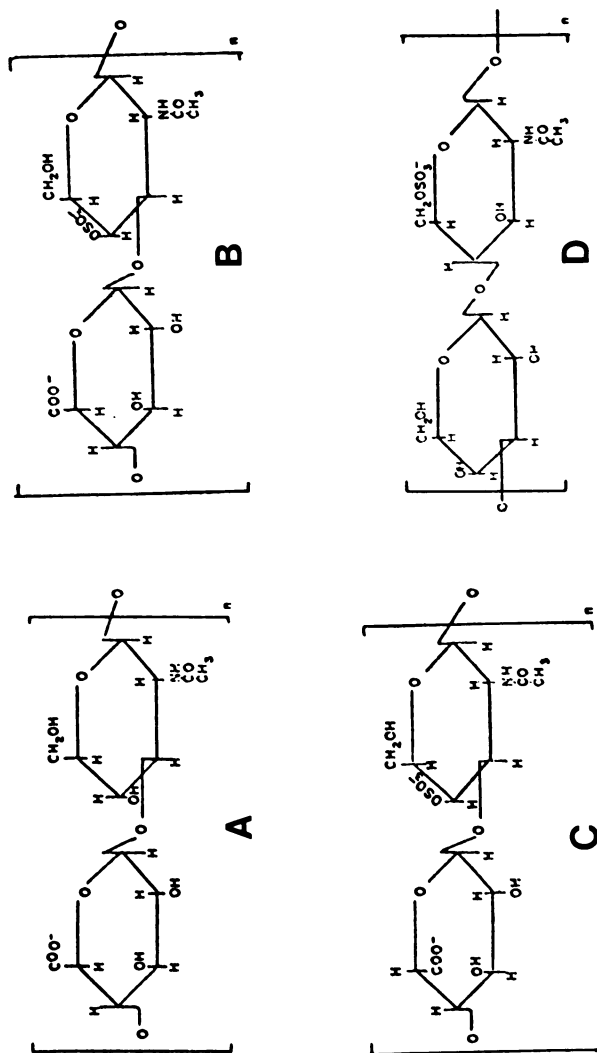


Figure 1. Primary structure of glycosaminoglycans: (A) hyaluronic acid; (B) chondroitin-4-sulfate; (C) dermatan sulfate; (D) heparin; (E) heparan sulfate.

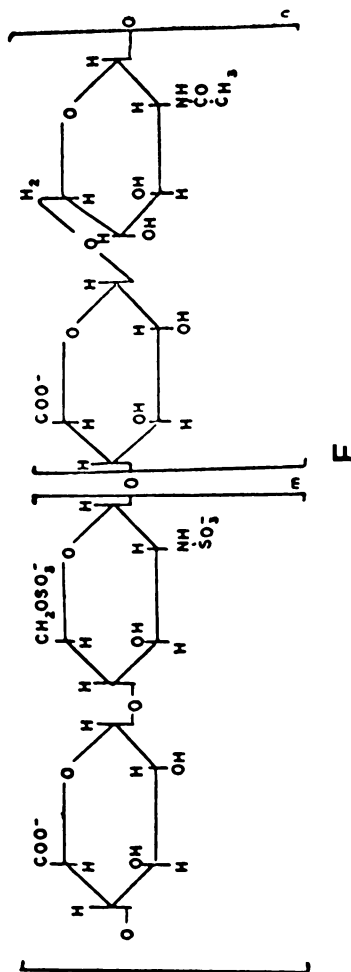
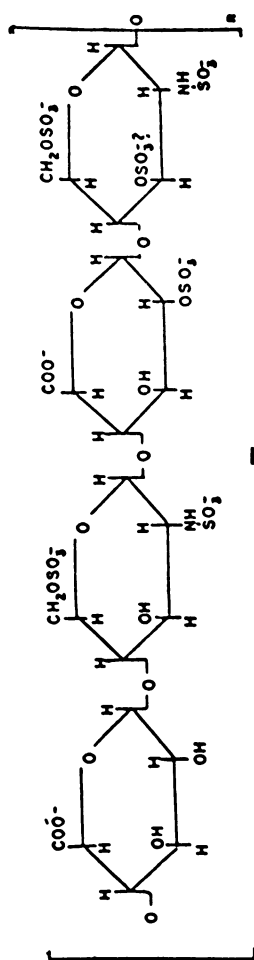


Figure 1 (continued)

exhibit a circular dichroism (CD) band near 210 nm and most of them show a second CD band around 190 nm (Figure 2). These CD bands have generally been assigned (6) to the $n-\pi$ and $\pi-\pi$ amide bands, respectively. Unfortunately, the transitions due to carboxyl received less attention although uronic acids have been shown to exhibit considerable optical activity (7,8,9). Almost in the same region of $n-\pi$ amide transition, uronic acid displays CD bands that have been assigned to the $n-\pi$ carboxyl transition. Glucuronic acid CD consists of a low-energy (234 nm) negative band and a higher-energy (207 nm) positive band. Listowski et al (7) first reported this long-wavelength band and, from solvent-dependent CD studies, assigned it to the $n-\pi$ transition of unsolvated molecules and the normal higher-energy band near 207 nm to the same transition in molecules hydrogen-bonded to water. This interpretation was later rejected, and the most widely accepted explanation of the two bands is that they arise from the $n-\pi$ transition of different rotational isomers of carboxyl groups (8,9,10). The property appears to be characteristic for uronic acids with the C-4 hydroxyl group as an equatorial substituent. In contrast, galacturonic or iduronic acid, in which this hydroxyl is axial, shows a single CD band around 210 nm attributable to the $n-\pi$ carboxyl transition (7,8). CD titration of sodium glucuronate shows an isodichroic point at 225 nm, which indicates the presence of only two species (9). Studies of the CD bands due to $\pi-\pi$ carboxyl transition of the monomeric sugars and of their polymer, which are located below 190 nm, were limited experimentally; the range of the commercial spectropolarimeter does not extend below 190 nm and in many cases includes artifacts. With the rapid development in instrumentation over the last few years, it is now possible to measure CD in the vacuum ultraviolet region (11). We have successfully utilized the technique and, for glucuronic acid and glucuronate, a CD band is observed at 182 nm, the rotational strengths of which are negative in solution of both species and in films of the acid; in films of the anion its rotational strength is positive (9). The location of the band is close to what is expected for a $\pi-\pi$ carboxyl transition although some contribution from a ring transition cannot be ruled out. The change in the sign of the CD band in the film relative to the solution was explained by intermolecular as well as carboxyl-cation interaction.

Circular Dichroism of Acetamido Sugar Residues

In GAG the amide occurs as an acetamido group; the monomers are either N-acetylglucosamine or N-acetylgalactosamine. The exception is heparin, where many amino sugars are N-sulfated rather than acetylated. Beychok and Kabat (12) first identified amide optical activity in sugars and noted the blue shift of the $n-\pi$ band relative to peptides (210 nm versus 220 nm in peptides) and the $\pi-\pi$ transition coinciding with that observed in peptides (190 nm). Their work along with that of Listowski (13) and Stone (6) established that acetamido CD is dependent on sugar configuration at C-2, C-4, and C-1. Kabat et al (14) have shown that the optical activity may be used to differentiate various intersaccharide linkages and substituent position. The anomeric configuration at C-1 has been shown to have a strong influence on the optical activity in the 220 nm region. They

have made a case for the importance of anomeric configuration in determining the CD of amido sugars at 210 nm. However, CD data of Coduti et al (15) do not tend to support this proposal; rather they show that CD in the $\pi-\pi^*$ region varies with anomeric configuration, substituent position, and linkage position. Bush and coworkers (15,16) have recently studied the CD of some mono-, di-, and trisaccharides of N-acetyl sugars in water and hexafluoro-isopropanol (HFIP). They found a strong dependence on CD of the $\pi-\pi^*$ amide band in aqueous solution and $n-\pi^*$ and $\pi-\pi^*$ in HFIP on both configuration and solvent. The vacuum ultraviolet CD of N-acetylglucosamine exhibits a positive CD band at 188 nm assigned to the $\pi-\pi^*$ amide transition in addition to a negative $n-\pi^*$ band at 210 nm (9). Both of these bands have been observed to be insensitive to protonation of amide chromophores.

* The assignments of the first transition to a $n-\pi^*$ and the second to a $\pi-\pi^*$ transition are well established for the acetamido sugars. The appearance of $n-\pi^*$ amide in the lower wavelength region (~ 210 nm) for these sugars as compared to that in α helical polypeptides (~ 222 nm) is believed to be due to extensive solvation of amido groups in saccharides (9).

Optical Activity of Glycosaminoglycans

Stone (6) made the first attempt to show that the CD of acetamido groups could be useful in probing GAG structure, conformation, and interaction. Although her pioneering work on the optical studies of glycosaminoglycans discovered certain important features of these polysaccharides, in the analyses of data she had tacitly neglected the contribution of carboxyl chromophore to the Cotton effect. It is true that in most cases amide chromophores play a major role in the spectral features of GAG, yet the CD of the carboxylate have been shown (8) to be useful in probing the structure of some acidic polysaccharides with no amide chromophores. In order to understand the conformational properties of glycosaminoglycans more fully, and place their theoretical interpretation on a firmer basis, we have undertaken a systematic study of the CD of these compounds. The optical activity of such polymers must be analyzed in terms of the transitions of both amide and carboxyl chromophores. However, our analysis has ignored any explicit contribution to the CD by the hemiacetal or acetal group. The validity of this assumption is obvious from Nelson and Johnson's (17) vacuum ultraviolet CD studies which showed that these groups make a very small contribution to the CD at wavelengths longer than 190 nm.

We may summarize our results on the CD of GAG in terms of the sign and relative intensities of the two bands (Table I). The rotational strengths of glucosamine monomers are relatively much higher than those of glucuronic acid (but not iduronic acid) (18). Thus, if we are to ignore the contribution of glucuronic acid in the CD of this uronic acid-containing polymer, the interpretation of the data should be straightforward. As regard to sign, the CD of all GAG at 210 nm is negative; on the other hand, the CD band at 190 nm is apparently dependent on anomeric configurations and intersaccharide linkages. As Stone (6) pointed out, 1,3-linked amino sugars display a negative CD and 1,4-linked, a positive one at

Table I
SIGN AND RELATIVE INTENSITIES OF CD
OF GLYCOSAMINOGLYCANS (GAG)

GAG	210 nm band	190 nm band
hyaluronic acid	S (-)	vW (-)* W (+) in acid
β 1,3-D-glucosamine β 1,4-D-glucuronic acid		
chondroitin sulfate	S (-)	vW (-)* W (+) in acid
β 1,3-D-galactosamine β 1,4-D-glucuronic acid		
dermatan sulfate	W (-)	S(-)
β 1,3-D-galactosamine α 1,4-L-iduronic acid		
heparin	W (-)	S (+)
α 1,4-D-glucosamine α 1,4-L-iduronic acid (major) D-glucuronic acid (minor)		
heparan sulfate	mS (-)	S (+)
α 1,4-D-glucosamine α 1,4-D-glucuronic acid (major) L-iduronic acid (minor)		
keratan sulfate	S (-)	S (+)
β 1,4-D-glucosamine β 1,3-D-galactose		

S = strong; mS = medium strong; W = weak; vW = very weak
(+) and (-) indicate the sign of the CD band

* These negative bands are not commonly observed.

the π - π^* amide transition region. However, in both hyaluronic acid and chondroitin sulfate the second negative CD band is often not observed. We will discuss more about this later. In the earlier studies, the relative intensities of the CD band at 210 nm were not a subject of discussion in terms of additivity of monomer contribution to polymer. For the 190 nm band it has been noted (6) that 1,3 linkages have small negative CD at 190 nm whereas those with 1,4 linkages have large positive CD at that wavelength. The effect is similar when the amido sugar is substituted at the 3 position (a small negative CD) or at the 4 position (a large positive CD) (15).

In order to evaluate the contribution of both carboxyl and amide transitions to the CD of GAG, we have included in our studies not only the acid and salt forms of the polymers but also some chemically substituted heparins and chondroitin sulfates (Table II). The ellipticity value at 210 nm of hyaluronate is considerably higher than for the rest of the series. Interesting differences can be observed between heparin (HP) and keratan sulfate (KS), and between dermatan sulfate (DS) and chondroitin sulfate (CHS). Although HP is α 1,4 linked as opposed to the β 1,4 linkage of KS, the lower value of DS cannot be explained on the same ground because CHS and DS are both β 1,3-linked amino sugars. We believe that the iduronic acid makes the difference. N-desulfated heparin may have very few acetamido groups; hence, the contribution to the 210 nm CD band is mostly due to iduronic acid only. The lower ellipticity values of HP, HPS, and DS near 210 nm compared to other GAG and even to their monomeric constituents, suggest that the n - π amide transitions are weakly optically active or virtually inactive. This is supported by the fact that even complete N-acetylation of heparin does not increase the rotational strength at 210 nm; rather it decreases it. Thus it has been proposed (18) that a disaccharide unit containing N-acetylamino sugar linked with iduronic acid would display a weak n - π amide CD band, or none. HPS shows a larger dichroism than N-acetylated heparin because of the former's relatively higher content of both glucuronic acid and N-acetylglucosamine. It may even be possible that the n - π amide band is positive when the adjacent sugar is iduronic acid. Unfortunately, we do not have any values for the ellipticity of L-iduronic acid. The value for methyl-iduronoside reported here (Table II) is of the D-isomer, not the L-isomer. Mirror-image spectra of the D-isomer (with a negative value) were assumed to be spectra of L-isomer. If this magnitude is reasonably true, then the lower negative values of HP and DS may also be due to a cancellation effect of the positive ellipticity of the n - π amide transition. This is supported by the fact that the calculated values for amide contribution are positive for those GAG the uronic acid component of which is mostly iduronic acid.

pH-Dependent CD of Glycosaminoglycans. Acidification of glycosaminoglycan solution results in significant changes in CD properties (18). Two general patterns are observed; CH, CHS, and HA (hyaluronic acid), which are glucuronic acid-containing polymers, show decreased negativity ellipticity near 210 nm and enhanced negative ellipticity near 230 nm with increasing acidity of the solution. For predominantly iduronic acid-containing polysaccharides, heparin and dermatan sulfate, the ellipti-

TABLE II
ANALYSIS OF pH-DEPENDENT CD OF GAG AND MONOMERS IN TERMS OF $n-\pi^*$ AMIDE
AND CARBOXYL TRANSITION (Ellipticity is expressed as deg/cm^2 per $\text{dmole} \times 10^{-3}$)

Sample ^a	Observed values ^b				Calculated amide contribution ^c			
	210 nm		230 nm		210 nm			
	$[\theta]$	$\Delta[\theta]$	θ	$\Delta[\theta]$	θ	$\Delta[\theta]$	θ	$\Delta[\theta]$
hyaluronic acid	-16.10	+1.50	-1.30	-1.50	-15.10	-1.70	5.80	-1.60
chondroitin	-6.80	+1.60	-0.52	-0.62	5.30	-1.50	4.90	1.40
chondroitin 4-sulfate	-6.30	+1.70	-0.56	-0.93	5.10	-3.30	1.71	+1.00
chondroitin 6-sulfate	-5.90	+1.80	-0.55	-0.89	1.69	0.00	—	0.00
chondroitin methylester	-5.50	+0.70	-1.97	+0.04	—	+0.10	—	+0.10
dermatan sulfate	-3.72	-0.84	-0.33	-0.68	—	-0.77	—	+0.10
heparin	-2.74	-1.84	-0.28	-1.10	—	-0.77	—	+0.10
N-desulfated heparin	-2.09	-1.94	-0.23	-0.77	—	-0.96	—	-0.54
N-acetylated heparin	-1.76	-2.38	-0.21	-0.96	—	-0.84	—	-1.80
heparan sulfate	-4.55	+0.41	-0.28	-0.84	—	-0.42	—	—
D-glucuronic acid	-1.00	+3.20	0.08	-0.42	—	0.0	—	—
N-acetylglucosamine	-4.60	-0.01	-0.25	0.0	—	0.0	—	-0.02
N-acetylglucosamine	-4.80	-0.02	-0.30	0.0	—	0.0	—	-0.02
methyl-D-glucuronoside ^d	-0.47	+4.00	-0.24	-0.19	—	-0.19	—	—
methyl-L-iduronoside	-5.43	-1.84	-0.46	-1.89	—	-1.89	—	—

^a Results of our sample analysis showed that dermatan sulfate has 99% iduronic acid and the rest glucuronic acid; heparin 90% idu and 10% glu; heparan sulfate 33% idu and 67% glu. Hyaluronic acid and chondroitins are all 100% glucuronic acid. ^b $[\theta]$ is the value at pH 7.5; $\Delta[\theta] = [\theta]_{\text{pH}2.5} - [\theta]_{\text{pH}7.5}$. ^c Assumption is made that the carboxyl contribution is additive. See text. ^d Taken from Ref. 8. See text.

city values at both 210 and 230 nm become more negative with decreasing pH. The difference in acid-induced dichroic behavior of polymers with epimeric variations is evident. Heparan sulfate, which contains both uronic acids, shows the combined effects of both glucuronic and iduronic acids.

If the change in CD features at a particular wavelength that occurs with change in pH is due solely to one chromophore, and no major conformational transition is associated with the change, then the relative variation of ellipticity is expected to follow an empirical equation:

$$\text{pH} = \text{pK}_a - n \log (\alpha/1-\alpha) \quad (1)$$

where α denotes the degree of dissociation and can be related to ellipticity change as $\alpha = (\theta - \theta_{\text{pH} \ll \text{pK}_a}) / (\theta_{\text{pH} \gg \text{pK}_a} - \theta_{\text{pH} \ll \text{pK}_a})$. n is an empirical constant

and depends on the ionic strength and the concentration of the solution. pK_a can thus be determined from equation 1.

With this rule of thumb, it has been possible for us to examine whether the pH variation can cause any change in conformation of the molecule (18). Results, indeed, provide significant information. The changes in ellipticity at 230 nm for HA, CH, and CHS follow equation 1, but the changes at 210 nm do not — the reverse is true for HP, N-desulfated HP, and N-acetylated HP. The fact that the 230 nm ellipticity values of the first group of polymers follow equation 1 indicates that the change in CD properties in this wavelength region is due entirely to the acid-base properties of the carboxyl group. The dichroic behavior at 210 nm with pH does not obey the equation, which suggests some conformational change of this group of polymers with change in hydrogen ion concentration. Except for DS, compounds of the second group contain both iduronic and glucuronic acids (Table II). Thus the ellipticity variations with pH at both 210 and 230 nm can be used for DS to determine the pK value. Even though heparin contains a small amount of glucuronic acid, the change in dichroism at 210 nm follows equation 1, because the variation with pH at this wavelength for an iduronic acid-containing polymer is so large that the effect of glucuronic acid is negligible. Because of the presence of appreciable amounts of both glucuronic and iduronic acids, the method is not applicable to heparan sulfate.

The spectral behavior of heparin in the $\pi-\pi^*$ transition region associated with change in pH might originate from conformational change but the CD features at 210 nm provide no evidence for conformational change as has been suggested (19). Instead, our results (18) demonstrate that variations of CD spectra of heparin arise mainly from the acid-base behavior of the uronic acid moieties.

X-ray studies (20) favor the 1-C conformation of iduronic acid in heparin as opposed to the C-1 in dermatan sulfate, but NMR studies (21) in solution do not suggest such a difference (Figure 3). The conformation of the L-iduronic acid in dermatan sulfate has been suggested (22) as C-1, based on analysis of optical rotatory dispersion curves. The striking dissimilarities in the dichroic properties of heparin and dermatan sulfate in

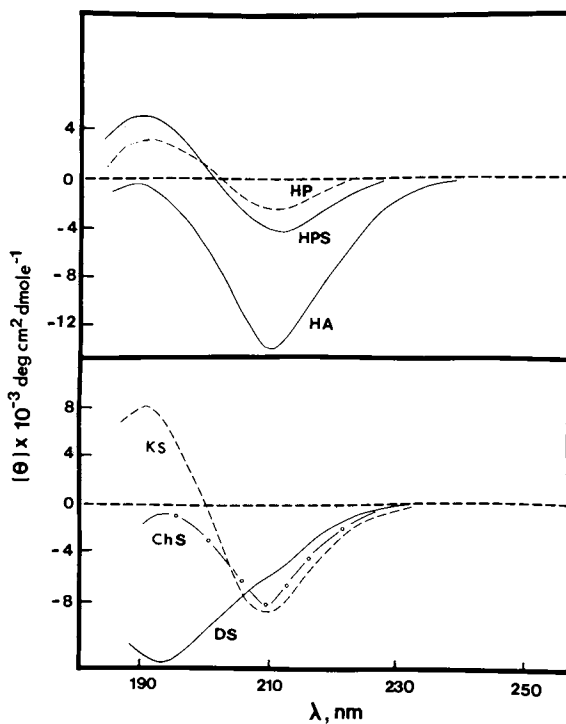


Figure 2. CD of glycosaminoglycans, pH 6.8. Area under square bracket indicates the transition region of amide and carboxyl chromophores of sugars.

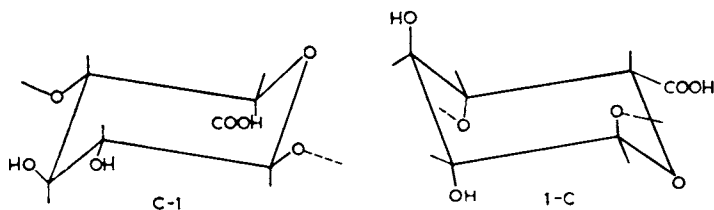


Figure 3. 1-C and C-1 conformation of iduronic acid

their acid and salt forms (18) and in the CD spectra of copper complexes (23) have been attributed to their difference in intersaccharide linkages or to the conformation of the iduronic acid moiety.

Dichroic Behavior of Carboxyl and Amide Chromophores in Polysaccharide. It is evident that the configurational differences of the uronic acid moiety are well reflected in the dichroic behavior of the polymer, and the carboxyl chromophore thus plays a significant role in the chiroptical properties of the molecules. Certain facts regarding carboxyl chromophores are apparent from this study: a) monomeric CD properties are well reflected in the Cotton effect of the polymer; b) similarities in $\Delta\theta$ values (Table II) between monomers and polymers containing similar uronic acids indicate the additivity of monomer contributions to polymer CD; c) iduronic acid shows considerably larger CD than glucuronic acid, which may have some origin in the observed difference in the NMR behavior (24) of methyl α -D-idopyranosiduronic acid from uronic acid with normal C-1 conformation. This has been interpreted in terms of either an equilibrium between the C-1 and 1-C chair forms or adoption of a hybrid 'skew boat' structure.

Dichroic behavior of the amide chromophores, on the other hand, shows a remarkable difference between the monomers and the polymers. Examples are: a) sign and intensity of π - π^* transition changes (Table I) with anomeric configuration and intersaccharide linkage; b) in most cases there is nonadditivity of the ellipticity values of both the CD bands from monomer to polymer; c) a drastic change in the relative rotational strengths of π - π^* and n - π^* occurs on conformational change of hyaluronic acid (discussed later). If we accept that the magnitude, sign, and position of the CD bands of carboxyl chromophore do not change from monomer to polymer, then we can calculate the amide contribution to the CD of GAG (Table II). Even change in pH causes a marked change in $\Delta\theta$ values (due to amide only) of the 210 nm band. Significant changes of the 190 nm CD band have been observed in HA (25), and in HP and DS (18). The phenomena might indicate a conformational change of the polymers with change in their hydrogen ion concentration. Nonadditivity of the amide transition from monomer to polymer is observed in most of these polysaccharides, but in hyaluronic acid it is significantly higher than in the rest.

CD of Oligosaccharides of Hyaluronic Acid

Among GAG, conformation of HA in solution (6,9,25-33) and in solid state (34,35,36,37) has been studied most. We have recently prepared oligosaccharides of HA, starting from di- to dodecasaccharide according to reported methods (38,39). We have also succeeded in making some trisaccharides by glucuronidase digestion of tetrasaccharides (39).

Figure 4 shows the CD of the equimolar mixture of N-acetylglucosamine and glucuronic acid and of disaccharide of HA. The sharp contrast between the two can be observed in the π - π^* amide transition region (190 nm) while the rotational strengths of the n - π^* region of both remain the same; the band at 190 nm, which does not exist in the mixture, is significantly intense for the disaccharide. At lower pH, however, the

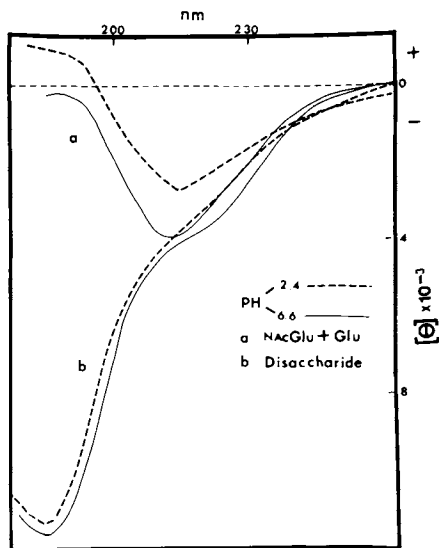


Figure 4. CD of equimolar mixture of N-acetylglucosamine and glucuronic acid (NacGlu + Glu) and disaccharide

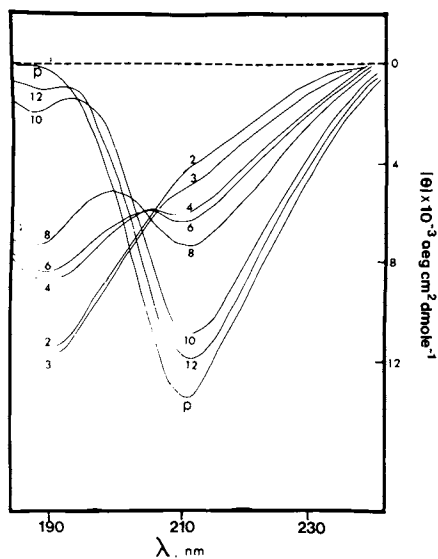


Figure 5. CD of oligosaccharides of hyaluronic acid: 2-12 indicates the number of saccharides; P is the polymer, hyaluronic acid; pH 6.8.

component mixture shows a positive ellipticity below 200 nm because of weaker negative dichroism of the glucuronic acid than glucuronate at that region (9). Clearly, the intersaccharide linkage makes a large difference in the dichroic properties of carbohydrates. Obviously, an equimolar mixture of the monomeric constituents cannot be a representative model for the CD of hyaluronic acid or any other GAG. The question is whether even the disaccharide can serve the purpose. One has to remember that HA is an alternate β -1,3- and β -1,4-linked polymer. Testicular hyaluronidase, used in our preparation, cleaves off the β 1,4 uronic acid linkage but retains the β 1,3 amino linkage sugar intact. Hence, the disaccharide is β 1,3 linked, the dichroic behavior of which may be significantly different from that of the 1,4 linked. By the same argument, trisaccharide, which has one 1,3 and other 1,4 linkages, should be different from disaccharide. However, the CD features of di- and trisaccharides are very similar (Figure 5), suggesting the need for an alternative explanation.

Although the parent molecule has both β 1,3 and β 1,4 linkages, it is possible that the end groups of oligosaccharides may be either α or β , or equilibrium anomeric mixtures. This anomeric difference of the end groups may influence the CD properties and the effect could be predominant in smaller oligosaccharides such as di- and trisaccharides. However, we have not observed any difference in dichroism between a freshly prepared solution and a solution kept a sufficiently longer time for any mutarotation to occur. It has been also suggested (see Bush and Ralapati, this volume) that the CD magnitude around 190 nm, particularly of the lower members of the oligosaccharides, may significantly change due to mutual coupling between the π - π amide transition and the n - σ band of the acetal chromophore. For reducing sugars, it is the hemiacetal, and for their corresponding glycosides, the acetal chromophore transition that are involved in this coupling. The mechanism, thus, reasonably explains the large rotational strength of the π - π amide band of di- or trisaccharides. The amide n - π CD band is insensitive to anomeric configuration or to such interaction (15). The n - π transition of both di- and trisaccharides are almost equal in magnitude with a mixture of N-acetylglucosamine and glucuronic acid, whereas from tetramer to polymer the 210 nm band increases with simultaneous decrease in the π - π amide transition. The fact that even in octasaccharide there is a considerable rotational strength of the 190 nm CD band makes it evident that the mechanism by which π - π amide is highly optically active in disaccharide is also operating in the higher oligosaccharides. The conformation of the end residues of the oligosaccharides is expected to be different from that of the internal residues and so also their contribution to the CD values. In that concept, the ellipticity of the disaccharide CD band is due entirely to the end residues, and increase (210 nm) or decrease (190 nm) in the CD magnitude of the higher oligomers can be explained by the weighted average contribution of internal repeating disaccharides and end residues. The abrupt change in the CD values from di- to tetrasaccharides and gradual change from tetramer to octamer validate this argument.

* There seems to be a drastic change in the values of both n - π and π - π amide transitions when the number of sugar units is ten or higher. It is evident from the plot of both the 210 nm band ellipticity and the ratio of

$\theta_{190}/\theta_{210}$, which show a drastic change in the values from lower oligosaccharide to decamer (Figure 6). Similarities in the shape of the curves indicate that the error in the concentration measurements (upper curve of Figure 6) is negligible. The values for di- and trisaccharide, as expected, are significantly different from the general trend of changes of the optical parameters in higher oligomers, and they are off from the curves. The results seem to indicate that some conformational variations exist among three sets of oligomers; the first set is the di- and trisaccharides, the second is tetra- to octasaccharides, and the third includes decasaccharides and higher polymers. The dissimilarity of the CD features in the π - π region of di- and trisaccharides from that of the component monomers suggests that there is some interaction between two chromophores of these saccharides and the interaction is likely to occur through the pyranose rings. The effect is still there in the next set of oligomers, but with increasing number of sugar units, a second factor, probably hydrogen bonding, tends to change the backbone conformation in such a way that the former interaction is less predominant as manifested in the decreasing n - π amide band amplitude. It has been proposed (34) from x-ray diffractograms of hyaluronate that the C-4 hydroxyl group of N-acetylglucosamine is involved in hydrogen bonding with ring oxygen of glucuronic acid. Such hydrogen bonding cannot be overruled even in solution state as the behavior of hyaluronate in solution is known (30) to be significantly different from chondroitin or chondroitin sulfate which differ from the former in C-4 hydroxyl configuration. In deca- and higher oligomers (including the polymer), there is some sort of cooperative conformational transition which is manifested in CD features. The predominant factor that leads to this conformation is likely to be associated with the hydrogen bonding mentioned above. Any orientation change of amide chromophore against the dissymmetric environment of the rest of the molecule will cause large changes in CD magnitude as observed in the amide transitions, particularly the nonadditivity of the n - π amide band from lower oligomers to decamer and polymer. Several possibilities for the nonadditivity of the CD band at 210 nm of hyaluronate have been considered (9) before: the change in the configuration of sugar ring and/or its hydroxyl groups in the presence of neighboring sugar rings, contributions of polarizability and static field to the optical activity of the n - π transition, or the alteration of the acetamido group. The study, however, has not ruled out the possibility of an ordered structure that could be responsible for the nonadditivity of the CD intensity at 210 nm. The large rotational strengths of the n - π amide transition in solution and the π - π transition in film of hyaluronate in comparison to those of chondroitin 4-sulfate have also been attributed (40) to some "conformational constraints" in hyaluronate.

It has been demonstrated (5,41) that amide transition, at least in hyaluronic acid, is very sensitive to conformational change. The CD spectra of hyaluronate in film, hyaluronic acid in aqueous-organic solvent, and Cu^{2+} hyaluronate differ from those of acid and neutral forms of hyaluronates. In all three spectra the appearance of a strong negative band in the π - π amide transition and apparent loss of n - π CD minima are evident, and the changes have been attributed to a conformational transition of the molecule to a 4-fold helix.

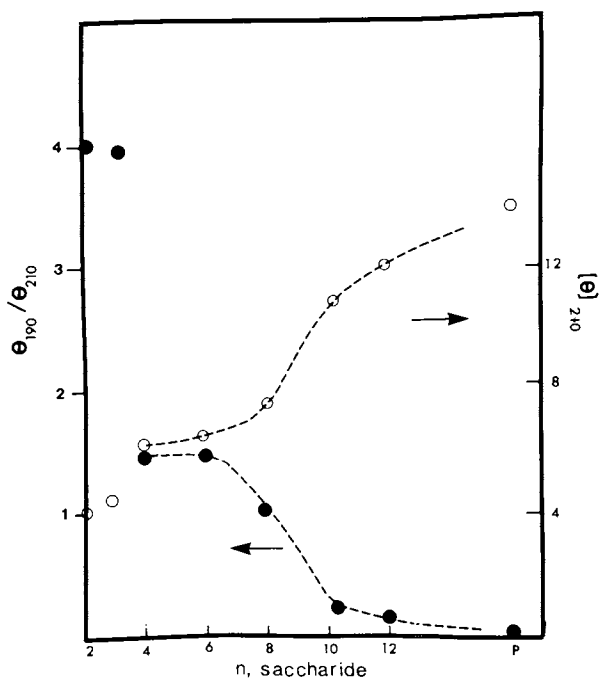


Figure 6. Plot of ratio $\theta_{190}/\theta_{210}$ and ellipticities at 210 nm vs. number of saccharides; pH 6.8.

Conformational feature of hyaluronate at neutral pH is still a matter of conjecture. Structural change of the molecule with $\text{pH} > 7$ has been suggested (32,33,42,43) from various physicochemical measurements. The changes in the CD spectra, of both $n-\pi$ and $\pi-\pi$ amide transitions, from lower oligosaccharides to polymer, are suggestive of some conformational order in the hyaluronate at neutral pH. Earlier hydrodynamic measurements (44) of hyaluronate in neutral solution have characterized the molecule as a 'random coil with some stiffness'. The description requires considerable modification in view of the new insights gained from recent hydrodynamic (45) and optical studies presented here. At neutral pH, hyaluronate is in extended conformation due to the repulsive interactions between the negative charges along the chain. The change in CD features from oligosaccharides to polymers can be accounted for by a suggestion that in neutral solution the molecule is in an extended helical form probably similar to a 2-fold helix (34). Such an assumption obviously requires support from further investigations but the interesting changes in the CD spectra of amide transitions cannot be explained by the earlier assumption of a random coil conformation of the molecule in the physiological range of pH.

ABSTRACT: Circular dichroism of glycosaminoglycans has been analyzed in terms of both carboxyl and amide transitions. Although the contribution of the carboxyl chromophore to polymer CD is significant and the epimeric variation of the uronic acid is well reflected in the dichroic behavior of the polysaccharides, there seems to be an additivity of the carboxyl spectral features from monomer to polymers. In contrast, the magnitude and sign of both $\pi-\pi$ and $n-\pi$ amide CD bands are sensitive to anomeric configuration, glycosidic linkage, and also the conformation of the polymers. The rotational strengths of the amide transitions in glycosaminoglycans may also vary with the epimeric variations of the adjacent uronic acids. The oligosaccharides of hyaluronic acid, for which data are presented here, show a remarkable difference in their chiroptical behavior between the lower and higher members of the series. A drastic change in the CD amplitude from lower oligomers to decamer suggests that hyaluronate at neutral pH probably exists as an extended helix rather than a random coil.

ACKNOWLEDGMENT: The study was supported by PHS research grant EY-01760 and Research Career Development Award K04 EY-00070.

Literature Cited

1. Mathews, M.B. "Connective Tissue: Macromolecular Structure and Evolution", Springer-Verlag, New York, 1975.
2. Bettelheim, F.A., in Veis, A., Ed. "Biological Polysaccharides"; Marcel Dekker, New York, 1970, p. 131.

3. Comper, W.D.; Laurent, T.C. *Physiol. Rev.*, 1978, 58, 255.
4. Stone, A.L., in Timasheft, S.N. and Fasman, G.D., Eds. "Structure and Stability of Biological Macromolecules", Marcel Dekker, New York, 1969, p. 353.
5. Chakrabarti, B.; Park, J.W. "Glycosaminoglycans: Structure and Interaction", *CRC Review in Biochemistry* (in press).
6. Stone, A.L. *Biopolymers*, 1971, 10, 739.
7. Listowski, I.; England, S.; Avigad, G. *Biochemistry*, 1969, 8, 1781.
8. Morris, E.R.; Rees, D.A.; Sanderson, G.R.; Thom, D. *J. Chem Soc. (Perkin II)*, 1975, 1418.
9. Buffington, L.A.; Pysh, E.A.; Chakrabarti, B.; Balazs, E.A. *J. Amer. Chem. Soc.*, 1977, 99, 1730.
10. Listowski, I.; Avigad, G.; England, S. *J. Org. Chem.*, 1970, 35, 1080.
11. Young, M.A.; Pysh, E.S. *Macromolecules*, 1973, 6, 790.
12. Beychok, S.; Kabat, E.A. *Biochemistry*, 1965, 4, 2565.
13. Listowski, I.; Avigad, G.; England, S. *Carbohyd. Res.*, 1968, 8, 205.
14. Kabat, E.A.; Lloyd, K.O.; Beychok, S. *Biochemistry*, 1969, 8, 747.
15. Coduti, P.L.; Gordon, E.C.; Bush, C.A. *Anal. Biochem.*, 1977, 78, 9.
16. Dickinson, H.R.; Coduti, P.L.; Bush, C.A. *Carbohyd. Res.*, 1977, 56, 249.
17. Nelson, R.G.; Johnson, W.C. *J. Amer. Chem. Soc.*, 1972, 94, 3343.
18. Park, J.W.; Chakrabarti, B. *Biochim. Biophys. Acta*, 1978, 544, 667.
19. Stone, A.L. *Nature (London)*, 1967, 216, 551.
20. Atkins, E.D.T.; Nieduszynski, I.A. *Fed. Proc.*, 1977, 36, 78.
21. Perlin, A.S.; Casu, B.; Sanderson, G.R.; Johnson, L.F. *Can. J. Chem.*, 1970, 48, 2260.
22. Davidson, E.A. *Biochim. Biophys. Acta*, 1965, 101, 121.
23. Mukherjee, D.C.; Park, J.W.; Chakrabarti, B. *Arch. Biochem. Biophys.*, 1978, 191, 393.
24. Perlin, A.S.; Casu, B.; Sanderson, G.R.; Tse, J. *Carbohyd. Res.*, 1972, 21, 123.
25. Chakrabarti, B.; Balazs, E.A. *J. Mol. Biol.*, 1973, 78, 135.
26. Chakrabarti, B.; Balazs, E.A. *Biochem. Biophys. Res. Commun.*, 1973, 52, 1170.
27. Chakrabarti, B. *Arch. Biochem. Biophys.*, 1977, 180, 146.
28. Park, J.W.; Chakrabarti, B. *Biopolymers*, 1978, 17, 2415.
29. Park, J.W.; Chakrabarti, B. *Biochim. Biophys. Acta*, 1978, 541, 263.
30. Figueroa, N.; Chakrabarti, B. *Biopolymers*, 1978, 17, 2415.
31. Hirano, S.; Kondo-Ikeda, S. *Biopolymers*, 1974, 13, 1357.
32. Mathews, M.B.; Decker, L. *Biochim. Biophys. Acta*, 1977, 498, 259.
33. Dark, A.; Finer, E.G.; Moorehouse, R.; Rees, D.A. *J. Mol. Biol.*, 1975, 99, 475.
34. Guss, J.M.; Hukins, D.W.L.; Smith, P.J.C.; Winter, W.T.; Arnott, S.; Moorehouse, R.; Rees, D.A. *J. Mol. Biol.*, 1975, 95, 359.
35. Winter, W.T.; Smith, P.J.C.; Arnott, S. *J. Mol. Biol.*, 1975, 99, 219.
36. Arnott, S.; Winter, W.T. *Fed. Proc.*, 1977, 36, 73.
37. Sheehan, J.K.; Gardner, K.H.; Atkins, E.D.T. *J. Mol. Biol.*, 1977, 117, 113.
38. Flodin, P.; Gregory, J.D.; Roden, L. *Anal. Biochem.*, 1964, 8, 424.
39. Hascall, V.C.; Heinegrad, D. *J. Biol. Chem.*, 1974, 249, 4242.

40. Buffington, L.A. Ph.D. Dissertation, Dept. of Chemistry, Brown University, 1978.
41. Chakrabarti, B.; Figueroa, N.; Park, J.W.; Gregory, J.D.; Jeanloz, R.J., Eds. "Glycoconjugate Research, Vol. I", Academic Press, New York, 1979, p. 119.
42. Chakrabarti, B.; Balazs, E.A. Fed. Proc., 1975, 34, 635.
43. Baret, T.W.; Harrington, R.E. Biopolymers, 1977, 16, 2167.
44. Laurent, T.C., in Balazs, E.A., Ed. "Chemistry and Molecular Biology of the Intercellular Matrix", Vol. 2, Academic Press, London, 1970, p. 703.
45. Cleland, R.L. Arch. Biochem. Biophys., 1977, 180, 57.

RECEIVED September 8, 1980.

Vacuum UV Circular Dichroism Spectroscopy of Acetamido Sugars

C. ALLEN BUSH and SURESH RALAPATI

Department of Chemistry, Illinois Institute of Technology, Chicago, IL 60616

The carbohydrate chains of glycoproteins and glycolipids have non repeating structures containing from four to approximately fifteen sugar residues. Since the chains are branched and feature sugars with such chemical functionality as amides and carboxylic acids, they are known as complex carbohydrates. Although the biological function of these complex oligosaccharides is not well understood, it is the subject of considerable study in connection with such biochemical phenomena as lectin stimulated mitogenesis, hormone binding to cell surfaces and inter-cellular communication generally.

The conformational properties and the physico chemical interactions of the complex oligosaccharides have not been extensively investigated. As a modest beginning for such studies we will pose certain questions regarding the influence of a sugar on its neighbors in a complex oligosaccharide chain. We will attempt to show how one can initiate studies of the conformation of the glycosidic linkage between sugars and between the sugar and the protein as well as the interactions among sugar residues and between the carbohydrate and the peptide chain of a protein. The biophysical techniques we have used are mainly spectroscopic, primarily circular dichroism (CD) and to a lesser extent NMR. Other methods which may be brought to bear on this problem include conformational energy calculations and x-ray crystallography. Small molecule crystallography has already provided some useful insights but protein crystallography has not yet made the major contributions which we would expect, apparently as a result of some fundamental problems in preparing x-ray quality crystals of glycoproteins.

I. CD of Amide Chromophores in Carbohydrates

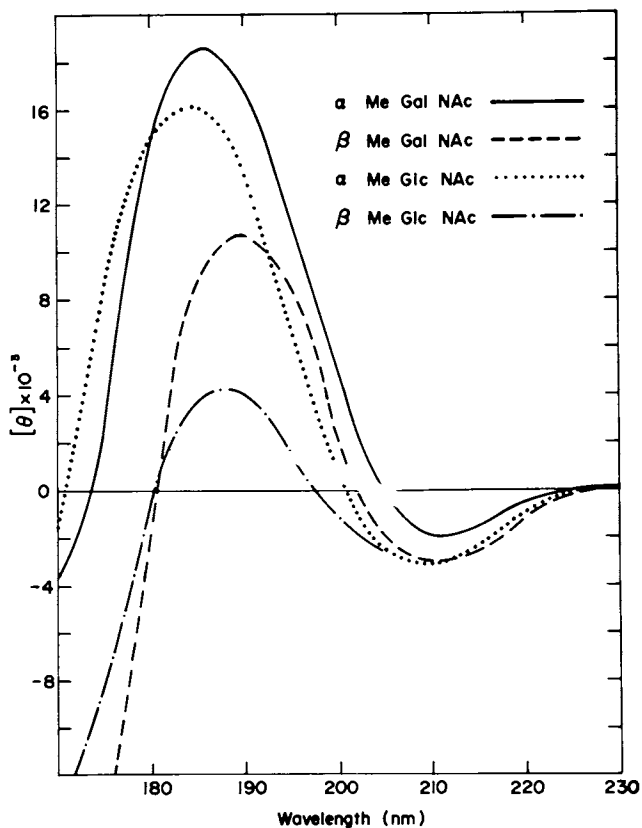
Peptide CD studies have revealed the importance of the amide $n-\pi^*$ transition in amide spectra. This transition which contributes an important CD band at 222 nm in the polypeptide α helix spectrum also appears in the CD spectra of N-acetyl

0097-6156/81/0150-0293\$05.00/0
© 1981 American Chemical Society

amino sugars near 210 nm (Figure 1). This band, although it occurs near the short wavelength limit of the range of conventional commercial CD instrumentation, has been studied by several research groups (1, 2, 3, 4). Also apparent in the spectra of Figure 1 is a band at shorter wavelength (185-192 nm). This band is associated with the strong amide $\pi-\pi^*$ transition which has its uv absorption maximum at 189 nm. Although some useful data on these shorter wavelength bands has been obtained from conventional commercial instruments, in our laboratory we have used a vacuum uv instrument which is optimized for use with samples in solution in the wavelength range 160-300 nm. The instrument features a short focal length monochromator with the cell compartment at atmospheric pressure following a design first introduced by Brahms et al. (5). The optical layout of the instrument in our lab is illustrated in Figure 2 (6). This machine is operated under computer control for repetitive scanning, signal averaging, and Fourier digital filtering of the CD spectra (7).

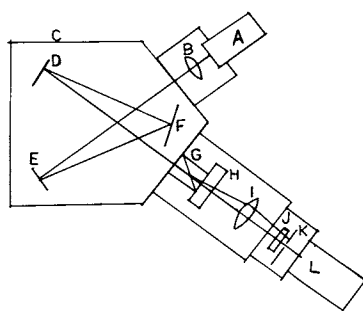
The data of Figure 1 illustrate the similarity of the longer wavelength $n-\pi^*$ bands for different anomeric glycosides of 2-acetamido-2-deoxy-glucose and -galactose (GlcNAc and GalNAc). Variations over a factor of two in magnitude without a change in sign of wavelength of the minimum are observed for this band in a wide variety of oligosaccharides containing these acetamido sugars in aqueous solution. At shorter wavelength, the β glycosides generally show a positive band near 192 nm while the α glycosides have a stronger band at 185 nm. These bands certainly arise from the amide chromophore as is shown by their absence in CD spectra of neutral sugar glycosides which lack the 2-acetamido functionality (8). The fact that the wavelength of the maximum of the CD band departs from the maximum of the absorbance (189 nm) suggests that there is mutual coupling between the amide $\pi-\pi^*$ transition and some other strong transition, perhaps an $n-\sigma^*$ band of the acetal chromophore.

The CD spectra of reducing sugars differ substantially from those of the corresponding glycosides. The data of Figure 3, taken with the instrument in our laboratory, are in substantial agreement with those of Bush (9) taken with the instrumentation in the laboratory of Dr. J. Brahms (5). The data reported by Buffington et al., (10) for GlcNAc differ in the 180-190 nm region perhaps as a result of a difference in anomeric composition. Our data represent an equilibrium anomeric mixture of approximately equal amounts of α and β pyranose. In addition to variability in the exact anomeric composition, a second feature contributes to differences between the CD spectra of reducing sugars and those of their corresponding glycosides. In the former case the amide is perturbed by the hemi-acetal chromophore while in the latter case it is the acetal chromophore which influences the $\pi-\pi^*$ rotational strength, perhaps by a coupling mechanism.



Dordrecht-Holland

Figure 1. CD spectra of methyl pyranosides of 2-acetamido-2-deoxy hexoses (9)



Analytical Chemistry

Figure 2. Schematic of the vacuum UV CD apparatus: (A) 200-W deuterium lamp; (B) CaF_2 collimating lens; (C) McPherson 218 monochromator vacuum chamber; (D, E) focusing mirrors; (F) plane grating; (G) MgF_2 rochon polarizer; (H) modulator; (I) CaF_2 lens; (J) sample chamber at atmospheric pressure; (K) mask for extraordinary beam, (L) photomultiplier (6).

II. Circular Dichroism Spectra of Oligosaccharides Containing Acetamido Sugars

The effect on the CD spectrum of linking two GlcNAc residues by a β 1-4 linkage is essentially that of forming a β glycoside as may be seen from comparison of the spectrum of chitobiose (Figure 4) with that of β -methyl-GlcNAc (Figure 1). This fact is also clear from a spectrum of chitotriose (9). It is also true for β 1-6 linked acetamido sugars as may be seen in the spectrum of GlcNAc(β 1-6)GlcNAc (9).

In contrast, sugars linked at the C-3 position, directly adjacent to the amide chromophore, show a strong negative band at 180 nm which is not seen in spectra of simple glycosides. Figure 5 shows the spectrum of Gal(β 1-3)GalNAc which has negative CD in the 190 nm region, a feature which is characteristic of three and four linked oligosaccharides having reducing terminal acetamido sugars. Lacto-N-tetraose (LNT) has a β linked GlcNAc residue which is also substituted at the C-3 position. Therefore its spectrum shows a positive band at 190 nm characteristic of a β linked acetamido sugar in addition to the negative band at 180 nm which is characteristic of C-3 substitution. Although data presently available for oligosaccharides containing acetamido sugars are sufficient to make a few generalizations, it will be necessary to examine a wider variety of linkages in order to recognize details of explicit interactions between residues.

III. Vicinal Diacyl Amino Sugars and Glycopeptides

In many glycoproteins the connection between the carbohydrate and peptide occurs through a glycosyl amide linked to an asparagine side chain in the protein. The linked sugar, invariably a β GlcNAc residue, is therefore a vicinal diacyl amino sugar. Such sugars have two amide chromophores in sufficiently close proximity to interact by exciton coupling in a manner analogous to that in polypeptides. The CD spectrum which arises from this interaction is characterized by a pair of strong positive and negative bands crossing the axis near the wavelength of the absorbance maximum for the coupled bands. The CD spectrum of 4-N-(2-acetamido-2-deoxy- β -D-glucopyranosyl)-asparagine (GlcNAc-Asn) of Figure 6 shows just such a pair of strong CD bands, crossing the axis near the maximum of the amide π - π^* absorbance. That these bands, which are much larger than those of the other acetamido sugars discussed above, arise from the interaction of the vicinal di-equatorial amides is shown by the CD spectrum of 2-acetamido-2-deoxy-1-N-Acetyl- β -D-glucopyranosyl amine (β 1,2 DAG). Its similarity to that of GlcNAc-Asn implies that the large bands arise from amide interaction, not from the amine and carboxyl functions of the amino acid. Since the CD due to this exciton coupling is quite sensitive to the geometric

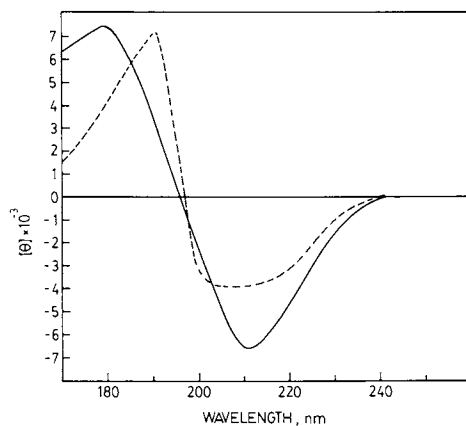


Figure 3. CD spectra of N-acetyl glucosamine (—) and of N-acetyl galactosamine (---)

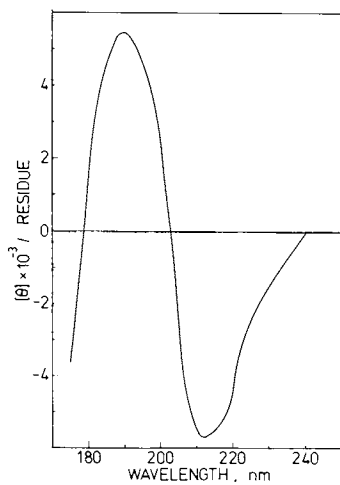


Figure 4. CD spectrum of GlcNAc (β -1,4)GlcNAc (chitobiose)

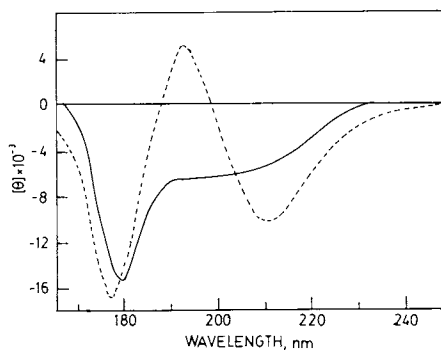


Figure 5. CD spectra of Gal (β -1,3)GalNAc (—) and of Gal(β -1,3)GlcNAc(β -1,3)Gal(β -1,4)-Glc (Lacto-N-tetraose) (---).

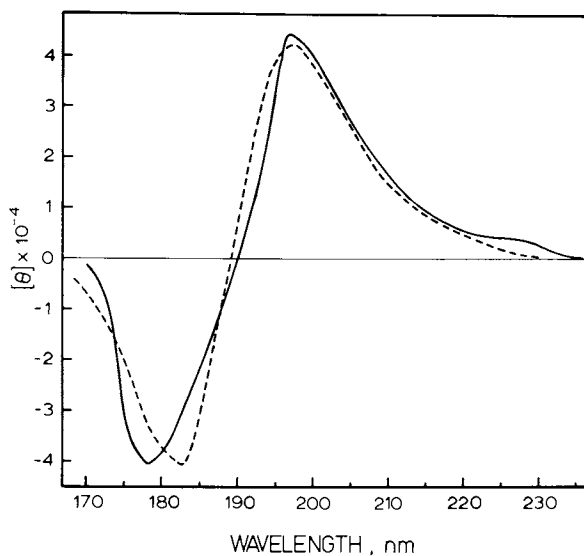


Figure 6. CD spectra of 4-N-(2-deoxy-2-acetamido glycosyl) asparagine (—) and of 2-acetamido-2-deoxy-1-N-acetyl- β -D-glucopyranosyl amine (---) (17)

Biochemistry

relationship of the two amides, we have been able by means of theoretical models to relate the CD spectrum to the geometric relationship of the amides. A model has been proposed for the conformation of GlcNAc-Asn based on these calculations (11).

IV. Conformation of the Amide in Acetamido Sugars

In acetamido sugars the amide is in the planar trans conformation as it is in most peptide bonds. This conformation, which is generally lower in energy than the planar cis amide, has been found in all x-ray crystallographic studies of 2-acetamido-2-deoxy sugars (12, 13, 14). For a planar trans amide there remains the question of rotation about the bond between the amide nitrogen and the pyranose ring carbon atom. There are two conformations allowed by steric contact between the amide and the adjacent groups. In one conformation the amide proton and the pyranose C-2 proton are cis to one another while in the second these protons are trans. Conformational energy calculations show these two conformations to be similar in energy with the cis conformation lying approximately 1 kcal. below the trans conformer (15).

Experimental methods capable of identifying these two conformations points firmly in favor of the trans conformer. In the proton nmr spectra of acetamido sugars, the amide proton resonance is located well down field and is easily assigned. The dihedral angle about the C-N bond is related to the amide proton coupling constant by a Karplus relation which has been extensively investigated because of its importance in peptide conformational studies (16). These studies show that coupling constants as large as 8 Hz are found only for conformations with very nearly trans related protons. The amide proton coupling constants of acetamido sugars have been investigated in a wide variety of solvents. In all cases studied the coupling constants were high (8 to 9 Hz) implying a trans relationship between the protons for both the amide at C-2 as well as at the anomeric center for glucopyranosyl amides (17). X-ray crystallography also points to the trans conformation in the solid state for GlcNAc (12), for chitobiose (14) and for both the amides of GlcNAc-Asn (13). Moreover the trans conformer has been assumed in successful CD calculations for 2-acetamido-2-deoxy sugars (18) as well as for vicinal diacyl amino sugars (11).

Since there is as yet no clear cut evidence for the existence of 2-acetamido sugars in which the amide proton is in a cis conformation with respect to the pyranose proton one must consider the possibility of some error in the conformational energy calculations. Such an error could arise from the neglect of the effects of solvation. This seems unlikely since the proton coupling constants are found to be similar in solvents of widely differing polarities (17). There remains the interesting

possibility that the *cis* conformer occurs under conditions which have not yet been experimentally investigated. The existence of these two conformational isomers could be of considerable biological significance.

V. Theoretical Interpretation of the CD Spectra of Acetamido Sugars

Theoretical interpretations of the CD of acetamido sugars draw heavily on the extensive studies of the CD spectra of polypeptides whose chromophoric properties are essentially identical to those of acetamido sugars. As in the case of polypeptides, it has been shown that the amide $n-\pi^*$ band is made optically active by the asymmetric electrostatic field of the groups surrounding the amide. Specifically it is the electric dipole moment of the hydroxyl function at C-3 which most influences the CD spectrum in the 210 nm region for 2-acetamido-2-deoxy sugars (18). Since the anomeric configuration of the sugar or its glycosides does not have a strong influence on the electrostatic field gradient, the CD in the 210 nm region is not very sensitive to anomeric configuration in oligosaccharides.

On the other hand, the perturbation of the C-3 hydroxyl group is found to be quite sensitive to the hydrogen bonding properties of the solvent. In contrast to water which is both a hydrogen bond donor and acceptor hexafluoro-2-propanol (HFIP) acts only as a hydrogen bond donor. Dickinson et al. (19) have shown that the CD spectra of GlcNAc and GalNAc in HFIP have positively signed CD bands at 210 nm in contrast to the negative bands seen in aqueous solutions (Figure 3). Both the absorbance and CD curve shapes are similar for samples in these two solvents implying that HFIP does not exert a profound effect on the chromophoric properties of the amide. Clear experimental support for the involvement for the C-3 hydroxyl in this effect has been given (19).

The amide $\pi-\pi^*$ transition in glycosides of GlcNAc and GalNAc gains its rotational strength not from electrostatic perturbation but rather from coupling with strong transitions of nearby chromophores, perhaps the $n-\sigma^*$ transitions of the acetal chromophore. Therefore it is reasonable to expect that the position and magnitude of the $\pi-\pi^*$ bands should depend on anomeric configuration as is observed experimentally (Figure 1). These effects have not yet been successfully treated theoretically since the exact electronic nature of the bands with which the $\pi-\pi^*$ transition is coupled is unknown. The improved understanding of the chromophoric properties of the acetal group which is emerging from CD studies on neutral sugar glycosides may make such a treatment possible. (See contribution to this volume by E.S. Stevens.)

For vicinal diacyl amino sugars, it is the two amide chromophores which interact. Therefore in this case coupling theories

developed for polypeptides are directly applicable. Complete calculations involving a consistent treatment of both the $n-\pi^*$ and $\pi-\pi^*$ amide transitions have given an adequate explanation of the large CD bands of GlcNAc-Asn (11).

Abstract

The title compounds have been studied over the wavelength range 170-220 nm using a new ultraviolet CD instrument whose design features a sealed 200 watt deuterium lamp, a wide aperture vacuum monochromator and a small sample compartment purged with N_2 at atmospheric pressure. The asymmetric electrostatic field causing the $n-\pi^*$ band at 210 nm to be optically active arises mainly from the hydroxyl group at C-3 in the case of the 2-acetamido-2-deoxy hexoses. As a result of free rotation of the C-3 hydroxyl group, the CD band at 210 nm is quite sensitive to solvent, the sign of the CD of 2-deoxy 2-acetamido hexoses in fluorinated alcohols being opposite to that found for aqueous solutions of amido sugars not substituted or hydrogen bonded at the C-3 oxygen. In vicinal diacyl amino sugars, strong exciton CD bands are seen at 178 and 200 nm due to coupling of the two amide $\pi-\pi^*$ transitions. Calculations following theories previously used in polypeptide CD correlate the observed CD bands with the amide orientation. In a conformational model of the glycopeptide linkage compound, 2-acetamido-2-deoxy-1-L-aspartamido- β -D-glucopyranosylamine, the amides at C-1 and C-2 are both oriented such that the amide protons are *trans* to their respective ring protons. This conformation has been confirmed by nmr measurements of the amide proton coupling constants.

Literature Cited

1. Kabat, E.A.; Lloyd, K.O.; Beychok, S. Biochemistry, 1969, 8, 747.
2. Stone, A.L. Biopolymers, 1971, 10, 739.
3. Park, J.W.; Chakrabarti, B. Biopolymers, 1978, 17, 1323.
4. Coduti, P.L.; Gordon, E.C.; Bush, C.A. Anal. Biochem., 1977, 78, 9.
5. Brahms, S.; Brahms, J.; Spach, G.; Brack, A. Proc. Natl. Acad. Sci. U.S.A., 1977, 74, 3208.
6. Duben, A.; Bush, C.A. Anal. Chem., 1980, 52, 635.
7. Bush, C.A. Anal. Chem., 1974, 46, 890.
8. Nelson, R.G.; Johnson, W.C. J. Am. Chem. Soc., 1976, 98, 4296.
9. Pullman, B.; Goldblum, N., Eds. "Excited States in Organic Chemistry and Biochemistry"; D. Reidel: Dordrecht-Holland., 1977; p. 209.
10. Buffington, L.A.; Pysh, E.S.; Chakrabarti, B.; Balazs, E.A. J. Am. Chem. Soc., 1977, 99, 1730.

11. Bush, C.A.; Duben, A. J. Am. Chem. Soc., 1978, 100, 4987.
12. Johnson, L.N. Acta. Crystallogr., 1966, 21, 885.
13. Delbaere, L.T.J. Biochem. J., 1974, 143, 197.
14. Mo, F.; Jensen, L.H. Acta. Crystallogr., 1978, 1334, 1562.
15. Pincus, M.R.; Burgess, A.W.; Scheraga, H.A. Biopolymers, 1976, 15, 2485.
16. Ramachandran, G.N.; Chandrasekaran, R.; Kopple, K.D. Biopolymers, 1971, 10, 2113.
17. Bush, C.A.; Duben, A.; Ralapati, S. Biochemistry, 1980, 19, 501.
18. Yeh, C.-Y.; Bush, C.A. J. Phys. Chem., 1974, 78, 1829.
19. Dickinson, H.R.; Coduti, P.L.; Bush, C.A. Carbohydr. Res., 1977, 56, 249.

Research supported by NSF Grant CHE 76-16783.

RECEIVED September 11, 1980.

Vacuum UV Circular Dichroism of D-Glucans

ARTHUR J. STIPANOVIC and E. S. STEVENS

Department of Chemistry, State University of New York at Binghamton,
Binghamton, NY 13901

We have measured the vacuum ultraviolet circular dichroism (VUCD) of a series of D-glucans containing α - and β -(1 \rightarrow 3), (1 \rightarrow 4) and (1 \rightarrow 6) linkages. Our general conclusions are threefold. (1) Gel formers, such as amylose and pustulan, show a negative band in the region 180-190 nm. In pustulan the band appears only after gelation begins; in amylose the band is seen in solution as well and is attributed to the local pseudohelical order in aqueous amylose solutions. Pullulan solutions display the band at much reduced intensity, and the band does not appear under any conditions for dextran. The 180-190 nm band we therefore take as diagnostic of particular local inflexibility in a polysaccharide chain. (2) Aqueous solutions and films of all D-glucans exhibit a CD band in the region 164-177 nm. For (1 \rightarrow 3)- and (1 \rightarrow 4)-glucans the sign of the band is correlated with anomeric configuration (positive for α -linkages, negative for β -linkages) but not for (1 \rightarrow 6)-glucans (the band is positive for both dextran and pustulan). (3) Except for cellulose, a band appears in all glucan film spectra in the region of 145-150 nm and its sign is always opposite to that of the 164-177 nm band. We describe the unique behavior of cellulose in terms of its special solid state structural features.

With the advent of vacuum ultraviolet circular dichroism (VUCD) spectroscopy it has become possible to examine the acetal and hydroxyl chromophores of underivatized polysaccharides (1,2). We have demonstrated for several polysaccharides that their VUCD behavior is strongly influenced by such factors as solvation, molecular conformation and degree of intermolecular association (3-10). In the present study we have investigated a series of glucan polysaccharides (Table 1). We describe the results in terms of comparisons between polymer and monomer (11,12,13) chiroptical properties, variations among solution, gel and film properties; and as a function of C(1) configuration and linkage type.

0097-6156/81/0150-0303\$05.00/0
© 1981 American Chemical Society

Table I. D-glucan Samples

D-Glucan	Branch Linkages ^b	Common Name	Sample Source	Solubility	Approximate DP _b
(1→3)-α-	-	Pseudonigeran	J.R. Merkel and Linda Neiman Lehigh University	Insoluble	700
(1→3)-β-	-	Curdian	W.S. Fulton U. of Bristol, U.K.	H ₂ O, 95°C (gel)	-
(1→4)-α-	-	Amylose	Sigma, Type III	H ₂ O, 120°C	6000
(1→4)-α-	~5% (1→6)-α-	Amylopectin	Sigma	H ₂ O, 25°C	6000
(1→4)-α-	~15% (1→6)-α-	Glycogen	Sigma, Type VII	H ₂ O, RT	-
(1→4)-β-	-	Cellulose	Eastman ^a	Insoluble	120
(1→6)-α-	~5% (1→3)-α-	Dextran	Pharmacia T10	H ₂ O, RT	35-62 ^c
(1→6)-β-	-	Pustulan	Calbiochem	H ₂ O, 90°C	>62 ⁹
(1→3)-α-	-	Nigeran	Calbiochem	H ₂ O, 100°C	-
(1→4)-α-	-	Pullulan	Calbiochem	H ₂ O, RT	-
{(1→6)-α- [(1→4)-α-]} ₂	-				

^a From cellulose triacetate.

^b Not determined experimentally. Based on supplier's data or literature values for samples similar in origin.

^c $M_n = 5200$, $M_w = 10000$.

Previous VUCD studies have been reported for amylose(14) and, by us, for pustulan (9), and dextran (10). Prior to those works, optical studies of glucan conformation in solution included optical rotation and optical rotatory dispersion measurements to approximately 200 nm (15-20), CD studies of chemically modified glucans (21,22,23,24,25), and perturbation methods applied to glucan-ligand complexes (26-33).

Experimental

Table I describes the *D*-glucans we examined, including their source, molecular weight, and solubility in H₂O. The samples were used without further purification, with the exception of pustulan (9), which was purchased as an unbleached and partially acetylated extract of the lichen *P. papullosa*. Deacetylation (saponification) of native pustulan was accomplished by dissolving the material in 1% aqueous NaOH at 90°C and allowing the solution to stand at 50-60°C overnight. Following neutralization with HCl, the brown colored solution was bleached with NaClO₄ yielding a faintly yellow solution. The bleached pustulan was precipitated with 95% ethanol and collected by vacuum filtration. After several washings with alcohol, the precipitate was redissolved in hot water, allowed to cool, and dialyzed using an Amicon ultrafiltration membrane apparatus. Solutions were then freeze dried.

Samples described as "insoluble" in Table I were acetylated by either of two procedures (34,35) to derivatives soluble in trifluoroethanol. It was then possible to obtain films of the underivatized polysaccharide by treating acetate films with 1% (w/v) aqueous or alcoholic NaOH.

Amylose, which is marginally soluble in boiling H₂O, was completely dissolved by autoclaving 10 mg/ml solutions at 120°-160°C for 15-30 min. These solutions became faintly opalescent after 1 hour, indicating that the polysaccharide had begun to retrograde.

Spectra of aqueous solutions and gels were recorded at room temperature in fused-silica vacuum UV cells 25μ-200μ in path-length. For solutions of amylose complete spectra were obtained within 20 min of autoclaving to eliminate the effect of retrogradation. Gels of curdlan were prepared directly in a VUCD cell by heating a 20 mg/ml aqueous suspension to 95°C.

Films were prepared by allowing a volume of polysaccharide solution (0.05-0.10 ml, 5-20 mg/ml) to evaporate on a CaF₂ disc (19 mm diameter) in a dessicating oven at 70-80°C. Films of curdlan were cast from 10 mg/ml aqueous solutions containing 1% NaOH, followed by extensive rinsing with H₂O to remove the base.

The VUCD instrument and typical operating conditions are discussed elsewhere. Molar ellipticities ($[\theta]$) were calculated based on a monomer residue molecular weight of 162.

Results

VUCD data for the series are summarized in Tables II, III and IV. Figure 1 contains amylose solution, gel and film VUCD spectra; in the region of overlap our solution spectrum is in agreement with that of Lewis and Johnson (14). Spectra of amylopectin and glycogen are shown in Figure 2, and Figure 3 shows spectra of pseudonigeran, nigeran and curdlan.

Discussion

180-190 nm Region. Generally the first band we observe in glucans is below 180 nm, but there are cases where, significantly, a low energy extremum appears in the region near 182 nm. Therefore, the CD exhibited in the region 180-190 nm is best discussed separately from the higher energy CD. The relevant data are summarized in Table II.

Evidence for a distinct optical transition above 180 nm has previously been observed in monosaccharides by Nelson and Johnson (11,12,13). They found that the CD of α - and β -D-glucose begins about 10 nm to the red of the corresponding xylose anomers (i.e., near 190 nm) even though the CD maxima are approximately the same for both pairs (~167 nm) (12). Nelson and Johnson suggest the presence of a second low-intensity positive band in glucose sugars, seen only as a tail at the red end of their spectra (Fig. 2 of Reference 12). Methyl α -D-glucopyranoside shows the same low-intensity tail and an actual extremum exists in the spectrum of methyl β -D-glucopyranoside (Fig. 3 of Reference 13).

We have seen a low energy CD band in our own detailed VUCD study of pustulan [(1 \rightarrow 6)- β -D-glucan] which has been published separately (9). In that work we found that freshly prepared aqueous solutions of pustulan show a positive band near 177 nm. As solutions gel, however, a negative band develops at 190 nm which blue shifts with continued aging. Furthermore, spectra of crystalline films of pustulan resemble blue shifted spectra of aged gels; and Na⁺ and Ca⁺⁺ accelerate gelation, presumably by decreasing the activity of the solvent (9). We concluded that the increase in intensity of the negative band with time and its blue shift reflect the development of ordered conformations and their aggregation to form the gel.

Figure 1 shows similar chiroptical behavior in amylose. Figure 1A is the spectrum of a freshly autoclaved solution and shows a well developed negative band near 182 nm. A gel (Figure 1B) shows an enhanced 182 nm band. Film spectra depend somewhat on whether the film is prepared from a freshly autoclaved solution (Figure 1D) or an aged solution (Figure 1C). Amylose differs from pustulan in that the 182 nm band is observed in solution as well as the gel. This result is in accord with a pseudohelical conformation of amylose in solution, which upon gelation is

Table II. D-Glucan CD in the 180-190 nm Region.

		λ nm	$[\theta]$ $10^3 \text{ deg cm}^2 \text{ dmol}^{-1}$
(1 \rightarrow 4)- α -	Solution	182	-0.90
	Gel	184	-0.90
	Film	184	-0.30, -0.40
Amylopectin	Solution	182	-0.90
	Film	182	-0.20
Glycogen	Solution	182	-0.45
	Film	-	-
(1 \rightarrow 6)- β -	Solution	-	-
	Gel	184	-1.2
	Film	180	-0.27
Pullulan	Solution	187	-0.20

Table III. D-Glucan CD in the 164-177 nm Region.

		λ	$[\theta]$
		nm	$10^3 \text{ deg cm}^2 \text{ dmol}^{-1}$
(1→3)- α	Film	173	+2.7
(1→3)- β	Gel	<175	-1.4 ^b
	Film	172	-1.4
(1→4)- α	Solution	<175	Positive
	Gel	<175	Positive
	Film	168	+1.2
Amylopectin	Solution	<175	Positive
	Film	166	+1.1
Glycogen	Solution	<175	Positive
	Film	166	+2.8
(1→4)- β ^a	Film	157 ^a	-13.0
(1→6)- α	Solution	\leq 177	+2.6
	Film	167	+1.6
(1→6)- β	Solution	<177	+1.0 ^b
	Gel	<175	Positive
	Film	164	+0.3
Nigeran	Film	164	+1.6
Pullulan	Solution	<180	Positive
	Film	166	+3.3

^a Cellulose is a special case. See text for discussion.

^b $[\theta]$ at 180 nm.

Table IV. D-Glucan CD in the 145–150 nm Region.

	λ nm	$[\theta]$ $10^3 \text{ deg cm}^2 \text{ dmol}^{-1}$
(1 \rightarrow 3)- α	145	-0.7
(1 \rightarrow 3)- β	145	Positive
(1 \rightarrow 4)- α	150	Negative
Amylopectin	<150	Negative
(1 \rightarrow 4)- β	150	Negative
(1 \rightarrow 6)- α	150	Negative

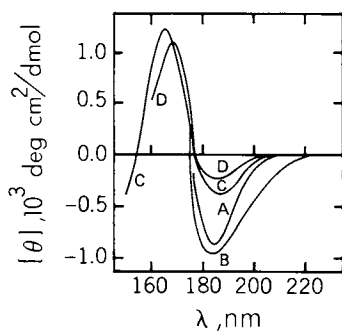


Figure 1. VUCD spectra of amylose: (A) solution (10 mg/mL) autoclaved at 120°C, 30 min; (B) gel (20 mg/mL), aged ~ 2 d; (C) film cast from aged solution (10 mg/mL); (D) film cast from Solution A.

Figure 2. VUCD spectra of amylopectin and glycogen: (A) amylopectin solution (20 mg/mL); (B) glycogen solution (20 mg/mL); (C) amylopectin film (0.04 mL, 20 mg/mL); (D) glycogen film (0.02 mL, 20 mg/mL).

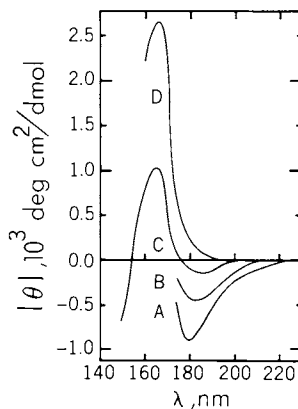
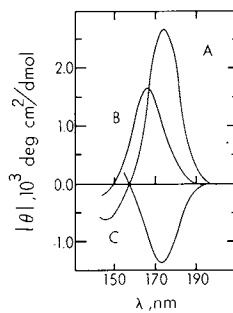


Figure 3. VUCD film spectra of (A) pseudonigeran [(1 → 3)- α -D-glucan], (B) nigeran [(1 → 3)- α -(1 → 4)- α -D-glucan], and (C) curdlan [(1 → 3)- β -D-glucan]



modified, but only slightly, through the association of helical molecules and formation of junction zones (36). This model is consistent with (1) Goebel *et al.*'s (37) theoretical calculations by which one percent of conformation (ϕ, ψ) space is responsible for 90% of the partition function, (2) Senior and Hamori's iodine binding kinetics study (31), and (3) Lewis and Johnson's finding (14) that the CD of amylose in aqueous solution and that of amylose in aqueous/butanol solution are similar.

Amylopectin solutions (Figure 2A, Table II) show the same intensity at 182 nm as do amylose solutions indicating that the approximately 5% (1 \rightarrow 6)- α -linkages present as branch points (Table I) do not significantly perturb the local order to which CD is sensitive. The decrease in the 180 nm band in glycogen (Figure 2B, Table II) reflects a relative randomization of molecular conformation resulting from the presence of approximately 15% (1 \rightarrow 6)- α -linkages. Films of amylopectin (Figure 2C) show a large decrease in the negative band, and in glycogen films (Figure 2D) no negative dichroism is observed.

We also observe a negative band at 190 nm in the solution spectrum of pullulan (Table II), but at much reduced intensity relative to amylose. We take this band to originate in the same local conformation responsible for the low energy dichroism in amylose. The intensity, however, is modified by the presence of 1 \rightarrow 6 linkages between repeating sequences of maltotriose.

Our conclusion, therefore, is that the negative CD band we see in the 180-190 nm region of some *D*-glucans reflects a high degree of local order in the polysaccharide chain; i.e., an inflexibility arising from substantially restricted rotation about the angles ϕ and ψ . That band is absent in cases where increased flexibility causes cancellation of oppositely signed CD contributions through conformational averaging.

We qualify that conclusion for cases where there is substantial negative dichroism near 170 nm [(1 \rightarrow 4)- β -*D*-glucan (cellulose) and (1 \rightarrow 3)- β -*D*-glucan (curdlan)], since a smaller negative band near 180 nm would probably not be separately observable.

164-177 nm Region. In the region 164-177 nm (Table III) all α -*D*-glucans show positive dichroism as does methyl α -*D*-glucopyranoside (13), suggesting that the chiroptical properties of the transition responsible for that dichroism are relatively independent of molecular conformation and linkage type for α -*D*-glucans.

Nelson and Johnson (11,12,13) have suggested that there is a correlation in the sign of the 164-177 nm band and the anomeric configuration of methyl pyranosides. Typical of the evidence for that suggestion is that methyl α - and β -*D*-xylopyranosides show positive and negative bands, respectively near 174 nm; other pairs of monosaccharides show a similar correlation (11,12,13). Significantly for the present work, however, they observed an exception to this correlation in the case of glucopyranosides; methyl

α -D-glucopyranoside has a positive band near 174 nm but the β -anomer shows virtually no dichroism. Furthermore, in the region near 167 nm, α - and β -D-glucose themselves both exhibit positive extrema, with the β -anomer being slightly less intense; and the same can be said for the xylose sugars (12). Therefore, even at the monosaccharide level, the correlation between sign of the 164-177 nm CD band and anomeric configuration is not strict.

Our present work shows that there is also no strict correlation in D-glucans between the sign of the CD in the 164-177 region and anomeric configuration. There is a correlation for 1 \rightarrow 3 and 1 \rightarrow 4 D-glucans (Table III), reminiscent of the xylopyranoside behavior. For 1 \rightarrow 6 D-glucans (dextran and pustulan) there is only a decrease in (positive) CD in the 164-177 nm region on going from the α - to β -linked chain, but no change in sign (Table III); this behavior is similar to the behavior of the methyl glucopyranosides. Thus, in D-glucans the dependence of CD on C(1) configuration is modulated by linkage site, with the C(6) hydroxymethyl group as linkage site playing a special role. This conclusion is consistent with the previously reported result (11, 12, 13) that the C(6) hydroxymethyl group also plays a significant role in determining the sign of the 164-177 nm CD of monomeric glucopyranoses.

Figure 3 illustrates the semiquantitative relation we observe for the positive band in this region for α -D-glucans. The (1 \rightarrow 3)-linked chain (pseudonigeran, Figure 3A) shows the largest dichroism. The alternating (1 \rightarrow 3), (1 \rightarrow 4)-linked chain shows reduced intensity (nigeran, Figure 3B), and in fact is intermediate in intensity between the (1 \rightarrow 3)-linked pseudonigeran and the (1 \rightarrow 4)-linked chain (amylose, Figure 1C and 1D). Figure 3 also illustrates the sign change on going from the (1 \rightarrow 3)- α -glucan [pseudonigeran, Figure 3A] to the (1 \rightarrow 3)- β -glucan [curdlan, Figure 3C].

145-160 nm Region. We have previously pointed out the general occurrence of two CD bands in the regions 165-180 nm and 145-160 nm, as in ι -carrageenan (3), agarose (5) and galactomannans (7). We find the same here as indicated in Tables III and IV. (The high energy band can only be observed in films.) For a given polysaccharide these two bands are always of opposite sign, but chemical structure and configuration appear to determine whether the positive band is the low energy or high energy band of the pair.

Cellulose. Cellulose appears to be a special case. Only one CD band, rather than two, appears in the high energy region; and the intensity of the band is an order of magnitude greater than in all other D-glucans. There is clearly a source of very large dichroism in cellulose which plays little or no role in other glucans. The X-ray study and conformational energy calculations by one of us (A.J.S.) (38) provides an explanation for

the unique chiroptical properties. In the predicted solid state structure of cellulose II (38,39) every hydroxyl group in the cellulose chain participates in a hydrogen bond, and the C(6) hydroxymethyl group is in the *tg* rotational position. These two structural features are absent in the solid state structures of the other glucans we studied. We suggest that one or both of these features lead to the enhanced dichroism in cellulose.

Assignments. Our approach to the assignments of saccharide CD bands is based on the theoretical work of Texter and Stevens (40,41). From that work it is clear that there is a low energy $\sigma^*/3s\leftarrow n$ transition originating from the non-bonding orbital of every oxygen atom, including the ring oxygen, linkage oxygen and hydroxyl oxygens. The observed dichroism in the low energy region is the result of summed contributions from each of those transitions, each contribution reflecting the relevant conformational average. In particular molecules the net result may be very small dichroism. When a CD band is observed, one or the other contribution may dominate. Assignment of the lowest energy CD band in saccharides to the ring oxygen (11,12,13) is compatible with this view.

The second (164-177 nm) and third (145-160 nm) CD bands we associate with a pair of transitions which also originate on each of the oxygen atoms. The observed dichroism is again the sum of contributions from each oxygen atom, some particular contribution possibly being dominant in specific cases. This view is compatible with the correlation of sign with anomeric configuration being only partial.

In the case of cellulose, this view naturally leads to the hypothesis that hydroxyl-localized transitions to the high energy CD band dominate the observed dichroism, even though (smaller) contributions are present from the linkage and ring oxygen atoms, perhaps to the same extent they are present in other glucans.

Acknowledgments

Acknowledgment is made to the donors of the Petroleum Research Fund, administered by the American Chemical Society, for partial support of this research. Partial support was also received from the U.S. National Science Foundation through Grant PCM79-04293. We are grateful to J. R. Merkel and Linda Neiman of Lehigh University for providing the pseudonigeran, and to W. S. Fulton of the University of Bristol for providing the curdlan.

Literature Cited

1. Pysh(Stevens), E.S. Ann. Rev. Biophys. Bioeng., 1976, 5, 63-75.
2. Johnson, Jr., W.C. Ann. Rev. Phys. Chem., 1978, 29, 93-114.
3. Balcerski, J.S.; Pysh(Stevens), E.S.; Chen, G.C.; Yang, J.T. J. Am. Chem. Soc., 1975, 97, 6274-6275.
4. Buffington, L.A.; Pysh(Stevens), E.S.; Chakrabarti, B.; Balazs, E.A. J. Am. Chem. Soc., 1977, 99, 1730-1734.
5. Liang, J.N.; Stevens, E.S.; Morris, E.R.; Rees, D.A. Biopolymers, 1979, 18, 327-333.
6. Buffington, L.A.; Stevens, E.S. J. Am. Chem. Soc., 1979, 101, 5159-5162.
7. Buffington, L.A.; Stevens, E.S.; Morris, E.R.; Rees, D.A. Int. J. Biol. Macromol., in press (1980).
8. Liang, J.N.; Stevens, E.S.; Frangou, S.A.; Morris, E.R.; Rees, D.A. Int. J. Biol. Macromol., in press (1980).
9. Stipanovic, A.J.; Stevens, E.S. Int. J. Biol. Macromol., in press.
10. Stipanovic, A.J.; Stevens, E.S.; Gekko, K., to be published.
11. Nelson, R.G.; Johnson, Jr., W.C. J. Am. Chem. Soc., 1972, 94, 3343-3345.
12. Nelson, R.G.; Johnson, Jr., W.C. J. Am. Chem. Soc., 1976, 98, 4290-4295.
13. Nelson, R.G.; Johnson, Jr., W.C. J. Am. Chem. Soc., 1976, 98, 4296-4301.
14. Lewis, D.G.; Johnson, Jr., W.C. Biopolymers, 1978, 17, 1439-1449.
15. Beychok, S.; Kabat, E.A. Biochemistry, 1965, 4, 2565-2574.
16. Purvinas, R.M.; Zobel, H.F. Carbohydrate Res., 1969, 10, 129-139.
17. Rao, V.S.R.; Foster, J.F. Biopolymers, 1963, 1, 527-544.
18. Kuge, T.; Ono, S. Bull. Chem. Soc., Jpn., 1961, 34a, 1264-1270.
19. Dintzis, F.R.; Tobin, R. Biopolymers, 1969, 7, 581-593.
20. Dintzis, F.R.; Tobin, R.; Babcock, G.D. Biopolymers, 1971, 10, 379-389.
21. Bittiger, H.; Keilich, G. Biopolymers, 1969, 7, 539-556.
22. Mukherjee, S.; Marchessault, R.H.; Sarko, A. Biopolymers, 1972, 11, 291-302.
23. Mukherjee, S.; Sarko, A.; Marchessault, R.H. Biopolymers, 1972, 11, 303-314.
24. Sarko, A.; Fischer, C. Biopolymers, 1973, 12, 2189-2193.
25. Merle, J-P.; Sarko, A. Carbohydrate Res., 1973, 30, 390-394.
26. Johnson, J.A.; Srisuthep, R. Cereal Chem., 1975, 52, 70-78.
27. Manners, D.J.; Stark, J.R. Staerke, 1974, 26, 78-80.
28. Szejtli, J.; Richter, M.; Augustat, S. Biopolymers, 1967, 5, 5-16; Szejtli, J.; Richter, M.; Augustat, S. Biopolymers, 1968, 6, 27-41.
29. Szejtli, J.; Augustat, R.; Richter, M. Biopolymers, 1967, 5, 17-26.

30. Thompson, J.C., Ph.D. thesis, University of Delaware (1970).
31. Senior, M.; Hamori, E. Biopolymers, 1973, 12, 65-78.
32. Hollo, J.; Szejtli, J., in Starch and Its Derivatives, 4th ed., Radley, J.A., Ed., Chapman and Hall, London, 1968, p. 203.
33. Hamori, E.; Senior, M.B. Ann. N.Y. Acad. Sci., 1973, 210, 34-38.
34. Jeanes, A.; Wilham, C.A. J. Am. Chem. Soc., 1952, 74, 5339-5340.
35. Sprague, B.S.; Riley, J.L.; Noether, H.D. Tex. Res. J., 1958, 28, 275-287.
36. Rees, D.A., Polysaccharide Shapes, Halstead Press, John Wiley and Sons, New York, 1977.
37. Goebel, C.V.; Dimpfl, W.L. Brant, D.A. Macromolecules, 1970, 3, 644-654.
38. Stipanovic, A.J., Ph.D. Thesis, SUNY College of Environmental Science and Forestry, Syracuse, New York, 1978.
39. Stipanovic, A.J.; Sarko, A. Macromolecules, 1976, 9, 851-857.
40. Texter, J.; Stevens, E.S. J. Org. Chem., 1979, 44, 3222-3225.
41. Texter, J.; Stevens, E.S. J. Chem. Phys., 1979, 40, 1440-1449.

RECEIVED September 8, 1980.

Interactions of Group II Cations and Borate Anions with Nonionic Saccharides

Studies on Model Polyols

R. M. WILLIAMS¹ and R. H. ATALLA

The Institute of Paper Chemistry, P.O. Box 1039, Appleton, WI 54912

Interactions of aqueous electrolytes with nonionic polysaccharides play an essential role in investigations of plant cell wall polysaccharides, where isolation and fractionation procedures are commonly based on different degrees of solubility in particular electrolytes. This is especially true of the beta-1,4-linked pentosans and hexosans which are the primary backbone structures of most of the cell wall polysaccharides; not infrequently solubility is the basis of identification as well. The beta-1,4-linked hexosans are a special subset which, because of constraints on the freedom of rotation about the bonds of the glycosidic linkage, tend to be less soluble than the pentosans or the hexosans with less constrained linkages.

One of the difficulties in investigating solutions of polysaccharides in aqueous electrolytes, is that most such electrolytes are either acidic or basic in nature, and therefore catalyze a variety of degradation reactions. An interesting exception in this respect are concentrated solutions of the calcium halides which, although neutral, are capable of swelling cellulose and solubilizing it if it is of sufficiently low DP. The studies reported here represent an effort to shed light on the mechanisms of their action by examination of a series of model systems. The first phase consisted of a study of interactions of the halides of Group II cations with ethylene glycol as the most simple polyol with vicinal hydroxyl groups. The second phase was concerned with interactions of calcium chloride, and in selected instances of magnesium chloride, with more complex polyols possessing some similarity to the pyranose structures occurring in most polysaccharides. Interactions of some of the polyols with borate anions were also investigated to provide some basis for comparison.

In the following section relevant studies of interactions of Group II cations with saccharides and polyols will be reviewed together with the first of our studies, focused on ethylene glycol, which has been reported in detail elsewhere (1). The results

¹ Current address: Champion International Corporation, Hamilton, OH 45020.

of the studies on the more complex polyols will then be presented. Finally the implications of these results with respect to solubilization of beta-1,4-linked polysaccharides will be discussed.

PRIOR INVESTIGATIONS. The complexes of carbohydrates with divalent cations have been investigated both in solution and in the solid phase. The work of Angyal *et al.* (2,3) on solution complexes, using NMR spectral measurements, indicated that three adjacent hydroxyl groups in axial-equatorial-axial configuration are prerequisite for complexation of the carbohydrate. In a study confined to zinc chloride solutions, Richards and Williams (4) found the prerequisite to be a minimum of three oxygen sites, two of which are vicinal hydroxyl groups, but without the constraint of configuration found by Angyal *et al.* The crystallographic studies of calcium complexes with a number of sugars (5-7) reveal complexation involving either 2 or 3 hydroxyl groups from each of two different sugar molecules. These suggest even fewer constraints on the structure of the carbohydrate component, though of course, stability in the solid phase does not necessarily imply stability in solution. A similar reduced level of constraints for complex formation in solution is suggested, however, by the work of Thompson and his coworkers on solutions of xylan (8,9). They developed evidence for complex formation between the xylans and some Group II cations, and in this instance it seems quite unlikely that more than 2 hydroxyl groups per residue can be coordinated to the same metal ions.

Our investigation of complex formation in solutions of ethylene glycol (1) was undertaken in an effort to clarify the prerequisites for complex formation. The approach adopted was a Raman spectral investigation of the interactions between the Group II cations and ethylene glycol in aqueous solution. For comparison purposes the effects of some of the ions on the spectra of a series of related molecules were explored. The series included methanol and ethanol, the cyclohexane 1,2-diols, and ethylene diamine. Some complementary IR spectral measurements on solutions in ethylene glycol were also included.

In this phase of the investigation the Raman spectra of aqueous solutions of ethylene glycol in the presence of several Group II cations, including calcium, barium, cadmium, zinc, magnesium, and strontium ions, were examined. Inspection of the spectra showed that the cations could be classified into two groups according to the extent to which they altered the vibrational spectrum of ethylene glycol. The presence of magnesium, barium, or cadmium ions, added as the chlorides, produced only minor changes in the 1000 to 1100 cm^{-1} region, but almost no change in other regions of the spectrum of ethylene glycol. An example of this group is illustrated in Figure 1 which shows only minor changes in the spectrum of an aqueous solution of ethylene glycol when magnesium chloride is added. In contrast, the addition of calcium, zinc, or strontium chloride was found to cause

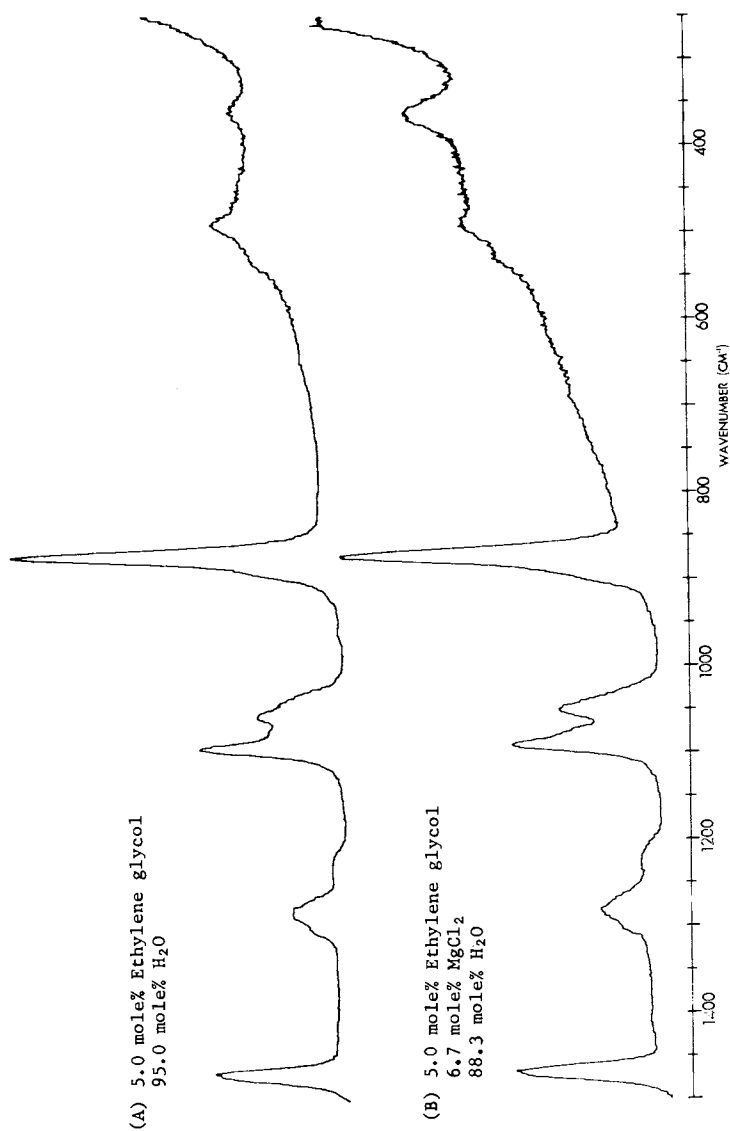


Figure 1. Raman spectra of the 1500–250 cm⁻¹ region for two ethylene glycol solutions

extensive changes throughout the 800 to 1300 cm^{-1} region. The characteristic changes observed are illustrated in Figure 2 where the addition of different levels of calcium chloride are shown to produce dramatic shifts in the strong skeletal band in the 850 to 900 cm^{-1} region. The relatively strong band at 866 cm^{-1} in the spectrum of ethylene glycol is replaced by the equally strong band at 887 cm^{-1} in the spectrum of the ethylene glycol together with the high concentration of calcium chloride. In addition in the region 1200 to 1300 cm^{-1} , as the calcium chloride concentration is increased the band at 1274 cm^{-1} in the ethylene glycol spectrum decreases in relative intensity while a new band at 1241 cm^{-1} increases in relative intensity. Band shifts were also noted in the 1000 to 1100 cm^{-1} region.

The relative changes produced in the vibrational spectrum of ethylene glycol by the two groups of cations suggested two different types of interactions with the ethylene glycol. The relatively minor changes produced by the presence of magnesium, barium, or cadmium ions were interpreted as corresponding to monodentate coordination of the metal ions with ethylene glycol hydroxyl groups. This interpretation was supported by additional experiments with methanol and ethanol solutions containing varying amounts of calcium chloride. In these cases, where monodentate coordination is the only mode of interaction possible, only minor changes in the region 1000 to 1100 cm^{-1} were observed.

The more pronounced changes in the ethylene glycol spectrum produced by the presence of calcium, zinc, or strontium ions were interpreted as resulting from bidentate coordination of the metal ions accompanied by conversion of the ethylene glycol molecules from the trans conformation to the gauche conformation in order to form the complex. The validity of this interpretation was also subjected to further experimental exploration.

Cis- and trans-cyclohexane 1,2 diols have the same capacity to form bidentate complexes as ethylene glycol, but without the possibility of conformational change. It was postulated that any electronic effects resulting from complex formation which could significantly perturb the vibrational frequencies would also occur in the case of the cyclohexane diols. The Raman solution spectra of the cyclohexane diols, with and without added calcium chloride, were recorded. For cis-cyclohexane diol virtually no change in the solution spectrum was observed after addition of calcium chloride. For trans-cyclohexane diol some changes in relative band intensities in the regions 1400 to 1325 and 1150 to 1100 cm^{-1} were observed after addition of calcium chloride. This suggests an electronic perturbation is occurring and its effect observed in the spectrum as a consequence of changes in the polarizability of the carbon-oxygen bonds. Since the changes observed with the cyclohexane diols were not unlike those in solutions of methanol and ethanol in the presence of the calcium ions, it was concluded that the electronic perturbation resulting from bidentate coordination of the calcium ions could not by itself account for the

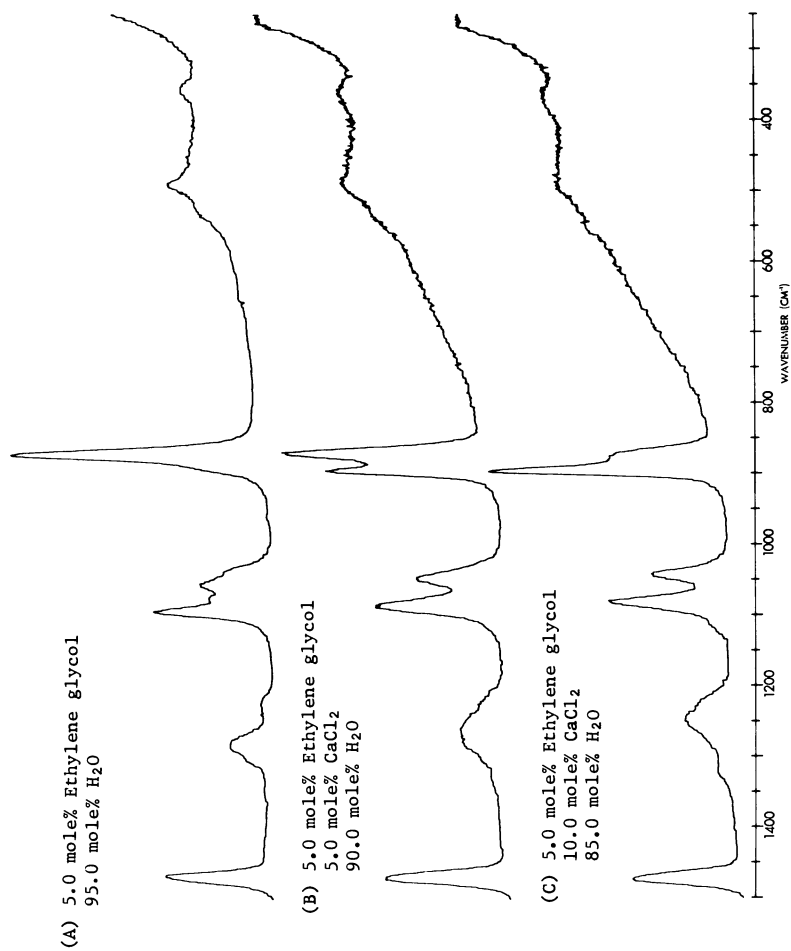


Figure 2. Raman spectra of the 1500–250 cm^{-1} region for three ethylene glycol solutions

major changes observed in the ethylene glycol spectrum in the presence of calcium ions.

The solution spectrum and calcium ion complex spectrum of ethylene diamine were also examined. As with ethylene glycol, it was postulated that ethylene diamine has the capability of bidentate coordination and conformational change. Furthermore, ethylene diamine is known to complex in the gauche conformation. The similarities between the geometries of ethylene glycol and ethylene diamine suggest that if the major changes in the spectrum of ethylene glycol upon bidentate coordination are indeed due to conformational changes, then similar changes should be detectable in the Raman spectrum of ethylene diamine upon bidentate coordination of metal ions. The addition of calcium chloride to aqueous solutions of ethylene diamine did indeed result in changes in the Raman spectra which closely parallel the changes observed in the spectra of ethylene glycol in the presence of calcium chloride. These observations further validate the interpretation of the changes in the ethylene glycol spectrum as consequences of conformational changes, from the trans to the gauche form, resulting from complex formation with calcium, zinc, or strontium ions.

STUDIES ON THE MORE COMPLEX POLYOLS. In 1961, Mills (10) reported electrophoretic mobilities for several carbohydrates, including cis-inositol and epi-inositol, when in the presence of such cations as calcium, strontium, barium, and magnesium. Nomenclature of the inositols is shown in Figure 3. The mobilities were interpreted as evidence of complexing between the carbohydrates and the cations. Angyal and his coworkers (2,11) studied the proton NMR spectra of several inositols in the presence of cations. They found that the addition of calcium chloride to a D₂O solution of epi-inositol resulted in a downfield shift of the proton signals. From the proton shifts, the largest shift being observed for the hydrogen attached to C1, it was concluded that the calcium ion was coordinated with the three hydroxyl groups as shown in Figure 4. The methine hydrogen attached to C1 is indicated in the figure. It was found that cis-inositol and allo-inositol also complexed strongly, but myo-inositol exhibited no pronounced proton signal shifts, indicating the absence of strong complexing. The strong complexing cyclitols, epi-inositol, cis-inositol, and allo-inositol, all have in common the axial-equatorial-axial sequence of hydroxyl groups. It was suggested that the axial-equatorial-axial sequence is favorable for complex formation. Myo-inositol and neo-inositol do not possess this hydroxyl group sequence and do not complex strongly. Further investigation substantiated the postulation that an axial-equatorial-axial sequence of hydroxyl groups is favorable for complex formation. For example, studies with D-allose (12,13) showed the equilibrium between the alpha-pyranose and alpha-furanose, beta-pyranose and beta-furanose forms in solution was altered by the presence of some cations. Complexes were preferentially formed with the alpha-

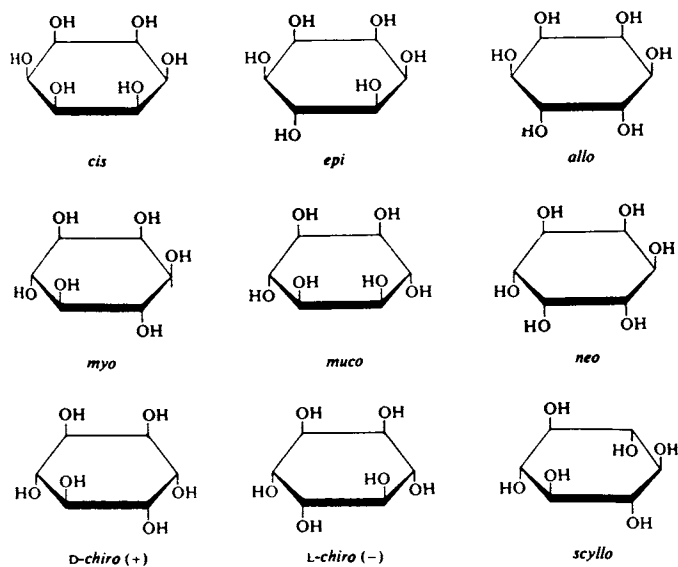


Figure 3. The nine inositol isomers

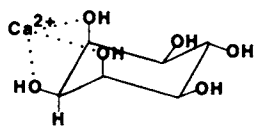


Figure 4. Representation of the epi-inositol-calcium ion complex

pyranose and alpha-furanose forms which contain the axial equatorial axial sequence. This resulted in a shift of the equilibrium to these forms from the beta forms which do not contain this hydroxyl group sequence.

The present investigation was undertaken with the thought that the Raman spectra of solutions of the inositols in the aqueous electrolytes could shed further light on the mechanism of interaction. The impetus behind this investigation was the desire to further clarify the results of the earlier work on the complexes with ethylene glycol and to extend this work to model systems which more closely approximated the pyranose structures. The intent was to complement reports previously presented in the literature. The inositols were chosen because their complexes with metal ions have been characterized using other techniques, whereas the ethylene glycol complexes had not been as extensively characterized. To assess the effect of complex stability on the ligand vibrational frequencies, the inositol complexes chosen for study ranged in strength from a relatively strong inositol complex [epi-inositol, calcium ion complex] to relatively weak complexes [epi-inositol, magnesium ion, and myo-inositol calcium ion complexes]. To observe the effect of complex formation with an attendant change in the geometry of the ligand molecule, the calcium ion complex of another model compound, the 1,5-anhydrosorbitol, was investigated. It was hypothesized that the 1,5-anhydrosorbitol would change conformation to the alternate chair form to enhance formation of the calcium ion complex because the alternate conformation has the axial-equatorial-axial sequence preferred for complex formation.

As noted earlier epi-inositol has been shown to complex with calcium ions in the preferred conformation as shown in Figure 4. Angyal and Hickman (11) reported a stability constant of $K = 2.2 \pm 0.2 \text{ mole}^{-1} \text{ liter}$ for the epi-inositol calcium ion complex, which in comparison to the other inositol complexes, is relatively strong. The effect of calcium ion complex formation on the Raman spectra of epi-inositol solution is shown in Figure 5 where it is clear that the only change resulting from complex formation is a change in the relative intensities of the two bands between 850 and 950 cm^{-1} . The epi-inositol and calcium chloride concentrations used are in the same range as those used by Angyal and Hickman.

For comparison purposes the spectra of the weaker complexes corresponding to epi-inositol and magnesium chloride and to myo-inositol and calcium chloride, were also recorded. No changes in the spectra of the inositols were observed upon addition of the electrolytes in these systems.

The three systems just discussed span the range from a relatively strong complex to a very weak complex. For the weak complexes the inositol vibrational spectra remain essentially unchanged upon complex formation. For the strong complex, the epi-inositol calcium ion complex, changes observed in the inositol spectrum were of a minor nature involving changes in the relative

intensities of two bands. The absence of major changes in the inositol spectra, such as sizeable shifts of bands or the appearance of new bands, suggests little or no change in the structural geometries of the inositols upon complex formation; large changes in inositol geometries would be expected to result in more pronounced changes in the spectra than those observed.

Perturbations of the electronic structure of the inositols almost certainly occur upon complex formation. The degree of the perturbation would be expected to be dependent on the strength of the complex. The relative band intensity changes observed in the epi-inositol spectrum upon complex formation are likely a manifestation of an electronic perturbation. If complex formation results in a change in electron distribution, this will affect the polarizability of the bonds in the immediate neighborhood of the cation, and, hence, the intensity of the bands associated with their vibrations.

To further explore the possible effects of major changes in ligand geometry, somewhat similar to those observed with ethylene glycol, the 1,5-anhydroribitol molecule was chosen. Its structure is shown in Figure 6 which depicts the equilibrium between the two alternate chair forms and the possibility of complexation with the calcium ion in the form with the axial-equatorial-axial configuration of the hydroxyl groups. Pitzner (14) calculated that approximately 26% of the 1,5-anhydroribitol molecules would be in the alternate conformation at equilibrium in solution, in the absence of any electrolyte. In analogy with the observations of Angyal (12,13), it was anticipated that addition of calcium chloride to solutions of the 1,5-anhydroribitol would shift the equilibrium toward the alternate conformation which is more favorable to complex formation. Figure 7 shows the vibrational spectra of the crystalline 1,5-anhydroribitol compared with that of the aqueous solution and with the spectrum of a solution containing calcium chloride. It is clear that the new bands which appear in the solution, and which Pitzner attributed to the alternate conformer, are significantly intensified upon addition of calcium chloride.

The observations of the spectra of the 1,5-anhydroribitol support the finding of Angyal that the formation of complexes with calcium can indeed shift the equilibria between different conformations, when one of the conformations is more favorable to complex formation. Furthermore it is clear that, when complex formation involves a significant change in the geometry of the ligand, many new bands characteristic of the alternate conformation appear in the spectrum. It is also interesting to note that most of the bands which are intensified in the presence of calcium chloride, are not significantly shifted relative to their position in the aqueous solution of 1,5-anhydroribitol. Thus the changes in the spectrum are primarily due to the change in geometry and not to the perturbation of the ligand molecule by the cation complexed to it. It seems clear from the nature of the spectral

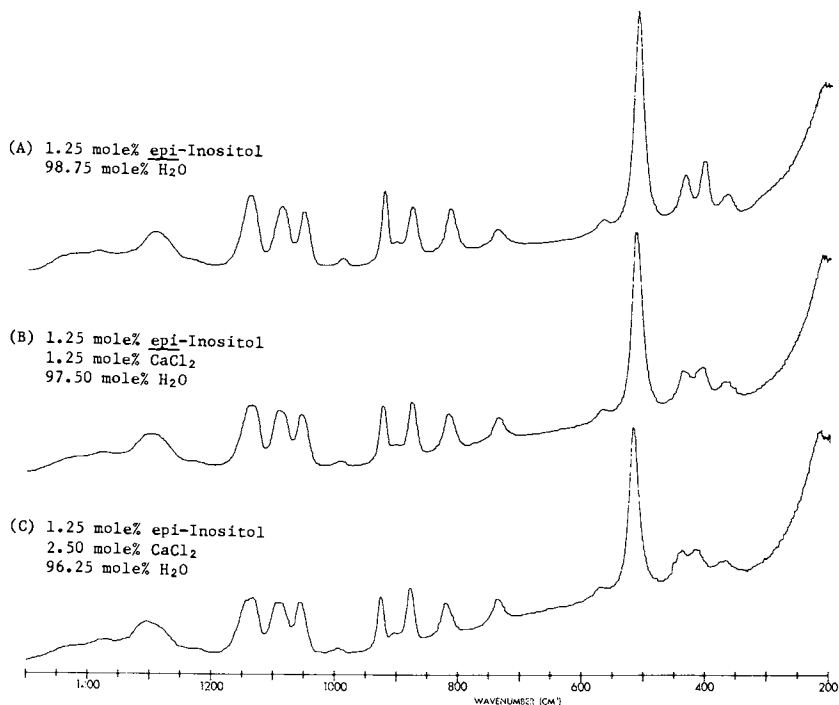


Figure 5. Raman spectra of the 1500–200 cm⁻¹ region for three epi-inositol solutions

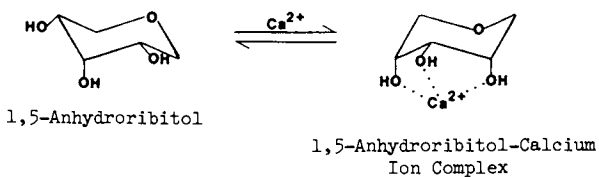


Figure 6. Representation of the 1,5-anhydroribitol chair inversion to form the 1,5-anhydroribitol-calcium ion complex

changes that the formation of the complex is such that the alternate conformation is stabilized with respect to the lower energy conformation with two equatorial and one axial hydroxyl group. The rather insignificant change in the frequencies of the alternate conformer bands which are intensified, suggest that the presence of the calcium ion does not in any way influence the internal coupling of the vibrations in the 1,5-anhydroribitol to a significant extent.

In an interesting extension of the application of the mechanism involved in the reaction of the 1,5-anhydroribitol with calcium chloride, the effect of aqueous calcium chloride on the solubility of neo-inositol was investigated. Neo-inositol has two axial hydroxyl groups on opposite carbons in the ring and four equatorial hydroxyl groups between them, and thus has a center of inversion as an element of its symmetry. It is the least soluble of the inositols, to the extent that it is not possible to record a Raman spectrum of a solution of neo-inositol in water. It was reasoned that if the calcium chloride solution could result in conversion of the neo-inositol from the more stable form to the alternate form where two ends of the molecule would have axial-equatorial-axial conformations, the solubility of the inositol might be enhanced. Such an experiment was carried out, and it was observed that the concentration of neo-inositol which entered into solution in the aqueous calcium chloride was indeed sufficient to permit acquisition of a Raman spectrum. The main bands in the spectrum of the solution did not coincide with those observed in the spectrum of the solid, and thus the indication is that the neo-inositol in solution is predominately in the alternate conformation and complexed to calcium cations.

The complexes of the borate anion with the inositols have been investigated quite extensively and it has generally been established that the most effective and stable complexes occur with conformations of the inositols that possess three axial hydroxyl groups on alternate carbon atoms permitting tridentate coordination with the anion. In the case of cis-inositol and epinositol particularly strong complexes have been detected (15). Though the Raman spectra of such complexes have been investigated (16) they will not be presented here because they are not immediately relevant to the problem of dissolution of polysaccharides in aqueous electrolyte systems. They are mentioned only as a point of reference to indicate that the spectra represent significant changes from what one might obtain from a linear superimposition of the spectra of the inositols and the borate anions. It is clear that the complexes with the borate anions represent formation of entirely new molecular species, the vibrational spectra of which must be interpreted in terms of the dynamics of multiring compounds. The nature of the species involved is illustrated in Figure 8.

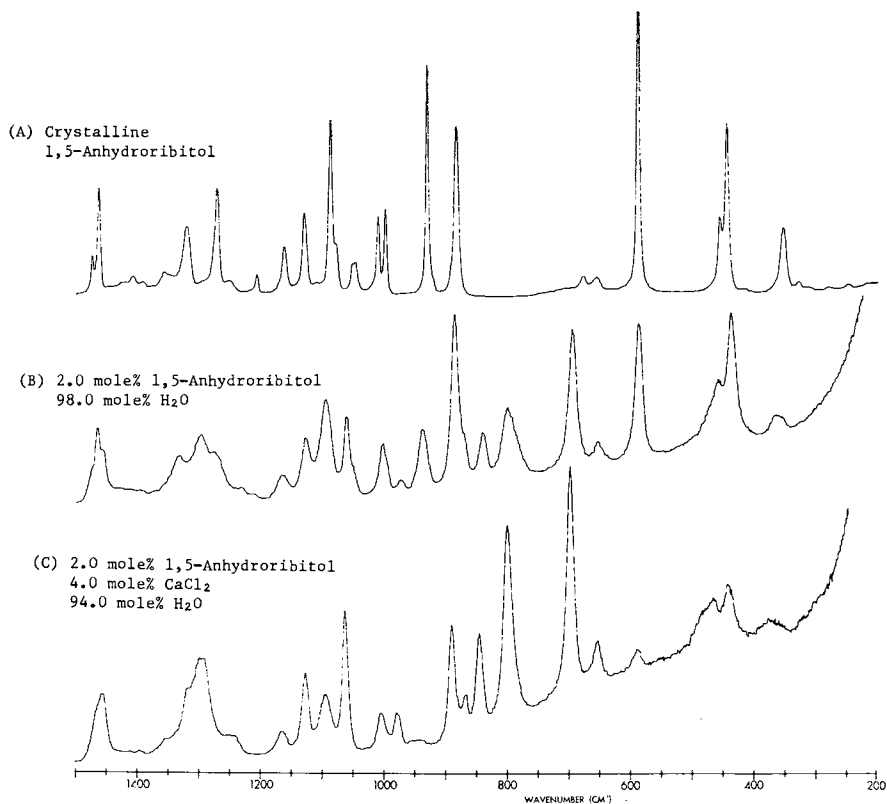


Figure 7. Raman spectra of crystalline 1,5-anhydrosorbitol and two aqueous solutions

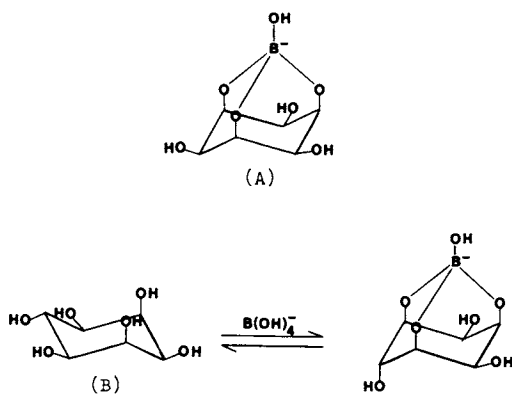


Figure 8. Representations of (A) cis-inositol borate and (B) the epi-inositol chair inversion to form the epi-inositol borate

CONCLUSIONS

It was noted in our earlier report that the pattern of variation in the interactions between ethylene glycol and the cations is not simply rationalized. Strong coordination by zinc in the case of ethylene glycol is not surprising in view of its position in the periodic table, the stability of many of its complexes, and the results reported by Richards (6). Equally strong coordination by calcium is not anticipated a priori however. Rationalization in terms of electro-negativity, or charge:radius ratio would require, for consistency, that either cadmium or magnesium coordinate as strongly as calcium. Angyal's observation (3) that a radius of approximately 1 Å is the common characteristic of the coordinating metal ions does not fit the pattern reported with ethylene glycol; the zinc ion has a radius of 0.74 Å while the radius of the cadmium ion is 0.97 Å.

More empirically, the indication of strong coordination of vicinal hydroxyl groups with calcium is consistent with the findings by Bugg and Cook (17) that bidentate coordination of calcium by carbohydrates is accompanied by significant distortions in the O...O distances and the skeletal angles of the vicinal hydroxyl groups involved in the coordination.

In attempting to relate the present and previous observations to the role of calcium chloride solutions, or the calcium cations in particular, one particular effect seems to stand out. This is the capacity of the calcium ion to induce conformational changes through multidentate coordination. In addition, the stability of the complex of the calcium cation at sites favorable to multidentate coordination seems clearly established. A plausible mechanism for the action of the calcium cation with the beta-1,4-linked polysaccharides may well be a two stage process. In the first stage the calcium cation interact with the polysaccharide entity to produce conformational adjustments favorable to multidentate coordination of the calcium ion. In the second stage the remaining gaps in the coordination sphere of the calcium ion are filled with water molecules thus promoting the hydration and solubilization of the beta-1,4-linked polysaccharides, which otherwise would be less soluble in water.

The reasons for the exceptional effectiveness of the calcium ion in comparison to the other Group II cations remains enigmatic, however. It may well be related to its particular position at the beginning of the 4th period; the relatively small separation between the energies of the $3d$ and $4p$ orbitals in calcium, and the penetration, in its instance, of the $3d$ orbitals closer to the nuclear charge (18) may expose coordinated species to a higher field. The effect certainly is deserving of further investigation, not only in relation to the beta 1,4-linked polysaccharides, but with respect to the important role of calcium in biological systems in general.

ABSTRACT

Interactions which influence solution behavior of nonionic polysaccharides in aqueous electrolytes were explored in Raman spectral investigations of a sequence of model systems. The studies included interactions of Group II cations with ethylene glycol, the cyclohexane diols, 1,5-anhydrosorbitol, and a number of inositols, as well as interactions between inositols and the borate anion. Different levels of interaction were identified. The weakest associations had no noticeable effects on the Raman spectra of the polyols. The next level involved chelation with a favorable configuration of adjacent hydroxyl groups, and resulted in small changes in the spectra which indicated minor perturbation of the polarization parameters of the affected hydroxyls. A higher level of interaction occurred in systems where one conformer could interact more strongly with the cations, and the association resulted in changes in relative intensities of bands assigned to the different conformers. The strongest interactions were with the borate anions, where the spectra were no longer superpositions of the spectra of the alternate conformers and the anion, but indicated the formation of new molecular species with highly coupled vibrations.

LITERATURE CITED

1. R. M. Williams and R. H. Atalla, J. Chem. Soc. Perkins II, 1975, 1155.
2. S. J. Angyal and K. P. Davies, Chem. Commun. 1971, 500.
3. S. J. Angyal, Austral. J. Chem. 1972, 20, 1957.
4. N. J. Richards and D. G. Williams, Carbohyd. Res. 1970, 12, 409.
5. D. C. Craig, N. C. Stephenson, and J. D. Stevens, Carbohyd. Res. 1972, 22, 494.
6. G. Richards, Carbohyd. Res. 1973, 26, 448.
7. C. E. Bugg, J.A.C.S. 1973, 95, 908.
8. B. D. E. Gaillard, N. S. Thompson, and A. J. Morak, Carbohyd. Res. 1969, 11, 509.
9. B. D. E. Gaillard and N. S. Thompson, Carbohyd. Res. 1971, 18, 137.
10. A. J. Mills, Biochem. Biophys. Res. Comm. 1961/62, 6(6), 418.
11. S. J. Angyal and R. J. Hickman, Austral. J. Chem. 1975, 28, 1279.
12. S. J. Angyal, Austral. J. Chem. 1972, 25, 1957.
13. S. J. Angyal, Pure Appl. Chem. 1973, 35, 131.
14. L. J. Pitzner, Doctoral Dissertation, IPC, Appleton, 1973.
15. S. J. Angyal and D. J. McHugh, J. Chem. Soc. 1957, 1423.
16. R. M. Williams, Doctoral Dissertation, IPC, Appleton, 1977.
17. C. E. Bugg and W. J. Cook, Chem. Comm. 1972, 727.
18. E. W. Condon and H. Odabasi, "Atomic Structure," Cambridge Univ. Press, N.Y. 1980.

RECEIVED September 25, 1980.

Polyelectrolytic Behavior of Ionic Polysaccharides

V. CRESCENZI, M. DENTINI, and R. RIZZO

Istituto di Chimica-Fisica, Università di Roma, Roma, Italy

An important aim of physico-chemical studies on natural and synthetic ionic-polysaccharides is to help elucidate the correlations between chemical structure-conformational characteristics of such polymers and their equilibrium properties in solution. In this context, attention is being given in our laboratory to the thermodynamics of macroion-counterion interactions and of polyion-polyion interactions, including (soluble) complex formation between polysaccharidic macroions and different polyampholites (e.g. proteins) in dilute aqueous solution.

Our experimental approach is mainly based on the use of microcalorimetric, potentiometric, and chiroptical techniques. Polymers considered include: 1) sulfated polysaccharides (i-carrageenan, dextran sulfate); 2) glycosaminoglycans (heparins); 3) microbial polysaccharides (Xanthan, PS-10).

Species listed above (sodium salts) have been characterized in water and/or aqueous NaCl solution in terms of Na^+ counterion activity coefficient, heat of dilution, and heat of Cu^{2+} ions binding. These experiments are part of a systematic investigation on the relationship between "charge-density" along polyelectrolyte chains and (metal) ion-binding, comparing experimental evidence with existing theories {1, 2, 3}.

Microcalorimetric and spectroscopic data have then been collected on the interaction of human serum albumin with dextran sulfate and heparin, respectively, in dilute aqueous solution. The purpose is to afford possible, original evidence on the energetics of complex formation between glycosaminoglycans and different proteins of the biological fluids.

Finally, the enthalpy of protonation as well as the circular dichroism of Xanthan have been studied in a rather wide range of pH values in water and in aqueous NaCl. This was done in order further characterize from a "structural" and thermodynamic standpoint the dissociation behavior of such a conformationally pecu-

0097-6156/81/0150-0331\$05.00/0
© 1981 American Chemical Society

liar polycarboxylic acid (4, 5). For comparison purposes, the same experiments have been done using another microbial polysaccharide, PS-10 (6, 7), whose chains are supposed to lack any conformational order. Work is now in progress to investigate solution properties of the Klebsiellae K-63 polysaccharide (8).

We wish to briefly summarize here a few of the results obtained so far in our laboratory from work on the three main research lines exemplified above.

Results and Discussion

1) Sulfated polysaccharides and heparin

a) Heat of dilution and of counterion binding (Na^+ , Cu^{2+}).

The activity coefficient of Na^+ counterions (γ_{Na^+}) for i-carrageenan, dextran sulfate, and heparin in water at 25°C, as evaluated from our potentiometric data, are reported in Fig. 1.

Although the concentration range investigated is rather limited, one observes that γ_{Na^+} is low, and quite insensitive to dilution, the more so the higher the charge-density along the chains. These results are in line with a number of similar data collected by various authors (9, 10): the agreement is however only qualitatively, when a comparison is feasible at all, given the lack of similarity among different samples used in different laboratories.

A more important property useful for the thermodynamic characterization of aqueous polyelectrolyte solutions is the enthalpy of dilution. Our microcalorimetric results (25°C) are reported in Fig. 2 for dextran sulfate, and in Fig. 3 for segmented i-carrageenan and for heparin, respectively. It is seen that, for a given dilution range: 1) the integral heat of dilution (ΔH_D : cal/polyel.equiv.) is higher the lower the charge density along the chains; 2) dilution in the presence of NaCl (at a fixed NaCl molarity) leads to distinctly smaller heat effects than in water.

To our knowledge no calorimetric data of comparable accuracy on ionic polysaccharide solutions can be found in the literature, with the notable exception of the results recently reported by R. L. Cleland (11) on the enthalpy of mixing glycosaminoglycans with aqueous NaCl.

Additional evidence on the complex interplay of factors which govern polysaccharide-counterion interactions is clearly afforded by the calorimetric data on the binding of Cu^{2+} ions reported in Fig. 4. Here the "charge-density" of the chains is not the only dominant parameter as, quite obviously, also the nature and relative configuration of fixed-charges (heparin) and the propensity of the chains to assume ordered conformations (i-carrageenan) contribute importantly to the observed overall energetic effects upon Cu^{2+} -binding. In the case of i-carrageenan the peculiar shape of the Q_B against $[\text{Cu}^{2+}]/N$ plot (see Fig. 4; Q_B = heat of mixing polyelectrolyte and $\text{Cu}(\text{NO}_3)_2$ solutions, corrected for dilution effects; N = polyelectrolyte concentration in equiv./l) should

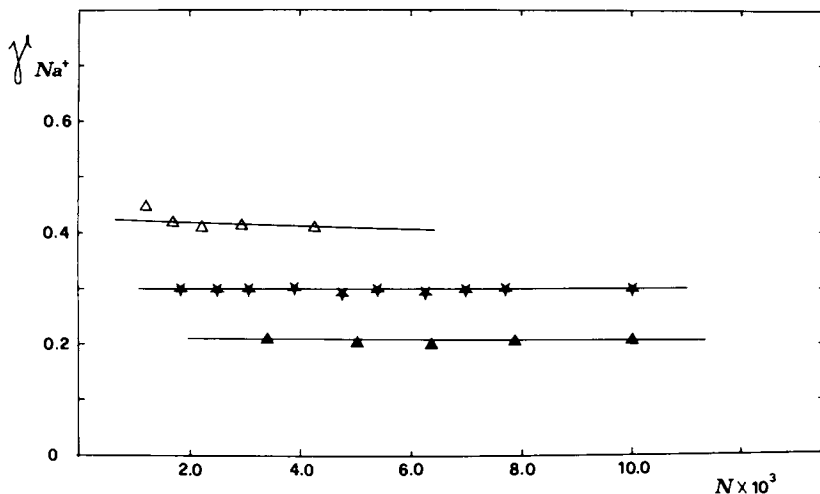


Figure 1. Activity coefficient of Na^+ counterions (γ_{Na^+}) of ionic polysaccharides in water ($25^\circ C$), N is the polyelectrolyte concentration in equivalents/liter: (Δ) isocarrageenan ($\xi = 1.2$); (\star) heparin ($\xi = 1.3$); (\blacktriangle) dextran sulfate. ($\bar{M} = 4 \cdot 10^4$; $\xi = 2.8$).

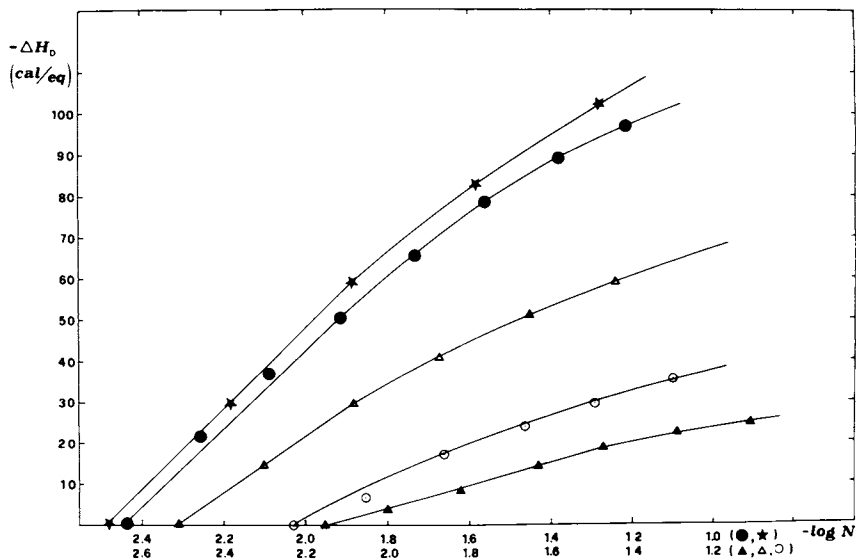


Figure 2. Enthalpy of dilution of dextran sulfate ($\bar{M} = 4 \cdot 10^4$) at $25^\circ C$: (\star) in water; (\bullet) in $1 \cdot 10^{-3} M NaCl$; (Δ) in $3 \cdot 10^{-3} M NaCl$; (\circ) in $5 \cdot 10^{-3} M NaCl$; (\blacktriangle) in $1 \cdot 10^{-2} M NaCl$.

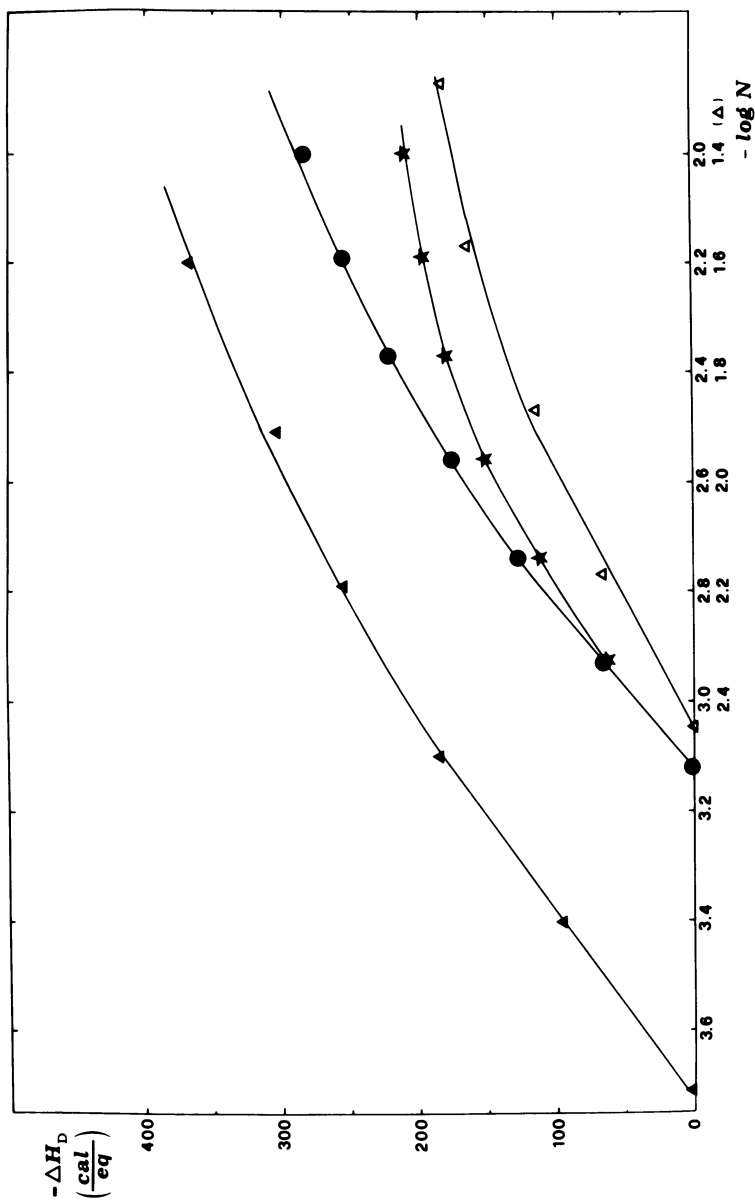


Figure 3. Enthalpy of dilution of iso-carrageenan segments and of heparin at 25°C: (▲) iso-carrageenan in water; (●) iso-carrageenan in $1 \cdot 10^{-3}$ M NaCl; (★) iso-carrageenan in $5 \cdot 10^{-3}$ M NaCl; (Δ) heparin in water.

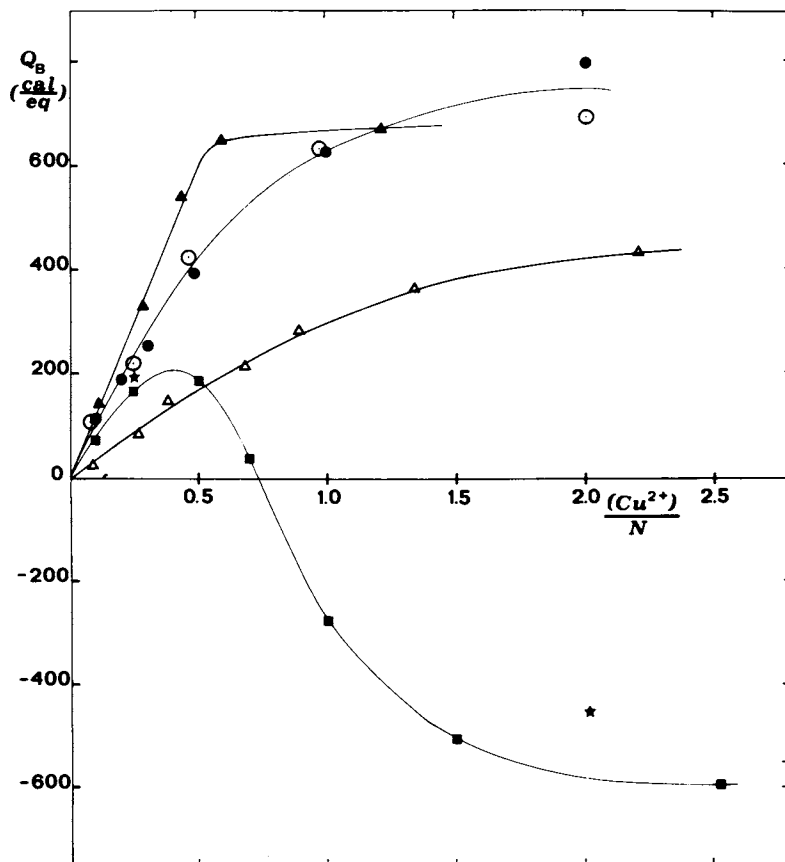


Figure 4. Enthalpy of Cu^{2+} ions binding in water (25°C): (▲) heparin; (○, ●) dextran sulfate ($\bar{M} = 4 \cdot 10^4$ and $\bar{M} = 8 \cdot 10^3$); (△) cellulose sulfate (D.S. = 1.0); (■) iso-carrageenan segments ((★) intact); polyelectrolyte concentration (N); $5 \cdot 10^{-3}$ equiv/L.

in fact be traced back to a disorder---► order transition, as clearly supported by optical activity measurements (12).

Critical comparison of our data (Figs 1-4) with current theories of polyelectrolyte solutions would entail a rather lengthy presentation and discussion of a number of equations and underlying assumptions. For sake of brevity let us simply point out here that, considering Manning's theory (13, 14), we find only a qualitative, rough agreement with our experimental results. In particular, the heat of dilution data in aqueous NaCl (Figs 2 and 3) seem "anomalous" with respect to theoretical predictions (11). A detailed discussion on these points with the presentation of data also for different polyelectrolytes will be given elsewhere (15).

b) Microcalorimetric and spectroscopic data on ionic polysaccharide-protein interactions. The association between different charged polymers is a well known phenomenon with important implications in the case of many biological processes. For instance, the extensive association of heparin with certain plasma proteins is currently thought to be the basis for the biological activity of this glycosaminoglycan (16). The interaction between ionic polysaccharides and a number of proteins leading to soluble complex formation has been characterized in vitro using different experimental techniques (17), but much remains to be understood about energetic aspects as well as specific mechanisms at the molecular level. In this field, our research program includes studies of the complexation processes between ionic-polysaccharides, in particular mucopolysaccharides, and selected proteins in aqueous solution by means of microcalorimetric and spectroscopic experiments. A few results of the latter experiments concerning the dilute aqueous systems: dextran sulfate-human serum albumin (NaDS-HSA), and heparin-human serum albumin (Hep-HSA), respectively, are reported in Figs. 5a, and 5b. Spectral data were collected for the above systems (at pH = 5.0; ionic strength 0.1 M) using two different optical probes, namely: fluoresceine and rhodamine-B. These dyes do not interact (fluoresceine) or interact only very weakly (rhod-B) with the ionic-polysaccharides considered.

For the particular experimental conditions used, fluoresceine may be considered as extensively bound on a single, primary binding site of HSA (18, 19) in the absence of extraneous polyelectrolytes.

Addition of NaDS ($\bar{M} = 4.10^4$) perturbs the fluoresceine spectrum in the direction of an extensive displacement of dye molecules from the protein with an apparent "equivalence-point" corresponding to a stoichiometric $N/[HSA]$ ratio close to 15, according to absorption and fluorescence data (see Fig. 5a). At pH = 6.5, on the contrary, any effect was barely detectable. This is in line with extensive complex formation between NaDS and HSA driven essentially by electrostatic forces, which would engage many of the fixed positive charges of HSA, probably including most of

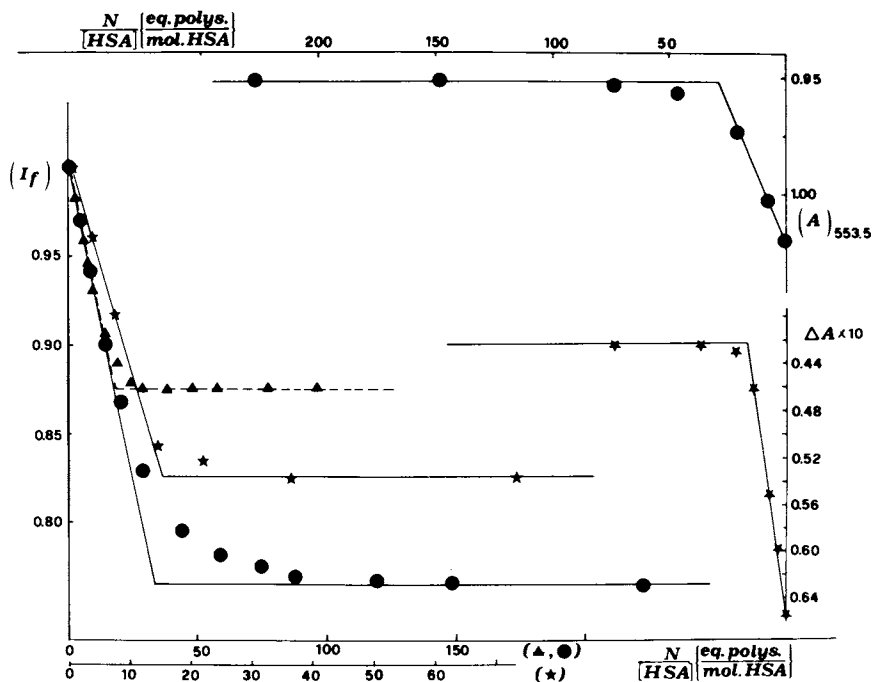


Figure 5a. ΔA and I_f data for the system: dextran sulfate-HSA-fluorescein. Albumin concentration ($[HSA]$), $1 \cdot 10^{-5}M$. Fluorescein concentration, $1 \cdot 10^{-5}M$, $pH = 5.02$, acetate buffer (0.1M). (\star) NaDS ($\bar{M} = 4 \cdot 10^4$). ΔA is the difference in ΔA of fluorescein at 500 and 550 nm. Data for the system: dextran sulfate-HSA-rhodamine B. Experimental conditions as above. (\bullet) NaDS, $\bar{M} = 4 \cdot 10^4$; (\blacktriangle) NaDS, $\bar{M} = 8 \cdot 10^3$.

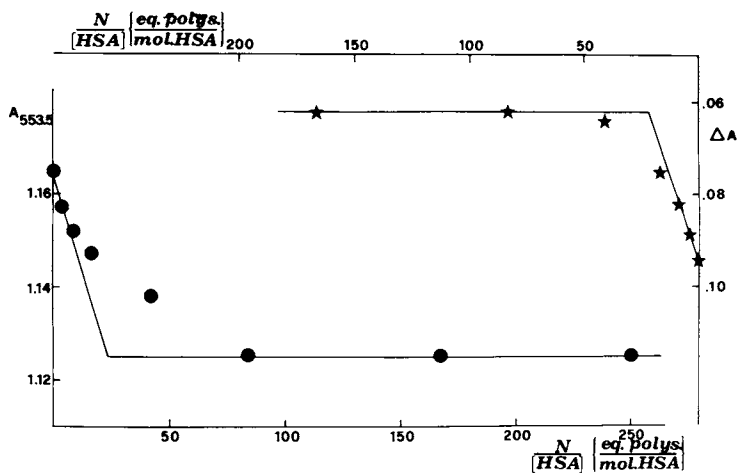


Figure 5b. ΔA data for the heparin-HSA system. Same experimental conditions as in Figure 5a: (\star) fluorescein; (\bullet) rhodamine-B.

those at the fluoresceine primary binding-site. Quite opposite is the behavior of rhodamine-B. Data of Fig. 5a show in fact that this dye is only very weakly bound to free HSA molecules (under our experimental conditions) but that addition of NaDS would promote its binding. The "equivalence-point" for NaDS of $\bar{M} = 4.10^4$ is in this case found at an $N/[\text{HSA}]$ ratio approximately 30.

In view of the zwitterionic nature of rhodamine-B a possible explanation of this effect may be that interaction of NaDS with HSA brings pairs of positive and negative fixed charges into sufficiently close proximity with the onset of "binding-sites" for rhodamine. It is interesting to point out that the "equivalence-point" for NaDS with $\bar{M} = 8.10^3$ is certainly lower than that for the higher \bar{M} sample, as shown in Fig. 5a.

Data collected using heparin instead of NaDS but for otherwise identical condition are given in Fig. 5b. The trend of the absorption data are quite similar to those found with NaDS: apparent "equivalence-points" are in this case discernible at $N/[\text{HSA}]$ values around 20 (fluoresceine) and 25 (rhod.B). These interesting features deserve further investigation. Here we limit ourselves to deduce from the data of Figs 5a and 5b that for a $N/[\text{HSA}]$ ratio of about 30, with $[\text{HSA}]$ ca $10^{-5} \bar{M}$, the majority of HSA molecules should be bound by NaDS or by heparin chains. Initially, more than one protein molecule would thus be bound per polysaccharide chain. It has to be pointed out however that the spectroscopic "equivalent-points" correspond to $N/[\text{HSA}]$ values minimal in order to nearly cancel (fluoresceine) or to fully develop (rhodamine) spectral perturbations of probe chromophores, for our working conditions.

Further addition of polysaccharides may in fact lead to further "interactions" with HSA no longer detectable by the dyes employed. This, among other things, is born out by the calorimetric experiments which indicate that at pH = 6 there is little polysaccharide-HSA interaction (in agreement with spectral observation) while at pH = 5.0 the ΔH_c (in Kcal per mole of HSA, corrected for dilution effects) values progressively increase with increasing polysaccharide concentration and appear to finally reach a plateau (Fig. 6). Evidently, electrostatic interactions are mainly responsible for the observed effects.

In the case of NaDS with $\bar{M} = 4.10^4$ one can estimate from the calorimetric data an apparent "equivalence-point" in fair agreement with the spectroscopic results ($N/[\text{HSA}]$ ca. 30). The influence of polysaccharide average molecular weight is also evident from data of Fig. 6, a lower \bar{M} producing a lowering and smearing out of the ΔH_c values. With NaDS $\bar{M} = 8.10^3$ we find in fact, at high $N/[\text{HSA}]$ values, a ΔH_c practically coincident with that for heparin but nearly half of that for NaDS with $\bar{M} = 4.10^3$ (but always with DS = 2). Moreover for the NaDS with $\bar{M} = 8.10^3$ and for heparin no equivalence-point may be estimated from Fig. 6.

The polydispersity of our NaDS samples, of unknown molecular weight distributions, precludes quantitative interpretation of

these interesting observations. A possible qualitative explanation may however be that at very low $N/[\text{HSA}]$ values the protein binding process takes place with practically identical mechanisms, independent of NaDS molecular weight. This is in agreement with both spectroscopic and calorimetric experimental evidence. For higher $N/[\text{HSA}]$ values, i.e. near to 20 (see Fig. 5a), differences in the "binding-sites" for HSA along short chains and longer polysaccharidic chains become evident. One may assume that with the longer chains more fixed charges may be engaged in the binding of each albumin globular molecule (at high $N/[\text{HSA}]$ values) so that more heat is evolved (Fig. 6) and more opportunity is given to rhodamine to participate in the complexation (Fig. 5a).

The same qualitative reasoning might apply as well to the Hep-HSA case (\bar{M} of heparin ca. 10^4) which, to a first approximation, may resemble the HSA-NaDS $\bar{M} = 8 \cdot 10^3$ case. It has to be recalled that the calorimetric experiments were performed using HSA solutions nearly ten times more concentrated than in the spectroscopic experiments. Finally, concerning the influence of NaDS molecular weight, it must be said that using a sample with $\bar{M} = 5 \cdot 10^5$ ($\text{DS} = 2$) protein precipitation occurred.

Findings reported here deserve further study inasmuch as the systems considered and the original experimental approaches used may yield valuable "reference" information for similar investigations on polysaccharide-proteins systems in which specific interactions do play an important role (e.g. heparin-antithrombin III).

II) Natural carboxylated polysaccharides

a) Dissociation equilibria of Xanthan and PS-10. Prior to a discussion of data concerning the protonation equilibria, it may be of interest to report briefly a few results on the enthalpy of dilution and on the enthalpy of Cu^{2+} ion binding for Xanthan and PS-10 in dilute aqueous solution. First of all it must be pointed out that while for Xanthan the chemical structure and conformational features have been already elucidated and/or thoroughly investigated, no similar information is available for PS-10. For the latter exocellular polysaccharide, in fact, it appears that, so far, chemical composition (6, 7) only is known (gluc : galact : glucA : fucose = 6:4:3:2, and an O-acetyl content of 4.5%). Nevertheless, we decided to use PS-10 in our studies essentially as a reference polysaccharidic compound devoid of chain conformational order at any pH or ionic strength, as opposed to the case of Xanthan.

For these two natural carboxylated polysaccharides which have equivalent weights: 633 (Xantahn) and 854 (PS-10), the heat of dilution data are given in Fig. 7. It once more appears that ΔH_D is a linear function of $\log N$, at least in the limited range of N values studied, as experienced with the sulfated polysaccharides (Figs 2 and 3: low N values). Here, however, correlation of this feature with theories based on line-charge models is out of the

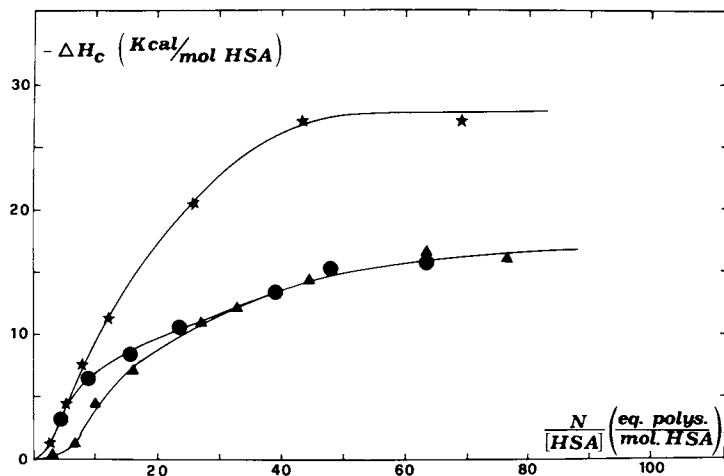


Figure 6. Calorimetric data on the interaction of HSA with dextran sulfate (●, ★) and with heparin (▲) in aqueous solution (25°C), pH = 5.04, acetate buffer ($7 \cdot 10^{-2}$ M), albumin concentration (constant) = $1.45 \cdot 10^{-4}$ mol/L. (★) dextran sulfate, $\bar{M} = 4 \cdot 10^4$; (●) dextran sulfate, $\bar{M} = 8 \cdot 10^3$; (▲) heparin.

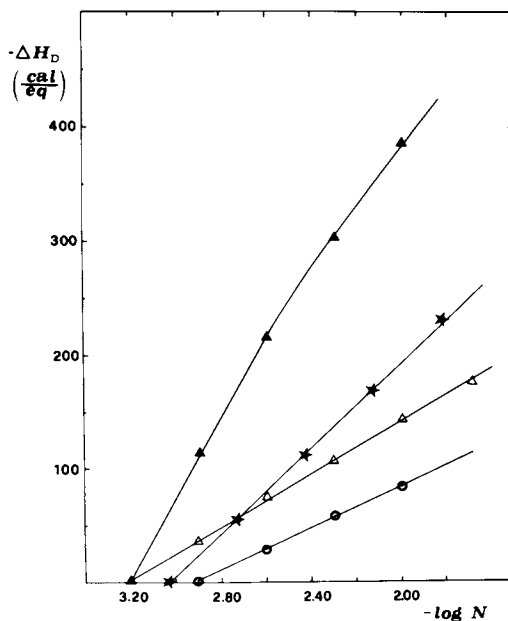


Figure 7. Enthalpy of dilution of xanthan and PS-10 (25°C): (▲) PS-10 in water; (★) xanthan in $5 \cdot 10^{-2}$ M NaCl; (△) PS-10 in $1 \cdot 10^{-2}$ M NaCl; (○) PS-10 in $5 \cdot 10^{-2}$ M NaCl.

question in view of the complex, branched structure of Xanthan. In other words, the linearity of calorimetric plots such as those of Fig. 7 (data in water and in aqueous NaCl, at 25 C) is not, in our opinion, a manifestation of the "polyelectrolytic" nature of species considered.

On the other hand data reported in Fig. 8 indicate that the higher charge-density of Xanthan compared to PS-10 shows up in a higher heat of Cu^{2+} ion binding and in a lower activity coefficient of Na^+ counterions. From the initial slope of the Q_B against $[\text{Cu}^{2+}] / N$ plots of Fig. 8 one estimates for Xanthan in water a differential enthalpy of Cu^{2+} binding of about 1 Kcal per mole of copper bound. In conclusion, as found with the sulfated polysaccharides (Fig. 4) as well as with different synthetic polycarboxylates (3), chelation of Cu^{2+} ions by polyanions is a process systematically driven by the entropy.

Passing to the protonation equilibrium experiments, our calorimetric results are reported in Fig. 9. It is evident that in the case of Xanthan in water the enthalpy of protonation is rather anomalous. Leaving aside possible aggregation \rightleftharpoons disaggregation phenomena which, in our experience, may render troublesome all physico-chemical measurements on aqueous Xanthan but which should be minimized for our thermally treated solutions (20) (see also Experimental Part), we propose that the anomalous $\bar{e}nthalpy$ trend may be ascribed to a conformational, isothermal change of Xanthan chains. This hypothesis appears to gain support from the circular dichroism data illustrated in Figs 10 and 11 for PS-10 and Xanthan respectively.

For PS-10 the change of the CD spectrum with pH essentially reflects the undissociated \rightleftharpoons dissociated equilibrium of carboxyl groups of glucA residues (21, 22).

For Xanthan the dependence of the CD spectra on pH is more complicated because different chromophores (23) participate in the above said equilibrium: one can, nevertheless, distinguish peculiar $[\theta]$ vs. pH features in correspondence with pH values for which anomalies are also detectable in the calorimetric plots (Fig. 8).

In 0.1 NaCl (25°) all anomalies are cancelled out, and the ordered conformation assumed by Xanthan in this milieu (4, 5) would thus resist any pH perturbation.

Experimental

The segmented i-carrageenan sample was a kind gift of Dr. S. Reid, Unilever Research Laboratory (England). The intact i-carrageenan sample was a SIGMA-4 (USA) product, purified and characterized in the CERMAV laboratory of the University of Grenoble (France). Dextran sulfate of $\bar{M} = 5.10^5$, 4.10^4 and 8.10^3 were PHARMACIA (Sweden) samples, which have been purified by dialysis.

Elemental analysis of the above polysaccharides (Na salts) and potentiometric titrations carried out after conversion to the

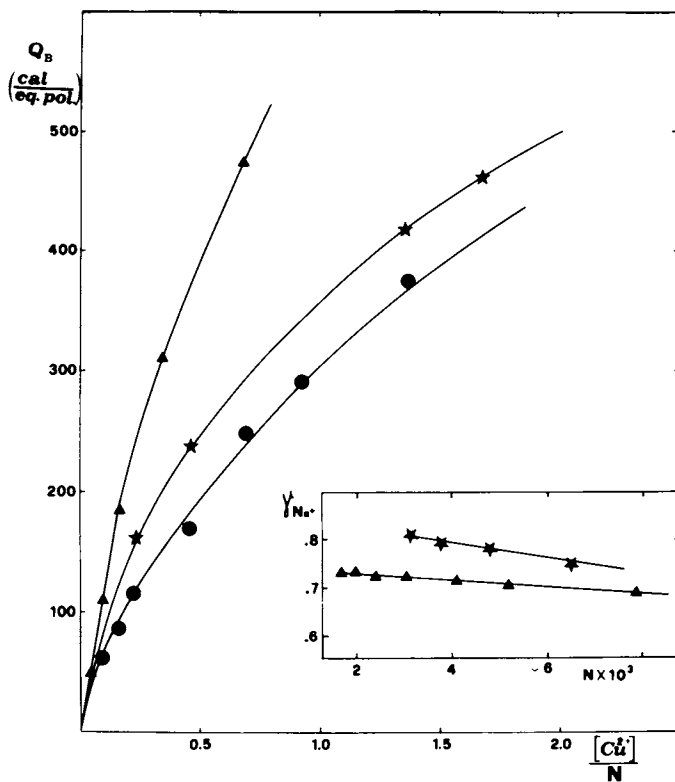


Figure 8. Calorimetric data on Cu^{2+} binding by xanthan and PS-10 in aqueous solutions ($25^\circ C$): (\blacktriangle) xanthan in $1 \cdot 10^{-2} M$ NaCl; (\star) PS-10 in water; (\bullet) PS-10 in $1 \cdot 10^{-2} M$ NaCl. In the insert γ_{Na^+} for (\star) PS-10 (in water) and (\blacktriangle) xanthan (in water).

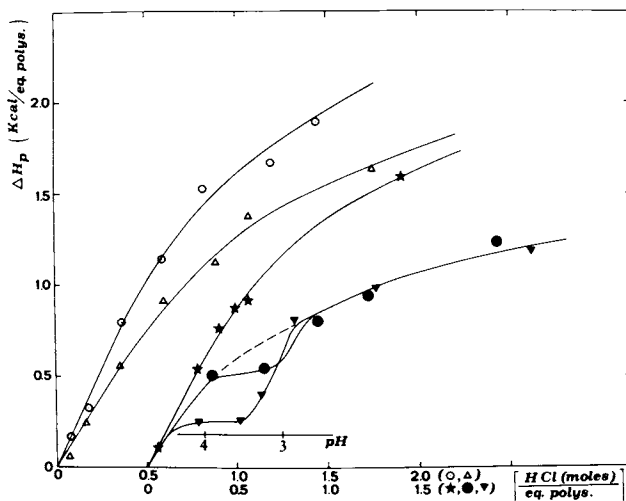


Figure 9. Enthalpy of protonation data for xanthan and PS-10 (25°C). Polymer concentration = $5 \cdot 10^{-3}$ equiv/L. (○) PS-10 in water; (△) PS-10 in 0.1M NaCl; (★) xanthan in 0.1M NaCl; (●, ▲) xanthan (degraded, undegraded) in water.

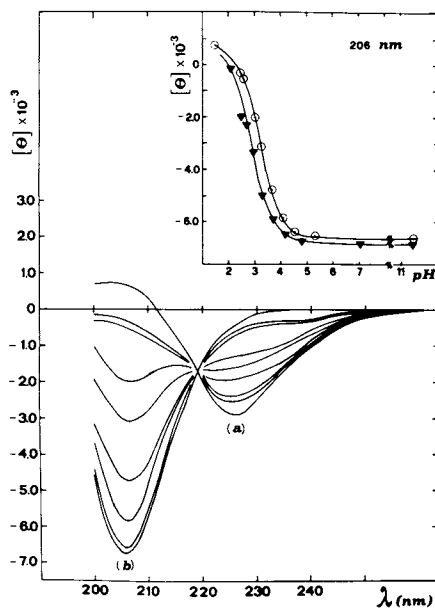


Figure 10. CD spectra of PS-10 in aqueous solution at different pHs. Polymer concentration $3 \cdot 10^{-3}$ monomol/L. The $[\theta]$ in $\text{deg cm}^2/\text{dmol}$ (mole of repeating units, assuming 2562 as the average unit's weight): (a) acid form; (b) sodium salt. In the insert: pH dependence of molecular ellipticity of PS-10 at 206 nm in water (○) and in 0.1M NaCl (▼).

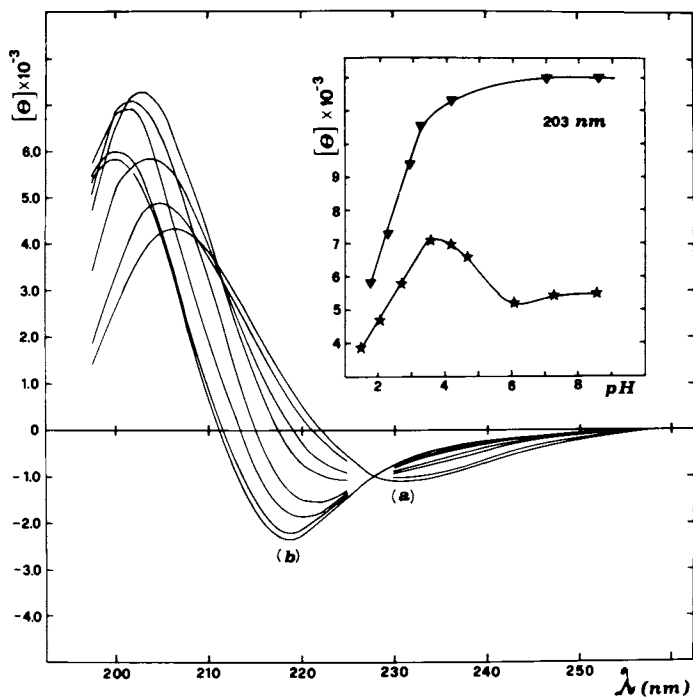


Figure 11. CD spectra of xanthan in water as a function of pH (25°C). Polymer concentration $5 \cdot 10^{-3}$ monomol/L. $[\theta]$ in $\text{deg cm}^2/\text{dmol}$ (mole of repeating units, assuming 1899 as the average unit's weight): (a) acid form; (b) sodium salt. In the insert: $[\theta]$ variation with pH at 203 nm for xanthan in water (\star) and in 0.1M NaCl (\blacktriangledown).

free acids by ion exchange have yielded the following equivalent-weight data: 1) i-carrageenan segments, 270; 2) intact i-carrageenan, 270; 3) dextran sulfate, 219, taking of course into account the different water contents of the samples.

These values correspond to a degree of substitution of 2.0 for dextran sulfate (number of sulfate groups per glucose residue) and of 1.7 for i-carrageenan segments (average number of sulfate groups per two sugar residues in the chain).

The heparin used was a purified sample from Prof. B. Casu laboratory (Milan), with the following characteristics: biological activity = 157 u.; equivalent weight = 168; ratio $[\text{COOH}] / [\text{SO}_3] = 1/2.3$. For the so called charge density parameter $\xi = e^2/DkTb$ where **b** is the distance between neighboring charges on the macroions, *e* the electronic charge, *D* the dielectric constant of the solvent, and *k* is the Boltzmann's constant, one can therefore calculate the following values: 1.2 (i-carrageenan); 1.3 (heparin); 2.8 (dextran sulfate).

Two Xanthan samples have been used; one was a purified, cellulase-degraded, ($\bar{M} = 2.10^5$) sample from Prof. Rinaudo laboratory (Grenoble); the other was a Kelco product, purified according to the literature (24). For both samples the equivalent weight (by NaOH titration of the acid forms) was 633. Solutions of Xanthan were heated at 80 for 10-15 hrs prior to measurements: such a treatment leaves unchanged the equiv. weight but efficiently reduces polymer aggregation.

PS-10 was a Kelco product. It was sonicated to reduce the viscosity, purified by centrifugation and precipitation from aqueous NaCl-EDTA solution with isopropyl alcohol. The polymer was redissolved in water and dialyzed exhaustively against redistilled water at 5 C, lyophilized and redissolved as required. The equivalent weight (854) was determined by NaOH titration of the acid form as well as by flame (Na^+) photometry. Human serum albumin was a Sigma product (lot No. A-9511).

Fluoresceine (sodium salt) was purchased from C. Erba (Italy) and Rhodamine-B from Merck (W. Germany): both were used without further purification.

Copper nitrate solutions were prepared using a pure $\text{Cu}(\text{NO}_3)_2 \cdot 3\text{H}_2\text{O}$ (C. Erba) sample: the titre of the solutions was controlled by titration of HNO_3 liberated upon passage through an ion-exchange column. All solutions were prepared using deionized, twice-distilled water.

Spectral measurements were carried out with a Cary-219 spectrophotometer; circular dichroism measurements with a Cary-61 dichrograph. The temperature of the cells was in all cases controlled ($\pm 0.1^\circ\text{C}$) by circulating water through an ultrathermostat (Haake).

Calorimetric measurements were performed using a LKB 10070-batch microcalorimeter at 25°C following a procedure similar to that already described elsewhere (3). The results of the dilution experiments are reported in Figs. 2, 3, and 7 as integral

heats of dilution ΔH_D (calories per equivalent of polyelectrolyte) against $\log N$ plots, where N is the polyelectrolyte concentration in equiv/l. The results of the Cu^{2+} ion binding experiments are collected in Figs 4 and 8 where the measured heats Q_B (calories per equivalent of polyelectrolyte, after correction for heats of dilution) are plotted against the $[\text{Cu}^{2+}] / N$ ratio.

Potentiometric measurements for the evaluation of Na^+ activity coefficients were carried out using a Orion 801 Analyser with a Orion Na-electrode in conjunction with a reference calomel electrode and a water jacketed titration cell.

Acknowledgements: This work has been carried out with financial support of the Italian C.N.R. The assistance of Dr. G. Paradossi and of Mr. L. Pietrelli in performing a number of experiments is acknowledged.

Literature Cited

1. Crescenzi V.; "Thermochemistry of Polyelectrolyte Solutions", Charged and Reactive Polymers, Ed. E. Selegny, D. Reidel Publ. Co., Holland-USA 1974, pgs. 115-135.
2. Crescenzi V., Delben F., Quadrifoglio F., Dolar D., J. Phys. Chem., 1973, 77, 539.
3. Paoletti S., Delben F., Crescenzi V. J. Phys. Chem., 1976, 80, 2564.
4. Rinaudo M., Milas M. Biopolymers, 1978, 17, 263.
5. Southwick J.G., McDonnell M.E., Jamieson A.M., and Blackwell J. Macromolecules, 1979, 12, 305.
6. Kang K.S., Veeder G.T., Richey D.D. "Extracellular Microbial Polysaccharides", Am. Chem. Soc. Symp. 45. Eds. P.A. Sandford, A. Laskin, Am. Chem. Soc., Washington, D.C., 1977, p.211-2119.
7. Sandford P.A.: "Exocellular, Microbial Polysaccharides" Adv. Carb. Chem. Biochem., 1979, 36, 297.
8. Joseleau J.P., Marais M.F. Carb. Res., 1979, 77, 183.
9. Milas M., Rinaudo M. Carb. Res., 1979, 76, 189.
10. Pass G., Phillips G.O., Wadlock D.J., Morley R.G. "Interaction of Sulfated Polysaccharides with counterions", chapt. 17 of: Carbohydrate Sulfates, R.G. Schweiger Ed., Am. Chem. Soc. Symp. 1878, 77.

11. Cleland R.L. Biopolymers, 1979, 18, 2673.
12. Crescenzi V., Dentini M., Paradossi G., and Rizzo R. Polymers Bull., 1979, 1, 777.
13. Manning G.S.; J. Chem. Phys., 1969, 51, 924.
14. Boyd G.E., Wilson D.P. J. Phys. Chem. 1976, 80, 805
15. Delben F., Paoletti S., and Crescenzi V.: in preparation.
16. Casu B.; Pharm. Res Commun., 1979, 11, 1.
17. Ledward D.A.: "Protein-polysaccharide Interactions" Polysaccharides in Food. J.M.V. Blandshard, and J.R. Mitchell Eds. Butterworths, 1979, p. 205-217.
18. Manzini G., Ciana A., and Crescenzi V. Biophys. Chem., 1979, 10, 389.
19. Manzini G., Crescenzi V. Biophys. Chem., 1979, 10, 297.
20. Rinaudo M., Milas M.; Intnl. J. Biol. Macromol. 1980, 2, 54.
21. Park J.W., Chakrabarti B. Biochem. Biophys. Res. Commun. 1977, 78, 604.
22. Morris E.H., Rees D.A., Sanderson G.R., Thom D. J. Chem. Soc. Perkin, 1975, 2, 1418.
23. Morris E.R., Rees D.A., Young G., Walkinshaw M.D., Darke A. J. Mol. Biol., 1977, 110, 1.
24. Holzwarth G.; Biochemistry, 1976, 15, 4333.

RECEIVED August 26, 1980.

American Chemical
Society Library
1155 16th St. N. W.

Interaction Between Metal Cations and Anionic Polysaccharides

G. PASS and P. W. HALES

Department of Chemistry, University of Salford, Salford, M5 4WT, U.K.

A wide variety of techniques has been used to investigate the interaction between inorganic cations and polyelectrolytes in aqueous solution. The results are usually given in the form of a sequence of metal cations listed in order of increasing interaction with the polyelectrolyte. For the alkali metal cations the sequence of increasing interaction with carboxylated (1, 2) and phosphated polyelectrolytes (3) parallels the decrease in ionic radius. The sequence is reversed for the interaction with sulphated polyelectrolytes. (4, 5, 6)

A theoretical model (7) has been developed to explain the behaviour of polyelectrolytes in aqueous solution in terms of a linear charge parameter, defined for monovalent charged groups and counterions as

$$\xi = \frac{e^2}{DkTb}$$

where e = the charge on the proton

D = the bulk dielectric constant of water

b = the average distance between charged groups

k = the Boltzmann constant

T = the thermodynamic temperature

When $\xi > 1$ a proportion of the counterions will condense on to the polyanion to give an effective value of $\xi = 1$, the remaining uncondensed counterions interact with the polyelectrolyte through Debye-Hückel forces.

The development from this theory of mathematical expressions for certain physical properties of polyelectrolyte solutions has allowed more quantitative investigations to be undertaken. Measurements have usually been made on the sodium salt of the polyelectrolyte and good agreement is obtained between theory and experiment. (8, 9, 10) When different salts of the polyelectrolyte are used the results reflect the sequential behaviour already described. (11, 12, 13)

0097-6156/81/0150-0349\$05.00/0

© 1981 American Chemical Society

An expression has been derived from the linear charge model for the enthalpy of dilution of polyelectrolyte solutions. (14) This has been applied to the enthalpy of dilution of samples of sodium carboxymethylcellulose and sodium polyacrylate. (15) Better agreement between theoretical and experimental values was obtained with sodium carboxymethylcellulose. This was attributed to the NaCMC chain more closely approaching the rod-like geometry required by the linear charge model of a polyelectrolyte. Satisfactory agreement between theory and experimental values was also reported for sodium polyvinylsulphonates. (14) The effect of cation size on the enthalpy of dilution of polystyrenesulphonates has been reported at low concentrations (16) and also at relatively high concentrations (17).

In the present work we have investigated the effect of the cation on the enthalpy of dilution of alkali metal salts of carboxymethylcellulose, alginate, and dextran sulphate.

An expression has also been derived from the linear charge model for the enthalpy change when a polyelectrolyte is mixed with a salt solution containing the same counterion. (18) We have now investigated the enthalpy of mixing of alkali metal salts of alginate and dextran sulphate with solutions of alkali metal chlorides to establish whether the cation has any influence on the enthalpy change.

Experimental

Sodium carboxymethylcellulose (7L2P) was supplied by the Hercules Company, U.K. The structure of the polyanion consists of repeating units of β -1,4 linked anhydroglucose residues, substituted by sodium carboxymethyl groups, with a repeating length of 0.515 nm. The sample (19) had a degree of substitution (DS) of 0.83. Sodium alginate (Manucol LB) was supplied by Alginate Industries, U.K. The polyanion contains anhydromannuronate and anhydroguluronate units, with a repeating length of 0.50 nm. The sample (20) had a DS = 0.92. Sodium dextran sulphate was supplied by the Sigma Chemical Co., USA. The main structural feature consists of linear chains of α -1,6 linked glucopyranose residues, containing the sulphate groups, with a repeating length of 0.51 nm. The sample had a DS = 2.13. All the samples were dialysed for 48 hours against distilled water before use. Dialysis tubing, Visking size 8, was obtained from Medicell International Ltd. The dialysed solutions were concentrated on a rotary evaporator at 40°C, and the concentrated solution was either freeze dried or used immediately to prepare solutions of the required concentrations.

The dialysed solutions of the sodium salts were converted to the lithium or potassium salt forms by passing the solutions through an ion exchange resin, Zerolit 325, supplied by B.D.H., UK. The acid form of the resin was converted to the appropriate cation form by passing the alkali metal chloride solution (1M) through the column, and the column washed until the washings were free of

chloride ion. A solution of the sodium polyelectrolyte, of suitably low viscosity, was passed through the column and collected with twice the volume of washings. The solutions were concentrated using the same procedure adopted for the sodium salts, and the purity of the products determined by flame photometry. The column was regenerated by first converting to the acid form.

Lithium chloride, sodium chloride and potassium chloride were dried at 105°C for 48 hours before use. A stock solution of each chloride was prepared containing $16 \times 10^{-2} \text{ mol l}^{-1}$. Aliquots of these solutions were diluted as required.

Calorimetric measurements were made using a flow calorimeter (LKB Produkter, Bromma, Sweden. Model 2107). The two solutions are pumped through the spiral tubing (1mm diam. x 60 cm) of the flow mixing cell at a rate of $14 \text{ cm}^3 \text{ h}^{-1}$, giving a residence time of approximately 1 minute. The heat change occurring in the cell flows through two thermopiles to or from a large aluminium block. The voltage generated in the thermopiles is amplified (Keithley Instruments Model 150B microvolt ammeter) and displayed on a chart recorder (LKB Model 2066) relative to a base line established with a flow of deionised water replacing the polyelectrolyte. Peak heights are calibrated against a known input of heat at controlled current and heater resistance. The calorimeter is kept in an insulated box which in turn is in a thermostatted air bath with a temperature stability of $\pm 0.02^\circ\text{C}$. The two solutions to be mixed are brought to the same temperature by two heat exchange coils before entering the flow mixing cell. Using the calibrated heater, heat changes in the mixing cell down to $50 \mu\text{W}$ could be determined to $\pm 2\%$. The performance of the calorimeter was checked by measuring the heat of dilution of sodium chloride which gave results $\pm 2\%$ of the literature values.

Results and Discussion

The enthalpy changes occurring in the interaction between polyelectrolytes and counterions may be considered in terms of at least three possible effects. The first involves the enthalpy changes occurring on dilution, the second involves enthalpy changes arising from interaction between the ion atmosphere of the polyelectrolyte and the counterion, and the third concerns the enthalpy changes involving the condensed counterions.

Enthalpy of dilution. The enthalpy of dilution of aqueous solutions of single salts of carboxymethylcellulose (CMC) was determined over the concentration range $8 \times 10^{-2} - 0.5 \times 10^{-2} \text{ equiv. l}^{-1}$. The CMC solution was diluted with an equal volume of water and the sum of the heat changes was calculated to allow determination of the enthalpy of dilution from a given initial concentration to a final concentration of $0.5 \times 10^{-2} \text{ equiv. l}^{-1}$.

The enthalpy of dilution of a polyelectrolyte may be calculated from the expression (14)

$$\Delta H_{m_p^i \rightarrow m_p^f} = \frac{-RT\xi^n}{2} \left(1 + \frac{T}{D} \frac{dD}{dT}\right) \ln \frac{m_p^f}{m_p^i} \dots\dots 1$$

where m_p^f = the final polyelectrolyte concentration
 m_p^i = the initial polyelectrolyte concentration
 $n = 1$ when $\xi < 1$ and $n = -1$ when $\xi > 1$

The expression is a limiting law in the Debye-Hückel sense and is strictly valid only in dilute solution. For a reaction at 25°C the enthalpy of dilution

$$\Delta H_{m_p^i \rightarrow m_p^f} = 1.067 \times 10^3 \xi^n \log \frac{m_p^f}{m_p^i} \text{ J mol}^{-1} \dots\dots 2$$

where $\left(1 + \frac{T}{D} \cdot \frac{dD}{dT}\right)$ is taken as equal to -0.374. (21)

The enthalpy of dilution is therefore dependent on the extent of the charge on the polyelectrolyte, which is given in terms of the linear charge parameter, ξ . For the sample of CMC the degree of substitution (DS) was 0.83 and taking the length (22) of a repeating unit in the polymer as 0.515 nm this gives a value of $\xi = 1.15$.

The experimental results for the lithium, sodium, and potassium salts of CMC are given in Figure 1 with the theoretical line obtained for $\xi = 1.15$. The results for the sodium salt are in satisfactory agreement with previously reported results. (15) The results in Figure 1 show that the enthalpy of dilution becomes increasingly exothermic in the sequence $K < Na < Li$, and in the case of the lithium salt the dilution is more exothermic than the theory predicts and give enthalpies approaching the theoretical maximum ($\xi = 1$). Although linear plots are obtained for the enthalpies of dilution of the lithium and sodium salts, from which effective values of the linear charge parameter may be calculated, (23, 24) this is not feasible for the potassium salt.

The enthalpies of dilution of single salts of alginate have also been measured. The alginate was found to have a DS = 0.92 and taking the length (22) of a repeating unit as 0.50 nm gives $\xi = 1.30$. The plots of the enthalpies of dilution of the lithium, sodium and potassium salts are given in Figure 2. The enthalpies of dilution of the two carboxylated polyanions show a dependence on the counterion which is present, and fall into the sequence $Li > Na > K$, but there is no apparent difference in the behaviour of a carboxyl and a carboxymethyl substituent in the polyanion. (18)

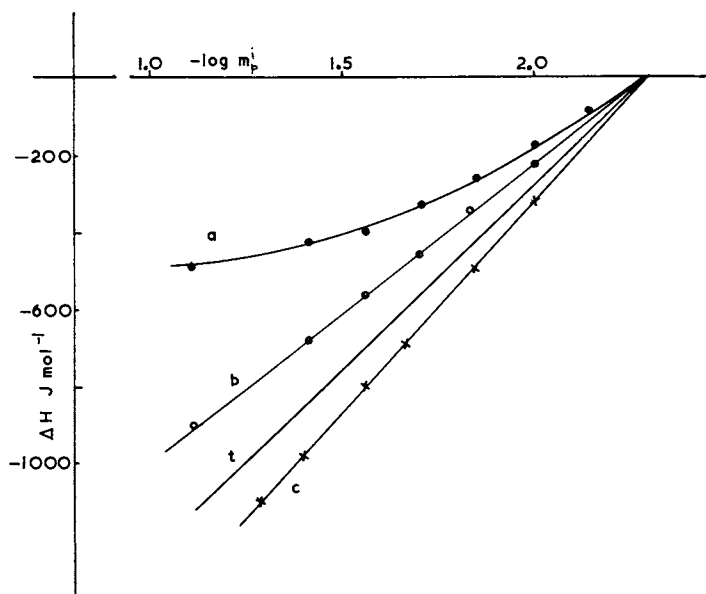


Figure 1. Enthalpy of dilution of salts of CMC: (a) KCMC; (b) NaCMC; (c) LiCMC; (t) theoretical line from Equation 2.

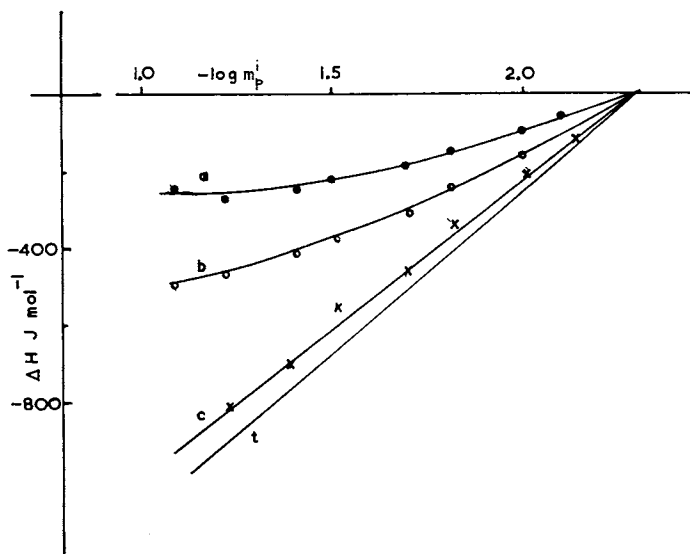


Figure 2. Enthalpy of dilution of alginates: (a) K alginate; (b) Na alginate; (c) Li alginate; (t) theoretical line.

Ion atmosphere effects. The enthalpy change occurring when a polyelectrolyte solution is mixed with a simple salt solution containing the same counterion may be calculated (18) from

$$\Delta H_{\text{mix}} = 1.067 \times 10^3 \xi^n \log \frac{(m_p^f + 2\alpha m_s^f)}{m_p^i} \dots \dots 3$$

where in addition to the terms defined in equations 1 and 2,

m_s^f = the final salt concentration

$\alpha = 1$ when $\xi < 1$ and $\alpha = \xi$ when $\xi > 1$.

$$Y = \frac{m_p^f + 2\alpha m_s^f}{m_p^i}$$

Solutions of a given salt form of alginate were prepared containing 10^{-2} equiv. l^{-1} and mixed with equal volumes of the alkali metal chloride solution. Thus samples of sodium alginate (10^{-2} equiv. l^{-1}), were mixed with a sequence of sodium chloride solutions of different concentrations. The enthalpy of mixing as calculated from the equation refers only to the contribution from the polyelectrolyte. The experimental enthalpy changes were corrected for the enthalpy of dilution of the sodium chloride solution, which was determined under identical reaction conditions, except that the sodium alginate solution was replaced by deionised water. The corrected enthalpies of mixing lithium alginate with lithium chloride and potassium alginate with potassium chloride were determined in the same way.

The results in Figure 3 show that the corrected enthalpy of mixing becomes progressively more endothermic as the concentration of the added salt is increased, although in the case of the potassium salt this trend is reversed at the highest salt concentrations. Dilution of the ion atmosphere of the polyelectrolyte produces a sequence $K < Na < Li$ in order of increasing exothermic enthalpies of dilution. When the concentration of the ion atmosphere is increased the opposite sequence is obtained $K < Na < Li$ in order of increasing endothermic enthalpies of mixing. This dependence of the enthalpy changes on the nature of the cation leads to speculation as to possible contributions to the overall enthalpy change. These might include changes in the structure of water which are dependent on the counterion which is present (25), or changes in hydration of the counterion, approaching behaviour usually postulated for condensed counterions (27).

Condensed ion effects. The enthalpy of mixing of a polyelectrolyte and a simple salt containing different counterions was next investigated. Sodium alginate solution was mixed with a sequence of lithium chloride solutions of different concentrations,

and the enthalpy of mixing measured. These results were compared with the enthalpies of mixing of lithium alginate with sodium chloride and the results are given in Figure 4, with the theoretical line for comparison. The mixing of lithium chloride with sodium alginate gives a more endothermic reaction than predicted, while the mixing of sodium chloride with lithium alginate gives a more exothermic reaction. Similar results are obtained when the enthalpies of mixing are determined for other combinations of polyelectrolyte and simple salt, which do not have a common counterion, and which may be considered as opposing reactions in a general equilibrium $AP_a + BCl \rightleftharpoons BP_a + ACl$. These results are given in Figures 5 and 6.

The mixing reaction, with unlike counterions, may be considered to not only alter the concentration of the counterions in the ion atmosphere of the polyelectrolyte but also to produce some exchange of the condensed counterions. For the alginate sample the fraction of condensed counterions (7) will be $(1 - \xi^{-1})$, 0.23. The common effect shown in Figures 4-6 is to make the enthalpy changes more endothermic when the alkali metal alginate is mixed with an alkali metal chloride, containing a lighter counterion. Conversely the enthalpy of mixing becomes more exothermic when the alkali metal alginate is mixed with an alkali metal chloride containing a heavier counterion. From this we conclude that the replacement of a condensed cation by a lighter cation is an endothermic process, and exothermic when the reaction is reversed.

The enthalpy changes resulting from exchange of a condensed counterion may be seen more clearly if it is assumed that in the mixing of solutions containing unlike cations the effects observed with solutions of like cations will still be operating. Thus when sodium chloride solution is mixed with sodium alginate (Fig. 3b) the corrected enthalpy of mixing is more exothermic than the theoretical line. We may assume that this is the result of the theory giving an incomplete interpretation of the ionic interactions. When $\log Y = 1.0$ the departure from theory = -540 J mol^{-1} . When sodium chloride solution is mixed with potassium alginate (Fig. 5a) the corrected enthalpy of mixing is more endothermic than the theoretical line. When $\log Y = 1.0$ the departure from theory = 60 J mol^{-1} . If we assume that the non-predicted effects operating in Figure 3b are still operating in Figure 5a then this results in an understatement of the endothermic nature of the reaction between potassium alginate and sodium chloride. The departure from the theoretical line at $\log Y = 1.0$ would then be $(60 + 540) = 600 \text{ J mol}^{-1}$. This value for the departure from theory at $\log Y = 1.0$ is plotted in Figure 7b. The other points in Figure 7b are obtained in similar fashion. Comparison of the results plotted in Figure 7b with the theoretical line may then be used to determine the additional enthalpy changes due to exchange of the condensed potassium ions with sodium ions from the solution.

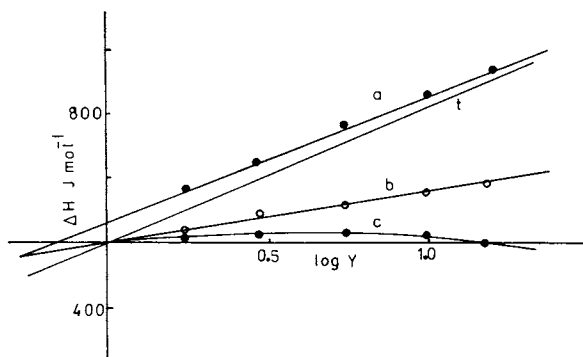


Figure 3. Enthalpy of mixing of alginates with alkali metal chlorides: (a) LiCl/Li alginate; (b) NaCl/Na alginate; (c) KCl/K alginate; (t) theoretical line from Equation 3.

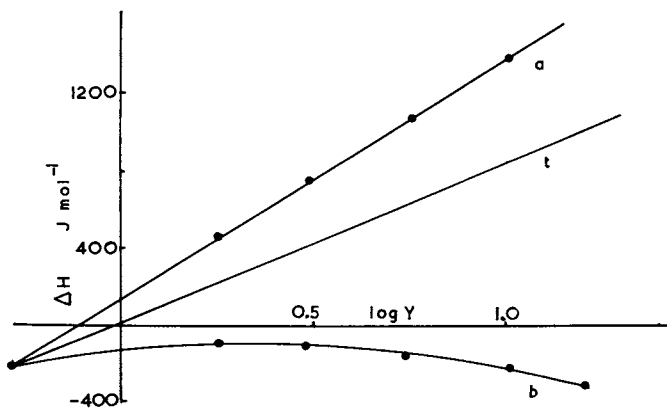


Figure 4. Enthalpy of mixing of alginates with alkali metal chlorides (unlike cations): (a) LiCl-Na alginate; (b) NaCl-Li alginate; (t) theoretical line.

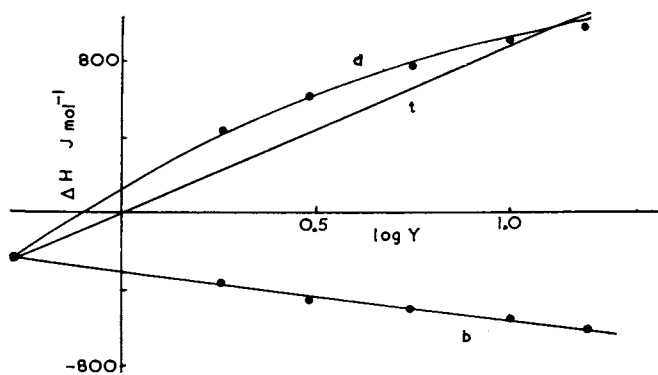


Figure 5. Enthalpy of mixing of alginates with alkali metal chlorides (unlike cations): (a) NaCl-K alginate; (b) KCl-Na alginate; (t) theoretical line.

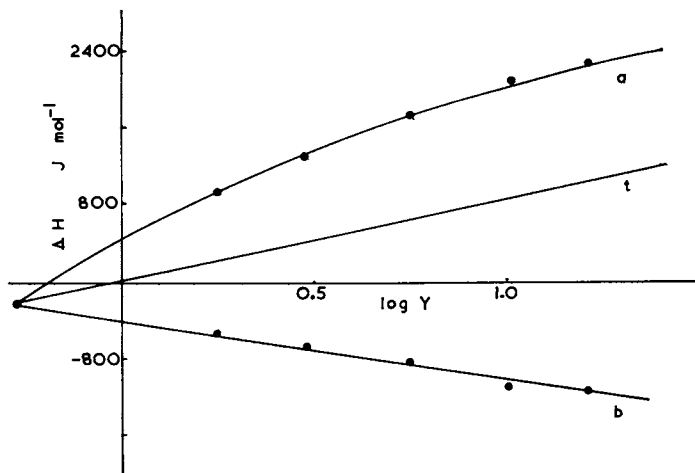


Figure 6. Enthalpy of mixing of alginates with alkali metal chlorides (unlike cations): (a) LiCl-K alginate; (b) KCl-Li alginate; (t) theoretical line.

A similar procedure may be applied to the results in Figure 3e, where the departure from theory at $\log Y = 1.0$ is -820 J mol^{-1} , and the results in Figure 5b where the departure from theory at $\log Y = 1.0$ is -1440 J mol^{-1} . This gives the value at $\log Y = 1.0$ of $(-1440 + 820) = -620 \text{ J mol}^{-1}$ for the departure from the theoretical line plotted in Figure 7e. The other points in Figure 7e are obtained by using the same procedure. The data plotted in Figures 3, 4 and 6 may then be treated in the same way to obtain the other plots in Figure 7.

The results may be compared with the observed sequences (1) for reactions involving equilibrium between the alkali metal cations and carboxylated polyanions, which give an order of affinity $\text{Li} > \text{Na} > \text{K}$. The equilibrium sequence, which is a measure of the free energy change in the reaction, can only be reconciled with the enthalpy data if the endothermic replacement of the condensed sodium ion by a lithium ion is accompanied by an increase in the total entropy. This would accord with the observed order of volume changes, $\text{Li} > \text{Na} > \text{K}$, for the site binding (condensation) of alkali metal cations to polycarboxylates, (26, 27), where the volume change is related to a change in the extent of hydration of the counterion. If the exchange of a cation from solution with a condensed cation involves a net loss of bound water molecules (28) this may produce a positive enthalpy change and also provide the necessary increase in entropy. The observation that a positive enthalpy change accompanies the transfer of a lithium cation from the solution to the polyanion has also been observed with polymaleic acid (29). It is also relevant to note that metal ion complex formation with carboxylated ligands has a positive enthalpy of formation and is also an entropy driven process (30).

It follows from these results that the bond strength between the condensed counterion and the carboxylated polyanion has no necessary dependence on the nature of the counterion. Any binding sequence is possible which allows that there is a greater release of water molecules by the lighter cation when it condenses. This does appear to be an area of confusion where sequences of binding affinity are based upon some form of equilibrium measurement, and thus relate to the free energy change in the reaction. However, in certain cases these orders of binding affinity have become synonymous with bond strengths, that is enthalpy changes, and there seems little justification for such an interpretation.

Sulfated polyanions. In the interaction of counterions with sulphated polyanions there is less dehydration of the counterions (1) and the reverse sequence of volume changes (26) is observed for the counterion interaction. The enthalpy changes for dilution and mixing of alkali metal salts of dextran sulphate were therefore measured and compared with the results for the carboxylated polyanions.

The sample of dextran sulphate had a D.S of 2.13, and with the

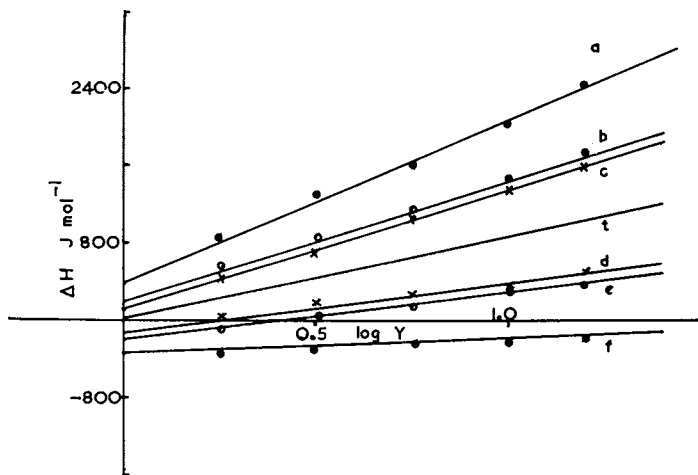


Figure 7. Enthalpy of mixing of alginates with alkali metal chlorides (unlike cations) corrected for ion atmosphere effects: (a) LiCl-K alginate; (b) NaCl-K alginate; (c) LiCl-Na alginate; (d) NaCl-Li alginate; (e) KCl-Na alginate; (f) KCl-Li alginate; (t) theoretical line.

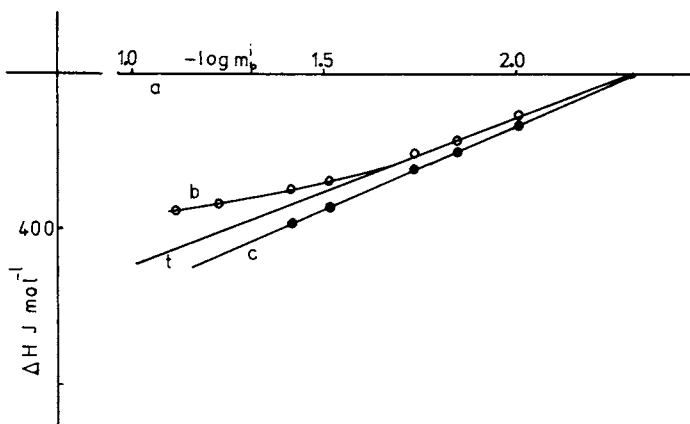


Figure 8. Enthalpy of dilution of dextran sulfates: (a) K dextran sulfate; (b) Na dextran sulfate; (c) Li dextran sulfate; (t) theoretical line Equation 2.

length (31) of the repeating unit taken as 0.51 nm this gives $\xi = 2.95$. The enthalpies of dilution of the lithium, sodium, and potassium salts, with the theoretical line are given in Figure 8. The sequence is the same as observed for CMC and alginate. The lithium salt is most exothermic, exceeding the theoretical value, the sodium salt gives values less exothermic than the theoretical value, and the potassium salt gave no measureable enthalpy of dilution over this concentration range. A similar decreasing series of enthalpies of dilution for lithium, sodium, and potassium salts of polystyrene sulphonates has also been reported (16). This sequence is again reversed when the dextran sulphate salts are mixed with a solution of simple salt containing the same counterion (Figure 9). The enthalpies of dilution and mixing of the dextran sulfates show the same marked dependence on the counterion as the enthalpies of dilution of CMC and alginate, and the enthalpies of mixing of alginate. The fact that this additional effect appears to be independent of the polyanion may be further support for the speculation that it arises from an interaction between the counterion and the solvent.

The enthalpies of mixing of the alkali metal dextran sulphates with simple salts containing a different counterion show increasing endothermic values when the dextran sulphate is mixed with an alkali metal halide containing a lighter counterion. These results are given in Figures 10-12, which qualitatively demonstrate the same general features found with the alginates. Note that with the dextran sulphates a larger fraction (0.66) of the counterions will be condensed. The enthalpy effects due to exchange of condensed counterions may be seen more clearly if the same empirical approach used to produce Figure 7 is applied to the results in Figures 9-12. This will produce the series of plots given in Figure 13. This again shows a general similarity with the results obtained for the alginates (Figure 7) with the exception that the sodium chloride/potassium dextran sulphate mixing has become relatively more endothermic and the reverse reaction relatively more exothermic.

The sequence of enthalpy changes where replacement of a condensed alkali metal counterion by a heavier alkali metal counterion is an exothermic process is now in the same sequence as the observed equilibrium data. (1, 5) For the interaction of alkali metal cations with sulphated polyelectrolytes this is $K > Na > Li$. Thus in the case of the sulphated polyanions the enthalpy change and the equilibrium, free energy change, follow the same sequence. The sequence of enthalpy changes seems to imply that the bond strength between the condensed alkali metal cation and the dextran sulphate increases in the sequence $Li < Na < K$.

Abstract

The enthalpy changes occurring when solutions of anionic polysaccharides are diluted or mixed with solutions of simple

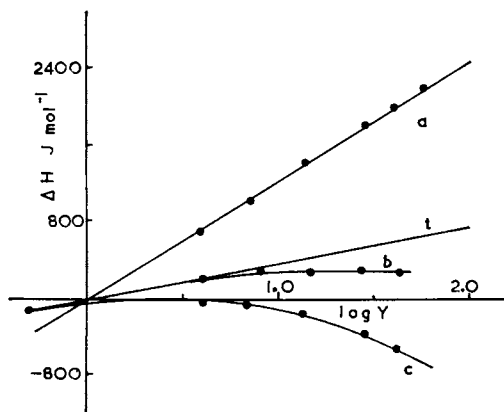


Figure 9. Enthalpy of mixing of dextran sulfates with alkali metal chlorides: (a) LiCl-Li dextran; (b) NaCl-Na dextran sulfate; (c) KCl-K dextran sulfate; (t) theoretical line Equation 3.

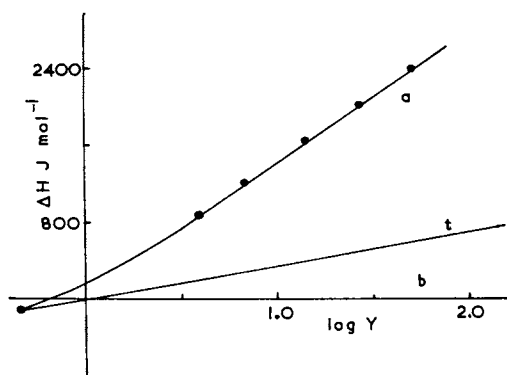


Figure 10. Enthalpy of mixing of dextran sulfates with alkali metal chlorides (unlike cations): (a) LiCl-Na dextran sulfate; (b) NaCl-Li dextran sulfate; (t) theoretical line.

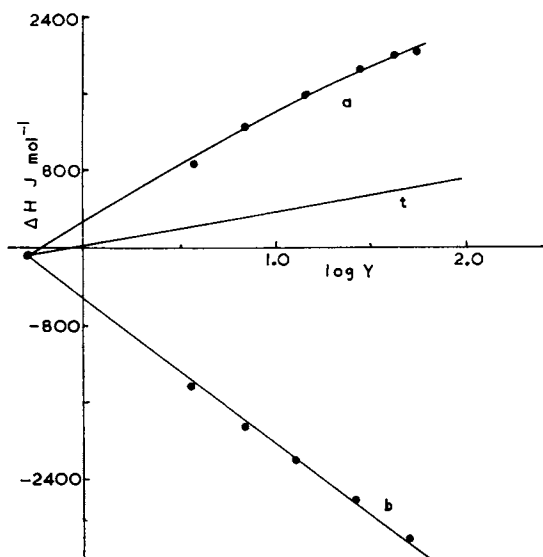


Figure 11. Enthalpy of mixing of dextran sulfates with alkali metal chlorides (unlike cations): (a) NaCl-K dextran sulfate; (b) KCl-Na dextran sulfate; (t) theoretical line.

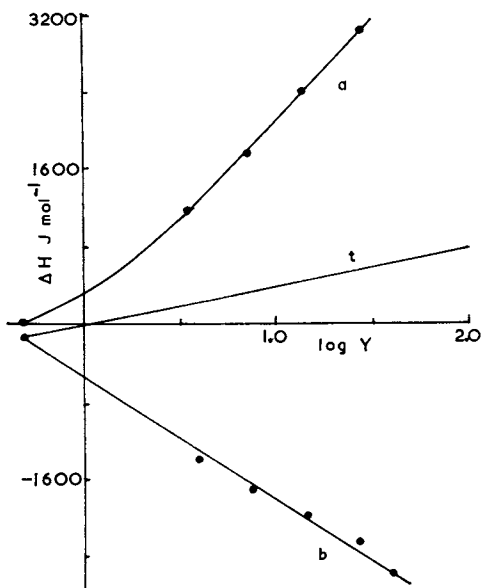


Figure 12. Enthalpy of mixing of dextran sulfates with alkali metal chlorides (unlike cations): (a) LiCl-K dextran sulfate; (b) KCl-Li dextran sulfate; (t) theoretical line.

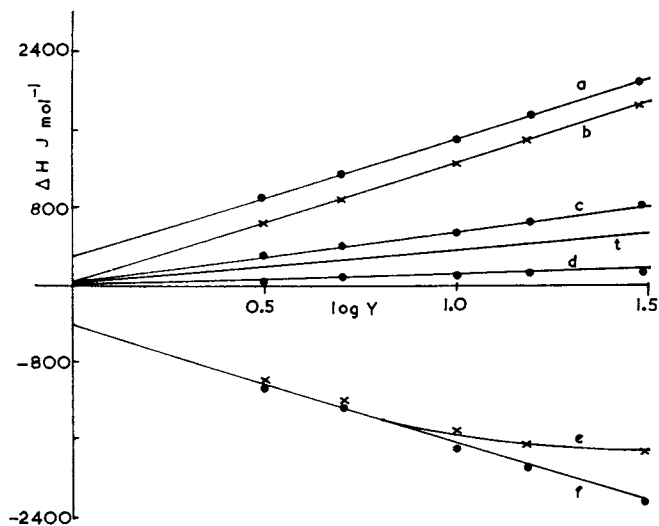


Figure 13. Enthalpy of mixing of dextran sulfates with alkali metal chlorides (unlike cations) corrected for ion atmospheric effects: (a) NaCl-K dextran sulfate; (b) LiCl-K dextran sulfate; (c) LiCl-Na dextran sulfate; (d) NaCl-Li dextran sulfate; (e) KCl-Li dextran sulfate; (f) KCl-Na dextran sulfate.

electrolyte have been determined. Different metal salts of a given polyanion were prepared and the observed enthalpy change on dilution was exothermic with a dependence on the nature of the metal cation. The enthalpy change occurring when a metal salt of a polyanion was mixed with a solution of simple electrolyte was found to become progressively more endothermic as the simple electrolyte concentration was increased. For a given salt of a polyanion the enthalpy change observed on mixing depended on the cation present in the simple electrolyte. The enthalpy changes occurring on dilution and mixing were compared with the predictions based on the line charge model of polyelectrolytes. It is suggested that one cause of the difference between theory and experiment is an additional enthalpy effect arising from interaction between the cation and the solvent.

Literature Cited

1. Bungenburg de Jong, H.G., 'Colloid Science', Vol II, Elsevier, Amsterdam (1949).
2. Gregor, H.P., Gold, D.H., Frederick, M., J. Poly. Sci. (1957), 23, 467.
3. Strauss, U.P., Ross, P.D., J. Amer. Chem. Soc. (1959), 81, 5295.
4. Satake, I., Fukuda, M., J. Poly. Sci. Poly. Phys., (1972), 10, 2343.
5. Jooyahdeh, F., Moore, J.S., Phillips, G.O., Davies J.V., J.C.S. Perkin II (1974), 1468.
6. Ashton, W.R., Pass, G., Phillips, G.O., Wedlock, D.J., J.C.S. Perkin II, (1977), 1229.
7. Manning, G.S., J. Chem. Phys., (1969), 51, 934.
8. Wingrove, D.E. and Ander, P., Macromolecules (1979), 12, 135.
9. Tomasula, M., Swanson, N., Ander, P., 'Carbohydrate Sulfates', Ed. Schweiger, R.G., ACS Symposium Series 77, (1978).
10. Wells, J.D., Biopolymers, (1973), 12, 223.
11. Kwak, J.C.T., Murphy, G.F., Spiro, E.J., Biophys. Chem. (1978), 7, 379.
12. Podlas, T.J., Ander, P., Macromolecules (1970), 3, 154.
13. Pass, G., Phillips, G.O., Wedlock, D.J., Macromolecules (1977), 10, 197.
14. Boyd, G.E., Wilson, D.P., J. Phys. Chem., (1976), 80, 805.
15. Mita, K., Okubo, T., J.C.S. Faraday I, (1974), 70, 1546.
16. Skerjanc, J., Dolar, D., Leskovsek, D., Z. Phys. Chem. (Frankfurt am Main), (1970), 70, 31.
17. Daoust, H., Hade, A., Macromolecules (1976), 9, 608.
18. Boyd, G.E., Wilson, D.P., Manning, G.S., J. Phys. Chem., (1976), 80, 808.
19. Eyler, R.S., Klug, E.D., Diephuis, F., Analyt. Chem., (1947), 19, 24.
20. Steiner, A.B., McNeely, W.H., in 'Natural Plant Hydrocolloids', Advances in Chemistry Series 11 (1954).

21. Robinson, A.L., J. Amer. Chem. Soc., (1932), 54, 1311.
22. Palmer, K.J., Hartzog, M.B., J. Amer. Chem. Soc., (1945), 67, 1865.
23. Katchalsky, A., Alexandrowicz, Z., Kedem, O., 'Chemical Physics of Ionic Solutions'. Eds. Conway, B.F., Barradas, R.G., ch. 15 Wiley, New York (1966).
24. Hales, P.W., Pass, G., J.C.S. Faraday 1 in press.
25. Sheehan, J.K., Gardner, K.H., Atkins, E.D.T., J. Mol. Biol., (1977), 117, 113.
26. Strauss, U.P., Lueng, Y.P., J. Amer. Chem. Soc (1965), 87, 1476.
27. Zana, R., Tondre, C., Rinaudo, M., Milas, M., J. Chim. Phys. Phys. Chim. Biol. (1971), 68, 1258.
28. Atkinson, G., Baumgartner, E., Fernandez-Prini, R., J. Amer. Chem. Soc. (1971), 93, 6436.
29. Quadrifoglia, F., Crescenzi, V., Delben, F., Macromolecules, (1973), 6, 301.
30. Christensen, J.J., Eatough, D.J., Izatt, R.M., 'Handbook of Metal Ligand Heats', 2nd Edn. Dekker, New York, (1975).
31. Wells, J.D. Proc. R. Soc., London, Ser B (1973), 183, 414.

RECEIVED September 24, 1980.

Investigations on Aqueous Solution Properties of κ -Carrageenans

M. RINAUDO and C. ROCHAS

Centre de Recherches sur les Macromolécules Végétales, Laboratoire propre du C.N.R.S., associé à l'Université Scientifique et Médicale de Grenoble, 53 X 38041 Grenoble Cedex, France

We established recently (1) that similarly to Xanthan (2) the melting temperatures for the helix-coil and sol-gel transitions in kappa carrageenan (Figure 1) are directly controlled by the total ionic concentration C_T . In Figure 2 the concentration dependence of the melting temperature T_M is determined from optical rotation and conductivities. On the heating and on the cooling curves, T_M is given as a function of C_T with

$$C_T = \bar{\gamma} C_p + C_s$$

C_p and C_s are the equivalent concentration of polyelectrolyte and external salt respectively and $\bar{\gamma}$ is the mean activity coefficient of the counterions. From our previous work $\bar{\gamma}$ is calculated at half transition for equal proportions of coil and helical structures. From Figure 2, it is clear that the nature of counterions (K^+ or Na^+) has a strong influence on the stability of ordered conformations and on the formation of gel in kappa carrageenan. For each counterion there exists a critical ionic concentration C^* above which hysteresis of optical rotation appears and a gel is formed. Above C^* the melting temperatures corresponding to heating and cooling cycles become different. These experimental results confirm the data given by Rees and coworkers (3).

1/ Helix-coil transition ($C_T < C^*$). In the first part of this work we investigate the influence of the macromolecular conformation (given by specific optical rotation $[\alpha]_{300}$) on the activity coefficient of Na^+ and K^+ (obtained by potentiometry).

The temperature and the concentration dependence of the activity coefficient of the sodium form is very slight (Figure 3A). At infinite dilution γ_{Na} is 0.72 ; the specific optical rotation $[\alpha]_{300}$ is constant corresponding to the coil conformation. We observe the same dependence for the potassium form at 35°C. But at 15°C a transition is observed both in γ and $[\alpha]_{300}$ (Figure 3A

0097-6156/81/0150-0367\$05.00/0

© 1981 American Chemical Society

Figure 1. Primary structure of κ -carrageenan

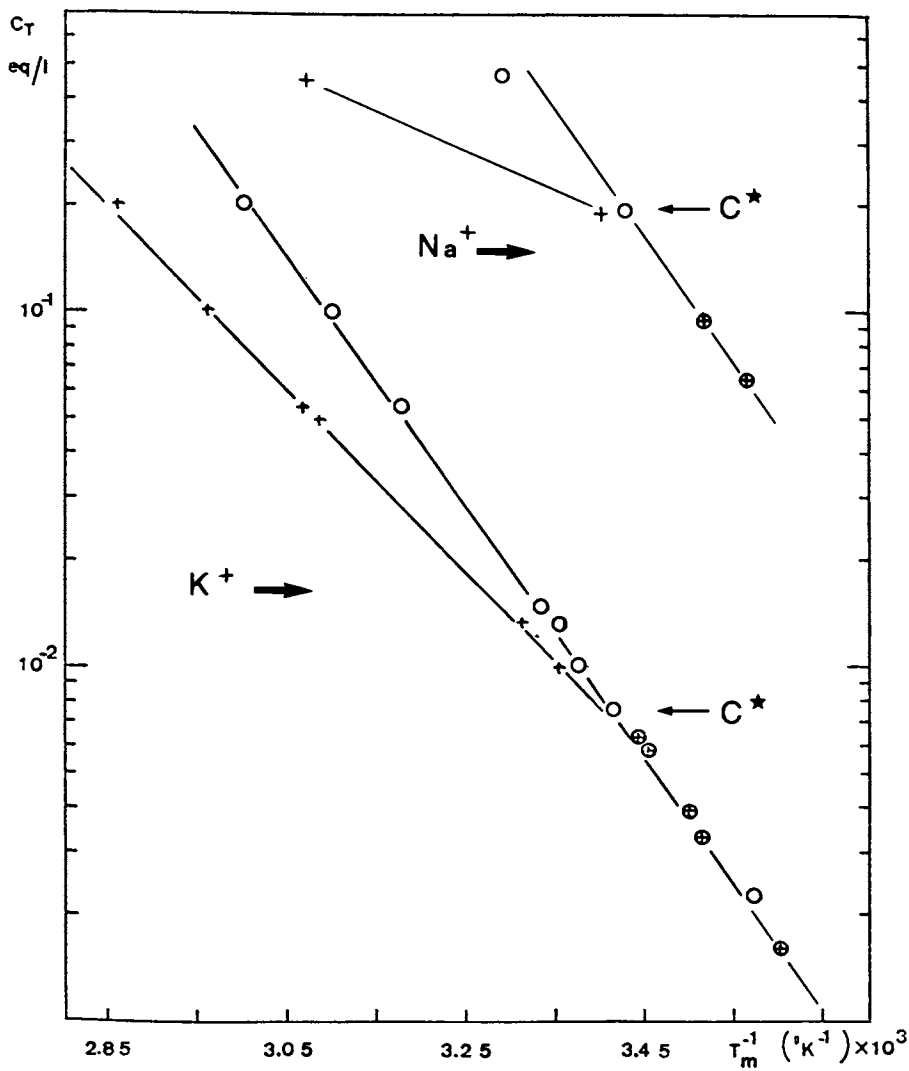
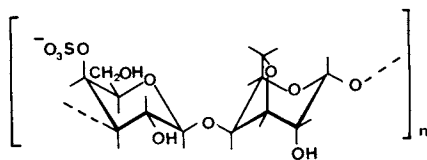


Figure 2. Variation of the melting temperature T_m with the logarithm of the free counterion concentration C_T ($C_T = C_s + \bar{\gamma}C_p$): (O) cooling; (+) heating.

and 3B). Over a given polymer concentration the helix conformation becomes established. The values ($\gamma_{\text{Na}^+} - \gamma_{\text{K}^+}$) normalized for the helix content are also plotted on the same figure as $[\alpha]_{300}$ (Figure 3B). The agreement is good and proves that it is the conformational transition which induces the change of γ ; moreover the experimental values are in agreement with Manning's theory (4). If the charge parameter is λ , the activity coefficient is given by the following relations :

$$\lambda \geq 1 \quad \ln \gamma = -\frac{1}{2} - \ln \lambda$$

$$\lambda \leq 1 \quad \ln \gamma = -\frac{1}{2} \lambda$$

Assuming that $\lambda(\text{coil})$ is calculated from the chemical structure (5) and that $\lambda(\text{double helix})$ is calculated from X-ray data (6) we get :

$$\lambda(\text{coil}) = 0.68 \quad \rightarrow \gamma_{\text{coil}}^{\text{calculated}} = 0.71$$

$$\lambda(\text{double helix}) = 1.65 \rightarrow \gamma_{\text{double helix}}^{\text{calculated}} = 0.37$$

The experimental values are $\gamma_{\text{coil}} = 0.72$ and $\gamma_{\text{ordered form}} \approx 0.35$.

These values agree with a dimerization of ordered form (double helix).

When $C_T < C^*$ the temperature dependence of the conformation investigated by optical rotation is perfectly reversible, without hysteresis.

The helix-coil transition of κ^+ carrageenan can be also observed by conductivity measurements (Figure 4A). The helix content calculated from the ratio ρ of the conductivity of the poly-electrolyte to that of a simple reference electrolyte corresponds well with the values of optical rotation (Figure 4B).

In conclusion it is apparent that a concentration and temperature reversible helix-coil transition takes place in solutions of kappa carrageenans as soon as the total ionic concentration C_T becomes lower than a critical value C^* . This critical value depends on the nature of the counterions.

2/ Sol-gel transition ($C_T > C^*$). For C_T larger than about $7 \cdot 10^{-3}$ eq/l (K^+ form) the hysteresis sets in as shown in Figure 2. Figure 5A shows the hysteresis in salt-free polymer solution in optical rotation ($C_p = 1.79 \cdot 10^{-2}$ eq/l ; $C_T = 0.96 \cdot 10^{-2}$ eq/l at half transition) ; the curves can't be obtained in their entirety due to the birefringence. In contrast the entire curves of conductivity are obtained (Figure 5B). These curves suggest a two step mechanism on heating and a continuous process on cooling with a melting temperature lower than for heating. The study of the ratio of the conductivities ρ between the polymer and a simple electrolyte used as a reference gives the same result as the conductivity, but it is more precise. This is due to the temperature

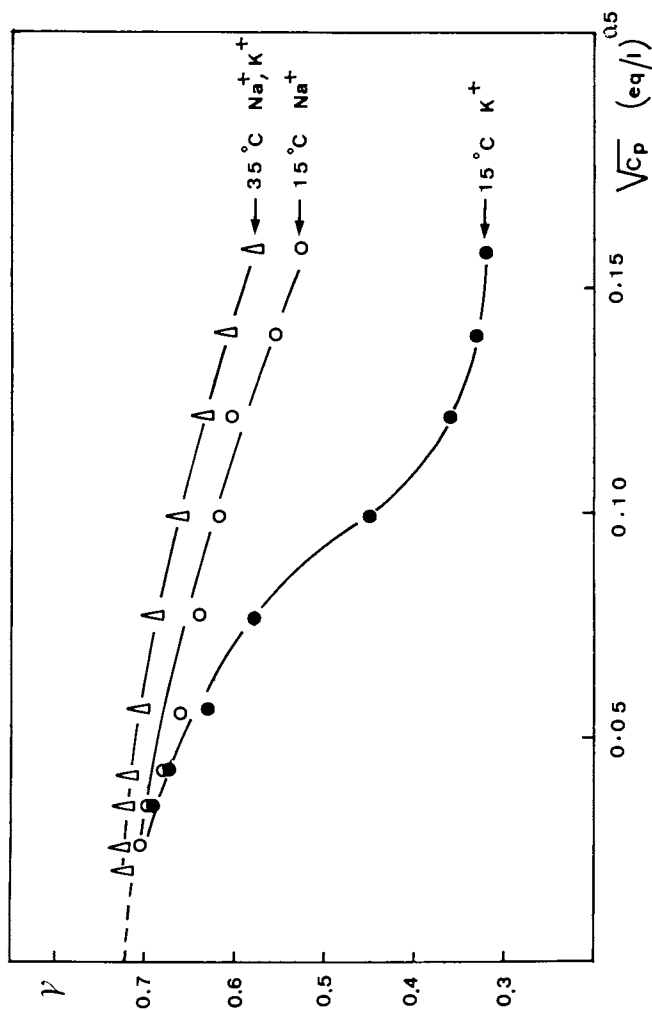


Figure 3.4. Variation of the activity coefficient of sodium and potassium counterions with polymer concentration C_p , at 15°C and 35°C in the absence of external salt

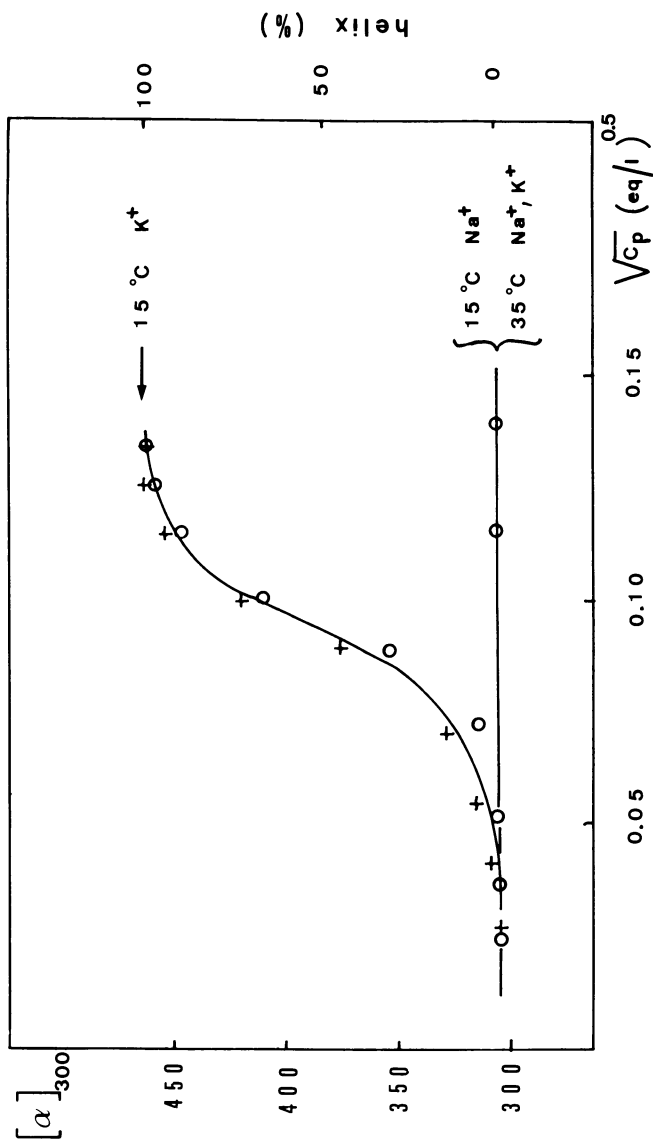


Figure 3B. Concentration dependence of specific rotation $[\alpha]_{300}$ and helix content (%) at 15°C and 35°C for potassium and sodium κ -carrageenan in the absence of external salt (O); helix content (%) at 15°C on potassium κ -carrageenan calculated from the values ($\gamma_{K^+} - \gamma_{Na^+}$) of Figure 3A (+).

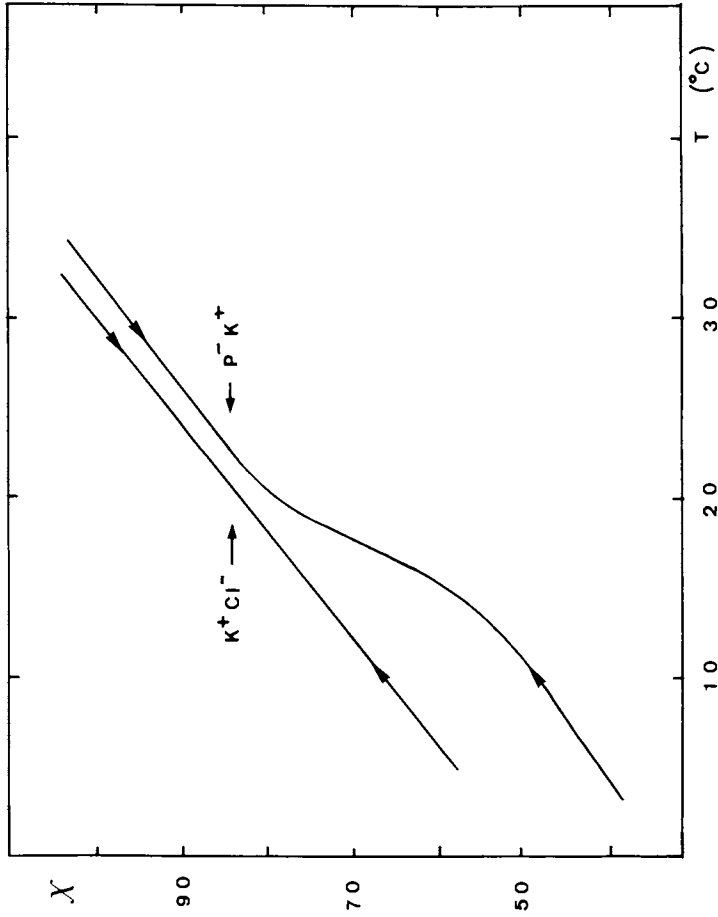


Figure 4A. Temperature dependence of conductivities χ (expressed in $\Omega^{-1} \cdot \text{cm}^{-1}$) for potassium κ -carrageenan in the absence of external salt and for potassium chloride. $C_p = 1.05 \times 10^{-2}$ equiv/L, $C_{KCl} = 0.65 \times 10^{-2}$ equiv/L.

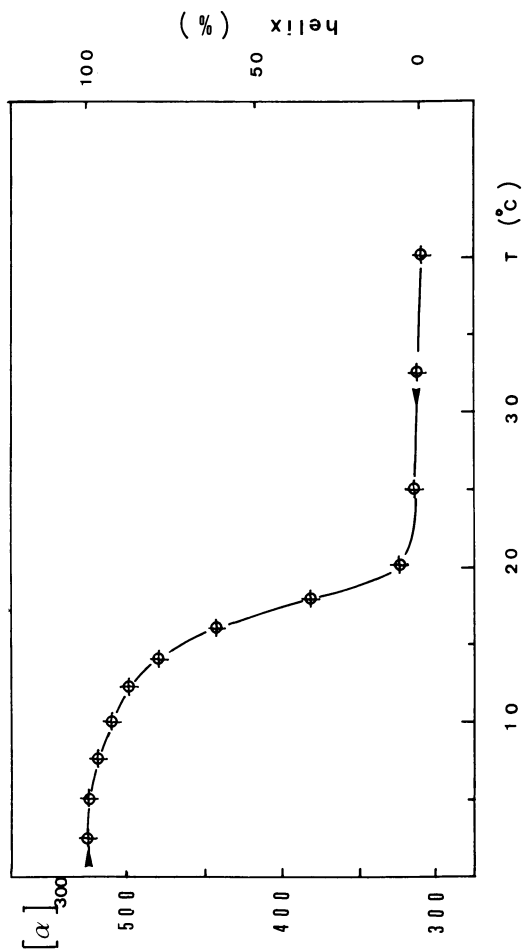


Figure 4B. Temperature dependence of specific rotation $[\alpha]_{300}$ and helix content (%) for potassium κ -carrageenan in the absence of external salt (O); helix content (%) calculated from the values of the ratio ρ of conductivities (+). $C_p = 1.05 \times 10^{-2}$ equiv/L; KCl, 0.65×10^{-2} equiv/L is used as the reference.

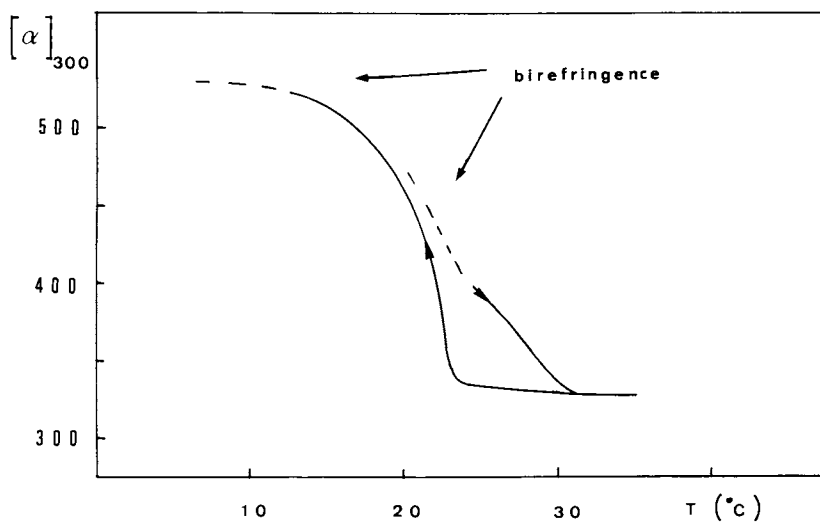


Figure 5A. Temperature dependence of specific rotation $[\alpha]_{300}$ of potassium κ -carrageenan in the absence of external salt $C_p = 1.79 \times 10^{-2}$ equiv/L.

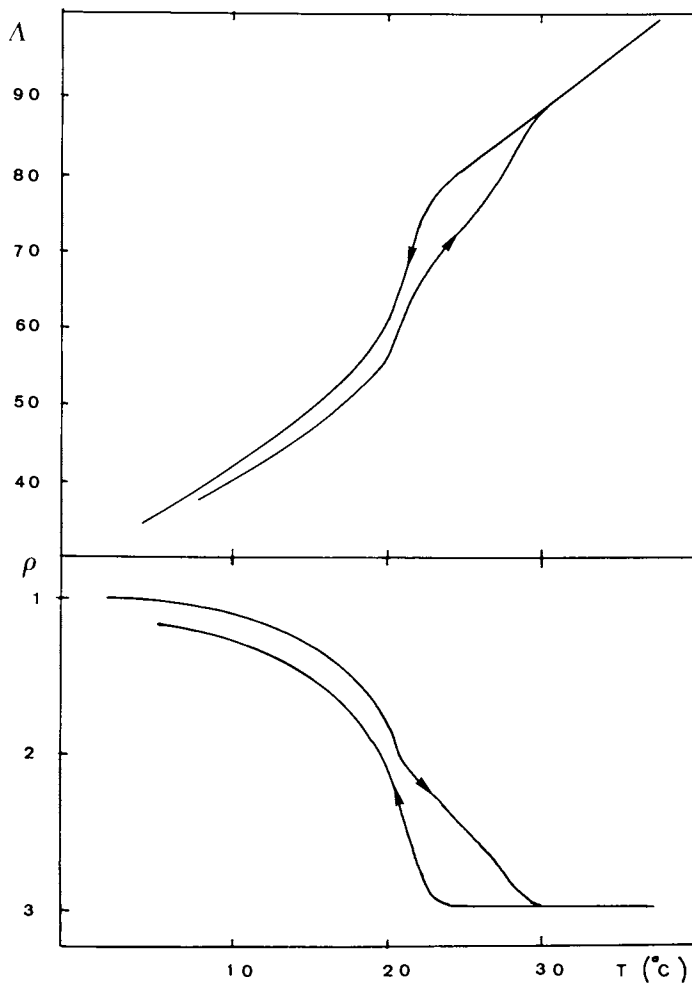


Figure 5B. Temperature dependence of equivalent conductivity Δ (expressed in $\Omega^{-1} \text{ cm}^2 \text{ equiv}^{-1}$) and ratio ρ of conductivities. $C_p = 1.79 \times 10^{-2} \text{ equiv/L}$; KCl , 10^{-2} equiv/L is used as the reference.

independence of ρ (in contrast to the conductivity, the ratio of two conductivities taken in the same range is about independent of the temperature). In addition the study of ρ demonstrates that for low temperature the rate of gel formation is small and that the conductivity remains lower for the heating than for the cooling cycle.

When the viscosity and the polymer concentration are lower ($C_p = 0.17 \cdot 10^{-2}$ eq/l ; $C_s = 0.9 \cdot 10^{-2}$ eq/l ; $C_T = 10^{-2}$ eq/l) the birefringence disappears and the gel formation is reversible within the time of the experiment ; also the temperature dependence of $[\alpha]_{300}$ and ρ are quite identical.

Similar types of curves are given for a "fresh" gel and a gel aged 15 hours at 21°C on Figure 7. The relative position and amplitude of both steps are modified by the ageing. Our interpretation of experimental curves (Figures 5, 6, 7) is as follows :

- When the gel is heated, first the isolated helical chains melt at a temperature T_{M1} ; in a second step, the aggregates of helical segments melt at a temperature T_{M2} . The weight fraction of isolated chains decreases during the ageing.

- When the gel is cooled, only one melting temperature is obtained near T_{M1} , with an initial increase of $[\alpha]$ which is abrupt than when the solution is heated. This temperature confirms the two-step mechanism of the heating curve, but when the sol is cooled, first the coil forms helical segments and immediately thereafter the helical segments gel.

Conclusion

In this work, optical rotation in dilute solutions of kappa carrageenans is used to interpret the activity coefficient of potassium counterions and to demonstrate a conformational transition associated with an increase of the charge parameter corresponding to a dimerization.

Above a critical ionic concentration a thermoreversible gel exists and a hysteresis of optical rotation and conductivity is present. When the rate of heating is low a two step mechanism for the gel melting is demonstrated by both methods. The relative importance of these steps is correlated to the ageing of the gel and thought to be due to the melting of isolated helical chains and aggregates of chains respectively. The melting temperature determined from the heating curve given in Figure 2 are mean values obtained for highest heating rate and are approximate. Accurate values of T_M computed from heating curves depend on a variety of experimental conditions including the heating rate, ageing of the gel and others.

In our opinion the new concept (3) of sol-gel transition given by Rees and coworkers is not enough to interpret the specific role of counterions in the double helix stabilization and consequently in the gel formation.

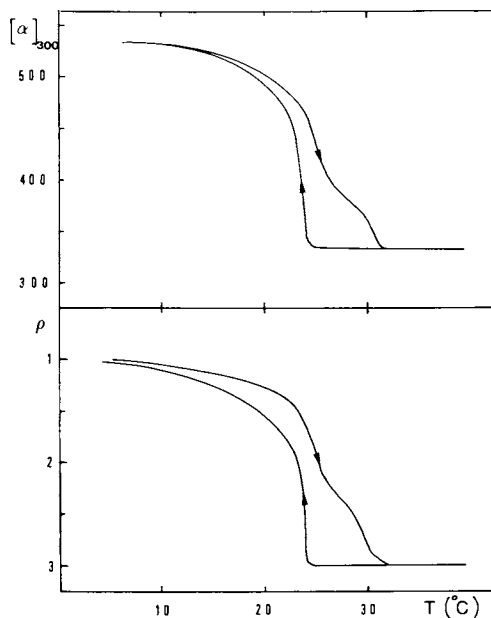


Figure 6. Temperature dependence of specific rotation $[\alpha]_{300}$ and ratio ρ of conductivities for potassium κ -carrageenan in the presence of KCl. $C_p = 0.179 \times 10^{-2}$ equiv/L, $C_s = 0.910 \times 10^{-2}$ equiv/L; KCl, 10^{-2} equiv/L is used as the reference.

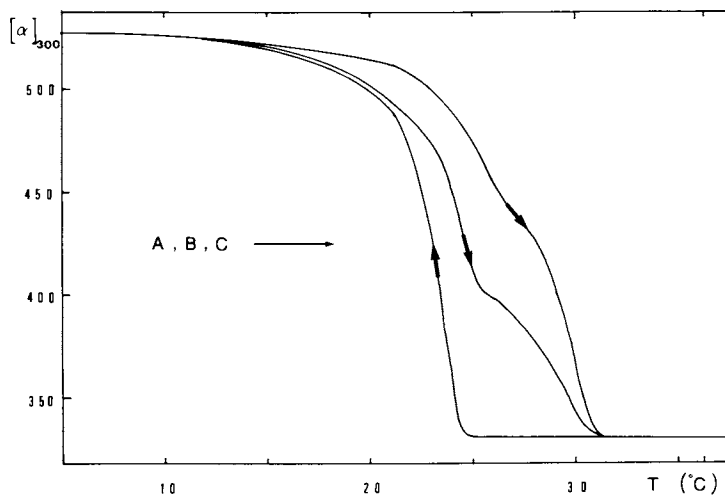


Figure 7. Temperature dependence of specific rotation $[\alpha]_{300}$ of potassium κ -carrageenan in the presence of KCl. $C_p = 0.179 \times 10^{-2}$ equiv/L; $C_s = 0.910 \times 10^{-2}$ equiv/L. (A) cooling curve; (B) heating curve (the heating is done directly after A); (C) heating curve after aging 15 h at 21°C after the melting.

Experimental

Materials. Kappa carrageenan, a copolymer of $\underline{0}$ - β -D galactopyranosyl-4-sulfate (1 \rightarrow 4)-0-3,6-anhydro- α -D-galactopyranosyl (1 \rightarrow 3) as confirmed by NMR spectroscopy (7) (Figure 1) was supplied by Sigma and used after purification. The aqueous solutions (10 g/l) were precipitated by ethanol in excess of salt (1M NaCl) and washed seven times with an ethanol water mixture (80/20 V/V). The sodium and potassium forms were obtained by exact neutralization of the acidic form by NaOH or KOH after percolation through an ion exchanger IR 120 H⁺. The experimental value of the capacity of the sodium form was $2.44 \cdot 10^{-3} \pm 0.02$ eq/l in good agreement with $2.45 \cdot 10^{-3}$ calculated from the molecular structure (equivalent weight 408).

Techniques. The specific rotation $[\alpha]_{300}$ was determined at 300 nm with a FICA Spectropol 1 spectropolarimeter in a 5 cm thermostated cell. Activities of potassium and sodium were determined with Tacussel ion-selective glass electrodes; a saturated calomel electrode was used as the reference. All e.m.f. measurements were made with a Tacussel Minisis 6000 pH-meter. A potential reading constant over a 20 min. period was regarded as a reliable e.m.f. Calibration curves were obtained using pure NaCl or KCl solutions before and after each set of measurements. The temperature control of all measurements was 0.01°C. Conductivity measurements were performed with platinized electrodes Tacussel CM 01 G and with a conductivity bridge Tacussel CD 78. A peculiarity of this bridge is its ability to measure the ratio between the conductivity of a sample and of a reference.

The temperature dependences of the specific rotation $[\alpha]_{300}$ and of the conductivities were performed with a constant cooling or heating rate of 17°C/h.

Literature Cited

1. Rochas, C. and Rinaudo, M., *Biopolymers* (1980) in press.
2. Milas, M. and Rinaudo, M., *Carbohydr. Res.* (1979) 76, 189-196
3. Morris, E.R., Rees, D.A. and Robinson, G., *J. Mol. Biol.* (1980) 138, 349-362.
4. Manning, G.S., *J. Chem. Phys.* (1969) 51, 924-933
5. Snoeren, T.H.N. Thesis (1976), Ede, (The Netherlands)
6. Bayley, S.T., *Biochem. Biophys. Acta* (1955) 17, 194-205.
7. Rochas, C., Rinaudo, M. and Vincendon, M., *Biopolymers* (1980) in press.

RECEIVED September 8, 1980.

Thermodynamics of Protonation and of Copper(II) Binding in Aqueous Alginate Solutions

Alginate Acid from *Azotobacter vinelandii*

S. PAOLETTI, A. CESÀRO, A. CIANA, F. DELBEN, and G. MANZINI
Institute of Chemistry, University of Trieste, Trieste, Italy

V. CRESCENZI

Institute of Physical Chemistry, University of Rome, Rome, Italy

The equilibrium properties in dilute aqueous solution of weakly ionized polysaccharides, e.g. carboxylated natural polysaccharides, have not been so thoroughly investigated in comparison with other natural and synthetic polyelectrolytes. For instance, a detailed thermodynamic characterization of acid ionization and of counterion binding in terms of combined experimental potentiometric, calorimetric and volumetric data has not been achieved so far for the above types of polysaccharides. Such a description, however, is of obvious relevance for a better understanding of structure-conformation dependent solution properties for this important class of biopolymers.

We wish to report here the results of a study on protonation equilibria and on copper(II) binding in aqueous alginate solution, performed using alginate acid from *Azotobacter vinelandii* (alginate S-35), whose solution properties have not as yet been studied in detail. Our data concern the changes in free energy, enthalpy (and entropy), as well as the volume changes associated with the uptake of protons or of Cu^{2+} ions, respectively, by alginate S-35 macroions.

Experimental

Materials. Alginate acid (sample S-35) produced by *Azotobacter vinelandii* (1) was a kind gift of Dr.K.C.Symes, Tate and Lyle

0097-6156/81/0150-0379\$05.00/0

© 1981 American Chemical Society

Limited, Reading, U.K. It was purified by dissolution in 0.05 M EDTA (0.2% polysaccharide) and centrifugation for two hours at 20,000 g. The supernatant was dialysed against 0.05 M EDTA and then exhaustively against pure water at 5°C. The intrinsic viscosity of the purified sample in 0.2 M NaCl at 25°C was 2.60 dl/g. For all measurements only freshly prepared solutions were used. Alginic acid concentration was determined by potentiometric titration with standard base using aliquots of stock alginate solutions, after conversion to free acid by passage through anion exchange column (H⁺-form). The titre of the solutions was also routinely determined by means of Na⁺ ion flame photometry. The results of the two methods agreed within experimental error (ca. 2% overall).

Copper(II) perchlorate was prepared by reaction of the carbonate with warm aqueous HClO₄. The resultant solution was filtered and cooled: the metal perchlorate precipitated was collected and recrystallized twice from water. The titre of the copper perchlorate solutions was determined using EDTA (2).

The equilibrium dialysis experiments were carried out using cellulose tubing (Union Carbide Co., Chicago, USA). Treatment of membranes prior to use has been previously reported (3). All the reagents used were C. Erba RP products of analytical reagent grade. HCl solutions employed both in calorimetry and in dilatometry were obtained by proper dilution of freshly prepared standard Normex 0.1N HCl solutions. The water employed had a specific conductivity of ca. $10^{-6} \Omega^{-1}\text{cm}^{-1}$. It was obtained by an all-glass deionizer-bidistillator.

Methods. Dilatometric measurements were performed using Carlsberg dilatometers (4). Both the procedure and the treatment of data have already been described (3). The n-heptane employed as dilatometric liquid was a C. Erba RP product: it has been purified as reported elsewhere (5). The thermostat bath in which the dilatometers were suspended has already been described (6); constancy of temperature was better than $\pm 0.001^\circ\text{C}$.

The potentiometric measurements, under N₂ flux, were performed as previously described (7). Similarly, the execution of the experiments and the treatment of the calorimetric data were the same as already described in detail elsewhere (7).

The equilibrium dialysis measurements were performed by introducing 2 ml of 1.2×10^{-3} M sodium alginate (in 0.05 M NaClO₄) and 2 ml of Cu(ClO₄)₂ at various concentrations (in 0.05 M NaClO₄) into the two compartments of each dialysis vessel. In all cases dialysis equilibrium was reached in about 2 days (at 25°C) and the concentration of copper(II) in both compartments was determined.

Copper concentrations as low as 10^{-5} M were determined adding a constant excess of EDTA sodium salt and measuring the absorbance at 270 nm, using as reference a solution of EDTA at the same concentration. In the absence of other divalent cations the method proved reproducible within $\pm 2\%$ and the absorbance followed the

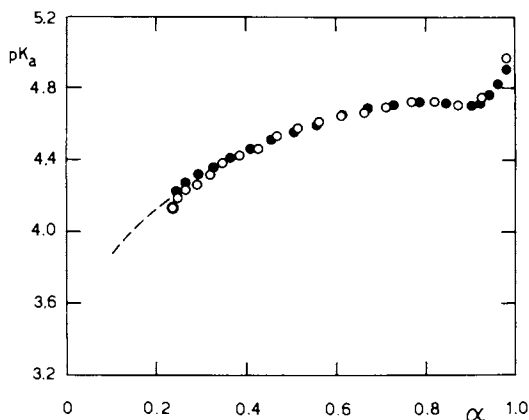


Figure 1. Apparent pK_a dependence on α for alginic acid S-35 in aqueous solution at 25°C, titrated with KOH (○) and NaOH (●) respectively; polymer concentration, 10^{-3} equiv/L.

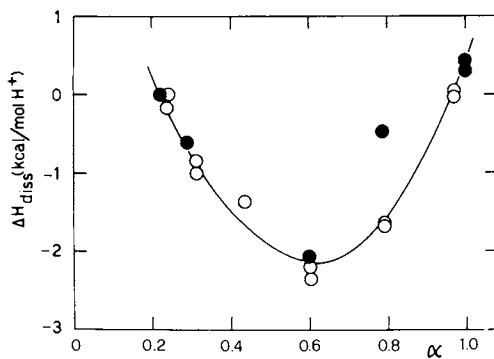


Figure 2. Enthalpy change (kilocalories/mole H^+) on proton dissociation of alginic acid S-35, partially neutralized with KOH (○) and NaOH (●) in water at 25°C; polymer concentration, 10^{-3} equiv/L.

Lambert-Beer law up to 5×10^{-4} M. The resulting absorption coefficient was $3.5 \times 10^3 \text{ M}^{-1} \text{ cm}^{-1}$ at 270 nm (the wavelength of maximum absorption being 260 nm).

Results and Discussion

1) Protonation equilibria. The potentiometric titration data are reported in Figure 1 as a plot of $\text{pK}_a (\equiv \text{pH} + \log \frac{1-\alpha}{\alpha})$ against the degree of ionization, α . Alginate S-35 in water is a weak polyacid, comparatively weaker than structurally similar polysaccharides (8,9). However, it appears feasible to extrapolate the experimental curve of Figure 1 so that the pK_0 value common to those alginates from other sources is attained for $\alpha = 0$ (9). The calorimetric data given in Figure 2 show that the enthalpy of dissociation, ΔH_{diss} , of alginic acid S-35 is always negative (except for $\alpha \approx 1$) with a distinct minimum at around $\alpha = 0.6$ of about $-2.2 \text{ kcal/mol H}^+$ (at 25°C). Considering together the potentiometric and calorimetric data one can readily estimate that the entropy of ionization, $\Delta S_{\text{diss}} (= \frac{\Delta H_{\text{diss}}}{-2.3 \text{ RpK}_a})$, is always negative with a minimum value of about -28 e.u. at $\alpha = 0.6$, while it is about -22 e.u. for α approaching unity.

In other words, the ΔH_{diss} and ΔS_{diss} values at near half neutralization happen to fall in their respective normal ranges found for other polycarboxylates (10) as well as for monomeric carboxylates (11); on the contrary the upturn of both ΔH and ΔS at higher α values seems somewhat anomalous. Indeed the potentiometric data also seem to disclose a somewhat anomalous behavior in the same range of high α values. These observations might be related to the ionization of configurationally different $-\text{COOH}$ groups which, progressively, could bring about some conformational perturbation along the alginate chains.

More remains to be learned with the aid of different techniques on the causes, presumably conformational ones, contributing to the overall, peculiar trend of both thermodynamic state functions with changing α from 0 to unity for our alginate sample.

On the other hand, the dilatometric data reported in Figure 3 do show that the volume change on dissociation of alginic acid S-35 is simply a linear function of α . This behavior, rather uncommon for a polyelectrolyte, demonstrates that dissociation of ionizable groups along alginate chains takes place without any interference among the hydration sheaths of such groups. From our data one can in fact characterize alginate S-35 with just one value for the differential volume of dissociation, i.e. : -11.5 cm^3 per mole of carboxyl groups (slope of the plot of Figure 3).

In conclusion, if a pH-induced conformational change is a possible qualitative explanation of the potentiometric data, such a change would have no bearing on the solvation of alginate S-35. It has to be pointed out, moreover, that the ionization behavior

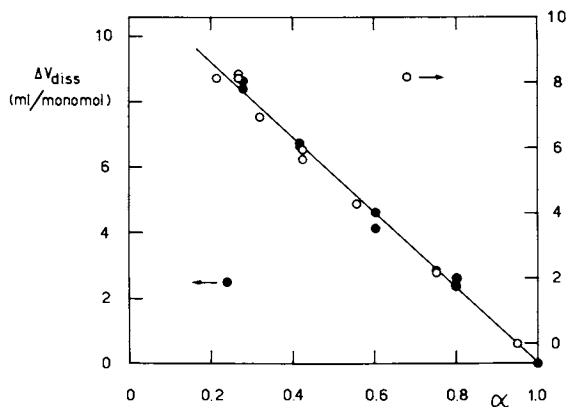


Figure 3. Volume change in milliliters/equivalent on proton addition to the K^+ (○) (ordinate right) and Na^+ (●) (ordinate left) salt forms, respectively, of alginic acid S-35 in water at 25°C; polymer concentration, 2×10^{-3} equiv/L in the former case and 2.5×10^{-3} equiv/L in the latter one. The abscissae are to be read from the right to the left.

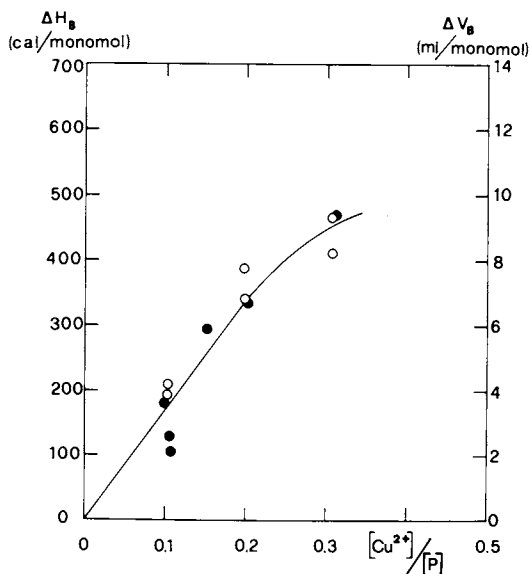


Figure 4. Enthalpy changes (●) (left scale) in calories per mole of the polymer repeating unit, and volume changes (○) (right scale) in milliliters per mole of the polymer repeating unit, on the addition of $Cu(ClO_4)_2$ to the sodium salt form ($\alpha = 1.0$) of alginic acid S-35 in 0.05M $NaClO_4$ at 25°C. $[Cu^{2+}]/[P]$ stands for the molar ratio of the total copper(II) to the polymer repeating unit.

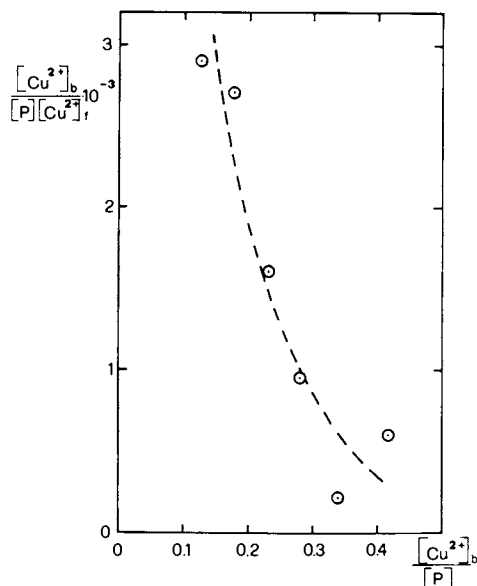


Figure 5. Scatchard plot from equilibrium dialysis measurements for the binding of Cu^{2+} onto sodium alginate S-35 in 0.05M NaClO_4 at 25°C . Polymer concentration, $[P]$, was 1.2×10^{-3} equiv/L. $[\text{Cu}^{2+}]_b$ and $[\text{Cu}^{2+}]_f$ stand for bound and free copper molar concentrations, respectively.

of this polycarboxylate does not depend at all on whether counterions are Na^+ or K^+ ions (see Figures 1-3).

II) Binding of Cu^{2+} ions. The results of the calorimetric experiments on the interaction of Cu^{2+} (added $\text{Cu}(\text{ClO}_4)_2$) with aqueous sodium alginate (in 0.05 M NaClO_4 solution) are reported in Figure 4.

The calorimetric data, expressed in calories per stoichiometric equivalent of polyelectrolyte, ΔH_B , as a function of the stoichiometric $[\text{Cu}^{2+}]/N$ ratio (moles of copper(II) per equivalent of alginate in solution), show that ΔH_B is always positive and steadily increases with increasing added Cu^{2+} ion concentration.

The dilatometric results shown in Figure 4 collected under experimental conditions identical to the calorimetric ones, demonstrate that there is a net volume increase upon binding of Cu^{2+} ions by sodium alginate. Finally, a few equilibrium dialysis data are reported in Figure 5 in the usual Scatchard-plot form.

From the latter data it is possible to estimate a value of 4.10^3 (1/equiv) for the apparent equilibrium constant of Cu^{2+} binding, on the hypothesis that it simply involves one fixed alginate charge per Cu^{2+} ion bound and no interdependence between binding sites. Consequently, one also estimates that $\Delta G_B = -4.9$ (kcal per mole of binding reaction), and that in the calorimetric and dilatometric experiments at, say, $[\text{Cu}^{2+}]/N = 0.05$ more than 90% of the Cu^{2+} ions present in solution are linked to alginate chains.

Deriving from the limiting slopes of the plots of Figure 4 the differential enthalpy ($\Delta \bar{H}_B$) and the differential volume ($\Delta \bar{V}_B$) of binding, respectively, one then finds: $\Delta \bar{H}_B = 2$ kcal, and $\Delta \bar{V}_B = 39 \text{ cm}^3$, always per mole of copper bound. Also: $\Delta \bar{S}_B = 23$ e.u. (per mole of complex).

In conclusion, it clearly appears that Cu^{2+} ions are extensively bound by alginate S-35 and that the process is entirely entropy driven. The link between the changes in $\Delta \bar{V}_B$ and $\Delta \bar{S}_B$ may be readily, although qualitatively, established assuming, in analogy with similar evidence for other polycarboxylates (3), that interaction between $-\text{COO}^-$ groups and Cu^{2+} ions loosens a relatively large number of water molecules from the solvation shells of both ionic species, thus producing a net gain of molecular degrees of freedom in the system. This occurs at $[\text{Cu}^{2+}]/N$ ratios not higher than about 0.4, inasmuch as relatively higher Cu^{2+} ion concentrations lead to gel formation and hence to systems intractable with our experimental approaches. It will be interesting to make a comparative analysis of the thermodynamic solution properties of alginate samples of different origin containing different proportions of mannuronic and guluronic acids as well as of the parent homopolymers. Work is now under way along these lines in our laboratory.

Acknowledgements. This work has been carried out with financial support of the Italian Consiglio Nazionale delle Ricerche, C.N.R.

Literature cited

1. Sandford, P.A. and Laskin, A., Eds. "Extracellular Microbial Polysaccharides"; ACS Symp. 45, American Chemical Society : Washington, D.C., 1977; p.14.
2. Flaschka, H. Mikrochemie, 1952, 39, 38.
3. Crescenzi, V.; Delben, F.; Paoletti, S.; Skerjanc, J. J.Phys. Chem., 1974, 78, 607.
4. Linderstrøm -Lang, K. and Lanz, H. Comp.Rend.Trav.Lab.Carlsberg, Sez.Chim., 1938, 21, 315.
5. Katz, S. and Ferris, T.G. Biochemistry, 1966, 5, 3246.
6. Delben, F. La Chimica & l'Industria, in press.
7. Fenyo, J.C.; Delben, F.; Paoletti, S.; Crescenzi, V. J.Phys. Chem., 1977, 81, 1900.
8. Mandel, M. J.Polymer Sci., A-2, 1970, 8, 1841.
9. Haug, A. Acta Chem.Scand., 1961, 15, 950.
10. Crescenzi, V.; Delben, F.; Quadrifoglio, F.; Dolar, D. J.Phys. Chem., 1973, 77, 539.
11. Delben F. and Crescenzi, V. J.Sol.Chem., 1978, 7, 597.

RECEIVED August 26, 1980.

Ion-Polyion Interactions in Chondroitin Sulfate Solutions

H. MAGDELENAT—Service de Radiopathologie, Institut Curie, 26, rue d'Ulm, 75005 Paris, France

P. TURQ—Laboratoire d'Electrochimie, Université P. et M. Curie, 4, place Jussieu, 75230 Paris, France

P. TIVANT and M. DRIFFORD—Laboratoire de Spectroscopie Optique, C.E.N. Saclay, 91190 Gif-sur-Yvette, France

The Nernst-Einstein relationship (1),

$$U^\circ / D^\circ = Z_s e/kT \quad (1)$$

relates the electrical mobility U° and the self-diffusion coefficient D° of an ionic species in solution through the structural charge Z_s (e = elementary charge, kT = Boltzman factor). It allows the determination of the structural charge of individual species such as simple or complex ions, since the transport parameters, U° and D° can be obtained experimentally, for instance with radioactive tracers (2). This relationship is strictly valid only in the limit of infinite dilution, i.e., in the absence of interactions between the ionic species. In the presence of such interactions, for instance in semi-dilute solutions, one can however define the apparent charge, Z_{ap} , by the following equation :

$$Z_{ap} = (U/D) (kT/e) \quad (2)$$

where U and D are the observed transport parameters. In many cases Z_{ap} is a good approximation to the effective charge (2).^{ap} It is the aim of this presentation to show how the determination of U , D , and subsequently Z_{ap} , reflects the nature and the extent of ion-polyion

interactions in aqueous solutions with or without added salts.

Theoretical Background.

In the frame of electrochemistry, polyelectrolytes are defined as macromolecular structures bearing a great number of charged sites. We consider the case where these sites are similar in nature (negative in most biological polyelectrolytes such as DNA, RNA or sulfated polysaccharides), so that the polyelectrolyte, or polyion, acquires a high charge density. Counterions are present in solution in order to maintain electro-neutrality or as constituents of an added simple salt which, in turn, introduces a co-ion.

The transport parameters U and D of the different ionic species in the polyelectrolyte solution depend both on the equilibrium properties and on specific effects which appear in relation with the motion of ions, i.e., "relaxation" and "electrophoresis".

Ion-polyion interactions and equilibrium properties. The high charge density of the polyion gives polyelectrolyte solutions their unique properties :

a) electrostatic repulsion between charged sites gives the polyion an extended conformation at low or semi-low ionic strength. The polyion can thus be considered as almost linear, at least over a distance of several charged sites.

b) consequently, the excess free energy (of electrostatic origin) can be derived -and subsequently all the equilibrium properties, from a cylinder, or rod-like, or linear chain model of distribution of charges, by solving a Poisson-Boltzmann equation with cylindrical symmetry for the potential.

The central parameter of modern polyelectrolyte theories is ξ_s , the linear charge density parameter in the model of Manning (3):

$$\xi_s = e^2 / \epsilon kTb \quad (3)$$

where ϵ = dielectric constant and b = axial distance between charged sites.

When ξ_s is sufficiently high, condensation of counterions on the polyion should be observed, and is effectively observed, so that ξ is reduced to $[z_i]^{-1}$, z_i being the valence of the counterion (3). The residual charge of the polyion is a fraction of the structural charge Z_s ,

$$\text{with } a = (\xi_s z_i)^{-1} \quad (4)$$

The above expressions apply to polyions with univalent charged sites. In the absence of added salt a is also the fraction f of counterions which are not condensed onto the polyion. The observed transport parameters for the counterions should therefore be the fraction-averaged mean of the transport parameters of the uncondensed (u) and condensed (c) entities.

$$\left[\frac{D}{U} \right] = f \cdot \left[\frac{D}{U} \right]^{(u)} \cdot A(\xi, r_i) + (1-f) \left[\frac{D}{U} \right]^{(c)} \quad (5)$$

Ion-polyion interactions and transport properties.

Relaxation effect. In equation (5), $A(\xi, r_i)$ represents the correction for relaxation. The relaxation effect is due to the temporary asymmetry of the ionic atmosphere around a given ion. The electric field which appears from charge separation slackens the motion of the ion. $A(\xi, r_i)$ has been calculated by Manning for polyelectrolyte solutions (4). Only at zero or low added salt concentration can $A(\xi, r_i)$ be significantly lower than 1.

Electrophoretic effect. It is due to the mutual hydrodynamic transmission of velocity between moving ions.

Material and Method.

The polyion. Chondroitin sulfate was elected for this work because of its biological interest: it is the main component of cartilage and plays a role in biological calcification and retention of multivalent cations (see paper by Rosenberg, this symposium)

Chondroitin sulfate (ChSO_4) is a polymer of glucuronic acid and glucosaminosulfate with two isomeric positions for the sulfate group (Fig. 1). We have mostly worked with the 4-isomer.

It is an adequate model of polyelectrolyte with relatively high charge density. It is almost linear in solution as shown by electron microscopy (5) or by physico-chemical determinations (6).

The average distance between charged sites can be estimated to be near 6 Å, which makes ξ_s about 1.2. As a comparison with other biological anionic polysaccharides, hyaluronic acid is less charged ($b \approx 20$ Å) while heparin is more ($b \approx 3 - 4$ Å).

The molecular weight of the polyion is 29-30,000 Daltons leading to a structural charge of about -120 and a contour length of about 600 Å. However, the

polyion is not exhaustively sulfated and Z_s is about -100 .

The self-diffusion coefficient and electrical mobility of the polyion (in excess sodium salt)₂ are respectively 34 ± 0.4 Ficks and $(5.7 \pm 0.5) 10^{-4} \text{ cm}^2 \text{ s}^{-1} \text{ V}^{-1}$.

Transport parameter measurements.

Transport parameters of small counterions were measured by radioactive tracer methods, the labeled ionic species moving amidst a chemically homogeneous solution :

- self-diffusion, by the "open and capillary" method described previously (7,8)
- electrical mobility, by electrophoresis on cellulose acetate strips (9).

Transport parameters of the macromolecular ionic species were measured by dynamic light scattering :

- apparent diffusion coefficient was derived from the broadening of the Rayleigh diffusion line measured by homodyne or heterodyne optical beating (10). If Γ is the linewidth of the power spectrum of Rayleigh diffusion, and k the modulus of the associated wave vector, $k = (2\pi n/\lambda_0) \sin(\theta/2)$, then :

$$\Gamma = D_t k^2 .$$

- the electrical mobility of the macroion is proportional to the shift of the heterodyne power spectrum in the presence of an external electric field (10). The optical mountings have been described previously (11,12).

Results.

We define r_i as the ratio of equivalent concentration $z_i n_i$ of the added counterion i of charge z_i to the equivalent concentration of the polyion n_e ($r_i = Z_i n_i / n_e$).

Transport parameters of counterions.

One counterion species : Figure (2) shows that the self-diffusion coefficient of Na^+ in chondroitin sulfate salt solution, D_{Na^+} , is lowered from its value in absence of polyelectrolyte ($D_{\text{Na}^+} = 133$ Ficks) to a little less than 100 Ficks in the absence of added NaCl ($r_i = 0$). Since half of this 30 percent decrease can be accounted for by the relaxation effect, it means that around 15 percent of the polyion charge is neutralized by condensed Na^+ ions. This is in agreement with the predicted lowering of ξ from $\xi = 1.2$ to $\xi_{\text{ef}} = 1 = [Z_i]^{-1}$. No significant specific effect, as regards condensation, was observed neither between Na^+

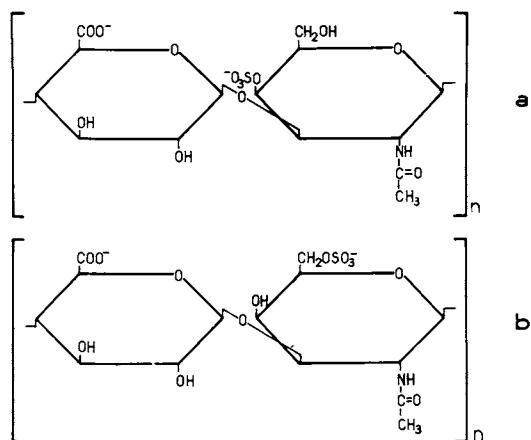


Figure 1. *Chondroitin sulfate: (a) Isomer 4; (b) Isomer 6.*

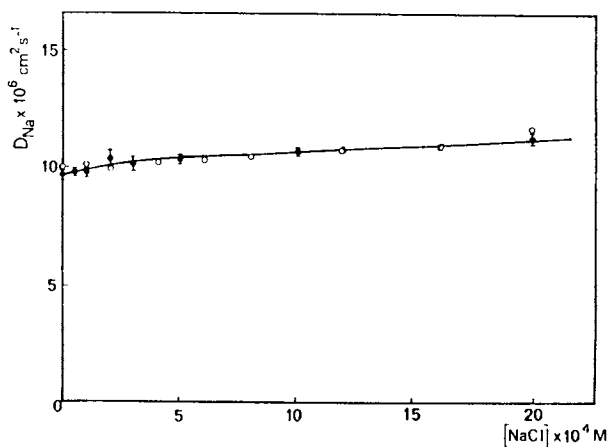


Figure 2. *Variation of D_{Na^+} when NaCl is added to: (1) $ChSO_4-Na$ (●); (2) $ChSO_4-N(CH_3)_4$ (○) ($n_e = 3.4 \times 10^{-3}$ equiv/L).*

and $N(CH_3)_4^+$ (Fig.2), nor between Na^+ and Cs^+ (Fig.3).

The variation of U_{Na^+} , the electrical mobility of Na^+ in chondroitin sulfate solutions where NaCl is added is quite similar to that of D_{Na^+} (Fig.2). The apparent charge for Na^+ equation (2) is always close to 1 (Table I).

Counterions with different charges. If we add divalent cations, like Ca^{2+} , Sr^{2+} or Co^{2+} to $ChSO_4$ -Na solutions, ξ_{ef} being initially 1 and $Z_i = 2$, condensation of M^{2+} occurs in order to lower ξ_i . The observed transport parameters, D_M and U_M , should be as low as the transport coefficients of the polyion. This is almost true for D_M (Fig.4) and it can be derived that up to about 50 percent of the polyion charge can be neutralized when sufficient divalent cations are added. No significant specific effect is observed between the three divalent counterions (Fig. 4 and reference (12)).

Figure 5 shows the variation of U_{Co} when $CoCl_2$ is added to $ChSO_4$ -Na. The curves for U_{Sr} and U_{Ca} are quite similar. They all show an anionic behavior at low added salt concentration, so that an anionic apparent charge is observed, which becomes positive and tends toward + 2 in excess added salt (Table II).

However the apparent charge of the counterions at low added salt is not as negative as expected, since it should be close to the charge of the polyion (about -100). Therefore some degrees of freedom remain for the cations which are allowed to move rapidly along the polyion. Indeed n.m.r. experiments have shown, at least for cobalt, that less than 40 percent of the condensed ions are site-bound (13).

We have also shown previously (12) by measuring D_{Na^+} when $CaCl_2$ is added to $ChSO_4$ -Na that the small fraction (15 percent) of the sodium ions initially condensed are expelled from the condensation layer by the newly condensing Ca^{2+} ions, which can be expected from Manning's theory.

On the contrary, that an excess of monovalent ions can compete with condensed divalent ones is out of the range of validity of Manning's model. However, the model of Iwasa (13) which introduces an entropic term contributing to the free energy of polyelectrolyte systems can explain that an excess NaCl displaces condensed divalent counterions. In the experiment described in Fig. 6, NaCl was added to a solution of chondroitin sulfate containing Sr^{2+} counterions, a fraction of which are condensed. The variation of D_{Sr} shows that Sr^{2+} are "decondensed" by an excess NaCl, in good agreement with Iwasa's model.

TABLE I

Apparent charge of Na^+ in $\text{ChSO}_4\text{-Na}$ solutions with added NaCl

r_{Na^+}	D_{Na^+} ($10^{-7} \text{ cm}^2 \text{ s}^{-1}$)	$U_{\text{Na}^+}/U_{\text{Cl}^-}$	Z_{Na^+}
0	100	0.50	0.90
0.25	104	0.55	0.92
0.5	110	0.58	0.97
1	115	0.60	1.00

$r_{\text{Na}^+} = n_s/n_e$; $U_{\text{Na}^+}/U_{\text{Cl}^-}$: observed electrical mobility of Na^+ relative to that of Cl^- in $\text{ChSO}_4\text{-Na}$ solutions; Z_{Na^+} = apparent charge of Na^+

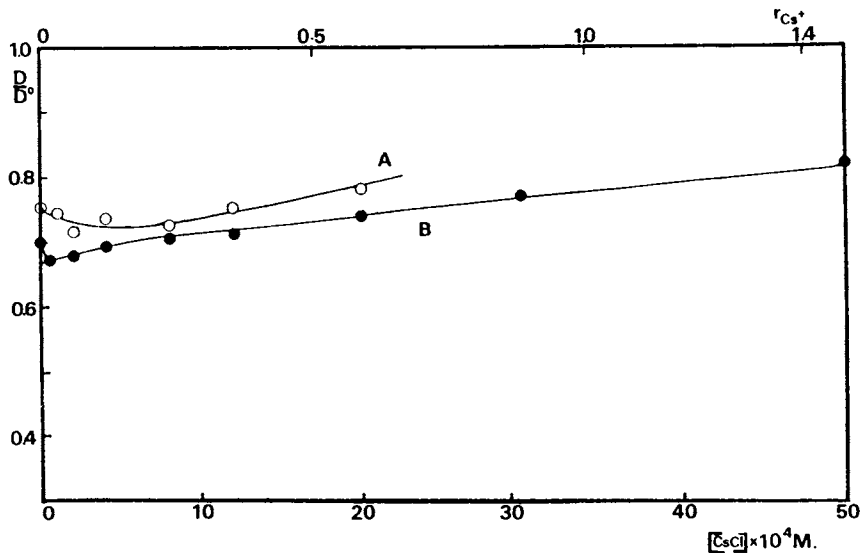


Figure 3. Variation of D/D° for Na^+ (A) and Cs^+ (B) when CsCl is added to $\text{ChSO}_4\text{-Na}$.

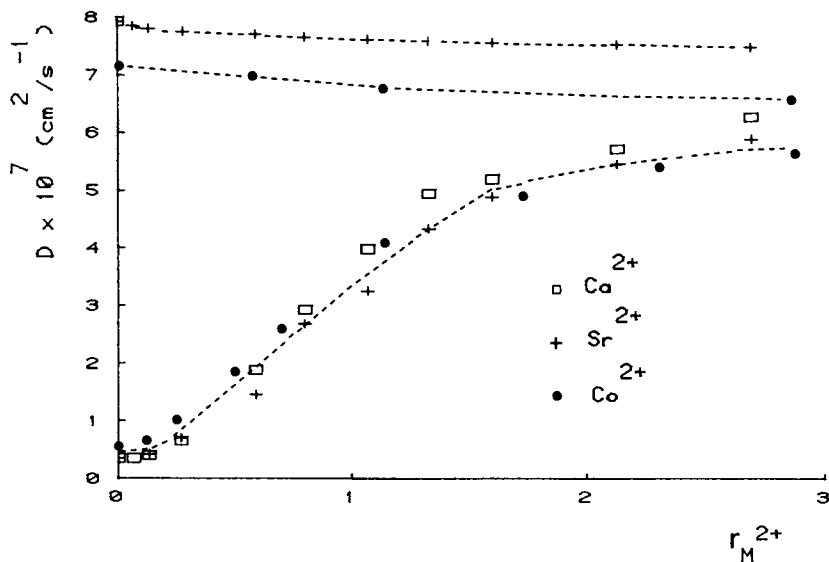


Figure 4. D of Ca^{2+} , Sr^{2+} , Co^{2+} counterions on adding CaCl_2 , SrCl_2 , or CoCl_2 ($r_M^{2+} = 2n_s/n_e$). Upper lines refer to the variation of D of Sr^{2+} (+) and Co^{2+} (●) in the absence of polyelectrolyte.

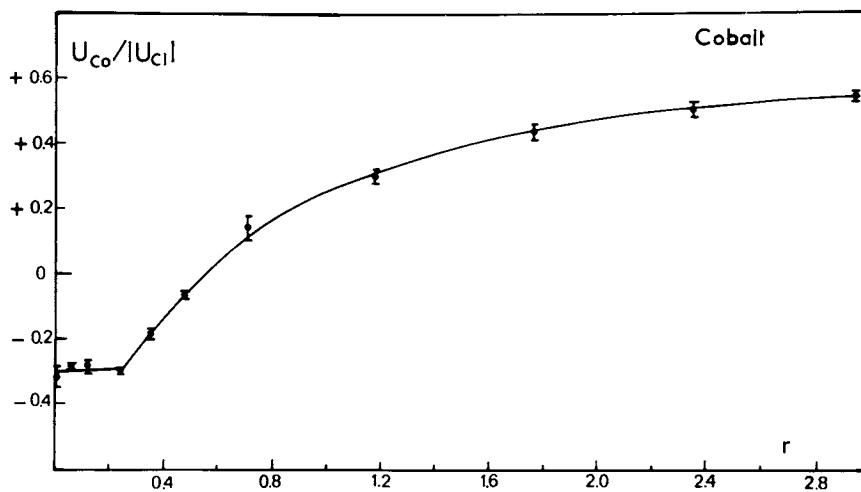


Figure 5. Variation of \bar{U}_{Co} (relative to the electrical mobility of Cl^-) when CoCl_2 is added to $\text{ChSO}_3\text{-Na}$

TABLE II

Apparent charges Z_{ap} of the divalent counterions Ca^{2+} , Sr^{2+} and Co^{2+} in $CH_2P(SO_3^-)_2Na$ solutions ($n_e = 5.4 \cdot 10^{-3} \text{ eq/l}$) as a function of their concentration ($r_i = 2n_i/n_e$). $Z_{M^{2+}}$ is the apparent charge of the cations in the absence of polyelectrolytes, at ionic strengths corresponding to r_i .

r_i	Apparent charge Z_{ap}				
	Ca^{2+}	Sr^{2+}	Co^{2+}	$Z_{M^{2+}}$	$n_s \times 10^{-4} M$
0	- 7.1	- 3.5	- 12	2.00	0
0.18	- 4.5	- 2.3	- 10	1.94	5
0.25			- 6		
0.36	- 1	- 1.2	- 4.5	1.90	10
0.55	+ 0.52	+ 0.50	+ 0.9	1.88	15
0.72	+ 1.40	+ 1.45	+ 1.1	1.86	19.5
0.88	+ 1.40	+ 1.60	+ 1.50	1.85	24
1.40	+ 1.60	+ 1.56	+ 1.80	1.81	38
1.84	+ 1.63	+ 1.54	+ 1.95	1.78	50
2.25	+ 1.64	+ 1.55	+ 1.95	1.75	60
2.58	+ 1.67	+ 1.55	+ 1.96	1.72	70
2.94	+ 1.70	+ 1.54	+ 1.99	1.70	80
3.68	+ 1.75	+ 1.49	-	-	100

Trivalent counterions such as La^{3+} , added to $\text{ChSO}_4\text{-Na}$, do not condense since ξ_{ef} is initially equal to $1/4$ and should be lowered to the critical value of $1/3$ in the presence of trivalent cations. Results published previously (12) clearly showed that up to about 70 percent of the polyion charge could be neutralized by La^{3+} ions. La^{3+} ions not only competed with Na^+ ions but also with Ca^{2+} or Sr^{2+} ions and the agreement with Manning's model was fairly good. It is a general observation that the higher the counterion charge, the better Manning's model fits the data concerning condensation. Indeed more anionic values than for divalent counterions were obtained (2) for the electrical mobilities of La^{3+} ions in the presence of $\text{ChSO}_4\text{-Na}$ ($Z_{\text{ap}} = -13$ for La^{3+} at low added LaCl_3 concentration compared to $Z_{\text{ap}} = -7$ for Ca^{2+}) indicating a more rigid condensation layer.

Trivalent counterions added to $\text{ChSO}_4\text{-Ca}$ solutions were also shown to condense (12) so that ξ_{ef} , which is initially equal to $1/2$ ($Z_{\text{Ca}} = 2$), is lowered to $\xi_{\text{ef}} = 1/3$ in the presence of trivalent counterions. On addition of LaCl_3 , the Ca^{2+} ions which are initially condensed (about 40 percent of the stoichiometric concentration) are expelled from the condensation layer as was shown by an increase of D_{Ca} (12).

Transport parameters of the polyion

Transport parameters of the polyion itself will be affected by two types of ion-polyion interactions :

Condensation, which reduces significantly the effective charge of the polyion and hence, its electrical mobility. Condensation should be less sensitive to the self-diffusion coefficient unless great conformational variation results from charge modification.

Electrokinetic effects, i.e. interactions between the polyion and its ionic atmosphere, since counterions cannot move independently from the polyion, in order to maintain electroneutrality. These effects are highly dependent on the ionic strength of the solutions and affect both self-diffusion and electrical mobility as measured by dynamic light scattering since they give rise to long-range spatial correlations between ions. These effects are expected to be larger in dilute solutions because of the large relative fluctuations there.

The variation of the translational diffusion coefficient measured at 20°C by homodyne detection at angles from 5° to 40° of $\text{ChSO}_4\text{-Na}$ when the ionic strength is

increased by addition of NaCl is reported in Table III. Figure 7 represents the experimental variation (lower values, \square) together with other values derived from three models, assuming an effective charge of the polyion $Z_{ef} = -88$. ($\text{ChSO}_4\text{-Na} : 10\text{g/l}$).

- \square : the model of Stephen (14) where the fluctuations of the macroions are the only ones to be taken into account gives :

$$D_t = D_P \left(1 + \frac{Z_{ef}}{1 + 2r} \right) \quad (6)$$

where D_P is the self-diffusion coefficient of the polyion and $r = n_s/n_e$ is the ratio of the equivalent concentration of the added salt to that of the polyion.

- Δ : the model of Turq (11, 15), where the fluctuations of the three components of the system are considered. This model leads to the following expression for D_t (11) :

$$D_t = \frac{(Z_{ef} + 1 + 2r) D_P D_1 D_2}{(Z_{ef} + 1 + r) D_P D_1 + (Z_{ef} + r) D_P D_2 + (Z_{ef} + 2r) D_1 D_2} \quad (7)$$

D_1 and D_2 are the self-diffusion coefficients of the counterion and the coion respectively.

- \bullet : a model of screened charge, that we propose originally here (15). The two preceding models based on the Debye-Onsager treatment of ion transport, consider the entire charge of the polyion to be concentrated in a point charge. This is totally misleading since the length of the polyion chain can be one hundred times that of the Debye-screening length (K^{-1}) at such ionic strengths. We propose that the effective charge of the polyion Z_{ef} be replaced in equation (7) by a screened charge, Z_D , of the form :

$$Z_D = \frac{1 + e^{-Kb}}{1 - e^{-Kb}} \quad (8)$$

b being the distance between charged sites and K the Debye screening parameter. Each unit charge on the polyion chain, at a distance nb from a central charge, contributes to this central charge by a screening factor e^{-Knb} so that the sum of contributions gives equation (8). In order to maintain the total concentration, n_e must be replaced by $n'_e = n_e Z_{ef} / Z_D$ in equation (7).

The agreement of this model with the experimental values is much better than by the other models.

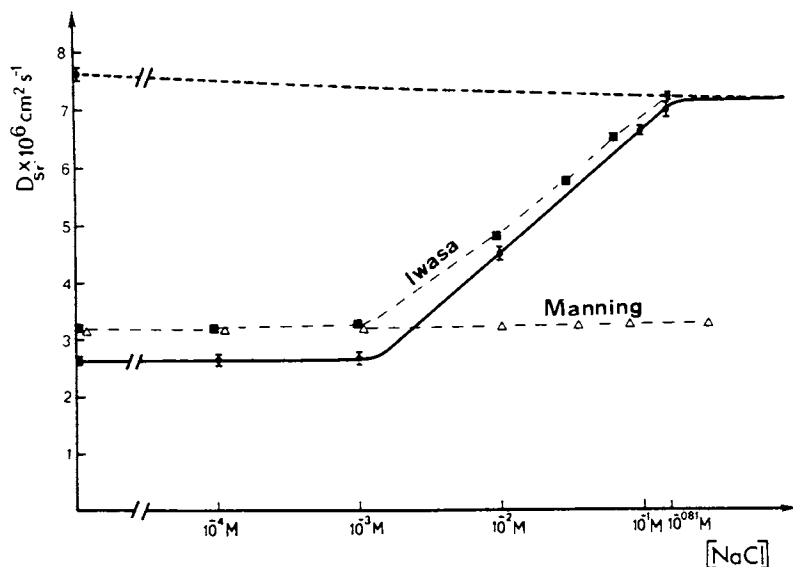


Figure 6. Substitution of Sr^{2+} ions condensed on $ChSO_4-Na$ by a large excess of Na^+ ions ($n_e = 1.7 \times 10^{-3}$ equiv/L; $r_{Sr^{2+}} = 0.7$).

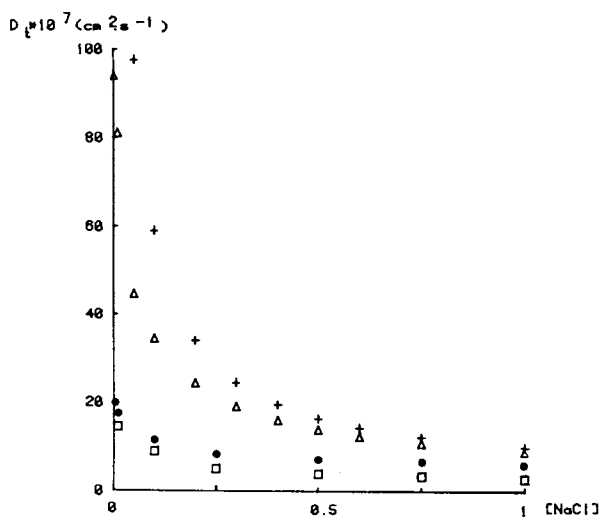


Figure 7. Variation of D_t of $ChSO_4-Na$ with added $NaCl$ concentration

The variation of the electrical mobility of ChSO_4^- measured by dynamic light scattering (heterodyne detection at an angle of 5°), is reported in Figure 8. The mobility decreases with the first addition of NaCl, then keeps a constant value from $2 \cdot 10^{-3}$ to 10^{-2}M added NaCl. The initial value is compatible with an effective charge of the polyion $Z_{\text{ef}} = -42$ (corresponding to a structural charge $Z = -50$). The initial decrease can be described by the Gorin-Henry model (16) for the electrical mobility of cylindrical macroions according to :

$$U = \frac{2 Z_{\text{ef}}}{\pi n l} \frac{1}{F} \left(\frac{K_0(K_a)}{K_a K_1(K_a)} + \ln \frac{a+r}{a} \right) \quad (9)$$

where a is the radius of the cylinder

l its length

r the hydration radius of the counterion (1.5 \AA)

K_0 et K_1 the zeroth and first order solutions of the modified Bessel function (17)

F : Henry's factor

$$K = \left(\frac{8 \pi N e}{1000 \epsilon k t} \right)^{1/2} \cdot \sqrt{I}, \quad I \text{ being the ionic strength.}$$

The best fit is obtained for values of $l : 300 \text{ \AA}$

$a : 25 \text{ \AA}$

$Z_{\text{ef}} : -50$

The leveling of the experimental values at higher ionic strength can be ascribed to a conformational change of the macromolecule, the polyion being less and less rigid and getting a more and more spherical conformation when the ionic strength increases.

Conclusion

From the experimental results that we have just presented, which were obtained by various independent techniques, it is obvious that electrostatic interactions have a predominant influence on ion-polyion interactions in aqueous solutions. This influence is exerted at three different levels :

1) Coulombic forces give rise, in ionic systems involving species with high charge densities, to short range interactions such as condensation in the sense of Manning and to long range interactions in the sense of Debye-Huckel. This leads to a separation of the counterions into two types :

- free counterions interacting only weakly with the polyion through long range Debye-Huckel interactions.

TABLE III

Variation of $D_t(\text{ChSO}_4\text{-Na})$ with the ionic strength :

$[\text{NaCl}] :$	10^{-2}	$5 \cdot 10^{-2}$	10^{-1}	0.25	0.5	0.75	1
D_t (Ficks)	14.5	9.4	8.9	5.0	4.0	3.5	3.4

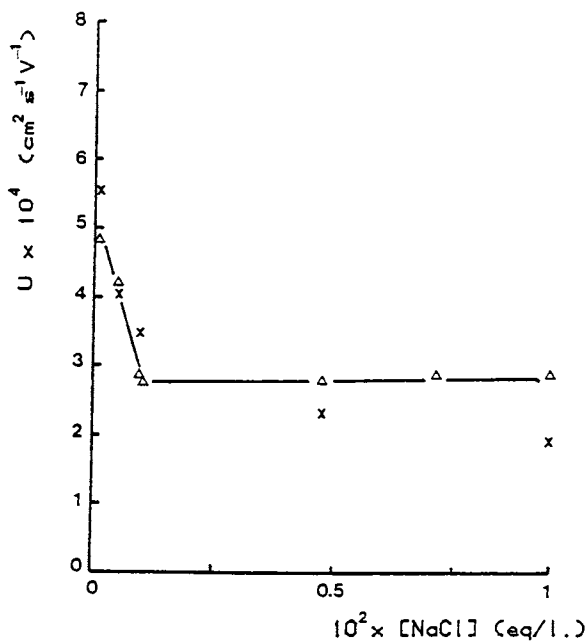


Figure 8. Variation of the electrical mobility of $\text{ChSO}_4\text{-Na}$ (1.5 g/L) with added NaCl concentration: (Δ) experimental values; (\times) values derived from Equation 9.

- condensed counterions, entrapped in the close atmosphere of the polyion, some of them being site-bound (as seen by n.m.r.), the other moving freely along the polyion.

These short range interactions are mostly evidenced by the variation laws of transport coefficients of the counterions while the long range interactions affect the electrical mobility of the polyion, as measured by dynamic light scattering.

2) The electroneutrality states that negative and positive charges cannot be macroscopically separated ; this leads to great variations between macroscopic transport parameters and individual ion transport parameters. Such effects appears significantly at low ionic strength. The case of the translational diffusion coefficient of $\text{ChSO}_3^- \text{Na}^+$ as measured by dynamic light scattering illustrates the amplitude of the variation and the need for new theoretical approach.

3) Ionic strength is responsible for conformational effects, the screening of coulombic repulsion between charged sites on the polyion leading to less extended conformation.

All these effects have to be considered when interpreting equilibrium properties or irreversible phenomena of polyelectrolyte solutions.

Abstract

The charge effects on ion-polyion interactions in chondroitin-sulfate solutions were studied by both tracer and dynamic light scattering techniques. The experimentally available quantities are therefore the transport coefficients of both counterions and polyions. The tracer techniques have provided the self-diffusion coefficients (D) and electrical mobilities (U) of counterions. The dynamic light scattering techniques with or without an applied electric field lead to the self-diffusion coefficient (D) and to the electrical mobility (U) of the polyion itself. An extensive use of the Nernst-Einstein relation expressed as $Z = (U/D) \cdot (e/kT)$ provides the apparent charges of the different ionic entities in solutions of mixtures of chondroitin sulfate with different added salts. The effects of counterion condensation are separated from those due to electroneutrality conditions and long range Coulomb interactions, especially for the polyion.

Literature Cited .

- 1 . Robinson, R.A.; Stokes, R.H. "Electrolyte Solutions" Butterworths : London, 1970.
- 2 . Magdelénat, H.; Turq, P.; Tivant, P.; Chemla, M.; Menez, R.; Drifford, M. J. Chem. Educ., 1978, 55, 12-17. Apparent ionic charge in electrolyte and polyelectrolyte solutions.
- 3 . Manning, G.S. J. Phys. Chem., 1969, 51, 924-933. Limiting laws and counterion condensation in polyelectrolyte solutions. I Equilibrium properties.
- 4 . Manning, G.S. J. Phys. Chem. ,1969, 51, 934-938 . Limiting laws and counterion condensation in polyelectrolyte solutions .II Self-diffusion of the small ions.
- 5 . Thierry, J.P. Personal communication.
- 6 . Tanaka, K. J. Biochem., 1978, 83, 647-653 & 655-659. Physicochemical properties of chondroitin sulfate. I Ion binding and secondary structure.
- 7 . Anderson, J.S.; Saddington, K. J. Chem. Soc., 1949, Sup 2, 381-386. The use of radioactive isotopes in the study of the diffusion of ions in solution.
- 8 . Magdelenat, H.; Turq, P.; Chemla, M. Biopolymers, 1974, 13, 1535-1548. Study of the self-diffusion coefficients of cations in the presence of an anionic polysaccharide.
- 9 . Magdelénat, H.; Turq, P.; Chemla, M.; Para, B. Biopolymers, 1976, 15, 175-186. Electric mobility of bivalent cations in the presence of an anionic polysaccharide.
- 10 . Berne, B.J.; Pecora, R. "Dynamic Light Scattering" John Wiley & sons :New York, 1976.
- 11 . Gouesin-Menez, R. "Applications de la diffusion quasi-élastique de la lumière à l'étude des propriétés dynamiques de macromolécules chargées", Thesis, Paris, 1979.

- 12 . Magdelénat, H.; Turq, P.; Tivant, P.; Chemla, M.; Menez, R.; Drifford, M. Biopolymers, 1979, 18, 187-201. The effect of counterion substitution on the transport properties of polyelectrolyte solutions.
- 13 . Tivant, P.; Turq, P.; Magdelénat, H.; Spegt, P.; Weill, G. Biopolymers, 1979, 18, 1849-1857. Condensation of Co^{2+} ions on chondroitin sulfate from transport coefficients and protons NMR measurements in aqueous solutions.
- 14 . Stephen, M.J. J. Chem. Phys., 1974, 61, 1598-1599. Doppler shifts in light scattering from macroion in solution.
- 15 . Tivant, P.; Turq, P.; Drifford, M.; Magdelénat, H.; Menez, R. submitted to Biopolymers.
- 16 . Abramson, H.A.; Gorin, M.H.; Moyer, L.S. Chem. Rev., 1939, 24, 345-366.
- 17 . Abramovitz, M.; Stegun, I.A. "Handbook of Mathematical functions", Dover : New York, 1965.

RECEIVED October 21, 1980.

The Charge Fraction of Ionic Polysaccharides

PAUL ANDER

Department of Chemistry, Seton Hall University, South Orange, NJ 07079

Equations are derived from the Manning theory of polyelectrolyte solutions that permit the calculation of the charge fraction of ionic polysaccharides using experimental counterion and coion diffusion coefficients. Results are reported for the sodium salts of heparin, dextran sulfate, alginate and the calcium salt of heparin.

The properties of biological polyelectrolytes in solution depend on the charge fraction of the polyelectrolyte, i.e., the fraction of stoichiometric charge on the polyelectrolyte uncompensated by bound counterions. The Manning theory of polyelectrolyte solutions emphasizes that counterion condensation onto the polyelectrolyte occurs for polyelectrolytes with $\xi > \xi_c$, where $\xi = e^2/\epsilon kTb$, b is the average axial distance between charges on the polyelectrolyte and $e^2/\epsilon kT$ is the Bjerrum length, with $\xi_c = |z_1|^{-1}$, z_1 being the charge on the counterion (subscript 1).¹⁻⁴ More recently, Manning has extended his theory to include those counterions that are "territorially bound" or trapped in the domain of the polyelectrolyte, but are somewhat free to move along the polyanion.⁵ Counterions that are neither condensed site-bound nor territorially-bound are in the ion atmosphere, along with the coions, if simple salt is added. The idea of counterion condensation has recently received substantiation from theoretical investigations of the Poisson-Boltzmann equation for polyelectrolyte solutions.^{6,7}

Since ionic polysaccharides are stiffer than most synthetic polyelectrolytes, they were thought to be appropriate experimental models to test theories based on cylindrical symmetry. Systematic determinations of counterion and coion diffusion coefficients and activity coefficients have been made in the presence of ionic polysaccharides; these measurements pertain to the interaction of small ions in the ionic atmosphere with the polyelectrolyte. Here, results are presented for estimating the fraction of ions dissociated from the ionic polysaccharide in simple salts solutions,

0097-6156/81/0150-0405\$05.00/0
© 1981 American Chemical Society

including the sodium salts of heparin, dextran sulfate and algin and the calcium salt of heparin. The results for heparin and dextran sulfate are compared with those for sodium polystyrene-sulfonate, whose charge densities are comparable.

Experimental: The determination of small ion tracer diffusion coefficients and the ionic polysaccharides employed have been discussed elsewhere.^{8,9,10}

Results and Discussion: Manning's formulation treats all uncondensed counterions and all coions in the Debye-Hückel approximation. In order to be correlated to Manning's theory, the experimental data ought to be extrapolated to zero concentration of all ionic species because the theory yields limiting laws. If one denotes z_p as the valence of a charge site on the polyion, $(z_1)_p$ as the valence of the counterion originally present with the polyion prior to the addition of salt, and $(z_1)_s$ and $(z_2)_s$ as the valences of the counterions and coions provided by the added salt, respectively, then in the common counterion case, where the added counterion and counterion originally present are the same, the Manning theory yields^{1,2,3}

$$D_i/D_i^0 = f_i [1 - z_i^2 A(\xi_c, \xi^{-1}X)/3] \quad (1)$$

where f_i is a condensation term which is unity for coions and for counterions it is

$$f_i = (\xi_c \xi^{-1}X + 1)/(X + 1) \text{ for } \xi > \xi_c \quad (2)$$

with

$$A(\xi, X) = \sum_{\substack{m^2 \rightarrow \infty \\ m^2 + n^2 = 0}}^{\infty} \sum_{\substack{n^2 \rightarrow \infty \\ m^2 + n^2 = 0}}^{\infty} [\pi(\xi z_p)^{-1}(m^2 + n^2) + |z_1|_p + (|z_1|_s + |z_2|_s)X^{-1}]^{-2} \quad (3)$$

with $X = n_p/n_s$, the ratio of the normality of polyelectrolyte to the molarity of simple salt.

It will now be shown how counterion and coion diffusion results can be used to estimate the degree of dissociation of a polyelectrolyte if the experimental diffusion coefficients approximate those predicted from the Manning theory. The Manning theory gives

$$(D_{Na^+}/D_{Na^+}^0) = f_{Na^+}^u [1 - A(1, \xi^{-1}X)/3] \quad (4)$$

$$(D_{Cl^-}/D_{Cl^-}^0) = 1 - A(1, \xi^{-1}X)/3 \quad (5)$$

and

$$(D_{\text{SO}_4^{2-}}/D_{\text{SO}_4^{2-}}^0) = 1 - 4A(1, \xi^{-1}X)/3 \quad (6)$$

where $f_{\text{Na}^+}^u$ is the fraction of sodium ions in the solution which are condensed. The fraction of sodium ions which are condensed is $f_{\text{Na}^+}^c = 1 - f_{\text{Na}^+}^u$ and rearranging eqs 4, 5 and 6,

$$f_{\text{Na}^+}^c = 1 - \frac{(D_{\text{Na}^+}/D_{\text{Na}^+}^0)}{(D_{\text{Cl}^-}/D_{\text{Cl}^-}^0)} \quad (7)$$

and

$$f_{\text{Na}^+}^c = 1 - \frac{(D_{\text{Na}^+}/D_{\text{Na}^+}^0)}{3 + (D_{\text{SO}_4^{2-}}/D_{\text{SO}_4^{2-}}^0)} \quad (8)$$

where it is understood that both diffusion ratios appearing are to be determined at the same X value. As rn_p equivalents of Na^+ of the total $(n_p + n_s)$ equivalents of Na^+ presumed bound, one has

$$f_{\text{Na}^+}^c = rn_p / (n_p + n_s) = rX / (X + 1) \quad (9)$$

Counterion condensation onto polyelectrolytes has been operationally defined as association such that the total fraction of polyion sites compensated for with counterion remains invariant over a wide range of X values. If the interaction of Na^+ with polyelectrolytes is properly described as "counterion condensation", then a plot of $f_{\text{Na}^+}^c (X + 1)$ vs. X should be linear with slope r . Note that this would indicate that the fraction of sodium ions dissociated from the polyelectrolyte is constant and independent of the concentrations of polyelectrolyte and of simple salt. It is clear that r is the fraction of the condensed or bound Na^+ ions which are originally on the polyelectrolyte and $(1-r)$ is the charge fraction of the polyelectrolyte.

The sodium ion diffusion ratios $D_{\text{Na}^+}/D_{\text{Na}^+}^0$ in aqueous Na_2SO_4 solutions are compared to the results predicted from the Manning theory. Since the molecular weight of heparin is rather low (about 12,000), its diffusion constant was approximated from Ca^{+2} ion diffusion results⁸, where the heparin diffusion coefficient is that of $D_{\text{Ca}^{+2}}$ for $X > 5$ because the added tracer calcium ion is condensed onto the heparin by exchanging with condensed sodium ion. Note in Figure 1 that better accord with theory is obtained when the solid Manning line is rectified for the heparin diffusion. Figure 2 shows that the Manning theory (solid line) predicts the chloride ion diffusion coefficients over the whole concentration range of heparin and of sodium chloride.⁸ It has been shown¹¹ that the counterion diffusion coefficient is independent of the

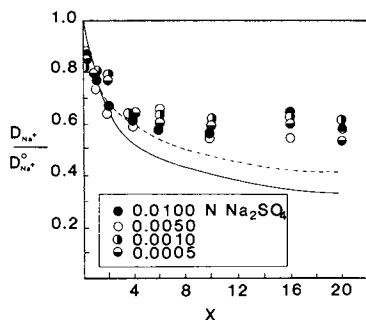


Figure 1. Sodium ion diffusion ratio in aqueous sodium heparin solutions containing sodium sulfate. The theoretical solid line is rectified to account for the diffusion of heparin to give the broken line (8).

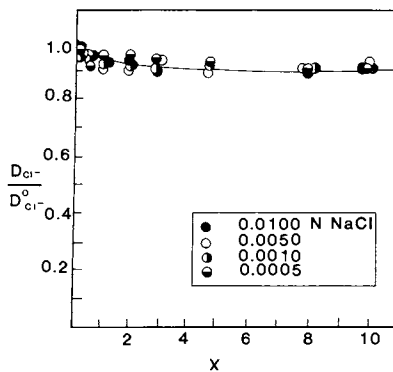


Figure 2. Chloride ion diffusion ratio in aqueous sodium heparin solutions containing sodium chloride. The solid line is predicted from the Manning theory (8).

Table I. A Comparison of the Experimental Charge Fraction with Those Predicted from the Manning Theory for Several Ionic Polysaccharides

	Ξ	Slope	Charge Fraction	
			$(l - r)$	$(z_i \Xi)^{-1}$
Sodium Heparin	3.0	0.43 ± 0.01	0.43	0.33
Sodium Dextran Sulfate	2.9	0.65 ± 0.02	0.35	0.34
Sodium Polystyrenesulfonate	2.6	0.66 ± 0.01	0.34	0.38
Sodium Alginate	1.4	0.36 ± 0.02	0.64	0.70
Sodium DNA ¹⁰	4.2	0.61 ± 0.05	0.39	0.24
Calcium Heparin	3.0	0.41 ± 0.03	0.18	0.17
Calcium DNA ¹⁰	4.2	0.43 ± 0.04	0.14	0.12

nature of the coion. Using the data for $D_{Na^+}/D_{Na^+}^0$ and $D_{SO_4^{2-}}^0 - 2/D_{SO_4^{2-}}^0 - 2$ for sodium heparin, $f_{Na^+}^c$ was calculated from eq 8 and a plot was made using eq 9, which is shown in Figure 3. The line in Figure 3 was drawn visually through the origin and the slope r given in Table 1, was computed from the points only. The experimental charge fraction $(1-r)$ for sodium heparin of 0.43 is in good agreement with the theoretical charge fraction $(z_1 \xi)^{-1}$ of 0.33 considering the corrections employed for the polyelectrolyte diffusion.

From the data for sodium dextran sulfate in 0.0005N Na_2SO_4 in reference 8 and using eqs 8 and 9, $f^c(1 + X)$ was plotted against X . The resulting linearity gave a slope of 0.65 ± 0.02 , which is the fraction of sites on sodium dextran sulfate having bound sodium ions. The charge fraction on 0.35 is in excellent agreement with the theoretical value of 0.34, as is listed in Table 1. Note that the linearity shown in Figures 1 and 2 indicate that the charge fraction of each polysaccharide is a constant value and independent of the ionic strength of the solution. It was of interest to compare these results with those obtained for a synthetic polyelectrolyte of comparable charge density. The reported diffusion results¹¹ for sodium polystyrenesulfonate of $\xi = 2.61$ in 0.001N NaCl and eqs 7 and 9 gave the linear plot of $f^c(1 + X)$ vs. X shown in Figure 3. The slope of 0.66 ± 0.01 results in a charge fraction of 0.34, which compares excellently with the theoretical value of 0.38. Then the charge fraction of polyelectrolytes as calculated from tracer diffusion results and the Manning theory appear to be constant, independent of ionic strength and depend only on the linear charge density parameter ξ . A similar treatment was tried using the data for sodium alginate, an ionic polysaccharide of lower charge density ($\xi = 1.43$) and whose ionic moieties are carboxyl groups compared to a mixture of sulfate and carboxyl groups on heparin and sulfate groups on dextran sulfate. Using the diffusion data in reference 9 for sodium alginate in 0.0005N NaCl for $X < 5$ and eqs 7 and 9, a plot of $f^c(1 + X)$ vs. X gave linearity with a slope of 0.36 ± 0.02 . The excellent agreement between the calculated charge fraction 0.64 and the theoretical one of 0.70 gives more credence to this method for determining the charge fraction of polyelectrolytes.

As Ca^{+2} ion is added to a polyelectrolyte in the Na^+ form, Ca^{+2} ion exchanges for the condensed Na^+ and the diffusion coefficient and the diffusion coefficient of Ca^{+2} , $D_{Ca^{+2}}$, is that of the polyelectrolyte. This exchange takes place until all the condensed Na^+ ions are replaced by the added Ca^{+2} ions. Because Ca^{+2} ion is now the counterion, $\xi (= |z_1|^{-1})$ changes from unity to $1/2$ at $X_c = 4\xi/(2\xi-1)$ and more Ca^{+2} can condense to reduce the charge density parameter to its effective value of $1/2$, which occurs at $X_{lc} = 2\xi/(\xi-1)$. As more Ca^{+2} ion is added, $X_c + 2 (= X)$ is decreased and the condensation term in the $D_{Ca^{+2}} + 2/D_{Ca^{+2}}^0$ expression is dominant over the Debye-Huckel term giving¹⁰ an important feature of the theoretical lines which is experimentally verified,

Figure 3. $f^c(1 + X)$ vs. X for sodium heparin

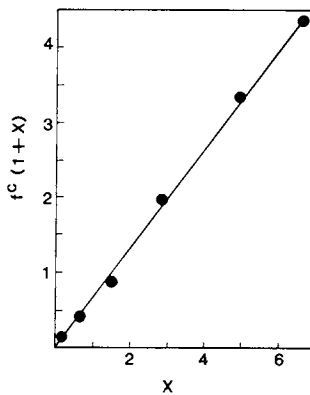
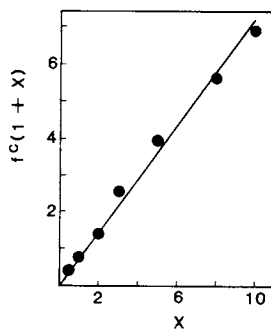


Figure 4. $f^c(1 + X)$ vs. X for sodium dextran sulfate



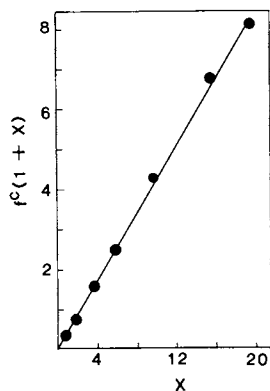


Figure 5. $f^c(1 + X)$ vs. X for sodium polystyrenesulfonate

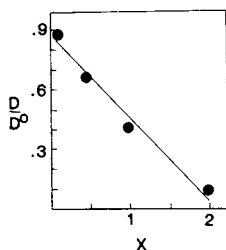


Figure 6. $D_{Ca^{2+}}/D_{Ca^{2+}}^0$ vs. X for sodium heparin, where X is the ratio of equivalents of polyelectrolytes to $CaCl_2$ molarity, i.e. $X = X_{Ca^{2+}} = n_p/n_s$

the linearity at low $X_{Ca^{2+}}$. At low $X_{Ca^{2+}}$ only the condensation term contributes significantly and one has

$$D_{Ca^{2+}}/D_{Ca^{2+}}^0 = [(X_{Ca^{2+}})_{lc} - X_{Ca^{2+}}]/(X_{Ca^{2+}})_{lc} \quad (10)$$

Of the n_p polyion "sites" available, let r be compensated with calcium, then

$$r_{Ca^{2+}}^c = rn_p/n_{Ca^{2+}} = rX_{Ca^{2+}}/2 \quad (11)$$

but from eq 11 one has

$$r_{Ca^{2+}}^c = X_{Ca^{2+}}/(X_{Ca^{2+}})_{lc} \quad (11)$$

Upon comparing eqs 12, 11 and 10, one notes that a low $X_{Ca^{2+}}$, the absolute value of the slope of the plot $D_{Ca^{2+}}/D_{Ca^{2+}}^0$ vs. $X_{Ca^{2+}}$ is equal to one half the fraction of sites compensated with calcium. The linearity of Figure 6 means that r is essentially independent of $X_{Ca^{2+}}$ at low $X_{Ca^{2+}}$, in the limit of infinite dilution. One obtains a slope of -0.41 ± 0.03 , which gives $r = 0.82$. The experimental charge fraction of 0.18 compares favorably with the theoretical value of 0.17. Not only does calcium heparin at low $X_{Ca^{2+}}$ values follow the counterion condensation concept defined by Manning, but so does CaDNA¹⁰, listed in Table 1, obtained using the same method. From the laser light scattering measurements Magdelanat et al.^{12,13} found excellent agreement between the charge fractions for the Na^+ , Ca^{2+} and La^{3+} salts of chondroitin sulfate ($\xi = 1.15$) and those predicted from the charge fraction rule of Manning.

Counterion binding to polyelectrolytes appear to be adequately accounted for in the operationally defined condensation term in the Manning theory. However, there are some experimental results that indicate that counterion binding may be present for polyelectrolytes where $\xi < \xi_c$,^{14,15} which is contrary to the Manning interpretation.

Acknowledgement: The author is grateful to Mr. Rosario Trifiletti and Dr. Marie Kowblansky for persuading him that the calculation of the charge fraction presented is sound. This project was partially supported by Grant No. GM21234, awarded by The Public Health Service.

References and Notes

- (1) G. S. Manning, J. Chem. Phys., 51, 924 (1969).
- (2) G. S. Manning, J. Chem. Phys., 51, 934 (1969).
- (3) G. S. Manning in Polyelectrolytes, E. Selegny, Ed., D. Reidel Publishing Co., Dodrecht, Holland, 1974.
- (4) G. S. Manning, Q. Rev. Biophys., 2, 179 (1978).
- (5) G. S. Manning, Acc. Chem. Res., 12, 443 (1979).
- (6) N. Yoshida, J. Chem. Phys., 69, 4867 (1978).
- (7) M. Gueron and G. Weisbuch, Biopolymers, 19, 353 (1980).
- (8) P. Ander, G. Gangi, and A. Kowblansky, Macromolecules, 11, 904 (1978).
- (9) A. Kowblansky, R. Sasso, V. Spagnuola, and P. Ander, Macromolecules, 10, 78 (1978).
- (10) R. Trifiletti and P. Ander, Macromolecules, 12, 1197 (1979).
- (11) M. Kowblansky and P. Ander, J. Phys. Chem., 80 297 (1976).
- (12) H. Magdelenat, P. Turq, P. Tivant, R. Menez, M. Chemla and M. Drifford, Biopolymers, 18, 187 (1979).
- (13) H. Magdelenat, P. Turq, P. Tivant, M. Chemla, R. Menez and M. Drifford, J. Chem. Educ., 55, 12 (1978).
- (14) Y. M. Joshi and J. C. T. Kwak, J. Phys. Chem., 83, 15 (1979).
- (15) P. Ander and L. Leung-Louie, to be published.

RECEIVED September 22, 1980.

Solution Properties of Dextran and Its Ionic Derivatives

KUNIIHIKO GEKKO

Department of Food Science and Technology, Faculty of Agriculture,
Nagoya University, Nagoya 464, Japan

Dextran, an anhydroglucose polymer consisting mainly of α -1,6-glucosidic linkages, has been used as a blood plasma volume expander and as a useful material for partition of biological materials in aqueous polymer two-phase systems and Sephadex gel chromatography. Ionic dextran derivatives, too, are known to have some important medical applications, e.g., dextran sulfate is a good anti-coagulant for blood. Their solution properties and interactions with proteins have been a matter of concern to many investigators, since such studies should present basic information for understanding the mechanism of these medical functions and for developing new applications for these products.

The present paper is devoted to a discussion of some physico-chemical solution properties of dextran and its ionic derivatives and focusses on the following two subjects: (1) the molecular weight dependence of dextran-water interactions in the transition region from oligomer to polymer and (2) the effects of the nature and degree of substitution of ionic or hydrophobic groups in ionic dextran derivatives on their interaction with water and metal ions. Dextran with 96% α -1,6-linkage (Meito Sangyo Co., Ltd. Nagoya), produced by *Leuconostoc mesenteroides* N-4, was used in these experiments. This material was hydrolyzed by acid and then fractionated by a fractional precipitation or solubilization method (1). Dextran with molecular weight of $4-5 \times 10^4$ was modified by introducing some ionic groups to different extents. The structure of the dextran derivatives used is illustrated in Figure 1.

I. Solution Properties of Oligodextran

What is the minimum degree of polymerization necessary for dextran to exhibit properties characteristic of a typical polymer? This question should be resolved by examining the molecular weight dependence of its solution properties, although this may be subject to the limitation that native dextran is not a linear polymer but a branched one. The optical rotation data in Figure 2 demonstrate the transition from oligomer to polymer around the

0097-6156/81/0150-0415\$06.00/0
© 1981 American Chemical Society

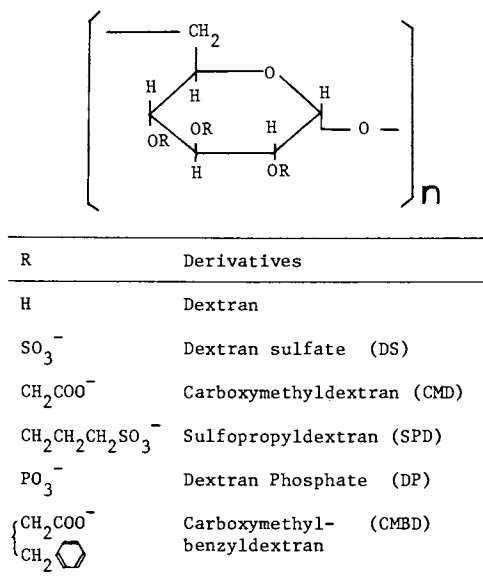


Figure 1. Structure of ionic dextran derivatives. The abbreviated sample names in the parenthesis will be used in the following discussion.

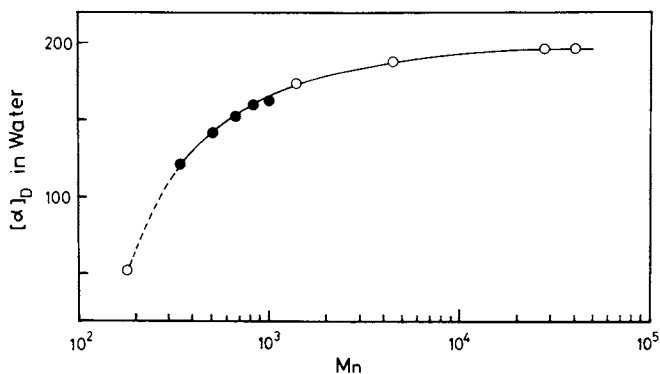


Figure 2. Molecular-weight dependence of the optical rotation of dextran. Data shown by (●) are taken from Turvey and Whelan (2).

molecular weight of a few thousand although a critical molecular weight cannot be definitely identified. For amylose the critical point in $[\alpha]_D$ is known to exist at degree of polymerization, $n=7$ (3). With these ideas in mind, some dextran solution properties have been examined in the transition region from oligomer to polymer.

(A) Viscosity. The intrinsic viscosity of low molecular weight dextrans with $410 < M_n < 32,100$ was measured in six solvents (water, formamide, dimethylformamide/water mixtures, methanol/water mixtures) (4). The viscosity data for the fractions with $M_n > 2,000$ in any solvent can be expressed by the Kuhn-Mark-Houwink equation as shown in Figure 3a,

$$[\eta] = K M_n^a \quad (1)$$

where $[\eta]$ is the intrinsic viscosity, M_n is the number average molecular weight of the polymer, and K and the exponent a are constants independent of the molecular weight of the polymer, but dependent on temperature and the nature of the solvent. Further, the following Stockmayer-Fixman equation holds for these high molecular weight fractions (Figure 3b)

$$[\eta]/M_n^{1/2} = K_\theta + 0.51\phi D M_n^{1/2} \quad (2)$$

$$K_\theta = [\eta]_\theta/M_n^{1/2} = \phi \langle L_o^2 \rangle / M_n^{3/2} \quad (3)$$

where ϕ is a universal constant, D is the long range interaction parameter, K_θ is the characteristic constant in a theta solvent, and $\langle L_o^2 \rangle$ is the mean square end-to-end distance of the unperturbed polymer chain. Parameters, K , a and K_θ obtained from Equations (1-3) are listed in Table I. Senti et al. (1) reported the equation $[\eta] = 1.09 \times 10^{-3} M_n^{0.50}$ for hydrolyzed dextran with $1.5 \times 10^4 < M_n < 1 \times 10^5$ in water at 25°C. Bianchi and Peterlin (5) also reported that the a -value was nearly 0.5 for many low molecular weight polymers. However, Granath (6) suggested that the a -value should increase for lower molecular weights because it had been found that branching in dextran diminishes rapidly when the molecular weight decreases to 10^4 . Our result ($a=0.60$) may be rather comparable with $a=0.675$ proposed by Wales et al. (7) for the hypothetical linear dextran with $1.1 \times 10^4 < M_n < 3.7 \times 10^5$. Such high molecular weight dextran would be considered to have a uniform conformation, that is, a random coil conformation characteristic of a typical polymer. Equations 1 and 2 also hold for $M_n > 2,000$ in other solvent systems. The addition of methanol and dimethylformamide into aqueous medium brings about an increase in K and a decrease in a and D . Clearly, both organic solvents act to reduce the expansion of the dextran molecule and its hydration, leading to phase separation. The value of $\langle L_o^2 \rangle / M_n^{1/2}$ was calculated to be 0.710Å by using $K_\theta = 0.91 \times 10^{-3}$ and $\phi = 2.5 \times 10^{21}$.

$$B_H^E = -(\Delta H_1^E / V_1 c^2) \quad (7)$$

where π is the osmotic pressure, c the concentration of solute, n the degree of polymerization expressed as $n = \bar{v}^\circ M / V_1$, \bar{v}° the partial specific volume of solute, V_1 the partial molar volume of solvent, B the second virial coefficient ($=RTA_2$, where A_2 is the second virial coefficient in $\text{mol}\cdot\text{ml}/\text{g}^2$), B_S^{id} the ideal entropy coefficient, B_S^E the excess entropy coefficient, B_H^E the excess enthalpy coefficient, ΔS_1^E the entropy of dilution, and ΔH_1^E the enthalpy of dilution. It should be noted that for high polymeric materials the value of B corresponds to the usual excess virial coefficient, $B^E (=B_S^E + B_H^E)$, but for oligomeric materials it involves the effect of the ideal entropy coefficient, B_S^{id} , besides the excess virial coefficient. Therefore, the quantity to be examined is not B but $B^E (=RTA_2^E)$ in order to compare the thermodynamic properties of a series of oligomeric materials. The parameter A_2^E is related to the Flory-Huggins interaction parameter, χ , by

$$\chi = 1/2 - \rho^2 V_1 A_2^E \quad (8)$$

where ρ is density of solute.

The values of A_2 , A_2^E and χ of oligodextran in water estimated by vapor pressure osmometry are listed in Table II (16). As M_n decreases, A_2 and A_2^E increase up to a maximum at around $M_n=2,000$, then decrease sharply to negative values. A similar tendency has been reported also for polystyrene (14) and poly(methyl methacrylate) (13) in various solvents. The difference between A_2 and A_2^E becomes larger with decreasing M_n since the B_S^{id} term becomes more significant. The interaction parameter, χ , for $M_n > 2,000$ assumes an almost constant value of 0.46, which is close to that common for polymer-good solvent systems. On the other hand, the χ -value increases with a decrease in M_n for $M_n < 2,000$, but it never exceeds its critical value, χ_c , expressed as $(1 + 1/\sqrt{n})^2/2$. Thus, it is evident that the dextran-water interaction becomes stronger with decreasing M_n for oligodextran.

The molecular weight dependence of B_H^E and B_S^E , determined from the temperature effect on B^E , reveals that both ΔH_1^E and ΔS_1^E change from positive to negative around $M_n=2,000$ (Figure 4). A similar molecular weight dependence of both parameters has been observed for polyethylene glycol aqueous solutions by Lakanpal et al. (17) and Kagemoto et al. (18). It has been proposed experimentally and theoretically that in an athermal system there is a maximum in the $B_S^E-M_n$ curves at the conformational transition point from the spherical molecule to the rodlike one (11, 12). Therefore, it seems that the observed molecular weight dependence of thermodynamic parameters for dextran supports the coil-rodlike conformational change postulated to explain the viscosity data. A large negative entropy and enthalpy of dilution suggests forma-

This value is very close to 0.740\AA which has been obtained for high molecular weight dextran (7). By using this value, the flexibility parameter, $\sigma (= [\langle L_o^2 \rangle / \langle L_f^2 \rangle]^{1/2})$, can be estimated to be 1.7-1.8, which is less than that of amylose (2.24) and cellulose (about 4.4). As shown above, the viscosity theories for typical polymer solutions appear to be applicable down to M_n of about 2,000 for dextran, independent of solvent and temperature.

The upward deviation of viscosity data from Equations 1 and 2 for $M_n < 2,000$ clearly indicates that the effective hydrodynamic volume of oligodextran increases with decreasing M_n . Similarly, a critical degree of polymerization in viscosity has been observed at $n=100$ for amylose (8, 9). The $\log[\eta]$ - $\log M$ plots for cellulose are known to begin a slightly downward curvature around $n=150$ and then change to an upward curvature around $n=10$ (10). The critical degree of polymerization seems to be related to the flexibility of polysaccharide chains. Although the theoretical equations for the semi-flexible chain or wormlike chain model may be useful for the transition region from oligomer to polymer, their compatibility with our viscosity data has not yet been established. However, such a relative increase in hydrodynamic volume for oligomers may be assumed to arise from two factors. The main origin would be a conformational transition of the dextran molecule from the random coil (spherical) form for polymer to a rodlike (ellipsoidal) form for oligomer. The second origin may be a resultant increase in hydration or dextran-water interaction.

(B) Thermodynamic Parameters. The variation with chain length of the dextran-water interaction should manifest itself in the thermodynamic parameters of the solutions. However, thermodynamic studies in the oligomer-polymer transition region have been limited by the technical difficulty that methods such as osmotic pressure and light scattering are often not applicable to the oligomers. A useful technique is a cryoscopic method, which has been applied to study the molecular weight dependence of the second virial coefficient for solutions of synthetic oligomers (11, 12). Another recently developed and convenient method is vapor pressure osmometry. The effectiveness of the latter method has been empirically confirmed in thermodynamic studies of a series of oligomers, although the second virial coefficient obtained by this method is an apparent one under pseudo-equilibrium conditions (13, 14, 15).

According to the analysis of Sotobayashi and Ueberreiter (11), the osmotic pressure of a dilute solution of oligomers is expressed as follows,

$$\pi = (RT/M)c + Bc^2 = (RT/M)c + (B_S^{id} + B_S^E + B_H^E)c^2 \quad (4)$$

$$B_S^{id} = (RT\bar{v}^2/2nV_1)(2 - 1/n) \quad (5)$$

$$B_S^E = (T\Delta S_1^E/V_1c^2) \quad (6)$$

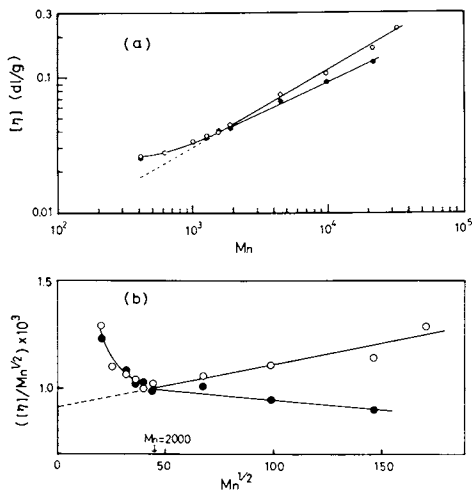
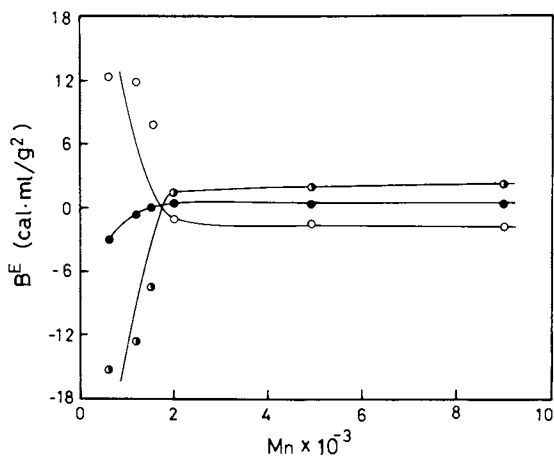


Figure 3. Molecular-weight dependence of intrinsic viscosity of dextran in water (○) and methanol-water mixture with a methanol mole fraction of 0.228 (●) at 25°C (4, 21): (a) $\log [\eta] - \log \bar{M}_n$ plots; (b) Stockmayer-Fixman plots.



Journal of Science of the Hiroshima University

Figure 4. Molecular-weight dependence of excess thermodynamic functions of dextran aqueous solutions at 37°C: (●) excess virial coefficient, B^E ; (○) excess enthalpy coefficient, B_H^E ; (◐) excess entropy coefficient, B_S^E (16).

Table I
The Parameters in Equations 1 and 2 Calculated for Dextran
with $2,000 < M_n < 32,100$

Solvent*	$K \times 10^4$		a		$K_\theta \times 10^3$	
	25°C	50°C	25°C	50°C	25°C	50°C
Water	4.93	3.93	0.60	0.61	0.91	0.78
Methanol/Water						
X =0.100	9.11	6.42	0.51	0.55	0.96	0.86
X =0.228	11.8	8.09	0.42	0.52	1.04	0.95
DMF/Water						
X =0.068	8.25		0.53		0.96	
X =0.189	16.1		0.45		1.09	
Formamide	16.5		0.49		ca. 1.5	

* X represents a mole fraction of organic solvent in the mixed solvents. DMF is an abbreviation for dimethylformamide (4).

Table II
Second Virial Coefficients^a and Interaction Parameter of
Dextran Aqueous Solutions

M_n	$A_2 \times 10^4$		$A_2^E \times 10^4$		χ	
	37°C	60°C	37°C	60°C	37°C	60°C
618	-40.5	-53.9	-50.1	-63.7	0.742	0.806
1,220	-5.36	-18.8	-10.3	-23.7	0.550	0.616
1,460	2.17	-6.19	-1.96	-10.4	0.509	0.549
2,040	10.9	12.0	7.83	9.01	0.464	0.458
4,930	7.66	9.36	6.40	8.14	0.469	0.462
8,980	6.42	8.60	5.71	7.89	0.473	0.464

^a A unit of A_2 and A_2^E is $\text{mol} \cdot \text{ml} / \text{g}^2$. J. Sci. Hiroshima Univ. (16).

tion of a highly ordered structure in oligodextran aqueous solutions or a stronger intermolecular hydrogen bond between oligodextran and water as compared with the high molecular weight dextran.

(C) Compressibility and Hydration. We will now consider whether the increased oligodextran-water interaction is reflected in its degree of hydration. Among many methods for estimation of the degree of hydration, a convenient technique is a compressibility method based on sound velocity measurements (19, 20, 21, 22). The principle of this method is as follows.

The partial specific adiabatic compressibility of solute, $\bar{\beta}_1^\circ$, is defined by

$$\bar{\beta}_1^\circ = -(1/\bar{v}^\circ)(\partial\bar{v}^\circ/\partial P) = (\beta_0/\bar{v}^\circ) \lim_{c \rightarrow 0} (\beta/\beta_0 - V_0)/c \quad (9)$$

$$(\beta/\beta_0 - V_0)/c = \beta_1/\beta_0 d_1 - (v_0 - v_2 \beta_2/\beta_0)/c \quad (10)$$

$$V_0 = (d - c)/d_0 \quad (11)$$

$$\bar{v}^\circ = \lim_{c \rightarrow 0} (1 - V_0)/c \quad (12)$$

where β , β_0 , β_1 and β_2 are the adiabatic compressibilities of solution, solvent, solute and bound water, respectively; d , d_0 and d_1 are the densities of solution, solvent and solute, respectively; c is the concentration of solute in grams per milliliter of solution; \bar{v}° is the partial specific volume of solute; v_0 is the apparent specific volume fraction of bound water; v_2 is the specific volume fraction of bound water. The adiabatic compressibility of solution can be determined from accurate measurement of sound velocity, U , and density, d , by using the following equation

$$U^2 = 1/d\beta \quad (13)$$

Thus, the amount of bound water, v_0/c , can be estimated from $\bar{\beta}_1^\circ$ at infinite dilution with the following assumptions: (1) the solute is incompressible ($\beta_1=0$), (2) the compressibility of bound water is the same as that of ice ($\beta_2=18 \times 10^{-12}$ cm²/dyne) since the hydration of neutral polysaccharide would be mainly due to hydrogen bonds between water and OH groups of the polymer, and (3) $v_0=v_2$.

The partial specific adiabatic compressibility and the bound water value of dextran estimated by this method are plotted against M_n in Figure 5 (21). A critical point is evidently observed at the same molecular weight as observed in the viscosity and thermodynamic studies. A negative value of $\bar{\beta}_1^\circ$ is attributed to the strong solvation around the solute molecule. The amount of bound water per mole of OH groups was calculated by assuming that the hydration occurs only at the OH groups of dextran. A hydroxyl group in high molecular weight dextran thus seems to be hydrated

to only about half the extent of monomer or dimer. The enhanced hydration of oligodextran may be regarded as a result of an increased probability of intermolecular hydrogen bonding between dextran and water. On the contrary, the intramolecular hydrogen bonding in oligodextran would be less than that of high molecular weight dextran. Whereas long-range intramolecular hydrogen bond may be formed in the flexible polysaccharide chains consisting of many segments, this is not expected in oligomeric materials. Recently, Stipanovic (23) has shown that stereochemically acceptable models for dextran contain an intramolecular O_5-O_2 hydrogen bond, but at present there is no direct evidence for the molecular weight dependence of such hydrogen bonds in aqueous oligodextran. However, it is noteworthy that for α -1,4-linked polyglucose in dimethylsulphoxide the tendency of O_2-O_3 hydrogen bond formation increases in the series, maltose < maltodextrin < amylose < cyclodextrin (24).

As discussed above, several solution properties of dextran show consistent changes around $M_n=2,000$ or $n=12$. A plausible explanation for these results is an assumed conformational or configurational change of dextran molecules from coiled (polymer) to rodlike (oligomer) form. This explanation, however, must be regarded as tentative because we lack information on the molecular weight dependence of the end group effect, on the molecular weight distribution, and on the degree of branching in the dextran samples used. Whatever origin may be assigned to these observations, it is likely that some properties of these dextrans and their derivatives, e.g., solute-solute interaction in solid state (25) and their interaction with protein (26), are different below and above the critical degree of polymerization.

II. Solution Properties of Ionic Dextran Derivatives

(A) Hydration. As mentioned in the previous section, an estimation of the amount of hydration is not too difficult for neutral polysaccharides, since their hydration occurs mainly through hydrogen bonds between water and the OH groups of the polymer. In general, however, for ionic derivatives one must take into consideration three hydration modes, the electrostriction around ionic groups, the hydrophobic hydration around non-polar groups, and the hydrogen-bonded hydration around polar groups. Usually, it is not simple to estimate separately the amounts of these three hydrations. Suzuki and Uedaira (27) determined the lower and upper limiting hydration numbers of potassium hyaluronate to be 9.22 and 18.4 mole per base mole, respectively, 70-80% of which was ascribed to hyaluronate ion.

In order to elucidate the influence of substituent ionic groups on the hydration, the partial molal volume and compressibility data of ionic dextran derivatives have been analyzed in terms of three kinds of hydration (22, 28). The partial molal volume of ionic dextran derivatives, \bar{V}° , may be written as the sum

of the partial molal volume of polyion, V_p , and that of counterion, V_g ,

$$\bar{V}^{\circ} = V_p + V_g \quad (14)$$

$$V_p = V_{\text{int},p} + H_p + P_p + E_p \quad (15)$$

$$V_g = V_{\text{int},g} + E_g \quad (16)$$

where E_p and E_g are the volume changes due to electrostriction by the polyion and the counterion, respectively, P_p is the volume change from hydrogen-bonded hydration around polar groups of the polymer, H_p is the volume change from hydrophobic hydration around nonpolar groups of the polymer, $V_{\text{int},p}$ is the intrinsic volume of polyion including the void, and $V_{\text{int},g}$ is the intrinsic counterion volume. The total volume change due to hydration of the polyion, $\Delta V_t (=H_p + P_p + E_p)$, can be determined through measurements of \bar{V}° since $V_{\text{int},p}$, $V_{\text{int},g}$ and E_g can be evaluated with some assumptions. The more negative the value of ΔV_t is, the larger the amount of hydration is. As seen in Figure 6, the total hydration of ionic dextran derivatives increases almost linearly with increasing degree of substitution of the ionic group and in the order of $\text{CMD} < \text{DS} < \text{SPD} < \text{DP}$ at the identical degree of substitution. This linearity suggests that there is no overlap of hydration shells around the ionic groups of the polyion. By considering the difference in ΔV_t between each ionic derivative and dextran, the volume change due to electrostriction by COO^- and SO_3^- groups was estimated to be -18.7 and -30.3 ml, respectively. These values correspond to about 7 and 11 mole of water per mole of COO^- and SO_3^- , respectively, since the electrostrictional volume change of water is known to be -2.7 ml/mole (29). The difference in ΔV_t , -7.5 ml, between DS and SPD can be ascribed to the hydrophobic hydration of the additional propylene group, $\text{CH}_2\text{CH}_2\text{CH}_2$, of SPD if E_p and P_p of SPD are assumed to be equivalent to those of DS. A similar result has been obtained from the pressure dependence of the dimerization constant of formic, acetic, propionic, and n-butyric acids in water (30); the estimated volume change due to hydrophobic interaction is 1 ml, 5 ml, and 8 ml per mole of CH_3 , CH_3CH_2 , and $\text{CH}_3\text{CH}_2\text{CH}_2$, respectively. These values are very small compared with the volume change due to dissolution of propane gas in water, -20 ml. At present, the values of -1 to -2 ml per mole of methylene group may be acceptable as a reasonable volume change due to hydrophobic hydration, instead of -20 ml which has been assumed for a long time (31).

If e milliliters of free water are bound electrostricturally to the ionic groups whereupon they occupy a volume of e' milliliters, the volume change due to the electrostriction, E_p , is expressed as $E_p = e' - e$. In the same way, $H_p = h' - h$ and $P_p = p' - p$, where h and p represent the volume of free water which are changed to volumes h' and p' , respectively, by the hydrophobic hydration

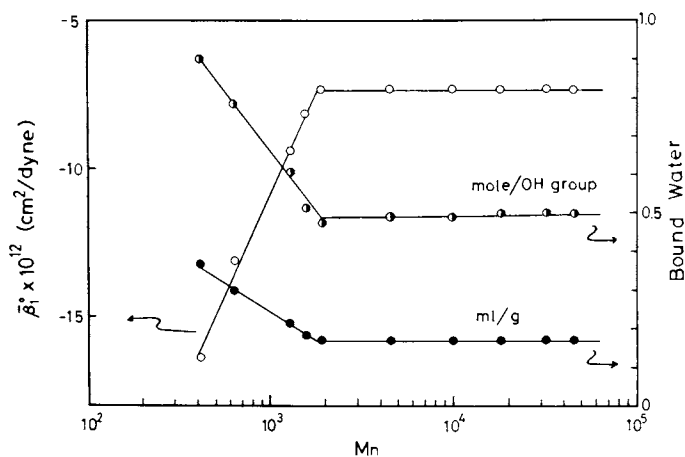


Figure 5. Molecular-weight dependence of partial specific compressibility and bound water of dextran at 25°C (21)

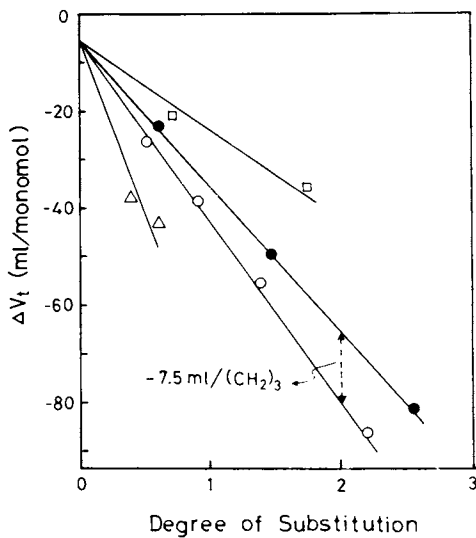


Figure 6. Relation between the total volume change by hydration and the degree of substitution for dextran derivatives at 25°C (22, 28): (□) CMD; (●) DS; (○) SPD; and (△) DP.

and hydrogen-bonded hydration. Since V_g and $V_{int,p}$ are regarded as incompressible volumes, the following equation is derived from Equations 9 and 15 (22),

$$\begin{aligned} -\bar{V}_1^{\circ}\bar{\beta}_1^{\circ} &= \partial\bar{V}^{\circ}/\partial P = \partial V_p/\partial P \\ &= \beta_w(h + p + e) - (h'\beta_h + p'\beta_p + e'\beta_e) \end{aligned} \quad (17)$$

where β_h , β_p , β_e , and β_w represent the adiabatic compressibilities of the water of hydrophobic hydration, hydrogen-bonded hydration, electrostricted hydration, and the free water, respectively. The term $-\bar{V}_1^{\circ}\bar{\beta}_1^{\circ}$ corresponds to the partial molal compression, i.e., the differential coefficient of the partial molal volume with pressure at infinite dilution. The observed positive values of $-\bar{V}_1^{\circ}\bar{\beta}_1^{\circ}$ for dextran derivatives (Figure 7) suggest that the volume change due to hydration is smaller under higher pressure. Neither the structure nor the compressibility of water participating in hydration of each derivative would be identical since the value of $-\bar{V}_1^{\circ}\bar{\beta}_1^{\circ}$ increases in the order of DS < SPD < CMD < DP at the identical degree of substitution, and this is different from the order for the total hydration, ΔV_t . By analyzing the difference in $-\bar{V}_1^{\circ}\bar{\beta}_1^{\circ}$ between DS and SPD a relation, shown in Figure 8, was derived between the mole number and the adiabatic compressibility of the water of hydrophobic hydration around the propylene group of SPD. If the volume change per mole of water participating in hydrophobic hydration is assumed to be -1 ml, the compressibility of hydrophobic hydration, β_h , is evaluated to be about 40×10^{-12} cm²/dyne. Thus, we may propose $\beta_e < \beta_p < \beta_h < \beta_w$ as the order of adiabatic compressibility of water participating in each kind of hydration. Further investigations should be aimed at finding out how these types of hydration affect the medical or biological functions of the several derivatives. It is interesting that the mixture of diethylaminoethyl dextran and bovine serum albumin forms a coacervate or soluble complex which is much enhanced by elevating the temperature (32). This effect must therefore depend predominantly on the hydrophobic interaction.

(B) Selective Counterion Binding. Physicochemical studies on the binding of metal ions such as Na⁺, K⁺, Ca²⁺ and Mg²⁺ to ionic polysaccharides should give basic information for understanding the roles of such polymers in ion accumulation and selective ion binding in biological systems. It is of special interest to know how selective ion binding to polysaccharides is affected by such factors as different ionic groups, charge density, constituent sugar structure, configuration of the glucosidic linkage, and the resulting conformation and flexibility of the polysaccharide chain. The degree of cation binding to polyions has been estimated by a variety of techniques, e.g., conductivity, membrane equilibrium measurements, dilatometry, etc. Recent development of ion-selective electrodes has made it possible to measure quantita-

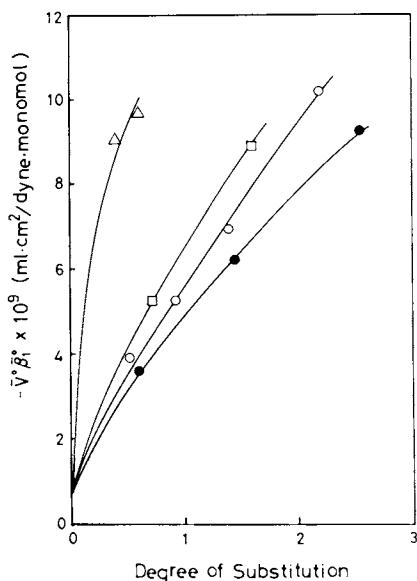
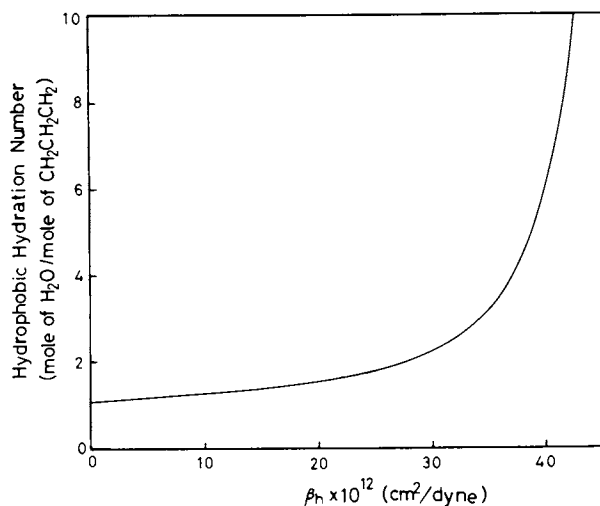


Figure 7. Relation between the partial molal compression and the degree of substitution of dextran derivatives at 25°C (22, 28): (□) CMD; (●) DS; (○) SPD; and (△) DP.



Macromolecules

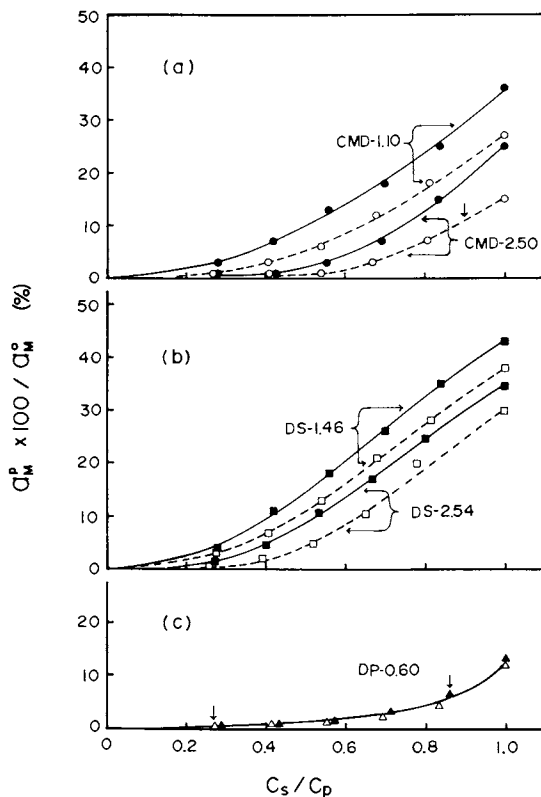
Figure 8. Relation between the mole number and adiabatic compressibility of the water of hydrophobic hydration around the propylene group of SPD at 25°C (22)

tively the counterion activity. Here, this potentiometric method has been utilized to examine the affinity of some cations to ionic dextran derivatives with different ionic groups and charge densities (28, 33, 34, 35).

As seen in Table III, in the case of CMD γ_{Na^+} was completely identical with γ_{K^+} at any degree of carboxyl substitution, indicating that CMD shows no selectivity in affinity for these two ions. However, a selective interaction with these cations is evident for the other three derivatives. There is a possibility of specific site binding of K^+ ion with DS since γ_{K^+} is extremely small, only 0.16 at degree of substitution of 2.54, in comparison with γ_{Na^+} which is 0.23. This specificity has been qualitatively observed through the measurement of the critical cation concentration required for the precipitation of 1% dextran sulfate (36). This is supported also by the observation that the additivity rule of counterion activity in added salt systems hold within 1.5% for the sodium dextran sulfate-NaCl system, but the deviation reaches 8.8% for the potassium dextran sulfate-KCl system. The decrease in sound velocity observed in the latter system demonstrates that the interaction between K^+ and DS is so strong that a part of the water of hydration is released from the ions. In contrast to DS, the affinity of Na^+ for DP and SPD is stronger than that of K^+ . This suggests that polysulfate ions and polyphosphate ions may have an opposite effect on the ion accumulation of Na^+ and K^+ ions in biological systems. For all derivatives, an increase in the degree of substitution extensively decreased the counterion activity and also enhanced the ion-selectivity for the two cations. This trend is especially significant for DS. A membrane system containing considerable condensed sulfate group might therefore be highly selective for the transport of K^+ over Na^+ .

The free fraction of divalent counterions, Ca^{2+} and Mg^{2+} , which was estimated potentiometrically by titrating the tetramethylammonium salt of dextran derivatives with $CaCl_2$ or $MgCl_2$, is plotted in Figure 9 as a function of the equivalent concentration ratio, C_s/C_p , of added divalent cation (C_s) to polyion (C_p) (35). The affinity of Ca^{2+} and Mg^{2+} ions for dextran derivatives increases in the order of DS < CMD < DP and most added cations are bound to polyion at small C_s/C_p . All derivatives show a higher affinity for Ca^{2+} than for Mg^{2+} ion. An increase in degree of substitution causes still higher affinity for both cations. The strong affinity of both cations for DP may be due to the divalent-anion character of the phosphate group. As with other carboxyl polymers, CMD shows an especially high selectivity for the two divalent cations. This may be ascribed to the higher chelating ability of Ca^{2+} ion with carboxyl groups and in part, to the difference in hydrated ion-radii of these cations.

As presented above, the degree of substitution of ionic groups or charge density is an important factor for ion-binding ability of these derivatives. An electrostatic free energy per ionic group, G_{el} , at the degree of ionization, α , may be estimated



Carbohydrate Research

Figure 9. Plots of the free fraction (%) of divalent cations, Mg^{2+} (●, ■, ▲) and Ca^{2+} (○, □, △), as a function of equivalent concentration ratio, C_s/C_p , of added cation (C_s) to polyion (C_p) for dextran derivatives: (a) CMD; (b) DS; and (c) DP. The numbers attached to the abbreviated sample names show the degree of substitution of ionic groups. The mark ↓ above the curves shows the appearance of turbidity (35).

from the potentiometric titration curves,

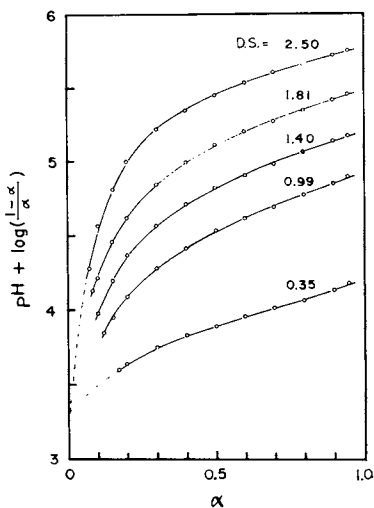
$$G_{el}(\alpha) = 2.3kTf_0^\alpha \{pH + \log[(1 - \alpha)/\alpha] - pK_0\} d\alpha \quad (18)$$

$$pK_a = pH + \log[(1 - \alpha)/\alpha] \quad (19)$$

where pK_0 is the negative logarithm of the intrinsic dissociation constant of an ionic group, k the Boltzman constant, and T the absolute temperature. As shown in Figure 10, the pK_a of CMD is a monotonic increasing function of α , indicating that there is no conformational change corresponding to coil-helix or globular-coil transition (34). The value of pK_0 was 3.30 and 3.25 for aqueous media containing no salt and 0.02M NaCl, respectively, independent of the degree of substitution. It is evident that a monotonous increase in G_{el} with degree of substitution (Figure 11) causes a comparable decrease in counterion activity as observed in Table III.

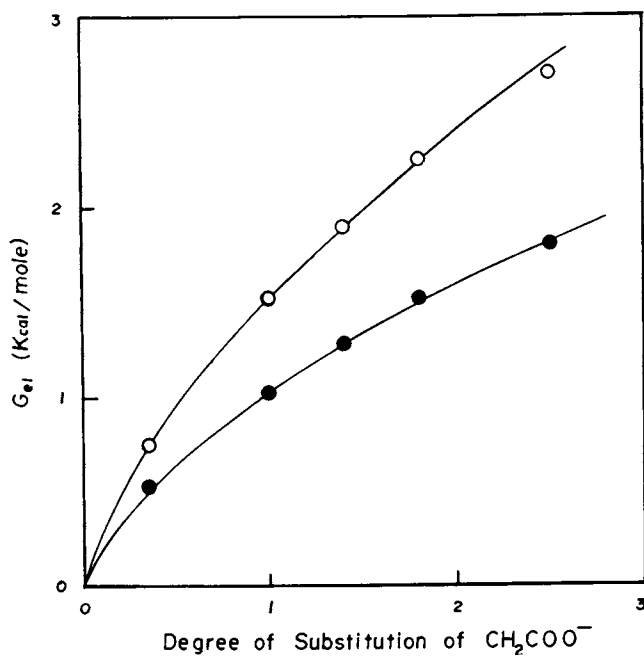
G_{el} and pK_0 are affected not only by ionic groups but also by hydrophobic groups surrounding the carboxyl group on the polymer. However, little has been known about whether the hydrophobic environment around the ionic group causes the selectivity in counterion binding or not. The ion-binding data for CMBD may offer a clue to the answer to this question. When the benzyl group is introduced into CMD, fixing the degree of substitution of carboxyl group at 0.35, the pK_a increased gradually with the benzyl group content as shown in Figure 12. The substituent benzyl groups presumably change the structure of water in the vicinity of a carboxyl group so that the resulting local decrease in dielectric constant of water depresses the dissociation of the carboxyl group. The activity of Na^+ and K^+ ions certainly decreased in the solution of CMBD as compared with CMD (Table IV). However, it should be noted that γ_{Na^+} is smaller than γ_{K^+} in the solution of CMBD, although both activity coefficients were completely identical in the CMD solution. This result indicates that a carboxyl group can manifest its potential selectivity for the two cations when it is surrounded by an hydrophobic environment. The difference in the two activity coefficients observed for CMBD may be successfully interpreted in terms of the difference in hydration energy of the cations. The dissociation free energy of K^+ ion would not be extensively affected by the hydrophobic medium since this ion has relatively few water molecules of hydration, so that its hydration energy is not influenced so much by the medium. However, the hydration structure of the ions having appreciable water of hydration, such as Na^+ ion, must be significantly disrupted in the hydrophobic environment so as to decrease its hydration energy. This results in the instability of the dissociated ion. A more drastic selectivity would be generated when the carboxyl group is buried in a much more hydrophobic environment.

Much work on selective counterion binding has been concerned with polyions having different ionic groups, such as COO^- , SO_3^-



Biopolymers

Figure 10. Potentiometric titration curves of CMD with various degrees of substitution in water at 25°C. Polymer concentration is 0.0100 equiv/L (34).



Biopolymers

Figure 11. Plots of $G_{e1}(\alpha = 1)$ as a function of the degree of substitution of the carboxyl group for CMD in H_2O (○) and in 0.02M NaCl (●) at 25°C. Polymer concentration is 0.0100 equiv/L (34).

Table III
Counterion Activity Coefficients of Ionic Dextran
Derivatives in Water at 25°C

Dextran Derivative	Degree of Substitution	γ_{Na^+}	γ_{K^+}
Carboxymethyldextran	0.35	0.672	0.672
	1.10	0.389	0.393
	2.50	0.266	0.264
Dextran Sulfate	0.61	0.481	0.477
	1.46	0.316	0.284
	2.54	0.228	0.164
Sulfopropyldextran	0.92	0.466	0.481
	1.41	0.377	0.396
	2.20	0.273	0.305
Dextran Phosphate	0.38	0.255	0.282
	0.60	0.224	0.249

Listed are the activity coefficients in the polymer concentration range of 0.02-0.04 equiv/l in which they were independent of the polymer concentration (28, 33).

Table IV
Counterion Activity Coefficients of Ionic Dextran
Derivatives in Water at 25°C

Polymer Conc. (equiv/l)	CMD ^a		CMBD ^b	
	γ_{Na^+}	γ_{K^+}	γ_{Na^+}	γ_{K^+}
0.0250	0.672	0.672	0.654	0.664
0.0100	0.681	0.682	0.658	0.680
0.0025	0.720	0.720	0.660	0.680

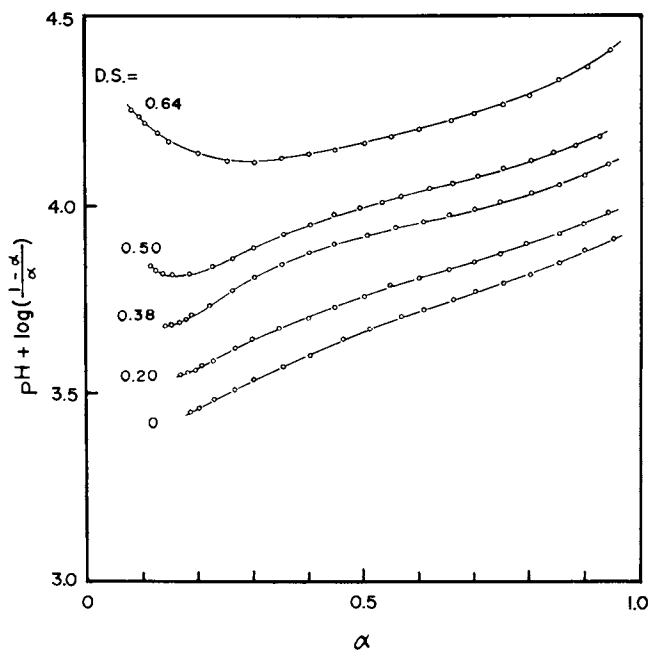
^a Carboxymethyldextran; degree of substitution of carboxyl group is 0.35.

^b Carboxymethylbenzylidextran; degree of substitution of carboxyl and benzyl groups is 0.35 and 0.64, respectively (34).

and PO_3^{2-} , but the mechanism remains unclear. Recently, the crown compounds, such as dicyclohexyl-15-crown-5 and valinomycin, have been found to be very effective in selection of Na^+ and K^+ , due mainly to the limiting geometric factors between the ionic radius of the guest ions and the annular space of the crown compounds. As a third origin, we may expect ion selectivity based on the hydrophobicity. A further study may be concerned with such hydrophobic effects, since the biological functions of biopolymers are often carried on in an hydrophobic environment.

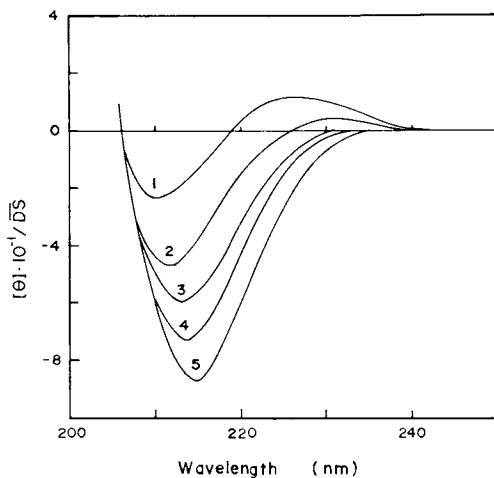
(C) Circular Dichroism of Carboxymethyl-dextran. While recent vacuum ultraviolet circular dichroism developments have made it possible to measure the spectra of the backbone pyranose chain (37, 38), many circular dichroism (CD) analyses of the polysaccharides have been carried out over the past ten years by studying chromophores such as the carboxyl and amide groups involved. However, a general rationalization for the polyelectrolytic effect on the $n-\pi^*$ transition of the carboxyl group has remained obscure, since the transition is perturbed by some factors in a complicated manner.

Here, we have examined how the charge density, polymer concentration, degree of neutralization, and added salts affect the CD spectra of CMD in order to elucidate the microscopic polyelectrolytic properties of this polymer (39). The negative CD band of CMD around 213 nm, which is ascribed to the carboxyl $n-\pi^*$ transition, is shifted to higher wavelength accompanying an increase in its intensity with increasing degree of carboxyl substitution, while the crossover point near 206 nm was not affected (Figure 13). The dependence of the CD band on degree of substitution must arise from the electrostatic perturbation of the carboxyl $n-\pi^*$ transition, since the ellipticity extremum of this negative band appears to increase in proportion to the electrostatic free energy for ionization, G_{el} , of the carboxyl group, and the effect of degree of substitution was not observed for dextran acetate (40). A notable point is that a positive band appears in addition to the negative band at small degrees of substitution. This positive band is more evident on decreasing neutralization or at low pH (Figure 14). It is well known that the magnitude and sign of the CD spectra associated with a particular electronic transition are critically dependent on molecular geometry, or, more specifically, on the disposition of other groups about the symmetry planes of the chromophore. The most widely adopted explanation of the two bands with different signs is that they arise from the $n-\pi^*$ transition of different rotational isomers of the carboxyl chromophore (37, 41, 42). It is probable that another stable rotational isomer may be caused by the increased hydrogen bond of the carboxyl group with other polar groups and the decrease in intra- and/or intermolecular electrostatic energy of CMD. The findings that the polymer concentration dependence of ellipticity in pure water disappears on adding salt are evidence that the intermole-



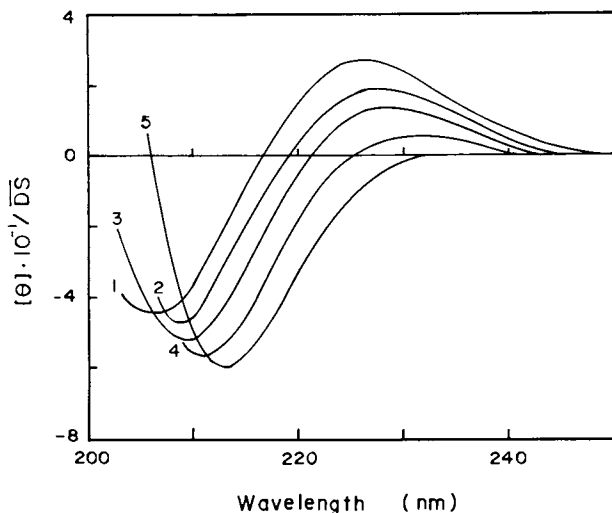
Biopolymers

Figure 12. Potentiometric titration curves of CMBD with various degrees of substitution of benzyl group in 0.02M NaCl at 25°C. The degree of substitution of the carboxyl group is fixed at 0.35. Polymer concentration is 0.0100 equiv/L (34).



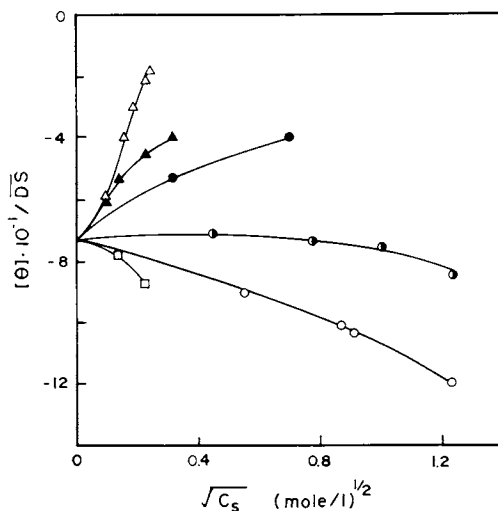
Biopolymers

Figure 13. CD spectra of CMD with various degrees of substitution of the carboxyl group: 0.35 (Curve 1); 0.68 (Curve 2); 0.99 (Curve 3); 1.40 (Curve 4); and 1.85 (Curve 5). Polymer concentration is 0.100 equiv/L (39).



Biopolymers

Figure 14. CD spectra of CMD with various degrees of neutralization: 0 (Curve 1); 0.25 (Curve 2); 0.50 (Curve 3); 0.75 (Curve 4), and 1.0 (Curve 5). The degree of substitution of the carboxyl group is 0.99. Polymer concentration is 0.100 equiv/L. (39).



Biopolymers

Figure 15. CD intensity of sodium CMD at 213 nm as a function of added salt concentration (C_s): (●) LiCl; (○) KCl; (○) NaCl; (△) CaCl₂; (▲) MgCl₂; and (□) BaCl₂. The degree of substitution of the carboxyl group is 1.40. Polymer concentration is 0.100 equiv/L (39).

cular and non-nearest (long-range) intramolecular electrostatic interactions contribute substantially to the perturbation of the carboxyl $n-\pi^*$ transition.

The negative band at 213-215 nm increased in the order of counterions, $\text{Li}^+ < \text{K}^+ < \text{Na}^+$, although no selectivity among Na^+ and K^+ ions was found by the measurement of their activities as mentioned above. This order is also different from that of the crystallographic radii of these cations. The effects of added monovalent salt, LiCl , KCl and NaCl , on the CD negative band of CMD (Figure 15) may be interpreted as a result of partial exchange of the counterion from Na^+ to K^+ or Li^+ . The influences of divalent cation salts, CaCl_2 , MgCl_2 and BaCl_2 , are more dramatic; the effect of Ba^{2+} is completely opposite to that of Ca^{2+} and Mg^{2+} . The n -orbitals of the carboxyl ion may undergo complicated perturbation due to the proximity of specifically bound divalent cations or chelate complex accompanying the discharge and dehydration of the ion.

As mentioned above, it is surprising that the CD spectra of CMD reflect rather sensitively its polyelectrolytic properties, certainly more so than those of other ionic polysaccharides examined in the past. This is probably because the asymmetric carbon atom of the pyranose ring fixes the symmetry plane of the carboxyl group only weakly on account of the existing ether linkage $-\text{OCH}_2-$ between them. The findings that the carboxyl $n-\pi^*$ transition is perturbed dominantly by intra- and intermolecular electrostatic interactions suggest that in general the CD magnitude of carboxylic polysaccharides will be larger compared to that of its constituent oligomer or monomer because of the condensed electrostatic field of polyion itself (the so-called polymer effect). At present the effects of different counterions and added salts, some of them deduced from the ion-binding data, cannot be easily explained by appeal to generalizations about polyelectrolyte behavior. It must await further investigation to decide whether or not the CD analysis will be applicable as a probe of the microstructure and the macroscopic solution properties of carboxylic polysaccharides.

Acknowledgment

The author wishes to thank Central Research Institute of Meito Sangyo Co., Ltd. Nagoya for supplying the dextran and its derivatives. He also thanks the late Professor Hajime Noguchi for his collaboration in this work.

Literature Cited

1. Senti, F. R., Hellman, N. N., Ludwig, N. H., Babcock, G. E., Tobin, R., Glass, C. A. and Lamberts, B. L., J. Polymer Sci. (1955) 17, 527-546.
2. Turvey, J. R. and Whelan, W. J., Biochem. J. (1957) 67, 49-52.
3. Suggett, A., "Water" (Frank, F., ed.), Vol. 4, p.548, Plenum Press, New York, (1975).
4. Gekko, K., Makromol. Chem. (1971) 148, 229-238.
5. Bianchi, U. and Peterlin, A., J. Polymer Sci. A2 (1968) 6, 1759-1772.
6. Granath, K. A., J. Colloid Sci. (1958) 13, 308-328.
7. Wales, M., Marshall, P. A. and Weissberg, S. G., J. Polymer Sci. (1953) 10, 229-240.
8. Burchard, W., Makromol. Chem. (1963) 64, 110-125.
9. Pfannemüller, B., Mayerhöfer, H. and Schulz, R. C., Makromol. Chem. (1969) 121, 147-158.
10. Vink, H., Makromol. Chem. (1966) 94, 15-19.
11. Sotobayashi, H. and Ueberreiter, K., J. Polymer Sci. A (1964) 2, 1257-1274.
12. Sotobayashi, H., Makromol. Chem. (1965) 81, 57-67; *ibid.* (1969) 123, 157-183.
13. Springer, J., Ueberreiter, K. and Möller, E., Ber. Bunsenges. Physik. Chem. (1965) 69, 494-499.
14. Nomura, H. and Miyahara, Y., Nippon Kagaku Zasshi (1968) 89, 142-144.
15. Wachter, A. H. and Simon, W., Anal. Chem. (1969) 41, 90-94.
16. Gekko, K., J. Sci. Hiroshima Univ. (1971) A35, 111-121.
17. Lakhnupal, M. L., Chhina, K. S. and Sharma, S. C., Indian J. Chem. (1968) 6, 505-509.
18. Kagemoto, A., Murakami, S. and Fujishiro, R., Makromol. Chem. (1967) 105, 154-163.
19. Shiio, H., J. Am. Chem. Soc. (1958) 80, 70-73.
20. Nomura, H., Yamaguchi, S. and Miyahara, Y., J. Appl. Polymer Sci. (1964) 8, 2731-2734.
21. Gekko, K. and Noguchi, H., Biopolymers (1971) 10, 1513-1524.
22. Gekko, K. and Noguchi, H., Macromolecules (1974) 7, 224-229.
23. Stipanovic, A. J., Ph. D. Dissertation, SUNY College of Environmental Science and Forestry, Syracuse, N. Y., (1978).
24. Casu, B., Reggiani, M., Gallo, G. G. and Vigerani, A., Tetrahedron (1966) 22, 3061-3083.
25. Gekko, K., Agric. Biol. Chem. (1978) 42, 1287-1288.
26. Gekko, K. and Noguchi, H., J. Agric. Food Chem. (1978) 26, 1409-1414.
27. Suzuki, Y. and Uedaira, H., Bull. Chem. Soc. Jap. (1970) 43, 1892-1894.
28. Gekko, K. and Noguchi, H., Repts. Prog. Polym. Phys. Japan (1978) 21, 683-684.
29. Conway, B. E., Desnoyers, J. E. and Smith, A. C., Phil. Trans.

- Roy. Soc. London, Ser. A (1964) 256, 389-437.
30. Suzuki, K., Taniguchi, Y. and Watanabe, T., J. Phys. Chem. (1973) 77, 1918-1922.
 31. Noguchi, H., Prog. Polymer Sci. Japan (1975) 8, 191-232.
 32. Gekko, K. Harada, H. and Noguchi, H., Agric. Biol. Chem. (1978) 42, 1385-1388.
 33. Noguchi, H., Gekko, K. and Makino, S., Macromolecules (1973) 6, 438-442.
 34. Gekko, K. and Noguchi, H., Biopolymers (1975) 14, 2555-2565.
 35. Gekko, K. and Noguchi, H., Carbohydr. Res. (1979) 69, 323-326.
 36. Kimizuka, H., Yamaguchi, A. and Mori, T., Bull. Chem. Soc. Jap. (1967) 40, 1281-1282.
 37. Buffington, L. A., Pysh, E. S., Chakrabarti, B. and Balazs, E. A., J. Am. Chem. Soc. (1977) 99, 1730-1734.
 38. Liang, J. N., Stevens, E. S., Morris, E. R. and Rees, D. A., Biopolymers (1979) 18, 327-333.
 39. Gekko, K., Biopolymers (1979) 18, 1989-2003.
 40. Mukherjee, S., Sarko, A. and Marchessault, R. H., Biopolymers (1972) 11, 303-314.
 41. Morris, E. R., Rees, D. A., Sanderson, G. R. and Thom, D., J. Chem. Soc. Perkin Trans. (1975) 2, 1418-1425.
 42. Barth, G., Voelter, W., Mosher, H. S., Bunnenberg, E. and Djerassi, C., J. Chem. Soc. Chem. Commun. (1970) 92, 875-886.

RECEIVED September 15, 1980.

Specificity of Interactions Between Polysaccharide Helices and β -1,4-Linked Polysaccharides

IAIN C. M. DEA

Unilever Research, Colworth Laboratory, Sharnbrook, Bedford MK44 1LQ, U.K.

It is now firmly established that agarose¹, ι -carrageenan² and probably also κ -carrageenan² can adopt double helical conformations in the condensed phase. The evidence is also very strong that, in favourable conditions of temperature and concentration, and (for the carrageenans) ionic strength and appropriate counterions, these double helices can survive in highly hydrated solutions and gels⁴. We have reported previously² that the double helices of agarose and κ -carrageenan (but not ι -carrageenan) could bind in an ordered, cooperative fashion, to the unsubstituted sequences of 1,4-linked β -D-mannopyranose residues in certain plant galactomannans, and that such mixed polysaccharide systems can lead to unexpected and useful rheological properties.

We proposed⁵, that the binding mechanism involves noncovalent association between unlike polysaccharide chains in ordered, complementary conformations - a double helix and a ribbon respectively - as shown schematically in Figure 1. We have not yet determined the stoichiometry of binding (ie. whether helices and ribbons combine in a 1:1 or some other molecular ratio), or the particle weight of the complex. The turbidity of the mixed systems, both for agarose and κ -carrageenan, does suggest qualitatively that many or all of these subunits exist in aggregated form. We further suggested⁵ that this system could represent a model mechanism for biological assembly of cell walls and other heterogeneous, carbohydrate-rich extracellular structures. It was therefore of interest to examine whether the binding shows the specificity for fine details of polysaccharide structure that we might expect (a) on physical grounds, because intimate stereochemical 'fit' should be disturbed by changes in the main chain and substituents, and (b) on biological grounds, because the wide and subtle variation of natural polysaccharide structure is presumed to represent a mechanism for control of their intermolecular interactions.

0097-6156/81/0150-0439\$05.00/0

© 1981 American Chemical Society

This paper is a preliminary communication of some more recent investigations of the specificity of the interactions between the two series of helix forming polysaccharides and four series of β 1,4-linked ribbon-forming polysaccharides.

Figure 2 shows the repeat structures for carrageenan and agarose, and illustrates their close similarity. (Agarose contains, 3,6-anhydro-L-galactose instead of the D-enantiomer in carrageenan). The agarose used had been purified by chromatography on DEAE-sephadex, and was a gift from Duckworth and Yaphe⁶. It is probably as near as one can get to the idealised non-substituted structure. In addition segmented agarose₁, prepared by "kink-splitting" at the L-galactose residues using Smith Degradation, was used. The κ -carrageenan was prepared from *Chondrus crispus* by Marine Colloids Inc., Rockland, Maine. Infra-red analysis indicates that it is not an ideal κ -carrageenan, but contains a high percentage (ca. 30%) of the 3,6-anhydro-D-galactose residues as the 2-sulphate. This sample was used in the potassium salt form.

TABLE 1

Ribbon-forming polysaccharides used in study.

1. β 1,4-linked Galactomannans	eg. locust bean gum guar gum
2. β 1,4-linked Glucomannans	eg. "konjac" mannan Spruce hemicellulose
3. β 1,4-linked Glucans	eg. Seed amyloids CMC
4. β 1,4-linked Xylans	eg. <i>Watsonia</i> polysaccharide Sapote gum

Table 1 lists the four series of ribbon-forming β 1,4-linked polysaccharides used in the study. For each of these a number of variants, differing in the pattern of specific substitution and modification, were used. The interaction of agarose and κ -carrageenan with each of these series of ribbon-forming polysaccharides will now be discussed in turn.

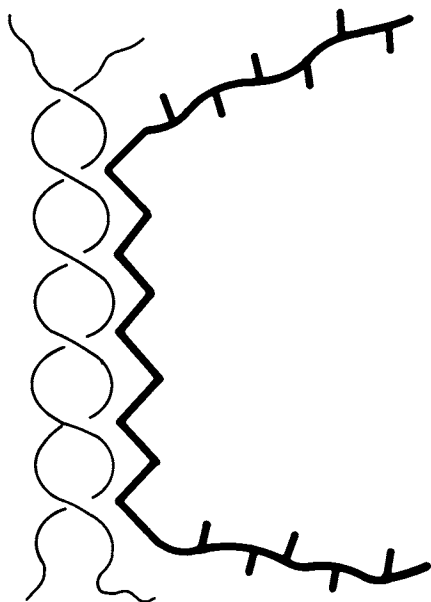


Figure 1. Proposed model for the interaction between the double helix of κ -carrageenan or agarose with galactomannan

Journal of Molecular Biology

(5)

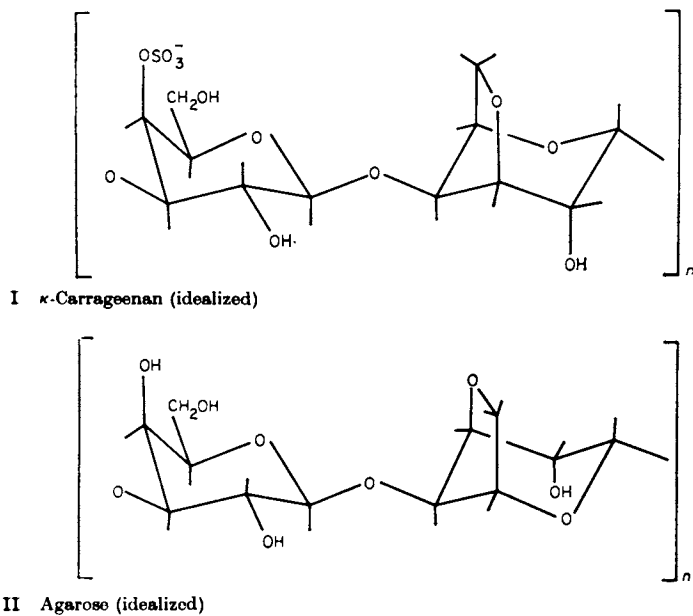


Figure 2. Idealized repeating structures for κ -carrageenan and agarose

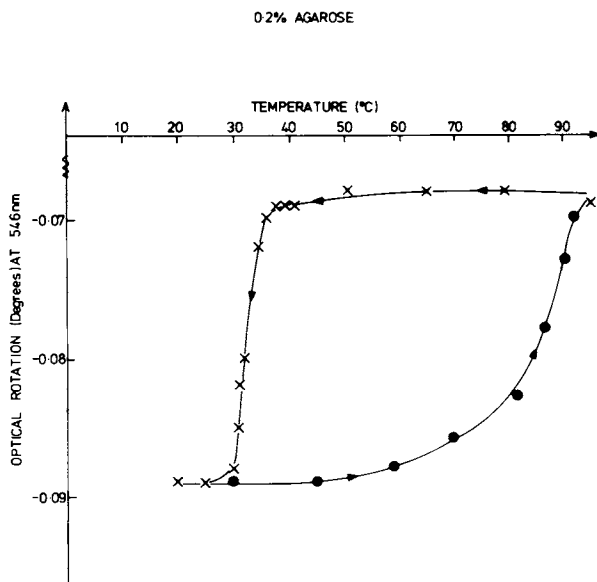
Interaction with Galactomannans

We have previously reported⁵ that the gelation of agarose by cooling a hot solution, is accompanied by a large negative shift in optical rotation which signals the formation of the double helical cross-links and that this shift is reversed when the gel is liquified and the helices are melted by re-heating (see Figure 3). The optical rotation traces for this cycle of cooling and heating shows a large hysteresis loop which reflects the hysteresis in bulk properties.

Agarose at a concentration of 0.05% does not form a continuous gel on cooling; however the optical rotation behaviour on cooling and reheating is identical². This indicates that the same change in conformation occurs, but that there are insufficient agarose chains to form a complete network. This refutes the possible objection that the optical rotation changes are merely artifacts of the change in bulk properties (eg. strain birefringence in the gel state). Indeed both the optical rotation data and X-ray diffraction data are consistent with a left-handed, 3-fold, double helix for agarose¹. We have also reported² that the addition of locust bean gum gels 0.05% agar and changes the form of the optical rotation trace; the cooling curve now seems to be a composite of the usual negative contribution from the agarose coil to helix conversion, and a new, positive contribution from a galactomannan transition which does not occur in the absence of agarose. The hysteresis now shows a complex butterfly form instead of the usual loop, and we interpret this as showing that, although the disorder-order conversions for the two polysaccharides occur together on the cooling curve, on re-heating, the order-disorder transition for the galactomannan can be caused to occur first (see Figure 4).

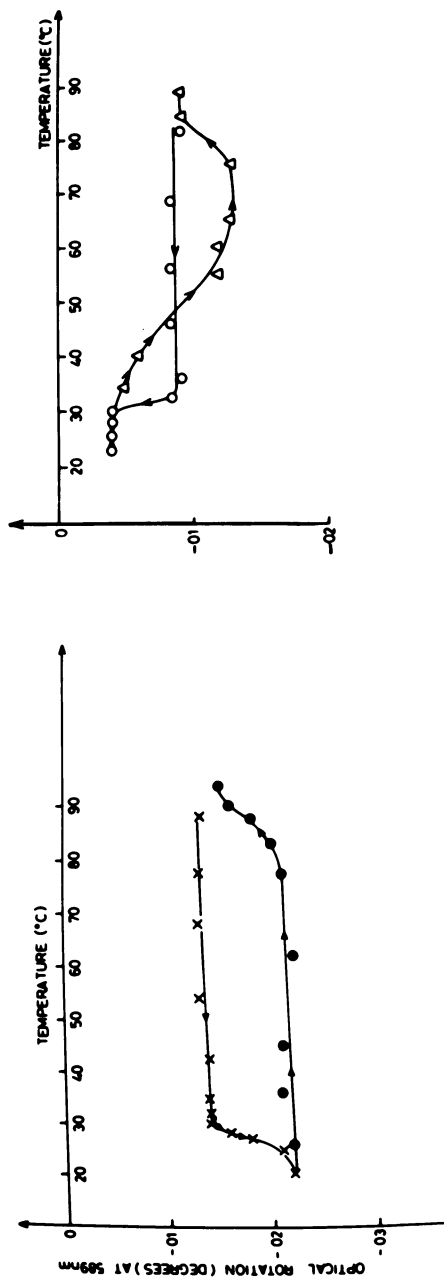
Addition of locust bean gum (1%) to the non-gelling segmented agarose (0.2%) results in a firm rubbery gel which is too cloudy to be examined by optical rotation. On halving the concentration of this mixture a non-gelling system is obtained which is clear enough for optical rotation studies. This mixture shows the "butterfly" hysteresis without gelation (see Figure 5). Therefore, this optical rotation behaviour also originates from molecular effects.

If the magnitude of the positive contribution to the cooling shift is used as a measure of the extent of interaction between non-gelling agarose concentrations and locust bean gum, we find that, as galactomannan concentration increases the extent of interaction increases in absolute terms until the agarose is saturated (see Figure 6). At the higher galactomannan concentrations the proportion of the interacting galactomannan decreases. All this would be expected if the binding obeyed any form of equilibrium law. Figure 7 shows the optical rotation hysteresis curves pertaining to some of



Advances in Carbohydrate Chemistry and Biology

Figure 3. Optical rotation changes during setting and liquefaction of an agarose gel (0.2%) (16)



Advances in Carbohydrate Chemistry and Biology

Figure 4. Comparison of the optical rotation variations with temperature (right) for agarose at a nongelling concentration (0.05%) and (left) for a gelling mixture of agarose (0.05%) and locust bean gum (0.1%). Measurements were at 589 mm (16).

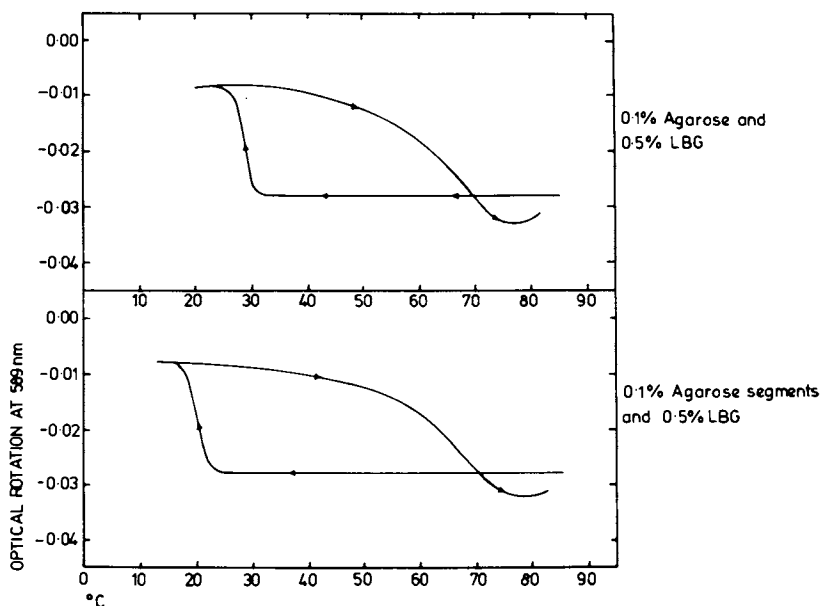


Figure 5. Comparison of the optical rotation variations with temperature (above) for a gelling mixture of agarose (0.1%) and locust bean gum (0.5%), and (below) for a nongelling mixture of segmented agarose (0.1%) and locust bean gum (0.5%)

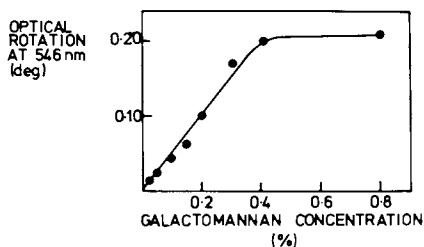


Figure 6. Variation of the positive contribution to optical rotation in mixtures of agarose (0.05%) and locust bean gum. Measurements were at 589 nm.

(5)

Journal of Molecular Biology

the points in Figure 6. It is clear that optical rotation changes between 20°C and 70°C on the heating curve, can be attributed to melting of the locust bean gum ordered conformation. It can be seen that the mid-point of this transition increases by as much as 20°C with locust bean gum concentration. By increasing the concentration of the galactomannan, we are evidently increasing the concentration of binding sites for the agarose helices, so driving the melting transition to higher temperature by a mass action phenomenon. This increases in hysteresis with locust bean gum concentration is also accompanied by an increase in the melting point of the gel.

We might suspect that, superimposed upon this effect, is an influence from microheterogeneity of the locust bean gum chains; they can be expected to carry a variety of binding sites with a spectrum of stabilities in the bound state with agarose. Higher locust bean gum concentrations will make available not only a higher population of total binding sites but also a higher population of sites with higher affinity for agarose. This hypothesis is confirmed by fractionation studies⁴ on locust bean gum on the basis of the water solubility.

The locust bean gum was stirred in distilled water for 12 hours at 10°C, and the solution was removed by centrifugation and freeze-dried to yield the "cold water soluble fraction". The insoluble residue was stirred in hot distilled water (90°C) for 2 hours and the solution again removed by centrifugation and freeze-dried to give the "hot water soluble fraction". The mannose to galactose ratios of the "whole", "cold water soluble fraction" and "hot water soluble fraction" were 3.35, 3.0 and 4.0 respectively. The materials were found to differ in their interaction properties with agarose, the hot water soluble, low galactose containing, fraction having the greatest reactivity (see Figure 8).

Some indication for the relative importance of microheterogeneity on the one hand, and mass action effects on the other, can be obtained by comparison of the behaviour of different galactomannans with agarose. Figure 9 shows a set of optical rotation curves for the interaction of agarose with locust bean gum (77% mannose, 23% galactose), tara gum (76% mannose, 24% galactose), cold water soluble extract of Gleditsia triacanthos seeds⁸ (73% mannose, 27% galactose), hot extract of Gleditsia triacanthos seeds⁸ (76% mannose, 24% galactose) and guar gum (61% mannose, 39% galactose). There is a trend from a large hysteresis for the positive rise in optical rotation in the case of locust bean gum to little or no hysteresis in the case of guar gum. Although the mannose to galactose ratios for the first four galactomannans are very similar, locust bean gum and tara gum give significantly different results, and both are quite different from the

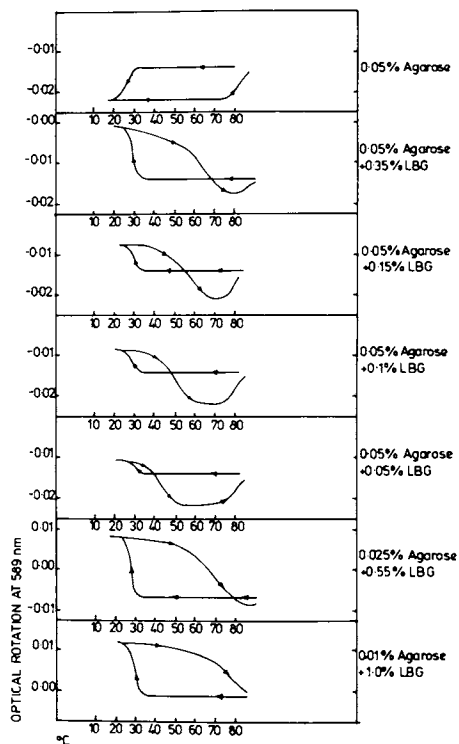
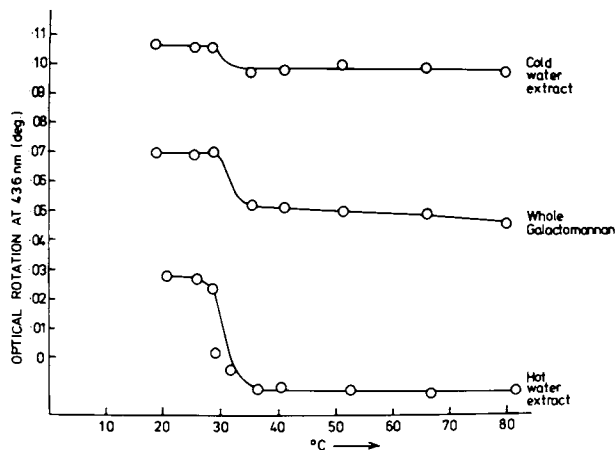


Figure 7. Comparison of the optical rotation variations with temperature for agarose at a nongelling concentration (0.05%) and a number of agarose-locust bean gum mixtures



Advances in Carbohydrate Chemistry and Biology

Figure 8. Comparison of the optical rotation variations with temperature for (top) a gelling mixture of agarose (0.05%) and the cold-water-soluble fraction of locust bean gum (0.4%), (middle) a gelling mixture of agarose (0.05%) and whole locust bean gum (0.4%), and (bottom) a gelling mixture of agarose (0.05%) and the hot-water-soluble fraction of locust bean gum (0.4%) (16).

American Chemical
Society Library

1155 16th St. N. W.

Washington, D. C. 20036

Gleditsia gums. This would indicate significant differences in fine structure for these galactomannans.

Moreover, comparison of different agarose to galactomannan ratios indicates similar hysteresis behaviour as shown by locust bean gum, but to varying extents. Thus the variation in hysteresis behaviour of agarose - tara gum mixtures with tara gum concentration is less than that of agarose - locust bean gum mixtures, while the hysteresis shown by agarose - Gleditsia galactomannan systems varies only slightly with galactomannan concentration. This large difference in the sensitivity of hysteresis to galactomannan concentration suggests that mass action plays a relatively minor role. Rather this hysteresis effect can be used as a probe for the width of the molecular spectrum of galactomannan, since at low ratios of agarose to galactomannan the agarose binds that fraction of galactomannan with which it interacts best. Thus locust bean gum has wide spectrum varying from weakly binding to quite strongly binding components, while Gleditsia galactomannans have a fairly narrow spectrum of weakly binding molecules. This is further emphasised by the fact that cold water extract of Gleditsia triacanthos seeds interacts with agarose to much the same extent as the hot extract of these seeds.

Interaction with Glucomannans

Pure β 1,4-D-glucomannan, like β 1,4-D-mannan, is insoluble in water. The solubility of 'konjac mannan' (actually a glucomannan) is caused by the low degree of acetylation (D.S. 0.15)². Evidently these occasional acetyl groups along the chain, sterically prevent the aggregation of the D-glucomannan backbone because deacetylation in dilute alkali leads to precipitation of pure glucomannan. It is not known whether there are regions of the backbone which are acetate rich and acetate free, or whether the acetates are relatively evenly distributed. The structural evidence available suggests that the mannose and glucose residues are distributed fairly evenly along the main chain, rather than in mannose rich and glucose rich blocks.

Since the backbone of 'konjac mannan' differs from galactomannans only in the orientation of the hydroxyls on C-2 of the glucose residues (38% of the main chain)¹⁰, tests were carried out to determine whether it interacts synergistically with agarose and κ -carrageenan. The ability to gel non-gelling agarose (0.05%) and κ -carrageenan (1%) ranked about equally with that of locust bean gum. Despite the fact the 'konjac mannan' and locust bean gum interact with agarose to similar extents, as shown by gelling experiments, the temperature dependence of optical rotation for agarose - 'konjac mannan' mixtures differs significantly from that shown

by agarose - locust bean gum mixtures. Thus while agarose/locust bean gum mixtures show net positive optical rotation changes on cooling, agarose/'konjac mannan' mixtures only show a reduced negative transition. The reason for this difference is not understood, but one possible explanation is that the ordered conformation adopted by the 'konjac mannan' backbone is different from that adopted by the mannan backbone of galactomannans. 'Konjac mannan' gels non-gelling concentrations of κ -carrageenan to the same degree as locust bean gum, and it induces the formation of the κ -carrageenan double helix in the same way. (See Figure 10).

An interesting interaction was also noted between agarose and a Spruce hemicellulose glucomannan which was a gift from Professor G.O. Aspinall. Since the preparation is water soluble, the glucomannan is presumed to be of low molecular weight as it contains less than 1% D-galactose. On cooling a non-gelling concentration of agarose (0.05%) with the Spruce hemicellulose preparation (1%), rapid precipitation occurred instead of gelation. However a mixture of 0.2% agarose with Spruce hemicellulose (1%) gave a gel with a greater gel strength than 0.2% agarose alone. In this interaction the D-glucomannan backbone is considered to associate with the agarose tertiary structure in the normal way, resulting in a more highly cross-linked framework. The precipitation of the lower agarose concentration probably results because the glucomannan is of low molecular weight, so that when they bind to the agarose they are too short to give the extra cross-linkages that are necessary for gelation. Similarly a non-gelling carrageenan solution (2%) set to a firm gel when the glucomannan was present at a level of 0.5%.

Interaction with Glucans

The plant seed amyloid and galactomannans have obvious similarities in structure. In the amyloids, a cellulosic backbone is substituted by disaccharide and sometimes monosaccharide stubs. The amyloids studied were from Tamarindus indica, in which approximately 75% of the glucose residues in the backbone are substituted by side chains, and Annona mucronata (a gift from Dr. P. Kooiman), in which approximately 25% of the glucose residues in the backbone were substituted¹⁴. These were found to gel 0.05% agarose at levels of 1%. The interaction is quite weak and similar to guar gum. Although this could indicate that the extent of substitution of the cellulosic backbone has little effect on the strength of the gelling interaction with agarose, the poor performance of the Annona mucronata could arise because it is of lower molecular weight. Examination by optical rotation indicates positive contributions from both amyloids, which are

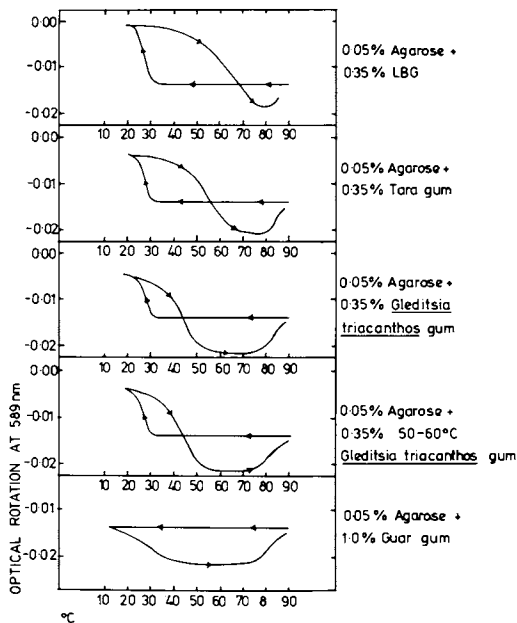


Figure 9. Comparison of the optical rotation variations with temperature for a range of agarose-galactomannan mixtures

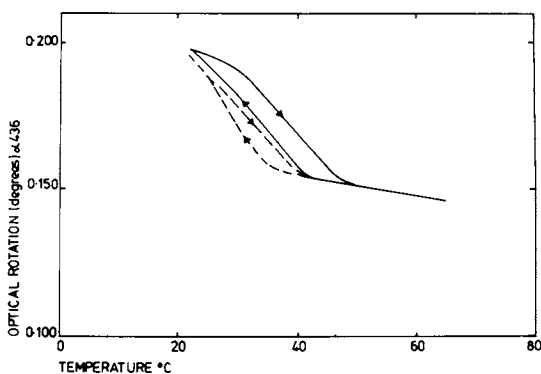


Figure 10. Comparison of the optical rotation variation with temperature for 2% κ -carrageenan (---) and a mixture of 2% κ -carrageenan 0.5% konjac mannan (—)

of the same order and similar to that found for guar gum when mixed with agarose (cf. Figure 9). (These small positive contributions to optical rotation are in line with that found for 'konjac mannan' with agarose, and could indicate that the β 1,4-D-mannan backbone exhibits this effect to the greatest extent.) On reheating, both agarose/amyloid mixtures give optical rotation behaviour similar to that of agarose/guar gum, and indicates that the amyloid/agarose associations break down rather easily.

Carboxymethylcelluloses (CMC) are another type of soluble cellulose which have been shown to be capable of replacing galactomannans in the interaction with agarose. Two low viscosity CMC's of different degree of substitution (D.S.) were investigated (D.S. 0.4 and 0.7). The same amount of both these CMC's (0.7%) was required to gel 0.05% agarose). Examination of the interaction between agarose and CMC by optical rotation gave closely similar results to those obtained with the amyloids.

Non-gelling κ -carrageenan solutions (2%) can also be gelled by the addition of polysaccharides with a β 1,4-D-glucan backbone, such as the *Tamarindus indica* amyloid (0.5%) and CMC (0.5%). The addition of 0.5% CMC has a similar effect on the optical rotation-temperature profile of κ -carrageenan as does locust bean gum and 'konjac mannan'. (cf. Figure 10). These results therefore give further evidence that β 1,4-D-glucan chains can interact with agarose and κ -carrageenan in a similar fashion to the β 1,4-D-mannan backbone of galactomannans. However, because of the possible differences in distribution of the side groups in galactomannans and these cellulosic derivatives it is not possible at this stage to decide whether the two types of backbone bind to the same or differing extents.

The bacterial polysaccharide Xanthan Gum comprises a regularly substituted cellulose backbone, and shows quite different solution properties from the plant amyloids. No ability to interact with agarose or κ -carrageenan was observed for Xanthan Gum.

Interaction with Xylans

The interaction of agarose with two heavily substituted β 1,4-linked D-xylans was studied. Using the same gelation and optical rotation criteria, the heavily substituted xylans from sapote gum¹³ and *Watsonia pyramidata* corm sacs¹⁴ were found to interact, albeit weakly, with agarose. It is significant that these heavily substituted xylans interact with agarose; almost all the xylose residues in sapote gum are substituted¹³ while some of the xylose residues in the *Watsonia* polysaccharide are even disubstituted¹⁴. Solution

studies¹⁵ with self-associating hemicellulose xylan system have indicated that the arabinofuranosyl side chains have an unusual function, in that they do not cause termination of binding sites. Rather the associations remain, but in a modified form. A similar role for side chains in the association of *Watsonia* polysaccharide and sapote gum with agarose would explain why these heavily substituted D-xylans interact as well as they do with agarose.

An interesting interaction was observed between agarose and the water soluble fraction of esparto xylan, which was gifted by Professor G.O. Aspinall. This is a lightly substituted and fairly low molecular weight xylan. As in the case of Spruce hemicellulose cooling a non-gelling concentration of agarose (0.05%) with the xylan (0.75%-1.5%) a rapid precipitation occurred instead of gelation. In this interaction the xylan chains are envisaged to associate with the agarose tertiary structure in the normal way, but due to its low molecular size the extra cross linking necessary for gelation cannot occur. Instead, the binding of the xylan chains to the agarose causes it to precipitate much faster than it would normally. κ -carrageenan also interacts with polysaccharides based on a β 1,4-D-xylan backbone. κ -carrageenan (2%) is gelled by addition of sapote gum (0.5%) but not by the xylan from *Watsonia pyramidata* corm sacs. The interaction with sapote gum (totally monosubstituted) is interesting as such a level of substitution prevents interaction of κ -carrageenan with the galactomannans. These results further emphasise the versatility of agarose and κ -carrageenan in their interaction with the β 1,4-linked series of polysaccharides. It is apparent that loss of the hydroxymethyl group does not prevent D-xylans binding to agarose and κ -carrageenan.

Conclusions

From the preliminary studies, the mechanism of the synergistic interaction between agarose or κ -carrageenan and galactomannans was considered to involve ordered binding between ribbon-like smooth regions on the galactomannan chains and the double-helical regions of agarose or κ -carrageenan, (Figure 1). This more thorough investigation of the phenomenon in general supports this description of the interaction. It is apparent that the β 1,4-D-mannan backbone is not a total requirement for the interaction. Substituted β 1,4-linked D-glucomannan, D-glucans and D-xylans all exhibit the same type of interactions as galactomannans. The comparative evidence is however, not yet good enough to determine whether these different backbones have identical or different binding activities with agarose. As in the case of galactomannans,

results for substituted D-glucans indicate that a certain degree of substitution along the chain is compatible with binding to agarose; totally substituted regions are however believed to be non-interacting. In the case of D-xylans however the situation is different since the results indicate that totally substituted β 1,4-D-xylan chains can bind agarose and κ -carrageenan although the strength of binding is modified.

Skeletal polysaccharides based on β 1,4-D-mannan and β 1,4-D-xylan backbones exist in the cell walls of red seaweeds which contain agarose or carrageenan in the intracellular matrix. It therefore seems reasonable to suggest that the associations described mimic the natural associations which may exist between the components of the cell wall and the matrix.

Literature Cited

1. S. Arnott, A. Fulmer, W.E. Scott, I.C.M. Dea, R. Moorhouse and D.A. Rees, J.Mol.Biol., 1974, 90, 269.
2. S. Arnott, W.E. Scott, D.A. Rees, and C.G.A. McNab, J.Mol.Biol., 1974, 90, 253.
3. S. Arnott, W.E. Scott, I.C.M. Dea and D.A. Rees, unpublished work.
4. D.A. Rees, in G.O. Aspinall, Ed., "Carbohydrates", MTP Int. Sci., Vol. 7, Butterworths, London, 1975, p.251-283.
5. I.C.M. Dea, A.A. McKinnon, and D.A. Rees, J.Mol.Biol., 1972, 68, 153.
6. M. Duckworth and W. Yaphe, Carbohyd. Res., 1971, 16, 189.
7. P.A. Hui and H. Neukom, Tappi, 1964, 47, 39.
8. C. Leschziner and A.S. Cerezo, Carbohyd. Res., 1970, 15, 291.
9. N. Sugiyana, H. Shimahara, and T. Andoh, Bull.Chem.Soc.Jap., 1972, 45, 561.
10. K. Kato and K. Matsuda, Agr.Biol.Chem.(Tokyo), 1969, 33, 1446.
11. P. Kooiman, Rec.trav.chim., 1961, 80, 849.
12. P. Kooiman, Phytochemistry, 1967, 6, 1665.

13. A.M. Stephen and E.A.G.L.E. Schelpe, Die suid-Africaanse Industriële Chem., 1964, 12.
14. D.H. Shaw and A.M. Stephens, Carbohyd. Res., 1966, 1, 400.
15. I.C.M. Dea, D.A. Rees, R.J. Reveridge and G.N. Richards, Carbohyd. Res., 1973, 29, 363.
16. I.C.M. Dea and A.A. Harrison, Advances in Carbohydrate Chemistry and Biochemistry, 1975, 31, 241-313.

RECEIVED September 16, 1980.

Deep Blueing Mechanism of Triiodide Ions in Amylose Being Associated with Its Conformation

TAKASHI HANDA, HIROFUMI YAJIMA, TADAHIRO ISHII,
and TAKESHI NISHIMURA

Department of Chemistry, Faculty of Science, Science University of Tokyo,
1-3, Kagurazaka, Shinjuku-ku, 162 Tokyo, Japan

It is generally accepted that the increase in the degree of polymerization (DP) of amylose is accompanied with the bathochromic shift of the blue band (1, 2, 3, 4, 5) and the bluing of iodine/iodide in amylose depends on their concentrations (6) and the mixing rate of iodine/iodide with amylose (7, 8). The bluing mechanism of triiodide ions in starch was first explained by Robin (9) using electronic theory. As an extension of his work, the change of circular dichroism (CD) spectra with the bathochromic shift of the blue band was studied by Handa and Yajima (10, 11) in correlation with the conformation of the amylose-triiodide complex in aqueous solution. However, the characteristics of CD bands correlated with the nature of the deep bluing band peculiar to high DP amylose have not yet been satisfactorily interpreted in accordance with the conformational change of amylose in aqueous solution.

The object of this paper is first to correlate the deep bluing of iodine/iodide with the characteristics peculiar to the conformation of high DP amylose on the basis of the changes in the CD spectra and secondarily to clarify the underlying mechanism governing the phenomena.

Experimental

Materials. Amyloses with average DP 10-500 were prepared by enzymatic degradation of the long polymer. Those samples with DP 10, 20, and 30 were obtained by fractionation through Sephadex-Gel columns. Amylose of DP 1000 was isolated from potato starch by Schoch's method (12). Amyloses with DP 2500 and 4500 were of commercial grade from Wako Pure Industries and Nagase Co., Ltd., respectively. The molecular weights of the amyloses were determined by reducing-end measurement (13) and viscometry (14).

Preparation of Amylose Solutions. Amylose (100 mg) was dissolved into 3 ml of 1 N KOH solution. Then, the solution was

neutralized through an Amberlite column and diluted to 0.1 %.

Preparation of Amylose-Iodine-Iodide Complex Solutions.

The complex solution was prepared at room temperature by mixing of an amylose solution with an equal volume of KI-I₂ solution using different mixing times.

Measurements. Measurements of absorption and CD spectra were made using a Hitachi EPS-3T spectrophotometer and Jasco J-20 spectropolarimeter, respectively. The spectra were always measured 24 hrs after preparation.

Results and Discussion

KI-Effect. It is known that an increase in KI concentration brings about a blue shift of the blue band at a relative low concentration of I₂. Cronan and Schneider (6) pointed out on the basis of a stoichiometric study that the composition of the bound species of iodine/iodide (I₂.I_b) varied from I₂ to I₃⁻ (b = 0 → 1) with increase of the KI concentration. Handa and Yajima (10) explained the bluing mechanism of triiodide ions bound cooperatively by amylose in the presence of excess KI as coming from the exciton-coupling in a dimeric unit, using electronic theory. They (15) also proposed the lengthening of the coloring unit constituting a segment of polyiodide chain from I₂²⁻ (I₃.I₃) to I₂²⁻ (I₃.I₂.I₂.I₃, I₂.I₃.I₃.I₂ or I₂.I⁻.I₂.I₂.I⁻.I₂)⁶ through I₈²⁻ (I₃.I₂.I₃) corresponding to decrease in the b value, on the basis of the assignment of the four fundamental resonance Raman lines which obviously appear at 159, 111, 55, and 27 cm⁻¹. Likewise, it should be mentioned that the coloring is strongly involved with the multiple charge transfer processes which combine the aforesaid species with the amylose lattice.

Figure 1 shows the change in the CD spectra with an increase of KI concentration at high I₂ concentration for high polymer DP 1000 in the rapidly mixed system. Therein, the composition of the bound species varies depending on the change of b-value in I₂.I_b from 0.5, 0.7, 0.9 through 1 corresponding to the increase of KI concentration from 1.2 x 10⁻⁴, 6.0 x 10⁻⁴, 4.8 x 10⁻³, 8.4 x 10⁻³, 1.2 x 10⁻², and 2.4 x 10⁻² M, respectively, based on the stoichiometric determination (6). The mutually split CD bands with opposite signs and symmetrical intensity in the blue band region at low iodide concentration give way to a mild asymmetry above 6.0 x 10⁻⁴ M of KI. At high iodide concentration above 8.4 x 10⁻³ M, the CD bands have the same positive sign. On the other hand, for low DP below 100, the change in intensities of the absorption and CD spectra with iodide concentration was insignificant, although the spectra did show a blue shift depending on the change of bound species. Therefore, it can be said that the behavior of the CD spectra in Fig.1 is peculiar to high DP amylose.

On the electronic aspect of the phenomena, the lowering of

the positive peak associated with the asymmetric shallowing of the negative valley can be ascribed first to the increase in the contributions from the interaction of in-plane oriented dipoles belonging to a pair or double pairs of ions in side-by-side aggregated helices and secondly from a skewed pair of ions at the intermolecular junctions of amylose chains (11). To conform the electronic interpretation of the phenomena at a submolecular level to the understanding from the light scattering study at a molecular level as described in later section, we had to consider that uncomplexed amylose chain in aqueous solution may possess intrinsically the parts for two kinds of junctions, i.e., intra- and intermolecular junctions. In this respect, the side-by-side association of partially or completely filled helices originates probably from the rearrangement of hydrogen bonds by iodine/iodide at the intramolecular junctions, whereas the occurrence of the binding of ions in a skewed pair is presumably specific to the rearrangement of hydrogen bonds at the intermolecular junctions.

From another aspect based on the kinetic study of the complex reaction (11, 16), it is believed that the binding of most of iodine/iodide with the lattice of a long polymer is achieved within 1 msec and the configuration of iodine/iodide in the single helices is almost attained close to that for DP 100 within 200 msec. The completion of the configuration of the bound iodine/iodide at the intra- and intermolecular junctions is conceivably achieved with a longer relaxation time. Hence, the extent to which the binding of iodine/iodide occurs in side-by-side associated helices and at intermolecular junctions in the aggregates must depend on the composition of the bound species. We suggest that with increasing KI concentration, the extent of the compact aggregation of helices and the intermolecular entanglement are pronounced not only due to the shielding of electrostatic repulsion but also due to the decrease in the flexibility of the polyiodide chain conforming to the unit segment length which depends on the nature of the bound species. The consideration that the intermolecular junctions increases with KI concentration is supported by the result of KI dependence of sedimentation coefficient of the complex by Dintzis et al (17).

DP-Effect. Figure 2 shows the DP dependence of the absorption and CD spectra for the complex in excess KI at the rapid mixed rate. The spectra are represented by displaying the molar extinction coefficient (ϵ) and molar ellipticity ($[\theta]$) of bound triiodide ions ($I_{3,b}^-$) in amylose. Those spectra were obtained from the observed ones as reported previously (11). The molarity of the $I_{3,b}^-$ ions was determined using dialysis. The I_2 concentration (5.1×10^{-2} mM) of the system corresponds to a degree of saturation of the $I_{3,b}^-$ ions (q) from 0.9 to 1.0 on the basis of the guide-line method (6) for the plot of the molarity of the $I_{3,b}^-$ ions vs. the dosage of I_2 . As shown in the absorption spectra, the bathochromic shift of the colored band from 440 to 800 nm was

Figure 1. Effect of KI concentration on the CD spectra in the rapidly mixed system KI (in moles): (a) 1.2×10^{-4} ; (b) 6×10^{-4} ; (c) 4.8×10^{-3} ; (d) 8.4×10^{-3} ; (e) 1.2×10^{-2} ; (f) 2.4×10^{-2} . Amylose (DP 1000), 0.05 g/L; I_2 , 5.1×10^{-2} mM.

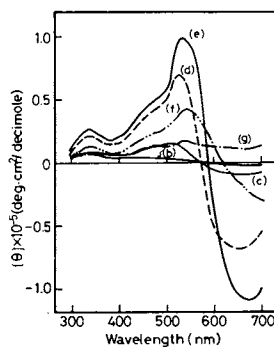
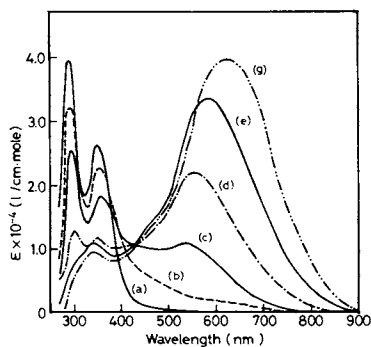
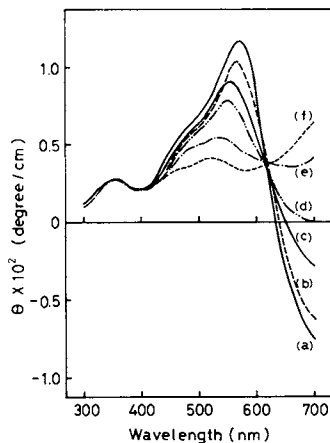


Figure 2. Effect of DP on the absorption and CD spectra of $I_{3,6}$ in amyloses in the rapidly mixed system DP: (a) 10; (b) 20; (c) 30; (d) 42; (e) 100; (f) 190; (g) 1000. Concentrations: amylose, 0.05 g/L; KI, 1.2×10^{-2} M; I_2 , 5.1×10^{-2} mM.

observed with the increase of DP above 10 which was taken as the apparent achromic point. A similar hyperchromic effect was observed in CD bands up to DP 100. The intensities of CD bands decreased significantly with the increase of DP above 100, associated with the gradual bathochromic shift of the blue band. CD bands for DP 1000 did not form a normal pattern. These results suggest that the high polymer complex possesses the deep bluing species in the aggregate of the amylose helices. The asymmetric shallowing of the CD bands can be ascribed to the increase of the foregoing exciton-coupled interactions as discussed in the previous section.

I₂-Effect. Figure 3 shows the effect of iodine concentration or q value on the CD spectra for high polymer DP 1000 in the rapidly mixed system. Up to $q \approx 0.8$, the mutually split CD bands with opposite signs remained almost unchanged in the pattern and intensities, but above $q \approx 0.8$, the intensities of the CD bands decreased asymmetrically and very pronouncedly. However, it should be noted that a symptom for the latter change was indicated at a q of 0.6. Then, the CD bands had the same signs around a q of 1, where the wavelength of maximum absorption shows a continuous red shift.

Normally, the intensities of CD bands (+,-) appear much weaker for long polymers than that for the DP 100 even at a q of 0.2. This implies that the bluing of the ions in side-by-side associated helices and in portions at intermolecular junctions occurs even at a low q . The anomalous change of CD pattern above $q \approx 0.8$ can be ascribed to an initiation of specific aggregation as affected by the extra-ions belonging to the second adsorption (6). The results of component analysis by the decomposition of each spectrum in Fig.3 reveal that above $q \approx 0.8$, a considerable part of the dipole interaction tends to occur in-plane with scanty rotatory strengths due to the side-by-side aggregation of filled helices through folding with a turn of ca. DP 100.

From the calorimetric data (18), an extra-change of the lattice is expected from the structural energy being involved with the packing of the ions above $q \approx 0.6$, despite of the fact that the energy of the cooperative adsorption in dimeric units did not vary below $q \approx 0.6$. Figure 3 shows the corresponding symptom at a q of 0.6 with regard to the change of CD spectral pattern for the rapidly mixed system.

Conformational Change with q at a Molecular Level. The resonance light scattering study with polarized lights from Ne-He laser provided information at a molecular level on the conformational change of the complex with q (19). The highlights of the study can be characterized first by a priority of rod character which suggests a specific extension of the conformation toward one direction at the binding of iodine/iodide as being manifested by an anomalously high value of the depolarization ratio ρ_u and its

pronounced increase with q . Secondly, the highlights can also be characterized by an outstanding contraction of the molecular volume even in a lower range of q in accordance with a decrease in the dissymmetry value Z being endorsed by a pronounced increase in ρ_u . Thirdly, the structure of the complex must preserve some coil nature intermixed with rod character as being suggested by a quasi-constancy of the ρ_h value which stayed always close to 1, irrespective of q .

To characterize the conformational change with q , the fitting of the results was pursued on computer with regard to ρ_u and Z on the basis of the model in a combination of coil and rod^u besides that in the worm-like chain. In the former model, the conformational change was characterized by the change in the rod factor, contour length and anisotropic factor at a given segmental number, whereas the conformational change was characterized by the change in the contour length, persistent length and anisotropic factor in the latter model. Both results conformed well to each other except some inconsistency on the estimates of the contour length at a low q below 0.2. However, the benefit in employing the latter model exists in that the simulated result can uniquely depict the process schematically in the q -dependent conformational change of the complex. The complex solutions contained in the rapidly mixed system: 0.01 g/l of amylose (DP 2000), 0.24–2.4 mM of KI, and 1.6×10^{-3} – 2.4×10^{-2} mM of I_2 .

As a result, the following are surmised:

(1) Uncomplexed amylose in aqueous solution must exist as an aggregate on average in tetramer-pentamer which was estimated from the best fit of the observed Z value (1.3) with the theoretical one using the persistent length of 13.6 Å (20).

(2) In so far as the rapidly mixed systems were concerned, the extreme shortening of the contour length even at a q within the range of 0.1–0.2 was uniquely confirmed by the fitting either in the former or in the latter model. Being based on an obvious increase in ρ_u or ρ_v , it was predicted that the anisotropy of the effective segment increases eminently and the persistent length of the complex chain elongates appreciably. The latter result relates to a serious decrease in the number of the effective segments. Accordingly, we have to admit the occurrence of some critical change similar to the phase transition in the conformation of the amylose matrix due to the binding of iodine/iodide even at a low dose. Hence, it seems likely that there is no other alternative explanation on these results except the following: First, a remarkable contraction occurs in an amylose molecule itself through some transition of coil to helix by a cooperative action in the propagation and rearrangement of hydrogen bonds resulting in the unravelling of intermolecular junctions. The unravelling must bring about an extra-contribution to the shortening of the contour length in an extent to which the dissociated molecules indicated a persistent length of ca. 300 Å at $q=0.1$ –0.2. This value was significantly longer than that of deformed helix

(ca. 40–70 Å) (21, 22). Therefore, it may be considered that the surplus in the elongation of the persistent length comes from the side-by-side association of partially filled helices. In respect of an pronounced increase in the anisotropy, the occurrence of a further aggregation of the side-by-side associated helices onto their traverse direction can hardly be considered in this range of q . The vertical progression in the side-by-side association of helices will result in the shortening of the contour length on one hand and on the other hand, in the elongating of the persistent length effectively even at a low dose of iodine/iodide with q below 0.2.

(3) In accordance with a pronounced increase in ρ_u with q in the range of 0.2–0.7 and the corresponding decrease in Z , the increase in the persistent length and anisotropy still continued despite of a slight difference in the shortening of the contour length with q in this range as compared to that in the former range of q . Taking account of a slight decrement in the contour length and a significant increment in the anisotropy with q , the remarkable increase in the persistent length can be understood as coming from the tightening of helices through the progression of the complexation. This stimulates the orientation of thin-rod segments toward the vertical direction. Therefore, the incidence of the aggregation to pile up the side-by-side associated helices toward their traverse direction must be yet rare in the q range of 0.2–0.7. Provided that the creation of skewed pairs of ions at the intermolecular junctions can be regarded as a difference between the incidence of the authentic unravelling and that of the unravelling by the intermolecular entanglement, the number of unravelled intermolecular junctions by the binding of iodine/iodide is presumably fewer than that in the former range of q .

(4) In accordance with a specific decrease in ρ_u and Z in the higher range of q above 0.7, a decrease in the anisotropy was predicted despite of a still further elongation of the persistent length associated with the levelling off in the decrease of the contour length. The simulated result predicts that a considerable aggregation of filled helices occurs toward their traverse direction through a propagation of folding action with a turn of ca. DP 100 in accordance with a promotion in the extent of aggregation toward the vertical direction. Thereby, the vertical growth may be promoted being associated with a coagulation probably end-to-end by the intermolecular entanglement in taking account of the balance between an anomalous elongation of the persistent length and an inferior thickening toward the traverse direction through folding.

At $q=1$, the persistent length reached finally ca. 1000 Å which was approximately equivalent to the contour length. Similar value of persistent length was found for DNA in an estimate by the worm-like model (23). The result seems somewhat unreal. Nevertheless, it looks adequate in representing the authentic character of the complexation leading to the formation of the rod-like

structure of Bittiger et al (24). It should be noted herewith that the results differed in the slowly mixed system and the final conformation of the complex must remain in a zig-zag rod structure. The conceptualized scheme on the process of the conformational change leading to the rod-like structure of Bittiger et al. will be illustrated later in Fig.14.

Amylose-Effect. Figure 4 shows the effect of amylose concentration on the CD spectra at a weight ratio of iodine to amylose, 0.26, which corresponds to $q \approx 1$. Up to 0.01 g/l of amylose, the split CD bands in the blue band region had opposite signs and the intensities were almost symmetrical. Above 0.01 g/l, the intensities of the CD bands decreased remarkably and above 0.025 g/l, the split CD bands had the same signs. However, at $q \approx 0.5$, the change in the spectral pattern with amylose concentration did not occur so susceptibly as described above.

The intensities of the mutually split CD bands (+,-) with a symmetric pattern at the low concentration (0.005 g/l) of amylose with DP 1000 was found to be still considerably smaller than those for DP 100 at $q \approx 1$. This is primarily ascribed to the side-by-side association of helices at the intramolecular junctions. An obvious increase in the asymmetry of the CD bands (+,-) with increasing amylose concentration can be explained by an increase in the contribution from a skewed pair of the ions at the intermolecular junctions, corresponding to the increase in the number of the junctions in uncomplexed amylose with amylose concentration.

Solvent-Effect. The effect of the intermolecular junctions in the uncomplexed conformation of amylose on the aggregation of helices was examined using the amylose complex solution in H_2O and in 95 % H_2O -5% DMSO, as shown in Fig.5. Thus, for the H_2O -DMSO system, 10 mg of amylose (DP 1000) was dissolved in 10 ml of DMSO by heating the mixture at 70°C for 2 hrs, and then the solution was stored at room temperature for a day. Subsequently, the stock solution was diluted to 0.1 g/l with H_2O and then equal volumes of the solution and $KI-I_2$ solution were rapidly mixed.

A similarity is observed in the spectral patterns between the complex solution in the H_2O -DMSO system and the complex solution in H_2O at a low amylose concentration. However, the complex in 99.7% H_2O -0.3 % DMSO solution with the ratio of DMSO to H_2O close to that in the system of Dintzis et al. (17) gave only a positive CD pattern similar to that in the H_2O system (b) in Fig.5. The phenomena can be interpreted by assuming that the perturbation occurs for hydrogen bonding contributing to the structure at the intermolecular junctions due to the complexation with DMSO. This will exclude the formation of tight bonding between the ions and the lattice occupied with DMSO in the junction portions.

⁻³ It should be noted that the complex solution containing 5.8×10^{-3} N NaCl as a product of neutralization of alkaline amylose solution gave a symmetric pair of CD bands with a normal pattern

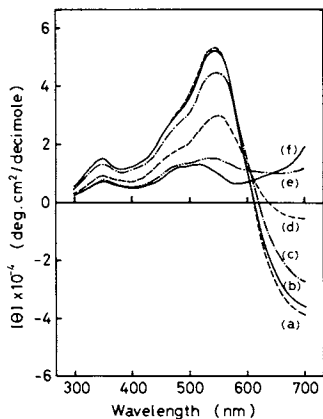


Figure 3. Effect of I_2 concentration on the CD spectra of $I_{3,b}$ in amylose (DP 1000) in the rapidly mixed system I_2 (in millimoles): (a) 7.9×10^{-3} ($q = 0.2$); (b) 2.4×10^{-2} ($q = 0.6$); (c) 3.1×10^{-2} ($q = 0.8$); (d) 3.9×10^{-2} ($q = 0.95$); (e) 5.1×10^{-2} ($q = 1$); (f) 1.2×10^{-1} . Amylose, 0.05 g/L; KI, 1.2×10^{-2} M.

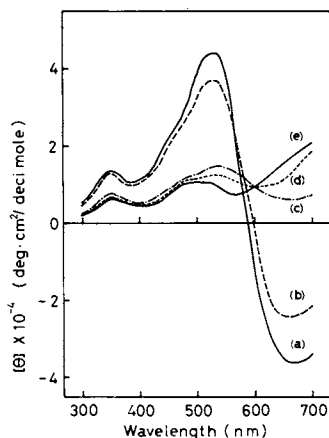


Figure 4. Effect of amylose concentration on the CD spectra of $I_{3,b}$ in amylose (DP 1000) at a weight ratio $(I_2)/(amylose) = 0.26$ and KI 1.2×10^{-2} M in the rapidly mixed system amylose (in grams/Liter): (a) 0.005; (b) 0.01; (c) 0.025; (d) 0.1; (e) 0.5.

(+,-) presenting high intensities close to those for DP 100 (a) in Fig.5. Therein, the complex solution was prepared by mixing the KI-I₂ solution with the neutralized solution of amylose which was prepared by intermixing the twentyfold diluted solution of 10 g/l amylose in 1N NaOH with HCl. However, the mere addition of an equivalent amount of NaCl to the present amylose solution was not effective in giving symmetric CD bands with a normal pattern (+,-) at the complexation with KI-I₂ solution. It only produced an asymmetric pattern close to that in H₂O system (b) in Fig.5. Therein, the amylose-NaCl solution was prepared by adding 1.2×10^{-3} mol NaCl to 100 ml of 0.1 g/l amylose solution which was prepared by the present method through an Amberlite column.

Consequently, the conformations of the complex in aqueous solution must be seriously affected by the in-situ conformation of uncomplexed amylose depending strongly on the method and cation-effect in the neutralization of alkaline amylose solution.

Mixing-Rate Effect. The effect of the rate of mixing iodine/iodide solution with amylose on CD spectra was examined to pursue the function and performance of hydrogen bonding at the intra- and intermolecular junctions in producing different conformations by the binding of iodine/iodide. Figure 6 shows the CD spectra for the complex using varying mixing rates. Slow mixing at 0.08 ml/min and rapid mixing at 300 ml/min is abbreviated by SM and RM, respectively. The spectra all had the same pattern under the mixing rate below 0.08 ml/min. As the mixing rate decreased, the CD bands for the complex reverted into the usual normal pattern, being associated with the blue shift of the band. This blue shift can be recognized as the extinction of deep bluing bands owing to the unravelling of a specific configuration of dipoles at the intermolecular junctions accompanied by the decline in the incidence of the side-by-side association of helices. However, the positive peak of the symmetric CD bands with a normal pattern (+,-) is still located in the longer wavelength side than that for DP 100, indicating a somewhat lower intensity than that for the latter. As for low polymers with DP below 1000, symmetric CD bands with a normal pattern appeared at the SM rate even for a considerably higher amylose concentration (0.1 g/l) and an I₂ concentration more than that corresponding to $q=1$. As for the long polymers with DP above 1000, the shallowing of the negative CD band tended to be magnified with DP at the SM rate, indicating an asymmetry for the CD bands (+,-). It is likely that the hydrogen bonding at the intermolecular junctions is comparatively stable in the long polymers (DP 2500 and 4500) and some parts of them still survive even at the SM rate, indicating an equivalent occupied ratio to that at the RM rate as a result of the component analysis by the resolution of spectra. Therein, the occupied ratio refers to the contribution ratio of each species in a mole of the I₃⁻ ions involved with the bluing.

The mixing rate dependence of CD spectra can be interpreted

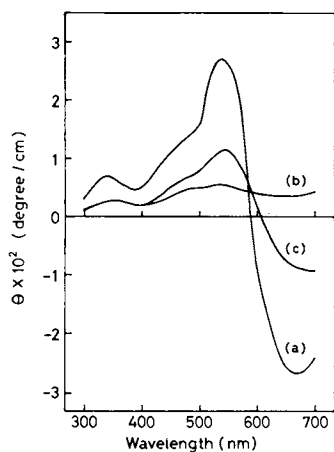


Figure 5. Effect of solvent on the CD spectra in the rapidly mixed system: (a) DP 100 in H_2O ; (b) DP 1000 in H_2O ; (c) DP 1000 in 95% H_2O -5% DMSO. Concentrations: amylose, 0.05 g/L; KI, $1.2 \times 10^{-2}M$; I_2 , $5.1 \times 10^{-2}mM$.

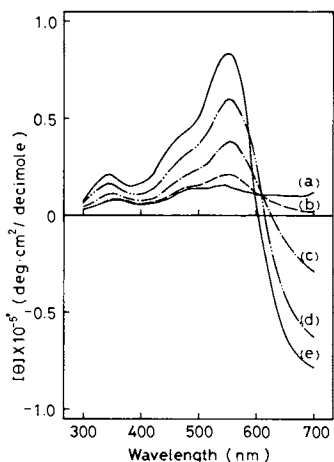


Figure 6. Effect of the mixing rate (in milliliters/min) of $KI-I_2$ solution with amylose (DP 1000) solution on the CD spectra of I_3^- : (a) 300 (RM); (b) 0.7; (c) 0.25; (d) 0.13; (e) 0.08 (SM). Concentrations: amylose, 0.05 g/L; KI, $1.2 \times 10^{-2}M$; I_2 , $5.1 \times 10^{-2}mM$.

in terms of the difference in a mode of the relaxation between the rearrangement of hydrogen bonding in the labile intramolecular junctions and that in the comparatively stable intermolecular ones. Therefore, the mode of relaxation must be governed by a time difference to attain a given value of q between two extremes (SM and RM). Taking account of these results, we propose that at rapid-mixing rate, the rearrangement of hydrogen bonds at the intra- and intermolecular junctions causes the propagation of side-by-side association of helices, whereas at slow-mixing rate, the rearrangement of the bonds particularly at the intramolecular junctions issues presumably another type of association, i.e., a braided double helix.

Decomposition and Assignment of Spectra. Following the method as applied to the decomposition of absorption and CD spectra for the DP 100 in the previous papers (10, 11), eight bands were isolated from both spectra of $I_{3,b}$ in amylose with DP below 1000 in the slowly mixed system, regardless of q . Those bands were named $S_1, S_2, S_3, \dots, S_8$ going from the long to the short wavelength. The isolated bands S_1 and S_2 in the blue band region were further decomposed into a pair of isolated bands, respectively. The species having the structure which produces the normal blue band equivalent to that of the DP 100 was named the A species whereas that producing another isolated band peculiar to long polymer was named the A' species. For the long polymer in the rapidly mixed system, the blue band composed of S_1 and S_2 bands plus a deep blue band S_0 around 700 nm was decomposed into three pairs of isolated bands: a pair of isolated bands around 570 and 700 nm with asymmetric rotatory strengths was named the C species, and the other two pairs of isolated bands with symmetric rotatory strengths were named as the A and B species, respectively.

Therefore, the conformation of the complex in the rapidly mixed system is presumed to consist of three structural parts: the normal single helix (A), the side-by-side associated helices (B) and the entangled packet around intermolecular junction (C). Thereby, the C part includes the subsidiarily created junction by intermolecular entanglement in the complexation besides the authentic junction existing in uncomplexed amylose. The complex in the slowly mixed system is composed of two structural parts for amylose with DP less than 1000 and three structural parts for higher DP amylose: the normal single helix (A), a braided double helix (A') and the entangled packet around intermolecular junction (C).

Figure 7 shows the characteristic spectral patterns of the A, A', B, and C species. Here, $S_1^A, S_1^{A'}, S_2^A,$ and $S_2^{A'}$ are called as $A_1, A_1', A_2,$ and A_2' , respectively, and also $S_1^B, S_1^C, S_2^B,$ and S_2^C as $B_1, B_2, C_1,$ and C_2 , respectively. The doubly split bands of the A' and B species are located close to those of the A species. The doubly split bands of each species have signs opposite to each other in the CD band. The dipole strengths of the twin bands (D_1, D_2) were estimated for each species in unit of 10^{-35} cgs:

4.9, 4.9; 9.9, 5.7; 9.6, 5.3, 9.5, 4.7 for the A, A', B, and C species, respectively. The rotatory strengths of the twin bands (R_1 , R_2) were estimated in unit of 10^{-38} cgs: -3.8, 3.8; -2.0, 2.0; -0.4, 0.4; 2.1, -0.4 for the A, A', B, and C species, respectively. The ratios of the dipole strengths D_1 to D_2 for the A, A', B, and C species are about 1.0, 1.7, 1.8, and 2.0, respectively. The absolute values of ratios of the rotatory strengths R_1 to R_2 are approximately equal to 1 for the A, A', and B species, while the ratio is about 6 for the C species.

In order to characterize the isolated bands, a simulation was carried out by using dimer as a coloring unit in the refinement of the exciton-coupled model proposed by Robin (9). As reported previously (10, 11), the characterization of the isolated bands for the A, A', and C species was made on the basis of a 12-th order secular equation. As for the B species, the simulation was made by using a tetramer model. As shown in Fig.8, the A' species is characterized by a configuration with a larger angle as compared with the A species. The B species is characterized by an approximately coplanar configuration with a wide fanning-out angle for each pair of dipoles in the side-by-side associated helices. The C species is characterized by the strong interaction between the long-axis transition dipoles of the ion and the short-axis transition dipoles of the other ion under asymmetric perturbation. Therein, the configuration of the short-axis transition in the skewed dimers was abbreviated for simplicity's sake. The C species is probably enclosed in a packet at the intermolecular junction portions or between the helices in the aggregate structure of side-by-side associated ones.

Conformation of the Bluing Species at a Submolecular Level.

Figure 9 shows the schematic diagram of the proposed amylose conformation at a submolecular level governing the characteristics of the bluing species. The conformation of the A species is represented by a normal helix which takes a rather looser conformation in solution than in solid. The conformation of the A' species is represented by a braided double helix which are more restricted in freedom of segmental motion than that of helix for the A species, being mutually tied together by hydrogen bonds at the braiding portions. As mentioned earlier, the A' species is suggested to originate from the transient binding at the intramolecular junctions which are also expected to take part in the formation of the B species in the rapidly mixed system. The conformation of the B species is represented by side-by-side associated helices, being considerably fixed by tight hydrogen bonds. The conformation of the C species is represented by a packet of the entangled helices among intermolecular chains.

Several Factors on the Occupied Ratios of the Bluing Species.

The factors which govern the formation of the A, A', B, and C species are examined in correlation with the solution characteris-

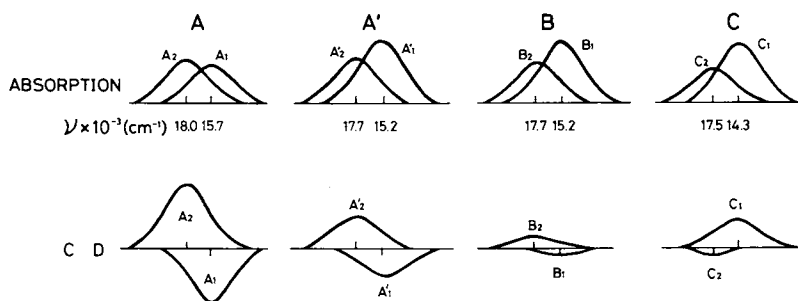


Figure 7. Spectral feature of the blueing species A, A', B, and C

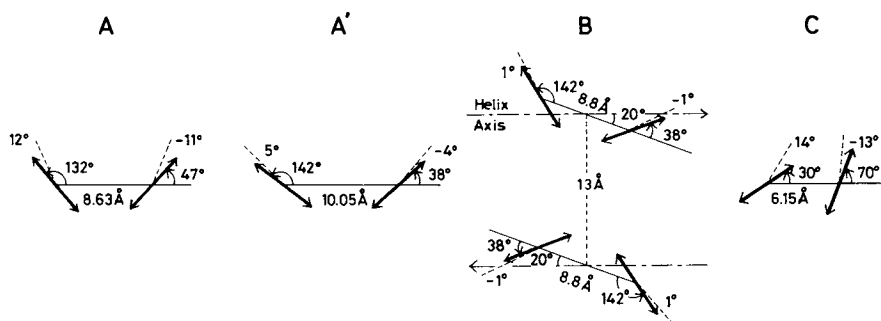


Figure 8. Configuration of the long-axis transition dipoles for the blueing species

tics of amylose in terms of the isolation of bands by spectral resolution and the results of component analysis. The dependence of the occupied ratios of these species on DP above 100 at $q = 0.5$ and 1.0 , in the SM and RM systems is shown in Fig.10. A similar dependence of the occupied ratios on the concentration of amylose for DP 1000 is shown in Fig.11.

The presumption that the C species originates primarily from the authentic intermolecular junctions peculiar to high polymer can be justified except in a low range of q : (1) the q -independence of the formation of the C species in the relation of the occupied ratio to DP and approximately the same level of the occupied ratio for the C species covering both SM and RM systems for high polymers; (2) the q -independence of the increase in the occupied ratio of the C species with amylose concentration.

The presumption that high DP amylose tends to be associated in aqueous solution is also supported by the level of threshold concentration of amylose for the onset of the formation of the C species, which occurs at a low concentration of amylose around 5×10^{-3} g/l even for the DP 1000. For higher polymers, the levels of the threshold concentration are expected to shift to a very low range around 10^{-3} g/l or less, in so far as the present method for the preparation of amylose aqueous solution is concerned.

From the q -independence of the occupied ratio for the C species in Fig.12, it is also revealed that the C species originates primarily from the intermolecular junctions existing intrinsically in uncomplexed amylose and is not created so much during complexation.

The threshold concentration of amylose for the formation of the B species is located considerably below that for the formation of the C species, as shown in Fig.11. This implies that the creation of the transient binding at the intramolecular junctions capable of yielding either B or A' species must occur independent of the creation of the binding at the intermolecular junctions. However, it is not too much exaggeration to say that the aggregation of helices through folding leading to the rod-like structure of Bittiger et al. can occur first in the concentration range of amylose above 0.005 g/l where the aggregation of uncomplexed amylose can be recognized corresponding to the revelation of the C species. It is expected that in the concentration range below 0.005 g/l, the conformation of the complex at $q = 1$ will stay in a zig-zag rod structure which consists of single helices and side-by-side associated helices even in the rapidly mixed system. Further, it is suggested that the conceptualized rod-structure coagulated end-to-end may be achieved first by a long time crystallization of these zig-zag rods in dilute solution through a quasi-static coagulation process associated with folding action.

The presumption for a correlation between the formation of the B species and that of the A' species is based on the approximate coincidence of the threshold time-interval in the mixing for the initiation of the decrease of the B species with that for the

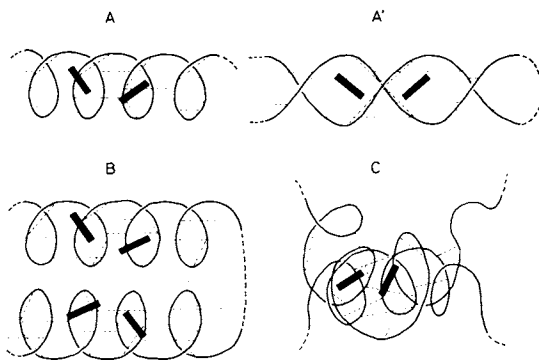


Figure 9. Schematic of the conformation of the blueing species at a submolecular level

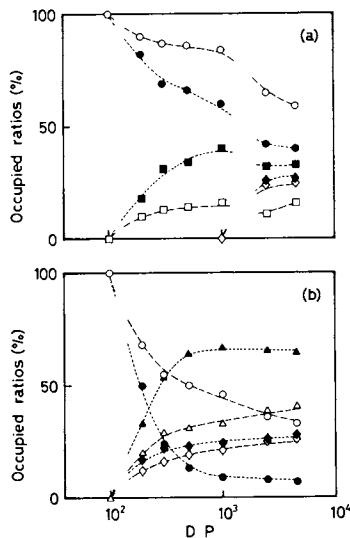


Figure 10. Change in the occupied ratios (percentages) of the blueing species with the DP above 100 at $q = 0.5$ ($\circ, \square, \triangle, \diamond$) and $q = 1$ ($\bullet, \blacksquare, \blacktriangle, \blacklozenge$) in the SM (a) and RM (b) systems: (\circ, \bullet) A; (\square, \blacksquare) A'; ($\triangle, \blacktriangle$) B; (\diamond, \blacklozenge) C. Amylose, 0.05 g/L; KI, 1.2×10^{-2} M. The occupied ratio refers to the contribution ratio of each species in a mole of the $I_{3,2}$ ion involved with the blueing.

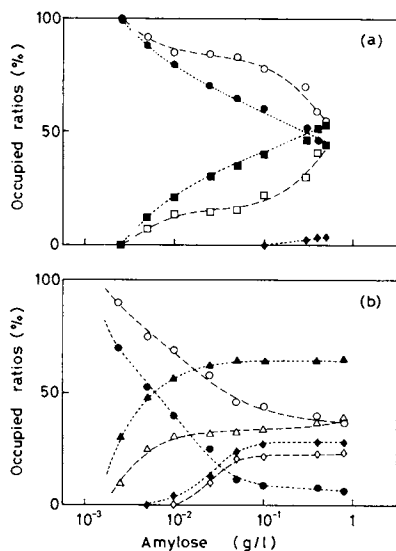


Figure 11. Change in the occupied ratios (percentages) of the blueing species with amylose (DP 1000) concentration at $q = 0.5$ (\circ , \square , \triangle , \diamond) and $q = 1$ (\bullet , \blacksquare , \blacktriangle , \blacklozenge) in the SM (a) and RM (b) systems: (\circ , \bullet) A; (\square , \blacksquare) A'; (\triangle , \blacktriangle) B; (\diamond , \blacklozenge) C. KI, 1.2×10^{-2} M.

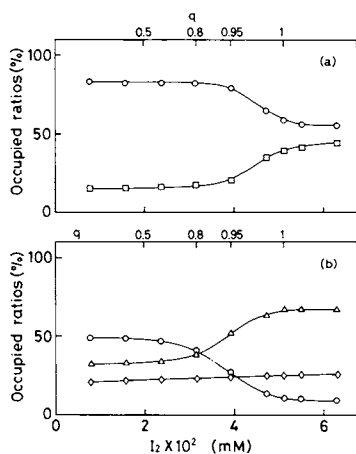


Figure 12. Change in the occupied ratios (percentages) of the blueing species with I_2 concentration or q in the SM (a) and RM (b) systems: (\circ) A; (\square) A'; (\triangle) B; (\diamond) C. Amylose (DP 1000), 0.05 g/L; KI, 1.2×10^{-2} M.

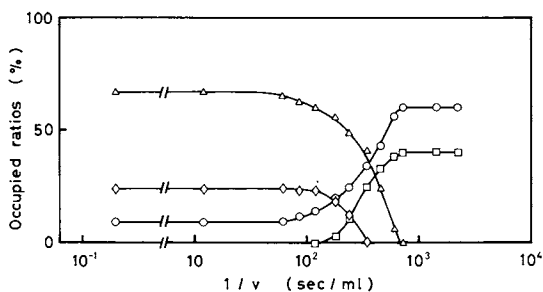


Figure 13. Change in the occupied ratios (percentages) of the blueing species with the reciprocal of the mixing rate (in milliliters per second) at $q = 1$: (\circ) A; (\square) A'; (\triangle) B; (\diamond) C. Amylose, 0.05 g/L; KI, 1.2×10^{-2} M.

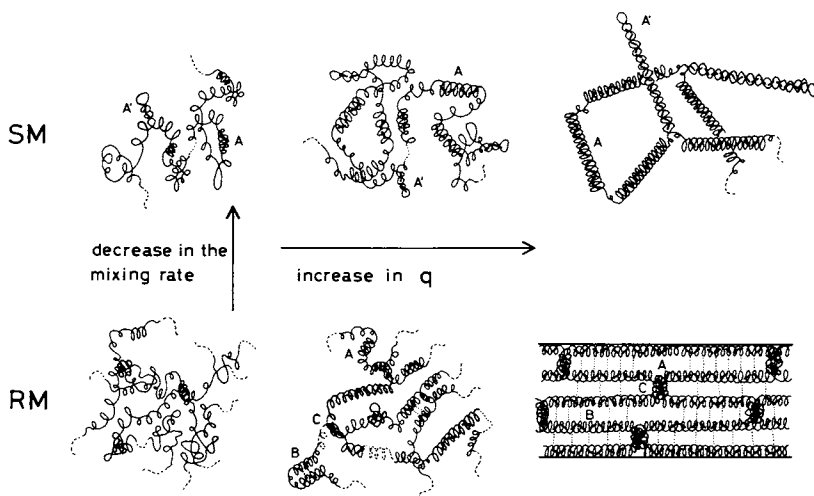


Figure 14. Schematic of the change of the complex conformation with q in aqueous solution for the slowly and rapidly mixed systems

initiation of the increase of the A species associated with that of the A species as shown in Fig.13.

Conformational Change of the Complex with q in Aqueous Solution. On the basis of the above results at a submolecular level, a schematic for the conformational change of the complex in aqueous solution with q is proposed in Fig.14 with regard to the slowly- and rapidly mixed systems and the correlation of the changes between both systems, being endorsed by the previous results at a molecular level.

In the slowly mixed system, the complex conformation is characterized by a worm-like helical chain or a randomly oriented zig-zag rod accompanied by the formation of braided double helices. The intramolecular side-by-side association of helices and intermolecular entanglement are scarcely developed due to the fractional mixing with a long interval periods exceeding the relaxation time for the rearrangement of hydrogen bonds. This may result in the exclusive formation of the A and A' species by suppressing the formation of the B species due to extinction of the C species as an anchor.

In the rapidly mixed system, the complex conformation is characterized by a rod-like structure with the intramolecular aggregation of side-by-side associated helices through folding of the chain involving intermolecular association, as presented by Bittiger et al (24).

Abstract

The deep bluing of iodine/iodide peculiar to high DP amylose was studied and a correlation of the abnormal CD spectral patterns with the conformational of the amylose-iodine complex is proposed. The conformational changes in excess KI were characterized by the characteristics of isolated bands (A, A', B, and C) from spectral decomposition of the observed blue band. Bands A, A', B, and C come from the exciton-coupling of the basic units of I_3^- ions in a normal helix, braided double helix, side-by-side associated helices, and an entangled packet of intermolecular junctions, respectively. The triiodide complex with high DP amylose can be characterized by the formation of stabilized binding of the ions with the lattice at intermolecular junctions and transient binding at intramolecular junctions. The former binding induces the aggregation of side-by-side associated helices through folding at the rapidly mixed system whereas the latter binding induces the braiding of double helices as well as the releasing helices singly in a zig-zag rod structure at the slowly mixed rate. These may intrinsically originate from the multiple characters of high DP amylose chain, which is prone to coagulate end-to-end,

fold in side-by-side helices and sometimes braid in double helices, depending on the conditions.

Acknowledgments

The authors wish to express their sincere thanks to Dr. Masao Kotani, President of the University for his kind advice and discussions. The authors also are indebted to Dr. Yaichi Ayukawa, the former director of Nakatani Memorial Laboratory, Far East Division of Corn Product Corporation USA, for financial aid and encouragement of this study and to Drs. W. Braun and Peterson, National Bureau of Standards USA, for their kind advice and helps in revising the manuscript. Finally, the authors sincerely express their hearty thanks to Dr. David A. Brant, Professor of Chemistry, University of California, Irvine, for his kind invitation to 179th ACS National Meeting, Houston, March, 1980.

Literature Cited

1. Baldwin, R. R.; Bear, R. S.; Rundle, R. E. J. Am. Chem. Soc. 1944, 66, 111.
2. Ono, S.; Tsuchihashi, S.; Kuge, T. J. Am. Chem. Soc., 1953, 75, 3601.
3. Murakami, H. J. Chem. Phys., 1954, 22, 367.
4. Ohashi, K. J. Agr. Chem. Soc. Jpn., 1959, 33, 576.
5. Banks, W.; Greenwood, C. T.; Khan, K. M. Carbohydr. Res., 1971, 17, 25.
6. Cronan, C. L.; Schneider, F. W. J. Phys. Chem., 1969, 73, 3990.
7. Pfannemüller, B. Carbohydr. Res., 1978, 61, 41.
8. Handa, T.; Yajima, H.; Kato, T.; Arisawa, H. JCS Meeting Abstract, 1975, 32, 1715.
9. Robin, M. B. J. Chem. Phys., 1964, 40, 3369.
10. Handa, T.; Yajima, H. Biopolymers, 1979, 18, 873.
11. Handa, T.; Yajima, H. Biopolymers, 1980, 19, 723.
12. Schoch, T. J. Adv. Carbohydr. Chem., 1945, 1, 247.
13. Hiromi, K.; Takasaki, Y.; Ono, S. Bull. Chem. Soc. Jpn., 1963, 36, 563.
14. Cowie, J. M. G. Makromol. Chem., 1961, 42, 230.
15. Handa, T.; Yajima, H.; Kajiura, T. Biopolymers, 1980, in press.
16. Hiromi, K.; Shibaoka, T.; Ono, S. J. Biochem., 1970, 68, 205.
17. Dintzis, F. R.; Beckwith, A. C.; Bebbcock, G. E.; Tobin, R. Macromolecules, 1976, 9, 471.
18. Handa, T.; Yajima, H.; Yamamura, T.; Ishii, T.; Aikawa, H. Stärke, 1980, 32, 194.

19. Handa, T.; Yajima, H. Biopolymers, submitted.
20. Jordan, R. C.; Brant, D. A.; Cesaro, A. Biopolymers, 1978, 17, 2617.
21. Rao, V. S. R.; Foster, J. F. Biopolymers, 1963, 1, 527.
22. Whistler, R. L.; Paschall, E. F., Eds. "Starch: Chemistry and Technology", Academic Press: New York, 1965; p. 371.
23. Hays, J. B.; Magar, M. E.; Zimm, B. H. Biopolymers, 1969, 8, 531.
24. Bittiger, H. E.; Husemann, E.; Kuppel, A. J. Polymer Sci., 1969, 28, 45.

RECEIVED September 30, 1980.

A Model for Amylose-Iodine Binding

ATTILIO CESARO and WALTER KONIC

Laboratory of Macromolecular Chemistry, University of Trieste, 34127 Trieste, Italy

DAVID A. BRANT

Department of Chemistry, University of California, Irvine, CA 92717

Perhaps the best known property of amylose in aqueous solution is its reaction with iodine in the presence of iodide to give a dark blue complex. Notwithstanding considerable study over a period of many years, a complete description of the conformation and stoichiometry of the dissolved complex has yet to emerge, in part because of the large number of independent variables that must be controlled and separately studied in order to carry out a complete investigation (1). It is furthermore evident that a full understanding of the aqueous complex has been elusive because it may exist in various states of aggregation, which depend upon kinetic as well as equilibrium factors (1, 2, 3, 4). Conflicting models continue to appear as an outgrowth of efforts to interpret hydrodynamic data (1, 3, 4, 5) and recent results from resonance Raman (6, 7, 8, 9), Moessbauer (8), and circular dichroism (9) spectroscopy. In what follows we review briefly some of these results in order to describe certain features of the complex on which general agreement seems to have been achieved. Subsequently we present a simple model, based on some widely accepted characteristics of the complex, which is capable of correlating a number of these features.

Structure and Stoichiometry of the Complex

There seems little doubt that the dissolved complex is an inclusion compound in which iodine resides within the annular cavity of a more or less regular helical amylose chain. This picture emerged early from the work of Rundle and coworkers on the crystalline (10) and dissolved (11) complex and has not been seriously challenged by any more recent studies. Despite the acknowledged helical character of the dissolved complex, it is very clear from hydrodynamic evidence that the complexed polymer does not adopt a rigid, rod-like conformation; indeed, the hydrodynamic volume of the polymer decreases upon complexation with iodine (1, 3, 5). The spectroscopic properties of the dissolved complex imply that the bound iodine is arrayed in linear sequences, but neither the

0097-6156/81/0150-0477\$05.00/0

© 1981 American Chemical Society

distribution of iodine chain lengths nor even the mean chain length has been established. The complex absorbs strongly near 600 nm, where the unbound iodine species have no significant absorption. Extensive investigations (12, 13, 14) have established that the wavelength of maximum absorption in this band, λ_{\max} , is a strong function of the mean degree of polymerization x of the amylose chains. This effect saturates above $x \approx 100$, where λ_{\max} achieves an asymptotic upper limit near 640 nm. Analogy with the Kuhn model for the polyenes (15) has been recognized (16) and exploited (3). The λ_{\max} also depends somewhat on the degree of saturation of the complex and moreso on the concentration of iodide ion (1).

Even the stoichiometry of the complex continues to be debated. If we denote the molar concentrations of I^- , I_2 , and I_3^- as $[I^-]_i$, $[I_2]_i$, and $[I_3^-]_i$, where i can be replaced, respectively, by t , b , or f to refer to the total, bound, and free (unbound) concentrations of these species, then we can express the stoichiometry of the complex in terms of the ratio R of bound triiodide to total bound iodine as $R = [I_3^-]_b / ([I_2]_b + [I_3^-]_b)$. It has now been repeatedly confirmed (1) that R cannot be zero; that is, iodide (or other negative) ions are mandatory for development of the blue color. Although some treatments (17, 18) of the complex assume that the bound species is I_3^- ($R = 1$), a careful analysis of the existing data reveals no evidence for a structure of such high charge density, at least in solution (1, 19, 20). The most recent work on the subject, using a variety of techniques, favors $R \approx 0.3$ (20) or $R = 0.5$ (8, 21). The latter value arises from X-ray crystallographic studies of the α -cyclodextrin- I_3^- complex (21) and resonance Raman and Moessbauer spectroscopy of the amylose-iodine complex and certain model compounds (8). Spectroscopic determinations of the free and bound iodine-containing species in dilute aqueous iodide solution (20) have suggested the stoichiometry of smaller charge density $R = 0.3 \pm 0.1$. These and other results thus support a stoichiometry with R in the range 0.2-0.5 and suggest that R may depend somewhat on such variables as mean polymer chain length, iodide and/or salt concentration, and physical state of the complex (i.e., crystalline or dissolved).

Some information also exists concerning the energetics of the complexation reaction. In particular, the cooperativity of the iodine binding process has been accepted for many years (22, 23). Direct charge transfer interaction between iodine and the oxygen atoms of the polysaccharide annulus has been proposed (9, 24, 25), but in the solid state no such interaction has been found for the α -cyclodextrin-pentaiodide structure (21). Even more interesting is the finding that α -cyclodextrin crystallized with I_2 in the absence of I^- does not have I_2 molecules in linear array but rather as isolated molecules within the dextrin cavity (26). The enthalpy of complexation is found to be constant for those changes in reaction conditions which leave λ_{\max} unchanged (20), and it varies with amylose chain length in a way that mimics the dependence of

λ_{max} on the degree of polymerization (14). We therefore believe that the rather large enthalpy change (ca. -17 kcal/mole of bound I_2) must sustain its largest contribution from the cooperative interactions between the atoms of the linear bound iodine chains and a much smaller contribution from interactions of the bound species with the polymer chain. These ideas are implicit in the amylose-iodine binding model of Schneider and coworkers (27) who treated the system using a cooperative one dimensional Ising model with variable R. They were able to fit their iodine binding data assuming a polyiodine chain of about 35 iodine atoms, a length considerably greater than the optimal iodine chain length suggested by most other workers (1, 9).

It is clear from the accumulated evidence that the stabilization energy of the complex can be realized only if the triiodide ion is present. Moreover, I_3^- has a considerably higher affinity for the polysaccharide matrix than does I_2 in the absence of cooperative interactions along the polyiodine chain (3, 28). These circumstances suggested to us that the complexation process is initiated by the binding of I_3^- to the polysaccharide with subsequent propagation of the polyiodine chain principally by molecules of I_2 (3). In what follows we pursue the consequences of this idea² using the matrix method originally developed by Zimm and Bragg (29) to treat the polypeptide helix coil transition and adapted by Schneider (27) and others (30) to treat the case of cooperative binding of ligands to a macromolecule. Given the pseudo-helical trajectory characterizing significant sequences aqueous amylosic chain (31), the present model allows the uncomplexed polymer to occur in both helical and random coil sequences (32). To be consistent with the known crystalline structure of the complex (10) and the observed changes in amylose chain dimensions which accompany iodine binding (3), the model permits binding only to helical sequences.

Theoretical Model

Let the polymer chain be capable of assuming two different conformational states, coil and helix, the latter capable of binding iodine as I_2 or I_3^- . Thus an amylose molecule may be described as a sequence of coil and helix sites, which for present purposes can each be taken to comprise approximately six glucose residues. Coil states can be denoted by c, unbound helix states by h, and helix states bound either to I_2 or I_3^- by b. We define "complex" as any uninterrupted sequence of b states, regardless of length. Then in the usual fashion (30) we define the statistical weight matrix \hat{U} indexed for sites $i-1$ and i as

$$\underset{S}{U} = \begin{matrix} & i-1 \setminus i & h & b & c \\ \begin{matrix} h \\ b \\ c \end{matrix} & \begin{bmatrix} 1 & \pi & \omega\rho \\ 1 & \eta & \omega\rho \\ 1 & \pi & \rho \end{bmatrix} \end{matrix} \quad (1)$$

where each element gives the relative probability (statistical weight) for finding site i in a particular state h , b , or c specified by the column index, given that site $i-1$ is in the particular state indicated by the row index. All statistical weights are defined relative to that for the unbound helical state which is consequently assigned unit weight regardless of the state of the preceding site. The parameter π is then the statistical weight for initiation of any new sequence of complex through binding of I_3^- at a site which follows any unbound site, h or c . Propagation of any sequence of complex, assumed for simplicity to occur only through addition of I_2 to the growing iodine chain, receives a weight η . Parameters ρ and ω are analogous, respectively, to the Zimm-Bragg (29) parameters s and σ . Thus, ρ describes the statistical weight of a coil state relative to unbound helix, and ω is a junction or initiation parameter to account for the possible cooperativity of the putative conformational transition in amylose in the absence of iodine.

The partition function Z for a chain of m sites is given (30) by

$$Z = \underset{S}{P} \underset{S}{U}^m \underset{S}{Q} \quad (2)$$

where

$$\underset{S}{P} = [1 \ 0 \ 0], \quad \underset{S}{Q} = \begin{bmatrix} 1 \\ 1 \\ 1 \end{bmatrix} \quad (3)$$

The average number of sequences of complex, n (i.e., the average number of sequence-initiating I_3^- ions), and the average number of propagating I_2 molecules, n_η , may be obtained by differentiation of Z (30), and these derivatives may also be computed as matrix products (33)

$$n_\pi = \frac{\partial \ln Z}{\partial \ln \pi} = Z^{-1} \underset{S}{S} \hat{\underset{S}{U}}^m \underset{S}{T} \quad (4)$$

$$n_\eta = \frac{\partial \ln Z}{\partial \ln \eta} = Z^{-1} \underset{S}{S} \hat{\underset{S}{U}}^m \underset{S}{T} \quad (5)$$

where

$$S = [1 \ 0 \ 0 \ 0 \ 0 \ 0] , \quad T = \begin{bmatrix} 0 \\ 0 \\ 0 \\ 1 \\ 1 \\ 1 \end{bmatrix} \quad (6)$$

and, letting $\alpha = \pi$ or η ,

$$\hat{S}_\alpha = \begin{bmatrix} S_U & U'_\alpha \\ S_O & S_U \end{bmatrix} \quad (7)$$

with O being the null matrix of order three and $U'_\alpha = \partial U / \partial \ln \alpha$. Connection of theory with experiment is made through the observable parameters θ , defined as the fraction of sites bound, and R , defined above. These are given by

$$\theta = \frac{n_\pi + n_\eta}{m} \quad (8)$$

$$R = \frac{n_\pi}{n_\pi + n_\eta} = L^{-1} \quad (9)$$

where L is the average length of the complex sequences measured in numbers of binding sites.

The number of observables described here is not sufficient to determine uniquely the several parameters of the theory. We can, however, assign ρ and ω on the basis of independent information concerning the conformation of aqueous amylose chains in the absence of iodine. A realistic model of aqueous amylose (31) discloses that perhaps 25% of an amylose chain in water might be classified as nearly regular helix at any instant, but the chain conformation is extremely labile, and there is no evidence for any conformational cooperativity in the absence of iodine. Hence, the cooperativity parameter ω may be set equal to unity, and for convenience we also take $\rho = 1$, which implies equal proportions of helix and coil in the absence of iodine. Calculations not reported in detail here reveal that the results described below are quite insensitive to the exact numerical value of ρ , provided $\omega = 1$ and ρ is of order unity.

Parameters π and η clearly must depend on the respective concentrations of I_3^- and I_2 present in the system. It is conventional to express the equations for ligand binding to macromolecules in terms of the concentrations of the free species, and it is readily shown (30) that π and η are appropriately expressed by

$$\pi = K_{\pi} [I_3^-]_f \quad (10)$$

and

$$\eta = K_{\eta} [I_2]_f \quad (11)$$

where K_{π} is the intrinsic association constant for binding of I_3^- to the π polymer and K_{η} is the constant for adding I_2 to the already-initiated complex sequence. The parameter m , which counts the binding sites per chain, might initially be thought to equal approximately one-sixth of the degree of polymerization x , but, as we shall see, this identity proves incorrect within the confines of the present simple model, and m must be left as an adjustable parameter of the data fitting procedure. Hence, the theoretical parameters π (or K_{π}), η (or K_{η}), and m exceed by one the number of experimental quantities available in the present work.

Let it be noted finally that the concentrations $[I_3^-]_f$ and $[I_2]_f$ are not independent, but, rather, related through the reaction stoichiometry



The equilibrium constant for triiodide formation is about 10^3 (34), but since measured values of K_{η} are normally one or two orders of magnitude larger than this, the above reaction is an effective buffer for I_2 . Thus propagation of the polyiodine chain of the complex sequence depends, in effect, on total free iodine $[I_3^-]_f + [I_2]_f$, and the equilibrium in Equation 12 has been taken into account in generating binding isotherms with the theory.

Experimental

In order to produce a continuous binding isotherm (25°C) under rigorously controlled conditions the method of gradient dilution (35) was used. A solution containing polymer and I^- at known concentrations was used to dilute continuously a second solution, identical except for the presence of I_2 at a known concentration high enough to saturate the amylose binding sites. The mixture, increasingly dilute in iodine, is pumped through a flow cell in the spectrophotometer and monitored at $\lambda = 640$ nm. The polymer sample was slightly substituted (DS = 0.3) carboxymethylamylose (CMA). Use of the ionic derivative as a model for amylose obviates problems with the solubility of unsubstituted amylose in the presence of iodine (3, 32). All materials and the gradient dilu-

tion spectrophotometric method have been described elsewhere (3, 20). Instrument parameters characteristic of the gradient mixing system were determined by diluting with water an aqueous solution of tris(ethylenediamine)cobalt(III) perchlorate, aqueous solutions of which conform to the Lambert-Beer Law over a wide range of concentration. Hence, the absorbance A at time t (corrected for the time lag between mixing chamber and spectrophotometer cell) is given for the exponential gradient used by

$$A = A_0 \exp(-at) \quad (13)$$

where $a = f/v$ is the ratio of the flow rate f to the volume of the mixing chamber v . In a typical experiment the measured $f = 1.503$ ml/min and $a = 0.0628 \text{ min}^{-1}$ to yield $v = 23.93$ ml. Direct measurement of v yielded 24.0 ml to confirm the reliability of Equation 13. Slight changes in flow rate from day to day made it necessary to determine this parameter for each experiment.

Results

Experimental Binding Isotherms. Experimental binding isotherms, plotted as A vs. $[I]_t \equiv [I_3^-]_t + [I_2]_t$, are shown in Figure 1 for CMA at pH 6 for three different potassium iodide concentrations, $[I^-]_t$. Under the conditions of these experiments no correction of $[I]_t$ for disproportionation of I_2 was required. For purposes of comparison with theory we convert A to θ using the definition $\theta \equiv (A - A_\infty)/(A_0 - A_\infty)$, where A_0 is the value of A at infinite dilution of I_2 ($t^0 = \infty$). It is also possible to convert $[I]_t$ to $[I]_f \equiv [I_3^-]_f + [I_2]_f$ using conservation of total iodine and spectrophotometric analysis of $[I_3^-]_b + [I_2]_b$. Alternatively, and as a control, direct spectrophotometric measurement of $[I_3^-]_f$ and $[I_2]_f$ is possible.

Theoretical Binding Isotherms. Figure 2 shows a typical plot of θ vs. $[I]_f$. The points represent experimental data taken from curve a of Figure 1, and the curves are theoretical isotherms calculated using Equation 8 and corresponding to the values for the parameters K_1 , K_2 , and m given in the figure legend. The position of the theoretical curves along the $[I]_f$ axis is governed primarily by the value of K_1 , while K_2 and m control the slope and symmetry of the isotherm. The search for theoretical parameters giving the best fit to the midpoint, $(\ln [I]_f)_{\theta=1/2}$, and slope at the midpoint, $(\partial\theta/\partial \ln [I]_f)_{\theta=1/2}$, of the experimental isotherms was carried out by a graphical procedure (36). In this way a series of binding isotherms for CMA at pH = 6, 25°C, and with $[I^-]_t$ in the range 10^{-2} – 10^{-4} M has been fit with $K_1 = (4.85 \pm 0.35) \times 10^5$, $K_2 = (1.30 \pm 0.08) \times 10^4$, and $m = 3$ – 4 . Figure 2 exemplifies the quality of fit achieved.

We take the discrepancy between the values of m required to fit the experimental data and the potential number of binding sites in the polymer chain, i.e., $x/6 \approx 300$, to be a clear reflec-

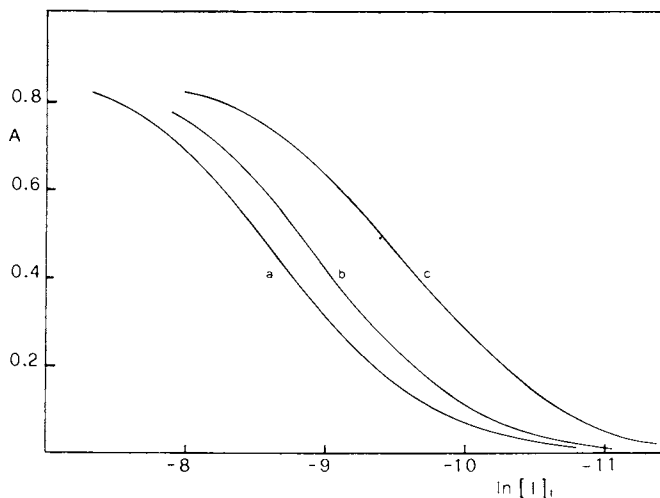


Figure 1. Experimental binding isotherms for CMA (0.1 g/L, pH 6) plotted as A (pathlength—0.2 cm) vs. the natural logarithm of $[I]_f$ for various $[I]_i$: (a) $1.0 \times 10^{-2}M$; (b) $2.0 \times 10^{-3}M$; and (c) $8.0 \times 10^{-4}M$.

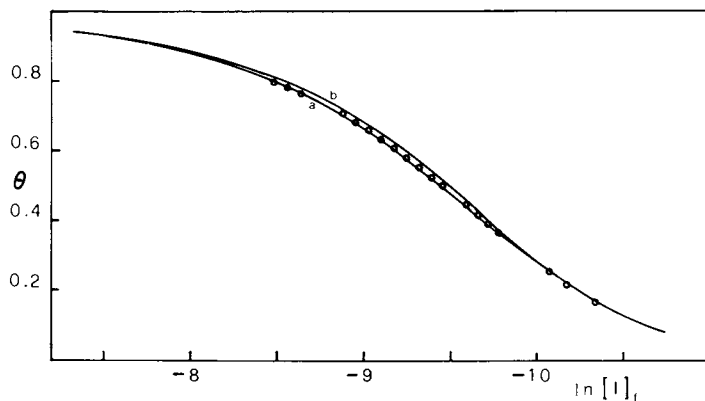


Figure 2. The experimental isotherm of Curve a in Figure 1 (O) plotted as the degree of saturation θ vs. the natural logarithm of $[I]_f$. Curves are theoretical isotherms corresponding to $[I]_i = 1.0 \times 10^{-2}$ and the choices of parameters: (a) $K_\pi = 1.22 \times 10^4$, $K_\eta = 5.25 \times 10^5$, $m = 3$; (b) $K_\pi = 1.37 \times 10^4$, $K_\eta = 4.50 \times 10^5$, $m = 4$.

tion of the inadequacy of Equation 11, which implies that the propagation constant K for extending the complex sequence is independent of sequence length. Whatever the origin of the cooperative interaction along the linear iodine chain, it clearly depends for its realization on the presence of I_3^- . It is therefore consistent with the fundamental assumptions of the present model, i.e., initiation of complex by I_3^- and propagation (predominantly) by I_2 , that the range of the cooperative interaction should be confined to 3-4 binding sites. This evidence that long polyiodine sequences do not develop in the complex at any degree of saturation is moreover consistent with the hydrodynamic results (1, 3, 4, 5) which show no indication of stiffening or extension of the dissolved amylose random coil when the iodine complex is formed, even at high θ . Inadequacies disclosed in the model by the discrepancy between m and $x/6$ could presumably be addressed by a revision of Equation 11 which would allow K to vary with polyiodine chain length. We will not address that question here but will instead pursue other attributes of the present model, which is not vitiated by the deficiencies of Equation 11 provided attention is restricted to modest values of θ for which the problems engendered by Equation 11 are avoided (cf. seq.).

Comparison of Theoretical and Experimental Complex Stoichiometries. With the values of K and K' established in fitting the CMA binding isotherms we have next used Equation 9 to compute L , the average length of the complex sequences, as a function of the number of binding sites m for oligomeric amyloses at $\theta = 1/2$. Restricting attention to $\theta = 1/2$ avoids the unrealistically long polyiodine chains predicted by the model for large m at high θ . The results for $[I^-]_t = 10^{-3}$ M are presented in Figure 3a as a plot of $L_{\theta=1/2}$ vs. $x_t = 6m$. Because the present model permits only one I_3^- per $\theta=1/2$ complex sequence, the stoichiometry R of the complex is related simply to L as given in Equation 9. Thus, the asymptotic value of $L_{\theta=1/2} \approx 3.7$ corresponds to $R_{\theta=1/2} \approx 0.27$, in excellent agreement with recent experimental observations of R for the same polymer (20). Furthermore, $L_{\theta=1/2}$ is quite similar to the values of m required to obtain the best fit to the binding isotherms. Thus, the mean stoichiometry of the bound species which emerges from the present model is approximately I_0^- . If these polyiodine sequence lengths are realistic, then the restriction of each sequence to a single negative charge as imposed by this model is probably quite reasonable.

In Figure 3b experimental values (14) of λ_{\max} vs. x are shown as open circles for conditions of $[I^-]_t$ comparable to those used to generate Figure 3a; the dashed curve is simply an empirical correlation of the experimental data. The results shown in Figures 3a and 3b can both be linearized by plotting the inverse of the ordinate values vs. x^{-1} . Since the experimental dependence of λ_{\max} on x is widely believed (1) to reflect changes in average complex sequence length, it is interesting to note the similar (linear) dependences of λ_{\max}^{-1} and $L_{\theta=1/2}^{-1}$ on x^{-1} . Eliminating x^{-1}

between the two linear expressions yields Equation 14

$$\lambda_{\max}^{-1} = 1.21 \times 10^{-3} + (1.7 \times 10^{-3}) L_{\theta=1/2}^{-1} \quad (14)$$

which relates λ_{\max}^{-1} and $L_{\theta=1/2}^{-1}$. This relationship, which evidently is meaningful only if the results in Figure 3a are correct, has been used to calculate λ_{\max}^{-1} from the values of $L_{\theta=1/2}^{-1}$ computed with the theory for several values of x ; these results are plotted as the filled squares in Figure 3b.

Dependence of Complex Stoichiometry on Iodide Concentration. Using the values of K_{π} and K_{η} previously established and taking $m = 20$, the value of $L_{\theta=1/2}^{\pi}$ has been calculated as a function of $[I^-]_f$. Results are plotted as the dashed curve in Figure 4a. As expected, the average length of the polyiodine chains declines with increasing $[I^-]_f$ for fixed $\theta = 1/2$, because higher $[I_3^-]_f$ results in more chain initiations under conditions of fixed total bound iodine. When $L_{\theta=1/2}^{\pi}$ is converted to λ_{\max} using Equation 14, the results shown as the lower dashed line in Figure 4b are obtained. Experimental data (16, 19) for λ_{\max} vs. $[I^-]_f$ are presented in Figure 4b for comparison; lines through the experimental points are empirical correlations only. It would appear that the predicted dependence of $L_{\theta=1/2}^{\pi}$ on $[I^-]_f$ is too strong, particularly in comparison with the experimental results of Ono et al. (16). This, we suppose, reflects a deficiency in Equation 10, which implies that the microscopic binding constant for I_3^- is independent of the number of I_3^- already bound. Because I_3^- is negatively charged, it is more realistic to imagine that the binding constant declines as the negative charge density on the polymer chain increases. This electrostatic effect can be taken into account most simply (37, 38) by replacing Equation 10 with Equation 15

$$\pi = K_{\pi} [I_3^-]_f \exp\left(-\frac{K_{\pi} [I_3^-]_f}{1 + K_{\pi} [I_3^-]_f}\right) \quad (15)$$

where the argument of the exponential factor is just the fraction of the I_3^- which is bound. With this simple modification only, the theory now yields the solid curves in Figures 4a and 4b, and agreement with experiment is significantly improved. Elaborations of Equation 15 could clearly improve the agreement still further, but such efforts are not justified in the present context owing to the simultaneous deficiencies in Equation 11 already discussed. Finally, let it be noted that attempts to calculate the dependence of λ_{\max} on θ with the present simple model were unsuccessful.

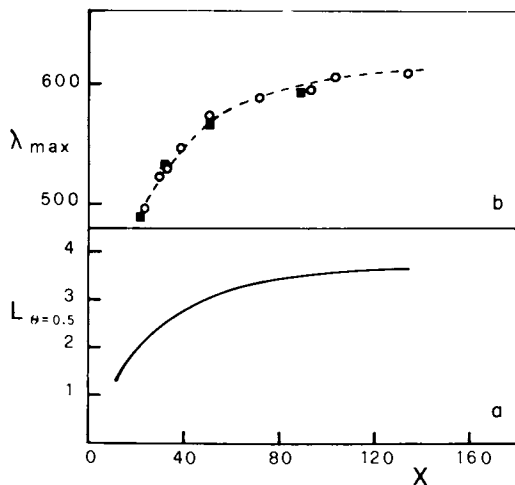


Figure 3. (a) Calculated average length of the complex sequences at $\theta = 1/2$, $L_{\theta=1/2}$, as a function of the amylose degree of polymerization x for $K_{\pi} = 1.37 \times 10^3$, $K_{\eta} = 4.50 \times 10^5$, and $[I_1] = 1.0 \times 10^{-3}M$. (b) Experimental results (14) for λ_{max} vs. the degree of polymerization x (○); an empirical correlation of these data (---). Values of λ_{max} calculated for various values of x as described in the text (■).

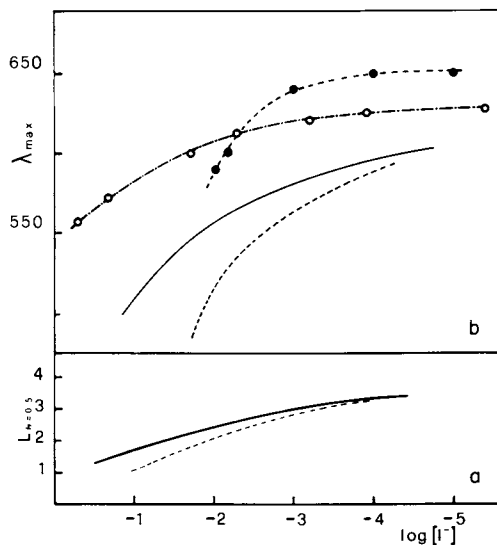


Figure 4. (a) Calculated average length of the complex sequences at $\theta = 1/2$, $L_{\theta=1/2}$, as a function of the base 10 logarithm of $[I_1]$ for the conditions of Curve b of Figure 2 using Equation 10 (---) and Equation 15 (—). (b) Experimental measurements of λ_{max} as a function of the base 10 logarithm of $[I_1]$ from Refs. 16 (○) and 19 (●); curves through these points are empirical correlations of the data. The solid and dashed curves are calculated, respectively, from $L_{\theta=1/2}$ given by the solid and dashed curves of Figure 4a using Equation 14.

Conclusions

We have shown that a model for amylose-iodine binding, based on initiation of binding by I_3^- and propagation (primarily) by I_2 , is consistent with many of the experimentally observed characteristics of the system. The qualitative dependence of λ_{\max} both on amylose chain length and iodide concentration has been reproduced. The model is furthermore quantitatively consistent with the observed stoichiometry R of the dissolved CMA-iodine complex and suggests strongly, consistent with independent evidence of various types, that the mean length of the complex sequences is only about 7-9 iodine atoms. Evident deficiencies in the present simple model relate principally to Equations 10 and 11, which characterize binding of I_2 and I_3^- , respectively, to the polymer by the single binding constants K_3 and K and thereby ignore (anti)-cooperative effects which are surely present. These shortcomings in the model force us to use the number of binding sites m as a fitting parameter rather than as a given physical characteristic of the system, and may explain our inability to reproduce the dependence of λ_{\max} on θ . We have pointed out ways in which the weaknesses of the model might be removed, but this would obviously be accomplished only at the cost of introducing additional parameters. It seems to us therefore that despite its approximate character, the present simple model may represent a constructive exercise that can illuminate some of the detailed features of the amylose-iodine system.

Acknowledgement

This work has been supported in part by National Science Foundation Research Grants PCM 79-23041 and PCM 77-23603 and by the Italian Research Council (CNR) through grant N.78.01129.03 and through a Travel Grant to A.C.

Abstract

A model for amylose-iodine binding is presented in which it is assumed that sequences of bound iodine are initiated by triiodide and propagated (principally) by iodine. The theory is developed using the matrix method of Zimm and Bragg; experimental isotherms for the binding of iodine to aqueous carboxymethylamylose (CMA) were generated using the gradient dilution method of Biltonen and coworkers. After establishing the best values of the theoretical parameters by fitting theoretical isotherms to the experimental data, the mean stoichiometry of the complex sequences was calculated with the theory to be $I_7^- - I_9^-$. The predicted charge density of the complex is thus in quantitative accord with experimental observations of Cesaro and coworkers on the aqueous CMA-iodine-iodide system. The theory also reproduces the qualitative dependence on amylose chain length and iodide concentration of the

wavelength of maximum absorbance of the complex. The experimental justification for the basic assumptions of the model are presented as are suggestions for rendering the simple theory more realistic.

Literature Cited

1. Banks, W., and Greenwood, C.T., "Starch and Its Components", Edinburgh University Press: Edinburgh, 1975.
2. PfannemueLLer, B., Carbohydr. Res. (1978) 61, 41.
3. Cesàro, A., and Brant, D.A., Biopolymers (1976) 16, 983.
4. Dintzis, F.R., Beckwith, A.C., Babcock, G.E., and Tobin, R., Macromolecules (1976) 9, 471, 478.
5. Senior, M.B., and Hamori, E., Biopolymers (1973) 12, 65.
6. Tasumi, M., Chem. Lett. (1972) 75.
7. Heyde, M.E., Rimal, L., Kilponen, R.G., and Gill, D., J. Am. Chem. Soc. (1972) 94, 5222.
8. Teitelbaum, R.C., Ruby, S.L., and Marks, T.J., J. Am. Chem. Soc. (1978) 100, 3215.
9. Handa, T., and Yajima, H., Biopolymers (1979) 18, 873.
10. Rundle, R.E., J. Am. Chem. Soc. (1947) 69, 1769.
11. Rundle, R.E., and Baldwin, R.R., J. Am. Chem. Soc. (1943) 65, 554.
12. Bailey, J.M., and Whelan, W.J., J. Biol. Chem. (1961) 236, 969.
13. PfannemueLLer, B., Mayerhoefer, H., and Schulz, R.C., Makromol. Chem. (1969) 121, 147.
14. Banks, W., Greenwood, C.T., and Kahn, K.M., Carbohydr. Res. (1971) 17, 25.
15. Kuhn, H., J. Chem. Phys. (1949) 17, 1198.
16. Ono, S., Tsuchihashi, S., and Kuge, T., J. Am. Chem. Soc. (1953) 75, 3601.
17. Reddy, J.M., Knox, K., and Robin, M.B., J. Chem. Phys. (1964) 40, 1082.
18. Robin, M.B., J. Chem. Phys. (1964) 40, 3369.
19. Cronan, C.L., and Schneider, F.W., J. Phys. Chem. (1969) 73, 3990.
20. Cesàro, A., Jerian, E., and Saule, S., Biopolymers (1980) 19, 1491.
21. Noltemeyer, M., and Saenger, W., Nature (1976) 259, 629.
22. Rundle, R.E., Foster, J.F., and Baldwin, R.R., J. Am. Chem. Soc. (1944) 66, 2116.
23. Stein, R.S., and Rundle, R.E., J. Chem. Phys. (1948) 16, 195.
24. Murakami, H., J. Chem. Phys. (1954) 22, 367.
25. Griffiths, D.W., and Bender, M.L., Adv. Catal. (1973) 23, 209.
26. McMullan, R.K., Saenger, W., Fayos, J., and Mootz, D., Carbohydr. Res. (1973) 31, 37, 211.
27. Schneider, F.W., Cronan, C.L., and Podder, S.K., J. Phys. Chem. (1968) 72, 4563.

28. Thoma, J.A., Stewart, L., in "Starch Chemistry and Technology" (Whistler, R.L., and Paschall, E.F., Eds.), Vol. 1, Academic Press: New York, 1965, Ch. IX.
29. Zimm, B.H., and Bragg, J.K., J. Chem. Phys. (1959) 31, 526.
30. Poland, D., "Cooperative Equilibria in Physical Biochemistry", Clarendon Press: Oxford, 1978.
31. Jordan, R.C., Brant, D.A., and Cesàro, A., Biopolymers (1978) 17, 2617.
32. Dubin, P.L., and Brant, D.A., Macromolecules (1975) 8, 831.
33. Flory, P.J., "Statistical Mechanics of Chain Molecules", Wiley-Interscience: New York, 1969.
34. Awtrey, A.D., and Connick, R.E., J. Am. Chem. Soc. (1951) 73, 1842.
35. Mountcastle, D.B., Friere, E., and Biltonen, R.L., Biopolymers (1976) 15, 355.
36. Konic, W., Laurea Thesis, University of Trieste: Trieste, Italy, 1978.
37. Tanford, C., "Physical Chemistry of Macromolecules", Wiley: New York, 1961, Ch. 8.
38. Sturgill, T., and Biltonen, R.L., Biopolymers (1976) 15, 337.

RECEIVED August 26, 1980.

The Interaction of Sodium Dodecyl Sulfate, a Competing Ligand, with Iodine Complexes of Amylose and Amylopectin

SHOBHANA V. BHIDE, MEENA S. KARVE, and N. R. KALE

Department of Chemistry, Division of Biochemistry, University of Poona,
Poona-411 007, India

Amylose and amylopectin are the isotactic homopolymers of α -D-glucose which interact with iodine (I_2) in aqueous systems to give the characteristic blue coloured complexes.

The helical nature of the amylose-iodine-complex, with six D-glucose units in the C-1 configuration per turn of the helix and the iodine molecules packed inside the lumen, parallel to the axis of the helix has been well established by X-ray diffraction studies (1). Electron microscopic studies of amylose-iodine-complex in the form of fibrils have revealed rod like structures with 40 nm in diameter and the length depending on the degree of polymerization of the polymer chain, and the helices folded parallel to the long axis (2). The recent studies of this complex by Raman resonance and iodine-129 Mössbauer spectroscopy have provided evidence for the presence of I_5^- species within the amylose helix (I-I-I \cdots I-I) (3).

Ultrafiltration studies have demonstrated that addition of excess of iodine to amylose solution completely prevents the passage of amylose molecules through the filter. This is attributed to the iodine induced coil \rightarrow helix transition, forming rather tight helices in the amylose-iodine-complex (4).

Amylose also forms crystalline helical complexes with a variety of organic compounds such as 1-butanol, fatty acids, dimethyl sulphoxide etc. (5,6,7). The helical complexes of amylose with SDS, 1-butanol and cyclohexanol are found to be resistant to the action of amylases (8,9).

Physicochemical methods employed for the study of conformation of amylose in the free and complexed state have failed to detect any significant change in conformation of amylose on complexing. The extensive work on hydrodynamic studies (10,11) suggests that

0097-6156/81/0150-0491\$05.25/0

© 1981 American Chemical Society

amylose in neutral aqueous solution exists as a flexible random coil and in the presence of complexing agents forms compact helical coils with ligand molecules caged inside the helices. The helical regions having 110-130 D-glucose units are interspersed by random coil regions, which contribute flexibility to the polymer chain (12).

Potentiometric studies by Bates, French and Rundle (13) have shown that amylose combines with iodine isopotentially and the potential is characteristic of amylose for its degree of polymerization and suggests a high cooperativity. However equilibrium (14) and kinetic (15) studies indicate moderate cooperativity of the reaction. On the basis of experimental evidence and computer model building, Brant and his coworkers (16,17) have concluded that amylose in aqueous solution behaves as a statistical coil with no helical character and in the presence of complexing agent acquires a helical conformation. A Monte Carlo study of amylose chain conformation has shown that an appropriate molecular model of amylose chain can generate a randomly coiled chain with perceptible regions of left handed pseudohelical backbone trajectory (18).

The extinction coefficient of the amylose-iodine-complex, the wavelength of the maximum absorption and the stability is influenced by the degree of polymerization of the amylose chain (19,20,21,22). Formation of the amylose-iodine-complex is affected by temperature, pH, ionic strength, concentration of iodide ions and the nature of amylose.

The study of the influence of solvents on the formation of the starch-iodine-complex has revealed that the water requirement is not related to either the dipole moment or the dielectric constant of the solvent (23). Moulík and Gupta have shown that surfactants and cosolvents, mainly destabilize the amylose-iodine-complex, and the overall polarity of the mixed medium is insufficient to systematize the solvent effect (24). Ono et al have reported that the blue colour of the amylose-iodine-complex is not formed in dimethyl sulphoxide-water mixtures containing less than 28 moles of water per litre (25).

All these observations indicate that coil→helix transition of amylose in the presence of complexing agents involves only minor structural changes. The enthalpy change of this complex formation is -11 to -20 k cal/mol iodine (26).

Our earlier studies on the ligand induced structural changes in amylose partially complexed with iodine have shown that competing ligand produces a

drop in absorbance at 640 nm and is accompanied by a blue shift (640-580 nm) in the absorption spectrum. We had chosen an iodine deficient system in order to avoid the stabilizing influence of iodine ions on the complex. Under these conditions, iodide ions generated by hydrolysis of iodine are sufficient to produce a stable, blue coloured amylose-iodine-complex, though the intensity is low. However, this system was found to be very sensitive to the generation of iodide ions, due to the oxidation of trace impurities in the ligand. In the homologous series of alcohols, the blue shift that was observed was more pronounced as the length of the hydrocarbon chain increased, implying that noncovalent interactions like H-bonds, Van der Waals forces, hydrophobic interactions and water play an important role in stabilizing these helical structures (27). Hollo'et al have also reported similar observations on the stability of amylose-alcohol complexes (28). Kim and Robinson have shown that the helical conformation of amylose was the most important factor in the binding of surfactant molecules in the helical cavity of amylose chain, resulting in a slight decrease in the intrinsic viscosity, fall in the β -amylolysis limit and the iodine binding capacity(29)

A recent report on the interaction of amylose with a hydrophobic fluorescent probe, has shown that it enhances the fluorescence indicating the presence of a hydrophobic environment (30).

In this paper, we present some of our observations on the nature of the amylose-iodine-complex/amylopectin-iodine-complex using SDS as a complexing ligand-probe which might shed some light on the ligand induced structural changes in amylose and amylopectin.

Materials and Methods

All reagents were of 'Analar' grade, and water distilled in all-glass apparatus was used. Sodium dodecyl sulphate (SDS), Fluka (Switzerland), 90-93% was recrystallized thrice from ethanol. Stearic acid, palmitic acid and myristic acid, all of extra-pure quality(99%) were obtained from SISCO Research Lab., Bombay.

A high molecular weight potato amylose was prepared by the urea dispersion method and it was preserved as a wet precipitate in ethanol(60%) at +4°C (31). Potato amylopectin was isolated from potato starch by the same method, and trace quantities of amylose from amylopectin fraction were removed by adsorption on defatted cellulose (32). Amylose and

amylopectin solutions were prepared by dispersion in NaOH(1.0 M) at room temperature(26-28°C) followed by neutralization with HCl(0.5 M) to pH 7.0, and centrifuged(2,418 g) before use. Freshly prepared solutions were used and the polysaccharide content was determined by the phenol-sulphuric acid method (33).

TABLE I

Characterization of potato amylose and amylopectin (31)

	Iodine Binding Capacity (IBC)	Blue Value (BV)	* β -amylolysis Limit(%)	Intrinsic viscosity $10^{-2} \cdot (\eta) / \text{cm}^3 \text{g}^{-1}$
Amylose	19.8	1.42	96-98	3.53
Amylopectin	0.21	0.16	48-50	1.49

*

* Expressed as percent conversion to maltose

Blue value reagent (BVR) - Iodine ($7.87 \times 10^{-4} \text{M}$) + KI ($1.21 \times 10^{-2} \text{M}$) was used for the iodine solution(I₃). The reactions were carried out in glass-stoppered test tubes maintained at 30°C ($\pm 0.05^\circ$) in a thermostat. The spectrophotometric records were made on SHIMADZU UV 300, at 30°C ($\pm 0.05^\circ$) in quartz cells (1.0 cm), using water as a blank.

Influence of iodine (BVR) on the formation of blue coloured amylose-iodine-complex(34): It was studied to determine the optimum concentration of iodine that gives maximum absorbance at 640 nm, without precipitation of the complex. A system containing amylose (0.07 mg) - 0.2 ml + acetate buffer(pH 4.8, 0.1 M) - 0.5 ml + iodine(BVR - 0.1→0.8 ml) + water to make the total volume to 5.0 ml, was maintained at 30°C for 30 minutes to attain the equilibrium and the spectra were recorded. The iodine concentration (BVR-0.6 ml) giving the maximum absorbance at 640 nm was chosen to study the influence of the competing ligands like SDS and fatty acids.

Influence of SDS on iodine complexes of amylose and amylopectin : (Figure 1) A system containing amylose(0.07 mg) - 0.2 ml/amylopectin(0.18 mg) - 0.3 ml + acetate buffer(pH 4.8, 0.1 M) - 0.5 ml + SDS ($1.0 \times 10^{-4} \text{M}$) - 0.2→3.0 ml was equilibrated at 30°C for 30 minutes followed by the addition of iodine(BVR) - 0.6 ml and the total volume was adjusted to 5.0 ml

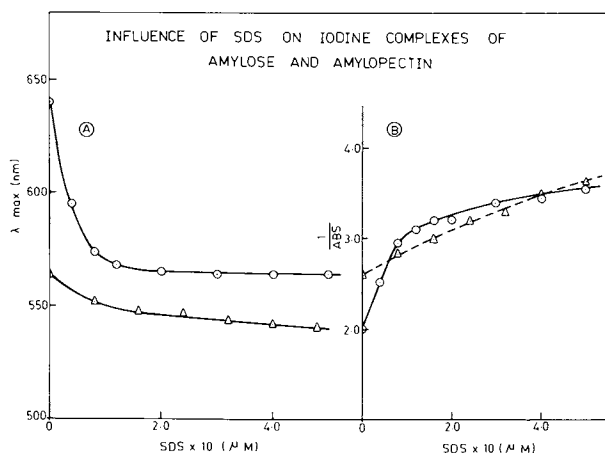


Figure 1. Amylose-SDS-iodine complex (\circ); amylopectin-SDS-iodine complex (\triangle); absorbance (ABS) (λ_{max}).

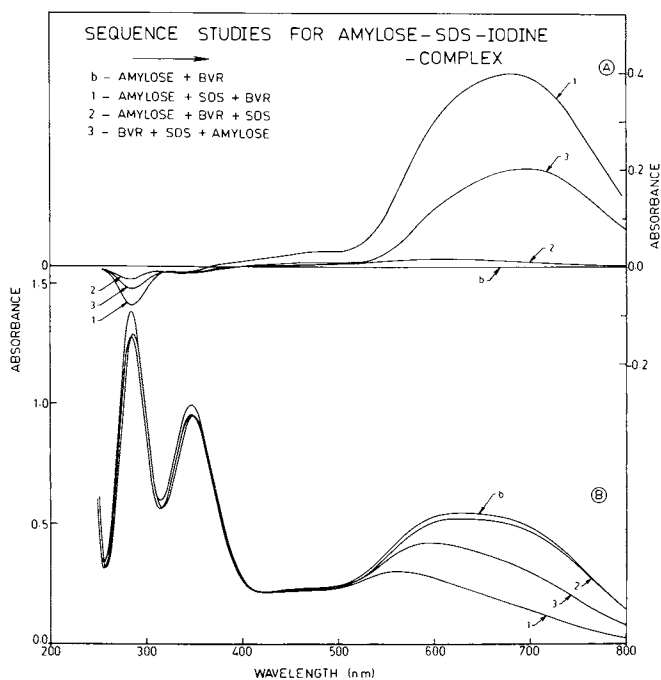


Figure 2. (A) Difference spectra: amylose-SDS-iodine complex minus amylose-iodine complex in acetate buffer, pH 4.8, for three different sequences (1, 2, and 3). (B) Absorption spectra for amylose-SDS-iodine complex in acetate buffer, pH 4.8, for three different sequences (1, 2, and 3).

with water. The system was maintained at 30°C for 30 minutes to attain the equilibrium and the absorbance was recorded at the respective λ_{max} .

Sequence studies : (Figure 2 & 3) The system was same as described above. The reagents were added in the sequence given in Figure-2. Iodine solution(BVR) - 0.6 ml and SDS solution ($1.0 \times 10^{-4}M$) - 2.0 ml were used in this system. The blank (b) was without SDS.

Perturbation studies : Reduction of iodine with sodium thiosulphate (Figure 4 & 5) The system was same as described for the sequence studies. Two sets of experiments were run under identical conditions. Iodine was completely reduced by adding required amount of sodium thiosulphate($1.0 \times 10^{-3}M$). One set was equilibrated at 30°C and the other at 60°C for 30 minutes respectively. The set maintained at 60°C was cooled to 30°C and both the sets were reiodinated by adding iodine(BVR) - 0.6 ml followed by equilibration for 30 minutes at 30°C.

Influence of urea on amylose-iodine-complex/ amylose-SDS-iodine-complex The destabilizing influence of urea on the absorbance of amylose-iodine-complex was investigated by recording the absorbance at 640 nm in the presence of urea(1.6→5.3 M). A system containing amylose(0.07 mg) - 0.2 ml + acetate buffer(pH 4.8, 0.1 M) - 0.5 ml + iodine(BVR) - 0.5 ml + urea (8 M) - 1.0→2.8 ml was adjusted to 5.0 ml with water. The system was equilibrated at 30°C for 30 minutes and absorbance was recorded at 640 nm (Figure 6A).

Influence of urea (1.6→5.3 M) on amylose-SDS-iodine-complex was studied by using essentially the same system as described for the sequence studies. The sequence-1 which gave maximum reduction in absorbance (640 nm) was chosen for this experiment. The increase in absorbance at 640 nm was recorded to study the perturbation caused by urea (1.6→5.3 M) to overcome the inhibitory influence of SDS (Figure 6B).

Perturbation with urea (Figure 7): The system contains amylose(0.07 mg) - 0.2 ml, acetate buffer (pH 4.8, 0.1 M) - 0.5 ml, SDS($1.0 \times 10^{-4}M$) - 1.0 ml, urea (8 M) - 2.8 ml. The reagents were mixed in the sequence (1, 2 & 3) as given in Figure 7. The blank (b) was without SDS. Two sets of experiments were conducted under identical conditions. One set was equilibrated at 30°C and the other at 60°C for 30 minutes respectively. The set maintained at 60°C was cooled to 30°C and iodine solution(BVR) - 0.5 ml was added to both the sets followed by equilibration for 30 minutes at 30°C.

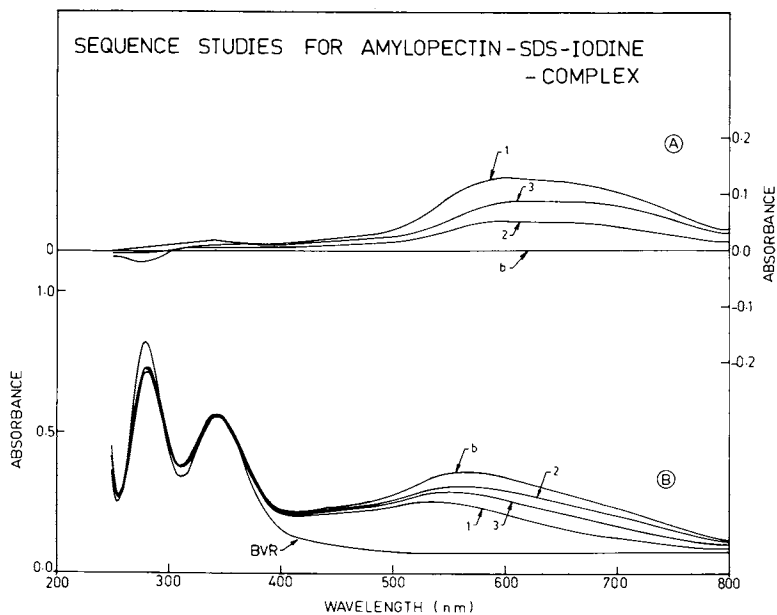


Figure 3. (A) Difference spectra: amylopectin-SDS-iodine complex - amylopectin-iodine complex in acetate buffer, pH 4.8, for three different sequences (1, 2, and 3) as given in Figure 2. (B) Absorption spectra for amylopectin-SDS-iodine complex in acetate buffer, pH 4.8, for three different sequences (1, 2, and 3) as given in Figure 2.

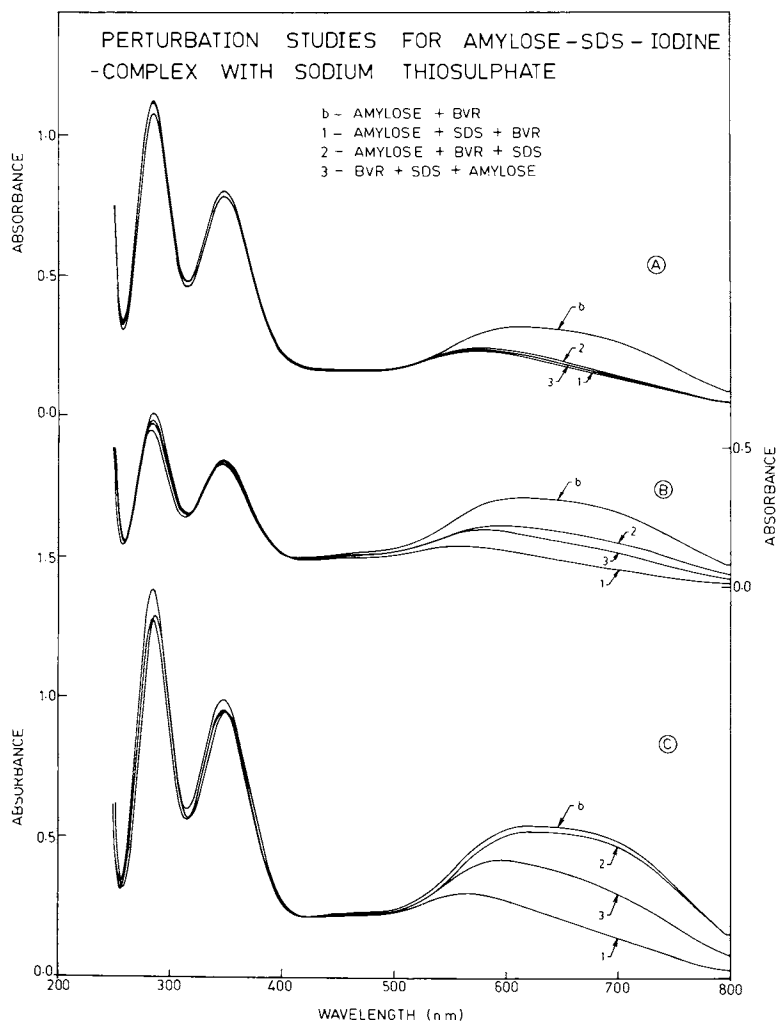


Figure 4. Absorption spectra of amylose-SDS-iodine complex in acetate buffer, pH 4.8, for three different sequences (1, 2, and 3). (A) The iodine was reduced with sodium thiosulfate, equilibrated at 60°C for 30 min, cooled to 30°C, and reiodinated. (B) The iodine was reduced with sodium thiosulfate, equilibrated at 30°C for 30 min, and reiodinated. (C) Control.

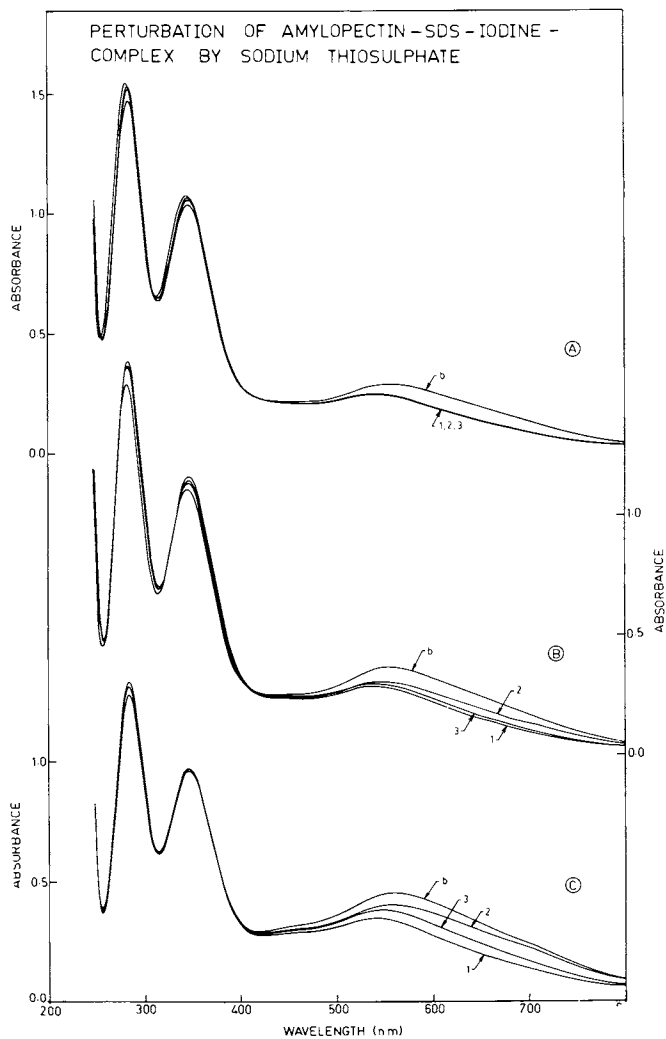


Figure 5. Absorption spectra of amylopectin-SDS-iodine complex in acetate buffer, pH 4.8, for three different sequences (1, 2, and 3) as given in Figure 4. (A) The iodine was reduced with sodium thiosulfate, equilibrated at 60°C for 30 min, cooled to 30°C, and reiodinated. (B) The iodine was reduced with sodium thiosulfate, equilibrated at 30°C for 30 min, and reiodinated. (C) Control.

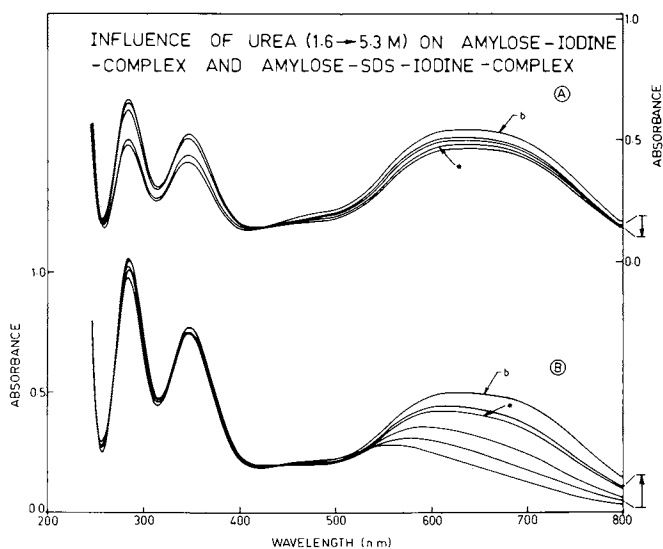


Figure 6. (A) The destabilizing influence of urea on the absorbance of the blue-colored amylose-iodine complex. (B) The inhibitory influence of SDS on the absorbance of amylose-iodine complex is overcome by urea; *, 4.5M urea. The arrow indicates the increasing concentration of urea (1.6 \rightarrow 5.3M).

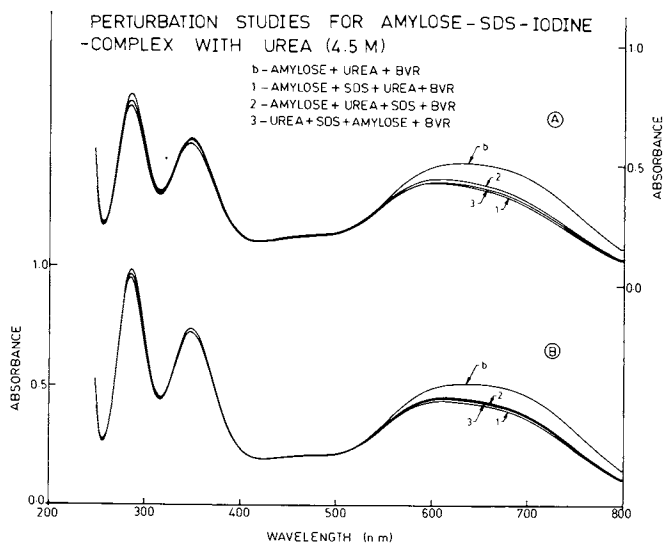


Figure 7. Absorption spectra of amylose-SDS-iodine complex in acetate buffer, pH 4.8, for three different sequences (1, 2, and 3) as given above. (A) Urea (4.5M) was added and the system was equilibrated at 60°C for 30 min, cooled to 30°C, followed by the addition of iodine. (B) Urea (4.5M) was added and the system was equilibrated at 30°C for 30 min, followed by the addition of iodine; b = blank without SDS.

Determination of $K_{0.5}$: The concentration of iodine ($K_{0.5}$) required to reduce the absorbance (640nm) to a value, half that of the saturation level is found to be very characteristic for a given polysaccharide. For these experiments the system described above for the determination of optimum concentration of iodine for the formation of blue coloured amylose-iodine-complex was used. The polysaccharide concentration was kept constant and the iodine concentration was varied (BVR - 0.1→0.8 ml). The concentration of polysaccharides used for the determination of their $K_{0.5}$ in this system were, amylose(0.07-0.09 mg), amylopectin(0.18-0.20 mg), potato starch(0.10-0.12 mg) and soluble starch(0.10-0.12 mg).

The concentration of the competing ligand ($K_{0.5}$) required to reduce the absorbance of amylose-SDS-iodine-complex (λ_{max}) to half, as compared with the blank(640 nm) was determined by using the sequence-1, which gave maximum reduction in the absorbance. For these experiments the system described for the study of influence of SDS on the amylose-iodine-complex was used. The concentration of amylose(0.07 mg) and iodine(BVR - 0.6 ml) was kept constant and the concentration of the competing ligands such as SDS-($1.0 \times 10^{-4}M$), sodium stearate-($5.0 \times 10^{-5}M$), sodium myristate-($4.0 \times 10^{-5}M$), sodium palmitate-($4.0 \times 10^{-5}M$) was varied (0.2→3.0 ml). The absorbance was recorded at the respective λ_{max} .

Studies on the inhibitory influence of SDS on amylose-iodine-complex : (Figure 10 & 11) The influence of the concentration of iodine(I_3^-) (BVR - 0.1→0.8 ml) on the formation of amylose-iodine-complex was studied by recording the absorbance at 640 nm (blank) and in the presence of SDS for the sequences 1, 2 & 3, at the corresponding λ_{max} . This system contained amylose(0.09 mg)- 0.2 ml and SDS($1.0 \times 10^{-4}M$) - 1.0 ml.

Results and Discussion

The competing ligand like SDS, appears to interact with the loose helical regions in amylose and amylopectin to form the corresponding compact helical complexes with SDS molecules trapped inside the helices. When iodine(I_3^-) is added to this system, a part of the SDS, which is loosely attached is displaced by iodine(I_3^-). The absorption spectra of the resulting amylose-SDS-iodine-complex/amylopectin-SDS-iodine-complex, when compared with their respective spectra in absence of SDS, show a reduction in

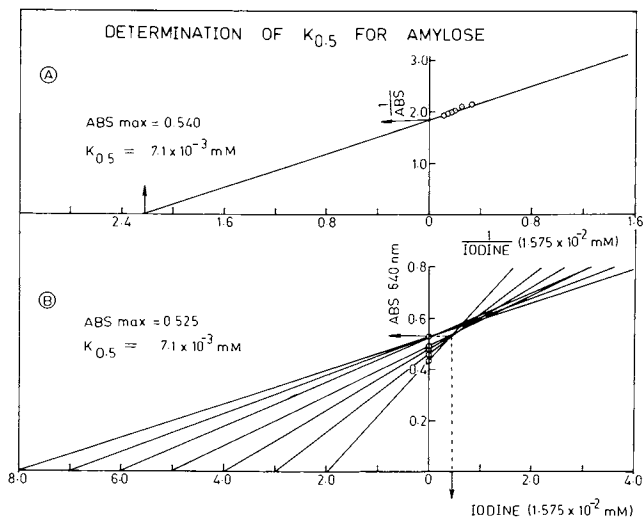


Figure 8. (A) Lineweaver Burk plot; (B) direct linear plot; ABS = absorbance (640 nm); BVR = blue value reagent (I_3^-).

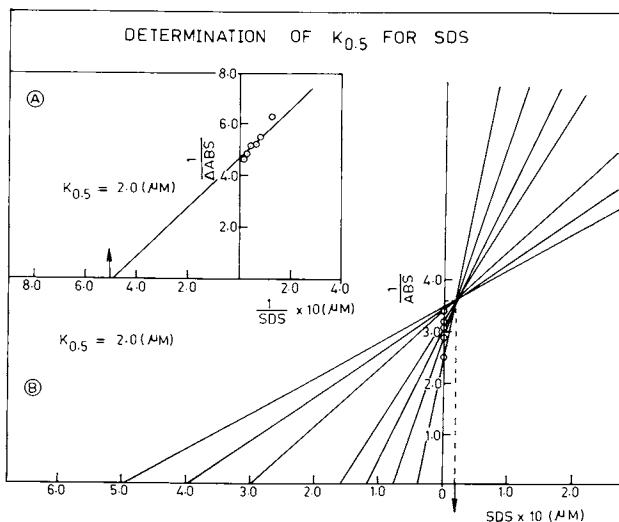


Figure 9. (A) Lineweaver Burk plot; (B) direct linear plot; (Δ) $ABS - ABS(\text{blank-}640 \text{ nm}) - ABS(\lambda_{max})$ ($ABS = \text{absorbance } (\lambda_{max})$). The reagents were added as per Sequence 1 (Amylose-SDS-BVR).

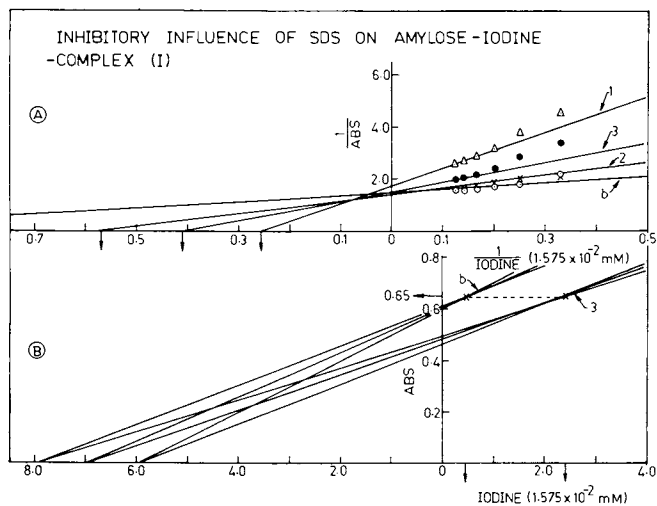


Figure 10. (A) Lineweaver Burk plot for three sequences (1, 2, and 3); (B) direct linear plot for Sequence 3 (BVR + SDS + amylose) ($ABS = \text{absorbance } (\lambda_{max})$; $b = \text{blank without SDS}$).

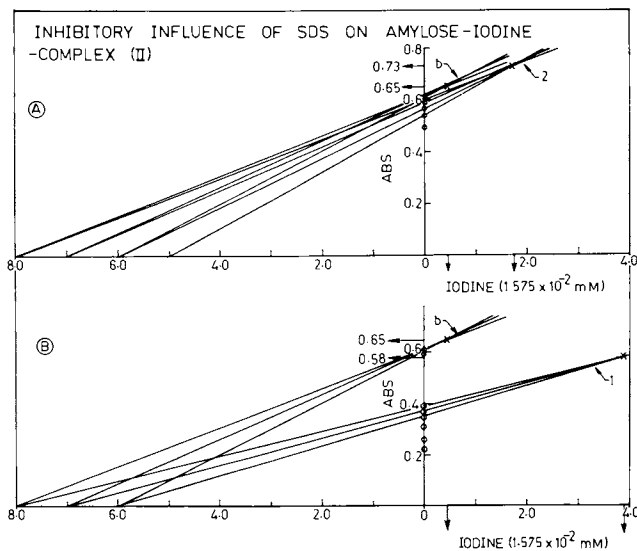


Figure 11. (A) Direct linear plot for Sequence 2 (amylose + BVR + SDS); (B) direct linear plot for Sequence 1 (amylose + SDS + BVR) ($ABS = \text{absorbance } (\lambda_{max})$; $b = \text{blank without SDS}$).

absorbance at 640 nm accompanied by a blue shift (640-570 nm) (Figure 1B & 1A). This change is more pronounced in the case of amylose (linear) than amylopectin (branched), as seen from their respective difference spectra (Figure 2A & 3A). The concentration of SDS used in these experiments is below the critical micellar concentration (CMC) and SDS has no interaction with iodine (I_3^-). The optimum concentration of iodine that gave maximum absorbance at 640 nm for the iodine complexes of amylose/amylopectin, without precipitation, was used. Under these conditions most of the iodine is bound inside the helical cavity and a small amount of iodine may be adsorbed on the surface of the complexed polymer chain (20).

The plot of $1/ABS$ vs SDS, in case of amylose-SDS-iodine-complex gives a typical rectangular hyperbola type curve, implying that after reaching the saturation level, there is no further drop in absorbance of the amylose-SDS-iodine-complex. Whereas in case of amylopectin-SDS-iodine-complex, there is a linear drop in the absorbance and the saturation level is not reached. This is probably due to low affinity of SDS/iodine for the short outer linear chains on amylopectin (Figure 1B).

Sequence studies : (Figure 2B & 3B) To our great surprise, it was observed that the reduction in absorbance at 640 nm and the blue shift (640-570 nm) caused by SDS was dependent on the sequence of addition of reagents, even though the system was equilibrated at 30°C for 30 minutes, after the addition of SDS and iodine, respectively. This time is sufficient to attain an equilibrium condition. The interaction of iodine (I_3^-) with the loose helical regions of amylose to produce blue coloured compact helical domains with iodine (I_3^-) molecules trapped inside the helices, is close to that of a diffusion controlled process ($7 \times 10^8 M^{-1} sec^{-1}$) and is independent of temperature (10-25°C) (35). Further, it was noticed that once the reagents were mixed in a given sequence, there was no change in the absorption spectrum of the amylose-SDS-iodine complex/amylopectin-SDS-iodine-complex, even after 16-18 hours of incubation at 30°C in glass-stoppered test tubes, protected from light. It appears that iodine (I_3^-)/SDS molecules once entrapped in the helix cannot diffuse out freely in the surrounding aqueous environment, due to the tight or stiff nature of the helix. This is more valid for the helical domains inside (endo) the polymer chain than at the end portion (exo). The influence of SDS was more prominent in sequence-1, intermediate in sequence-3 and minimum in sequence-2 as compared with the blank (Figure 2 & 3)

Perturbation studies : Reduction of iodine(I_3^-) with sodium thiosulphate - It was of great interest to know how the system behaves when one of the ligands such as iodine(I_3^-) was removed by reduction with sodium thiosulphate under extremely mild conditions (30°C), in the presence of SDS. One would normally expect that the SDS molecules from the solution would diffuse in the helical cavity to occupy the vacant spaces of iodine(I_3^-). On reiodination the absorption spectra of the systems generated by the sequences (2 & 3) should be identical to the absorption spectrum of the system generated by sequence-1. However, the results indicate that at 30°C the entry of SDS molecules in the empty helical regions of the polymer chain is rather a slow process (Figure 4B & 5B). This process can be accelerated by increasing the temperature to 60°C (Figure 4A & 5A). It appears that the helical domains of the polymer chain devoid of iodine molecules retain their conformational 'memory' over a short period. This is more prominent in case of amylose than amylopectin (Figure 4 & 5, sequence-2).

Influence of urea on amylose-iodine-complex/amylose-SDS-iodine-complex : Urea is known to have a destabilizing influence on the amylose-iodine-complex, resulting in a reduction in the absorbance at 640 nm. This is evident from the study of influence of urea on amylose-iodine-complex (Figure 6A). Urea also increases the flexibility of the polymer chain by affecting the intramolecular H-bonds (36). The inhibitory influence of SDS on the absorbance of amylose-iodine-complex at 640 nm was rapidly overcome at 30°C when urea (4.5 M) was added to amylose-SDS-iodine-complex. This is clearly evident from the study of influence of urea on amylose-SDS-iodine-complex (sequence-1 : Figure 6B). The sequence of addition of reagents had a little influence (Figure 7A) on the system equilibrated at 30°C and 60°C (Figure 7A & 7B). Further, addition of urea to amylose-SDS-complex before or after the addition of iodine(I_3^-) made no difference. These results imply that hydrophobic interactions and H-bonds play an important role in the formation of amylose-SDS-iodine-complex/amylopectin-SDS-iodine-complex.

Determination of $K_{0.5}$ and K_1 : A plot of concentration of iodine(I_3^-) vs absorbance (640 nm) in the case of the amylose-iodine-complex/amylopectin-iodine-complex gives a typical rectangular hyperbola curve (34), most often encountered in the field of enzyme kinetics. Similarly, the behaviour of many physical and biological systems can be described in

terms of a hyperbolic relationship between a measured response and a controlled variable. Hence Michaelis-Menten equation with suitable substitutions can be used to calculate $K_{0.5}$ from Lineweaver Burk plot and in particular the $K_{0.5}$ direct linear plot developed by Eisenthal and Cornish-Bowden (37,38) (Table II).

TABLE II

Michaelis-Menten Equation

$$v = \frac{V(s)}{K_m + (s)} \quad ; \quad \text{ABS} = \frac{\text{ABS}_{\text{max}} (\text{Iodine})}{K_{0.5} + (\text{Iodine})}$$

Lineweaver Burk Plot

$$\frac{1}{v} = \frac{1}{V} + \frac{K_m}{V} \cdot \frac{1}{(s)} \quad ; \quad \frac{1}{\text{ABS}} = \frac{1}{\text{ABS}_{\text{max}}} + \frac{K_{0.5}}{\text{ABS}_{\text{max}}} \cdot \frac{1}{(\text{Iodine})}$$

Eisenthal and Cornish-Bowden

Direct Linear Plot

$$\frac{V}{v} - \frac{K_m}{(s)} = 1 \quad ; \quad \frac{\text{ABS}_{\text{max}}}{\text{ABS}} - \frac{K_{0.5}}{(\text{Iodine})} = 1$$

Competitive Inhibition

$$K_m' = K_m \left(1 + \frac{1}{K_1}\right) \quad ; \quad K_{0.5}' = K_{0.5} \left(1 + \frac{1}{K_1}\right)$$

.....

TABLE III

Polysaccharide	Iodine (mM)	
	$K_{0.5}$	
Amylose	7.1×10^{-3}	
Amylopectin	7.4×10^{-2}	
Potato starch	3.8×10^{-2}	
Soluble starch	4.3×10^{-2}	

.....

The concentration of iodine $K_{0.5}$ required to reduce the absorbance (640 nm) to a $K_{0.5}$ value, half that of

the saturation level is very characteristic for amylose (linear) and amylopectin (branched), and can be determined accurately (Table III).

Similarly a plot of $1/ABS$ vs SDS in case of amylose in sequence-1 gives a typical rectangular hyperbola curve (Figure 1B). Hence $K_{0.5}$ values for different competing ligands can be obtained similar to that of SDS (Figure 9) by using sequence-1. Here the $K_{0.5}$ value gives the concentration of the complexing ligand required to reduce the absorbance of amylose-SDS-iodine-complex (λ_{max}) to half, as compared with the blank (640 nm) under standard conditions (Figure 9). It is interesting to know that $K_{0.5}$ values for SDS and sodium stearate having the same aliphatic hydrocarbon chain are identical and they decrease as the chain length increases (Table IV). The dissociation constant (K_1) can be calculated from this data for SDS (Table II & V). The values of $K_{0.5}$ and K_1 are very characteristic of the species of the ligand(s)-polymer complexes and they differ according to the sequence of addition of the reagents. Thus in sequence-1 the polymer chain is predominantly complexed with SDS and in the sequence-2, with iodine (I_3^-). In the sequence-3, the iodine and SDS molecules are randomly distributed in the helical domains. Hence the values of $K_{0.5}$ and K_1 for the sequence-3 are the mean values of the sequence (1) and (2) (Table V). Since the resultant parameters $K_{0.5}$ and K_1 depend on the mixing sequence, they cannot be understood as equilibrium constants in the usual sense. It also suggests that the helical domains of the polymer chain containing the ligands are identical. This is expected in case of amylose, a homopolymer made of D-glucose units linked through α -D(1 \rightarrow 4) linkages. The $K_{0.5}$ values obtained by Lineweaver Burk plots and direct linear plots were found to be similar (Figure 8,9,10,11).

Mechanism of interaction of SDS with amylose-iodine-complex : The inhibitory influence of SDS on the formation of amylose-iodine-complex can be investigated by studying the influence of iodine concentration (I_3^-) on the absorbance of amylose-iodine-complex in the presence (λ_{max}) and in the absence of SDS (640 nm). It is interesting to note that the mechanism of this inhibitory process is governed by the sequence of addition of the reagents. The sequence-3 shows a typical competitive mechanism, wherein iodine (I_3^-) and SDS molecules interact in a random way with the loose helical regions of the amylose chain to form compact helical domains containing SDS- I_3^- molecules. The

TABLE IV

Influence of Ligands on the Absorbance of Amylose-iodine-complex

Ligand		$K_{0.5}$ $\times 10^{-3}\text{mM}$
SDS	$\text{CH}_3 \cdot (\text{CH}_2)_{11} \cdot \text{OSO}_3\text{Na}$	2.0
Sodium Stearate	$\text{CH}_3 \cdot (\text{CH}_2)_{11} \cdot \text{COONa}$	2.0
Sodium Myristate	$\text{CH}_3 \cdot (\text{CH}_2)_{12} \cdot \text{COONa}$	0.8
Sodium Palmitate	$\text{CH}_3 \cdot (\text{CH}_2)_{14} \cdot \text{COONa}$	0.2
.		

TABLE V

 $K_{0.5}$ and K_1 for Amylose-SDS-iodine-complex

Sequence	(b)	(1)	(2)	(3)	Mean (1)&(2)
$K_{0.5} \times$					
10^{-2}mM Iodine	0.70	6.1	2.8	3.8	3.75 $(1)+(2)/2-(b)$
$K_1 \times$					
10^{-3}mM SDS	-	2.6	6.9	4.6	4.79
ABS_{max}	<u>0.65</u>	0.58	0.73	<u>0.65</u>	0.65
.					

K_d - Amylose-iodine-complex = 7.87×10^{-3} mM, Iodine

outstanding feature of competitive inhibition is that it is overcome by increasing the concentration of the competing ligand (substrate in case of enzyme). This precisely happens when iodine concentration is increased (Figure 10, Table V - ABS_{max} values). The sequence 1 and 2 showed a mixed type of inhibitory mechanism. (Figure 11).

Acknowledgements

Financial assistance in support of this work from :

1. University Grants Commission - New Delhi
2. Council of Scientific and Industrial Research - New Delhi
3. Youth Service Dept. (Science & Technology Cell) Govt. of Maharashtra - Bombay
4. S. H. Kelkar Charity Trust - Bombay
5. National Science Academy - New Delhi
6. Department of Science & Technology - New Delhi, is gratefully acknowledged.

Abstract

Amylose is a unique polysaccharide which forms a helical blue-coloured complex with iodine (I_3^-). It also forms helical complexes with a variety of organic compounds such as 1-butanol, 1-pentanol, cyclohexanol, SDS etc. The interaction of SDS, a competing ligand with iodine (I_3^-) complexes of amylose and amylopectin is studied spectrophotometrically. It is observed that the reduction in absorbance at 640 nm accompanied by the blue shift (640-570 nm) in the absorption spectrum is governed by the sequence of addition of the reagents, implying that this interaction is closely associated with the coil→helix transition of the polymer chain. Perturbation of this complex with sodium thiosulphate and urea has revealed that the transition from helix→coil is rather sluggish and hydrophobic interactions play an important role in the stability of this complex.

Literature cited

1. Rundle, R. E. and Edwards, F. C., J. Am. Chem. Soc. (1943) 65, 2200-2203.
2. Bittiger, H., Husemann, E. and Pfannemüller, B., Stärke. (1971) 23, 113-117.
3. Teitelbaum, R. C., Ruby, S. L. and Marks, T. J., J. Am. Chem. Soc. (1978) 100, 3215-3217.

4. Nguyen, Q. T., Aptel, P. and Neel, J.,
Biopolymers. (1976) 15, 2097-2100.
5. Mikus, F. F., Hixon, R. M. and Rundle, R. E.,
J. Am. Chem. Soc. (1946) 68, 1115-1123.
6. Valletta, R. M., Germino, F. J., Lang, R. E. and
Moshy, R. J., J. Polymer Sci. (1964) 2(A) 1085-1094.
7. Purvinas, R. M. and Zobel, H. F., Carbohydr. Res.
(1969) 10, 129-139.
8. Bhide, S. V., Indian J. Biochem. Biophys.
(1980) 17, 73-75.
9. Sakon, K., Watanabe, T. and Ono, S.,
Bull. Chem. Soc. Jap. (1970) 43, 1000-1005.
10. Banks, W. and Greenwood, C. T., Carbohydr. Res.
(1972) 21, 229-234.
11. Szejtli, J. and Augustat, S., Stärke.
(1966) 18, 38-52.
12. Szejtli, J., Richter, M. and Augustat, S.,
Biopolymers. (1967) 5, 5-16.
13. Bates, F. L., French, D. and Rundle, R. E.,
J. Am. Chem. Soc. (1943) 65, 142-148.
14. Cronan, C. L., Schneider, F. W. and Podder, S. K.,
J. Phys. Chem. (1968) 72, 4563-4568.
15. Cronan, C. L. and Schneider, F. W.,
J. Phys. Chem. (1969) 73, 3990-4004.
16. Goebel, C. V., Dimpfl, W. L. and Brant, D. A.
Macromolecules. (1970) 3, 644-654.
17. Brant, D. A. and Dimpfl, W. L.,
Macromolecules. (1970) 3, 655-664.
18. Jordan, R. C., Brant, D. A. and Cesàro, A.,
Biopolymers. (1978) 17, 2617-2632.
19. Pfannemüller, B., Meyerhöfer, H. and Schulz, R. C.,
Makromol. Chem. (1969) 121, 147-158.
20. Kuge, T. and Ono, S., Bull. Chem. Soc. Jap.
(1960) 33, 1273-1278.
21. Banks, W., Greenwood, C. T. and Khan, K. M.,
Carbohydr. Res. (1971) 17, 25-33.
22. Praznik, W. and Ebermann, R., Stärke.
(1979) 31, 288-293.
23. Smith, Jr. W. T. and Smith, G. T.,
Carbohydr. Res. (1969) 10, 598-600.
24. Moulik, S. P. and Gupta, S.,
Carbohydr. Res. (1979) 71, 251-264.
25. Ono, S., Watanabe, T., Ogawa, K. and Okazaki, M.,
Bull. Chem. Soc. Jap. (1965) 38, 643-648.
26. Takahashi, K. and Ono, S., J. Biochem. (Tokyo)
(1972) 72, 1041-1043.
27. Bhide, S. V. and Kale, N. R.,
Biochim. Biophys. Acta. (1976) 444, 719-726.
28. Hollo, J., Szejtli, J., László, E., Gatner, G. S.,
and Toth, M., Stärke. (1960) 12, 287-295.

29. Kim, Y. J. and Robinson, R. J.,
Stärke. (1979) 31, 293-300.
30. Nakatani, H., Shibata, K., Kondo, H. and Hiromi,
K., Biopolymers. (1977) 16, 2363-2370.
31. Patil, N. B., Gupte, S. P. and Kale, N. R.,
Makromol. Chem. (1974) 175, 1979-1994.
32. Patil, N. B., Taskar, S. P. and Kale, N. R.,
Carbohydr. Res. (1974) 33, 171-174.
33. Dubois, M., Gilles, K. A., Hamilton, J. K., Rebers,
P. A. and Smith, F., Anal. Chem. (1956) 28, 350-356.
34. Karve, M. S., Bhide, S. V. and Kale, N. R.,
This symposium.
35. Yamagishi, A., Imamura, T. and Fujimoto, M.,
Bull. Chem. Soc. Jap. (1972) 45, 2304-2308.
36. Amari, T. and Nakamura, M.,
J. Appl. Polym. Sci. (1976) 20, 2031-2043.
37. Eisenthal, R. and Cornish-Bowden, A.,
Biochem. J. (1974) 139, 715-720.
38. Cornish-Bowden, A. and Eisenthal, R.,
Biochem. J. (1974) 139, 721-730.

RECEIVED October 27, 1980.

Monte Carlo Calculations of the Debye Scattering Function and Diffusion Coefficient of Amylosic Chains

ATTILIO CESARO

Laboratory of Macromolecular Chemistry, University of Trieste, 34127 Trieste, Italy

DAVID A. BRANT

Department of Chemistry, University of California, Irvine, CA 92717

The aqueous solution configuration of amylosic chains has been studied extensively. Many of the findings have been reviewed in the recent literature (1, 2, 3, 4), and no general review will be undertaken here. A detailed statistical mechanical model (5), based on the known structural characteristics and estimated conformational energy surface of the dimeric subunit maltose (6), has been developed and shown to be consistent with the observed unperturbed dimensions of aqueous amylosic chains and also with the temperature and molecular weight dependences of these dimensions (7). Such theoretical polymer chain models are grounded in the most fundamental parameters of chemical structure, i.e., bond lengths, bond angles, etc., rather than on generic idealizations, e.g., the random flight model, of the polymer chain (2, 8). They allow not only for the prediction of important macromolecular properties which may be inaccessible to experimental investigation but also for a simple, yet realistic, conceptualization of macromolecular structure-property relationships. Examples of the latter capability are provided in another paper in this volume (9), where computer-generated "snapshots" of the instantaneous conformations of several dissolved polysaccharides are presented.

We have recently computed some mean properties of aqueous amylosic chains using a Monte Carlo technique (10) based on the refined theoretical amylosic chain model of Brant and Dimpfl (2, 5, 8). In the Monte Carlo technique a large number of polymer chain conformations are generated in the computer in a way which guarantees that all conformations are consistent with some preselected conformational energy function for the chain (10). Provided the Monte Carlo sample is large enough to approximate the parent distribution, averaged geometric, mechanical, and spectroscopic properties of the system may be obtained as simple arithmetic means over the members of the sample. Evidently, distribution functions for the several properties of the chain are available as well (10). Likewise, the characteristics of

0097-6156/81/0150-0513\$05.00/0

© 1981 American Chemical Society

individual (representative) members of the sample may be examined (9, 10).

The description that emerges from our current theoretical model (5, 10) suggests that amylosic chains in aqueous solution are tortuous random coils which possess at any instant many discernible sequences of short-range helical structure that is both irregular and short-lived (4, 10). Although this picture is generally satisfying, further refinement is desirable. In the first place, it must be recognized that the theoretical model (5) has been parameterized to produce agreement between calculated and observed measures of the overall chain dimensions, i.e., the unperturbed mean square radius of gyration or end-to-end distance, accessible through visible light scattering and hydrodynamics experiments (7). It is evident that the polymer end-to-end distance alone cannot provide a very detailed indication of the short-range conformational features of the chain. Hence the irregular pseudo-helical regions apparent in member chains of Monte Carlo samples based on the present model (2, 9, 10) may not reflect accurately the local chain trajectory of the real amylosic chain. Indeed, radial distribution functions of the end-to-end distance in the present Monte Carlo samples disclose a disturbing tendency of the chains to collide with themselves at a range of 6-10 residues in the chain sequence (10). It is not yet known whether this unrealistic feature is truly a serious defect in the current chain model.

Various experimental probes of local conformational character in macromolecules are available. Among these, magnetic resonance (11, 12, 13, 14) and circular dichroism spectroscopy (15, 16, 17, 18) come immediately to mind. Likewise, information about local structural and conformational characteristics is implicit in scattered radiation collected at relative large values of the scattering vector μ , i.e., at high angle and/or short wavelength (19). Normally such data are available from low angle X-ray (20) and neutron (21) scattering experiments. The present paper describes an investigation of the sensitivity of the Debye scattering function $P(\mu)$ to the details of the amylosic chain conformation at relatively large μ . We report also the preliminary results of a related calculation of the diffusion coefficients of the maltooligomers.

The Debye Scattering Function

Elastically scattered radiation reaching a detector from different scattering centers in a macromolecule will be subject to interference effects, provided the dimensions of the macromolecule are comparable to or larger than the wavelength of the radiation (22). The Debye scattering function $P(\mu)$ describes the variation, arising from intramolecular interference effects, of the scattered

intensity on observation angle θ and wavelength λ . It is defined to approach unity at $\theta = 0$, where the detector is aligned parallel with the incident radiation and phase shifts must vanish for scattering from different centers regardless of macromolecular size. The scattering function is given for an isolated chain with N scattering centers by (22)

$$P(\mu) = N^{-2} \sum_{i,j} \left\langle \frac{\sin \mu r_{ij}}{\mu r_{ij}} \right\rangle \quad (1)$$

where μ is defined by $\mu \equiv (4\pi/\lambda)\sin(\theta/2)$, r_{ij} is the distance between scattering centers i and j , and the double summation is over all such pairs of scattering centers. Integration over all orientations of the macromolecule with respect to the incident beam (and observer) is already implicit in Equation 1; the angle brackets express the remaining requirement for an appropriately weighted (statistical mechanical) average over all the conformations of any flexible macromolecule.

The limiting behavior of $P(\mu)$ at small μ is well known to reveal directly the overall dimensions of the macromolecule (mean square radius of gyration) without any assumption about macromolecular shape or form (22). cursory inspection of the expression in Equation 1 will disclose that as μ increases, the predominant contributions to $P(\mu)$ arise from terms with successively smaller r_{ij} . Thus, observation of $P(\mu)$ at larger μ can serve as a probe of shorter range structural characteristics of the macromolecule; normally some sort of macromolecular model is required to interpret $P(\mu)$ in this range of μ . We investigate here the potential for obtaining information about the local conformational features of amylosic chains from $P(\mu)$ at larger μ by examining the sensitivity of $P(\mu)$ to various changes in the amylosic chain model.

The Translational Diffusion Coefficient

The translational diffusion coefficient of a chain molecule is measurable using quasi-elastic light scattering (23, 24). It can be calculated from an appropriate chain model using the Kirkwood (25) equation

$$D = \frac{kT}{n\zeta} + \frac{kT}{6\pi\eta_0 n^2} \sum_{i \neq j} \langle r_{ij}^{-1} \rangle \quad (2)$$

where k is Boltzmann's constant, T is the absolute temperature, η_0 is the viscosity of the solvent, and ζ is the frictional coefficient of one frictional element in a chain of n such elements. The quantity r_{ij} is the distance between frictional elements i and j , and the angle brackets have the same meaning as in Equation 1. The initial term in Equation 2 represents the contribution to D from a "free draining" chain comprising n frictional elements while the second term reflects the contribution from "hydrodynamic interaction" among these elements. Although approximate, Equation 2 is quite accurate. Its reliability is discussed extensively elsewhere (26, 27, 28) and will not be dealt with here. The calculated value of D depends on the details of the macromolecular conformation through the hydrodynamic interaction term. It is our purpose here to assess the sensitivity of D to variations in the amylosic chain model employed.

Monte Carlo Averaging

The required configurational averaging of $\sin \mu r_{ij} / \mu r_{ij}$ in Equation 1 can be accomplished by Monte Carlo methods. We have followed an approach developed by Zierenberg, Carpenter, and Hsieh (29). For a Monte Carlo sample containing J_T chains generated as described above we obtain $P(\mu)$ from

$$P(\mu) = N^{-1} + 2N^{-2} \sum_{k=1}^{N-1} (N-k) \left\langle \frac{\sin \mu r_k}{\mu r_k} \right\rangle \quad (3)$$

where

$$\left\langle \frac{\sin \mu r_k}{\mu r_k} \right\rangle = J_T^{-1} \sum_{J=1}^{J_T} \frac{\sin \mu r_k(J)}{\mu r_k(J)} \quad (4)$$

The second term in Equation 3 arises from the assumption, normally made in treating the configurational statistics of homopolysaccharide chains (8, 10, 30), that mean geometric properties of chain segments depend only on $k \equiv |i - j|$ and not upon the positions of i and j in the chain sequence. Within a given chain there are, for each value of k , $(N-k)$ subchains comprising k scattering centers with (mean) end-to-end length r_k ; the term N^{-1} in Equation 2 accounts for the diagonal ($k = 0$) terms in the double summation of Equation 1. In practice we have taken for the (mean) distance $r_k(J)$ in Equation 4 only the single distance from scattering element 1 to scattering element $k + 1$ for each chain J ; provided J_T is large enough no loss of precision is incurred by this approximation (29).

In the present calculations we have identified glucose residues with scattering centers in the chain so that N is equal to the degree of polymerization, x . A Monte Carlo sample size $J_T = 205$ was employed for chains with various values of x up to 290 glucose residues. For regular helical amylosic chain models we took $J_T = 1$, since no configurational averaging is required for rigid macromolecules. Calculations were designed particularly to explore the range $0.1 < \mu < 1$. In this domain of the scattering vector $P(\mu)$ has converged to asymptotic behavior in its dependence on x for $x = 290$. The sample of 205 members was found sufficiently large to yield well-converged average properties for all chain models save the most flexible model (broken helix) for which the statistics were somewhat poorer than for the others.

The summation in Equation 2 is evaluated analogously. Thus

$$D = \frac{kT}{r_0} + \frac{kT}{3\pi\eta_0 n^2} \sum_{k=1}^{n-1} (n-k) \langle r_k^{-1} \rangle \quad (5)$$

with

$$\langle r_k^{-1} \rangle = \frac{1}{J_T} \sum_{J=1}^{J_T} r_k(J)^{-1} \quad (6)$$

Frictional elements were identified with glucose residues so $n = x$ and, again, the quantity $\langle r_k^{-1} \rangle$ is averaged over a sample of J_T chains taking $r_k(J)$ as the distance from the first glucose residue in the chain to residue $k + 1$ of that chain. For these calculations the sample size J_T was 945 for flexible chain models, and D was evaluated for all degrees of polymerization in the range $2 < x < 50$. For all flexible chain models D had converged to better than $\pm 1\%$ for $J_T = 945$.

Amylosic Chain Models

A realistic chain model (5), consistent with the observed mean squared unperturbed amylosic coil dimensions and their temperature and chain length dependences (7), was based on the average glucose residue geometry observed in crystalline cyclohexaamylose by Hybl et al. (31) and on conformational energy estimates after Goebel et al. (6). This is referred to as Model R in what follows. The refined conformational energy surface of Figure 2 in reference 10 was used to generate the Monte Carlo sample. For a chain with $x = 290$ the (mean) squared unperturbed radius of gyration R_G^2 calculated for Model R is given in the last column of Table I.

Table I

Characteristics of the Amylosic Chain Models

<u>Model</u>	<u>Type</u>	<u>h/\bar{A}</u>	<u>$\phi, \psi/\text{deg}$</u>	<u>R_G^2/\bar{A}^2</u>
R	random coil	--	--	0.41×10^4
A	helix	1.33	340,357	1.24×10^4
B	helix	1.53	340,353	1.64×10^4
C	helix	1.73	343,349	2.10×10^4
W	wormlike	--	--	1.00×10^4
J	jointed helix	--	--	0.25×10^4

Three rigid helical chain models were also investigated. In each case the Hybl et al. (31) residue geometry was used. The first of these, Model A, is based on the helical characteristics of crystalline V-amylose (1). It has six glucose residues per turn and a pitch of 8\AA ; the axial translation per residue h is thus 1.33\AA . A left-handed helix was chosen to conform with experimental indications (32). Given the residue geometry employed (31) and an assumed glycosidic bridge angle of 117° , this helix is characterized by glycosidic torsion angles $\phi, \psi = 357, 340$ (6). Models B and C are likewise left-handed, six-fold helices which differ from Model A only in having greater pitch. These models are inspired in part by the fact that crystalline B-amylose, which crystallizes spontaneously from aqueous solution (1), has a more extended helical structure than V-amylose (33). (Labels A, B, and C used arbitrarily to differentiate the present helical models should not be confused with similar notation frequently employed for the several crystalline modifications of amylose.) The characteristics of all of the helical models are given in Table I, where the dependence of R_G^2 on h is reported for chains with $x = 290$. Note that R_G^2 for all of the helical models exceeds that for the random coil chain of Model R as expected.

Two additional models, both corresponding to flexible chains, have been investigated. Model W is intended to represent a weakly bending or wormlike amylosic chain, which we understand to be one for which the direction of chain propagation changes gradually and continuously so that the radius of curvature of all chain segments is relatively large and no abrupt changes in direction occur (10,34). Models of this sort have been advanced for dissolved amylosic chains by other workers (35, 36, 37). Chains with this character may be generated using our Monte Carlo methods by imposing a conformational energy surface that restricts the torsional angles ϕ, ψ to some range of accessible values symmetric with respect to a particular point, i.e., rigid helical conformation, in conformation space (10). For Model W this energy surface was chosen so as to generate a parabolic probability surface with its maximum corresponding to the left-handed V-amylose helix (Model A); the probability was equated to zero for all ϕ and ψ more than $\pm 15^\circ$ different in either dimension from the maximum. The squared dimensions for the wormlike model exceed those of the presumably more realistic Model R by a factor of 2.5 for a chain with $x = 290$, while the wormlike chain is, as expected, more compact than the rigid V-amylose helix of corresponding x . A jointed or broken helix, Model J, was made by constructing 25-residue sequences in regular, left-handed

V-helical conformation and connecting these by glycosidic linkages at which both the ϕ and ψ torsions were permitted to undergo unhindered (free) rotation. This model, suggested by Szejtli and Augustat (38) and by Senior and Hamori (39), is the least extended of the several investigated, as seen by comparing the values of R_G^2 in Table I.

All calculations were carried out on the assumption that the chain consists of x identical scattering (frictional) centers, each corresponding to one glucose residue. The scattering (frictional) elements were taken to lie at the centers of mass of the several residues. This approximation should be quite satisfactory in calculations of $P(\mu)$ for small and intermediate values of μ . At large enough μ so that the predominant contributions to $P(\mu)$ come from intramolecular distances with dimensions of the order of one or a few glucose residues, it will fail. Under these circumstances the model used to calculate $P(\mu)$ must incorporate a realistic distribution of atomic centers along with a recognition of differences in the inherent atomic scattering power. Emphasis in calculations of D is on the chain length dependence of this parameter for the maltooligomers. It must be anticipated that end effects may become quite important at short chain lengths (28), and choice of a unique value for the frictional coefficient ζ may be inappropriate for calculations of D at low degrees of polymerization. For the preliminary results reported here, however, we have equated ζ with the frictional coefficient of glucose, $6.11 \times 10^{-9} \text{ g sec}^{-1}$, calculated from the diffusion coefficient of glucose in water (40). The viscosity of water, η_0 , has been taken as $0.01 \text{ g cm}^{-1} \text{ sec}^{-1}$, and all calculations have been made for $T = 298 \text{ K}$.

Results and Discussion

The Debye Scattering Function. The scattering function calculated for the chain models listed in Table I is reported in Figure 1 as $F(\mu) \equiv N\mu^2 P(\mu)$ vs. μ following Kratky and Porod (41) for values of μ up to 1 \AA^{-1} . For all of the models a broad maximum occurs centered near $\mu = 0.2 \text{ \AA}^{-1}$; significant differences between the models appear in Figure 1 only in the range of μ greater than about 0.3 \AA^{-1} . The positions of the principal maxima for the helical models (A, B, and C) differ substantially, presumably for reasons related to some periodicity specific to each helical geometry. This conclusion is reinforced by the observation that the principle maximum in $F(\mu)$ for the wormlike chain (W), although broader than that for helical model A, occurs at the same value of

μ as for helix A, the geometry of which serves as the reference or most probable conformation in model W. Likewise for model J, the jointed version of model A, the principal maximum in $F(\mu)$ appears to coincide on the μ axis with those for models A and W; results for model J are not plotted in Figure 1 because the Monte Carlo sample size was too small to yield adequate statistics with this model at the higher values of μ .

In the range of μ where the helical and wormlike models display their absolute maxima in Figure 1, the presumably more realistic random coil model R has a much lower and broader maximum. A minimum occurs in $F(\mu)$ for model R near $\mu = 0.5\text{\AA}^{-1}$, but at approximately the same value of μ the scattering function vanishes for helical models A, B, and C and the wormlike model W. Hence, it would appear that model R could be distinguished experimentally from the more regular models A, B, C, and W by the behavior of $F(\mu)$ in the range $0.3 \leq \mu \leq 1.0\text{\AA}^{-1}$. Likewise, regular helical or wormlike models may apparently be characterized in terms of their (most probable) axial translation per residue by using the position on the μ axis of the principal maximum in $F(\mu)$ in this range of μ . It is not so clear, however, that minor variations in models of type R could be differentiated experimentally.

These conclusions should be valid for chains with $x \geq 100$, because the present calculations reveal that $P(\mu)$ is independent of chain length in this range of x for $\mu \geq 0.1\text{\AA}^{-1}$. At sufficiently large μ the current approximation, which identifies scattering centers with glucose residues, will fail for reasons cited above. Under these conditions absolute comparison with experiment will require a more realistic description of atomic scattering power. We believe nevertheless that the qualitative distinctions described here between $F(\mu)$ vs. μ curves for several amylosic chain models will persist in any refined calculation. Thus, scattering experiments in the range $0.3 \leq \mu \leq 1.0\text{\AA}^{-1}$ may indeed be capable of distinguishing among the various generic models that have been proposed for amylosic chains.

If we examine in greater detail the behavior of the function $F(\mu)$ at smaller values of μ (Figure 2), we find, as expected (22), that the limiting dependence of $F(\mu)$ reflects the overall dimensions of the molecule. Thus, the curve in Figure 2 for the most flexible and compact model (J) displays the largest initial slope whereas the initial slope for the most extended helical model (C) is least. There is some indication in Figure 2 that the two more flexible models (J and R) have a more complex limiting behavior than do the helical and wormlike models. The results in Figure 2 are, of course, restricted to chains with $x = 290$, because the asymptote in the dependence of $F(\mu)$ on x has not

Figure 1. $F(\mu) \equiv N\mu^2P(\mu)$ vs. $\mu \equiv (4\pi/\lambda) \sin(\theta/2)$ for helical amylosic chain models A, B, and C, wormlike amylosic chain model W, jointed helical model J, and realistic random coil model R. Details of the models are described in the text.

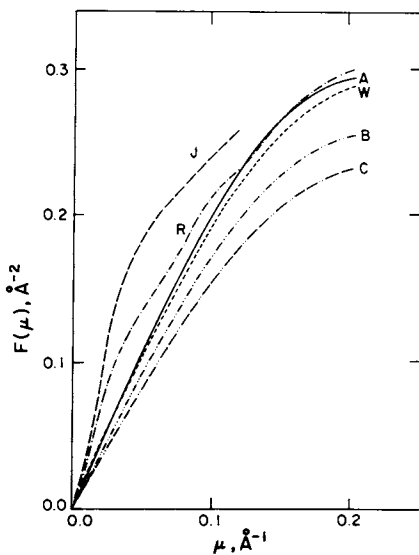
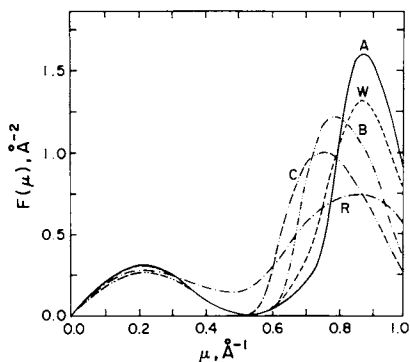


Figure 2. Same as Figure 1 but showing detail in the range of small μ .

achieved at $x = 290$ throughout the range $0 \leq \mu \leq 0.2\text{\AA}^{-1}$. For the regular helical chain models (A, B, and C) the initial slope of $F(\mu)$ vs. μ shows a steady decrease with increasing x , since R_G and x are directly proportional. In the case of flexible chains (models J, R, and W) R_G becomes proportional to approximately $x^{1/2}$ at large x , but this asymptotic behavior is achieved at a rate which depends on the directional persistence or stiffness of the chain. Clearly, interpretation of the experimentally derived scattering behavior at low μ requires a proper accounting in the model calculations for the chain length distribution of the sample.

The Translational Diffusion Coefficient. The calculated translational diffusion coefficient D of the maltooligomers up to $x = 18$ is shown in Figure 3 for models J, R, and C. The curves for models W and A (not shown) lie intermediate between those for models J and R while that for model B (not shown) lies between those for models R and C. In general, the less extended the model chain, the larger the diffusion coefficient. There is some crossing of the theoretical curves which arises from the differing dependence of the dimensions of rigid helical and flexible chains on chain length mentioned above and described elsewhere (10). In any case the similar, and essentially featureless, dependence of D on x calculated for all of the chain models suggests that they will not be differentiable on the basis of experimental measurements of D vs. x for the maltooligomers. It nevertheless remains of interest to compare the calculated and measured values of these quantities, particularly to assess the possible influence of solvation on the properties of the oligomers (28).

Conclusions

Monte Carlo calculations of the Debye scattering function $P(\mu)$ for several amylosic chain models suggest that it may be possible to distinguish experimentally between popular generic models for the amylosic chain by investigating the angular dependence of elastic scattering in the range $0.3 \leq \mu \leq 1.0\text{\AA}^{-1}$ of the scattering vector. Low angle X-ray scattering on dilute polymer solutions appears to be the method of choice, although lack of contrast between the carbohydrate chain and aqueous solvents may render the experiment difficult. Comparison of calculated and measured values of the translational diffusion coefficient for the maltooligomers may be useful in assessing the influence of solvation on the conformation and hydrodynamic shapes of the oligomers.

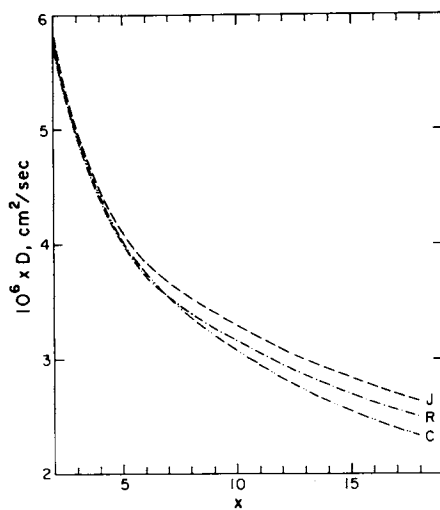


Figure 3. The calculated chain length dependence of D for the maltooligomers in the degree of polymerization range $2 \leq x \leq 18$ for chain models C, J, and R described in the text

Abstract

Monte Carlo calculations of the Debye scattering function and the translational diffusion coefficient of amylosic chains have been carried out for a variety of amylosic chain models. Helical, wormlike, and jointed helical models have been investigated as has a presumably more realistic random coil model which is based on detailed analysis of the conformational characteristics of the amylose molecular structure. It is concluded that the several chain models should be distinguishable experimentally on the basis of the angular dependence of low angle X-ray scattering from dilute amylose solutions. The calculated chain length dependence of the translational diffusion coefficients of the maltooligomers is quite similar for all of the models investigated. Measurements of this quantity therefore may not be very useful in distinguishing between the models, but comparison of calculated and measured diffusion coefficients may nevertheless yield information concerning the influence of solvation on the behavior of the maltooligomers.

Acknowledgements

This work has been supported in part by National Science Foundation Research Grants PCM79-23041 and PCM77-23603 and by the Italian Research Council (CNR) through Grant N.78.01129.03 and through a travel grant to A.C.

Literature Cited

1. Banks, W., and Greenwood, C.T., "Starch and Its Components", Edinburgh University Press: Edinburgh, 1975.
2. Brant, D.A., in "The Biochemistry of Plants" (Preiss, J., Ed.), Vol. 3, Chapter 11, Academic Press: New York, 1980.
3. Kodama, M., Noda, H., and Kamata, T., Biopolymers (1978) 17, 985.
4. Jordan, R.C., and Brant, D.A., Macromolecules (1980) 13, 491.
5. Brant, D.A., and Dimpfl, W.L., Macromolecules (1970) 3, 655.
6. Goebel, C.V., Dimpfl, W.L., and Brant, D.A., Macromolecules (1970) 3, 644.
7. Goebel, K.D., and Brant, D.A., Macromolecules (1970) 3, 634.
8. Brant, D.A., Quart. Rev. Biophys. (1976) 9, 527.

9. Brant D.A., and Burton, B.A., in "Solution Properties of Polysaccharides" (Brant, D.A., Ed.), ACS Symposium Series, Chapter 7, American Chemical Society: Washington, 1980.
10. Jordan, R.C., Brant, D.A., and Cesaro, A., Biopolymers (1978) 17, 2617.
11. St. Jacques, M., Sundararajan, P.R., Taylor, K.J., and Marchessault, R.H., J. Am. Chem. Soc. (1976) 98, 4386.
12. Parfondry, A., Cyr, N., and Perlin, A.S., Carbohydr. Res. (1977) 59, 299.
13. Dorman, D.E., and Roberts, J.D., J. Am. Chem. Soc. (1971) 93 4463.
14. Vollter, W., Bilik, V., and Breitmaier, E., Collect. Czech. Chem. Commun. (1973) 38, 1054.
15. Lewis, D.G., and Johnson, W.C., Jr., Biopolymers (1978) 17, 1439 (1978).
16. Chakrabarti, B., in "Solution Properties of Polysaccharides" (Brant, D.A., Ed.), ACS Symposium Series, Chapter 19, American Chemical Society: Washington, 1980.
17. Bush, C.A., and Ralapati, S., in "Solution Properties of Polysaccharides (Brant, D.A., Ed.), ACS Symposium Series, Chapter 20, American Chemical Society: Washington, 1980.
18. Stevens, E.S., and Stipanovic, A.J., in "Solution Properties of Polysaccharides (Brant, D.A., Ed.), ACS Symposium Series, Chapter 21, American Chemical Society: Washington, 1980.
19. Kratky, O., Pure Appl. Chem. (1965) 12, 483.
20. Ishimuro, Y., Hamada, F., and Nakajima, A., Macromolecules (1978) 11, 382.
21. Akcasu, A.Z., Summerfield, G.C., Jahshan, S.N., Han, C.C., Kim, C.Y., and Yu, H., J. Polym. Sci.: Polym. Phys. Ed. (1980) 18, 863.
22. Tanford, C., "Physical Chemistry of Macromolecules", Chapter 5, John Wiley and Sons: New York, 1961.
23. Chu, B., "Laser Light Scattering", Academic Press: New York, 1974.
24. Berne, B.J., and Pecora, R., "Dynamic Light Scattering" Wiley-Interscience: New York 1976.

25. Kirkwood, J.G., J. Polym. Sci. (1954) 12, 1.
26. Yamakawa, H., "Modern Theory of Polymer Solutions", Chapter 6, Harper and Row: New York, 1971.
27. Stockmayer, W.H., in "Molecular Fluids—Les Houches Lectures, 1973", (Balian, R., and Weill, G., Eds.), Gordon and Breach: London, 1976.
28. Mokrys, I.J., Rigby, D., and Stepto, R.T.F., Ber. Bunsenges. Phys. Chem. (1979) 83, 446.
29. Zierenberg, B., Carpenter, D.K., and Hsieh, J.H., J. Polym. Sci.: Polym. Symp. (1976) 54, 145.
30. Brant, D.A., and Goebel, K.D., Macromolecules (1975) 8, 522.
31. Hybl, A., Rundle, R.E., and Williams, D.E., J. Am. Chem. Soc. (1965) 87, 2779.
32. Winter, W.T., and Sarko, A., Biopolymers (1974) 13, 1447.
33. Wu, H.-C.H., and Sarko, A., Carbohydr. Res. (1978) 61, 7.
34. Dubin, P.L., and Brant, D.A., Macromolecules (1975) 8, 831.
35. Pfannemuller, B., Mayerhoefer, H. and Schulz, R.C., Biopolymers (1971) 10, 243.
36. Rao, V.S.R., and Foster, J.F., Biopolymers (1963) 1, 521.
37. Fujii, M., Honda, K., and Fujita, H., Biopolymers (1973) 12, 1177.
38. Szejtli, J., and Augustat, S., Staerke (1966) 18, 38.
39. Senior, M.B., and Hamori, E., Biopolymers (1973) 12, 65.
40. Longworth, L. G., J. Am. Chem. Soc. (1953) 75, 5705.
41. Kratky, O., and Porod, G., Rec. trav. chim. (1949) 68, 1106.

RECEIVED October 3, 1980.

Properties of Aqueous Amylose and Amylose-Iodine Solutions¹

B. PFANNEMÜLLER and G. ZIEGAST

Institute of Macromolecular Chemistry, University of Freiburg,
D-7800 Freiburg i. Br., Federal Republic of Germany

Aqueous solutions of natural amylose possess the undesirable property of retrogradation, i.e. the solutions are unstable and tend to precipitate spontaneously. From studies with enzymatically-synthesized, almost monodisperse amyloses we have shown that mainly molecules of intermediate length, around DP 80, are responsible for this effect (1). Shorter and longer chains are much more stable in solution. In this respect amylose shows behavior distinctly different from other polymers. The retrograded amylose gives a B-type X-ray diagram and an electron diffraction pattern (2), which is compatible with the double helix structure recently deduced by Wu and Sarko (3). The question remains whether a pre-formed, ordered conformation already exists in solution, or if not, at which stage (association, aggregation or crystallization) the double helix is formed.

A reasonable explanation of the unusual solution properties of aqueous amylose may be found in a certain chain stiffness, which in the critical DP range of high retrogradation rate favors intermolecular hydrogen bonding. Longer chains show a larger coiling tendency and a stabilization can occur predominantly by intramolecular hydrogen bonds (4,5,6). This interpretation is based on light scattering measurements of the radii of gyration and the second virial coefficient as a function of the DP (6). A_2 shows a maximum at a DP, for which intermolecular association is inhibited by the coiling of the chains. No change of the radii of gyration was found using retrograding solutions (4,5).

The problem whether or not a helical structure of amylose is retained in solution is nearly as old as the discovery of the V-amylose helix from X-ray data in 1943 (7) and has been the subject of extensive investigation and controversy. (For review see (8)). At present mainly two models are considered: the "extended helix chain" (9) and the "randomly coiled pseudohelical chain" (10). According to Senior and Hamori (9) the amylose chain conformation is characterized by loose, extended helical regions, which are interrupted by short, disordered regions. Hydrogen bonds between O(2) and O(3') of neighboring residues are

¹ Dedicated to Professor G. V. Schulz on the occasion of his 75th birthday.

assumed to account for stabilization. The model of Brant and co-workers (10) has been derived from a theoretical treatment of configurational statistics, experimental observations and recent Monte Carlo studies of the unperturbed chain conformation (10,11,12,13,14). A typical feature of this model are self-intersections of the helix loops at short distance of 5-20 residues. They are ascribed to short-range, nearest-neighbor interactions leading to a constraint of the glycosidic linkage torsion angles. Hydrogen bonds are assumed to play no role in determining the conformation of amylose in aqueous solution. The persistence length calculated using this model is very short (2.8 nm) (10) and out of the critical range of a DP 80 amylose.

In earlier ORD and CD measurements with amylose-iodine solutions we observed a maximum of the Cotton effect near DP 50 and a time dependent increase of the Cotton effect on standing of the solutions (1,15). This time dependent change of ORD and CD was considered to arise mainly from rearrangements of the amylose, since the absorption spectra remained virtually unchanged.

Because of the inherent instability of the aqueous amylose solutions viscosity changes on binding of complexing agents, e.g. butanol or iodine, have often been used for deducing the initial chain conformation (8,9,11,14,16). Observations with amylose-iodine solutions also contribute valuable information.

This paper is an extension of earlier studies and deals with the following points:

1. Time dependent change in CD spectra of amylose-iodine complexes; do they directly reflect the different stages of order for a V-amylose helix, or do they show the development of a regular supermolecular structure with characteristics, which depend on chain length ?

2. To which extent is the high tendency to retrogradation around DP 80 related to the conformation of the molecules in solution; more specifically, how does retrogradation lead to the formation of a double helix ?

For the amylose-iodine solutions information was expected from

- resonance Raman studies: In order to obtain a better understanding of the phenomena observed by CD and a further resolution of the CD curves, information on the electronic transitions of the polyiodine chromophore are needed, and may be obtainable from resonance Raman spectroscopy.
- CD studies: Measurements under selected conditions should help to differentiate between *intramolecular* and *intermolecular* ordering processes.
- fractional precipitation of amylose mixtures with iodine and GPC separation of the fractions: A preferential aggregation according to chain length should be an indication for a preformed or quickly developing order.

For the aqueous amylose solutions information was expected from

- CD measurements in the region of the sugar chromophores: They may give a direct observation of the discussed helical structure.
- Stepwise retrogradation of amylose mixtures and GPC separation of the fractions should reveal whether a preferential precipitation exists, possibly as a result of preformed double helices in solution.

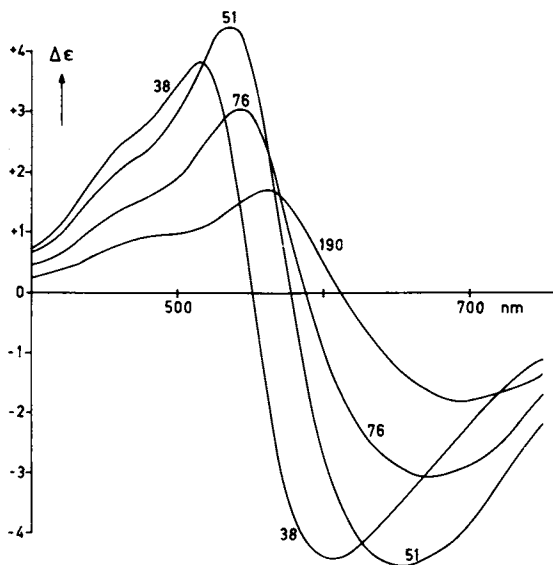
In view of the tremendous work dedicated to amylose and amylose-iodine complexes and the largely conflicting theories and results we can not yet offer a clearcut decision. We feel at the present stage of our knowledge there is now more need for experimental facts rather than for new theories.

Results and Discussion

Studies with Amylose-Iodine Solutions

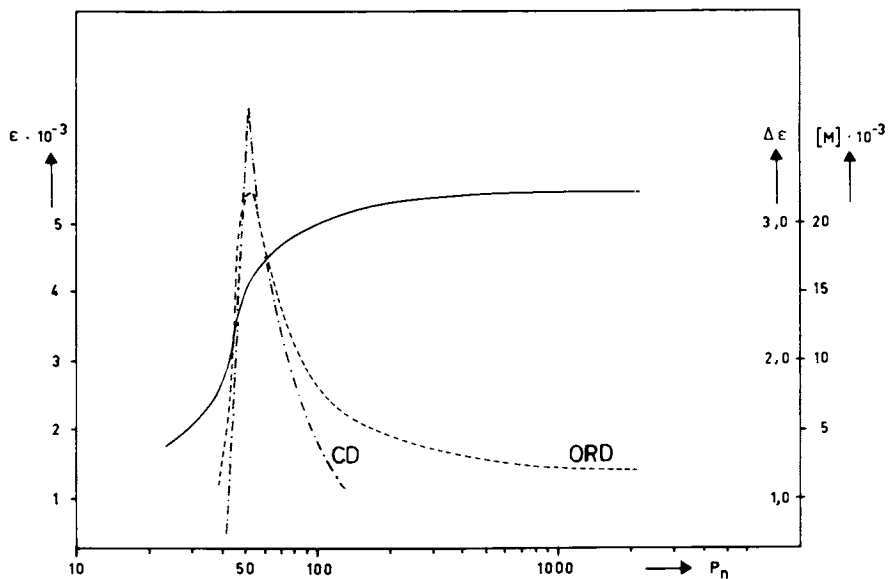
CD and Resonance Raman Measurements. Using synthetic amyloses we had earlier observed a maximum of the Cotton effect at a chain length of about DP 50 (1,15). This is demonstrated with the CD curves of a series of iodine-complexed amyloses DP 38, 51, 76 and 190 shown in Figure 1. While maxima of the long wavelength CD bands are continuously shifted to longer wavelengths the magnitude of the Cotton effect reaches an optimum value with DP 51. As seen from Figure 2 the decrease of the molar optical rotation (M) and dichroic absorption ($\Delta\epsilon_{\max}$) above DP 50 is not in line with the continued increase of the extinction coefficient (ϵ_{\max}) and with the further shift of λ_{\max} to longer wavelengths (15,18). At first sight this behavior appears not to be in agreement with theory.

The relationship between absorption, ORD and CD can be outlined briefly: When circularly polarized light is incident on an optically active medium the left and right circularly polarized component will have different velocities. This is conveniently expressed as the difference in refractive indices, $n_L - n_R$, the "circular birefringence", which is proportional to the angle of rotation α . When the wavelength dependence of α is measured in the range of an absorption band, the left and right circularly polarized wave will not only propagate with different speeds, but will also be absorbed to different extents. The difference, $\Delta\epsilon = \epsilon_L - \epsilon_R$, is the "circular dichroism" (CD). As a consequence of a CD the normal plain curve of the wavelength dependence of α , the "optical rotatory dispersion" (ORD) becomes anomalous and the plain curve is superposed by an S-shaped curve. Both, CD and anomalous ORD, are called "Cotton effect". Quantitatively CD and ORD are linked through the Kronig-Kramers relationship. No stringent coupling of the extinction coefficient (ϵ_{\max}) with the CD effect ($\Delta\epsilon_{\max}$) exists, because ϵ_{\max} contains



Carbohydrate Research

Figure 1. CD spectra of amylose-iodine complexes DP 38, 51, 76, and 190 (17)



Biopolymers

Figure 2. Extinction (—), molar optical rotation (· · ·), and dichroic absorption (— · —) of the long wavelength maxima as a function of the degree of polymerization (P_n) (1)

contributions from electron transitions, which do not necessarily arise from optically active chromophores.

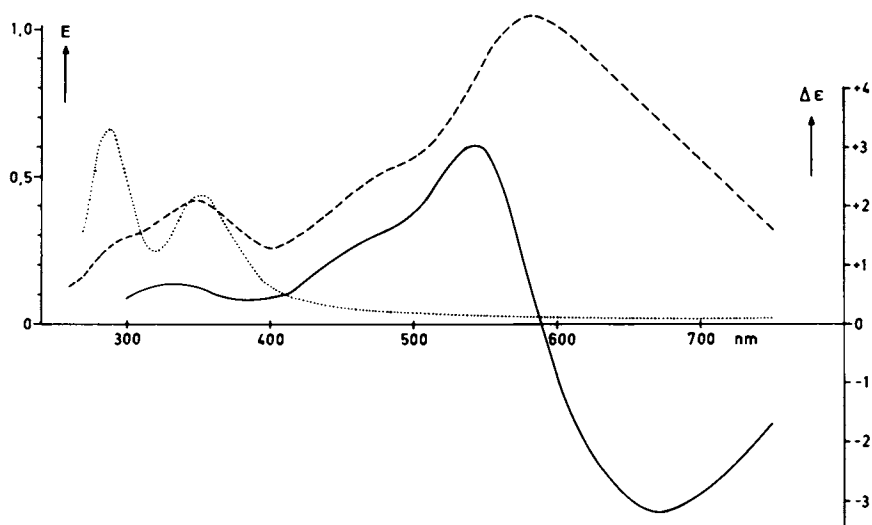
Our results indicate that $\Delta\epsilon$ (CD) changes in a different way as ϵ . The absorption and CD spectrum of an amylose-iodine complex DP 76 are shown in Figure 3. In the low wavelength region the absorption and CD curve have a similar shape. A weak positive CD and a shoulder are seen corresponding to the absorption maximum at 353 nm and the shoulder at 480 nm. The CD band corresponding to the long wavelength absorption maximum at 582 nm, however, is obviously split into two bands of opposite sign. This splitting, first recognized with oligonucleotides (19), and also found with amylose carbanilates (20,21) is caused by a bending or twisting of the iodine chromophore induced by the asymmetric environment of the helical amylose chain.

Helix formation probably arises from a co-operative action of amylose and iodine partners. Different models have been proposed; despite extensive investigation the nature of the interaction producing the intense visible absorption spectrum of the amylose-iodine complex is by no means clear. (For review see (8,16,22)).

Resonance Raman studies were begun in order to interpret the results from CD measurements and in the hope of a further resolution of the CD curves. To this end we needed a reliable assignment of the broad long wavelength absorption band and the shoulder band at 480 nm. An attempt at detailed assignment of the electronic transitions, based on model calculations of an exciton-coupled, one-dimensional polymeric I_3^- chain, was first published by Robin (23,24). Handa and Yajima (25) have recently extended these calculations to a I_3^- chain based on dimeric subunits with the assumption of strong interaction with the amylose oxygens. An analysis of the mentioned absorption bands should be possible by the application of resonance Raman spectroscopy.

The resonance Raman effect depends on the occurrence of a strong absorption band. An intensity enhancement of the normal Raman spectrum is observed when the frequency of the exciting radiation approaches an electronic absorption of the scatterer. We applied this method to the investigation of the red and blue colored complexes in order to find out whether changes in the Raman spectra occur. Furthermore, we had the idea that the blue band and the shoulder band in the absorption spectrum may arise from different iodine species bound in the complex.

Measurements were carried out with iodine solutions of various composition: (a) iodine solution free of I^- (iodine dissolved in 0.1 M perchloric acid) (26); (b) 1 I_2 /1.6 I^- ; (c) 1 I_2 /2.6 I^- ; (d) 1 I_2 /65 I^- . With all iodine solutions (without amylose) containing I^- (b-d) a main signal is observed at 111 cm^{-1} . Based on the vibrational analysis of the I_3^- ion by Maki and Forneris (27), this signal was assigned by Tasumi (28) to the symmetric stretching vibration of I_3^- . With the



Carbohydrate Research

Figure 3. CD (—) and absorption (---) spectra of amylose-iodine complex DP 76; absorption of I₂-KI solution (· · ·) (17).

solution containing the largest excess of I^- (d) an additional broad band centered at 159 cm^{-1} is found. With decreasing content of I^- (c) this band appears as a weak shoulder at about 152 cm^{-1} . The origin of this band, possibly from a polyiodine species (29), is still open to discussion (28,29,30,31). However, in the absence of I^- (a) only the symmetric stretching vibration band of molecular iodine at 207 cm^{-1} is found.

The resonance Raman spectra of solutions of iodine-complexed amyloses with DP 18, 47 and 190 are shown in Figure 4. Most strikingly, the resonance Raman spectra are almost identical inspite of the considerably different absorption spectra of these samples. A main band at 162 cm^{-1} , typical of complexed iodine (25,28,30,32), and a band at 111 cm^{-1} are observed. Heyde et al. (30) found two additional bands at 27 and 57 cm^{-1} ; the former can be seen in the spectra of DP 47 and 190 in Figure 4. The 57 cm^{-1} band is superposed by a group of signals located between 80 and 35 cm^{-1} , which turned out to be due to instrumental artifacts. Overtones and combination vibrations were found at 185, 217, 272 and 322 cm^{-1} .

Resonance Raman theory (33) predicts an enhancement of the scattering intensity, when the excitation wavelength approaches λ_{max} from the long wavelength side. This effect is clearly seen for the iodine complexes of DP 18 with $\lambda_{\text{max}}=518\text{ nm}$ in Figure 5 and of DP 190 with $\lambda_{\text{max}}=593\text{ nm}$ in Figure 6. It is worthy of note that the enhancement of the 162 cm^{-1} band is related to $\lambda_{\text{max}}/\lambda$ excitation as expected, but that the position of the 162 cm^{-1} Raman line remains unchanged from DP 18 to 190. This invariance of the Raman band position with amylose chain length indicates, that this vibration mode is independent of the polyiodine chain length.

The spectra do not show time dependent changes. In the range of the sugar vibrations, $500-1500\text{ cm}^{-1}$, resonance enhanced signals, which would have indicated strong interactions between iodine and amylose, were not observed.

Tasumi (28) has assigned the signals observed at 163, 115 and 56 cm^{-1} to the antisymmetric stretching, symmetric stretching and bending vibrations, respectively, of I_3^- included in the helix. This interpretation deviates from that of Teitelbaum et al. (32). Teitelbaum has combined resonance Raman and Mössbauer studies and his results indicate the presence of I_5^- units. The 163 cm^{-1} transition is therefore assigned to a fundamental, normal mode involving the symmetrically coupled internal stretching of two I_2 units flanking I^- . He states: "That the force constant is perturbed less from the free I_2 (207 cm^{-1}) than in I_3^- (108 cm^{-1}) reflects the fact that the available electron density of the I^- donor must now be distributed between two I_2 acceptors." His spectra show only very weak scattering at 109 cm^{-1} (I_3^-) and 56 cm^{-1} (not assigned). The question remains as to whether the conditions of his studies, freeze dried samples

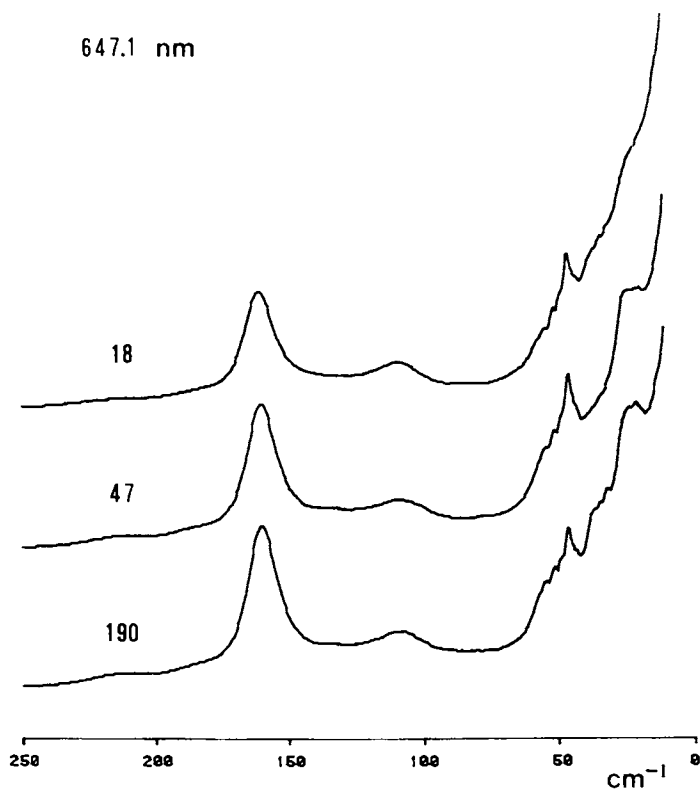


Figure 4. Resonance Raman spectra of amylose-iodine complexes DP 18, 47, and 190 ($\text{Kr}, 647.1$). (Amylose DP 18, concn = 0.2 g/L; DP 47 and 190, concn = 0.07 g/L; 1 I_3^- per 6 anhydroglucose residues; 1 I_2 per 1.6 I^- .)

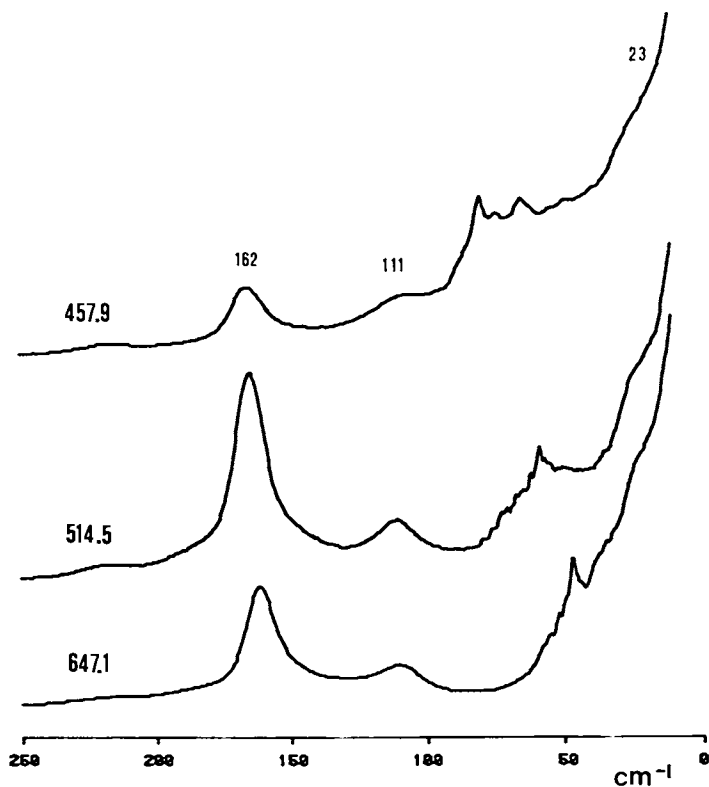


Figure 5. Resonance Raman spectra of amylose-iodine complex DP 18, $\lambda_{max} = 518 \text{ nm}$, for laser wavelengths 457.9, 514.5, and 647.1 nm

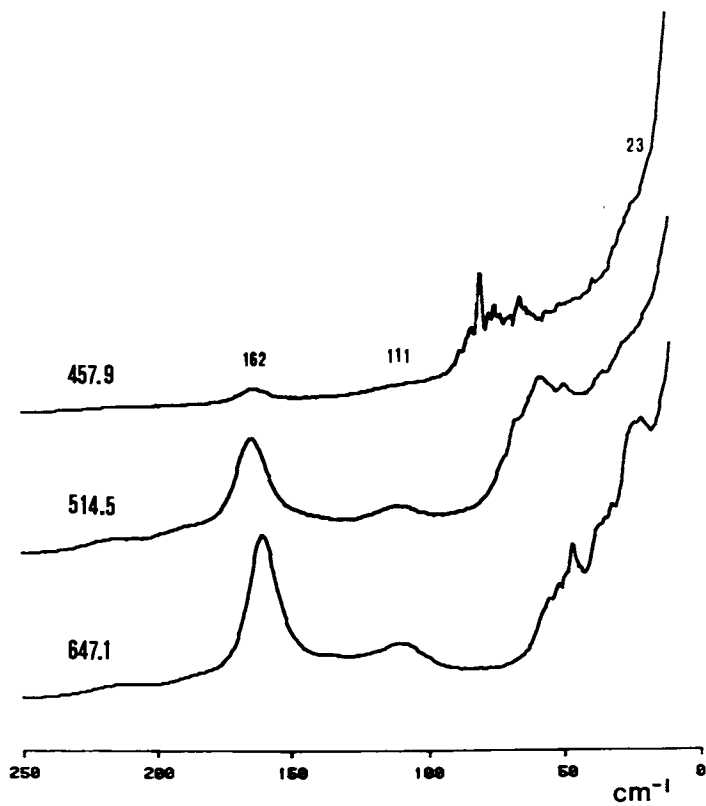


Figure 6. Resonance Raman spectra of amylose-iodine complex DP 190, $\lambda_{\text{max}} = 593 \text{ nm}$, for laser wavelengths 457.9, 514.5, and 647.1 nm

and a temperature of 4 K in Mössbauer studies, are comparable with dilute solutions at room temperature, which produce a comparatively stronger band at 111 cm^{-1} .

At the present stage we can say, that there is no indication for any change of the Raman excited modes of the enclosed iodine species with increasing λ_{max} , i.e. the length of the polyiodine chain. No difference in the spectra of red and blue colored amylose complexes is detectable (34,35). Preliminary experiments also give no indication of a change in the spectra with the I^- content of the iodine solutions used (b-d). Experiments with improved instrumentation and still shorter amylose chains are in progress. These studies may reveal a chain length limit for the observation of the characteristic signals. We are especially interested in a detailed investigation of the 27 cm^{-1} band because this band has been assigned by Heyde et al. (30) to an iodine chain length of 28 iodine atoms corresponding to optimal stability in the range of DP 72. However, this assignment appears doubtful since the signal is clearly seen with a DP 47 amylose (Figure 4).

Ordering Processes of Amylose-Iodine Solutions. A second feature observed in earlier ORD and CD measurements with amylose-iodine solutions was a time dependent increase of the Cotton effect (1). As mentioned above, *intra-* and *intermolecular* ordering processes may be considered. In order to differentiate between these two possibilities, we initially carried out studies in very dilute solutions to prevent association as far as possible (Figure 7).

There is a marked difference in the CD spectra measured immediately after addition of iodine and after 24 hours. This is in contrast to only a minor change in the absorption spectrum, which indicates that little happens to the polyiodine chain. Note, the optically active transitions ($\Delta\epsilon$) contribute very little to the overall extinction coefficient (ϵ).

The course of the development of the CD during the first two hours may be seen in Figure 8 for a DP 47 amylose. The negative and positive band increase almost uniformly. λ_{max} and λ_0 are simultaneously shifted to shorter wavelengths. This shift, typically found for slowly-ordering, longer chains (17) is an indication of a change, though small, in the polyiodine chain and is the subject of further investigation. A reasonable explanation of the time dependent increase of CD observed with the short chain amyloses is the transition from a loosely-wound helical chain to a more densely packed, regular one. Such ordering of asymmetric optically active centers of the amylose chain does not necessarily imply a change of polyiodine chain length upon passing from an imperfect to a well organized helix. In this way the increase in the number of asymmetric sites for iodine binding can be understood without a change of λ_{max} . Chain folding should also be kept in mind and will be more likely for

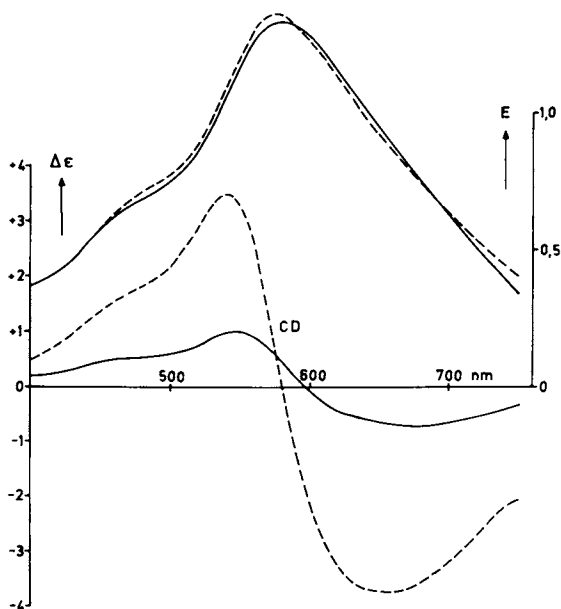
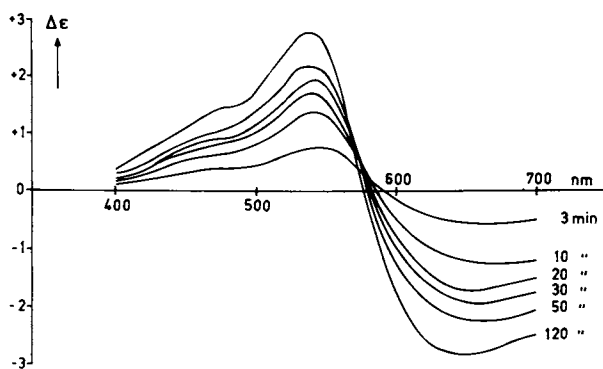


Figure 7. Absorption and CD spectra of amylose-iodine complex DP 51 in dilute solution 10 min (—) and 24 h (---) after adding iodine. (Amylose, concn = 0.07 g/L; 1 I_3^- per 6 anhydroglucose residues; 1 I_2 per 1.6 I^- .)



Carbohydrate Research

Figure 8. Time-dependent increase of CD of amylose-iodine complex DP 47. (Amylose, concn = 0.07 g/L (17).)

longer chains. The formation of associated particles is unlikely since we found no residue after ultrafiltration using an 800 Å Nucleopore filter. Thus an *intramolecular* ordering process must be responsible for the time dependent increase of the Cotton effect in dilute solutions.

In order to examine whether interaction between chains also leads to an increase of the Cotton effect we studied amylose-iodine solutions under aggregating conditions. In experiments using iodine solutions of different I^- content we observed at standard amylose concentration (0.4 g/l) a considerable tendency towards aggregation with the initially I^- free iodine solution and with solution containing a large excess of I^- (1 $I_2/65 I^-$). As was accidentally observed, addition of large amounts (5-15 g/l) of potassium iodate also promotes aggregation (salting out effect). The results from CD measurements show an increase of CD (i) proportional to the KIO_3 concentration added when visible aggregation has not yet taken place and (ii) during the course of the formation of insoluble aggregates (solution a and d). Aggregated solutions were resuspended by shaking before measurement. The formation of soluble and insoluble aggregates is obviously compatible with a time dependent increase of the Cotton effect. Whether the increase of the Cotton effect is due to an *intermolecular* alignment and/or to a preceding *intramolecular* ordering process, which also could be folding, remains an open question. However, we wish to point out that an ordering of the asymmetric centers along the chain (helix formation) could be facilitated by contact between different chains. Thus *intermolecular* interaction would give an additional contribution to the time dependent increase of $\Delta\epsilon$.

Fractional Precipitation of Amylose-Iodine Solutions. Fairly concentrated amylose solutions containing a mixture of two to five components (DP 90-5600) were precipitated by successive addition of KI_3 solution. The purified fractions were converted into tricarbanilate derivatives and were then separated over a high performance GPC column. The ratio of the components was obtained from careful evaluation of the peak areas using the concentration dependence of the single components and various mixtures of known composition. Figure 9 shows the elution curves of fractions a-d obtained from a two component system (DP 90 and DP 1800, 1:1).

We found that the higher molecular weight product is precipitated preferentially; this is the typical behavior for polymers. Different behavior would be expected if an association of lower molecular weight products or chain folding took place prior to the eventual precipitation. The results support the interpretation that the time dependent increase of the Cotton effect in dilute solutions (0.07-0.4 g/l) is not due to the formation of aggregated particles but rather the result of *intra-*

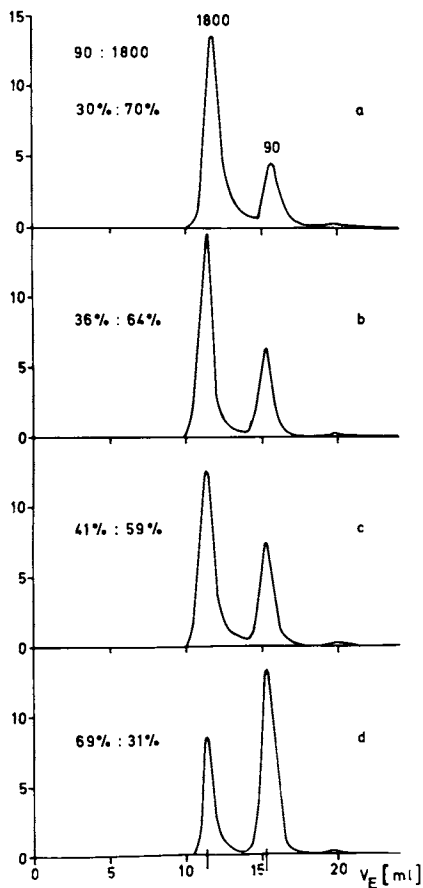


Figure 9. Fractional precipitation of amylose-iodine complexes DP 90 and 1800 (1:1). Elution curves of tricarbanilates in THF from HPLC-GPC. (Amylose solution: 200 mg DP 90 and 200 mg DP 1800 dissolved in 4 mL DMSO and diluted with water to 40 mL. Iodine solution: 0.05M I_2 , 0.76M KI, 0.1M KCl; fractions a-d were obtained by successive addition of 1 mL iodine solution.)

molecular ordering. Note a pronounced time dependent CD was found for the low molecular weight samples DP 38-125 but not for DP 2100.

Studies with Aqueous Amylose Solutions

Vacuum Ultraviolet CD Measurements. In order to investigate whether a preformed helical conformation exists in aqueous solution, we carried out CD measurements in the region of the sugar chromophores with one of the new instruments. These measurements were performed in collaboration with W. C. Johnson at Oregon State University in Corvallis, who recently studied maltooligomers including maltohexaose and a commercial amylose (37). We completed the series with readily soluble synthetic amyloses of DP 18 to 35; results for DP 25 are shown in Figure 10 along with the results of Lewis and Johnson (37).

All spectra show a weak negative band at about 182-184 nm and a strong positive band with a maximum at or below 164 nm. No abrupt change was observed in the shape of the CD curves with increasing chain length; there is a continuous increase of the negative band maximum near 182 nm. (Compared with the earlier measurements the CD curve of the synthetic sample DP 25 is shifted to longer wavelengths. To some extent this may be due to the higher temperature used in the later studies (38)).

Remarkably, all polysaccharides measured thus far give a similar pattern of two CD bands of opposite sign, one at about 180 nm and a second at about 164 nm (39,40,41). The signs and the relative magnitudes of these bands are characteristic of the polysaccharides. The band at 182 nm is tentatively assigned to the ring oxygen (42). The intense band at 164 nm is mainly attributed to hydroxyl groups absorbing in this region (42). The beginning of a helix formation may be expected to cause a splitting of the 182 nm band. However, no splitting and no change of even the shape of the CD curves is observed, when passing from maltose to amylose and this means that there is no twisting of adjacent chromophores in this region. The increase in CD, which is found, is most probably due to a stronger spatial fixation of the chain with increasing DP. These observations do not completely rule out a helix conformation; we can only state, that if helix formation takes place the 182 nm chromophore is insensitive to this process. Measurements in the region below 165 nm may give more information, but because of the absorption of water there these measurements have to be done with films and are therefore not directly comparable.

Fractional Retrogradation of Aqueous Amylose Solutions. In previous studies we investigated the association behavior of natural amylose with a broad molecular weight distribution and of synthetic monodisperse amyloses by light scattering measurements (1,5). In order to obtain quantitative data on the degree

of preferential retrogradation we studied solutions containing a sample of high association tendency (DP100) and a very stable one (DP 2270). Fractions were successively removed by centrifugation as soon as the solution became turbid. As described above amylose fractions were converted into tricarbonylates and then separated over a GPC column. Elution curves of fractions a-c obtained from a 1:1 mixture are shown in Figure 11.

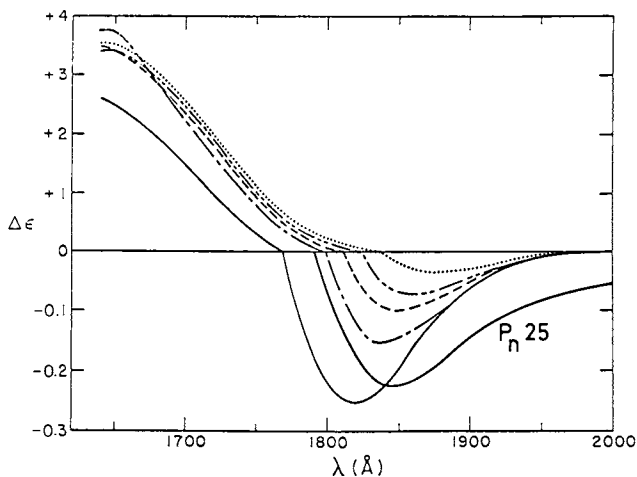
In retrograding solutions we expected a preferential precipitation of the DP 100 amylose. However, the ratio of the components in each fraction was found to be similar to the 1:1 composition of the solution. The same results were obtained with a 1:3 or a 3:1 composition ratio in the starting solution. The results show clearly that the high molecular weight product is involved in the association process from the very beginning.

Kodama and Noda (43) recently reported light scattering and sedimentation-equilibrium measurements on aqueous amylose solutions covering a wide range of molecular weights. Remarkably, in the range of DP 40 to 100 they observed associated particles with molecular weights corresponding to "dimers". The authors suggest that a B-type amylose aggregate, i.e. a double helix, has been formed in solution. This is supported by the rigid-coil conformation of these aggregates, which the authors found in contrast to the random coil behavior of the higher molecular weight fractions.

Conclusions

1. Resonance Raman measurements with iodine-complexed amyloses have shown that the vibration modes typical of the iodine species bound in the complex do not depend on the length of the polyiodine chain. Evidently these signals only give information about short sections of the polyiodine chain, as could be expected on the basis of Raman spectroscopy. Even at DP 18 no change in the position of the signals at 162 and 111 cm^{-1} is detectable. Thus resonance Raman spectra do not give the desired information about the nature of the polyiodine absorption bands. The assignment of both resonance Raman bands is still controversial (28,32) and it is not certain whether two different iodine species are involved.

2. The splitting of the CD corresponding to the long wavelength absorption maximum into a negative and positive contribution is a sign of asymmetric centers such as are found in helices. λ_{max} of absorption and λ_0 of the split CD are shifted simultaneously to longer wavelengths with increasing amylose chain length (Figure 1). Thus the split CD is related to the polyiodine chain length but the amylose need not necessarily be a perfect helix. A change from a less ordered to regularly ordered helix wound around the polyiodine chain would cause an increase of the Cotton effect but no shift in λ_0 provided that there was no change of the polyiodine chain length. The magni-



Biopolymers

Figure 10. CD spectra of amylose (—), maltohexaose (---), maltotetraose (-·-·-), maltotriose (-·-·-), and maltose (·-·-·) in aqueous solution at 10°C. Note that the scale of the negative range is enlarged 10 times. CD spectrum of synthetic amylose DP 25 in aqueous solution at 22°C (—) (37).

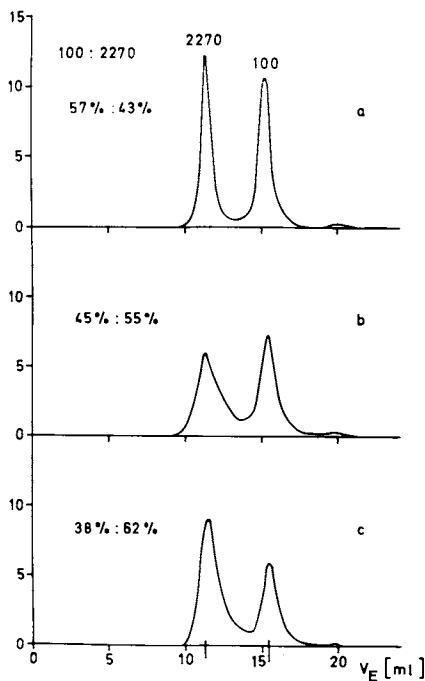


Figure 11. Stepwise retrogradation of amyloses DP 100 and 2270 (1:1). HPLC-GPC of tricarbonylates in THF. (Amylose solution: 200 mg DP 100 and 200 mg DP 2270 in 4 mL DMSO and diluted with water to 100 mL.)

tude of the Cotton effect is a measure of the asymmetric sites around the polyiodine chain. The time dependent increase of the Cotton effect on standing of amylose-iodine solutions results mainly from an *intramolecular* ordering process. In dilute solutions, where aggregates were shown to be absent, the ordering of short chains (DP 35-125) can be attributed to the transition from a loosely wound helical chain to a well organized helix leading to the observed increase of asymmetric sites for iodine binding. Both models, that of Senior and Hamori (9) and that of Brant and coworkers (10), would fit these results. An additional effect from chain folding may take place at larger DP. Similarly aggregation, studied under various conditions, may contribute to the increased CD by means of further spatial fixation of the polyiodine chain.

3. CD measurements with aqueous amylose solutions (37) give no evidence for a splitting of the CD in the region of 182 nm. Thus there is no twisting of directly coupled adjacent chromophores in the region of the negative CD band assigned to the transition of ring oxygen. Also with other polysaccharides, known to form helical structures, a splitting of this CD band has not been observed in solution. Measurements in the absorption range of the hydroxyl groups, i.e. below 164 nm, are not possible in aqueous solution. Results obtained with films in this region can not be taken as representative for the situation in solution.

4. The results from stepwise retrogradation of a mixture of two amyloses with largely differing association tendency give no evidence for preformed double helices in solution, even in the critical range of high retrogradation rate. The double helix formation probably takes place simultaneously with precipitation. The retrogradation maximum around DP 80 seems to be connected with a critical size of crystallization nuclei rather than with the persistence length or a specially preordered conformation.

Acknowledgements

This work was financially supported by the Deutsche Forschungsgemeinschaft. We thank Dr. M. Moschallski for the resonance Raman measurements and stimulating discussions.

Literature Cited

1. Pfannemüller, B.; Mayerhöfer, H.; Schulz, R.C. Biopolymers, 1971, 10, 243.
2. Chanzy, H.; Pfannemüller, B., unpublished results.
3. Wu, H. H.; Sarko, A. Carbohydr. Res., 1978, 61, 7.
4. Husemann, E.; Burchard, W.; Pfannemüller, B. Stärke, 1964, 16, 143.

5. Husemann, E.; Pfannemüller, B.; Burchard, W. Makromol.Chem., 1963, 59, 1.
6. Burchard, W. Makromol. Chem., 1963, 59, 16.
7. Rundle, R. E.; French, D. J. Am. Chem. Soc., 1943, 65, 558.
8. Banks, W.; Greenwood, C. T., "Starch and Its Components"; Edinburgh University Press, Edinburgh, 1975.
9. Senior, M. B.; Hamori, E. Biopolymers, 1973, 12, 65.
10. Jordan, R. C.; Brant, D. A.; Cesàro, A. Biopolymers, 1978, 17, 2617.
11. Goebel, K. D.; Brant, D. A. Macromolecules, 1970, 3, 634.
12. Goebel, C. V.; Dimpfl, W. L.; Brant, D. A. Macromolecules, 1970, 3, 644.
13. Dimpfl, W. L.; Brant, D. A. Macromolecules, 1970, 3, 655.
14. Dubin, P. L.; Brant, D. A. Macromolecules, 1975, 8, 831.
15. Pfannemüller, B.; Mayerhöfer, H.; Schulz, R. C. Makromol. Chem., 1969, 121, 147.
16. Cesàro, A.; Brant, D. A. Biopolymers, 1977, 16, 983.
17. Pfannemüller, B. Carbohydr. Res., 1978, 61, 41.
18. Bailey, J. M.; Whelan, W. J. J. Biol. Chem., 1961, 236, 969.
19. Bush, C. A.; Brahm, J. in "Physico-Chemical Properties of Nucleic Acids", Ed. J. Duchesne, Academic Press, New York, 1967, Vol. 2, p. 147.
20. Bittiger, H.; Keilich, G. Biopolymers, 1969, 7, 539.
21. Pfannemüller, B.; Berg, A. Makromol. Chem., 1979, 180, 1201.
22. Noltemeyer, M.; Saenger, W. J. Am. Chem. Soc., 1980, 102, 2710.
23. Robin, M. B. J. Chem. Phys., 1964, 40, 3369.
24. Reddy, J. M.; Knox, K.; Robin, M. B. J. Chem. Phys., 1964, 40, 1082.
25. Handa, T.; Yajima, H. Biopolymers, 1979, 18, 873.
26. Awtrey, A. D.; Connick, R. E. J. Am. Chem. Soc., 1951, 73, 1842.
27. Maki, A. G.; Forneris, R. Spectrochim. Acta, 1967, 23A, 867.
28. Tasumi, M. Chem. Lett., 1972, 75.
29. Loos, K. R.; Jones, A. C. J. Chem. Phys., 1974, 78, 2306.
30. Heyde, M. E.; Rimai, L.; Kilponen, R.G.; Gill, D. J. Am. Chem. Soc., 1972, 94, 5222.
31. Kaya, K.; Nikami, N.; Udagawa, Y.; Ito, M. Chem. Phys. Lett. 1972, 16, 151.
32. Teitelbaum, R. C.; Ruby, S. L.; Marks, T. J. J. Am. Chem. Soc., 1978, 100, 3215.
33. Behringer, J. in "Raman Spectroscopy", Ed. H. A. Szymanski, Plenum Press, New York, 1967.
34. Mould, D. L.; Syngé, R. L. M. Biochem. J., 1954, 58, 571, 585, 593.
35. French, D. A.; Effenberger, J. A. Abstracts of Papers, 140th National Meeting of the American Chemical Society, 1961, 25T.
36. Handa, T.; Yajima, H. Biopolymers, 1980, 19, 723.

**American Chemical
Society Library
1155 16th St. N. W.**

Washington, D. C. 20036

37. Lewis, D. G.; Johnson Jr., W. C. Biopolymers, 1978, 17, 1439.
38. Lewis, D. G., Ph. D. Thesis, Oregon State University, 1976.
39. Balcerski, J. S.; Pysh, E. S.; Chen, G. C.; Yang, J. T. J. Am. Chem. Soc., 1975, 97, 6274.
40. Pysh, E. S. in "Excited States in Organic Chemistry and Biochemistry", Eds. B. Pullman; N. Goldblum, Reidel, Dordrecht, Holland, 1977, p. 409.
41. Liang, J. N.; Stevens, E. S.; Morris, E. R.; Rees, D. A. Biopolymers, 1979, 18, 327.
42. Nelson, R. G.; Johnson Jr., W. C. J. Am. Chem. Soc., 1976, 98, 4296.
43. Kodama, M.; Noda, H. Biopolymers, 1978, 17, 985.

RECEIVED August 26, 1980.

Initial Rapid Processes in Retrogradation of Amylose Observed by the Light-Scattering, Stopped-Flow Method

MASATAKE OHNISHI and KEITARO HIROMI

Department of Food Science and Technology, Kyoto University
Kitashirakawa, Sakyo Ward, Kyoto City, Kyoto 606, Japan

Retrogradation of amylose and starch has been studied by digestibility with amylase (1), X-ray diffraction (2), light-scattering (3, 4), amperometric titration (2), and other physico-chemical methods (5) over rather long time ranges, usually hours or days, or, at the shortest, minutes. No attempt seems to have been made to search for initial nucleation processes in a much shorter time range, milliseconds to seconds, to elucidate the mechanism of retrogradation. We found that the light-scattering stopped-flow method is quite suitable for this purpose.

Potato amylose retrogradation caused by pH-jump down from pH 12 to 6 has been studied by the digestibility method with glucoamylase and an amperometric titration as a function of time over range of days (1). The retrogradation becomes complete within one day. Thus, an investigation of the initial stage in the retrogradation is important and interesting.

A solution (pH 12-13, dissolved with 1 M alkali) of amylose having an average degree of polymerization (\overline{DP}) ca. 100 was mixed in a Union Giken stopped-flow apparatus with an acetic acid solution of various concentrations to give a final pH 2 to 7. At least two kinetic phases of different rates were clearly distinguished. Apparent first-order rate constants, k_{app} of the fast phase ($\sim 10 \text{ sec}^{-1}$) show a steep increase with decreasing pH between 6 and 4. The rate constants are much dependent on the concentration of amylose, suggesting that the initial fast phase proceeds by an intermolecular mechanism. The slow phase, on the other hand, which has rate constants in order of 10^{-2} sec^{-1} , was independent on the amylose concentration. Thus it is concluded that the fast intermolecular process plays an important and decisive role in the nucleation of amylose retrogradation.

Amylose of \overline{DP} 600 was examined to see the effect of chain length on rate constant of the initial rapid reaction. However, no initial rapid reaction was observed, only the slow reaction. Presumably, the concentration of \overline{DP} 600 amylose was too low to find the initial rapid reaction.

0097-6156/81/0150-0549\$05.00/0
© 1981 American Chemical Society

Other amyloses having \overline{DP} 18 and 40 were found to show little change in light-scattering in the time range examined. No slow phase of these, thus no retrogradation was observed. Moreover, corn amylopectin showed no change in light-scattering in any time range studied.

Amyloses, Amylopectin and Chemicals

Amylose of \overline{DP} ca. 100 and amylopectin were corn products purchased from Kanto Chemical Co., Inc. Other kinds of amylose from corn were obtained from Hayashibara Biochemical Laboratories and from Dr. John Robyt of Iowa State University, U.S.A. These samples of amylose were separated using the Sephadex column chromatography and were certified to have narrow distribution of molecular weight. Sodium hydroxide and other chemicals were guaranteed products of Wako Pure Chemical Industries Ltd.

Light-Scattering Stopped-flow Method

Weighed samples of dry amylose were placed in 1 M sodium hydroxide solution to dissolve at room temperature overnight, and the alkaline amylose solutions were diluted with water before use. The alkaline solutions (pH 12-13) of amylose were rapidly mixed, "pH-jump", with an acetic acid solution of suitable concentration to give the desired final pH, where the final pH was measured with a Radiometer PHM64 Research pH-meter after the reaction. The change in scattered light intensity caused by the downward pH-jump was followed by a Union Giken RA-1300 stopped-flow apparatus, gas-pressure driven type, with a quartz observation cell (2 mm bore). The light-scattering was observed at right angles to the incident beam (320 nm) through a cut-off filter (half transmittance wavelength at 295 nm). A schematic diagram is shown in Figure 1. Figures 2 and 3 show the mixing part and the whole apparatus, respectively. Dead time of the apparatus is about 1 msec. Data averaging was carried out by a Union Giken RA-450 microprocessor in connection with the stopped-flow apparatus as described elsewhere (6). All measurements were made at 25°C.

Light-Scattering Change of Amylose Induced by the pH-Jump

When the pH in the alkaline solution of amylose (pH 12-13) was jumped down to pH 3-5 in the stopped-flow apparatus, a rapid increase in the scattered light intensity was observed in the time range of milliseconds to seconds. Some examples of the time curves, which were obtained by the pH-jump from pH 12.0 to 3.4, are shown in Figures 4 and 5. An increase in light-scattering can be seen obviously. Another time curve scanned for several seconds (Figure 5) indicates clearly that the fast increase is followed by a slow increase in the light-scattering.

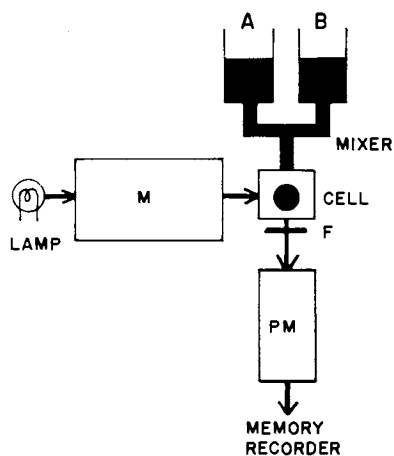


Figure 1. Schematic of the light-scattering stopped-flow apparatus. Samples (alkaline amylose and acetic acid solutions) are placed in the reservoirs A and B. M, monochromator ($\lambda = 320$ nm); F, a cut-off filter with half-transmittance wavelength at 295 nm; PM, photomultiplier; PM was set at 90° to the incident beam.

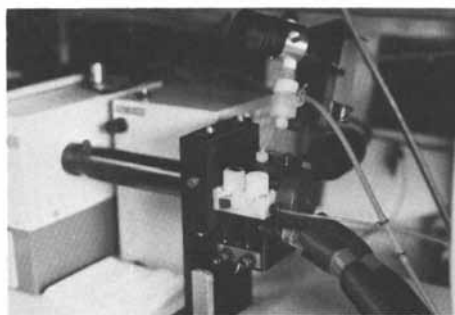


Figure 2. View of the mixing part of the apparatus (gas-pressure-driven type). The photomultiplier is set at right angles to the incident beam (black cylinder). The two sample reservoirs (with white caps) are in front of the mixer.

Figure 3. View of the whole apparatus. Right, a Union Giken RA-1300 stopped-flow spectrophotometer, gas-pressure-driven type) in light-scattering mode; left, a Union Giken RA-450 rapid data processor with a cathode ray monitor on the processor. The recorder is on the upper center shelf.

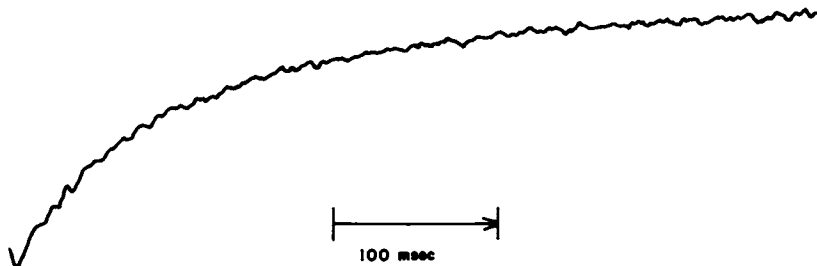
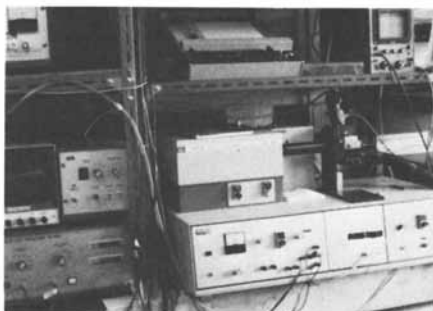


Figure 4. An example of the reaction curves obtained on the indicated time scale. Amylose ($\overline{DP} \approx 100$), 0.041% (final amylose concentration); pH jumped down from 12.0 to 3.4; 25°C.

Doppert and Staverman measured the rate of amylose retrogradation, which sets in as soon as the alkaline solutions are neutralized, with the light-scattering method and interpreted the retrogradation by the effective collisions of amylose molecules (7). The association rate of amylose was also measured to investigate the retrogradation by means of light-scattering in relation to degree of polymerization of amylose by Husemann *et al.* (8). The phenomenon observed by the light-scattering method is difficult to be interpreted briefly, in fact, but can be reasonably understood as the association of amylose molecules.

Kinetics of the Retrogradation of Amylose

Apparent first-order rate constants, k_{app} were evaluated for various concentrations of amylose from the reaction curves by using the method of Guggenheim (9). The analyzed values clearly indicate that at least two kinds of rate constants can be discriminated; the larger value ($\sim 10 \text{ sec}^{-1}$) and the smaller one ($\sim 10^{-2} \text{ sec}^{-1}$), which will be called the fast phase and the slow phase, respectively. Figure 6 shows that the rate constant of the fast phase is much dependent upon the concentration of amylose, that is, increases with increasing concentration of amylose. The points at concentration of amylose less than 0.1 % do not fall exactly on a linear plot, suggesting that a certain number of amylose molecules are involved cooperatively, if any, with a weak cooperativity, in the association reaction. In Figure 7, logarithms of the rate constant were plotted against logarithms of concentration of amylose. The logarithmic plots are linear, with a slope of about 1.2, indicating that the fast phase proceeds with second or higher order kinetics.

The slow phase, on the other hand, was independent on the amylose concentration, suggesting an intramolecular mechanism, and its rate constants were in order of 10^{-2} sec^{-1} in the concentration range studied. In this study, however, only the fast phase was examined and analyzed in detail, because the fast phase is the initial process of retrogradation, which carries an important and decisive role in the nucleation of amylose retrogradation.

Some models on the molecular configuration change of amylose (5, 10, 11) and a mechanism on the fibril formation similar to the amylose retrogradation (12) have been proposed on the basis of the results observed by the static techniques and the measurements of slow reaction, however, the initial fast nucleation process in such a short time range, milliseconds to seconds, has not been found and pointed out at all. Thus, the fast intermolecular process (second-order rate constant, in order of $1.5 \times$

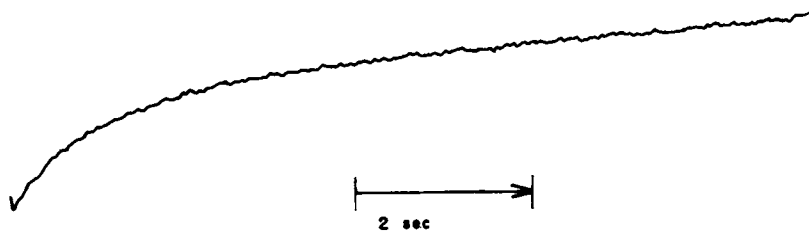


Figure 5. Another example of the reaction curves scanned for seconds. Amylose ($\overline{DP} \approx 100$); 0.041% (after mixing), pH jumped down from 12.0 to 3.4; 25°C.

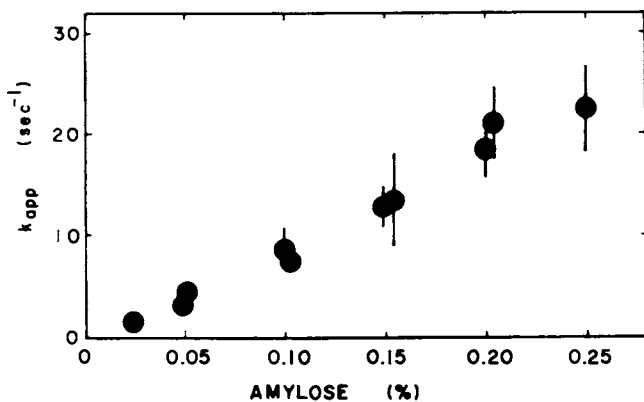


Figure 6. Dependence of k_{app} on the concentration of amylose. Amylose ($\overline{DP} \approx 100$); pH jumped down from 12.3 to 2.3; 25°C. The concentration indicated on the abscissa is the final concentration of amylose.

$10^5 \text{ M}^{-1} \text{ sec}^{-1}$) is tentatively concluded to carry a key role in the nucleation of the amylose retrogradation.

Dependency of the Rate Constant on the Final pH Value Obtained After the pH-Jump Down

Figure 8 shows the results obtained by the downward pH-jump to the various final pH values indicated in the figure. The rate constant, k_{app} , of the fast phase is very much dependent on pH, suggesting participation of some ionic group(s) in the process. Essentially, amylose has no ionic group in its molecular structure except pH higher than 12 (13, 14). One possibility is the existence of phosphate groups in the amylose molecule (15), and we are now going to measure phosphate in the amylose sample used.

Effect of \overline{DP} of Amylose on the Retrogradation Kinetics

The light-scattering change was also much dependent on the degree of polymerization of the amylose samples employed. Amylose having \overline{DP} of 18 and 40 were found to show little change in the scattered light intensity and to proceed in no retrogradation. Amylose of \overline{DP} 600 was observed to show no rapid increase, the fast phase, in the light-scattering, only the slow phase over the concentration range studied. The experimental result can be understood as follows; the concentrations of \overline{DP} 600 amylose, examined by 0.25 % (final concentration), were too low to find out the initial fast phase. These findings on the degree of polymerization support the results obtained by French, who has pointed out adequately that an exaggerated tendency of amylose to retrograde is greatly enhanced using amylose having \overline{DP} ca. 150-200 (16). It is also pointed out by Foster that the rate of retrogradation is markedly dependent upon the molecular size of amylose (17). Pfannemüller *et al.* have studied the dependences of rate of the retrogradation and of complex formation with iodine on chain length of amylose (18). They found a maximum rate of retrogradation at \overline{DP} 80 and suggested the presence of a well ordered, rigid structure in the molecular weight of amylose around \overline{DP} 80. Thus, \overline{DP} 80-100 seems to be a unit for the conformation of amylose; stiff helical segment or wormlike helical chain (18). \overline{DP} 100 amylose, employed mainly in the present study, is considered to be one of the best materials for the investigation of mechanism of the retrogradation and solution properties of amylose. It is, however, interesting and important to study the retrogradation of a serial amyloses in the wide range of molecular size by using the stopped-flow light-scattering method. Unfortunately, we cannot get the amylose samples having a serial and wide range of molecular weight.

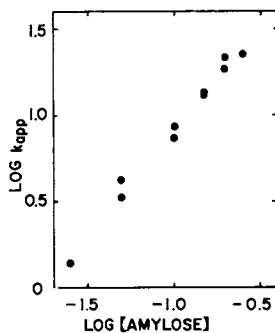


Figure 7. Logarithmic plots of k_{app} against the concentration of amylose. Experimental conditions are the same as those in Figure 6.

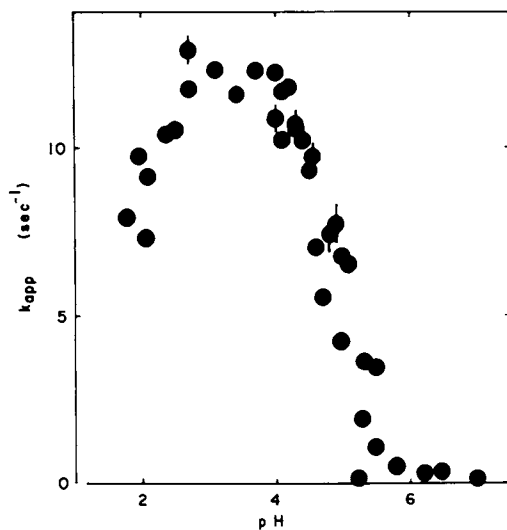


Figure 8. The pH dependence of k_{app} . Amylose ($\overline{DP} \approx 100$), 0.038% (after mixing; pH jumped down from 12.0 to the pH values indicated on the abscissa).

Abstract

An attempt to measure fast nucleation processes at the initial stage of retrogradation was carried out by the light-scattering stopped-flow method and with amylose having an average degree of polymerization (\overline{DP}) ca. 100. A solution of amylose in alkali (pH 12-13) was mixed in the stopped-flow apparatus with acetic acid solution of various concentration to give a final pH 2 to 7. The reaction was monitored by measuring the increase in light-scattering following neutralization. At least two phases were clearly distinguished. Rate constants of the fast phase are about 10 sec^{-1} , and show a steep increase with decreasing pH between 6 and 4. The rate constants increase with increasing concentration of amylose, suggesting that the initial fast process involves an intermolecular mechanism. On the other hand, the slow phase has rate constants of about 10^{-2} sec^{-1} and was independent on the amylose concentration. It is concluded that the fast intermolecular process is the key reaction in the nucleation of amylose retrogradation.

Symbols used

\overline{DP} , Average degree of polymerization; M, Molar concentration; λ , Wavelength; k_{app} , apparent first-order rate constant.

Acknowledgments

This study was supported in part by a grant from the Towa Foods Society for Promotion of Research, 東和食品研究振興会. We greatly appreciate their assistance. We are also grateful to Dr. D. French, Iowa State University and Dr. D. A. Brant, University of California, for helpful discussions and kind reviewing the manuscript.

This study has been reported in part at the Annual Meeting of the Japanese Society of Starch Science, June 20 (1979).

Literature Cited

1. Hizukuri, S.; Toyama, T.; Nikuni, Z. *Denpun Kogyo Kaishi* (in Japanese), 1971, **18**, 16-21.
2. Hizukuri, S. *Agric. Biol. Chem.* 1961, **25**, 45-49.
3. Kodama, M.; Noda, H.; Kamata, T. *Biopolymers*, 1978, **17**, 985-1002.

4. Burchard, W. Makromol. Chem., 1963, 59, 16-27.
5. Kuge, T.; Ono, S. Bull. Chem. Soc. Japan, 1961, 34, 1264-1271.
6. Ohnishi, M.; Hiromi, K. Carbohydr. Res., 1978, 61, 335-344.
7. Doppert, D. L.; Staverman, A. J. J. Polymer Sci., 1966, 4, 2353-2366.
8. Husemann, E.; Pfannemüller, B.; Burchard, W. Makromol. Chem. 1963, 59, 1-15.
9. Guggenheim, E. A. Phil. Mag., 1926, 2, 538.
10. Rao, V. S. R.; Foster, J. F. Biopolymers, 1963, 1, 527-544.
11. Szejtli, J.; Richter, M.; Augustat, S. Biopolymers, 1967, 5, 5-16.
12. Wood, G. C. Biochem. J., 1960, 75, 598-605.
13. Doppert, H. L.; Staverman, A. J. J. Polymer Sci., 1966, 4, 2367-2372.
14. Doppert, H. L.; Staverman, A. J. J. Polymer Sci., 1966, 4, 2373-2379.
15. Tabata, S.; Hizukuri, S. Starch, 1971, 23, 267-272.
16. French, D. "Biochemistry of Carbohydrates, Biochemistry, Series One"; University Park Press: Baltimore, 1975; 5, 267-335.
17. Foster, J. F. "Starch, Chemistry and technology"; Academic Press, 1965, Vol. I, 349-391.
18. Pfannemüller, B.; Mayerhofer, H.; Schulz, R. C. Biopolymers, 1971, 10, 243-261.

RECEIVED October 6, 1980.

Separation of Starch Components by Affinity Chromatography

MEENA S. KARVE, SHOBHANA V. BHIDE, and N. R. KALE

Department of Chemistry, Division of Biochemistry, University of Poona,
Poona-411 007, India

The polysaccharides deposited in starch granules normally consists of a heterogeneous mixture of linear (amylose) and branched (amylopectin), isotactic homopolymers of D-glucose. Amylose consists of linear chains of D-glucopyranose units linked through α -(1 \rightarrow 4) bonds and is heterogeneous with respect to molecular weight (1.5×10^5 - 2.4×10^6). Amylopectin contains short linear chains of α -(1 \rightarrow 4) linked D-glucopyranose residues, which are interlinked mainly by α -(1 \rightarrow 6) linkages to form a highly branched structure. Amylopectin is heterogeneous with respect to degree of branching and molecular weight (1×10^6 - 6×10^7). There is some evidence for the presence of a material (5-10%) in starch granules which is intermediate between amylose and amylopectin (1). This fraction is characterized as amylose with few α -(1 \rightarrow 6) linkages which are resistant to the action of β -amylase but hydrolysed by pullulanase (2).

Chromatographic methods commonly employed for the separation of starch components are chiefly based on the differences in solubility, preferential adsorption of one of the components or its complexes with a suitable ligand. Gel filtration has also been used for the separation of starch components (3) and to study their interactions with iodine (4). The iodine complexes of amylose and amylopectin have been separated on a micro-scale by paper chromatography (5) using perchloric acid (40%) as a solvent. Similarly sodium hydroxide (0.2 M) has been used as a solvent to separate starch components on filter paper (6). The use of strong acids and alkalis in presence of oxygen is bound to cause some degradation of starch components.

Amylose is the only homopolysaccharide of D-glucose which exhibits the unique property of forming a blue coloured amylose-iodine-complex in aqueous

solution. The helical nature of the amylose-iodine-complex, having six glucose residues per helical turn and iodine molecules packed inside the helix has been well established by X-ray diffraction studies (7). In solution amylose exists as a flexible random coil and in the presence of complexing agents, forms compact helical coils, with the ligand molecules entrapped inside the helix (8-13). The helical regions containing 110-130 D-glucose units are interspersed by random coil regions which contribute flexibility to the polymer chain (14). The outer linear chains of amylopectin containing 12-17 D-glucose residues interact with iodine (I_2) in a similar manner forming a blue-violet coloured complex (15).

We have reported a novel reversible interaction of amylose-iodine-complex with proteins, which is closely associated with the coil→helix transition of amylose chain, and the high adsorptive capacity of this complex appears to be due to hydrophobic interactions (16).

Here we describe a method for the separation of starch components, wherein crosslinked gelatin gel granules are used as an affinity matrix to retain amylose-iodine-complex (17).

Materials and Methods

All reagents were of 'Analar' grade and water distilled in all glass apparatus was used. Sodium dodecyl sulphate (SDS), Fluka (Switzerland) 90-93% was recrystallized thrice from ethanol and Ammonium persulphate, May & Baker (England) was used.

Blue value reagent (BVR) : Iodine ($7.87 \times 10^{-4} M$) +
KI ($1.21 \times 10^{-2} M$)

Reagent I : Acetate buffer (pH 4.8, 0.1 M) + BVR +
Urea (2 M)

Reagent II : Reagent I + SDS ($1.0 \times 10^{-3} M$)

Potato starch was prepared according to the method described by Schoch (18) and defatted by repeated extraction with hot chloroform : methanol (2:1). The defatted starch granules were equilibrated with saline (0.145 M) containing EDTA ($1 \times 10^{-3} M$) at room temperature (26-28°C), for 16-18 hours and further treated with 1-butanol : chloroform (3:1) to remove the trace amount of proteins (19). The starch solution was prepared by dispersing wet starch granules in sodium hydroxide (1.0 M) at room temperature (26-28°C) for 12-14 hours, followed by neutralization with HCl (0.5M) to pH 7.0 and centrifuged (2,418 g) before use. The enzyme, β -amylase (EC 3.2.1.2) was isolated from sweet

potatoes (20,21). It had a specific activity of 460 units/mg and was devoid of α -amylase (EC 3.2.1.1) and maltase (EC 3.2.1.20) activity.

Affinity gel matrix : the crosslinked gelatin granules were prepared from pig-skin gelatin (10%,w/v) essentially according to the method of Polson, Donnelly and Hodgkiss (22). The gel granules with particle size, 149 microns \pm 25 were obtained by sieving and the fines were removed by repeated decantation. The gelatin gel granules were iodinated with excess of Blue value reagent containing ammonium persulphate (0.15%) at room temperature (26-28°C) for 16-18 hours. On iodination, the gel granules were washed free of ammonium persulphate and equilibrated with Reagent I/II.

Column chromatographic system : A glass column (ϕ 2.5 x L 6.0 cm) with a capacity of \approx 20 ml was packed with crosslinked gelatin granules equilibrated with Reagent I/II. Both the ends of the column were plugged with polythene-mesh and connectors to attach polythene capillary tubings (1.0 mm ϕ). The column was covered with a black paper to protect it from light. The solutions were monitored under gravity (20-25 ml/hr) at room temperature (26-28°C). The fractions (5.0 ml) were collected on a fraction collector.

Soluble starch : A clear solution of starch (4.0 ml, 5 mg/ml) was mixed with 12.0 ml of Reagent I, centrifuged (2,418 g) and the clear solution of starch-iodine-complex was loaded on the column under gravity (20 ml/hr). The solution was recycled twice to ensure the complete retention of amylose-iodine-complex. The column was washed free of amylopectin-iodine-complex with Reagent I. The amylose-iodine-complex was eluted with acetate buffer (pH 4.8, 0.1 M) containing urea (2 M) (Figure 1).

Potato starch I : A clear solution of starch (4.0 ml, 5mg/ml) was mixed with 80.0 ml of Reagent I, centrifuged (2,418 g) and the clear solution of starch-iodine-complex was loaded on the column under gravity. The same procedure was followed as in the case of soluble starch, except that the amylose-iodine-complex was desorbed with acetate buffer (pH 4.8, 0.1 M) containing urea (8 M) (Figure 2).

Potato starch II : A clear solution of starch (4.0 ml, 5mg/ml) was mixed with 6.0 ml of acetate buffer (pH 4.8, 0.2 M + SDS - 2×10^{-3} M + Urea - 4 M) followed by 6.0 ml of iodine solution (1.575×10^{-3} M + KI - 2.410×10^{-2} M). The solution was centrifuged (2,418 g) before loading. The amylose-SDS-iodine-complex was eluted with acetate buffer (pH 4.8, 0.1 M) containing SDS (1.0×10^{-2} M) + Urea (8 M). The column was regenerated by passing 4-5 bed volumes of Reagent I/II and

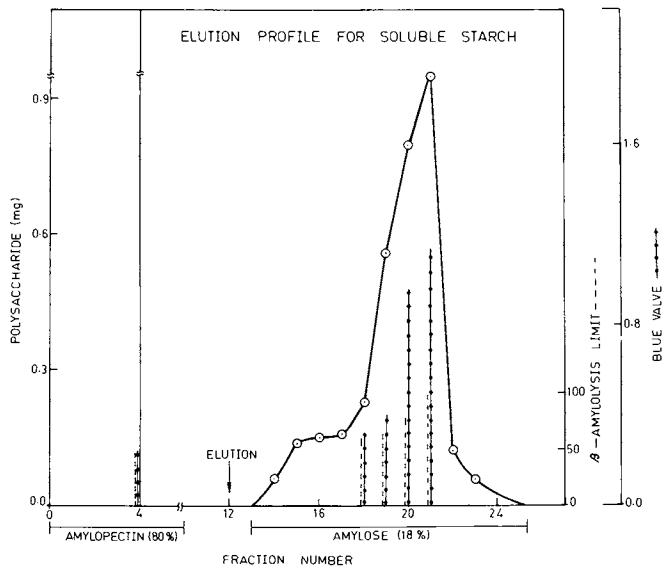


Figure 1. The amylose-iodine complex was eluted with acetate buffer (pH 4.8, 0.1M) containing urea (2M)

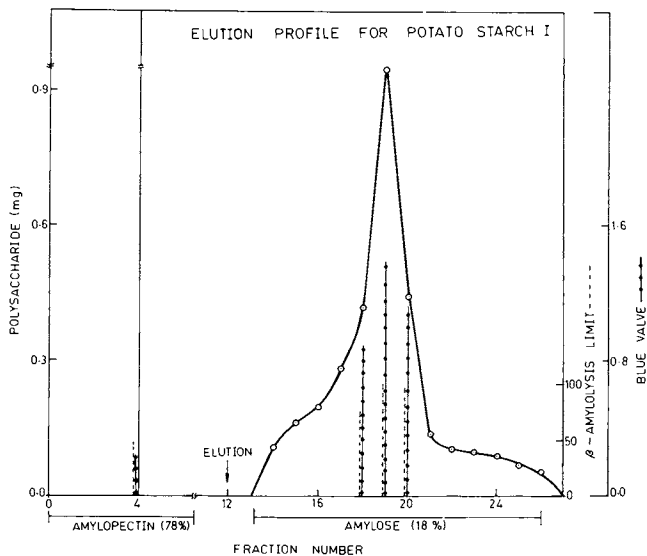


Figure 2. The amylose-iodine complex was eluted with acetate buffer (pH 4.8, 0.1M) containing urea (8M)

used for 2-3 times. The iodine in the collected fractions was reduced with sodium thiosulphate (0.1M) and the fractions were dialyzed against water to remove urea, SDS and salts. The fractions containing SDS were dialyzed against sodium bicarbonate (0.1M) followed by water. Further, 1-butanol treatment was given to remove the traces of SDS from the fractions containing amylose. These fractions were characterized by determining their blue value and β -amylolysis limit. The total polysaccharide content in the fractions was determined by Phenol-sulphuric-acid method (23).

Blue value : It is the absorbance of the blue colour, recorded at 680 nm at 30°C in 1.0 cm cuvette containing polysaccharide (0.1 mg) + BVR (1.0 ml) + acetate buffer 1.0 ml (pH 4.8, 0.1 M) in a total volume of 10.0 ml adjusted with water. For comparison, the optical density readings were multiplied by factor 4, since the values reported by McCready and Hassid (24) were taken in cuvette with an optical path of 4.0 cm. The β -amylolysis limit of the fractions was determined by incubating the polysaccharide (0.10 mg) with β -amylase (100 units/ml) in acetate buffer (pH 4.8, 0.1 M) for 6-8 hours, at 37°C, and the liberated maltose was estimated by the method of Park and Johnson (25).

Constant volume titration : (Figure 6)

A system containing polysaccharide (Amylose - 0.155 mg/Amylopectin - 0.50 mg/ Starch - 0.25 mg) 0.6 ml + Acetate buffer (pH 4.8, 0.1 M) 0.5 ml + Iodine solution (BVR + KCl - 1.21×10^{-2} M, 2:3 v/v) 0.1 ml \rightarrow 2.0 ml diluted with water, was incubated at 30°C ($\pm 0.05^\circ$) for 30 minutes. The absorbance at 286 nm was recorded on spectrophotometer (Shimadzu - UV 300) in 10 mm quartz cuvettes at 30°C using water as a blank.

Results and Discussion

Amylose in solution exists essentially as a random coil with short regions of extended loose helical conformation. In the presence of iodine (I_3^-), these loose helical regions undergo contraction, forming a compact V type helical domains with iodine molecules trapped in the helical lumen. These helical domains are interspersed by random coil regions, which contribute flexibility to the complexed polymer chain as revealed by the hydrodynamic studies (8, 26). This coil \rightarrow helix transition induced by iodine (I_3^-) probably generates some hydrophobic regions on the surface of the complex. Interaction of these hydrophobic regions with the hydrophobic pockets on the crosslinked gelatin gel matrix results in the retention of amylose-iodine-

complex. The amylopectin-iodine-complex with short terminal helices is not retained, probably due to weak interaction with gel matrix. When amylopectin-iodine-complex was loaded on the column, it was observed that almost all the polysaccharide (98-99%) appeared in the effluent, indicating that it has no affinity for the crosslinked gel matrix.

The experiments with soluble starch-iodine-complex have clearly shown that amylose-iodine-complex is strongly adsorbed on the gel matrix and occupies a blue coloured zone at the top of the column. It is clearly visible when the column is washed free of amylopectin-iodine-complex with Reagent I. The amylose-iodine-complex could not be desorbed by increasing the urea concentration (1→4 M - stepwise gradient) in presence of iodine (Reagent I). Hydrophobic interactions are weakened by polarity reducing solvents like ethylene glycol. However, ethylene glycol (40%) in Reagent-I did not desorb amylose-iodine-complex. Sodium thiosulphate (0.1 M) in acetate buffer (pH 4.8, 0.1 M) rapidly reduced the iodine and amylose was eluted as a sharp peak. Elution with acetate buffer (pH 4.8, 0.1 M) containing urea (2 M) produced a desired gradient of decreasing concentration of iodine, resulting in a gradual transition from helix→coil conformation, accompanied by the slow desorption of partially complexed amylose chains. The experiments with soluble starch gave very reproducible results. The elution profile of amylose was asymmetrical and the blue value and β -amylolysis limit of the amylose fraction revealed its heterogeneity. This was expected because soluble starch is a partially hydrolyzed starch (Figure 1).

The low molecular weight amylose-iodine-complex could be eluted with acetate buffer (pH 4.8, 0.1 M) containing 2 M urea (Figure 1), but in case of high molecular weight amylose-iodine-complex (Figure 2), it was necessary to increase the concentration of urea to 8 M to achieve complete desorption.

In case of potato starch it was necessary to dilute the solution (5 mg/ml - 4.0 ml + 80 ml Reagent-I) to avoid the precipitation of starch-iodine-complex. Attempts to avoid precipitation of potato starch-iodine-complex (5 mg/ml) by addition of amylopectin (2%), sucrose (10-20%) and ethylene glycol (10-40%) were not successful. Only sodium dodecyl sulphate helped to keep the potato starch-SDS-iodine-complex (5 mg/ml) in solution. Hence the influence of SDS concentration (3.5×10^{-4} - 3.5×10^{-3} M) on the retention of amylose-SDS-iodine-complex from potato starch was investigated. Under these conditions amylopectin-

-SDS-iodine-complex was quantitatively recovered in the effluent. The SDS also helped to maintain the flow rates during loading, washing and elution.

TABLE I

Characterization of Potato Amylose

Polysaccharide	Blue Value	β -amylolysis Limit (%)	Peak Fraction (%)
*			
Amylose	1.42	98	-
Amylose (Figure 2)	1.38	99	9.0
Amylose (Figure 3)	0.9	98	7.5

.

* Isolated by 1-butanol fractionation procedure (27)

The potato amylose eluted from the column constitutes 18-20% of the total polysaccharide. The pooled amylose fraction had a blue value-1.3 and β -amylolysis limit-91%. However the amylose from the peak fraction (9-10%) fairly compares with the potato amylose isolated by 1-butanol fractionation procedure (Table I). The blue value of amylose was low (Figure 3), because it was not possible to remove the traces of SDS even after repeated extraction with 1-butanol. The absorption spectra of this amylose-iodine-complex was identical with that of purified amylose-SDS-iodine-complex showing a characteristic blue shift. However, the β -amylolysis limit was same as that of the purified amylose. The amylose fractions with low blue value and β -amylolysis limit indicate the presence of amylose chains linked through bonds other than α -(1 \rightarrow 4). Though this column is able to pick-up amylose-iodine-complex/amylose-SDS-iodine-complex almost quantitatively, the subfractionation of amylose according to its degree of polymerization into discrete fractions is not achieved. Further work on the adsorption and elution of amylose of known degree of polymerization will provide valuable information for improving this resolution. The elution profiles for potato amylose (Figure 2 & 3) are asymmetrical and the blue value and β -amylolysis limit of the eluted fractions indicate the heterogeneity of amylose.

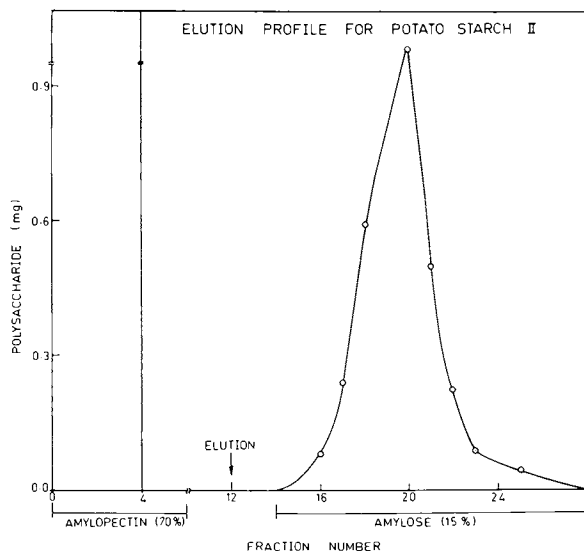


Figure 3. The amylose-SDS-iodine complex was eluted with acetate buffer (pH 4.8, 0.1M) containing SDS (1.0×10^{-3} M) + urea (8M)

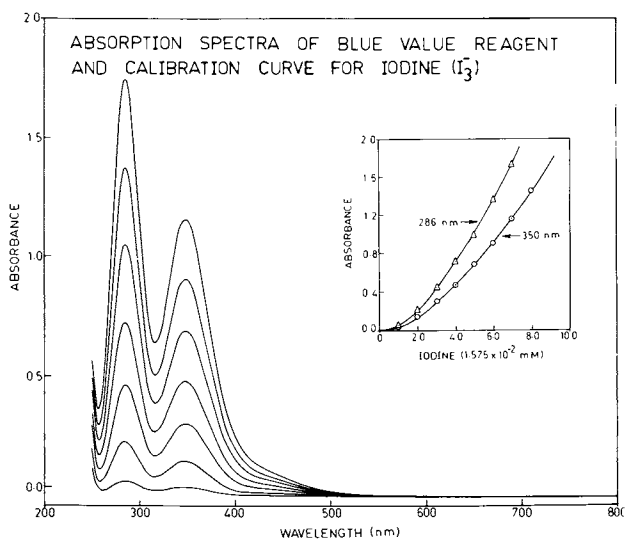


Figure 4. The system contains acetate buffer (pH 4.8, 0.1M) - 0.5 mL + iodine solution (BVR + KCl - 1.21×10^{-2} M, 2:3 v/v) - 0.125 mL \rightarrow 1.0 mL in a total volume of 5.0 mL adjusted with water

The pooled amylopectin fraction (Blue value-0.24; β -amylolysis limit-48%) fairly compares with that of purified potato amylopectin (Blue value-0.16; β -amylolysis limit-51%).

The high recovery (85-95%) of the polysaccharide suggests that this method can be used for the quantitative separation of starch components from defatted tuber and cereal starches, on a micro-scale.

A spectrophotometric method is developed for the determination of iodine binding capacity for starch and its components on a micro-scale. The absorption spectra of iodine in aqueous solution in acetate buffer pH 4.8, exhibits three distinct peaks at 286, 350 and 460 nm respectively (28). In the presence of sufficient amount of KI (Reagent-I) the peak at 460 nm is repressed which is attributed to iodine (Figure 4). The peaks at 286 and 350 nm are due to iodide (I_3^-) ions, since they are completely repressed by iodic acid. On addition of amylose to Reagent-I, a new peak appears at 640 nm while the peak at 350 nm is slightly enhanced (Figure 5). On increasing the concentration of iodine the absorbance at 640 nm increases and reaches a saturation level. The absorbance at 286 and 350 nm also increases and at the saturation level the absorbance is equal in case of amylose but not in the case of amylopectin or starch (Figure 6A). The concentration of free iodine (I_3^-) and absorbance at 286 nm can be correlated by a calibration curve (Figure 4). By using a constant volume titration method, bound iodine can be calculated by subtracting the free iodine from the total iodine. A plot of free iodine vs bound iodine shows a break point which on extrapolation gives the bound iodine (Figure 6B). The iodine binding capacity (IBC) of polysaccharide is expressed as the amount of iodine bound per 100 mg of the polysaccharide. The values of IBC obtained by this method are in good agreement with those obtained by conventional potentiometric and amperometric methods (29,30) (Table II).

TABLE II

Iodine Binding Capacity (IBC) of Potato Starch and its Components

Polysaccharide	Spectrophotometry	Potentiometry(31)
Amylose	19.8	19.8
Amylopectin	0.20	0.20
Potato Starch	4.4	4.2

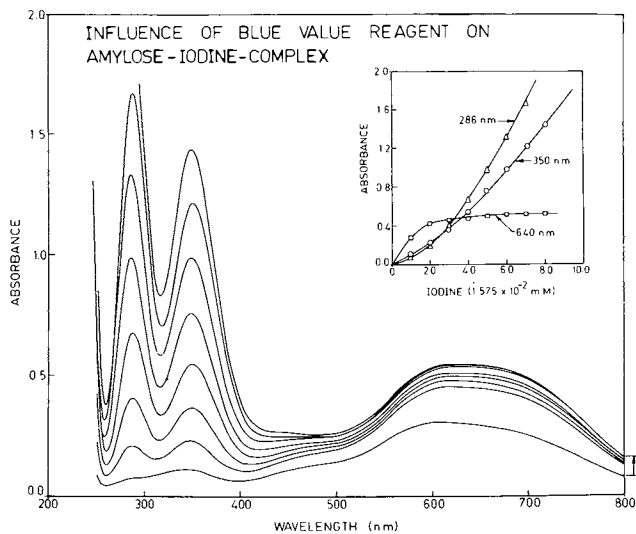


Figure 5. The system is the same as given in Figure 4 + amylose (0.07 mg)

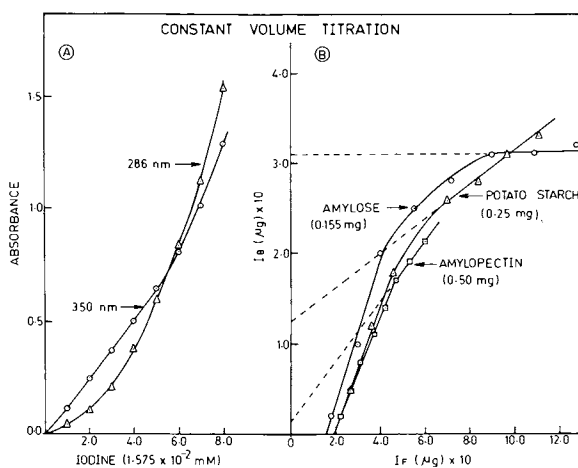


Figure 6.

Acknowledgements :

- Financial assistance in support of this work from;
1. University Grants Commission - New Delhi
 2. Council of Scientific & Industrial Research - New Delhi
 3. Youth Service Dept. (Science & Technology Cell) Govt. of Maharashtra - Bombay
 4. S. H. Kelkar Charity Trust - Bombay
 5. National Science Academy - New Delhi
 6. Department of Science & Technology - New Delhi
- is gratefully acknowledged.

Abstract

We have observed that proteins in solution display strong hydrophobic interaction with amylose-iodine-complex, forming insoluble precipitates which can be dissociated by reduction of iodine with a suitable reducing agent (16). Based on this observation we have developed a simple method for the separation of starch components by affinity chromatography on crosslinked gelatin granules in acetate buffer (pH 4.8, 0.1 M) containing urea (2 M) + Iodine ($7.87 \times 10^{-4}M$) + KI ($1.21 \times 10^{-2}M$) + SDS ($1.0 \times 10^{-3}M$). The amylose-SDS-iodine-complex is retained on the column and the amylopectin-SDS-iodine-complex appears in the effluent. The column is washed free of amylopectin-SDS-iodine-complex with the same solution and the amylose-SDS-iodine-complex was eluted with acetate buffer (pH 4.8, 0.1 M) containing urea (8 M) + SDS ($1.0 \times 10^{-3}M$). The amylose and amylopectin fractions were characterized by determining their blue value and β -amylolysis limit. A spectrophotometric method for the determination of iodine binding capacity of amylose, amylopectin and starch on a micro-scale is developed.

Literature Cited

1. Whistler, R.L. in 'Starch: Chemistry and Technology' Vol. I, Whistler, R.L. and Paschall, E.F. Eds. Academic Press, N.Y. (1965) pp. 331-347.
2. Banks, W. and Greenwood, C.T., Arch. Biochem. Biophys. (1966) 117, 674-675.
3. Yamada, T. and Taki, M., Stärke. (1976) 28, 374-377.
4. Kodama, M. and Sasaki, T., Bull. Chem. Soc. Jap. (1974) 47, 1368-1372.
5. Taki, M., Agr. Biol. Chem. (1962) 26, 1-9.
6. Ulmann, M., Stärke. (1964) 16, 151-157.
7. Rundle, R.E. and Edwards, F.C., J. Am. Chem. Soc. (1943) 68, 2200-2203.

8. Banks, W. and Greenwood, C.T., Carbohydr. Res. (1972) 21, 229-234.
9. Purvinas, R.M. and Zobel, H.F., Carbohydr. Res. (1969) 10, 129-139.
10. Bittiger, H., Husemann, E. and Pfannemüller, B., Stärke. (1971) 23, 113-117.
11. Senior, M.B. and Hamori, E., Biopolymers. (1973) 12, 65-78.
12. Foster, J.F. in 'Starch: Chemistry and Technology' Vol. I. Whistler, R.L. and Paschall, E.F. Eds. Academic Press, N.Y. (1965) pp 349-389.
13. Nguyen, Q.T., Aptel, P. and Neel, J., Biopolymers. (1976) 15, 2097-2100.
14. Szejtli, J., Richter, M. and Augustat, S., Biopolymers. (1967) 5, 5-16.
15. Pfannemüller, B., Carbohydr. Res. (1978) 61, 41-52.
16. Bhide, S.V. and Kale, N.R., Carbohydr. Res. (1979) 68, 161-167.
17. Karve, M.S., Bhide, S.V. and Kale, N.R., Paper presented at the Poster Session 'XIth International Congress of Biochemistry' Toronto, Canada, July 8-13, 1979.
18. Schoch, T.J., Methods. Enzymol. (1957) 3, 5-7.
19. Hirst, E., Manners, D.J. and Pennie, I. R., Carbohydr. Res. (1972) 22, 5-11.
20. Balls, A.K., Thomson, R.R. and Walden, M.K., J. Biol. Chem. (1946) 163, 571-572.
21. Nakayama, S. and Amagase, S., J. Biochem. (Tokyo) (1963) 54, 375-377.
22. Polson, S., Donnelly, M. and Hodgkiss, M., Prep. Biochem. (1976) 6, 421-430.
23. Dubois, M., Gilles, K.A., Hamilton, J.K., Rebers, P.A. and Smith, F., Anal. Chem. (1956) 28, 350-356.
24. McCready, R.M. and Hassid, W.Z., J. Am. Chem. Soc. (1943) 65, 1154-1157.
25. Park, J.T. and Johnson, M.J., J. Biol. Chem. (1949) 181, 149-151.
26. Cesa'ro, A. and Brant, D.A., Biopolymers. (1977) 16, 983-1006.
27. Patil, N.B., Gupte, S.P. and Kale, N.R., Makromol. Chem. (1974) 175, 1979-1994.
28. Bhide, S.V. and Kale, N.R., Biochim. Biophys. Acta. (1976) 444, 719-726.
29. Bates, F.L., French, D. and Rundle, R.E., J. Am. Chem. Soc. (1943) 65, 142-148.
30. Gilbert, G.A. and Marriott, J.V.R., Trans. Faraday Soc. (1948) 44, 84-93.
31. Patil, N.B. and Kale, N.R., J. Chromatogr. (1973) 84, 75-85.

RECEIVED August 26, 1980.

INDEX

- A**
- Acetamido groups, CD of 279
- Acetamido sugar(s)
- CD spectra of 300
 - oligosaccharides containing 296
 - conformation of amide in 299
 - residues, CD of 278
 - VUCD spectroscopy of 293-302
- 2-Acetamido-2-deoxy-1-*N*-Acetyl- β -D-glucopyranosyl amine 298f
- 2-Acetamido-2-deoxy sugars 299
- CD spectrum of 296
- 2-Acetamido-2-deoxy-galactose (GalNAc) 294
- 2-Acetamido-2-deoxy- β -D-glucopyranose 169
- 2-Acetamido-2-deoxy-glucose (GlcNAc) 161, 294
- 2-Acetamido-2-deoxy-D-glucose 162
- 4-*N*-(2-Acetamido-2-deoxy- β -D-glucopyranosyl)-asparagine (GlcNAc-Asn), CD spectrum of 296
- Acetyl substitution 61
- N*-Acetyl sugars 279
- N*-Acetylgalactosamine 278, 297f
- N*-Acetylglucosamine 238, 278, 281, 285, 287, 297f
- and glucuronic acid, CD of 286f
- N*-Acetylglucosamine 275
- Acetyltetraglycylethyl ester (ATGEE) 231
- Acid hydrolysis of *S. Salivarius* 102
- Acid mucopolysaccharides in fish cornea 274
- Acridine orange bound to heparin 252
- Acridine orange-heparin fluorescence, photochemical fading of 262
- Affinity chromatography, separation of starch components by 559-570
- Affinity gel matrix 561
- Agarose 441f, 443f, 445f, 450f
- Agglomeration of xanthan gum 32
- Aggregation of CTA 61-80
- Albumin, bovine serum 426
- Albumin, human serum 336, 345
- Algin, sodium salts of 406
- Alginate
- S-35 macro-ions 379
 - salts of 352
 - metal 350
 - solutions, protonation in 379-386
- Alginate acid from *Azobacter vinelandii* 379-386
- Alkali metal cations to polycarboxylates 358
- Amide(s)
- in acetamido sugars, conformation of 299
 - chromophores, CD of 293
 - chromophores, dichroic behavior of carboxyl and 285
 - glucopyranosyl 299
 - n*- π * transition 293
- Amino sugars, vicinal diacyl 296
- β -Amylase 559
- Amylopectin 494, 501, 504, 550, 559
- characterization of potato amylose and 494f
 - and glycogen, VUCD spectra of 310f
 - interaction of SDS with iodine complexes of amylose and 491-511
 - SDS-iodine complex 565
 - tricarbanilate 55, 56f
- Amylose 83-88, 559
- aggregate, B-type 544
 - and amylopectin, interaction of SDS with iodine complexes of 491-511
 - aqueous 529-548
 - carbanilates 533
 - chain conformation 529
 - Monte Carlo study of 492
 - decomposition and assignment of spectra 466
 - deep bluing mechanisms of triiodide ions in 455-475
 - effect 462
 - iodine binding 477-490
 - complex(es) 492, 495f, 497f, 560, 563-564
 - /amylose-SDS-iodine complex, influence of urea on 496, 505
 - CD spectra of 530
 - influence of iodine (BVR) on formation of 494
 - SDS on, inhibitory 500f, 501
 - urea on, destabilizing 500f
 - interaction of SDS with 507
 - iodide solutions 456

Amylose (<i>continued</i>)	
-iodide (<i>continued</i>)	
solution(s)	529-548
fractional precipitation of	541
ordering processes of	539
potato	565
and amylopectin, characteriza-	
tion of	494 <i>t</i>
retrogradation	549
retrogradation	549-558
kinetics	553-555
effect of DP on	555
solutions, fractional	543
-SDS-iodine complex	495 <i>f</i> , 497 <i>f</i> , 498 <i>f</i> , 499 <i>f</i> , 501
/amylopectin-SDS-iodine	
complex	501
influence of urea on amylose-	
iodine complex/	496, 505
spectra of	500 <i>f</i>
tricarbanilate (ATC)	55, 56 <i>f</i>
VUCD spectra of	309 <i>f</i>
V-Amylose helix	530
Amylose chain(s)	
Debye scattering function of	513-527
diffusion coefficient of	513-527
models	518-520
β -Amylolysis	565
3,6-Anhydro-L-galactose	440
Anionic polysaccharides, interaction	
between metal cations and	349-365
Anticoagulancy	261
Anticoagulant activity,	
heparin	251, 258 <i>f</i> , 260 <i>f</i> , 262
correlation of anionic density with	257
Antigen, polysaccharide	
of Group B <i>Streptococcus</i>	163 <i>f</i>
native Type 1a	170 <i>f</i>
Type III	170 <i>f</i>
native Type III streptococcal	166 <i>f</i>
Type 1a	165
Antigens, Group B streptococcal	162
Antithrombin-binding oligosaccharide	
sequence	261
<i>Aspergillus fumigatus</i>	150 <i>t</i>
<i>Aspergillus niger</i>	150 <i>t</i>
spectrum of galactomannan of	155 <i>f</i>
ATGEE (acetyltetraglycylethyl	
ester)	231
<i>Aureobasidium pullulans</i>	81
ATC (amylose tricarbanilate)	55
Axial birefringence	229
<i>Azobacter vinelandii</i> , alginate acid	
from	379-386
B	
<i>B. subtilis</i> levan	102
Bathochromic shift	455
Bead and spring model, xanthan	22
Bidentate coordination	322
Binding	
amylose-iodine	477-490
counterion	332
ionic-atmosphere-	230, 231
stoichiometric	230
territorial	230, 231
Birefringence	8, 28, 229, 247, 369
circular	531
radial	229
strain	442
Bjerrum length	405
Blood plasma	415
Blue value reagent (BVR)	560
Borate anions	327
with nonionic saccharides, Group II	
cations	317-330
Borate-treated xanthan gum	38-40
Bovine serum albumin	426
Butterfly hysteresis	442
BVR (blue value reagent)	560
C	
Cadmiummethylenediamine hydroxide	
(cadoxen)	55
Carbanilates, amylose	533
Carbazole procedure	112
Carbon-13 NMR	125-147
characteristics of gels	125-126
spectrum(a)	
of curdlan	132 <i>f</i> , 133 <i>f</i>
of (1 \rightarrow 3)- β -D-glucans	134 <i>f</i>
branched	140 <i>f</i>
of lentinan	142 <i>f</i>
of solid-state curdlan, CPMAS	132 <i>f</i>
Carboxyl and amide chromophores,	
dichroic behavior of	285
Carboxylated	
ligands	358
polyanions	352, 358
polysaccharides, natural	339-341
Carboxylates, monomeric	382
Carboxymethyl dextran	
(CMD)	428, 430, 432 <i>t</i> , 433
CD of	433
spectra	434 <i>f</i> , 435 <i>f</i>
Carboxymethylcellulose(s)	
(CMC)	351, 360, 451
metal salts of	350
ι -Carrageenan(s)	312, 332, 341, 345, 439
κ -Carrageenan(s)	441 <i>f</i> , 450 <i>f</i>
solution properties of	367-378
Cartilage, proteoglycan	213
monomer from whale nasal	214
CD (<i>see</i> Circular dichroism)	
CED (cupriethylenediamine	
hydroxide)	55
Cellulose	
acetate, properties of	61-80

- Cellulose (*continued*)
 triacetate (CTA) 65*t*, 69, 76
 aggregation of 61–80
 light scattering of 61
 polymer 74*t*
 tricarbaniolate (CTC) 44, 48–50, 57*f*
 structural formula for 45*f*
 trinitrate 57*f*
 viscosity–molecular weight
 relationships 43–59
Ceratocystis paradoxa 151*f*
Ceratocystis stenoceras 150*t*
 galactomannan 158*t*
 spectrum of 157*f*
 Cereal starches 567
 Chain dynamics, theory of 19
 Chain, free draining 516
 Chondroitin ABC lyase 220
 Chondroitin sulfate(s) (CHS) 213, 281
 chains 220
 solutions, ion–polyion interaction
 in 387–401
 Chondroitinase ABC 222*f*, 223*f*
 Chromophore(s)
 CD of amide 293
 dichroic behavior of carboxyl
 and amide 285
 iodine 533
 CHS (*see* Chondroitin sulfate)
 Circular dichroism (CD) 278, 293
 of acetamido groups 279
 of acetamido sugar residues 278
 of *N*-acetylglucosamine and
 glucuronic acid 286*f*
 of CMD 433
 of D-glucans, VU 303–315
 of glycosaminoglycans 275–292, 284*f*
 pH-dependent 281
 of hyaluronic acid 287
 of oligosaccharides 285, 287*f*
 of GAG, pH-dependent 282*t*
 and resonance Raman measure-
 ments 531–539
 spectrum(a)
 of acetamido sugars 300
 of oligasaccharides containing
 of 2-acetamido-2-deoxy-1-*N*-
 Acetyl- β -D-glucopyranosyl
 amide (β 1,2 DAG) 296
 of 4-*N*-(2-acetamido-2-deoxy-
 β -D-glucopyranosyl)-aspara-
 gine (GlcNAc-Asn) 296
 spectroscopy of acetamido sugars,
 UV 293–302
 of uronic acid residues 275
 CMA–iodine complex 488
 CMA, isotherms for 484*f*
 CMD 434*f*
 ion-binding data for 430
 CMC (carboxymethylcellulose) 351, 360
 CMD (*see* Carboxymethyl dextran)
 Coefficient
 self-diffusion 390
 translational diffusion 515, 523
 virial 529
 Condensed ion effects 354–358
 Configurational entropy of tethered
 polymers 265–274
 Conformational energy functions 81
 Conformational transition 376
 of (1 \rightarrow 3)- β -D-glucans,
 NaOH-induced 141–144
 Coil–helix transition 563
 polypeptide 479
 Copper(II) binding in alginate
 solutions 379–386
 Cornea, acid mucopolysaccharides
 in fish 274
 Cornea, osmiumtetroxide stained rabbit 266
 Corneal stroma, swelling tendency of 265
 Cotton effect 279, 530, 531, 541, 546
 Counterion binding 332
 Counterions, free 399
Crithidia fasciculata 150*t*
 Cross-polarization magic angle
 spinning (CPMAS) 125
 C-13 NMR spectrum of solid state
 curdlan 132*f*
 Cryoscopic method 418
 CTA (*see* Cellulose triacetate)
 CTC (*see* Cellulose tricarbaniolate)
 Cuprammonium hydroxide 55
 Cupriethylenediamine hydroxide
 (CED) 55
 Curdlan 126–138
 C-13 NMR spectra of 132*f*, 133*f*
 conformation of 129–131
 conformational transition of 131–136
 CPMAS C-13 NMR spectrum of
 solid state 132*f*
 gel network and gelation
 mechanism 136–137
 gelation behavior of 126, 128–129
 molecular-weight dependence of
 conformation of 136
 VUCD film spectra of 310*f*
 Cyclitols 322
 Cyclodextrins 129
 Cyclodextrin–I₅⁺ complex 478
 Cyclodextrin–pentaiodide structure 478
 Cyclohexaamylose 518
- D**
- Debye scattering function 514, 520–523
 of amylosic chains 513–527
 Debye–Hückel approximation 406
 Degradation of levan, hydrolytic 108
 Degradation product, methylated
 oligosaccharide 163*f*

4- <i>N</i> -(2-Deoxy-2-acetamido glycosyl)- asparagine	298f
Dermatan sulfate (DS)	281
Dextran(s)	88-92
derivative(s)	
hydration of	423
solution properties of	415-438
structure of ionic	416f
tetramethylammonium salt of	428
optical rotation of	416f
phosphate (DP)	432t
of amylose on retrogradation	
kinetics, effect of	555
-effect	457
solutions, thermodynamic parame- ters of	418
sulfate (DS)	332, 345, 358, 360, 415, 428, 432t
metal salts of	350
sodium salts of	406
viscosity of	417, 420f
Dextrin	478
Dichroic behavior of carboxyl and amide chromophores	285
Diethylaminoethyl dextran	426
Diffusion coefficient(s)	
of amylosic chains	513-527
histograms of	186f
translational	
of PGS	205f, 206f
self particle	203
z-averaged	193
translational	203
Dilution, enthalpy of	350-354
Dispersibility of xanthan gum	40
factor affecting	31
and hydration of glyoxal-treated	34-38
improvement	31-32
Dissipative shear modulus	241
Dissociation equilibria of xanthan and PS-10	339
DNA	388
DS (dermatan sulfate)	281

E

Electrostatic potential, Poisson- Boltzmann	243
Electrostatic repulsion	388
Electrostricted hydration	426
Encapsulation of xanthan gums	32
Energy functions, conformational	81
Enthalpy of dilution	351-354
Equilibria, protonation	382
Equilibrium properties, ion-polyion interactions and	3-8
Ethylene glycol hydroxyl groups	320
Exocellular polysaccharide	339
Exopolysaccharide	31

F

Fibril formation	553
Fish cornea, acid mucopolysaccha- rides in	274
Flory-Fox equation	108
Fluoresceine	338, 345
Fluorescence fading	257, 260f
Fluorescence, photochemical fading	
acridine orange-heparin	262
Free counterions	399
Free draining chain	516
D-Fructofuranose	101

G

GAG (<i>see</i> Glycosaminoglycans)	
Gal(β 1-3)GlcNAc(β 1-3)Gal(β 1-4)- Glc	298f
β -D-Galactofurano- α -D-mannopyranans, galactose to galactose structures in	149-159
β -D-Galactofurano- α -D-mannopyranans, galactose to mannose structures in	149-159
β -D-Galactofuranosyl	149
mannose	152
units	150t
2- <i>O</i> - β -D-Galactofuranosyl- α -D- mannopyranose	152
2- <i>O</i> - β -D-Galactofuranosyl-(methyl- α -D-mannopyranoside), spectrum of	153f
3- <i>O</i> - β -D-Galactofuranosyl-(methyl- α -D-mannopyranoside), spectrum of	153f
6- <i>O</i> - β -D-Galactofuranosyl-(methyl- α -D-mannopyranoside), spectrum of	155f
Galactomannan(s)	441f, 442-448, 450f, 451
of <i>Aspergillus niger</i> , spectrum of ..	157f
<i>C. stenoceras</i>	158t
spectrum of	157f
<i>Sporothrix schenckii</i>	152, 154t
of <i>Trichophyton interdigitale</i> , spectrum of	155f
of <i>Trypanosoma cruzi</i> , spectrum of ..	157f
D-Galactopyranose	162
β -D-Galactopyranose	167, 169
residues	165
β -D-Galactopyranosyl unit	149
β -D-Galactopyranosyluronic acid	162
Galactose to galactose structures in β -D-galactofurano- α -D-manno- pyranans	149-159
Galactose to mannose structures in β -D-galactofurano- α -D-manno- pyranans	149-159
D-Galactose	162, 449

- L-Galactose 440
- Gel(s)
- of branched (1 → 3)- β -D-glucans 138
 - C-13 NMR characteristics of 125-126
 - network of branched (1 → 3)- β -D-glucans 144
 - network and gelation mechanism, curdlan 136-137
 - thermoreversible 376
- Gelation mechanism, curdlan, gel network and 136-137
- Gibb-Duhem equation 269
- Gleditsia* galactomannan 448
- Glucans 449-451
- characterization of branched 138
- D-Glucan(s)
- CD 307*t*-309*t*
 - chains 96
 - VUCD of 303-315
- α -D-Glucan(s) 311
- chain segments, dimeric 84*f*
- (1 → 3)- β -D-Glucans
- C-13 NMR spectra of 134*f*
 - branched 140*f*
 - gel(s)
 - of branched 138
 - network of branched 144
 - state 125-147
 - NaOH-induced conformational transition of 141-144
- Glucmannans 448-449
- Glucopyranosides 311
- α -D-Glucopyranoside 312
- Glucopyranosyl amides 299
- 3,5-Glucopyranosyl residues 138
- Glucose, α -D-(1 → 4)-linked 131
- Glucose residues, β -D-(1 → 6)-linked 141
- D-Glucose 162, 492
- isotactic homopolymers of 559
 - residue 141
- α -D-Glucose 306
- β -D-Glucose 306
- α -1,6-Glucosidic linkages 415
- Glucuronic acid, CD of *N*-acetylglucosamine and 286*f*
- D-Glucuronic acid 229
- Glucuronidase digestion of tetrasaccharides 285
- Glycans 275
- Glycogen, VUCD spectra of amylopectin and 310*f*
- Glycosamine 275
- monomers, rotational strengths of 279
- Glycosaminoglycan(s) (GAG) 261, 275, 332
- CD of 275-292, 284*f*
 - pH dependent 281, 282*t*
 - HP 253, 259
 - nonheparin 252
 - optical activity of 279
- Glycosaminoglycan(s) (GAG) (*continued*)
- polysaccharide 229
 - primary structure of 276*f*-277*f*
 - side-chains 201
 - sulfated 215
- α -O-Glycosylation effects 152
- Glyoxal-treated xanthan gum 40
- dispersibility and hydration of 34-38
- Glyoxal treatment of polyhydroxyls 32-34
- GPC/LALLS 50
- accuracy of 48
 - configuration 45*f*
 - methodology 46
 - reproducibility of 48
- Group B streptococcal antigens 162
- Group II cations and borate anions with nonionic saccharides 317-330
- Guar gum derivatives 38
- Gyration, radius(ii) of 194*f*, 195
- z-averaged 179

H

- Heat of dilution 332
- Helix chain, extended 529
- Helix-coil transition 136, 244, 367-369
- Hemiacetals, hydrolysis of 34
- Heparins 251-264, 281, 332, 336, 345, 407
- acridine orange bound to 252
 - anticoagulant activity 258*f*, 260*f*, 262
 - correlation of anionic density with 257
 - calcium salt of 406
 - chains 338
 - characterization of 253
 - dynamic conformational properties
 - of 252
 - isolation of 253
 - N-desulfated 281
 - properties of 256
 - sodium salts of 406
 - sulfated polysaccharides and 332-339
- Hexafluoro-isopropanol (HFIP) 279, 300
- Hyaluronate interaction with PGS 208, 211
- Hyaluronate, x-ray diffractograms of 288
- Hyaluronic acid 213
- CD of 287
 - oligosaccharides of 285, 287*f*
 - dynamic viscoelasticity of 219*f*
 - solution properties of 229-250
 - on viscosity of proteoglycan
 - monomer, effect of 216*f*
- Hyaluronidase, testicular 287
- Hydration
- of dextran derivative 423
 - electrostricted 426
 - hydrogen-bonded 426
 - hydrophobic 426
 - of oligodextran 423

- Mixing-rate effect 464
Molecular-weight transformation 196*t*
Monte Carlo
 averaging 516-517
 study of amylose chain
 conformation 492
 technique 513
Mucopolysaccharides in fish cornea,
 acid 274
- N
- Nasal cartilage, proteoglycan mono-
 mer from whale 214
Nasal septum, structural characteri-
 zation of PGS from 202-212
Nernst-Einstein relationship 387
Newtonian viscosity 1
Nigeran, VUCD film spectra of 310*f*
NMP (*N*-methyl propionamide) 232
NMR, C-13 125-147
Nuclear Overhauser enhancements 136-137
NVP (*N*-vinylpyrrolidone) 126
- O
- Oligodextran, hydration of 423
Oligodextran, solution properties of .. 415
Oligonucleotides 533
Oligosaccharide(s)
 containing acetamido sugars,
 CD spectra of 296
 degradation product, methylated 163*f*
 of hyaluronic acid, CD of 285, 287*f*
 sequence, antithrombin-binding 261
Optical
 activity of glycosaminoglycans 279
 rotation of dextran 416*f*
 rotatory dispersion (ORD) 531
ORD (*see* Optical rotatory dispersion)
Osmiumtetroxide stained rabbit
 cornea 266
Ovalbumin in urea, denaturation of .. 231
- P
- P. papulosa*, lichen 305
PGA (proteoglycan aggregate) 201
PGS (*see* Proteoglycan subunit)
PS-10, dissociation equilibria of
 xanthan and 339
PS-60 111-124
 deacetylated 116-119
 clarified 119
 fermentation conditions 111
 native 114-116
 viscosity 115*f*
pH-dependent CD of GAG 281, 282*t*
Plaque pH depression 102
Plasma, blood 415
- Poisson-Boltzmann electrostatic
 potential 243
Poisson-Boltzmann equation 388, 405
Polyanions, carboxylated 352, 358
Polyanions, sulfated 358, 360
Polycarboxylates 382
 alkali metal cations to 358
Polelectrolytes
 carboxylated 349
 phosphated 349
 sulfated 360
Polelectrolytic behavior of ionic
 polysaccharides 331-347
Polyhydroxyls, glyoxal treatment of .. 32-34
Polyiodine chains 486
Polyion-polyion interactions,
 thermodynamics of 331
Polymers, configurational entropy of
 tethered 265-274
Polysols 317-330
Polypeptide helix-coil transition 479
Polysaccharide(s)
 antigen
 of Group B *Streptococcus* 163*f*
 native Type 1a 170*f*
 Type III 170*f*
 native Type III streptococcal 166*f*
 Type 1a 164
 -counterion interaction 332
 exocellular 339
 glycosaminoglycan 229
 of Group B *Streptococcus*, structure
 and conformation of capsu-
 lar 161-172
 histograms for 184*f*
 interaction(s) between
 helices and β 1,4-linked
 polysaccharides 439-454
 metal cations and anionic 349-365
 polysaccharide helices and
 β 1,4-linked 439-454
 ionic
 charge fraction of 405-413
 polelectrolytic behavior of 331-347
 -protein interactions 336
 microbial 331
 natural carboxylated 339-341
 ribbon-forming 440*t*
 sulfated 331, 388
 and heparin 332-339
 type III streptococcal 164*t*
 Polystyrene sulfonated, salts of 360
 Poly(*N*-vinylpyrrolidone) (PVP) 126
 Potassium dextran sulfate-KCl
 system 428
 Potato amylose 565
 and amylopectin, characterization
 of 494*t*
 retrogradation 549

- Stockmayer-Fixman equation 417
- Stokes-Einstein equation 10
- Strain birefringence 442
- Streptococcal
- antigens, Group B 162
 - infections in new born 161
 - polysaccharide antigen, native
 - Type III 166*f*
 - polysaccharides, type III 164*t*
- Streptococcus*, Group B
- native Type 1a polysaccharide
 - antigen of 170*f*
 - polysaccharide antigen of 163*f*
 - structure and conformation of capsular polysaccharides of 161-172
 - Type III polysaccharide antigen of 170*f*
- Streptococcus salivarius* (*S. salivarius*)
- acid hydrolyses of 101
 - levan, properties of 101-110
- Streptomyces* hyaluronidase 221*f*
- Stroma, swelling tendency of corneal 265
- Sugar(s)
- acetamido
 - CD spectra of 300
 - oligosaccharides containing 296
 - conformation of amide in 299
 - residues, CD of 278
 - VUCD spectroscopy of 293-302
 - 2-acetamido-2-deoxy 299
 - N*-acetyl 279
 - vicinal diacyl amino 296
- Sulfaminohexose (SAH) 252
- Sulfate, dextran 345
- Sulfated
- polyanions 358, 360
 - polyelectrolytes 360
 - polysaccharides 331, 388
 - and heparin 332-339
- Sulfonates, salts of polystyrene 360
- Sulfopropyl dextran (SPD) 432*t*
- Swelling
- pressure 273
 - properties of connective tissue 265-274
 - tendency of corneal stroma 265
- T**
- Tamarindus indica* amyloid 451
- Teeth, demineralization of 102
- Testicular hyaluronidase 287
- Tetramethylammonium salt of dextran derivatives 428
- Tetrasaccharides, glucuronidase digestion of 285
- Thermoreversible gel 376
- Tissue, swelling properties of connective 265-274
- Transition
- conformational 376
 - helix-coil 267-269
 - sol-gel 369-376
- Translational diffusion coefficient (D_t) 515, 523
- of PGS 205*f*, 206*f*
 - self particle 203
 - for xanthan 3
 - z-averaged 203
- Translational diffusional motions 192
- Transport parameter measurements 390
- Trichophyton interdigitale* 150*t*
- spectrum of galactomannan of 155*f*
- Triiodide ions in amylose, deep bluing mechanisms of 455-475
- Trypanosoma cruzi* 150*t*
- spectrum of galactomannan of 157*f*
- Tuber starches 567
- U**
- UA (uronate) 252
- Urea
- on mylose-iodine complex/amylose-SDS-iodine complex, influence of 496, 505
 - on amylose-iodine complex, destabilizing influence of 500*f*
 - denaturation of ovalbumin in 231
 - perturbation with 496
 - solution, xanthan in 10
- Uronate (UA) 252
- Uronic acid residues, CD 275
- UV CD of D-glucans, vacuum 303-315
- UV CD spectroscopy of acetamido sugars, vacuum 293-302
- V**
- Vacuum UV CD (VUCD) 303, 433, 543
- of D-glucans 303-315
 - spectra of amylose 309*f*
 - spectra of amylopectin and glycogen 310*f*
 - spectroscopy of acetamido sugars 293-302
- Vicinal diacyl amino sugars 296
- Vinylpyrrolidone, *N*- (NVP) 126
- Virial coefficient 529
- Viscoelasticity, dynamic
- of hyaluronic acid 219*f*
 - of proteoglycan 218*f*
 - solution 216
- Viscosity
- of dextran(s) 417, 420*f*
 - Newtonian 10
 - of proteoglycan monomer, effect of hyaluronic acid on 216*f*
 - vs. shear stress data for xanthan 17-19
- VUCD (*see* Vacuum UV CD)

W		Xanthan (continued)	
Water, free	426	gum(s) (continued)	
Whale nasal cartilage, proteoglycan monomer from	214	encapsulation of	32
Whitcomb and Macosko, ellipsoid model of	16	glyoxal-treated	40
Worm-like chain model	62-63	dispersibility and hydration of	34-38
Worm-like model of xanthan	20	hydrodynamic radii of	8, 10
		hydrodynamic size of	3
		and PS-10, dissociation equilibria of	339
		rigid rod model	22
		rod	15
		solution, effect of molecular weight on structure of	28-29
		in solution, QELS studies of	1-13
		solutions, thermal transition in	8
		temperature, effect of	26
		translational diffusion coefficient (<i>D</i>) for	3
		in urea solution	10
		viscosity vs. shear stress data for ...	17-19
		worm-like model of	20
		X-ray diffraction studies of	1
		Xylans	451-452
		α -D-Xylopyranosides	311
		β -D-Xylopyranosides	311
X		Z	
Xanthan	331, 341, 367	Zimm	
in aqueous solution, conformation and interactions of	1-13	-Bragg parameters	480
bead and spring model	22	plot	179, 197, 204
behavior above 40°C	26	for PGS	207f
behavior below 40°C	26	-Rice model	244
chain	15		
stiffness of	15		
concentration, effect of	4		
conformational properties of	25-30		
conformational transition, depend- ence on pH, the dependence of	25		
gum(s)	188, 451		
agglomeration of	32		
borate-treated	38-40		
cross-linking agents of	32		
dispersibility	40		
factor affecting	31		
improvement of	31-32		